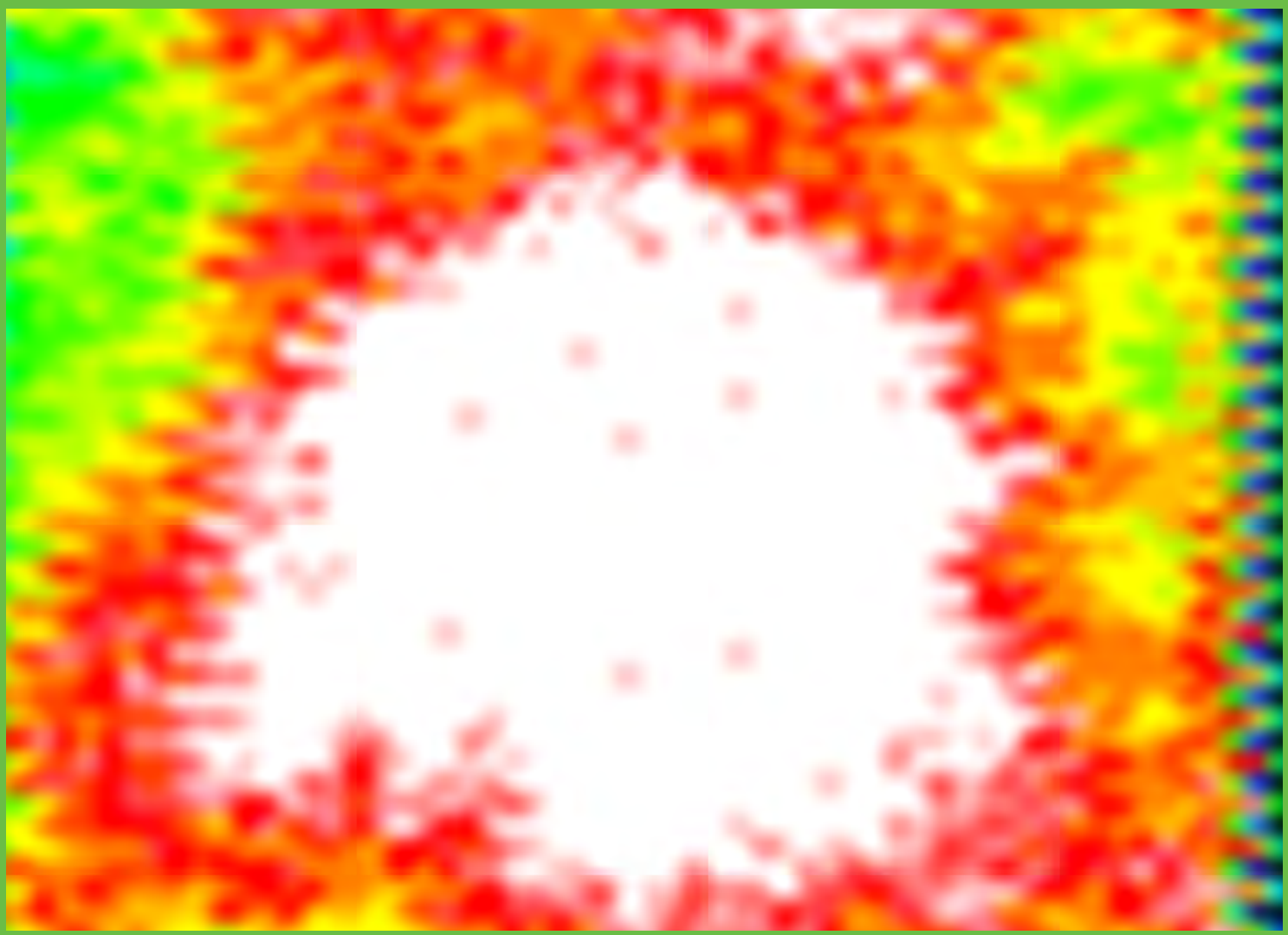
DYNA

Journal of the Facultad de Minas, Universidad Nacional de Colombia - Medellin Campus



DYNA 82 (194), December, 2015 - ISSN 0012-7353
Tarifa Postal Reducida No. 2014-287 4-72
La Red Postal de Colombia, Vence 31 de Dic. 2015.

UNIVERSIDAD NACIONAL DE COLOMBIA
SEDE MEDELLÍN
FACULTAD DE MINAS

UNIVERSIDAD NACIONAL DE COLOMBIA
SEDE MEDELLÍN
FACULTAD DE MINAS

DYNA
http://dyna.medellin.unal.edu.co/

DYNA is an international journal published by the Facultad de Minas, Universidad Nacional de Colombia, Medellín Campus since 1933. DYNA publishes peer-reviewed scientific articles covering all aspects of engineering. Our objective is the dissemination of original, useful and relevant research presenting new knowledge about theoretical or practical aspects of methodologies and methods used in engineering or leading to improvements in professional practices. All conclusions presented in the articles must be based on the current state-of-the-art and supported by a rigorous analysis and a balanced appraisal. The journal publishes scientific and technological research articles, review articles and case studies.

DYNA publishes articles in the following areas:

Organizational Engineering
Civil Engineering
Materials and Mines Engineering
Geosciences and the Environment
Systems and Informatics
Chemistry and Petroleum
Mechatronics
Bio-engineering
Other areas related to engineering

Publication Information

DYNA (ISSN 0012-73533, printed; 2346-2183, online) is published by the Facultad de Minas, Universidad Nacional de Colombia, with a bimonthly periodicity (February, April, June, August, October, and December). Circulation License Resolution 000584 de 1976 from the Ministry of the Government.

Contact information
Web page: http://dyna.unalmed.edu.co
E-mail: dyna@unal.edu.co
Mail address: Revista DYNA
Facultad de Minas Universidad Nacional de Colombia - Medellín Campus
Carrera 80 No. 65-223 Bloque M9 - Of.:107
Telephone: (574) 4255068 Fax: (574) 4255343
Medellín - Colombia

© Copyright 2014. Universidad Nacional de Colombia
The complete or partial reproduction of texts with educational ends is permitted, granted that the source is duly cited. Unless indicated otherwise.

Notice
All statements, methods, instructions and ideas are only responsibility of the authors and not necessarily represent the view of the Universidad Nacional de Colombia. The publisher does not accept responsibility for any injury and/or damage for the use of the content of this journal.
The concepts and opinions expressed in the articles are the exclusive responsibility of the authors.

Institutional Exchange Request
DYNA may be requested as an institutional exchange through the e-mail canjebib_med@unal.edu.co or to the postal address:

Biblioteca Central “Efe Gómez”
Universidad Nacional de Colombia, Sede Medellín
Calle 59A No 63-20
Teléfono: (57+4) 430 97 86
Medellín - Colombia

Indexing and Databases

DYNA is admitted in:

The National System of Indexation and Homologation of Specialized Journals CT+I-PUBLINDEX, Category A1

Science Citation Index Expanded
Web of Science - WoS, Thomson Reuters
Journal Citation Reports - JCR
SCImago Journal & Country Rank - SJR
Science Direct
SCOPUS
Chemical Abstract - CAS
Scientific Electronic Library on Line - SciELO
GEOREF
PERIÓDICA Data Base
Latindex
Actualidad Iberoaméricana
RedALyC - Scientific Information System
Directory of Open Acces Journals - DOAJ
PASCAL
CAPES
UN Digital Library - SINAB
CAPES
EBSCO Host Research Databases

Publisher’s Office
Juan David Velásquez Henao, Director
Mónica del Pilar Rada T., Editorial Coordinator
Catalina Cardona A., Editorial Assistant
Amilkar Álvarez C., Diagrammer
Byron Llano V., Editorial Assistant
Landsoft S.A., IT

Reduced Postal Fee
Tarifa Postal Reducida # 2014-287 4-72. *La Red Postal de Colombia,* expires Dec. 31st, 2015

UNIVERSIDAD NACIONAL DE COLOMBIA
SEDE MEDELLÍN
FACULTAD DE MINAS

DYNA

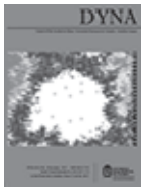


UNIVERSIDAD NACIONAL DE COLOMBIA

SEDE MEDELLÍN

FACULTAD DE MINAS

UNIVERSIDAD NACIONAL DE COLOMBIA
SEDE MEDELLÍN
FACULTAD DE MINAS



DYNA
http://dyna.medellin.unal.edu.co/

COUNCIL OF THE FACULTAD DE MINAS

Dean
Pedro Nel Benjumea Hernández PhD

Vice-Dean
Ernesto Pérez González, PhD

Vice-Dean of Research and Extension
Santiago Arango Aramburo, PhD

Director of University Services
Carlos Alberto Graciano, PhD

Academic Secretary
Francisco Javier Díaz Serna, PhD

Representative of the Curricular Area Directors
Luis Augusto Lara Valencia, PhD

Representative of the Curricular Area Directors
Wilfredo Montealegre Rubio, PhD

Representative of the Basic Units of Academic-Administrative Management
Gloria Inés Jiménez Gutiérrez, MSc

Professor Representative
Jaime Ignacio Vélez Upegui, PhD

Delegate of the University Council
León Restrepo Mejía, PhD

FACULTY EDITORIAL BOARD

Dean
Pedro Nel Benjumea Hernández, PhD

Vice-Dean of Research and Extension
Santiago Arango Aramburo, PhD

Members
Oscar Jaime Restrepo Baena, PhD
Juan David Velásquez Henao, PhD
Jaime Aguirre Cardona, PhD
Mónica del Pilar Rada Tobón, MSc

JOURNAL EDITORIAL BOARD

Editor-in-Chief
Juan David Velásquez Henao, PhD
Universidad Nacional de Colombia, Colombia

Editors
George Barbastathis, PhD
Massachusetts Institute of Technology, USA

Tim A. Osswald, PhD
University of Wisconsin, USA

Juan De Pablo, PhD
University of Wisconsin, USA

Hans Christian Öttinger, PhD
Swiss Federal Institute of Technology (ETH), Switzerland

Patrick D. Anderson, PhD
Eindhoven University of Technology, the Netherlands

Igor Emri, PhD
Associate Professor, University of Ljubljana, Slovenia

Dietmar Drummer, PhD
Institute of Polymer Technology University Erlangen-Nürnberg, Germany

Ting-Chung Poon, PhD
Virginia Polytechnic Institute and State University, USA

Pierre Boulanger, PhD
University of Alberta, Canadá

Jordi Payá Bernabeu, Ph.D.
Instituto de Ciencia y Tecnología del Hormigón (ICITECH)
Universitat Politècnica de València, España

Javier Belzunce Varela, Ph.D.
Universidad de Oviedo, España

Luis Gonzaga Santos Sobral, PhD
Centro de Tecnología Mineral - CETEM, Brasil

Agustín Bueno, PhD
Universidad de Alicante, España

Henrique Lorenzo Cimadevila, PhD
Universidad de Vigo, España

Mauricio Trujillo, PhD
Universidad Nacional Autónoma de México, México

Carlos Palacio, PhD
Universidad de Antioquia, Colombia

Jorge Garcia-Sucerquia, PhD
Universidad Nacional de Colombia, Colombia

Juan Pablo Hernández, PhD
Universidad Nacional de Colombia, Colombia

John Willian Branch Bedoya, PhD
Universidad Nacional de Colombia, Colombia

Enrique Posada, Msc
INDISA S.A, Colombia

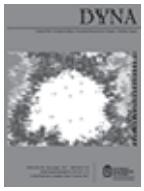
Oscar Jaime Restrepo Baena, PhD
Universidad Nacional de Colombia, Colombia

Moisés Oswaldo Bustamante Rúa, PhD
Universidad Nacional de Colombia, Colombia

Hernán Darío Álvarez, PhD
Universidad Nacional de Colombia, Colombia

Jaime Aguirre Cardona, PhD
Universidad Nacional de Colombia, Colombia

UNIVERSIDAD NACIONAL DE COLOMBIA
SEDE MEDELLÍN
FACULTAD DE MINAS



DYNA
http://dyna.medellin.unal.edu.co/

DYNA 82 (194), December, 2015. Medellín. ISSN 0012-7353 Printed, ISSN 2346-2183 Online

CONTENTS

Simulation of a hydrogen hybrid battery-fuel cell vehicle
Víctor Alfonsín, Andrés Suárez, Rocío Maceiras, Ángeles Cancela & Ángel Sánchez 9

Using waste energy from the Organic Rankine Cycle cogeneration in the Portland cement industry
José Pablo Paredes-Sánchez, Oscar Jaime Restrepo-Baena, Beatriz Álvarez-Rodríguez, Adriana Marcela Osorio-Correa & Gloria Restrepo 15

The production, molecular weight and viscosifying power of alginate produced by Azotobacter vinelandii is affected by the carbon source in submerged cultures
Mauricio A. Trujillo-Roldán, John F. Monsalve-Gil, Angélica M. Cuesta-Álvarez & Norma A. Valdez-Cruz 21

Supply chain knowledge management: A linked data-based approach using SKOS
Cristian Aarón Rodríguez-Enríquez, Giner Alor-Hernández, Cuauhtémoc Sánchez-Ramírez & Guillermo Córtes-Robles 27

The green supplier selection as a key element in a supply chain: A review of cases studies
Rodrigo Villanueva-Ponce, Liliana Avelar-Sosa, Alejandro Alvarado-Iniesta & Vianey Guadalupe Cruz-Sánchez 36

The effect of crosswinds on ride comfort in high speed trains running on curves
Miguel Aizpun-Navarro & Ignacio Sesma-Gotor 46

Valorization of vinasse as binder modifier in asphalt mixtures
Mª José Martínez-Echevarría-Romero, Gema García-Travé, Mª Carmen Rubio-Gámez, Fernando Moreno-Navarro & Domingo Pérez-Mira 52

Comparison of consistency assessment models for isolated horizontal curves in two-lane rural highways
Danilo Cárdenas-Aguilar & Tomás Echaveguren 57

Competition between anisotropy and dipolar interaction in multicore nanoparticles: Monte Carlo simulation
Juanita Londoño-Navarro, Juan Carlos Riaño-Rojas & Elisabeth Restrepo-Parra 66

Broad-Range tunable optical wavelength converter for next generation optical superchannels
Andrés F. Betancur-Pérez, Ana Maria Cárdenas-Soto & Neil Guerrero-González 72

Numerical analysis of the influence of sample stiffness and plate shape in the Brazilian test
Martina Inmaculada Álvarez-Fernández, Celestino González-Nicieza, María Belén Prendes-Gero, José Ramón García-Menéndez, Juan Carlos Peñas-Espinosa & Francisco José Suárez-Domínguez 79

Validating the University of Delaware's precipitation and temperature database for northern South America
Juan Sebastián Fontalvo-García, José David Santos-Gómez & Juan Diego Giraldo-Osorio 86

Experimental behavior of a masonry wall supported on a RC two-way slab
Alonso Gómez-Bernal, Daniel A. Manzanares-Ponce, Omar Vargas-Arguello, Eduardo Arellano-Méndez, Hugón Juárez-García, & Oscar M. González-Cuevas 96

Synthesis of ternary geopolymers based on metakaolin, boiler slag and rice husk ash
Mónica Alejandra Villaquirán-Caicedo & Ruby Mejía-de Gutiérrez 104

New tuning rules for PID controllers based on IMC with minimum IAE for inverse response processes
Duby Castellanos-Cárdenas & Fabio Castrillón-Hernández 111

Low-cost platform for the evaluation of single phase electromagnetic phenomena of power quality according to the IEEE 1159 standard
Jorge Luis Díaz-Rodríguez, Luis David Pabón-Fernández & Jorge Luis Contreras-Peña 119

Self-assessment: A critical competence for Industrial Engineering
Domingo Verano-Tacoronte, Alicia Bolívar-Cruz & Sara M. González-Betancor 130

Maintenance management program through the implementation of predictive tools and TPM as a contribution to improving energy efficiency in power plants
Milton Fonseca-Junior, Ubiratan Holanda-Bezerra, Jandecy Cabral-Leite & Tirso L. Reyes-Carvajal 139

Numerical modelling of Alto Verde landslide using the material point method
Marcelo Alejandro Llano-Serna, Márcio Muniz-de Farias & Hernán Eduardo Martínez-Carvajal 150

The energy trilemma in the policy design of the electricity market
Carlos Jaime Franco-Cardona, Mónica Castañeda-Riascos, Alejandro Valencia-Ariasc & Jonathan Bermúdez-Hernández 160

UNIVERSIDAD NACIONAL DE COLOMBIA
SEDE MEDELLÍN
FACULTAD DE MINAS

DYNA
http://dyna.medellin.unal.edu.co/

Influence of seawater immersion in low energy impact behavior of a novel colombian fique fiber reinforced bio-resin laminate 170
Fabuer Ramón-Valencia, Alberto Lopez-Arraiza, Joseba Múgica-Abarquero, Jon Aurrekoetxea, Juan Carlos Suarez & Bladimir Ramón-Valencia

Effect of V addition on the hardness, adherence and friction coefficient of VC coatings produced by thermo-reactive diffusion deposition 178
Fredy Alejandro Orjuela-Guerrero, José Edgar Alfonso-Orjuela & Jhon Jairo Olaya-Flórez

Multi-level pedagogical model for the personalization of pedagogical strategies in intelligent tutoring systems 185
Manuel F. Caro, Darsana P. Josyula & Jovani A. Jiménez

Impact of working conditions on the quality of working life: Case manufacturing sector colombian Caribbean Region 194
Laura Martínez-Buelvas, Oscar Oviedo-Trespalacios & Carmenza Luna-Amaya

Application of a prefeasibility study methodology in the selection of road infrastructure projects: The case of Manizales (Colombia) 204
Diego Alexander Escobar-García, Camilo Younes-Velosa & Carlos Alberto Moncada-Aristizábal

Simulation of a thermal environment in two buildings for the wet processing of coffee 214
Robinson Osorio-Hernandez, Lina Marcela Guerra-Garcia, Ilda de Fátima Ferreira-Tinôco, Jairo Alexander Osorio-Saraz & Iván Darío Aristizábal-Torres

A comparative study of multiobjective computational intelligence algorithms to find the solution to the RWA problem in WDM networks 221
Bryan Montes-Castañeda, Jorge Leonardo Patiño-Garzón & Gustavo Adolfo Puerto-Leguizamón

Determination of the Rayleigh damping coefficients of steel bristles and clusters of bristles of gutter brushes 230
Libardo V. Vanegas-Useche, Magd M. Abdel-Wahab & Graham A. Parker

Estimate of induced stress during filling and discharge of metallic silos for cement storage 240
Wilmer Bayona-Carvajal & Jairo Useche-Vivero

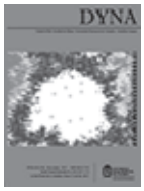
An early view of the barriers to entry and career development in Building Engineering 249
Margarita Infante-Perea, Marisa Román-Onsalo & Elena Navarro-Astor

Our cover
Image alluding to Article:
Influence of seawater immersion in low energy impact behavior of a novel colombian fique fiber reinforced bio-resin laminate

Authors:
Fabuer Ramón-Valencia, Alberto Lopez-Arraiza, Joseba Múgica-Abarquero, Jon Aurrekoetxea, Juan Carlos Suarez & Bladimir Ramón-Valencia



UNIVERSIDAD NACIONAL DE COLOMBIA
SEDE MEDELLÍN
FACULTAD DE MINAS



DYNA
http://dyna.medellin.unal.edu.co/

DYNA 82 (194), December, 2015. Medellín. ISSN 0012-7353 Printed, ISSN 2346-2183 Online

CONTENIDO

Simulación de un vehículo híbrido de hidrógeno con batería y pila de combustible 9
Víctor Alfonsín, Andrés Suárez, Rocío Maceiras, Ángeles Cancela & Ángel Sánchez

Aprovechamiento del calor residual por cogeneración con Ciclo Rankine Orgánico en la industria del cemento Portland 15
José Pablo Paredes-Sánchez, Oscar Jaime Restrepo-Baena, Beatriz Álvarez-Rodríguez, Adriana Marcela Osorio-Correa & Gloria Restrepo

La producción, el peso molecular y el poder viscosificante del alginato producido por Azotobacter vinelandii es afectado por la fuente de carbono en cultivos sumergidos 21
Mauricio A. Trujillo-Roldán, John F. Monsalve-Gil, Angélica M. Cuesta-Álvarez & Norma A. Valdez-Cruz

Administración del conocimiento en cadenas de suministro: Un enfoque basado en Linked Data usando SKOS 27
Cristian Aarón Rodríguez-Enríquez, Giner Alor-Hernández, Cuauhtémoc Sánchez-Ramírez & Guillermo Córtes-Robles

Selección de proveedores verde como un elemento clave en la cadena de suministro: Una revisión de casos de estudio 36
Rodrigo Villanueva-Ponce, Liliana Avelar-Sosa, Alejandro Alvarado-Iniesta & Vianey Guadalupe Cruz-Sánchez

Influencia del viento lateral en el confort de vehículos ferroviarios de alta velocidad circulando en curvas 46
Miguel Aizpun-Navarro & Ignacio Sesma-Gotor

Revalorización de la vinaza como modificador de betún para mezclas bituminosas 52
Mª José Martínez-Echevarría-Romero, Gema García-Travé, Mª Carmen Rubio-Gámez, Fernando Moreno-Navarro & Domingo Pérez-Mira

Comparación de modelos de análisis de consistencia para curvas horizontales aisladas en carreteras de dos carriles 57
Danilo Cárdenas-Aguilar & Tomás Echaveguren

Competición entre la anisotropía y la interacción dipolar en nanopartículas multi-núcleo: simulación Monte Carlo 66
Juanita Londoño-Navarro, Juan Carlos Riaño-Rojas & Elisabeth Restrepo-Parra

Conversor de longitud de onda óptico sintonizable de banda ancha para la siguiente generación de supercanales ópticos 72
Andrés F. Betancur-Pérez, Ana Maria Cárdenas-Soto & Neil Guerrero-González

Análisis numérico de la influencia de la dureza de la muestra y la forma de placa en el ensayo Brasileño 79
Martina Inmaculada Álvarez-Fernández, Celestino González-Nicieza, María Belén Prendes-Gero, José Ramón García-Menéndez, Juan Carlos Peñas-Espinosa & Francisco José Suárez-Domínguez

Validación de la precipitación y temperatura de la base de datos de la Universidad de Delaware en el norte de Suramérica 86
Juan Sebastián Fontalvo-García, José David Santos-Gómez & Juan Diego Giraldo-Osorio

Comportamiento experimental de un muro de mampostería apoyado sobre una losa de concreto reforzado 96
Alonso Gómez-Bernal, Daniel A. Manzanares-Ponce, Omar Vargas-Arguello, Eduardo Arellano-Méndez, Hugón Juárez-García, & Oscar M. González-Cuevas

Síntesis de geopolímeros ternarios basados en metakaolin, escoria de parrilla y ceniza de cascarilla de arroz 104
Mónica Alejandra Villaquirán-Caicedo & Ruby Mejía-de Gutiérrez

Nuevas reglas de sintonía basadas en IMC para un controlador PID con IAE mínimo en procesos con respuesta inversa 111
Duby Castellanos-Cárdenas & Fabio Castrillón-Hernández

Plataforma de bajo costo para la evaluación de fenómenos electromagnéticos monofásicos de calidad de la energía según el estándar IEEE 1159 119
Jorge Luis Díaz-Rodríguez, Luis David Pabón-Fernández & Jorge Luis Contreras-Peña

Autoevaluación: Una competencia crítica para la Ingeniería Industrial 130
Domingo Verano-Tacoronte, Alicia Bolívar-Cruz & Sara M. González-Betancor

Programa de gestión de mantenimiento a través de la implementación de herramientas predictivas y de TPM como contribución a la mejora de la eficiencia energética en plantas termoeléctricas 139
Milton Fonseca-Junior, Ubiratan Holanda-Bezerra, Jandecy Cabral-Leite & Tirso L. Reyes-Carvajal

Modelamiento numérico del deslizamiento Alto Verde usando el método del punto material 150
Marcelo Alejandro Llano-Serna, Márcio Muniz-de Farias & Hernán Eduardo Martínez-Carvajal

El trilema energético en el diseño de políticas del mercado eléctrico 160
Carlos Jaime Franco-Cardona, Mónica Castañeda-Riascos, Alejandro Valencia-Ariasc & Jonathan Bermúdez-Hernández

UNIVERSIDAD NACIONAL DE COLOMBIA
SEDE MEDELLÍN
FACULTAD DE MINAS



DYNA
http://dyna.medellin.unal.edu.co/

Influencia del agua de mar en el comportamiento frente a impacto de baja energía de un nuevo laminado de resina natural reforzada con fibra de fique colombiano 170
Fabuer Ramón-Valencia, Alberto Lopez-Arraiza, Joseba Múgica-Abarquero, Jon Aurrekoetxea, Juan Carlos Suarez & Bladimir Ramón-Valencia

Efecto de la adición de V en la dureza, adherencia y el coeficiente de fricción de recubrimientos de VC producidos mediante deposito termo-reactiva/difusión 178
Fredy Alejandro Orjuela-Guerrero, José Edgar Alfonso-Orjuela & Jhon Jairo Olaya-Flórez

Modelo pedagógico multinivel para la personalización de estrategias pedagógicas en sistemas tutoriales inteligentes 185
Manuel F. Caro a, Darsana P. Josyula b & Jovani A. Jiménez

Impacto de las condiciones de trabajo en calidad de vida laboral: Caso del sector manufacturero de la Región Caribe colombiana 194
Laura Martínez-Buelvas, Oscar Oviedo-Trespalacios & Carmenza Luna-Amaya

Aplicación de una metodología a nivel de prefactibilidad para la selección de proyectos de infraestructura vial. El caso de Manizales (Colombia) 204
Diego Alexander Escobar-García, Camilo Younes-Velosa & Carlos Alberto Moncada-Aristizábal

Simulación del ambiente térmico en dos edificaciones para beneficio húmedo de café 214
Robinson Osorio-Hernandez, Lina Marcela Guerra-Garcia, Ilda de Fátima Ferreira-Tinôco, Jairo Alexander Osorio-Saraz & Iván Darío Aristizábal-Torres

Estudio comparativo de algoritmos de inteligencia computacional multiobjetivo para la solución del problema RWA en redes WDM 221
Bryan Montes-Castañeda, Jorge Leonardo Patiño-Garzón & Gustavo Adolfo Puerto-Leguizamón

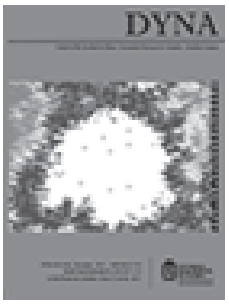
Determinación de los coeficientes de amortiguamiento de Rayleigh de cerdas y grupos de cerdas de acero de cepillos laterales 230
Libardo V. Vanegas-Useche, Magd M. Abdel-Wahab & Graham A. Parker

Estimación de esfuerzos inducidos durante el llenado y vaciado de silos metálicos para almacenamiento de cemento 240
Wilmer Bayona-Carvajal & Jairo Useche-Vivero

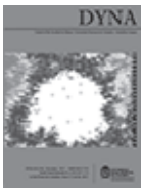
Una visión temprana de los obstáculos de acceso y deqsarrollo profesional en Ingeniería de edificación 249
Margarita Infante-Perea a, Marisa Román-Onsalo b & Elena Navarro-Astor

Nuestra carátula
Imagen alusiva al artículo:
Influencia del agua de mar en el comportamiento frente a impacto de baja energía de un nuevo laminado de resina natural reforzada con fibra de fique colombiano

Autores:
Fabuer Ramón-Valencia, Alberto Lopez-Arraiza, Joseba Múgica-Abarquero, Jon Aurrekoetxea, Juan Carlos Suarez & Bladimir Ramón-Valencia



UNIVERSIDAD NACIONAL DE COLOMBIA
SEDE MEDELLÍN
FACULTAD DE MINAS



DYNA
http://dyna.medellin.unal.edu.co/

Simulation of a hydrogen hybrid battery-fuel cell vehicle

Víctor Alfonsín [a], Andrés Suárez [b], Rocío Maceiras [c], Ángeles Cancela [d] & Ángel Sánchez [e]

[a] Centro Universitario de la Defensa, Escuela Naval Militar, Marín, España, valfonsin@cud.uvigo.es
[b] Centro Universitario de la Defensa, Escuela Naval Militar, Marín, España, asuarez@cud.uvigo.es
[c] Centro Universitario de la Defensa, Escuela Naval Militar, Marín, España, rmaceiras@cud.uvigo.es
[d] Escuela de Ingeniería Industrial, Universidad de Vigo, Vigo, España, chiqui@uvigo.es
[e] Escuela de Ingeniería Industrial, Universidad de Vigo, Vigo, España, asanchez@uvigo.es

Received: March 11th, 2014. Received in revised form: November 1rd, 2014. Accepted: October 25th, 2015

Abstract
This paper describes a vehicle simulation toolbox developed under Matlab® environment, which can be used to estimate the range of a vehicle battery, or a fuel cell/battery hybrid system. The model is function of mechanical and physical variables that depend not only on the vehicle but also on the ground. This toolbox can be extended to GPS tracking files by means of reading data file plug-ins. Even standard drive cycles can be simulated. Battery and hydrogen consumption, hydrogen storage tank level, battery state of charge, power consumption and fuel cell energy production, maximum range and maximum number of cycles for a real route can be determined. The model facilitates the prediction of the vehicle range and the hydrogen and energy consumption. Real route simulation gives a good approximation of the vehicle speed close to real-life services instead of using driving cycles that are quite arbitrary approximations to a real route.

Keywords: fuel cell vehicles; hydrogen, hybrid vehicles; simulation tool, battery.

Simulación de un vehículo híbrido de hidrógeno con batería y pila de combustible

Resumen
Este artículo describe una herramienta de simulación bajo el entorno de Matlab®, que puede ser utilizada para estimar la autonomía de un vehículo con baterías o híbrido con pila de combustible y baterías. El modelo es función de variables mecánicas y físicas que dependerán no solo del propio vehículo sino también del terreno. Su uso es extendido para recorridos obtenidos mediante dispositivos GPS y para ciclos estándar. Pueden obtenerse diferentes variables de salida tales como: el consumo de hidrógeno y batería, el nivel hidrógeno, el estado de carga de la batería, la potencia consumida, la producción de energía por parte de la pila, el máximo alcance del vehículo y el máximo número de ciclos finalizados. La simulación de rutas reales proporciona una buena aproximación de la velocidad del vehículo para usos, en lugar de utilizar ciclos de conducción estándar, obteniendo así aproximaciones bastante arbitrarias para una ruta real.

Palabras clave: Pila de combustible, hidrógeno, vehículos híbridos, simulación, batería.

1. INTRODUCTION

Automobiles are the major cause of urban pollution in the 21st century [1-3]. Fuel cell hybrid vehicles are a new emerging automotive technology that could reduce urban pollution, facilitate compliance with the Kyoto Protocol and reduce our dependence on oil [4,5].

Some automotive manufacturers have made commitments to introduce electric and fuel cell vehicles and hybrid fuel cell systems [6]. The prediction of performance and range is very important for their viability. Computing tools allow us to perform a rapid and economical evaluation of a proposed vehicle's performance [7].

Currently controllers for hybrid electric cars are based on parallel schemes with batteries and fuel cells, and the introduction of fuel cells into hybrid electric power systems principally extends the autonomy of the vehicle and the demanded power peak is only managed by the reversible energy storage system (batteries), allowing a drastic reduction on the fuel cell size [8,9].

© The author; licensee Universidad Nacional de Colombia.

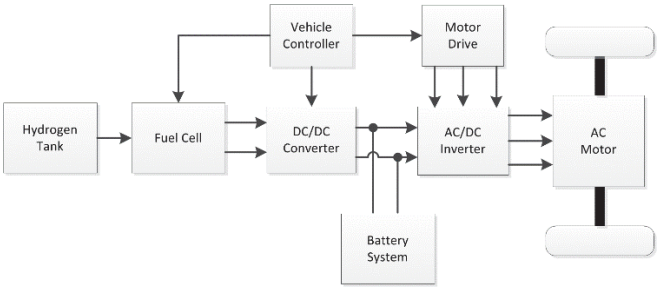


Figure 1. Fuel cell hybrid vehicle configuration.
Source: The authors

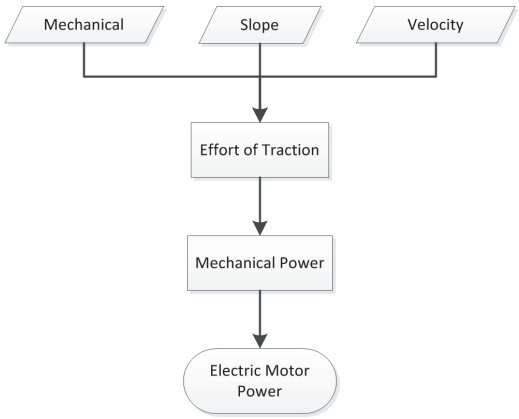


Figure 2. Electrical motor power output estimation.
Source: The authors

Fuel cells usually work in a steady-state mode for the average power demanded, and the excess of power yielded is then available to be used in the recharging process [10].

A tool to analyze and evaluate all of these vehicles is necessary so that a study of their technical and economic viability can be conducted [11].

2. Modelization Issues

The numerical model used for the hybrid vehicle simulation consists of several components. These components are specialized simulation modules separated in several m files. Every file has input and output parameters to be defined by the user before running the simulation. In the model, the vehicle dynamics, the electric motor, the battery block and the fuel cell have been considered [12,13].

Fig. 1 shows the fuel cell hybrid vehicle configuration used in the toolbox "SimuBus".

Vehicle dynamics Mechanical Power Simulation Model

This component consists of a longitudinal dynamic model of the vehicle. In Fig. 2, the flux diagram corresponding to the electrical motor power output calculation is presented. The variables considered are the vehicle mechanical features, road slope and instantaneous vehicle speed.

The mechanical traction effort should be directed toward moving the vehicle [14]:

$$P_{mechanical} = (F_{rr} + F_{ad} + F_{hc} + F_{la}) \cdot v \cdot \eta_g \qquad (1)$$

where F_{rr} is the force required to overcome the rolling resistance; F_{ad} is the force required to overcome the aerodynamic drag; F_{hc} is the component necessary to overcome the weight of the vehicle when it is climbing; F_{la} is the linear acceleration of the vehicle and η_g is the efficiency of the gearbox.

In terms of function inputs, vehicle mechanical properties must be known:

- Vehicle mass and front area.
- Rolling and aerodynamic coefficients.
- Gear ratio and efficiency.
- Regenerative ratio, in the case of a self-generation hybrid vehicle circulating over a negative slope path.

As output, the electric motor power output can be obtained.

Electric Motor Model. Input Electrical Power

Once the output mechanical power of the electric motor is calculated, the electrical power demand can be calculated too. To do this, the motor efficiency, or if that is not possible, the motor losses must be known. The losses are classified in four types [12,15,16]:

- Copper conductor losses
- Iron losses
- Friction and windage losses
- Constant losses (due to electronic control)

By calculating the efficiency and using the angular speed and motor torque, the electric power input can be determined. Adding the auxiliary element power demand, the total electric power demand that the batteries and/or the fuel cell must supply can be obtained.

Thus, the equation to calculate the electric power as a function of the mechanical power, the electric motor efficiency (η_m) and the auxiliary power (P_{aux}) is as follows:

$$P_{electric} = P_{mechanical} \cdot \eta_m + P_{aux} \qquad (2)$$

In this model, the user can set a limit factor to prevent the electric motor from exceeding a specific torque value. In Fig. 3, a flux diagram representing the calculation algorithm based on the input mechanical power and the electric motor efficiency is presented.

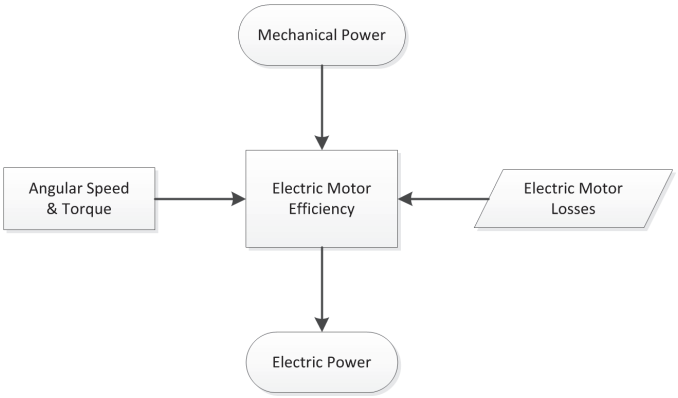


Figure 3. Electric motor efficiency.
Source: The authors

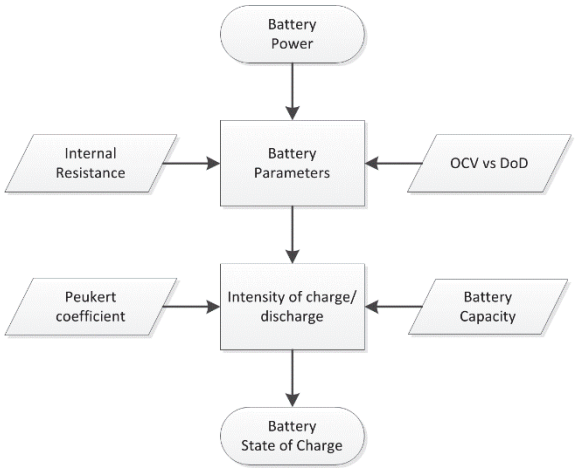


Figure 4. Battery model. Battery state of charge estimation
Source: The authors

Battery Model

The battery model is constructed from a simple equivalent circuit. For the model, it is necessary to know the internal battery resistance (R), the charge/discharge plot (open circuit electric potential versus depth of battery discharge), which is different for every type of battery technology considered in this simulation (lead acid, nickel-cadmium, lithium, etc.). With this value and the power required, the discharge current can be calculated:

$$I_{discharge} = \frac{E - \sqrt{E^2 - 4RP_{bat}}}{2R} \qquad (3)$$

For the charge, the same calculation is used, but with a different sign. In addition, the Peukert effect will be considered [6]. This effect is considered because the maximum battery capacity changes as a function of the discharge intensity, decreasing for high discharge intensities.

The Peukert equation makes it possible to correct the battery discharge by means of Peukert's Coefficient (k). Therefore, the equation modeling the discharge depth of the battery depends on the ratio between the amounts of charge spent or supplied (different signs) and the battery capacity corrected by Peukert's Coefficient [14].

$$DoD = \frac{\delta t \times I^k}{C_p} \qquad (4)$$

The necessary inputs are as follows:

- Battery type (Lead Acid, Nickel-Cadmium, Metal-Hydride, Lithium-Ion or Zebra).
- Number of cells.
- Peukert's Coefficient.
- Minimum allowed battery state of charge.

Fig. 4 shows the flux diagram for the battery state of charge estimation model:

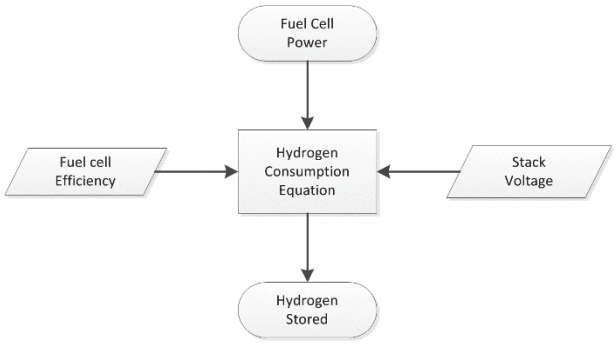


Figure 5. Flow diagram for the hydrogen utilization rate
Source: The authors

Fuel Cell Model

Considering that this is a hybrid vehicle simulation, what has actually been constructed is a hydrogen consumption model rather than a fuel cell electric power model.

An equation to model the hydrogen intake as a function of power demanded by the fuel cell (by the motor and the auxiliary systems) can be used.

Thus, based on the simple reaction stoichiometry [17], Faraday's Constant, the fuel cell efficiency [18] and the stack potential, the following equation is obtained:

$$H_{2_{usage}} = \frac{P_{electric}}{2V_c F} \qquad (5)$$

This equation depends only on the power demanded by the fuel cell. It yields the hydrogen mass flux, in moles per second, which makes it possible to know the hydrogen tank fill level at every moment. The inputs are the demanded power, the minimum hydrogen tank level and the maximum power output of the fuel cell, as shown in Fig. 5.

Logic Controller

A logic control model for the vehicle energy management was developed (Fig.6).

The management depends on the parameter SoC_HYB and SoC_MIN. Both parameters are related to the battery state of charge (SoC). Therefore, their values are critical to obtain the best battery performance. The SoC_HYB is used to change the energy management from an electric pure mode (serial mode) to a hybrid mode with battery and fuel cell (parallel mode).

If SOC is below SoC_HYB the energy management changes from the serial mode to the parallel one. For example, if the SoC_HYB is 0.5 (Fig.7) the energy management would change from serial mode to parallel mode when the SoC is below 50%.

In the parallel mode the battery is recharged with energy provided by the fuel cell and therefore the SoC rises. If SOC reaches Soc_HYB, the energy management changes from the parallel mode to the serial one. This algorithm will produce a constant switching energy management reflected in the saw-tooth graph of Fig. 7.

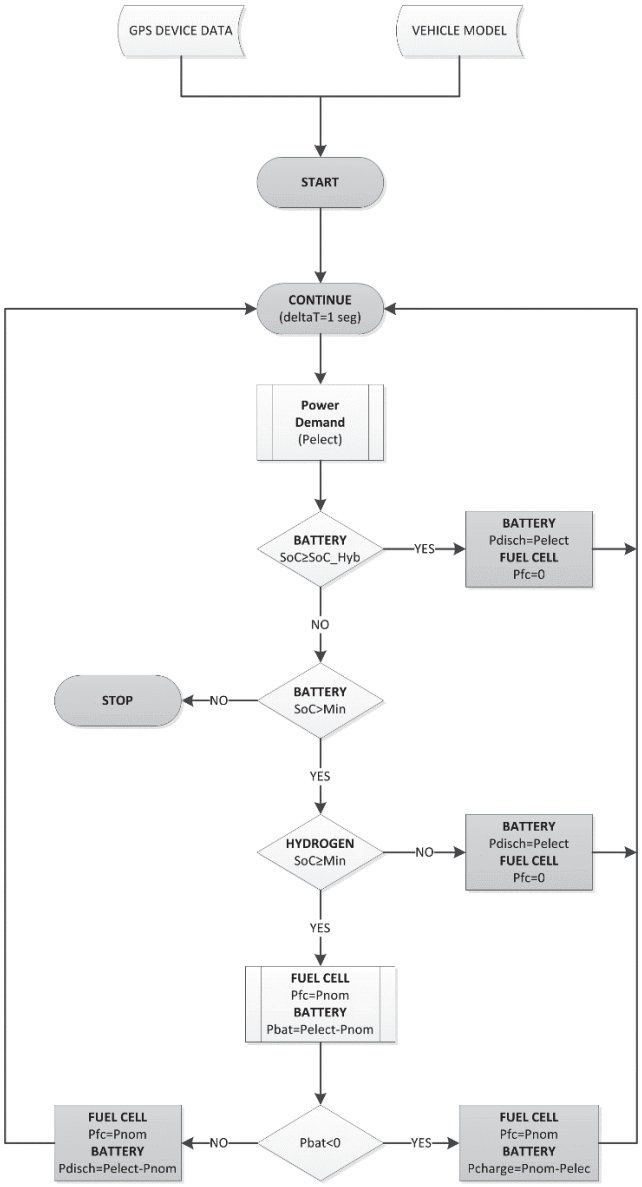


Figure 6. Summary of controller's algorithm.
Source: The authors

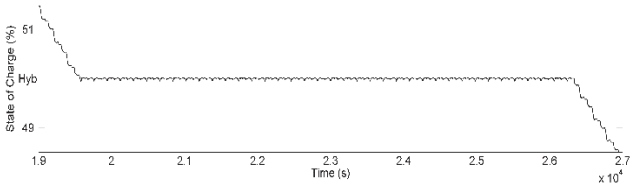


Figure 7: Example of SoC_HYB Parameter set for SoC=50%
Source: The authors

The parameter SoC_MIN specifies the minimum value of the battery state of charge. This parameter is important for almost all types of batteries since it conditions their state of health, and it could have a real influence on vehicle autonomy [19,20]. All battery manufacturers recommend an optimal SoC_Min to achieve a greater amount of life cycles.

Power distribution between the battery and fuel cell can be set in the main menu establishing a nominal power for the fuel cell. The remaining demanded power would complete by the battery every time step. This strategy about power distribution allows fuel cell to work on the steady-state mode.

The battery charge process is also considered in this simulation tool. Under the hybrid mode, when it is not demanded energy from the battery, and electric power demand of the vehicle is lower than fuel cell nominal power, then energy excess is used to charge the battery. Furthermore, the existence of a regenerative brake is taken into account.

By means of these adjustable parameters, it's possible to set several configurations in order to optimize the energy control strategy and to obtain minimum emissions from the vehicle.

3. Simulation

The principal aim of this tool is to estimate the range of an electric battery hydrogen hybrid vehicle, which is achieved by applying precedent equations to a standard drive cycle (or a real path). Fig. 8 shows a toolbox's screen scheme where it is possible to select standard or real cycles and choose if the slope component is taken into account. A few standard drive cycles are preprogrammed, but it is possible to create drive cycles from GPS data (the tool permits only one-second interval cycles at present). In this case, the tool transforms standard GPS data to speed, acceleration and slope.

The other necessary inputs are vehicle characteristics (weight, aerodynamical coefficient, front area, and other parameters). In the toolbox scheme depicted by Fig. 8 it is possible to set all configuration parameters for the vehicle simulated (mechanical parameters, battery and fuel cell systems or electrical losses). Once the drive cycle is defined, a step-by-step simulation can be performed [21].

The principal output is the range, but other variables can be obtained and plotted, including the hydrogen consumption, battery system depth of discharge and remaining range.

Of course, it is possible to simulate all-electric vehicles as hybrid vehicles by assuming that the volume of hydrogen and the power of the fuel cell are equal to zero. The toolbox is designed for any type of hydrogen storage system because of the use of hydrogen mass as a variable instead of pressure or volume. The system considers only moles of hydrogen in calculations.

After the simulation has finished, several plots can be obtained, including plots of the motor torque, acceleration, demanded power for each energy system, energy efficiency, motor efficiency, charge and discharge intensities, battery status and hydrogen consumption.

Fig. 9 shows the speed profile obtained from a GPS mounted on a bus traveling a real urban route, plotted as a time function. In the same figure, the altitude profile is represented.

As an example of this, Fig. 10 shows the battery state of charge and the stored hydrogen variation (both versus the time variable) for the previous GPS cycle simulation with a fuel cell hybrid vehicle (an urban buss). In this case there are three examples with several configurations about fuel cell power and stored hydrogen.

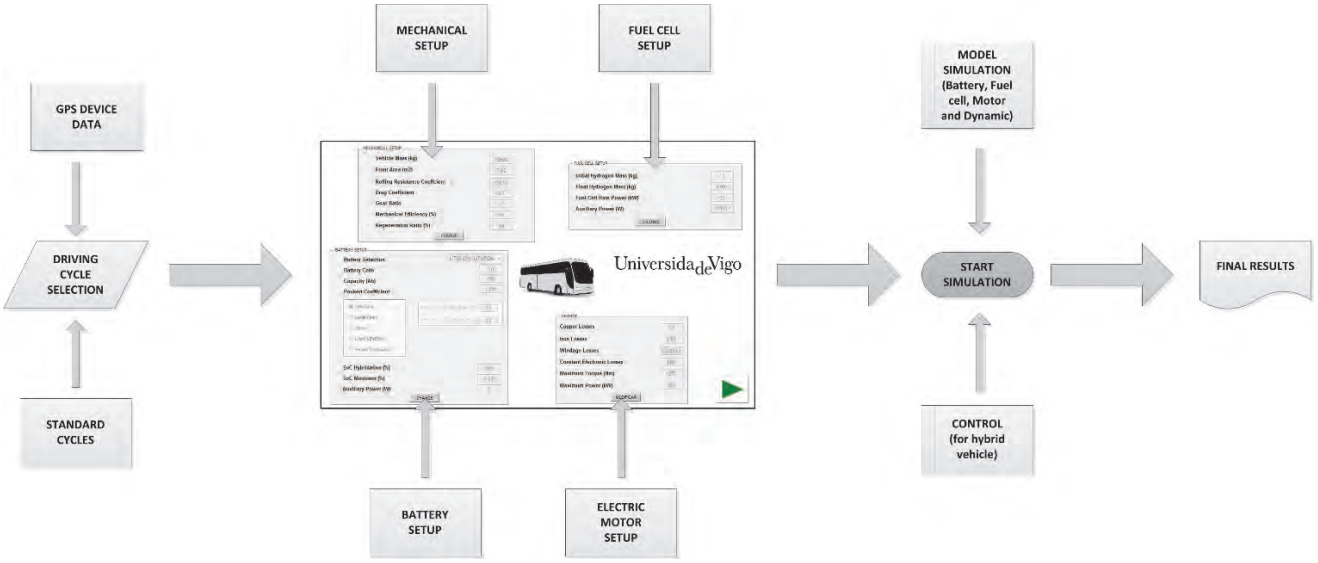


Figure 8. Toolbox scheme
Source: The authors

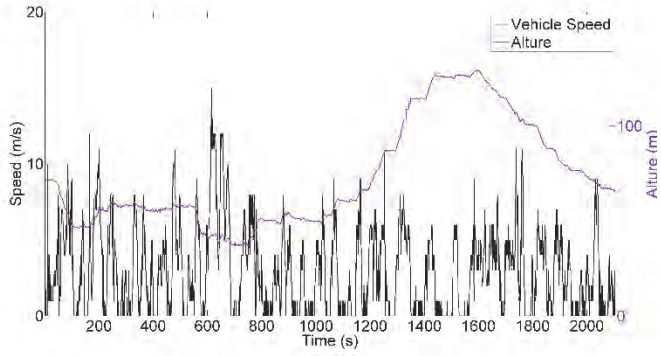


Figure 9. Urban bus GPS data
Source: The authors

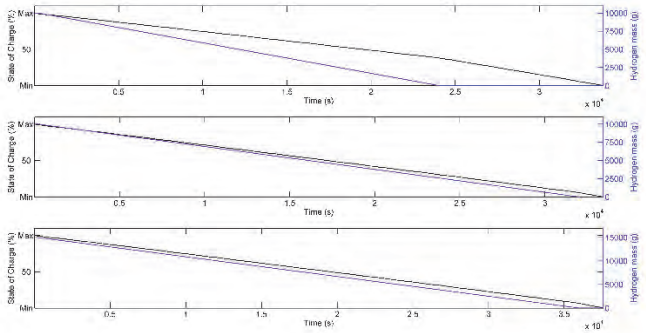


Figure 10. Simulation of an urban bus route for three different configurations of fuel cell power and stored hydrogen: 20 kW and 10 kg H2 (up), 15 kW and 10 kg H2 (middle), 20 kW and 15 kg H2 (down)
Source: The authors

A toolbox for the simulation of electric-only or hybrid electric hydrogen vehicles is presented.

The principal scope is to predict the range of batteries and/or a hydrogen tank. Moreover, the linear acceleration, angular velocity, motor torque, battery and fuel cell power, electric motor power, efficiency and hydrogen rates can be obtained.

This toolbox facilitates the evaluation of vehicle range (autonomy) for real travel, taking into account physical variables that are not taken into account in tools based on standard cycles.

The principal advantage of this tool is that it can be used in the vehicle design stage because all components are parameterizable. Also, GPS data simulation makes it possible to obtain a more precise range value than can be obtained by means of standard drive cycles because real data can be affected by parameters such as traffic density and weather and the influence of these parameters on the vehicle speed is considered

References

[1] Pollet, B.G., Staffell, I. and Shang, J.L., Current status of hybrid, battery and fuel cell electric vehicles: From electrochemistry to market prospects. Electrochim Acta, 84, pp. 235-249, 2012. DOI: 10.1016/j.electacta.2012.03.172

[2] Achour, H., Carton, J.G. and Olabi, A.G., Estimating vehicle emissions from road transport, case study: Dublin city, Appl. Energy, 88, pp. 1957-1964, 2011. DOI: 10.1016/j.apenergy.2010.12.032

[3] Kuramochi, T., Ramírez, A., Turkenburg, W. and Faaij, A., Techno-economic prospects for CO2 capture from distributed energy systems, Renewable and Sustainable Energy Reviews, 19, pp. 328-347, 2013. DOI: 10.1016/j.rser.2012.10.051

[4] Wang, C., Zhou, S., Hong, X., Qiu, T. and Wang, S., A comprehensive comparison of fuel options for fuel cell vehicles in China, Fuel Process Technol, 86, pp. 831-845, 2005. DOI: 10.1016/j.fuproc.2004.08.007

[5] Van Mierlo, J., Van den Bossche, P. and Maggetto, G., Models of energy sources for EV and HEV: Fuel cells, batteries, ultracapacitors, flywheels and engine-generators, J. Power Sources, 128, pp. 76-89, 2004. DOI: 10.1016/j.jpowsour.2003.09.048.

[6] Conte, M., Di Mario, F., Iacobazzi, A., Mattucci, A., Moreno, A. and Ronchetti, M., Hydrogen as future energy carrier: The ENEA point of view on technology and application prospects, Energies, 2, pp. 150-179, 2009. DOI: 10.3390/en20100150
[7] Hernandez, J.A., Velasco, D. and Trujillo, C.L., Analysis of the effect of the implementation of photovoltaic systems like option of distributed generation in Colombia, Renew Sust. Energ. Rev, 15, pp. 2290-2298, 2011. DOI: 10.1016/j.rser.2011.02.003
[8] Taymaz, I. and Benli, M., Emissions and fuel economy for a hybrid vehicle, Fuel, 115, pp. 812-817, 2014. DOI: 10.1016/j.fuel.2013.04.045
[9] Simmons, K., Guezennec, Y. and Onori, S., Modeling and energy management control design for a fuel cell hybrid passenger bus, J. Power Sources, 246, pp. 736-746, 2014. DOI: 10.1016/j.jpowsour.2013.08.019
[10] Hervello, M., Alfonsín, V., Sánchez, A., Cancela, A. and Rey, G., Simulation of a stand-alone renewable hydrogen system for residential supply, DYNA (Colombia), 81(185), pp. 116-123, 2014. DOI: 10.15446/dyna.v81n185.37165
[11] Markel, T., Brooker, A., Hendricks, T., Johnson, V., Kelly, K., Kramer, B. et al., ADVISOR: A systems analysis tool for advanced vehicle modeling, J. Power Sources, 110, pp. 255-266, 2002. DOI: 10.1016/S0378-7753(02)00189-1
[12] Larminie, J. and Lowry, J., Electric vehicle technology explained. Oxford: John Wiley & Sons; 2003.
[13] Hannan, M.A., Azidin, F.A. and Mohamed, A., Hybrid Electric vehicles and their challenges: A review, Renewable and Sustainable Energy Reviews, 29, pp. 135-150, 2014. DOI: 10.1016/j.rser.2013.08.097
[14] Gao, L. and Winfield, Z.C., Life cycle assessment of environmental and economic impacts of advanced vehicles, Energies, 5, pp. 605-620, 2012. DOI: 10.3390/en5030605
[15] Auinger, H., Determination and designation of the efficiency of electrical machines, Power Eng. J., 13, pp. 15-23, 1999. DOI: 10.1049/pe:19990106
[16] Kumar. L. and Jain. S,. ,Electric propulsion system for electric vehicular technology: A review, Renewable and Sustainable Energy Reviews, 29, pp. 924-940, 2014. DOI: 10.1016/j.rser.2013.09.014
[17] Larminie, J., and Dicks, A., Fuel cell systems explained. Oxford: John Wiley & Sons, Ltd., 2003.
[18] Kazim, A., A novel approach on the determination of the minimal operating efficiency of a PEM fuel cell, Renew Energy, 26, pp. 479-488, 2002. DOI: 10.1016/S0960-1481(01)00083-0
[19] Barré, A., Deguilhem, B., Grolleau, S., Gérard, M., Suard, F. and Riu, D., A review on lithium-ion battery ageing mechanisms and estimations for automotive Applications, J. Power Sources, 241, pp. 680-689, 2013. DOI: 10.1016/j.jpowsour.2013.05.040
[20] Lu, L., Han, X., Li, J., Hua, J. and Ouyang, M., A review on the key issues for lithium-ion battery management in electric vehicles, J. Power Sources, 226, pp. 272-288, 2013. DOI: 10.1016/j.jpowsour.2012.10.060
[21] Sanchez, A., Cancela, A., Urréjola, S., Maceiras, R. and Alfonsín, V., Simulation framework to evaluate the range of hydrogen fuel cell vehicles, I RE CH E, 2, pp. 840, 2010.

V. Alfonsín, has the Mining Engineering degree at University of Vigo, Spain. Currently, he is an assistant professor in the Defense University Center. His research interests include biofuels, fuel cells, renewable energy and simulation.
ORCID: 0000-0002-6807-2268

A. Suarez, has the Industrial degree at University of Vigo, Spain, he is an assistant professor in the Defense University Center. His research interests include batteries, fuel cells, renewable energy and simulation
ORCID: 0000-0001-6471-0261

A. Sánchez, is professor of Chemical Engineering Department at the University of Vigo, Spain, teaching Chemical Engineering at the Industrial Engineering Faculty. PhD. on Chemical Engineering, his main research area are the hydrogen and fuel cells technologies, bieofuels and the chemical engineering.
ORCID: 0000-0001-9069-698

R. Maceiras, has the Chemical degree at University of Vigo, Spain, and PhD. on Chemical Engineering. Currently she is an assistant professor in the Defense University Center. His research interests include biofuels, fuel cells, renewable energy and simulation.
ORCID: 0000-0003-4798-3510

A. Cancela, is assistant professor of Chemical Engineering at the University of Vigo, Spain, teaching Chemical Engineering at the Industrial Engineering Faculty. PhD. on Chemical Engineering her main research area are the Renewable Energies, CO_2 capture, Rheology and biofuels
ORCID: 0000-0002-0218-9850

UNIVERSIDAD NACIONAL DE COLOMBIA
SEDE MEDELLÍN
FACULTAD DE MINAS

Área Curricular de Ingeniería
Química e Ingeniería de Petróleos

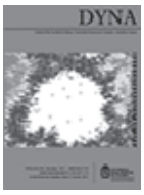
Oferta de Posgrados

Maestría en Ingeniería - Ingeniería Química
Maestría en Ingeniería - Ingeniería de Petróleos
Doctorado en Ingeniería - Sistemas Energéticos

Mayor información:

E-mail: qcaypet_med@unal.edu.co
Teléfono: (57-4) 425 5317

UNIVERSIDAD NACIONAL DE COLOMBIA
SEDE MEDELLÍN
FACULTAD DE MINAS



DYNA
http://dyna.medellin.unal.edu.co/

Using waste energy from the Organic Rankine Cycle cogeneration in the Portland cement industry

José Pablo Paredes-Sánchez [a], Oscar Jaime Restrepo-Baena [b], Beatriz Álvarez-Rodríguez [c], Adriana Marcela Osorio-Correa [d] & Gloria Restrepo [d]

[a] *Departamento de Energía, Universidad de Oviedo, Oviedo, España. paredespablo@uniovi.es*
[b] *Facultad de Minas, Universidad Nacional de Colombia, Medellín, Colombia. ojrestrepo@unal.edu.co*
[c] *Escuela Superior y Técnica de Ingenieros de Minas, Universidad de León, León, España. balvr@unileon.es*
[d] *Facultad de Ingeniería, Universidad de Antioquia, Medellín, Colombia. adriana.osorio@udea.edu.co, gloma@udea.edu.co*

Received: June 16th, 2014. Received in revised form: September 13th, 2015. Accepted: October 25th, 2015.

Abstract
Cement production is intensive in terms of energy consumption. An analysis of the resources involved in manufacturing clinker needs a corresponding mass and energy balance. This balance may indicate the existence of residual heat flows that are not used. This paper summarizes the development of a protocol for the evaluation of a cement plant rotary kiln to implement an Organic Rankine Cycle (ORC) system for cogeneration. The results show that 19.2% of the energy preheater exhaust gas can be recovered to be used in producing 5.5 GWh/year of electricity and 23.7 GWh/year of thermal energy in the cement plant. The electricity generated would represent annual savings of 1.18 $/t cement. The thermal energy produced in cogeneration, equivalent to coal in the plant itself, represents cement savings of 0.51 $/t cement and emissions reductions of 8 kt CO_2/year.

Keywords: energy balance; heat recovery; Portland cement; Organic Rankine Cycle (ORC).

Aprovechamiento del calor residual por cogeneración con Ciclo Rankine Orgánico en la industria del cemento Portland

Resumen
La producción de cemento es intensiva en consumo de energía. Un análisis de los recursos involucrados en la fabricación del clinker requiere de su correspondiente balance de materia y energía. Este balance puede indicar la existencia de flujos de calor residual que no son aprovechados. Este trabajo resume el desarrollo de un protocolo de evaluación de un horno rotatorio de planta cementera para la implementación de un sistema Ciclo Orgánico de Rankine (ORC) para cogeneración. Los resultados permiten la recuperación de 19.2% de la energía del gas de escape del precalentador para su aprovechamiento en la producción de 5.5 GWh/año de electricidad y 23.7 GWh/año de energía térmica en la planta de cemento. La electricidad generada supondría un ahorro anual de 1.18 $/t cemento. La energía térmica producida, equivalente al carbón de la planta, supone un ahorro de 0.51 $/t cemento y una reducción de emisiones de 8 kt CO_2/año.

Palabras clave: balance de energía; recuperación de calor; Cemento Portland; Ciclo Orgánico de Rankine (ORC).

1. Introduction

1.1. Paper size, margins, columns and paragraphs

Cement is essential within the current economic development, but it requires large quantities of resources. Portland cement manufacturing is one of the most costly processes in the production of non-metallic minerals, in terms of energy consumption, as its production costs are above 25% [1,2]. Theoretically, this activity requires a minimum of 1.6 GJ to produce a tonne of clinker [3]. Added to this are the CO_2 emissions resulting from the use of fossil fuels, necessary for the calcination process and the emissions from the limestone decarbonation. This means that the cement sector is responsible for about 5% of the total anthropogenic CO_2 emissions [4].

© The author; licensee Universidad Nacional de Colombia.

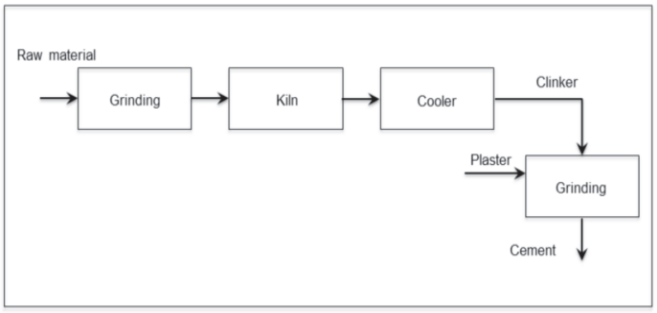


Figure 1. Diagram of the Portland cement manufacturing process.
Source: The authors.

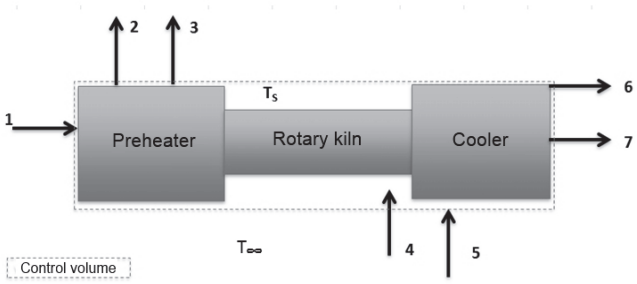


Figure 2. Control volume.
Source: The authors.

A number of studies have been carried out to evaluate Portland cement manufacturing´s energy consumption and CO_2 emissions [5-7], due to the growing interest in energy efficiency in the cement industry [3,8]. The high cost of energy makes it necessary to perform audits to analyze the possibilities of reducing the consumption in the clinker production process [9]. The study of mass and energy flows allows the possibilities of recovery of the residual heat [10-12] to be analyzed, which is recognized as a potential means to improve energy efficiency in the cement manufacturing process.

The Organic Rankine Cycle (ORC) is commonly accepted as a viable technology to convert heat at low temperature to electricity. Further benefits include low maintenance, favorable operating pressures and autonomous operation [13]. Having been proven in other industries, the interest in the ORC is increasing in the cement industry due to the fact that improvements in clinker production have led to lower exhaust gas temperatures [14].

The analysis of mass and energy balances of a typical rotary kiln cement plant is performed in this paper. The objectives are to evaluate the mass and energy balances in the cement plant, in order to determine the overall energy efficiency of the process and to enable their recovery by installing an ORC plant cogeneration system.

2. Process description and data collection

A dry process Portland cement production plant with a production capacity of about 1.7 kt/day has been chosen as a reference. The rotary kiln is located in the intermediate part of the production process; this can be seen in Fig. 1

The assessed oven has a cylindrical tubular geometry, measuring about 3.5 m x 54 m; it is longitudinally inclined with a slope of about 1º. It is lined with refractory brick inside and it is made of steel outside. The assembly rotates at a speed of about 30 rpm. In the kiln, the raw material is heated up to 1450 °C in such a way that it reacts to form clinker (a mixture of calcium silicates and aluminates). The process requires the introduction of air so that it operates with an excess of oxygen, otherwise there may be deficiencies, either by the formation of other phases or by incomplete formation of the components [15].

Due to the complexity of cement production [16] and energy flows that occur around the rotary kiln, a number of considerations were contemplated:

- Raw material, fuel and slag create a constant chemical composition.
- There is loss of negligible air.
- There are constant average ambient temperatures ($T\infty$ = 303 K), kiln surface (Ts = 581 K), cooler surface (Ts = 353 K) and preheater surface (Ts = 348 K).
- Combustion is complete.
- The operation is undertaken at a steady state and there are equilibrium conditions.

The methodology used follows these steps:

1) Definition of the control volume.
2) Identification and characterization of the main flows.
3) Formulation of mass balance.
4) Formulation of energy balance

2.1. Control volume

The control volume includes a preheater, a rotary kiln and a clinker cooler, Fig. 2

Where:

5) Raw material.
6) Preheater exhaust gas.
7) Preheater dust.
8) Coal.
9) Cooling air.
10) Clinker.
11) Cooler hot air.

2.2. Identification and characterization of the main mass flows

The inflow is the raw material in the control volume preheater (1); the raw material in the rotary kiln is the fuel (4) and, in the cooler, it is the air (5), Fig. 2.

The composition of the raw materials, the fuel (coal in this case), the clinker and the preheater exhaust gas are shown in Tables 1-4, respectively.

Table 1.
Composition of raw material.

Component	Percentage (%)
CaO	68.58
SiO_2	19.78
Al_2O_3	4.91
Fe_2O_3	4.04
MgO	2.69

Source: The authors.

Table 2.
Composition of coal.

Component	Percentage (%)
C	68.60
O	7.19
H	4.39
N	1.59
S	1.11
Ash	17.12

Source: The authors.

Table 3.
Composition of clinker.

Component	Percentage (%)
CaO	66.97
SiO_2	21.66
Al_2O_3	4.82
Fe_2O_3	4.04
MgO	2.51

Source: The authors.

Table 4.
Composition of preheater exhaust gas.

Component	Percentage (%)
N_2	60.54
CO_2	22.74
H_2O	10.03
O_2	6.69

Source: The authors.

2.3. Mass balance

The following reactions produced in the system must be considered, eq. (1-5).

- Calcination:

$$CaCO_3 \rightarrow CaO + CO_2 \quad (1)$$

$$MgCO_3 \rightarrow MgO + CO_2 \quad (2)$$

- Combustion:

$$C + O_2 \rightarrow CO_2 \quad (3)$$

$$2H_2 + O_2 \rightarrow 2H_2O \quad (4)$$

$$S + O_2 \rightarrow SO_2 \quad (5)$$

The main component of the gas produced is CO_2, which is derived from the combustion and decarbonation reactions. It is considered that, to manufacture cement, about half of the CO_2 emissions come from combustion and the other half are produced in the decomposition of the calcium carbonate in clinker production [17]. Only traces of SO_2 are present due to the combustion of the fuel sulphur. In the final part of the cement producing process, approximately 5% gypsum is added to the clinker.

2.4. Energy balance

The energy balance uses the physical data and equations described in the Peray manual [18]; these have been used in several papers about mass and energy balances in cement plants [1,11,19]. The first step is to carry out a balance of the enthalpy variation flows. To do this, both the temperature and calorific value of the fuel (28,000 kJ/kg) are characterized.

The results are presented as percentage of the total energy released by combustion of fuel in the kiln.

Table 5.
Mass balance.

Flow	Mass (kg/s)	Temperature (ºC)
1	29.61	70
2	57.11	330
3	2.50	159
4	4.25	70
5	67.86	30
6	18.36	130
7	23.75	215

Source: The authors.

Table 6.
Input energy flows.

Description	Result (kJ/kg-clinker)	Distribution (%)
Coal combustion	3,612	94.01
Raw material heat	102	2.65
Cooling air heat	98	2.55
Raw material Organics	19	0.49
Coal sensible heat	11	0.29
Total heat input	**3,842**	**100.00**

Source: The authors.

Table 7.
Output energy flows.

Description	Result (kJ/kg-clinker)	Distribution (%)
Clinker formation	1,783	46.41
Preheater exhaust gas	1,100	28.63
Cooler hot air	285	7.42
Heat losses by radiation from the kiln surface	155	4.03
Clinker discharge	90	2.34
[(1)]Heat losses by convection from the kiln surface	54	1.41
Heat losses by dust from the electrofilter	37	0.96
Moisture in the raw material and coal	28	0.73
Heat losses due to preheater surface radiation	2	0.05
[(2)]Heat losses due to preheater surface convection	2	0.05
Heat losses from cooler surface radiation	1	0.03
[(2)] Heat losses from cooler surface convection	1	0.03
Unaccounted losses	304	7.91
Total heat output	**3,842**	**100.00**

Note: Churchill & Bernstein[(1)] and Saunders & Weise[(2)] equations were used [19]. The starting point was the evaluation of the characteristics and operating conditions of every piece of industrial equipment used in the process.

Source: The authors.

3. Results and Discussion

The results of the mass balance are shown in Table 5.

The heat flows described have been considered for the energy balance. It is important to note that the moisture content in the raw materials due to energetic potential may be affected. The calculations have been made considering amounts per kg

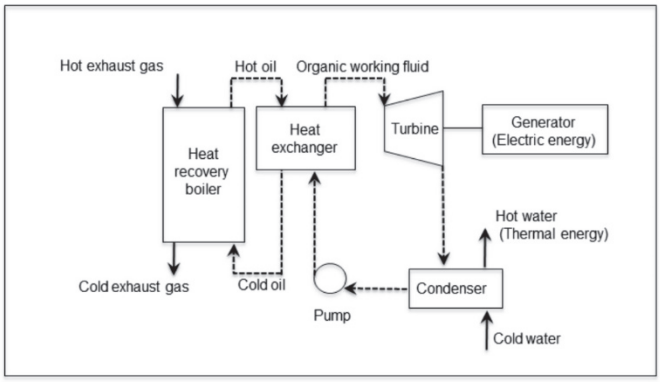


Figure 3. ORC cogeneration scheme.
Source: The authors.

of produced clinker. Tables 6 and 7 show the results of the energy balance for the different flows.

Energy recovery in cement plants has been studied in different works [10,11,21], as has the importance of ORC as an energy production system [22,23] and the use of cogeneration systems in the industry [1,24]. According to the results, (Table 7), there are opportunities for residual heat flow energy recovery. Thus, emissions and heat loss into the environment would be avoided. The largest residual heat flow corresponds to the preheater exhaust gas, which reaches 330 ºC, accounting for 53.4% of total losses. Part of this flow can be recovered by an ORC cogeneration system, Fig. 3

The proposed cogeneration system is shown in Fig. 3. The energy is transferred from the preheater exhaust gas to the organic fluid, used in the system's Rankine cycle, by means of a thermal oil. The circuit operates with a minimum temperature of 250 °C, which, to prevent intensive modifications to the plant, comes from the preheater exhaust gas at the outlet of the heat exchanger. The system allows it to be used as thermal energy for the hot water leaving the condenser manufacturing process. According to the final temperatures and operating conditions, it is possible to calculate the total available thermal energy ($\dot{Q}_T$) from the preheater exhaust gas mass flow ($\dot{m}_2$) [25], eq. (6).

$$\dot{Q}_T = \dot{m}_2 \cdot \left(h_{\text{Hot exhaust gas (330ºC)}} - h_{\text{Cold exhaust gas (250ºC)}} \right) \quad (6)$$

$$\dot{Q}_T = 57.11 \text{ kg/s} \cdot (610.4 - 527.0) \text{ kJ/kg} = 4{,}763 \text{ kW}$$

In order to determine the power of the electric generator, an overall efficiency (η) of 85% is estimated for the recovery of heat in this flow by the cogeneration ORC process ($\dot{Q}_{ORC}$), eq. (7)[26].

$$\dot{Q}_{ORC} = \eta \cdot \dot{Q}_T = 4{,}049 \text{ kW} \quad (7)$$

Considering that 18% of the recovered energy can be transformed into electricity, it is possible to achieve a power of 729 kW [26]. 7,500 operating hours per year at the plant would allow energy savings of 5.5 GWh/year. Taking energy costs to be 0.13 $/kWh [27] the value of such energy savings would amount to 1.18 $/t cement.

A preliminary estimation of the costs associated with the implementation of the ORC cogeneration system would need to include the necessary equipment and installation expenses. The investment and profitability significantly depend on the location and size of the ORC plant. For the whole system (Fig. 3) a 3 million dollar budget is estimated, which includes shipping, installation and commissioning. Therefore, an estimate of the period of a simple return on investment (p) can be shown in eq. (8).

$$p = (\text{Implementation costs})/(\text{Annual savings}) \quad (8)$$

$$p = (3 \cdot 10^6 \$)/(0.72 \cdot 10^6 \$/\text{year}) = 4.2 \text{ years}$$

It was calculated that 82% of the unused energy for electricity production is available for thermal use. If 4% of it is deducted due to heat losses in the system, the remaining 78% can be collected in hot water at 80 °C at the condenser outlet, which is equivalent to 23.7 GWh per year. This thermal energy, calculated annually, is equivalent to about 3 kt/year of coal used at the plant at a cost of 100 $/t [27], which represents about 0.31 million dollars. The use of this energy is equivalent to 8 kt CO_2 annual emissions. However, the particular characteristics of each plant, due to economic, environmental and technical factors, determine the viability of these types of projects.

Energy savings, through using an ORC cogeneration system, would also improve the energy efficiency of the plant. It should be noted that these calculations might vary according to the plant operating conditions and other economic factors.

4. Conclusions

The proposed methodology can be quickly applied to any cement plant with a rotary kiln that is used as a first assessment. The results of the audit, depending on the input and output thermal energy, indicate that the clinker production system has an efficiency of 46.4%. The main heat losses that occur in the kiln are with the preheater exhaust gas (28.6%), the hot air from the cooler (7.4%) and in radiation and convection (5.6%).

Recovering waste heat from the preheater exhaust gas flow is feasible and can provide about 0.7 MW of electric power, by using an ORC cogeneration system. The results obtained would allow the recovery of 19.2% from the preheater exhaust gas energy to produce 5.5 GWh/year of electricity and 23.7 GWh/year of thermal energy.

The use of the electricity generated in cogeneration would save about 0.72 million dollars per year (1.18 $/t cement). The equivalent in thermal energy, in terms of coal used by the plant itself, represents a cost of 0.31 million dollars (0.51 $/t cement) and would avoid 8 kt/year of CO_2 emissions. The expected payback period for the investment in the proposed facility is 4.2 years.

Acknowledgement

Adriana Marcela Osorio Correa and Gloria Restrepo are grateful to COLCIENCIAS and the Sustainability Strategy Program 2013-2014 of Antioquía University (Colombia).

References

[1] Khurana, S., Banerjee, R. and Gaitonde, U., Energy balance and cogeneration for a cement plant. Applied Thermal Engineering, 22(5), pp. 485-494, 2002. DOI: 10.1016/S1359-4311(01)00128-4

[2] Madlool, N.A., Saidur, R., Rahim, N.A., Islam, M.R. and Hossian, M.S., An exergy analysis for cement industries: An overview. Renewable and Sustainable Energy Reviews, 16(1), pp. 921-932, 2012. DOI: 10.1016/J.Rser.2011.09.013

[3] Liu, F., Ross, M. and Wang, S., Energy efficiency of China's cement industry. Energy, 20(7), pp. 669-681, 1995. DOI: 10.1016/0360-5442(95)00002-X

[4] Humphreys, K. and Mahasenan, M., Toward a sustainable cement industry. Substudy 8, Climate change [online], World Business Council for Sustainable Development, 2002 [accessed 21th, May, 2014]. Available at: http://wbcsdcement.org/pdf/battelle/final_report8.pdf

[5] Capros, P., Kouvaritakis, N. and Mantzos, L., Economic evaluation of sectoral emission reduction objectives for climate change: Top–down analysis of greenhouse gas emission possibilities in the EU [online], European Comission, Contribution to a Study for DG Environment, 2001 [accessed 21th, May, 2014]. Available at: http://ec.europa.eu/environment/enveco/climate_change/pdf/top_down_analysis.pdf

[6] Gartner, E., Industrially interesting approaches to "low-CO_2" cements. Cement and Concrete Research, 34(9), pp. 1489-1498, 2004. DOI: 10.1016/j.cemconres.2004.01.021

[7] Alvarez-Rodriguez, B., Menendez-Aguado, J.M., Rosa-Dizioba, B. y Coello-Velázquez, A.L., Evaluación de materias primas en una planta de beneficio de arena de sílice para aumentar la eficiencia energética del proceso de molienda DYNA, 80(177), pp. 95-100. 2013. DOI: 10.15446/dyna

[8] Hasanbeigi, A., Price, L., Lu, H. and Lan, W., Analysis of energy-efficiency opportunities for the cement industry in Shandong Province, China: A case study of 16 cement plants. Energy, 35(8), pp. 3461-3473, 2010. DOI: 10.1016/j.energy.2010.04.046

[9] Osorio, A., Restrepo, G. and Marín, J., Cement clinker grinding: Evaluation of mill spin speed, residence time and grinding media. DYNA, 76(158), pp. 69-77, 2009. DOI: 10.15446/dyna

[10] Sogut, M.Z., Oktay, Z. and Hepbasli, A., Energetic and exergetic assessment of a trass mill process in a cement plant. Energy Conversion and Management, 50(9), pp. 2316-2323, 2009. DOI: 10.1016/j.enconman.2009.05.013

[11] Kabir, G., Abubakar, A.I. and El-Nafaty, U.A., Energy audit and conservation opportunities for pyroprocessing unit of a typical dry process cement plant. Energy, 35(3), pp. 1237-1243, 2010. DOI: 10.1016/j.energy.2009.11.003

[12] Söğüt, Z., Oktay, Z. and Karakoç, H., Mathematical modeling of heat recovery from a rotary kiln. Applied Thermal Engineering, 30(8-9), pp. 817-825, 2010. DOI: 10.1016/j.applthermaleng.2009.12.009

[13] Lecompte, S. et al., Review of organic Rankine cycle (ORC) architectures for waste heat recovery. Renewable and Sustainable Energy Reviews, 47, pp. 448-461, 2015. DOI: 10.1016/j.rser.2015.03.089

[14] Schneider, M., Process technology for efficient and sustainable cement production. Cement and Concrete Research. In press. 2015. DOI: 1016/j.cemconres.2015.05.014

[15] Tobón, J.I., Restrepo, O.J. and Payá, J., Comparative analysis of performance of Portland cement blended with nanosilica and silica fume. DYNA 77(163), pp 37-46, 2010. DOI: /10.15446/dyna

[16] Giraldo, C., Mendoza, O., Tobón, J.I., Restrepo, O. y Restrepo, J.C. Durabilidad del cemento Pórtland blanco adicionado con pigmento azul ultramar. DYNA 77(164), pp 45-51, 2010. DOI: 10.15446/dyna

[17] Anand, S., Vrat, P. and Dahiya, R.P., Application of a system dynamics approach for assessment and mitigation of CO_2 emissions from the cement industry. Journal of environmental management, 79(4), pp. 383-398, 2006. DOI: 10.1016/j.jenvman.2005.08.007

[18] Peray, K.E., Cement Manufacturers Handbook. New York Chemical Publishing Company, 1979.

[19] Engin, T. and Ari, V., Energy auditing and recovery for dry type cement rotary kiln systems-A case study. Energy Conversion and Management, 46(4), pp. 551-562, 2005. DOI: 10.1016/j.enconman.2004.04.007

[20] Prieto, M.M. y Suárez, I., Tablas y gráficos para la resolución de problemas de transmisión de calor. Oviedo; Servicio de Publicaciones de la Universidad de Oviedo, 2008.

[21] Castrillon, R.P., González, A.J. and Quispe, E.C., Energy efficiency improvement in the cement industry by wet process through integral energy management system implementation. DYNA, 80(177), pp. 115-123, 2013. DOI: 10.15446/dyna

[22] Raj, N.T., Iniyan, S. and Goic, R., A review of renewable energy based cogeneration technologies. Renewable and Sustainable Energy Reviews, 15(8), pp. 3640-3648, 2011. DOI: 10.1016/j.rser.2011.06.003

[23] Madlool, N.A., Saidur, R., Hossain, M.S. and Rahim, N.A., A critical review on energy use and savings in the cement industries. Renewable and Sustainable Energy Reviews, 15(4), pp. 2042-2060, 2011. DOI: 10.1016/j.rser.2011.01.005

[24] de Oliveira, R.C., de Souza, R.D. and de Lima Tostes, M.E., A methodology for analysis of cogeneration projects using oil palm biomass wastes as an energy source in the Amazon. DYNA, 82(190), pp. 105-112, 2015. DOI: 10.15446/dyna.v82n190.43298

[25] Nellis, G.F. and Klein, S.A., Heat Transfer. New York: Cambridge, 2009.

[26] Turboden [online].Technical Reports, 2014 [accessed 12th, July, 2015]. Available at: http://www.turboden.eu/

[27] Ministerio de Minas y Energía. Gobierno de Colombia. Informe de precios Energéticos Observados en el Sector Industrial [online], 2012 [accessed 24th, May, 2014]. Available at: http://www.sipg.gov.co/Portals/0/Precios/Industria/Precios%20Industria%20Enero2012.pdf

J.P. Paredes-Sánchez, is a lecturer in the Department of Energy at the University of Oviedo, Spain. He received his PhD in Energy Engineering in 2010, at the University of Oviedo, Spain and has been associated with renewable energy projects at the Oviedo Higher Technical School of Mining and Engineering since 2007. He is the author or co-author of papers and conferences on renewable energy. He has published several books about university education. He is also involved in EU programs for updating renewable energy research and higher education.
ORCID: 0000-0002-1065-904X

O.J. Restrepo-Baena, obtained his BSc. degree in Mining and Metallurgy Engineering at the Universidad Nacional de Colombia, Medellín, Colombia; MSc. in Environmental Engineering and PhD in Metallurgy and Materials at the Universidad de Oviedo, Spain. He works in the Facultad de Minas at the Universidad Nacional de Colombia, Medellín, Colombia, and his research interests are focused in extractive metallurgy and materials of engineering: cements, ceramics, pigments.
ORCID: 0000-0003-3944-9369

B. Álvarez-Rodríguez, has a PhD in Mining Engineering from the Universidad de Oviedo, Spain. She works at the Universidad de León (UNILEON) and worked at the Universidad Politécnica de Cataluña (UPC), Spain. She has completed a Master's in renewable energies. She has taught and directed courses on mineral processing and renewable energies at the Universidad de Oviedo, Spain, Universidad Nacional de San Luis, Argentina, Universidad Nacional de La Rioja, Argentina and Universidad Nacional de Colombia. She is currently involved in a European research project on mineral processing (OptimOre). Her research focuses on extractive metallurgy, mineral processing and energy efficiency.
ORCID: 0000-0002-2194-4604

A.M. Osorio Correa, received her BSc. Eng in Chemical Engineering in 2006, her M.Sc. in Engineering with emphasis on Chemistry in 2009, and her Ph.D. in Engineering with emphasis in Materials in 2014, all from the Universidad de Antioquia, Medellin, Colombia. From 2006 until now, she worked as a researcher in the Procesos Fisicoquímicos Aplicados research group. Currently, she teaches a solids operations course in the Chemical Engineering Department, at the Facultad de Ingeniería, Universidad de Antioquia. Her research interests include: solids handling, grinding and

classification process, soil stabilization, mass balance and energy balance in processes.
ORCID: 0000-0002-6413-9023

G. Restrepo, obteined his BSc. in Chemical Engineering in 1988 at Universidad Pontificia Bolivariana; Medellín, Colombia, is PhD in Chemical Sciences in 1999, from the Universidad de Sevilla and the Instituto de Ciencias de Materiales de Sevilla, Spain. She has a certified in the area of foundations, modelling and management of air quality. Currently is a titular professor at Universidad de Antioquia, Colombia, attached at Facultad de Ingeniería where she teachs undergraduate and postgraduate courses and coordinates the research group Procesos Fisicoquímicos Aplicados, PFA. She has led and participated in more than forty research projects, mainly in materials and solids processing areas, technology of particles, environmental physicochemical and advanced oxidation processes; she is author and coauthor of several national and international papers.
ORCID: 0000-0001-6716-8834



UNIVERSIDAD NACIONAL DE COLOMBIA
SEDE MEDELLÍN
FACULTAD DE MINAS

Área Curricular de Ingeniería
Geológica e Ingeniería de Minas y Metalurgia

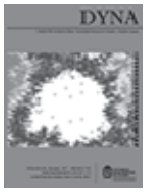
Oferta de Posgrados

Especialización en Materiales y Procesos
Maestría en Ingeniería - Materiales y Procesos
Maestría en Ingeniería - Recursos Minerales
Doctorado en Ingeniería - Ciencia y Tecnología de Materiales

Mayor información:

E-mail: acgeomin_med@unal.edu.co
Teléfono: (57-4) 425 53 68

UNIVERSIDAD NACIONAL DE COLOMBIA
SEDE MEDELLÍN
FACULTAD DE MINAS



DYNA
http://dyna.medellin.unal.edu.co/

The production, molecular weight and viscosifying power of alginate produced by *Azotobacter vinelandii* is affected by the carbon source in submerged cultures

Mauricio A. Trujillo-Roldán [a], John F. Monsalve-Gil [b], Angélica M. Cuesta-Álvarez [c] & Norma A. Valdez-Cruz [d]

[a.] *Instituto de Investigaciones Biomédicas, Universidad Nacional Autónoma de México, México DF, México, maurotru@gmail.com*
[b.] *Facultad de Minas, Universidad Nacional de Colombia, Sede Medellín, Medellín, Colombia. angelmcuesta@yahoo.com*
[c.] *Facultad de Minas, Universidad Nacional de Colombia, Sede Medellín, Medellín, Colombia. monsalvegil@hotmail.com*
[d.] *Instituto de Investigaciones Biomédicas, Universidad Nacional Autónoma de México, México DF, México. adrivaldez1@gmail.com*

Received: June 29th, 2014. Received in revised form: September 13th, 2015. Accepted: October 25th, 2014.

Abstract
Alginate is a linear polymer composed of β-1,4 linked mannuronic acid and its epimer, α-L-guluronic acid, and frequently extracted from marine algae, as from bacteria such as *Azotobacter* and *Pseudomonas*. Here, we show the impact of conventional and unconventional carbon sources on *A. vinelandii* growth, alginate production, its mean molecular weight (MMW) and its viscosifying power. Starting with 20 g/L of sugars, the highest biomass concentration was obtained using deproteinized and hydrolyzed whey (6.67±0.72 g/L), and sugarcane juice (6.68±0.45 g/L). However, the maximum alginate production was achieved using sucrose (5.11±0.37 g/L), as well the highest alginate yield and specific productivity. Otherwise, the higher alginate MMW was obtained using sugarcane juice (1203±120 kDa), and the higher viscosifying power was obtained using deproteinized/ hydrolyzed whey (23.8±2.6 cps L/g_{alg}). This information suggests that it is possible to manipulate the productivity and molecular characteristics of alginates, as a function of the carbon source used. All this, together with the knowledge of the effects of environmental conditions will allow for high yields of high added value biopolymers.

Keywords: alginates; *Azotobacter vinelandii*; viscosifying power; unconventional carbon sources.

La producción, el peso molecular y el poder viscosificante del alginato producido por *Azotobacter vinelandii* es afectado por la fuente de carbono en cultivos sumergidos

Resumen
El alginato es un polímero lineal compuesto por ácidos β-1,4 manurónico y su epímero, α-L- gulurónico y con frecuencia se extrae de algas marinas, como también de bacterias como *Azotobacter* y *Pseudomonas*. En este trabajo, se presenta el impacto de diferentes fuentes de carbono convencionales y no convencionales en el crecimiento de *A. vinelandii*, producción de alginato, su peso molecular promedio (PMP) y su capacidad viscosificante. Todos los experimentos se iniciaron con 20 g/L de azúcares totales, donde la más alta concentración de biomasa se obtuvo utilizando suero de leche hidrolizado y desproteinizado (6.67±0.72 g/L), y jugo de caña de azúcar (6.68±0.45 g/L). Sin embargo, la producción máxima de alginato se logró utilizando sacarosa (5.11±0.37 g/L), así como el más alto rendimiento de alginato y productividad específica. Por otra parte, el mayor PMP de alginato se obtuvo con jugo de caña de azúcar (1203±120 kDa). Además, la capacidad viscosificante más alta se obtuvo utilizando suero de leche desproteinizado e hidrolizado (23.8±2.6 cpsL/g_{alg}). Esta información sugiere que es posible manipular la productividad y las características moleculares de alginatos como función de la fuente de carbono utilizada. En conjunto con el conocimiento de los efectos de las condiciones ambientales se lograrían altos rendimientos de biopolímeros de alto valor agregado.

Palabras clave: alginatos, *Azotobacter vinelandii* , capacidad viscosificante, fuentes de carbono no convencionales.

© The author; licensee Universidad Nacional de Colombia.

1. Introduction

Alginates are polysaccharides composed of β-1,4 linked to mannuronic acid and its epimer, α-L-guluronic acid, and is used as a thickener, stabilizer, and gelling agent in the textile, pharmaceutical, and food industries [1,2]. These polymers are extracted from marine algae, and can also be obtained from bacterial sources such as the *Azotobacter* and *Pseudomonas* species [2-4]. The industrial importance of alginates is their ability to modify rheological properties of aqueous systems, and this is determined by the composition of the polymer. Alginate composition (or quality) is ruled by many factors, such as: the mean molecular weight (MMW), the polydispersity index (PI), the monomers ratio (mannuronic and guluronic acid residues, M/G ratio), the sequence pattern and the *O*-acetylation degree in mannuronic acid residues [5-9]. One of the main challenges in the production of microbial alginates is the ability to influence their quality by controlling the environmental conditions (such as dissolved oxygen, pH and temperature) and the culture medium, on bioreactors. This has been widely reported and reviewed [2,10].

Previous work has demonstrated the significant role of the culture medium components on alginate productivity by *A. vinelandii*, such as carbon source (C-source), calcium and phosphates concentration [6,11-13], and carbon to nitrogen ratio (C/N) [12,14]. In recent years, the effect of different nutrients on the alginate molecular characteristics has been reported, such as the effect of different nitrogen sources and the C/N ratio on MMW [14]. Moreover, other components of the culture medium such as 3-(N-morpholino)-propane-sulfonic acid (MOPS) affect the acetylation of alginate but not the MMW [15]. Also, the alginate produced by *A. vinelandii* by using 4-hydroxybenzoic acid as C-source is different to these produce by using glucose in terms of its M/G ratio and acetyl groups [6].

The growth of *A. vinelandii*, the alginate production and its molecular characteristics are affected by operational factors in bioreactors, such as agitation speed [16-18], the concentration of dissolved CO_2 [19], and dissolved oxygen tension (DOT) [17, 20-22]. In particular, DOT affects the M/G ratio [18], the acetylation degree [9] and the MMW [17,20,21,23]. Other studies succeeded in demonstrating that under the manipulation of the specific growth rate, the productivity and the MMW of alginate can be controlled. This through modification of the influx of carbon sources by setting up the dilution rate (D as the ratio of flux inlet/tank volume), in fed-batch cultures [24] and in continuous cultures [25,26]. However, in these continuous cultures both the manipulation of the growth rate and the concentration of the C-source in the influent medium modify the MMW of the alginate obtained [25].

Previous research reported that the specific consumption rate of sucrose is highly related with changes in alginate productivity [17]. Furthermore, a possible link between the specific carbon source consumption rate and the MMW of alginate has been proposed [25]. It can be assumed that the changes in metabolizing different C-sources may modify the production rate of mannuronic acid residues (through the enzymes AlgA, AlgC and AlgD), and in turn might be affecting the polymerization rate, where the key enzymes Alg8, Alg60 and Alg44 are involved [21,23]. As far as we know, there are no previous papers documenting the direct effects of non-conventional and conventional C-sources on alginate molecular weight, and its polydispersity index by *A. vinelandii.* Therefore, In the search for higher value-added alginates, we evaluated different carbon sources on the production, the mean molecular weight, the polydispersity index, the viscosifying power of alginate, the growth of *A. vinelandii* and the consumption of these sources.

2. Materials and Methods

2.1. Microorganism, culture media and growth conditions

The strain of *Azotobacter vinelandii* ATTC-9046 was used, and maintained by monthly subculture on Burk's agar (18%) slopes, and stored at 4°C [16,17]. *A. vinelandii* was grown in a modified Burk's medium of the following composition (in g/l): yeast extract (Difco) 3.0, K_2HPO_4 0.66, KH_2PO_4 0.16, MOPS 1.42, $CaSO_4$ 0.05, NaCl 0.2, $MgSO_4$-$7H_2O$ 0.2, Na_2MoO_4-$2H_2O$ 0.0029, $FeSO_4$-$7H_2O$ 0.027 [16]. The C-source for each experiment was added at a concentration of 20 g/L. A concentrated NaOH solution was used to adjust the initial pH to 7.2 in all cultures. 500X solution of salts $MgSO_4$-$7H_2O$, $FeSO_4$-7H2O and Na_2MoO_4-$2H_2O$ were prepared and sterilized independently to avoid precipitation. The required volume of sterile salts was added at the moment of inoculation. Previously to sterilization, sugarcane juice was filtered through 0.45 μm filter membrane (Millipore™, USA). Acid hydrolysis of the whey was conducted at pH 5.5, 90°C for 20 minutes, protein was recovered by centrifugation at 5000 xg for 10 min. The pH was adjusted to 1.5 with HCl, and brought to 121°C for 30 minutes. Pre-cultures were performed in a rotary shaker (with a rotatory diameter of 2.54 cm) at 200 rpm and 29ºC, for 24 h [16] by using three colonies (from Petri dishes) inoculated in 250-mL flasks, containing 50 mL of the medium.

Washed cells from pre-cultures were inoculated to start with an optical density near 0.15 absorbance units in 250 mL shake flask, containing 50 mL of modified Burk's medium, and incubated in a rotary shaker (with a rotatory diameter of 2.54 cm) at 200 rpm and 29ºC. Under these conditions, the cells were grown under oxygen limitation [16]. The aim of using washed cells as inoculum was to avoid the exhaust inoculum broth components (as extracellular alginate-lyase activity and alginate). It has been shown that the exhausted broth components from the inoculum play important regulatory roles in alginate biosynthesis, and in determining its molecular weight [27]. Two flasks were removed from the incubator for kinetic analysis as needed [16].

2.2. Analytical determinations

Biomass and alginate were determined gravimetrically as previously described [16]. The total reducing sugars (TRS) were evaluated by the dinitrosalicylic acid (DNS) method, and an acidic hydrolysis was undertaken when necessary. A standard correlation was made for each carbon source. Viscosity was measured on a cone and plate viscometer (Wells-Brookfield,

USA) using a CP-52 cone at a rotational speed of 6 rpm, which corresponds to a shear rate of 12 s^{-1} at room temperature [16]. Mean molecular weight (MMW), polydispersity index (PI) and molecular weight distributions (MWD) of alginates were estimated by gel-permeation chromatography as previously reported [16,21], and pullulans from *Aureobasidium pullulans* (from 5,800 to 1,600,000 Da) were used as standards. The polydispersity index (PI) was defined as the ratio of MMW (weighting the polymer molecules based on the weight of those having a specific molecular mass) to mean number weight (weighting the molecules based on the number of those with a specific molecular mass) [12,13]. All cultures were carried out at least in triplicate. Figs 1 and 2 show the mean value of at least three independent cultures and the standard deviation among replicas.

3. Results and Discussion

Five different carbon sources were evaluated (fructose, galactose, glucose, lactose, and sucrose) in modified Burk´s medium. Moreover, hydrolyzed and deproteinized liquid whey and sugarcane juice were also evaluated alone, or as a complement of Burk´s medium, always maintaining an initial concentration of 20 g/L of total reducing sugars (TRS). All cultures were carried out for 120 h and the final concentrations of biomass, alginate and TRS are shown in Fig. 1. If considering just the conventional carbon sources, the carbon source that yields the highest biomass (5.51±0.3 g/L) and alginate (5.11±0.37 g/L) production was sucrose, followed by glucose (5.47±0.65 and 3.1±0.70 g/L for biomass and alginate, respectively). Lower biomass growth and alginate production was obtained using fructose and galactose (Fig. 1A and 1B). These results confirm that *A. vinelandii* can use any of these three monomers to produce alginate as previously reported by Pindar and Bucke [28]. However, no biomass growth (nor alginate production) was observed using lactose as a carbon source in Burk´s medium [28].

Page et al. [29] demonstrated that large production of PHB (19 to 22 g/L) is supported when *A. vinelandii* is grown with complex, unrefined carbohydrate sources such as cane and beet molasses. In addition, these complex substrates may have other desirable effects on the production of PHB, such as culture growth promotion and reducing the time for PHB formation. Taking into account data reported by Page et al. [29], we evaluated two complex carbon sources (hydrolyzed and deproteinized whey and sugarcane juice) in the production of alginates by *A. vinelandii* and determined the effect of this process on their molecular characteristics, *i.e.* mean molecular weight and polidispersity index.

In cultures using hydrolyzed and deproteinized whey, a biomass concentration of 3.55±0.79 g/L and 1.20±0.13 g/L of alginate were obtained. While, using sugarcane juice 1.87±0.59 g/L of biomass and 0.45±0.20 g/L of alginate were obtained. It should be mentioned that those unconventional C-source cultures were carried out by just adjusting the initial pH to 7.2, TRS to 20 g/L and adding any buffer or salt. However, by complementing these unconventional C-sources with Burk´s medium (without sucrose), 6.67±0.72 g/L and 6.68±0.45 g/L of biomass were obtained, and 2.42±0.28 g/L and 3.55±0.45 g/L of alginate were achieved by using hydrolyzed and deproteinized whey or sugarcane juice, respectively.

When reviewing the consumption of C-sources, measured as total reducing sugars, as shown in Fig. 1C, no C-source uptake was observed using lactose, which is congruent with no obtaining biomass growth, nor alginate production. Furthermore, when hydrolyzed and deproteinized whey or sugarcane juice (without Burk´s medium) were used, less than half the C-source was consumed (Fig. 1C). In glucose, sucrose, galactose, hydrolyzed and deproteinized whey and sugarcane juice with Burk´s medium, the consumption of the C-source was nearly complete, and only residual values of less than 2.0 g/L were observed (Fig. 1C).

The highest alginate/biomass yield was found using sucrose as C-source with a value of 0.928±0.048 $g_{alginate}/g_{biomass}$ (Table 1), and also the best alginate/C-source yield was obtained (0.281±0.043 $g_{alginate}/g_{sucrose}$). Alternatively, the best yield biomass/C-source was obtained using hydrolyzed and deproteinized whey (0.454±0.064 $g_{biomass}/g_{whey}$) and sugarcane juice (0.406±0.042 $g_{biom}/g_{sugarcane}$) not fortified with Burk´s medium (Table 1). However, the lowest alginate/C-source yields of all were obtained for hydrolyzed and deproteinized whey (0.153±0.046 $g_{alginate}/g_{C\text{-}source}$) and sugarcane juice (0.098±0.018 $g_{alginate}/g_{C\text{-}source}$). This might be due to the lower concentrations of a nitrogen source, decreasing alginate production, but increasing biomass growth [14].

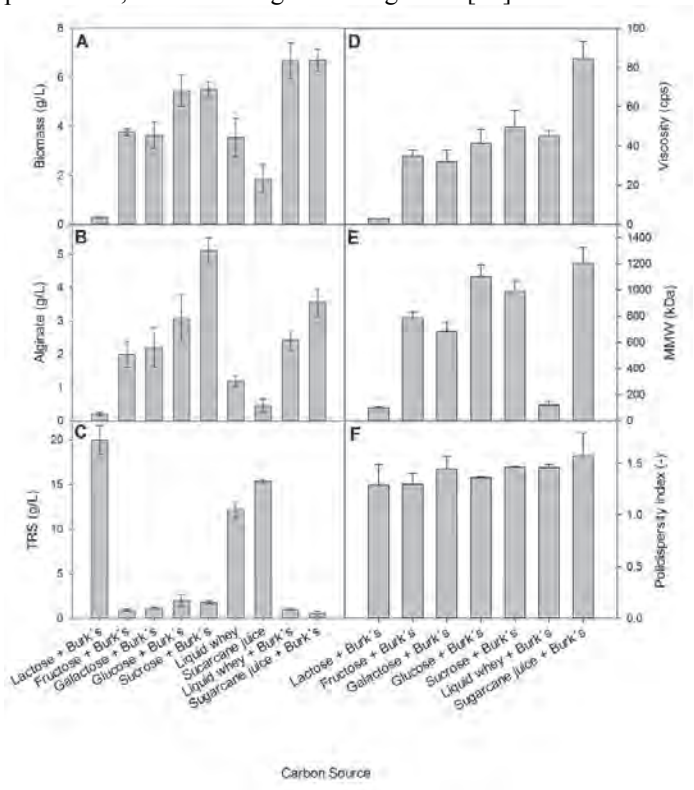


Figure 1. Effect of different carbon sources on the final concentrations of *A. vinelandii* growth (A), alginate production (B), and total reducing sugars (C), culture broth viscosity (D), alginate mean molecular weight (E), and polidispersity index (F) in cultures carried out in 250 mL shake flask, containing 50 mL of modified Burk's medium and incubated at 200 rpm and 29ºC.
Source: The Authors

Table 1.
Impact of the carbon source on the kinetics and stoichiometric parameters of alginate production in cultures of A.vinelandii, by using 20 g/L of different carbon sources with and without Burk´s medium components. Source: Authors' own

C-source	$Y_{alg/biom}$ (g_{alg}/g_{biom})	$Y_{alg/C\text{-}souce}$ ($g_{alg}/g_{C\text{-}source}$)	$Y_{biom/C\text{-}souce}$ ($g_{biom}/g_{C\text{-}source}$)	Viscosifying power (cps/g_{alg}/L)
Lactose + Burk´s medium	0.667±0.003	0.100±0.010	0.150±0.005	15.5±2.5
Fructose + Burk´s medium	0.531±0.038	0.105±0.029	0.197±0.006	17.5±1.8
Galactose + Burk´s medium	0.608±0.045	0.117±0.090	0.193±0.030	14.5±2.2
Glucose + Burk´s medium	0.564±0.307	0.171±0.068	0.303±0.082	13.4±1.6
Sucrose + Burk´s medium	0.928±0.048	0.281±0.043	0.303±0.036	9.7±0.9
Liquid whey	0.338±0.110	0.153±0.046	0.454±0.064	ND
Sugarcane juice	0.242±0.138	0.098±0.018	0.406±0.042	ND
Liquid whey + Burk´s medium	0.362±0.005	0.127±0.017	0.351±0.048	18.6±2.2
Sugarcane juice + Burk´s medium	0.532±0.098	0.182±0.021	0.343±0.022	23.8±2.6

ND: not determined
Source: The Authors

Using sugarcane juice-Burk culture medium, the highest viscosity was obtained (85±9 cps), with 3.55±0.42 g/L of alginate, and a MMW of 1203±120 kDa (Fig. 1B, 1D and 1E). Compared to sucrose-Burk medium, the viscosity was 50±9 cps with a final alginate concentration of 5.11±0.37 g/L and a MMW of 990±80 kDa. In glucose, the viscosity was 41±7 cps with 3.08±0.70 g/L of alginate and MMW of 1100±90 kDa (Fig.s 1B, 1D and 1E). The polydispersity index of alginates obtained from all C-sources was less than 2.0. These values demonstrated that alginates are monodisperse, without significant differences (Fig. 1F), at least in the experiments carried out in this work for shake flasks.

Peña et al. [10] propose "viscosifying power" as the way to compare the viscosifying capacity of alginates from different sources or processes, which can be defined as the viscosity generated per unit of polymer concentration. In order to compare the differences in the viscosifying power of alginates obtained from each C-source, viscosity/concentration ratio were calculated from final cultures of *A. vinelandii* (Table 1). The higher viscosifying power was found in those cultures carried out with sugarcane juice + Burk´s medium (23.8±2.6 cps L/$g_{alginate}$), and was twice the lowest viscosifying power obtained by using sucrose + Burk´s components (9.69±0.95 cps L/$g_{alginate}$). The most interesting result was the viscosifying power of 18.57±2.16 cps L/$g_{alginate}$ obtained from cultures carried out with hydrolyzed and deproteinized whey + Burk´s components (Table 1), due to the lower MMW of the alginate obtained (121±27 kDa) (Fig. 1D). These results cannot be explained only by MMW differences, because there are other factors such as the monomers ratio (M/G ratio), the sequence pattern and the O-acetylation degree in mannuronic acid residues that might also affect viscosifying power [6,9,10]. On the other hand, Peña et al. [30] reported that the viscosifying power, the degree of O-acetylation and the MMW of the alginate produced by *A. vinelandii* in shake flasks are determined by the oxygen transfer rate (OTR). Those data are in agreement with our data in terms that the OTR might be affected by the C-source used, as previously reported in *E. coli* cultures [31,32]. There is a well documented strong relationship between alginate production, its molecular characteristics and OTR [9, 10,33,34].

The alginate viscosity production and MMW differences between this work and those reported by Peña et al. [16], where sucrose + Burk´s medium were used, might be due to the Erlenmeyer shake flasks dimensions, volumes and inoculation form. Peña et al. [16] used shake flasks of 500 mL containing 100 mL of medium, inoculating 10% of the pre-culture (around 0.1-0.3 g/L, dry weight), reporting a maximum alginate concentration (obtained at 72 h) of 4.5 g/L, viscosity of 520 cps and a MMW of $1.98x10^6$ Da with a polidispersity index (PI) of 1.50, whereas, in this work, we used 250 mL shake flasks with 50 mL of culture medium, inoculated with washed cells. On the other hand, Peña et al. [16] reported that alginate production change as a function of the filling volume in shake flasks, modifying also its MMW. Thus, it is not surprising—comparing our results with those previously reported—that alginate molecular characteristics were different in spite of using the same strain of *A. vinelandii*.

In order to dissect the role of non-conventional carbon sources in *A. vinelandii* growth, C-source consumption and alginate molecular characteristics, a complete kinetics of *A. vinelandii* growth and alginate production was undertaken by using sucrose, deproteinized and hydrolyzed whey and sugarcane juice in Burk´s medium (Fig. 2). A similar final biomass was obtained using whey and sugarcane juice in Burk´s medium (6.7±0.7 g/L and 6.7±0.4 g/L, respectively), with similar specific growth rates (0.047±0.003 and 0.046±0.004 h^{-1}, respectively). But lower biomass was obtained using sucrose (5.5±0.2 g/L) with a higher specific growth rate (0.052±0.002 h^{-1}) (Fig. 2.A). However, lower alginate production, and lower specific alginate production rates were obtained by using hydrolyzed whey (2.4±0.3 g/L and $3.77x10^{-3}$±$0.3x10^{-3}$ $g_{alginate}/g_{biomass}h$, respectively), and sugarcane juice (3.6±0.4 g/L and $5.54x10^{-3}$±$0.6x10^{-3}$ $g_{alginate}/g_{biomass}h$, respectively) in Burk´s medium, than in sucrose (5.1±0.4 g/L and $25.8x10^{-3}$±$2x10^{-3}$ $g_{alginate}/g_{biomass}h$, respectively) (Fig. 2.B). In terms of C-source consumption, almost all were consumed, but no significant differences were obtained in specific consumption rates with an average of $3.46x10^{-3}$±$0.27x10^{-3}$ $g_{C\text{-}source}/g_{biomass}.h$ (Fig. 2.C). A similar viscosity kinetics was found between those cultures grown using deproteinized and hydrolyzed whey and sucrose in Burk´s medium (Fig. 2.D). These similarities are not correlated to MMW kinetics, where an almost five times lower MMW was obtained in those cultures grown using hydrolyzed and deproteinized whey (Fig. 2.E). To explain this behavior, the viscosifying power was plotted as a function of culture time (Fig. 3). This relation can

be a quantitative approach to define the quality of alginates [10]. Viscosifying power increases during culture, and decreases at the end of the exponential phase, possibly due to the action of alginate lyases [21,35]. Moreover, there is no relationship between biomass growth kinetics, Alginate MMW and its production and the viscosifying capacity. This may be due to differences in the biopolymer molecular characteristics, such as the M/G ratio and the acetylation degree [15,30]. Table 1 outlines the final viscosifying power of cultures. The highest viscosifying power was obtained using deproteinized and hydrolyzed whey, and sugarcane juice in Burk´s culture medium. However, it is clear that higher values of viscosifying capacity can be achieved during cultivation (Fig. 3) as a response of the increases in the MMW [2,9,15,30], and the final values presented in Table 1 are the result of the alginate lyase activity [21,23,35].

Here, we could suggest that using alternative C-sources, and consequently more complex but less expensive ones, alginates with different molecular properties than those obtained with conventional C-sources can be produced.

4. Concluding remarks

To our knowledge, this is the first work reporting the effect of non-conventional and conventional C-sources on alginate MMW and viscosifying power produced by *A. vinelandii*. Although the highest concentration of biomass was obtained with the use of alternative C-sources (deproteinized and hydrolyzed whey and sugarcane juice),

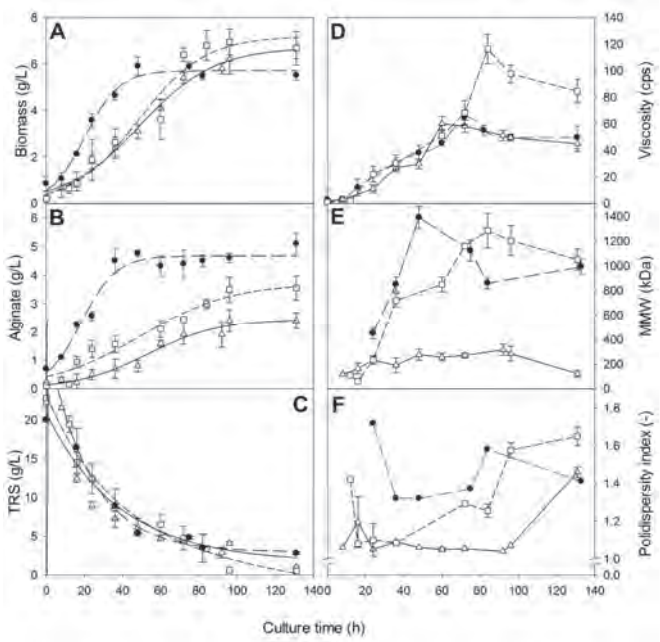


Figure 2. Kinetics of biomass growth (A), alginate production (B), total reducing sugars (C), culture broth viscosity (D), alginate mean molecular weight (E), and polidispersity index (F) of cultures carried out in 250 mL shake flask, containing 50 mL of modified Burk's medium and incubated at 200 rpm and 29ºC, by using sucrose (closed dots), deproteinized and hydrolyzed whey (open triangles), and sugarcane juice (open squares) as a carbon source in Burk´s medium.
Source: The Authors

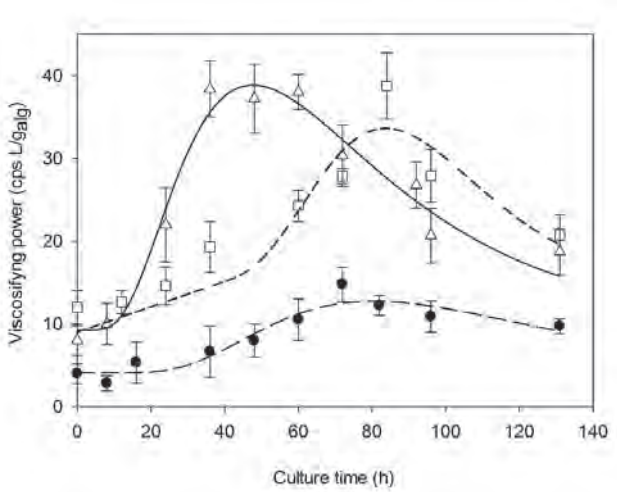


Figure 3. Kinetics of the relation viscosity/alginate concentration (viscosifying power) in culture media carried out using sucrose (closed dots), deproteinized and hydrolyzed whey (open triangles), and sugarcane juice (open squares) as a carbon source in Burk´s medium.
Source: The Authors

the highest concentration of alginate was obtained using sucrose in Burk´s medium. Furthermore, the best alginate yields and specific alginate production rates were obtained using sucrose, compared to unconventional C-sources. Moreover,differences in viscosifying power clearly demonstrated that the alginates produced by *A. vinelandii* when using deproteinized and hydrolyzed whey are surely different in composition than those produced with sugar cane or sucrose, said differences lying depending on the monomers ratio (M/G), the sequence pattern and the acetylation degree in mannuronic acid residues. Based on the data presented here, it can be assumed that it is possible to produce alginates with different molecular characteristics by modifying only the components of the culture, such as the C-source. This knowledge associated with the understanding of the effects of environmental conditions, would yield high concentrations of high added value alginates.

Acknowledgements

This work was financed by Consejo Nacional de Ciencia y Tecnología (CONACyT 178528, CONACYT-INNOVAPYME 214404), and Programa de Apoyo a Proyectos de Investigación e Innovación Tecnológica, Universidad Nacional Autónoma de México (PAPIIT-UNAM IN-210013 and IN-209113). The authors would like to thank Drs. Enrique Galindo, Carlos Peña and Celia Flores for technical assistance. We also thank Ana Carmen Delgado for reviewing the English version of the manuscript.

References

[1] Rehm, B.H. and Valla, S., Bacterial alginates: Biosynthesis and applications. Appl Microbiol Biotechnol 48, pp. 281-288, 1997. DOI: 10.1007/s10529-006-9156-x

[2] Galindo, E., Peña, C., Nuñez, C., Segura, D. and Espin, G., Molecular and bioengineering strategies to improve alginate and polydydroxyalkanoate production by *Azotobacter vinelandii*. Microb Cell Fact. [online]. 6:7, 2007. Avalilable at: http://www.microbialcellfactories.com/content/6/1/7. DOI: 10.1186/1475-2859-6-7

[3] Rehman, Z.U., Wang, Y., Moradali, M.F., Hay, I.D. and Rehm, B.H., Insight into assembly of the alginate biosynthesis machinery in *Pseudomonas aeruginosa*. Appl Environ Microbiol, 79(10), pp. 3264-3272, 2013. DOI: 10.1128/AEM.00460-13

[4] Hay, I.D., Wang, Y., Moradali, M.F., Rehman, Z.U. and Rehm, B.H.A., Genetics and regulation of bacterial alginate production. Environ Microbiol. 16(10), pp. 2997-3011, 2014. DOI:10.1111/1462-2920.12389.

[5] Skjåk-Braek, G., Grasdalen, H. and Larsen, B., Monomer sequence and acetylation pattern in some bacterial alginates. Carbohydr Res. 154, pp. 239-250, 1986. DOI: 10.1016/S0008-6215(00)90036-3

[6] Vargas-Garcia, M.C., Lopez, M.J., Elorrieta, M.A., Suarez, F. and Moreno, J., Properties of polysaccharide produced by *Azotobacter vinelandii* cultured on 4-hydroxybenzoic acid. J App Microbiol, 94, pp. 388-395, 2003. DOI: 10.1046/j.1365-2672.2003.01842.x

[7] Moresi, M., Bruno, M. and Parente, E., Viscoelastic properties of microbial alginate gels by oscillatory dynamic tests. J Food Eng., 64, pp. 179-186, 2004. DOI: 10.1016/j.jfoodeng.2003.09.030

[8] Remminghorst, U and, Rehm, B.H., Bacterial alginates: From biosynthesis to applications. Biotechnol Lett, 28, pp. 1701-1712, 2006. DOI: 10.1007/s10529-006-9156-x

[9] Castillo, T., Galindo, E. and Peña, C., The acetylation degree of alginates in *Azotobacter vinelandii* ATCC9046 is determined by dissolved oxygen and specific growth rate: Studies in glucose-limited chemostat cultivations. J Ind Microbiol Biotechnol, 40(7), pp. 715-723, 2013. DOI: 10.1007/s10295-013-1274-6

[10] Peña, C., Castillo, T., Nuñez, C. and Segura, D., Bioprocess design: Fermentation strategies for improving the production of alginate and poly-beta-hydroxyalkanoates (PHAs) by *Azotobacter vinelandii*. In Carpi, A. (ed). Progress in molecular and environmental bioengineering - From analysis and modeling to technology applications, 2011. DOI: 10.5772/20393.

[11] Horan, N.J., Jarman, T.R. and Dawes, E.A., Effects of carbon source and inorganic phosphate concentration on the production of alginic acid by a mutant of *Azotobacter vinelandii* and on the enzymes involved in its biosynthesis. J Gen Microbiol, 127, pp. 185-191, 1981. DOI: 10.1099/00221287-127-1-185

[12] Clementi, F., Fantozzi, P., Mancini, F. and Moresi, M., Optimal conditions for alginate production by *Azotobacter vinelandii*. Enzyme Microb Tech. 17, pp. 983-988, 1995. DOI: 10.1016/0141-0229(95)00007-0

[13] Clementi, F., Alginate production by *Azotobacter vinelandii*. Crit Rev Biotechnol, 17, pp. 327-361, 1997. DOI:10.3109/07388559709146618

[14] Zapata-Vélez, A.M. and Trujillo-Roldán, M.A., The lack of a nitrogen source and/or the C/N ratio affects the molecular weight of alginate and its productivity in submerged cultures of *Azotobacter vinelandii*. Ann Microbiol, 60, pp. 661-668, 2010. DOI: 10.1007/s13213-010-0111-7

[15] Peña, C., Hernandez, L. and Galindo, E., Manipulation of the acetylation degree of *Azotobacter vinelandii* alginate by supplementing the culture medium with 3-(N-morpholino)-propane-sulfonic acid. Lett Appl Microbiol, 43, pp. 200-204, 2006. DOI: 10.1111/j.1472-765X.2006.01925.x

[16] Peña, C., Campos, N. and Galindo, E., Changes in alginate molecular mass distributions, broth viscosity and morphology of *Azotobacter vinelandii* cultured in shake flasks. Appl Microbiol Biotechnol, 48 pp. 510-515, 1997. DOI: 10.1007/s002530051088

[17] Peña, C., Trujillo-Roldán, M.A. and Galindo, E., Influence of dissolved oxygen tension and agitation speed on alginate production and its molecular weight in cultures of *Azotobacter vinelandii*. Enzyme Microb Technol, 27, pp. 390-398, 2000. DOI: 10.1016/S0141-0229(00)00221-0

[18] Kivilcimdan, M.C. and Sanin, F.D., An investigation of agitation speed as a factor affecting the quantity and monomer distribution of alginate from *Azotobacter vinelandii* ATCC(R) 9046. J Ind Microbiol Biotechnol, 39, pp. 513-519, 2012. DOI: 10.1007/s10295-011-1043-3

[19] Seañez, G., Peña, C. and Galindo, E., High CO_2 affects alginate production and prevents polymer degradation in cultures of *Azotobacter vinelandii*. Enzyme Microb Technol, 29, pp. 535-540, 2001. DOI: 10.1016/S0141-0229(01)00435-5

[20] Trujillo-Roldán, M.A., Peña, C., Ramirez, O.T. and Galindo, E., Effect of oscillating dissolved oxygen tension on the production of alginate by *Azotobacter vinelandii*. Biotechnol Prog. 17, pp. 1042-1048, 2001. DOI: 10.1021/bp010106d

[21] Trujillo-Roldán, M.A., Moreno, S., Espin, G. and Galindo, E., The roles of oxygen and alginate-lyase in determining the molecular weight of alginate produced by *Azotobacter vinelandii*. Appl Microbiol Biotechnol, 63, pp. 742-747, 2004. DOI: 10.1007/s00253-003-1419-z

[22] Díaz-Barrera, A., Silva, P., Avalos, R. and Acevedo, F., Alginate molecular mass produced by *Azotobacter vinelandii* in response to changes of the O_2 transfer rate in chemostat cultures. Biotechnol Lett, 31, pp. 825-829, 2009. DOI: 10.1007/s10529-009-9949-9

[23] Flores, C., Moreno, S., Espin, G., Peña, C. and Galindo, E., Expression of alginases and alginate polymerase genes in response to oxygen, and their relationship with the alginate molecular weight in *Azotobacter vinelandii*. Enzyme Microb Technol, 53, pp. 85-91, 2013. DOI: 10.1016/j.enzmictec.2013.04.010

[24] Priego-Jimenéz, R., Peña, C., Ramírez, O.T. and Galindo, E., Specific growth rate determines the molecular mass of the alginate produced by *Azotobacter vinelandii*. Biochem Engin J., 25, pp. 187-193, 2005. DOI: 10.1016/j.bej.2005.05.003

[25] Díaz-Barrera, A., Silva, P., Berrios, J. and Acevedo, F., Manipulating the molecular weight of alginate produced by *Azotobacter vinelandii* in continuous cultures. Bioresour Technol, 101, pp. 9405-9408, 2010. DOI: 10.1016/j.biortech.2010.07.038

[26] Díaz-Barrera, A., Soto, E. and Altamirano, C., Alginate production and *alg8* gene expression by *Azotobacter vinelandii* in continuous cultures. J Ind Microbiol Biotechnol, 39, pp. 613-621, 2012. DOI: 10.1007/s10295-011-1055-z

[27] Trujillo-Roldán, M.A., Peña, C. and Galindo, E., Components in the inoculum determine the kinetics of *Azotobacter vinelandii* cultures and the molecular weight of its alginate. Biotechnol Lett, 25, pp. 1251-1254, 2003. DOI: 10.1023/A:1025027010892

[28] Pindar, D.F. and Bucke, C., The biosynthesis of alginic acid by *Azotobacter vinelandii*. Biochem J., 152, pp. 617-622, 1975.

[29] Page, W.J., Manchak, J. and Rudy, B., Formation of poly(hydroxybutyrate-co-hydroxyvalerate) by *Azotobacter vinelandii* UWD. Appl Environ Microbiol, 58(9), pp. 2866-2873, 1992.

[30] Peña, C., Galindo, E. and Büchs, J., The viscosifying power, degree of acetylation and molecular mass of the alginate produced by *Azotobacter vinelandii* in shake flasks are determined by the oxygen transfer rate. Process Biochem, 46, pp. 290-297, 2011. DOI: 10.1016/j.procbio.2010.08.025

[31] Kunze, M., Huber, R., Gutjahr, C., Mullner, S. and Büchs, J., Predictive tool for recombinant protein production in *Escherichia coli* shake-flask cultures using an on-line monitoring system. Biotechnol Prog. 28, pp. 103-113, 2012. DOI: 10.1002/btpr.719

[32] Ukkonen, K., Veijola, J., Vasala, A. and Neubauer, P., Effect of culture medium, host strain and oxygen transfer on recombinant Fab antibody fragment yield and leakage to medium in shaken *E. coli* cultures. Microb Cell Fact, 12, 73 P., 2013. DOI: 10.1186/1475-2859-12-73

[33] Díaz-Barrera, A., Aguirre, A., Berrios, J. and Acevedo, F., Continuous cultures for alginate production by *Azotobacter vinelandii* growing at different oxygen uptake rates. Process Biochem, 46, pp. 1879-1883, 2011. DOI: 10.1016/j.procbio.2011.06.022

[34] Lozano, E., Galindo, E. and Peña, C., Oxygen transfer rate during the production of alginate by *Azotobacter vinelandii* under oxygen-limited and non oxygen-limited conditions. Microb Cell Fact, 10, 13 P., 2011. DOI: 10.1186/1475-2859-10-13

[35] Trujillo-Roldán, M.A., Moreno, S., Segura, D., Galindo, E. and Espin, G., Alginate production by an *Azotobacter vinelandii* mutant unable to produce alginate lyase. Appl Microbiol Biotechnol, 60, pp. 733-737, 2003, DOI: 10.1007/s00253-002-1173-7

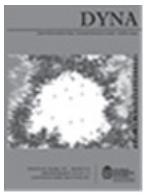
M.A. Trujillo-Roldán, *Corresponding autor*, is Ph.D. Head of the Unidad de Bioprocesos, Instituto de Investigaciones Biomédicas, Universidad Nacional Autónoma de México.
ORCID: 0000-0002-7497-4452

J.F. Monsalve-Gil, is Chemical Engineeering of the Facultad de Minas, Universidad Nacional de Colombia, Sede Medellín, coolombia.
ORCID: 0000-0001-7400-9372

A.M. Cuesta-Álvarez, is Chemical Engineering of the Facultad de Minas, Universidad Nacional de Colombia, Sede Medellín, Colombia.
ORCID: 0000-0003-3374-9715

N.A. Valdez-Cruz, is Ph.D., Departamento de Biología Molecular y Biotecnología, Instituto de Investigaciones Biomédicas, Universidad Nacional Autónoma de México, México.
ORCID: 0000-0002-8581-1173

UNIVERSIDAD NACIONAL DE COLOMBIA
SEDE MEDELLÍN
FACULTAD DE MINAS



DYNA
http://dyna.medellin.unal.edu.co/

Supply chain knowledge management: A linked data-based approach using SKOS

Cristian Aarón Rodríguez-Enríquez [a], Giner Alor-Hernández [b], Cuauhtémoc Sánchez-Ramírez[c] & Guillermo Córtes-Robles[d]

[a] *Instituto Tecnológico de Orizaba, Orizaba, México. crodriguezen@gmail.com*
[b] *Instituto Tecnológico de Orizaba, Orizaba, México. galor@itorizaba.edu.mx*
[c] *Instituto Tecnológico de Orizaba, Orizaba, México. csanchez@itorizaba.edu.mx*
[d] *Instituto Tecnológico de Orizaba, Orizaba, México. grobles@itorizaba.edu.mx*

Received: November 6th, 2014. Received in revised form: February 24th, 2015. Accepted: November 03rd, 2015.

Abstract
Nowadays, knowledge is a powerful tool in order to obtain benefits within organizations. This is especially true when semantic web technologies are being adapted for the requirements of enterprises. In this regard, the Simple Knowledge Organization System (SKOS) is an area of work developing specifications and standards to support the use of knowledge organization systems. Over recent years, SKOS has become one of the sweet spots in the linked data (LD) ecosystems. In this paper, we propose a linked data-based approach using SKOS, in order to manage the knowledge from supply chains. Additionally, this paper covers how SKOS can be enriched by ontologies and LD to further improve semantic information management. This is due to the fact that the supply chain literature focuses on assets, data, and information elements of exchange between supply chain partners, despite improved integration and collaboration requiring the development of more complex features of know-how and knowledge.

Keywords: knowledge; linked data; management; semantic; SKOS; supply chain.

Administración del conocimiento en cadenas de suministro: Un enfoque basado en Linked Data usando SKOS

Resumen
Hoy en día, el conocimiento es una poderosa herramienta para obtener beneficios en cualquier organización. Especialmente cuando las tecnologías de la Web semántica son adaptadas a los requerimientos de las empresas. En este sentido, el sistema simple de organización de conocimiento (SKOS) es un área de trabajo que ha desarrollado especificaciones y estándares para trabajar con sistemas de organización de conocimiento. Tomando esto en cuenta, en los últimos años SKOS se ha convertido en uno de los puntos clave en el ecosistema de Linked Data (LD). En este artículo, proponemos un enfoque basado en LD usando SKOS, con la finalidad de administrar el conocimiento en las cadenas de suministro. Adicionalmente este artículo cubre como SKOS puede ser enriquecido por ontologías y LD para mejorar la semántica en la administración del conocimiento. Esto se debe a que la literatura de cadenas de suministro se enfoca en los recursos, los datos y la información que se intercambian entre los socios de la cadena de suministro, a pesar del hecho que para mejorar la integración y colaboración entre socios requiere del desarrollo de características complejas de "saber-hacer" y conocimiento.

Palabras clave: administración; cadena de suministro; conocimiento; Linked Data; semántica; SKOS.

1 Introduction

Nowadays, the efficient use of knowledge has been critical to the organization's survival as well as its success in competitive global markets. It has a strong potential to problem solve, make organizational performance enhancements, undertake decision-making, and innovate. There is a growing recognition that supply chain management (SCM) offers significant opportunities for organizations to create strategic advantages Wen and Gu [1]. In this regard, knowledge management (KM) is the process of capturing, developing, sharing, and effectively using

© The author; licensee Universidad Nacional de Colombia.

organizational knowledge [2]. The term SCM was coined in 1982 by Laseter and Oliver [3]. According to Mentzer, DeWitt, Keebler, Min, Nix, Smith and Zacharia [4], supply chain management (SCM) is "the systemic, strategic coordination of the traditional business functions and the tactics across these business functions within a particular company and across businesses within the supply chain, for the purposes of improving the long-term performance of the individual companies and the supply chain as a whole". Due to the relevance of KM in organizations, several pieces of research and industry efforts have been focused on the topic in order to improve supply chain knowledge management (SCKM). In the literature, there are seminal research works with different approaches to KM, for instance, Capó-Vicedo, Mula and Capó [5] propose a social network-based model to improve knowledge management in multi-level supply chains formed by small and medium-sized enterprises (SMEs);Shih, Hsu, Zhu and Balasubramanian [6] propose a knowledge management architecture to facilitate knowledge management within a collaborative supply chain; and Raisinghani and Meade [7] explore the linkage between organization performance criteria and the dimensions of agility, e-supply-chain drivers, and knowledge management, among other approaches. Lopez and Eldridge [8] presented a working prototype to promote creation and control in a knowledge supply chain with the objective of diffusing the best practices among supply chain practitioners. In this sense, the adoption of best practices in conjunction with information technologies represents an advantage for organizations.

In addition to the relevance of knowledge management in organizations, collaboration between supply-chain partners is one of the most promising areas of study for academics and practitioners. This is because there are several benefits that can be achieved by companies and supply chains such as, intelligent inventory management, new product development, collaborative product design management, to mention but a few.

According to Andreas Blumauer, since 2014 the Simple Knowledge Organization System (SKOS) has become one of the 'sweet spots' in the linked data ecosystems. This is due to SKOS playing a key role in order to improve semantic information management, especially in terms of its following capabilities, taxonomy and thesaurus management, text mining and entity extraction, and finally knowledge engineering and ontology management. SKOS is an area of work in which there are developing specifications and standards to support the use of knowledge organization systems (KOS), such as thesauri, classification schemes, subject heading systems, and taxonomies within the framework of the Semantic Web.

However, even though many studies have reported theoretical and practical foundations for knowledge management, there has been very little research reported using semantic technologies and SKOS.

In this regard, Linked Data based IT-architectures cover all of SKOS's capabilities, and provide the means for agile data, information, and knowledge management. SKOS can increase the value of organizations data and better use of existing data can be fostered by semantic searches, agile data integration and content personalization. Taking this into consideration, a linked data-based approach in combination with SKOS is feasible for organizing knowledge management in organizations, specifically for supply chain management, due to its ability to coordinate and synchronize interdependent processes, and to integrate information systems and to cope with distributed learning [9].

The aim of this paper is to introduce a linked data based approach-using SKOS in order to improve and facilitate knowledge management between supply chain partners. The importance of using a new approach relies on the benefits of linked data and SKOS. These benefits are: 1) obtaining open data sources of knowledge (linked open data), 2) automatizing data organization and procurement for non-expert organizations, 3) improving organizations' process, 4) improving operational and organizational performance, and 5) improving the decision-making process, to mention but a few. This paper is structured as follows: in section 2, the related works are discussed, in section 3 the linked data-based approach using SKOS for supply chain knowledge management is presented, in section 4 a brief case study is conducted, section 5 discusses future work possibilities in order to talk about this research limitations and implications, and, finally, section 4 concludes with this research's findings.

2 Related works

Recent advances in the field of knowledge management and semantic technologies have increased the significance of knowledge management in organizations using information technologies. Through electronic networks, organizations can achieve integration by tightly coupling processes at the interfaces between each stage of the value chain. According to Williams Jr [10], electronic linkages in the value chains have been fundamentally changing the nature of inter-organizational relationships. Organizations are redesigning their internal structure and their external relationships, creating networks of knowledge to facilitate the communication of data, information, and knowledge, while improving coordination, decision making, and planning. Taking into account these organizational changes, the use of flexible and scalable information technologies is preferred in order to take advantage of the know-how from the supply chains. In this section, each of the most significant papers related to this work will be presented, starting with the exploitation of knowledge sharing across the supply chain.

Wu [11] addressed the problem of coordination among multi-agent systems. The issue of coordination problems in supply chains was presented, and how to design multi-agent systems to improve information and knowledge sharing was highlighted. Becker and Zirpoli [12] carried out research on the theme of knowledge transfer in outsourcing activities. In particular, the focus was on designing an outsourcing strategy to improve knowledge integration. Holtbrügge and Berg [13] carried out a study of the knowledge transfer process in German multinational corporations (MNCs). These three works focused on knowledge sharing and how exploit it. This is due to the fact that one of the most suitable ways to improve processes in organizations is through knowledge exploitation. In this regard, Sivakumar and Roy [14] proposed the concept of knowledge redundancy as a critical factor for supply chain value creation. Knowledge

redundancy deals with there being a sufficient knowledge overlap to provide the opportunity to have good communication and, thus, effective operation activities. At the moment that an organization exploits the knowledge, some benefits can be obtained; for instance, Raisinghani and Meade [7] investigated the links between the supply chain, the firm's agility, and knowledge management. Their focus was on the strategic decision making perspective. In this perspective, knowledge comes from every relationship in the supply chain. Hult, Ketchen and Arrfelt [15] stated that knowledge acquisition activities, knowledge distribution activities and shared meaning were related with faster cycle time. For instance, Piramuthu [16] developed a knowledge-based framework for a dynamic re-configuration of supply chains over time.

In García-Cáceres, Perdomo, Ortiz, Beltrán and López's research [17], the authors analyzed the supply and value chains of the Colombian cocoa agribusiness, in order to detect the agents, phases, stages, and factors influencing the planting and harvesting of the product. They also analyzed =the chocolate and confection production process, as well as the final consumption. Within the supply chain stage identification and effects context, Avelar-Sosa, García-Alcaraz, Cedillo-Campos and Adarme-Jaimes's [18] work analyzes the effects of regional infrastructure and the services in supply chain performance in manufacturing companies found in Ciudad Juarez, Chihuahua, Mexico. The results indicate that if regional infrastructure has a good level then there will be a positive impact on logistics services, and as a consequence, on costs. In addition to these works, Espinal and Montoya's research [19] identifies the state of the art and the current use of Information and Communications Technologies (ICT) in the supply chain as well as its application level in Colombian industry. The research does this through analysis of existing studies and, at the end of the review, the authors observed that most of these technologies contribute to cost reduction and improvement of the information flow among the actors in the supply chain.

Other approaches were also seen in the literature, for example, Lau, Ho, Zhao and Chung [20] analyzed a process mining system for supporting knowledge discovery in daily logistics operations. Niemi, Huiskonen and Kärkkäinen [21] pointed out the process of knowledge accumulation. They presented it as an ongoing procedure in which the implementation of organizational processes and inventory techniques takes place gradually. Niemi, Huiskonen, and Karkkainen's aim [22] was to evaluate the adoption of complex supply chain management practices. In order to do this, Niemi et al. used the knowledge maturity model and strategies to accelerate knowledge creation as theoretical frameworks. The purpose of their approach was to intend to provide meaningful knowledge management. Halley, Nollet, Beaulieu, Roy, and Bigras [23] suggested that the management of the relationships present in the supply chain could be useful to share and acquire knowledge, instead of building external business relationships.

Apart from the previous research, Douligeris and Tilipakis [24] carried out a study on the new opportunities provided by the semantic web. They focused their attention on the introduction of web technologies on supply chain management. In particular, the use of ontologies in improving knowledge management applications was described. Taking this into consideration, Huang and Lin [25] addressed the problem of managing knowledge heterogeneity in the context of interoperability among multi-entities in a supply chain. They proposed a solution for sharing knowledge using the semantic web. Their solution was based on a semi-structured knowledge model to describe knowledge, not only in an explicit and sharable way, but knowledge that also had a meaningful format, an agent-based annotation process to determine issues related with the heterogeneity of knowledge documents, and an articulation mechanism to improve the efficiency of interoperability between two heterogeneous ontologies.

The aforementioned research works emphasized the importance of integrating information and knowledge flows within the manufacturing supply chain, and highlighted the importance of handling distributed knowledge. For instance, Craighead, Hult, and Ketchen Jr [26] used an economics perspective to measure the impact of a knowledge development capacity on supply chain performance. They measured the effects of an innovation-cost strategy on the supply chain. They found that knowledge development capacity and intellectual capital efforts are a good complement to other supply chain strategies. However, these works lack the availability of data sources due to the requirements of managing and organizing data in organizations. Additionally, this task it's very complex for small and medium size organizations. Moreover, some of the techniques used for knowledge management were conceived to manage the data, and not to infer knowledge from raw data. Finally, some organizations do not have the right tools to manage knowledge. This is due to the nature of the data; in some domains the same words have different meanings. In this regard, we propose a linked data-based approach for supply chain knowledge management using SKOS.

3. Linked data-based approach for supply chain knowledge management using SKOS

Interest in supply chain management has steadily increased since the 1980s when firms saw the benefits of collaborative relationships within and beyond their own organization. Firms are finding that they can no longer compete effectively while isolated from their suppliers or other entities in the supply chain [27]. The term supply chain management has a variety of different meanings, some related to management processes, others to the structural organization of businesses. Supply chain management itself integrates the management of supply and demand. According to the Council of Supply Chain Management Professionals (2014), it encompasses "the planning and management of all activities involved in sourcing and procurement, conversion and logistics." Supply chain management also covers coordination and collaboration with channel partners, such as customers, suppliers, distributors, and service providers.

According to Thomas and Griffin [28] historically, there are three fundamental stages of the supply chain, procurement, production, and distribution. These have been managed independently and buffered by large inventories. Increasing competitive pressures and market globalization

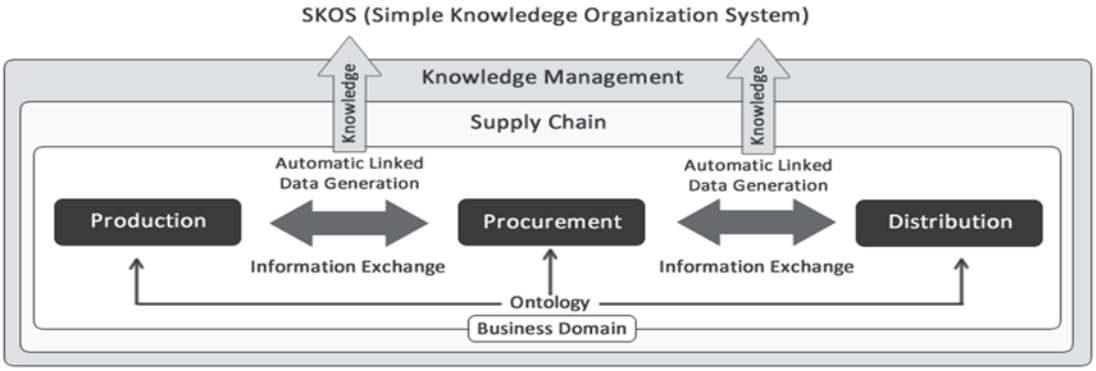


Figure 1. Conceptual schema.
Source: Authors

are forcing firms to develop supply chains that can quickly respond to customer needs. To remain competitive, these firms must reduce operating costs while continuously improving customer service. Taking this into consideration, with recent advances in communications and information technology, especially in semantic Web technologies, organizations have had an opportunity to reduce operating costs by coordinating the planning of these stages. In order to manifest the general idea about this proposal, in Fig. 1 a conceptual schema was depicted.

As can be seen from the conceptual schema, this proposal focuses its efforts on the automatic knowledge generation and management through linked data using SKOS and ontologies. These efforts were focused on technical information flows across the supply chain. This is due to the strong positive relationship that was found between the knowledge management process and the operational and organizational performance. In general terms, as a result of the information exchange across the supply chain among production, procurement, and distribution, Linked Data was produced in an automated way. This was due to domain specific knowledge (business domain) that was inferred from the ontology, and finally passed out to SKOS in order to provide both meaningful information and benefits for organizations. Due to the ontologies' relevance on this scenario, in the next subsection a brief table of highlights is included in order to explain the ontology used for this proposal in the context of a particular business domain.

3.1. Ontology

Originally, the term ontology has its roots in philosophy. An ontology denotes ''the science of what is, of the kinds and structures of objects, properties events, processes, and relations in every area of reality" [29]. Ontologies can be a component of knowledge-based systems, but also provide a "common language" for communication between domain analysts, developers, and users. In our proposal, SKOS can be improved with the use of ontologies. In this sense, a brief comparative analysis was performed on the results of the initial search query for "supply chain" AND "ontology" using online databases which were used for a keyword-based search. We also used the following alternative terms to reflect the actual use of various terms for the key concepts: "supply network", "supply chain management", "knowledge model", "semantic model", and "ontology model". These terms were based on the parameters proposed by Scheuermann and Leukel [30] in their literature review. The literature provides various SCM ontologies for a range of industries and tasks. Table 1 lists the suitable ontologies reported in the literature for this work.

A more detailed discussion about the ontologies presented in Table 1 was found in Scheuermann and Leukel's research [30], which is a review about ontologies for supply chain management. Taking into consideration the results discovered in the literature, IDEONTM and SCOntology are suitable for the purposes of this work. In this sense, these approaches have been used in the design of the software architecture used as a basis for Linked Data generation and knowledge management using SKOS.

IDEONTM is an extensible ontology for designing, integrating, and managing collaborative distributed enterprises, and SCOntology is a formal approach that gives a unified and integrated view of the supply chain. We found that IDEONTM and SCOntology are suitable for the purposes of this work due to the support it gives for processes, activities, resources, deliveries, and return schemas provided for each one.

3.2. SKOS

Using SKOS, concepts can be identified using URIs (strings of characters used to identify the name of a resource). These are labeled with lexical strings in one or more natural languages (for instance, a business domain language), they are assigned notations (lexical codes), documented with various types of note, linked to other concepts and organized into informal hierarchies and association networks, aggregated into concept schemes, grouped into labeled and/or ordered collections, and mapped to concepts in other schemes. All these features allow the integration and management of knowledge in a particular domain, for instance in supply chain management. In Fig. 2 the main elements of the SKOS data model was depicted.

Table 1.
Ontologies for Supply Chain Management

Author(s)	Language	Knowledge Representation Paradigm	Ontology Evaluation	Name	Key Concepts
de Sousa [31]	Thesaurus, UML class diagram	Algebra of sets	Not reported	Not reported	Organizational unit, plan, resource, order, product, activity.
Madni, Lin and, Madni [32]	UML class diagram	Algebra of sets	Application	IDEON™	Enterprise, process, resource, objective, plan, activity.
Pawlaszczyk, Dietrich, Timm, Otto and, Kirn [33]	Frames	F-Logic	Not reported	Not reported	Activity, plan, product, organization, time, event, transfer-object, flow, performance.
Fayez, Rabelo and, Mollaghasemi [34]	OWL	DL	Not reported	Not reported	Functional units, processes, materials, objects, information, information resources.
Matheus, Baclawski, Kokar and, Letkowski [35]	OWL, SWRL	DL	Application	Not reported	Airbases, aircraft, parts, facilities, remote supply depots, event object attribute.
Chandra, and Tumanyan [36]	Algebra, XML Schema	Algebra of sets	Scenario	Not reported	Agent, input, output, environment, objectives, functions, processes, products.
Gonnet, Vegetti, Leone, and Henning [37]	OWL (UML)	DL	Scenario	SCOntology	Organizational unit, process, resource, plans, source, make, deliver, and return.
Grubic, Veza, and Bilic [38]	Frames	F-Logic	Case studies & Scenario	Not reported	Asset, coordination, location, metric, process/activity, buyer, flow, person, supplier, system.
Sakka, Millet, and Botta-Genoulaz [39]	OWL	DL	Scenario	Not reported	Top level, configuration level, and process category level.
Anand, Yang, Van Duin, and Tavasszy [40]	OWL	DL	Informed argument & Case studies	GenCLOn	Stakeholders, objectives, KPI, resources, measures, activity, R&D.
Scheuermann and Hoxha [41]	OWL	DL	Experiment Scenario	Not reported	Logistics actor, Logistics role, logistics service, logistics object, logistics KPI, logistics resource, logistics location.

Source: Authors

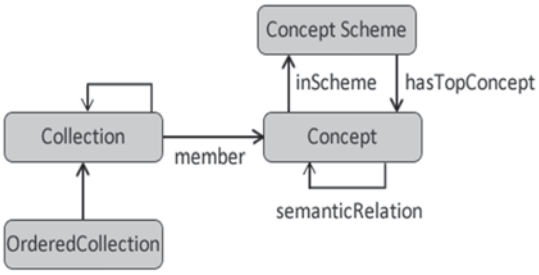


Figure 2. Main elements of the SKOS data model
Source: Authors

The SKOS data model enables the features [42] listed above by defining the elements depicted in Fig. 2. These features are:

- Identifying
- Labeling
- Documenting
- Linking and mapping concepts (even in other schemas)
- Aggregating concepts into concept schemes or collections

Taking into consideration SKOS' features, for the purposes of this research, SKOS has been used to express, in an interoperable way, different types of Knowledge Organization Systems (specifically for a supply chain model)—sets of terms or concepts, whether listed with definitions (glossaries), in hierarchical structures (basic classifications or taxonomies), or characterized by more complex semantic relations (thesauri, subject heading lists, or other advanced structures). In the next section an overview of the proposed architecture was described.

3.3. Architecture

The knowledge management focuses on the supply side; in contrast, knowledge creation is located on the demand side. Johnson and Whang [43] proposed the term e-collaboration for systems that facilitate the Internet-based coordination of decisions for all members of the supply chain. Taking this into consideration, our approach is focused on the demand side, through an Internet-based coordination of knowledge. The use of the proposed technologies was intended to generate raw knowledge in an automated way.

Our architecture has a layered design in order to organize its components. This layered design allows scalability and easy

maintenance because its tasks and responsibilities are distributed.

The general architecture is shown in Fig. 3. Each component has a function explained as follows:

Data layer: This layer stores supply chain management data; additionally, it contains all the configuration tables allowing the operation of the modules and services offered by our proposal. This layer comprises two key components, the business data and the ontology; these components are the core of the knowledge of the entire software architecture.

Data Management layer: This layer communicates with the Data layer in order to obtain business data and provide their representation through the ontology mapper in order to converting it to RDF.

Linked Data Generator: All data retrieved from Data layer through the Data Management layer is parsed in RFD in order to publish a local dataset of Linked Data.

Integration Layer [API]: This allows the creation of new educational applications through a series of public interfaces, which provide easy access to a set of services provided by the architecture. Service compositions are presented and defined in this layer. Specifically, the Data Manager component is responsible for providing interaction through raw data and the user interface.

Presentation Layer: In this layer, the architecture determines the best way to display the business data by using XHTML when HTML5 is not supported. The Presentation Layer does not know what events are taking place inside inferior layers and how the services are provided; it only uses them to show the end-user interface. It is worthwhile to mention that, for the purposes of this work, a graphic user interface was not used. However, the software architecture has been designed in order to support a Web-based user interface.

In additionally to the layer descriptions, there are a few main components that also need to be described:

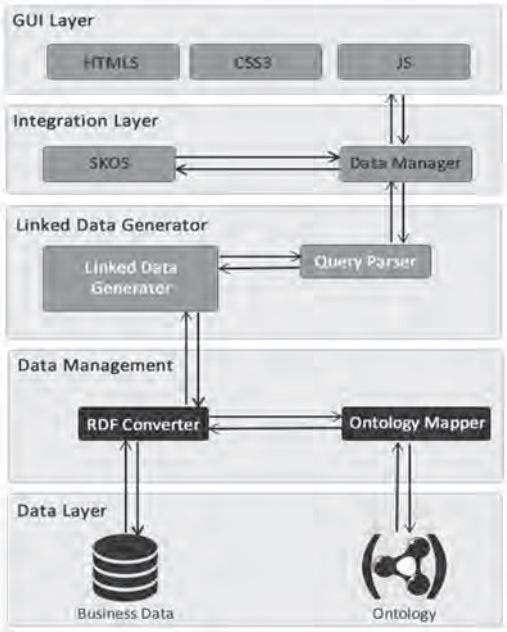


Figure 3. Architecture
Source: Authors

Business Data: As part of the Data Layer, in this repository (actually a database of structured or non-structured data), this component is responsible for the storage of the raw data from information exchanges across the supply chain.

Ontology: This component is responsible for managing the data representation and structure of the supply chain knowledge. In this component the IDEONTM and SCOntolgy has been used.

RDFConverter: In order to generate a Linked Data dataset, this component converted raw data mapped through the Ontology Mapper component to RDF (Resource Description Framework).

Linked Data Generator: This component is responsible for Linked Data Generation. In this component a local dataset of Linked Data is managed through the Query Parser component. At the end of the process, a set of structured RDF data is created and managed by a Linked Data engine.

Query Parser: This was used in order to translate a user-defined query into a natural language (a business domain specific language). This component translates the original query into SPARQL in order to retrieve the desired data, in this case the supply chain knowledge.

SKOS: In thesauri and other structured Knowledge Organizations Systems, concepts can be classified into semantically meaningful bundles. For example, arrays are used to group specializations of a concept that share a common feature: the concept "cars" might be primarily grouped by a feature "cars by engine" (''V8'', 'V6'', among others), and a second group of "cars by function" ("transport", "family", "sport", among others). Taking this as starting point, the SKOS component is responsible for the classification and management of the vocabulary used by the Data Manager component to retrieve processed and managed knowledge from the presentation layer.

Data Management: This component is responsible for managing the petitions performed by the GUI Layer, specifically the user request for data and knowledge.

It is worthwhile mentioning that Carrer-Neto, Hernández-Alcaraz; Valencia-García, and García-Sánchez; [44] and Ruiz-Martínez, Valencia-García, Martínez-Béjar, and Hoffmann's work [45] present the use of a top level ontology based framework to populate biomedical ontologies from texts and a social knowledge-based recommender system represent. These can be used to improve our software architecture in future work with the use of their techniques to extract knowledge from texts as a data source, and recommend knowledge resources through social network interactions among supply chain customers.

3.4. Data acquisition

This knowledge is related to the following aspects, which should be improved in supply chain management:

- **Demand:** Demand management is an essential element in supply chain management. It focuses companies and their partners on meeting the needs of customers, rather than the production process.
- **Integration:** Integrating supply chain processes helps each member to reduce their inventory costs.
- **Collaboration:** Collaboration in the supply chain

strengthens relationships between members by improving teamwork and helping all members increase their business.

- **Communication:** Effective communication helps the entire supply chain improve the efficiency and productivity of its operations by enabling all members to share the same demand and operational information.

For this research, the information required was obtained from broker web pages, ERPs, CRMs, and intranet applications, to mention but a few. In Fig. 4 a conceptual schema for data acquisition was depicted.

4. Case study: Detecting processing issues in a milk supply chain

The purpose of this case study was to put our knowledge management approach into practice. This case study should encourage supply chain practitioners and managers to use the experience and learning of this application to be able to develop and refine the application of knowledge management by using semantic web technologies.

Let us suppose that a supply chain in the field of milk production in the United States requires information (knowledge) about the delay that occurs between the procurement stage and distribution stage. This will be caused, in some scenarios, as a result of the product expiring because of the transit time, which represents losses and extra fees for the organization. The eight stages in the milk supply chain are:

a) Production of feed for cows: The dairy supply chain begins with growing crops such as corn, alfalfa hay, and soybeans to feed dairy cows.
b) Milk production: Dairy cows are housed, fed, and milked on dairy farms across the country.

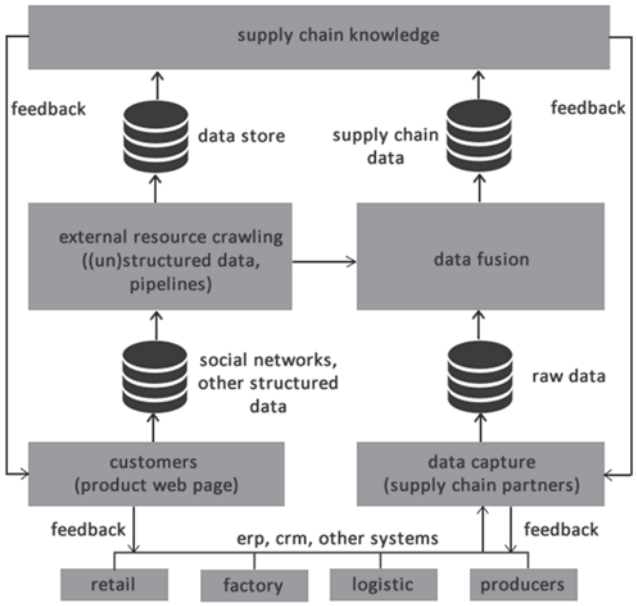


Figure 4. Conceptual schema for data acquisition and feedback
Source: Authors

c) Milk transportation: Milk is transported from the farm to the processing company in insulated tanker trucks. The average truck carries 5800 gallons of milk and travels approximately 500 miles on a round trip.
d) Processing: There are more than 1,000 U.S. processing plants that turn milk into cheese, yogurt, ice cream, powdered milk, and other products.
e) Packaging: This is typically done by the dairy processor. Both paperboard and plastic containers are designed to keep dairy products fresh, clean and wholesome.
f) Distribution: Distribution companies deliver dairy products from the processor to retailers, schools, and other outlets in refrigerated trucks.
g) Retail: Milk and dairy products are available at 178,000 retail outlets of all shapes and sizes.
h) Consumer: Milk and milk products deliver nine essential nutrients to consumers.

These stages should be grouped into the three main categories previously mentioned in the conceptual schema contained in section 3. The groups are: 1) production (production of feed for cows and milk production), 2) procurement (processing and packaging), and 3) distribution (distribution and retail).

In order to understand the full supply chain cycle, Fig. 5 shows the value chain of milk production.

Following the previously mentioned scenario, knowledge acquisition through the SKOS approach retrieved the following information:

- Production of feed for cows either increases or decreases the milk production.
- Production of feed for cows affects the quality of the produced milk.
- Due to the lack of communication between the processing and packaging phases, the milk spends a lot of time in the packaging process. The packaging unit does not accurately know way which milk product is to be released first. This is due to of the variation in milk quality. Some derivate products cannot be produced within the same processing time.



Figure 5. Milk supply chain
Source: Authors

In general terms, the lack of communication affects the operation of all stages in the milk supply chain. The degree of implication is directly proportional to the time needed to take countermeasures to change the production process in early stages. In order to take advantage of the knowledge produced in the supply chain, a more detailed analysis about production implications in the retail stage (sales, profits, among others) is required. In this sense, analysts can use data mining and big data tools. In future work, an analytic module must be added to our architecture in order to complete the cycle of knowledge management and data exploitation.

6. Conclusions and future directions

The primary contribution of this paper to the literature is to show how supply chain knowledge management can be improved with semantic web technologies. Fast evolving Web-based and semantic technologies provide, not only platforms for the development of powerful applications, but also opportunities to alleviate linguistic barriers to supply chain data across partners. In this study, a linked data-based approach using SKOS for supply chain knowledge management was presented. The findings showed how SKOS can be enriched using ontologies. Additionally, with automatic generation of linked data from supply chains, small and medium organizations without expertise, infrastructure, or resources to organize information can benefit from knowledge management. In this regard, knowledge sharing and reuse are important factors that affect the performance of supply chains. Due to this, a novel approach that combines the generation of Linked Data and ontology enriched SKOS was presented in this work, which can improve supply chain knowledge management.

Thinking about possible future directions, this research potentially has two key limitations or opportunities. First, the proposal contained in this case study addressed one particular business domain. In this regard, we need to prove this approach can be effectively used in other domains, which has to do with the Linked Data generation mechanism and their ontology-based knowledge management and acquisition. Second, there is a need to know and control the full scenario of the supply chain management. What will happen if one of the three stages (production, procurement, and distribution) it is out of scope, and the information exchange is not accessible for analysis and interaction? These two key limitations represent an opportunity to improve this proposal. Consequently, we plan to elaborate on this research in order to fulfill this gap.

Acknowledgments

This work was supported by the Tecnológico Nacional de México. Additionally, it was sponsored by the National Council of Science and Technology (CONACYT) and the Public Education Secretary (SEP), through PROMEP.

References

[1] Wen, H. and Gu, Q., The elements of supply chain management in new environmental era. Springer Berlin Heidelberg, City, 2014.

[2] Davenport, T.H. Saving IT's soul: Human-Centered information management. Harvard Business Review, 72(2), pp. 119-131, 1994.

[3] Laseter, T. and Oliver, K., When will supply chain management grow up? Strategy and Business. pp. 32-37, 2003.

[4] Mentzer, J.T., DeWitt, W., Keebler, J.S., Min, S., Nix, N.W., Smith, C.D. and Zacharia, Z.G., Defining supply chain management. Journal of Business Logistics, 22(2), pp. 1-25, 2001. DOI: 10.1002/j.2158-1592.2001.tb00001.x

[5] Capó-Vicedo, J., Mula, J. and Capó, J., A social network-based organizational model for improving knowledge management in supply chains. Supply Chain Management: An International Journal, 16(5), pp. 379-388, 2011. DOI: 10.1108/13598541111155884

[6] Shih, S.C., Hsu, S.H.Y., Zhu, Z. and Balasubramanian, S.K., Knowledge sharing—A key role in the downstream supply chain. Information & Management, 49(2), pp. 70-80, 2012. DOI: 10.1016/j.im.2012.01.001

[7] Raisinghani, M.S. and Meade, L.L., Strategic decisions in supply-chain intelligence using knowledge management: An analytic-network-process framework. Supply Chain Management: An International Journal, 10(2),pp. 114-121, 2005. DOI: 10.1108/13598540510589188

[8] Lopez, G. and Eldridge, S., A working prototype to promote the creation and control of knowledge in supply chains. International Journal of Networking and Virtual Organisations, 7(2), pp. 150-162, 2010. DOI: 10.1504/IJNVO.2010.031215

[9] Simatupang, T.M., Wright, A.C. and Sridharan, R., The knowledge of coordination for supply chain integration. Business process Management Journal, 8(3), pp. 289-308, 2002. DOI: 10.1108/14637150210428989

[10] Williams Jr, P.L., Factors affecting the adoption of E-business: An automotive industry study. ProQuest, 2008.

[11] Wu, D.-J., Software agents for knowledge management: Coordination in multi-agent supply chains and auctions. Expert Systems with Applications, 20(1), pp. 51-64, 2001. DOI: 10.1016/S0957-4174(00)00048-8

[12] Becker, M.C. and Zirpoli, F., Organizing new product development: Knowledge hollowing-out and knowledge integration–the FIAT auto case. International Journal of Operations & Production Management, 23(9), pp. 1033-1061, 2003. DOI: 10.1108/01443570310491765

[13] Holtbrügge, D. and Berg, N., Knowledge transfer in multinational corporations: Evidence from German firms. Springer, City, 2004.

[14] Sivakumar, K. and Roy, S., Knowledge redundancy in supply chains: A framework. Supply Chain Management: An International Journal, 9(3), pp. 241-249, 2004. DOI: 10.1108/13598540410544935

[15] Hult, G.T.M., Ketchen, D.J. and Arrfelt, M., Strategic supply chain management: Improving performance through a culture of competitiveness and knowledge development. Strategic Management Journal, 28(10), pp. 1035-1052, 2007. DOI: 10.1002/smj.627

[16] Piramuthu, S., Knowledge-based framework for automated dynamic supply chain configuration. European Journal of Operational Research, 165(1), pp. 219-230, 2005. DOI: 10.1016/j.ejor.2003.12.023

[17] García-Cáceres, R.G., Perdomo, A., Ortiz, O., Beltrán, P. and López, K., Characterization of the supply and value chains of Colombian cocoa. DYNA, 81(187), pp. 30-40. 2014. DOI: 10.15446/dyna.v81n187.39555

[18] Avelar-Sosa, L., García-Alcaraz, J.L., Cedillo-Campos, M.G. and Adarme-Jaimes, W., Effects of regional infrastructure and offered services in the supply chains performance: Case Ciudad Juarez. DYNA, 81(186) pp. 208-217, 2014.

[19] Espinal, A.C. y Montoya, R.A.G., Tegnologías de la información en la cadena de suministro information technologies in supply chain management. Dyna, 76(157), pp. 37-48, 2009.

[20] Lau, H.C.W., Ho, G.T.S., Zhao, Y. and Chung, N.S.H., Development of a process mining system for supporting knowledge discovery in a supply chain network. International Journal of Production Economics, 122(1), pp. 176-187, 2009. DOI: 10.1016/j.ijpe.2009.05.014

[21] Niemi, P., Huiskonen, J. and Kärkkäinen, H., Understanding the knowledge accumulation process—Implications for the adoption of inventory management techniques. International Journal of Production Economics, 118(1), pp. 160-167, 2009. DOI: 10.1016/j.ijpe.2008.08.028

[22] Niemi, P., Huiskonen, J. and Karkkainen, H., Supply chain development as a knowledge development task. International Journal of Networking and Virtual Organisations, 7(2), pp. 132-149, 2010. DOI: 10.1504/IJNVO.2010.031214
[23] Halley, A., Nollet, J., Beaulieu, M., Roy, J. and Bigras, Y., The impact of the supply chain on core competencies and knowledge management: Directions for future research. International Journal of Technology Management, 49(4), pp. 297-313, 2010. DOI: 10.1504/IJTM.2010.030160
[24] Douligeris, C. and Tilipakis, N., A knowledge management paradigm in the supply chain. EuroMed Journal of Business, 1(1), pp. 66-83, 2006. DOI: 10.1504/IJTM.2010.030160
[25] Huang, C.-C. and Lin, S.-H., Sharing knowledge in a supply chain using the semantic web. Expert Systems with Applications, 37(4), pp. 3145-3161, 2010. DOI: 10.1016/j.eswa.2009.09.067
[26] Craighead, C.W., Hult, G. T.M. and Ketchen Jr, D.J., The effects of innovation–cost strategy, knowledge, and action in the supply chain on firm performance. Journal of Operations Management, 27(5), pp. 405-421, 2009. DOI: 0.1016/j.jom.2009.01.002
[27] Lummus, R.R. and Vokurka, R.J., Defining supply chain management: A historical perspective and practical guidelines. Industrial Management & Data Systems, 99(1), pp. 11-17, 1999. DOI: 10.1108/02635579910243851
[28] Thomas, D.J. and Griffin, P.M., Coordinated supply chain management. European Journal of Operational Research, 94(1), pp. 1-15, 1996. DOI: 10.1016/0377-2217(96)00098-7
[29] Smith, B. and Ontology, L.F., Blackwell guide to the philosophy of computing and information. Blackwell Guide to the Philosophy of Computing and Information, 2003.
[30] Scheuermann, A. and Leukel, J., Supply chain management ontology from an ontology engineering perspective. Computers in Industry, 2014. DOI: 10.1016/j.compind.2014.02.009
[31] de Sousa, J.P., Distributed planning and control systems for the virtual enterprise: Organizational requirements and development life-cycle. Journal of Intelligent Manufacturing, 11(3), pp. 253-270, 2000. DOI: 10.1023/A:1008967209167
[32] Madni, A.M., Lin, W. and Madni, C.C., IDEONTM: An extensible ontology for designing, integrating, and managing collaborative distributed enterprises. Systems Engineering, 4(1), pp. 35-48, 2001. DOI: 10.1002/1520-6858(2001)4:1<35::AID-SYS4>3.0.CO;2-F
[33] Pawlaszczyk, D., Dietrich, A.J., Timm, I.J., Otto, S. and Kirn, S., Ontologies supporting cooperation in mass customization. A pragmatic approach. Citeseer, City, 2004.
[34] Fayez, M., Rabelo, L. and Mollaghasemi, M., Ontologies for supply chain simulation modeling. IEEE, City, 2005.
[35] Matheus, C.J., Baclawski, K., Kokar, M.M. and Letkowski, J.J., Using SWRL and OWL to capture domain knowledge for a situation awareness application applied to a supply logistics scenario. Springer, City, 2005.
[36] Chandra, C. and Tumanyan, A., Organization and problem ontology for supply chain information support system. Data & Knowledge Engineering, 61(2), pp. 263-280, 2007. DOI: 10.1016/j.datak.2006.06.005
[37] Gonnet, S., Vegetti, M., Leone, H. and Henning, G., SCOntology: A formal approach toward a unified and integrated view of the supply chain. Adaptive technologies and business integration: Social, managerial and organizational dimensions, IGI Global, Hershey, 2007, pp. 137-158.
[38] Grubic, T., Veza, I. and Bilic, B., Integrating process and ontology to support supply chain modelling. International Journal of Computer Integrated Manufacturing, 24(9), pp. 847-863, 2011. DOI: 10.1080/0951192X.2011.593047
[39] Sakka, O., Millet, P.-A. and Botta-Genoulaz, V., An ontological approach for strategic alignment: A supply chain operations reference case study. International Journal of Computer Integrated Manufacturing, 24(11), pp. 1022-1037, 2011. DOI: 10.1080/0951192X.2011.575798
[40] Anand, N., Yang, M., Van Duin, J.H.R. and Tavasszy, L., GenCLOn: An ontology for city logistics. Expert Systems with Applications, 39(15), pp. 11944-11960, 2012. DOI: 10.1016/j.eswa.2012.03.068
[41] Scheuermann, A. and Hoxha, J., Ontologies for intelligent provision of logistics services. City, 2012.
[42] Baker, T., Bechhofer, S., Isaac, A., Miles, A., Schreiber, G. and Summers, E., Key choices in the design of Simple Knowledge Organization System (SKOS). Web Semantics: Science, Services and Agents on the World Wide Web, 20, pp. 35-49, 2013. DOI: 0.1016/j.websem.2013.05.001
[43] Johnson, M.E. and Whang, S., E-Business and supply chain management: An overview and framework*. Production and Operations management, 11(4), pp. 413-423, 2002. DOI: 10.1111/j.1937-5956.2002.tb00469.x
[44] Carrer-Neto, W., Hernández-Alcaraz, M.L., Valencia-García, R. and García-Sánchez, F., Social knowledge-based recommender system. Application to the movies domain. Expert Systems with Applications, 39(12), pp. 10990-11000, 2012. DOI: 10.1016/j.eswa.2012.03.025
[45] Ruiz-Martínez, J.M., Valencia-García, R., Martínez-Béjar, R. and Hoffmann, A., BioOntoVerb: A top level ontology based framework to populate biomedical ontologies from texts. Knowledge-Based Systems, 36, pp. 68-80, 2012. DOI: 10.1016/j.knosys.2012.06.002

C.A. Rodríguez-Enríquez, is a full-time student of the Division of Research and Postgraduate Studies at the Instituto Tecnologico de Orizaba, Mexico. He received his BSc. Eng. in Systems Engineering in 2009, his MSc. in Systems Engineering in 2011, and is currently a PhD candidate in Engineering Sciences. All of these qualifications were undertaken at the Instituto Tecnológico de Orizaba. Orizaba, México. His research interests include: semantic web, linked open data, web development, software generation, and multi-modal user interfaces.

G. Alor-Hernandez, is a full-time researcher of the Division of Research and Postgraduate Studies at the Instituto Tecnologico de Orizaba, Mexico. He received his MSc. and a PhD. in computer science at the Center for Research and Advanced Studies of the National Polytechnic Institute (CINVESTAV), Mexico. He has led ten Mexican research projects that were granted money from CONACYT, DGEST and PROMEP. He is the main author of the book entitled *Frameworks, Methodologies, and Tools for Developing Rich Internet Applications,* published by IGI Global Publishing. His research interests include Web services, e-commerce, Semantic Web, Web 2.0, service-oriented and event-driven architectures, and enterprise application integration. He is an IEEE and ACM Member. He is a National Researcher recognized by the National Council of Science & Technology of Mexico (CONACYT).
ORCID: 0000-0003-3296-0981
Scopus Author ID: 17433252100

C. Sánchez-Ramírez, is a full-time researcher of the Division of Research and Postgraduate Studies at the Orizaba Technology Institute, Mexico. He received his PhD. in Industrial Engineering from COMIMSA, the center for research of the National Council of Science & Technology of Mexico (CONACYT). His research projects have been granted money from CONACYT, DGEST, and PROMEP. Dr. Sánchez is member founding of the Mexican Logistics and Supply Chain Association (AML) and a member of the CONACYT National Research System. His research interests are modeling and simulation of logistical processes and supply chains from a system dynamics approach. He is author/coauthor of around 30 Journal and conference papers in logistics and Supply Chain Management.

G. Cortes Robles, received his BSc. in Electronic Eng. in 1995from the Instituto Tecnologico de Orizaba (ITO), Mexico. He obtained his MSc. in Science in Industrial Eng. from the same institution and a PhD. in Industrial Systems from the Institut National Polytechnique de Toulouse in France. His doctoral thesis combined the TRIZ theory with the Case-Based Reasoning solving process. He is currently professor of engineering science at the ITO's postgraduate school, and specifically focuses on the Master's in engineering management and science engineering doctoral students. His research interests are the application of TRIZ theory combined with several approaches, knowledge management, decision support systems, simulation, different design approaches, lean manufacturing, and creativity techniques, which have the aim of accelerating the innovation process. He is currently the general secretary of the Mexican TRIZ association (AMETRIZ) and responsible for the www.innovasolver.com initiative.

UNIVERSIDAD NACIONAL DE COLOMBIA
SEDE MEDELLÍN
FACULTAD DE MINAS



DYNA
http://dyna.medellin.unal.edu.co/

The green supplier selection as a key element in a supply chain: A review of cases studies

Rodrigo Villanueva-Ponce [a], Liliana Avelar-Sosa [b], Alejandro Alvarado-Iniesta [c] & Vianey Guadalupe Cruz-Sánchez [d]

[a] *Instituto de Ingeniería y Tecnología, Universidad Autónoma de Ciudad Juárez, Juárez, México. villanueva.rodrigo@outlook.com*
[b] *Instituto de Ingeniería y Tecnología, Universidad Autónoma de Ciudad Juárez, Juárez, México. liliana.avelar@uacj.mx*
c Instituto de Ingeniería y Tecnología, Universidad Autónoma de Ciudad Juárez, Juárez, México. alejandro.alvarado@uacj.mx
d Instituto de Ingeniería y Tecnología, Universidad Autónoma de Ciudad Juárez, Juárez, México. vianey.cruz@uacj.mx

Received: November 6th, 2014. Received in revised form: February 20th, 2015. Accepted: November 17rd, 2015.

Abstract
The current pressure of global competition is demanding faster, reliable, flexible, and cheaper products. Thus, in order to keep up with customer demands, companies need to continuously improve their manufacturing systems and develop new strategies. Supply chain management (SCM) is currently the most important tactic for modern companies to maintain their competitiveness. Supplier selection process (SSP) plays an important role in SCM and has been studied extensively in the past years as a tool to provide guidance and help to researchers and decision makers. Green supply chain management (GSCM) arose due to the recent increase in environmental protection. Consequently, the correspondent green supplier selection process (GSSP) has become more and more critical in GSCM. This paper presents a review of studies published in scientific journals during the last five years about green criteria utilized in multi-criterion decision making (MCDM) techniques for GSSP. Furthermore, it identifies the most commonly used MCDM techniques, in journals, universities, and academic departments where this type of research is being developed.

Keywords: Supply Chain Management (SCM); Green Supply Chain Management (GSCM); Supplier Selection Process (SSP); Green Supplier Selection Process (GSSP); Multi-criteria Decision Making (MCDM); Case Studies.

Selección de proveedores verde como un elemento clave en la cadena de suministro: Una revisión de casos de estudio

Resumen
La presión actual de la competencia global está demandando productos más rápidos, confiables, flexibles y más baratos; por lo tanto, con el fin de mantenerse al día con las demandas de los clientes, las empresas necesitan mejorar continuamente sus sistemas de fabricación y desarrollar nuevas estrategias. La gestión de la cadena de suministro (GCS) es actualmente la táctica más importante que utilizan las empresas modernas para mantener su competitividad. El proceso de selección de proveedores (PSP) desempeña un papel importante en la GCS y ha sido ampliamente estudiado en los últimos años como una herramienta para orientar y ayudar a los investigadores y tomadores de decisiones. La gestión de la cadena de suministro verde (GCSV) surge debido al reciente incremento en la protección del medio ambiente. Entonces, el proceso de selección de proveedores verde (PSPV) se ha convertido en un elemento crítico en la GCSV. El presente manuscrito muestra una revisión de los trabajos publicados en revistas científicas en los últimos 5 años sobre los criterios verdes utilizados en la decisión multicriterio. Además, identifica las técnicas de selección multicriterio (TSM) más utilizadas, revistas, universidades y departamentos académicos, donde este tipo de investigación se está desarrollando.

Palabras Clave: Gestión de la Cadena de Suministro (GCS); Gestión de la Cadena de Suministro Verde (GCSV); Proceso de Selección de Proveedores (PSP); Proceso de Selección de Proveedores Verde (PSPV); Técnicas de Selección Multicriterio (TSM); Casos de estudio.

1. Introduction

Supply chain management (SCM) is an important strategy used by contemporary companies. The members of the supply chain (SC) need to be able to solve the most critical processes concerning the correct supplier selection. Making the appropriate decision helps to reduce costs, improves quality, and promotes long-term relationships

© The author; licensee Universidad Nacional de Colombia.

between companies and suppliers, increasing company competitiveness. Therefore, the objective of supplier selection process (SSP) is to identify suppliers with the highest potential to fulfill the company's necessities.

Selecting a supplier is an extremely important step in the SC. The supplier will provide an organization with the adequate raw material or products at a competitive price. A supplier will also help improve environmental performance while avoiding hazardous substances and considering green design. With increasing government regulations and stronger public awareness in environmental protection, firms today cannot ignore environmental issues when selecting a supplier if they want to survive in the global market [1]. In order to respond to increasing environmental regulations, new terms have been created: green supply chain (GSC) and green supplier selection (GSS).

This paper presents a careful review of studies about the GSS process, highlighting the methods utilized to select a supplier. The studies reviewed were published in international journals from 2007 to 2013 that present a case of study related to GSS and emphasize the main green criteria and multi-criteria decision making (MCDM) techniques utilized in green supply chain management (GSCM).

The rest of this paper is organized as follows: In Section 2, a series of useful definitions related to SCM, GSCM, SSP, and GSS is provided. Section 3 presents the details of the methodology used for the literature review. Section 4 presents the information obtained in Section 3 and is organized by the following subsections: Distribution of papers published, green criteria utilized, MCDM techniques applied, journals publishing papers about GSS, countries, universities, and academic departments developing this type of research. The analysis of the results are shown in Section 5. Finally, in Section 6 the conclusions are shown.

2. The supplier selection process (SSP)

The evolution of supply relationships is underlined by the fact that suppliers are required to have an adequate set of competencies to be part of a supply system capable of facing market competition. Therefore, this section will describe the main concepts involved in the SSP within a SC.

2.1. Supply chain (SC)

Blanchard [2] defines the SC as the sequence of events that covers the entire lifecycle of a product or service from the beginning to the end, as can be seen in Fig. 1. It requires companies to be attentive throughout the whole manufacturing process, considering material delivery, material costs, manufacturing processes, distribution packaging, methods, and costs.

The SC can be extremely complex, since it integrates independent organizations that interact together to control and manage a product that will be used by an end customer [3]. If a member of the SC fails to deliver a component on time, there will be an impact in all of the other members of the SC. Therefore, the good integration of these independent companies will lead to a successful SC.

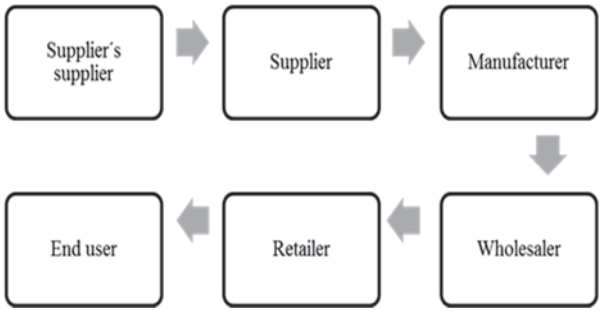


Figure 1. Supply chain's scope in a global company.
Source: [2]

2.2. Supply chain management (SCM) and Green supply chain management (GSCM)

In the following subsections, we explain the SCM and GSCM systems.

2.2.1. Supply Chain Management (SCM)

According to Li and Wang [4], SCM integrates internal operational decisions and activities with external customer demands to be able to enhance competitiveness and profit (after production process). Su et al. [5] state that SCM reveals the advantages of coordination with suppliers (before production process). Thus, SCM has become a critical strategy for organizations to create competitive advantages, transforming suppliers and customers into partners. One of the reasons why a supplier is so important is because the cost of raw materials frequently represents 70% of the final product's cost. Therefore, the purchasing department plays an important role in reducing this total figure [6,7].

2.2.2. Green Supply Chain Management (GSCM)

Lee et al. [8] note that with growing worldwide awareness of environmental protection, green production has become an important issue for almost every manufacturer and will determine the sustainability of a manufacturer in the long term. GSCM is generally involves suppliers based on their environmental performance and business is only done with those that meet certain environmental regulations or standards [9].

Due to some violations in regulations, certain countries have taken action. For example, in 2001 more than 1.3 million boxes of PlayStation 2 games consoles, produced by the Sony Corporation, were blocked by the Dutch government due to an excessive amount of the toxic element Cadmium found in the cables of the game controls. This led to losses exceeding $130 million, and indirectly led to the re-inspection of over 6,000 factories and the establishment of a new supplier management system [10].

The previous is an example of the focus given to environmental care around the world and the importance that this trend has among leading companies in all fields. The fact that firms assess their environmental impact, regardless of the driver, represents significant growth in environmental awareness.

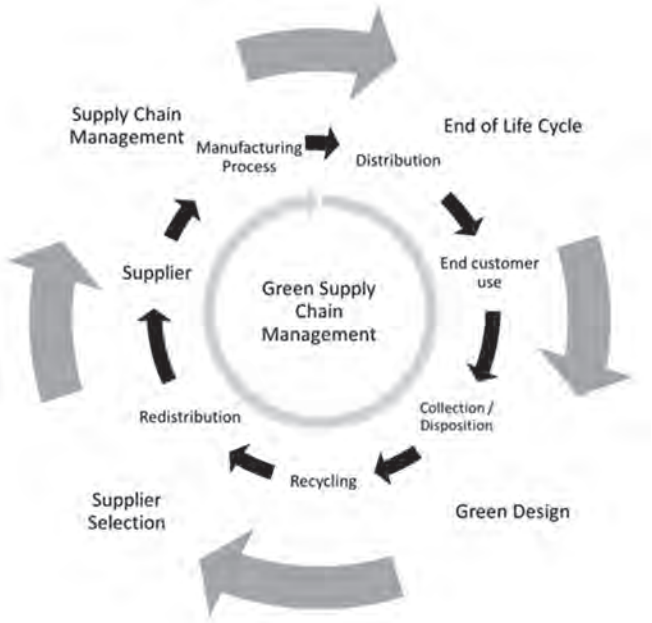


Figure 2. Work flow of a GSCM process.
Source: [11]

GSCM has been adopted as a strategy by leading industry companies to put pressure on their suppliers in order to achieve a certain level of environmental performance, stimulating operational cooperation of all SC members. The GSC approach seeks to reduce a product's ecological impact to a bare minimum. GSCM is, in essence, the same as a typical SCM. A typical example of how a GSCM works is shown in Fig. 2.

2.3. Supplier selection process (SSP)

As the first element in a SC, suppliers have a direct impact on the quality, cost, and delivery time of new products [12-14]. The supplier selection (SS) consists of measuring the performance of a group of suppliers to select the best option improving the effectiveness of the whole supply system.

SS is not an easy task, since various potential suppliers may have similar performance characteristics for different attributes. For many years, the traditional approach to SSP has mainly considered quality, cost, and lead time. However, currently, due to the environmental care issue, this is no longer enough, and companies have had to incorporate the environmental culture into the common SSP criteria.

A green supplier is expected, not only to achieve environmental compliance, but also to undertake efficient, green product design, and end-of-life cycle studies. Thus, in a GSC, companies need to have extensive SSP and performance evaluation processes [15]. A green supplier evaluation system is needed for a company to be able to meet the GSCM requirements and establish competitiveness. GSS is clearly a critical activity in purchasing, and buyers need to focus on the procurement of products and services from suppliers that can provide these with a low cost, good quality, short lead time, and environmental responsibility.

2.4. Evaluating attributes and Multi-criteria decision making (MCDM)

Decision making has always been a matter of concern for humankind. One of the most important tasks in decision making is to structure decision problems into a formal and manageable format [16]. Decision-making situations typically involve more than one attribute. MCDM has been created to help researchers and decision makers find the best solution to decision problems. There are several techniques, depending on the problem to be evaluated; however, all techniques follow the methodology suggested by De Boer et al. [17] for selecting a supplier:

- SSP definition
- Identification of criteria
- Supplier evaluation by chosen technique
- SS

In order to apply De Boer's methodology for SS, there has to be a way to determine and define the main attributes to be integrated into a technique for the SSP. The attributes used to evaluate a supplier fall into two classifications: quantitative and qualitative attributes.

2.4.1. Quantitative attributes

In simple terms, these attributes are composed of everything that can be measured and physically describe elements of a product, such as cost, speed, size, capacity, etc.

2.4.2. Qualitative attributes

These types of attributes are subjective; their application depends on the assigned weight, depending on the importance given to them by the organization. They describe products that need to be evaluated in a decision-making process to fulfill a requirement.

3. Material collection methodology

The literature review was undertaken in the 3 following steps: a) *Material collection*: The material to be collected is defined. b) *Review of articles*: The articles found were reviewed in order to obtain information to establish a categorization. c) *Information analysis*: For easy management of the article's information, classification software was used to generate tables and crosstabs showing data groups.

3.1. First step: Material collection

During this first step, a literature review was completed of English-language articles published in high-quality, peer-reviewed international journals between 2007 and 2013. The article search was performed in major databases such as: Science Direct, as a leading full-text scientific database that offers journal articles and book chapters; IEEE, which is considered the world's largest professional association for the advancement of technology; and ProQuest, which is a widely recognized dissertation database.

The selected journals were *Experts Systems with Applications*, *Journal of Cleaner Production*, *International Journal of Production Economics*, and *Industrial Engineering and Engineering Management*.

The search was performed by entering the keywords "green supplier evaluation" and "green supplier selection". The word "green" was then replaced by "environmental" and "ecologic". The word "supplier" was also replaced by "vendor". The words "evaluation" and "selection" were replaced by "assessment" and "qualification". A second set of keywords was then entered: "environmental criteria for supplier selection", "green multi-criteria decision making", and "green criteria for supplier selection".

The screening process consisted of looking for articles presenting a case of study in which a GSS problem was identified and a multi-criteria technique was used to solve the selection problem.

3.2. Second step: Review of articles

The articles were gathered and reviewed by obtaining information to establish a classification. The articles presented a SS case of study. The information obtained from the articles was then entered into software for easy management of the data.

3.3. Third step: Data entry using software

The classification categories used for the review were:

3.3.1. Year of publication

The search was limited to the period of time from 2007 to 2013. All the papers were classified according to their year of publication, in order to establish the progress in time.

3.3.2. Universities

The university in which the study was performed is important in order to understand the region in the planet that is working in this topic.

3.3.3. Journal Name

The journal category identifies the different disciplinary areas that contribute to the GSSP.

3.3.4. Case of study

The study provides a wide variety of applications in which a SS problem may exist. The case presents the different stages in an SS process, the technique, and the environmental criteria utilized.

3.3.5. SS Technique implemented

The multi-criteria technique used in the cases studies is one of the main objectives in the categorization. It is imperative to understand the main techniques utilized in the SS problem.

Table 1.
Papers considering GSS.

Year of publication	Number of papers considering GSS case studies
2007	2
2008	3
2009	6
2010	9
2011	9
2012	3
2013	2

Source: The authors

3.3.6. Green attributes employed in the selection

The case studies presented particular decision problems being solved. In most of the cases, the problem was related to a green supplier selection decision, for which attributes help evaluate the provided options. The attributes used in the GSS may vary depending on the type or product being supplied.

4. Material collection results

A total of 34 articles were found in the material collection process, and these were reviewed and grouped as is described in Section 3. This section shows the material collection results.

4.1. Year of publication

The distribution of the articles from 2007 to 2013 is shown in Table 1. It can be seen that 2010 and 2011 are the years with the highest number of publications.

4.2. Universities and academic departments

An additional way to present the information gathered in this review is to identify the university and academic department at which the first author works, providing work on the GSS topic.

Fig. 3 shows the universities at which the first authors conducted their research.

	University																														
Country	Chung Hua University	Tungan University	National Taipei University of Technology	Federal University of Sao Carlos	The Overseas Chinese Institute of Technology	National Tsing Hua University	Henan Polytechnic	Naresuan Phayao University	Tianjin Metallurgical Vocation-Technology Institute	Shandong University of Finance	Xi'an Polytechnic	Tianjin University	Science and Technology Beijing	Indian Institute of Delhi	Beijing Wuzi University	Tianjin University of Finance and Economics	Tungan University	Malaya University	Concordia University	National Taiwan University of Science and Technology	Aalborg University	Kocaeli University	Dalian University of Technology	Galatasaray University	Lung Hwa University of Science	National Institute of Technology	Greenwich	Total
China	0	0	0	0	0	0	4	0	1	1	1	1	1	0	1	1	0	0	0	0	0	0	1	1	0	0	0	13
Taiwan	1	1	2	0	1	2	0	0	0	0	0	0	0	0	0	0	1	0	0	1	0	0	0	0	1	0	0	10
India	0	0	0	0	0	0	0	0	0	0	0	0	0	2	0	0	0	0	0	0	0	0	0	0	0	1	0	3
Denmark	0	0	0	0	0	0	0	0	0	0	0	0	0	0	0	0	0	0	0	0	1	0	0	0	0	0	1	2
Turkey	0	0	0	0	0	0	0	0	0	0	0	0	0	0	0	0	0	0	0	0	0	1	0	1	0	0	0	2
Brazil	0	0	0	1	0	0	0	0	0	0	0	0	0	0	0	0	0	0	0	0	0	0	0	0	0	0	0	1
Thailand	0	0	0	0	0	0	0	1	0	0	0	0	0	0	0	0	0	0	0	0	0	0	0	0	0	0	0	1
Malasya	0	0	0	0	0	0	0	0	0	0	0	0	0	0	0	0	0	1	0	0	0	0	0	0	0	0	0	1
Canada	0	0	0	0	0	0	0	0	0	0	0	0	0	0	0	0	0	0	1	0	0	0	0	0	0	0	0	1
	1	1	2	1	1	2	4	1	1	1	1	1	1	2	1	1	1	1	1	1	1	1	1	2	1	1	1	34

Figure 3. Universities working on GSS
Source: The authors

The universities with the highest number of published articles are The Henan Polytechnic (4), located in China, followed by The University of Technology (2), National Tsing Hua University (2), and National Taipei Malaya University (2), all located in Taiwan, and then the Indian Institute of Delhi (2), located in India. The rest of the universities produced only one article. It can clearly be seen that China and Taiwan are the places where there are more research groups investigating aspects related to GSS techniques -representing 67.6% of this review- followed by India, Denmark, and Turkey with 20.5%, and finally, Brazil, Thailand, Malaysia, and Canada with 11.76%.

Table 2 presents the academic department within the universities that developed this type of research. It can be seen that the department with the most studies over these years is the Industrial Engineering Department, followed by the Environmental Management, and Energy and Science Departments.

4.3. Journals

The journal distribution shown in Fig. 4 identifies the different disciplinary areas contributing to the GSS process.

Table 2.
Academic department working on GSS

Department	Frequency
Industrial Engineering	6
Environmental Management	4
School of Energy and Science	4
Industrial Engineering and System Management	4
Management	3
Business Administration	2
Decision Sciences	2
School of Economics and Management	2
Department of Marketing	1
Engineering Design and Manufacture	1
Engineering Technology	1
International Trade	1
Mechanical Engineering	1
Metallurgic Engineering	1
School of Science	1

Source: The authors

Journal	Year of published							Total
	2007	2008	2009	2010	2011	2012	2013	
Experts Systems with Applications	0	0	1	1	2	1	0	5
Industrial Engineering and Engineering Management (IE&EM)	1	1	1	1	1	0	0	5
Journal of Cleaner Production	0	0	1	1	1	0	2	5
International Journal of Production Economics	0	0	0	2	1	0	0	3
Wireless Communications (WiCom)	1	1	0	0	0	0	0	2
Applied Soft Computing	0	0	0	0	0	1	0	1
Computers and Industry	0	0	0	0	1	0	0	1
Electronics, Communications and Control (ICECC)	0	0	0	0	1	0	0	1
Emerald Group Publishing Limited	0	0	1	0	0	0	0	1
I C on Automation and Logistics (AL)	0	0	0	0	1	0	0	1
I C on Supply Chain Management and Information Systems (SCMIS)	0	0	0	1	0	0	0	1
IC on Business Management and Electronic Information (BMEI)	0	0	0	0	1	0	0	1
IC on Machine learning and Cybernetics (MLC)	0	1	0	0	0	0	0	1
International Conference of management and Service Science (MASS)	0	0	1	0	0	0	0	1
International Conference on Mechanical and Electrionics Engineering (ICMEE)	0	0	0	1	0	0	0	1
International Conference on Signal Processin Systems (ICSPS)	0	0	1	0	0	0	0	1
International Conference on Systems, Man, and Cybernetics (SMC)	0	0	0	0	0	1	0	1
Internet Technology and Application	0	0	0	1	0	0	0	1
Supply Chain Management: an International Journal	0	0	0	1	0	0	0	1
	2	3	6	9	9	3	2	34

Figure 4. Journals with GSCM publications
Source: The authors

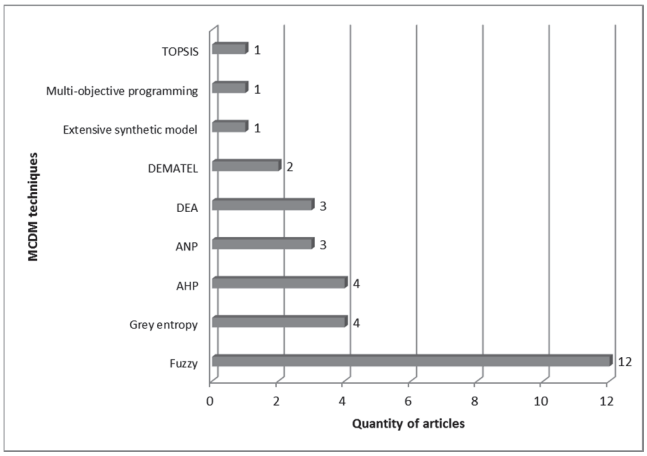


Figure 5. Multi-criteria techniques.
Source: The authors

There are three main journals identified in this literature review with the highest number of published articles on this topic: *Experts Systems with Applications*, *Industrial Engineering and Engineering Management* (IE and EM), and *Journal of Cleaner Production, all* with five published articles. The list continues with the *International Journal of Production Economics* with three published articles, followed by the *Wireless Communications* (WiCom) with two. The rest of the journals listed in the table have only one paper published on the topic. The information in this figure shows that the interest in green issues and environmental concern is being addressed in different areas.

4.4. Multi-criteria Techniques

There were 34 articles reviewed, and all but two considered a case study being applied where a SS problem was presented, and a MCDM technique was developed using traditional and green criteria in the selection process. Fig. 5 provides a summary of these techniques.

A total of 12 articles present a review using fuzzy logic models. A comparison of the GSS between the American, Japanese, and Taiwanese electronics industry in China is shown in [35]. The case of a printed circuit board manufacturer in Taiwan that seeks to implement GSCM is illustrated in [36]. A fuzzy multi-criteria decision problem approach with vague sets in an iron and steel company is shown in [37] and [38]. A new ranking method on the basis of fuzzy inference system (FIS) is applied in [27].

The next MCDM used was the Grey entropy model, which was in four papers: Chiou et al. [39] developed a model where subjectivity can be avoided in ascertaining weights of lower hierarchy factors. An improved grey correlative method applied in a previous publication is shown in [39] and [40]. An introduction of additional levels of analysis and application of grey entropy is presented in [41]. Finally, four papers are related to the use of Analytic Hierarchy Process (AHP) models [42-45].

4.5. Green attributes

In the traditional SCM, SS criteria consisted of the common qualities, cost and time, but due to the increased

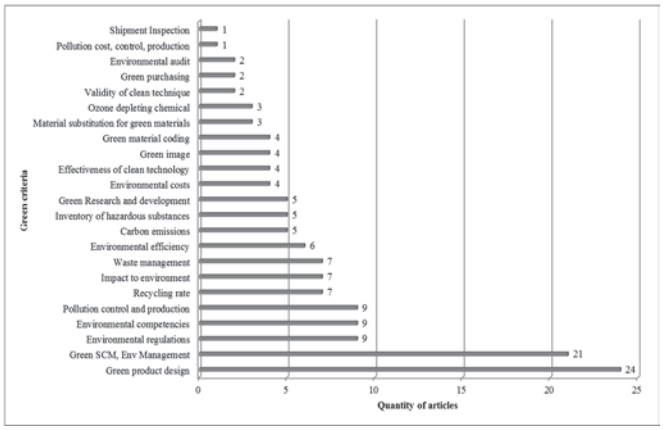


Figure 6. Green criteria
Source: The authors

awareness of environmental protection these are no longer important. Therefore, the traditional SSP incorporates green criteria in order to comply with environmental regulations, social consciousness, and industry performance.

From a total number of 34 published articles, 24 concurred that green product design is a criterion to be used when evaluating and selecting a supplier, 21 saw green supply management as being important, 9 environmental regulations, 9 environmental competencies, 9 pollution control and production, 7 recycling rate, 7 impact to the environment, 7 waste management, 6 environmental efficiency, 5 carbon emissions, 5 inventory of hazardous substances, and 5 green research and development. This can be seen in Fig. 6.

5. Analysis of the results and discussion

In this section, the key findings that resulted from the material collection are presented. The main goal of this study was to identify how GSS has evolved over recent years and which characteristics are discernible. Then, based on the review as well as the results, this section explains how the green criteria are useful in any GSS.

5.1. Analysis of publication distribution

There was a growing trend from 2007 to 2011 that showed an evolution in awareness regarding environmental impact issues. Based on the wider awareness of environmental concerns over the last decade, it is foreseen that research on the topic will continue to progress.

5.2. Analysis of environmental criteria in GSS

Environmental consideration of SS is a key competitive issue for large and medium-sized enterprises, and thus maintaining long-term relationships with these suppliers should be taken into account. De Boer et al. [17] proposed a knowledge-based system to evaluate the supplier's environmental performance, which can be sectioned into several categories: environmental costs, management competencies, green image, green design, environmental management system, and environmental competencies.

This section explores the broad environmental criteria of either quantitative or qualitative attributes with regard to environmental cost, production process, product, and management systems.

5.2.1. Environmental competencies

The percentage of companies that have established a GSC in order to incorporate ecological care is low. Nevertheless, there are companies that have a big concern for environmental issues and have actually established a plan to respond to regulations and social concern. In some cases the bigger the company, the greater the interest in integrating a GSC.

The development of environmental plan must include some important points in order for the response to be successful:

- Environmental impact assessments that define the current situation and areas that have opportunities.
- Environmental education and training, to provide information and develop environmental culture.
- Green design training, to increase design core groups' eco-engineering skills.
- Environmental policies and standards development, to establish an efficient operating system.
- Pollution prevention and control systems, to continuously improve and innovate product designs and manufacturing processes.
- Waste management systems implementation, to establish future re-use, recycling, and disposal of material.
- Strategic planning, monitoring, and reporting systems.

5.2.2. Green product design

One of the most important criteria in SSP is the capability for green design, which can promote product-oriented GSC implementation. According to Humphreys et al. [18], the strongest testament to the greening of international markets is the expanding number of companies seriously addressing environmental concerns as part of their product development process. A product is considered eco-friendly if it does not represent a threat to the environment when released into the air, water, or earth, either when it is in use or at the end of its life cycle. Green product design is extremely important because it is a key element in establishing a GSC. Green design can indicate the direction that each SC component will follow. Companies need to invest in design core groups and help to develop an understanding of how design decisions impact the products' entire life cycle.

5.2.3. Carbon emissions management

Carbon (CO2) emissions result from a variety of activities that humans undertake in their daily lives. Growing levels of anthropocentric CO2 emissions are known to cause global warming [20]. As the public becomes more aware of environmental issues and global warming, consumers will be asking more questions about the products they are purchasing. The term carbon footprinting refers to the total

amount of CO2 or greenhouse gases emissions an individual or organization is responsible for. Companies will have to expect questions about the state of their green manufacturing processes, their SC, their carbon footprint, and how they recycle. Luckily, CO2 emissions can safely be dealt with and predicted if a well-defined green design and manufacturing process is established within the company.

5.2.4. Energy/Resource consumption

Due to global competition, it is crucial for an enterprise to enhance its ability to improve energy utilization and efficiency through the enterprise's inner energy audit and energy management [21]. Energy conservation management projects promoted by the government, and energy audits have been undertaken in developed countries since the 1970s [22].

As shown by Zhang et al. [23], the case study detailed in this paper's main objective is to discover energy auditing and energy management problems in regions such as China. The case study reveals that if enterprises are unwilling to cooperate actively with the energy audit, then the government should improve the energy performance assessment system, increase capital investment, and develop energy-saving tax incentives.

All the current lean manufacturing methods, which have the primary objective of eliminating waste in a production process, are associated with energy and resource consumption. This attribute is really important, as can be seen in modern GSCs. When selecting a supplier, not only the traditional evaluation criteria is used, green criteria is also incorporated. In order to eliminate waste, there has to be better consumption of the current resources (raw materials, water, air, etc.,), as well as more consideration of the energy needed to manufacture a product.

5.2.5. Green material coding

ISO 11496 specifies a system for the uniform marking of products that have been fabricated from plastic materials. It intends to help identify plastic products for subsequent decisions concerning handling, waste, recovery, or disposal. These days, a common company practice is to incorporate the material specification code on a visible location on the part; this helps distinguish materials from a pile of products. There are companies that can handle a variety of plastic parts, and having the material code engraved in the component will easily help with the disposal of these parts at the end of their lives.

Material coding is also important when disposing of the products that have reached their end of their lives. It provides an immediate identification of hazardous and non-hazardous materials. Eveloy et al. [24] recommend that all lead-free materials, components, and boards should be assigned new part numbers to distinguish them from lead-based ones.

5.2.6. Management of hazardous substances

There is a serious-restricted use of hazardous substances during the production; therefore, companies have taken special interest in reducing the utilization of these substances and complying with environmental regulations. The International Electrotechnical Commission (IEC) set up the Hazardous Substance Process Management (HSPM) standard — namely, IECQ QC 080000 HSPM. As shown by Hsu and Hu [25], obtaining a certification helps companies mitigate risks associated with hazardous substances.

5.2.7. Waste management system

Waste is produced in all human activity; there is always something leftover. Therefore, the key point is to reduce the impact of this residue on the environment. In order to ensure the protection of the environment, a waste management system needs to be established. For example, all of the current lean manufacturing methods like SMED, Six Sigma, or Kaisen help companies achieve this reduction in operational costs and waste. For instance, according to Zúñiga-Ceron and Gandini-Ayerbe [26], the final disposal of sugar cane waste represents a huge environmental challenge. Therefore, the industry is looking for solutions such as the conversion of their residues into sub products to obtain economic gain, and at the same time reduce the environmental impact.

After the establishment of Waste Electrical and Electronic Equipment (WEEE), Restriction of Hazardous Substances (RoHS), and Eco-design for Energy-using Products (EuP), directives have been passed by the European Union (EU), and GSCM has been adopted as a strategy by leading electronics companies, including Dell, HP, IBM, Motorola, Sony, Panasonic, NEC, Fujitsu, and Toshiba [27].

A proper waste management system may integrate the following:

- Green product design can define the easy disposal of the product at its end-of-life cycle.
- Reduce waste releases to water, land, or air by resource management consumption.
- Reuse of discarded waste products will help reduce generation of unnecessary material.
- Recycling materials will lower the waste rate.

5.2.8. Recycling

According to Yi and Wang [28], there are three types of reverse SC recycle models in developed countries:

1. Manufacturer Take-Back (MT). This recycling model requires that the manufacturer build an enormous recycling network at an excessive cost.
2. Retailer Take-Back (RT). This recycling model can effectively utilize the stronger marketing network of a retailer, but the manufacturer has to face some coordination problems with the retailer, such as recycle pricing.
3. Third Party Take-Back (TPT). This category includes companies that lack investment and knowledge to develop their own reverse logistic system. The companies outsource this requirement to a third party, requiring less effort from them.

5.2.9. Green purchasing

The purchasing department has become much more important due to the recent agile improvement of network

technology and economic globalization [29]. Buyers in an SC are in the ideal position to identify an environmental risk and formulate requirements for suppliers to meet. The purchasing department needs to be at the forefront of all the environmental regulations in order to maintain a close relationship with the engineering group developing the product. This will help eliminate mistakes or conditions that lead to selecting an incorrect supplier. Environmental standards in purchasing provide a basis for constructive dialogue with suppliers within a joint commitment to quality progress context, and should motivate suppliers to promote these activities with their own suppliers [30].

5.2.10. Green research and development

The technology, method, and tool research relating to a green product has also become important [31]. The different GSC approaches — green sourcing, green manufacturing processes, green design, and reverse logistics —together provide new sources of innovation and continuous improvement of current management systems. For instance, as shown by Chen [32], the printed circuit board construction process is currently migrating from traditional eutectic Pb-Sn alloy to different lead-free alloys. This replacement attempts to alleviate the problem of the Pb-Sn solder alloy, which is toxic. However, this does not change the component separation problem for reuse and/or disposal of these materials without harming the environment. This means that, regardless of implementing an action to reduce the impact of one material or practice, the action needs to be deeply explored in order to measure its future impact as well.

5.2.11. Green image

Enhancing a companies' image is one of the most common reasons for assuming a green strategy, and, according to Canal-Marques et al. [33], companies that invest in environmental efforts are able to improve their corporate image and develop new markets, as well as increase their competitive advantages. People's awareness has pushed companies to act and incorporate green practices in complying with environmental regulatory constrains for the purpose of gaining market profit. Companies that embrace the green environment concept with environmentally friendly products and packaging can charge relatively high prices for their products, and thus increase their products' differentiation advantages [34, 35].

5.2.12. Environmental Regulations

Suppliers who have acquired environmental management systems (EMS) certifications (ISO14001) can state that an organization has implemented a management system that documents the its environmental aspects and impacts, and has identified a pollution prevention process that is continually improved over time [34,35]. Having this certification helps companies acquire a green public image, looks after the environment, and confers external legitimacy [35]. Companies may also be able to use ISO 14001 to increase their internal efficiencies and create competitive advantage opportunities and economic benefits [36].

There are several reasons, as mentioned by Coglianese and Nash [37], why companies implement ISO 14001:

- It is the best external valuation and they improve their corporate reputation.
- They prove their social responsibility and commitment to the environment.
- They will have continuous improvement.
- It helps with and ensures the legality of compliance with environmental legislation.
- It is different from the competition.
- Its administration is easy and its implementation is promoted.
- It improves competition scores and is mandatory.
- It improves safety at work.
- It promotes growth.

6. Conclusions and further work

SC professionals are under pressure to build a successful SC strategy that will raise productivity and competitiveness, respond to demand variations and environmental regulations, while at the same time empower product innovation and promote continuous improvement. Several years ago, there was a lack of environmental care and social awareness, with no connection to investment and profitability. This is no longer the situation. Social concern about environmental issues and global warming is causing consumers to demand that the products they are purchasing go green. Companies are being questioned about how green their manufacturing processes and SCM are, and what they are currently doing to reduce their carbon footprint and tackle global warming.

This paper informed the reader of the following: that GSCM is being adopted; that green criteria are being incorporated within evaluation techniques; that selecting a supplier is an important decision. This is the case, not only with respect to providing the organization with the right products at the right cost, but also taking into consideration environmental performance by eliminating contaminants, and reducing the energy to produce the products, etc.

It could be worthwhile to undertake further research on topics such as how companies deal with balancing the different GSS practices and how this practice could be more effective.

References

[1] Lee, A.H.I., A fuzzy supplier selection model with the consideration of benefits opportunities, costs and risks, Expert Systems with Applications, 36(2), pp. 2879-2893, 2009. DOI: 10.1016/j.eswa.2008.01.045

[2] Blanchard, D., Supply chain management best practices, 2nd. Edition. John Wiley and Sons, 2010.

[3] Wu, C.H., Chen, C.W. and Hsieh, C.C., Competitive pricing decisions in a two-echelon supply chain with horizontal and vertical competition, International Journal of Production Economics, 135(1), pp. 265-274, 2012. DOI: 10.1016/j.ijpe.2011.07.020

[4] Li, X. and Wang, Q., Coordination mechanism of supply chain systems, European Journal of Operational Research, 179(1), pp. 1-16, 2007. DOI: /10.1016/j.ejor.2006.06.023

[5] Su, Q., Shi, J.H. and Lai, S.J., Study on supply chain management of Chinese firms from the institutional view, International Journal of

Production Economics, 115(2), pp. 362-373, 2008. DOI: 10.1016/j.ijpe.2007.11.016

[6] Ghodsypour, S.H. and O'Brien, C., A decision support system for supplier selection using an integrated analytic hierarchy process and linear programming, International Journal of Production Economics, 56-57(1), pp. 199-212, 1998. DOI: 10.1016/S0925-5273(97)00009-1

[7] Aksoy, A. and Öztürk, N., Supplier selection and performance evaluation in just-in-time production environments. Expert Systems with Applications, 38(5), pp. 6351-6359, 2011. DOI: 10.1016/j.eswa.2010.11.104

[8] Lee, A.H.I., Kang, H.Y., Hsu, C.F. and Hung, H.C., A green supplier selection model for high-tech industry. Expert Systems with Applications, 36(4), pp. 7917-7927, 2009. DOI: 10.1016/j.eswa.2008.11.052

[9] Rao, P., Greening the supply chain a new initiative in southeast Asia. International Journal of Operations and Production Management, 22(6), pp. 632-55, 2002. DOI: 10.1108/01443570210427668

[10] Esty, D.C. and Winston, A.S. Green to gold: How smart companies use environmental strategies to innovate, create value, and build competitive advantage, Thesis,Yale University Press, New Haven, CT, USA, 2009.

[11] Diabat, A. and Govindan, K., An analysis of the drivers affecting the implementation of green supply chain management, Resources, Conservation and Recycling, 55, pp. 659-667, 2011. DOI: 10.1016/j.resconrec.2010.12.002

[12] Vokurka, R.J. and Fliedner, G.J., The journey toward agility, Industrial Data and Management Systems, 98(4), pp. 165-171, 1998. DOI: 10.1108/02635579810219336

[13] Meade, L. and Sarkis, J., Analyzing organizational project alternatives for agile manufacturing processes: An analytical network approach, International Journal of Production Research, 37(2), pp. 241-261, 1999. DOI: 10.1080/002075499191751

[14] Humphreys, P., Huang, G., Cadden, T., and McIvor, R., Integrating design metrics within the early supplier selection process, Journal of Purchasing and Supply Management, 13(1), pp. 42-52, 2007. DOI: 10.1016/j.pursup.2007.03.006

[15] Kainuma, Y. and Tawara, N., A multiple attribute utility theory approach to lean and green supply chain management, International Journal of Production Economics, 101(1), pp. 99-10, 2006. DOI: 10.1016/j.ijpe.2005.05.010

[16] Rezagholizadeh, M., Fereidunian, A.R., Dehghan, B., Moshiri, B. and Lesani, H., Multi criteria decision making (MCDM): A modified partial order theory (POT) approach, 3th International Conference on Advanced Computer Control (ICACC), pp. 650-655, 2011. DOI: 10.1109/icacc.2011.6016495

[17] De Boer, L., Labro, E. and Morlacchi, P., A review of methods supporting supplier selection, European Journal of Purchasing and Supply Management, 7(2), pp. 75-89, 2001. DOI: 10.1016/S0969-7012(00)00028-9

[18] Humphreys, P.K., Wong, Y.K. and Chen, F.T.S., Integrating environmental criteria into the supplier selection process, Journal of Materials Processing Technology, 138(1-3), pp. 349-356, 2003. DOI: 10.1016/S0924-0136(03)00097-9

[19] Lewis, H., Gertsakis, J., Grant, T., Morelli, N. and Weatman, A., Design and environment: A global guide to designing greener goods, Greenleaf Publishing, Sheffield, UK, 2001.

[20] Kumar, A. and Jain, V., Supplier selection: A green approach with carbon footprint monitoring, 8th IEEE International Conference on Supply Chain Management and Information Systems (SCMIS), pp. 1-8, 2010.

[21] Kipnis, A.B., Audit cultures: Neoliberal govern mentality, socialist legacy, or technologies of governing? American Ethnologist, 35(2), pp. 275-289, 2008. DOI: 10.1111/j.1548-1425.2008.00034.x

[22] Rosen, D.H. and Houser, T., China energy: A guide for the perplexed. [Online] 2007. Available at: http://www.iie.com/publications/papers/rosen0507.pdf

[23] Zhang, J., Zhang, Y., Chen, S. and Gong, S., How to reduce energy consumption by energy audits and energy management: The case of province Jilin in China, The International Conference on Technology Management in the Energy Smart World (PICMET), pp. 1-5, 2011.

[24] Eveloy, V., Ganesan, S., Fukuda, Y., Wu, J. and Pecht, M.G., Are you ready for lead-free electronics? IEEE Transactions on Components and Packaging Technologies, 28(4), pp. 884-889, 2005. DOI: 10.1109/TCAPT.2005.859353

[25] Hsu, C.W. and Hu, A.H., Applying hazardous substance management to supplier selection using analytic network process, Journal of Cleaner Production, 17(2), pp. 255-264, 2009. DOI: 10.1016/j.jclepro.2008.05.004

[26] Zúñiga-Ceron, V. y Gandini-Ayerbe, M.A., Caracterización ambiental de las vinazas de residuos de caña de azúcar resultantes de la producción de etanol, DYNA, 80(177), pp. 124-131, 2013.

[27] Zhu, Q. and Sarkis, J., An inter-sectoral comparison of green supply chain management in China: Drivers and practices, Journal of Cleaner Production, 14(5), pp. 472-486, 2006. DOI: 10.1016/j.jclepro.2005.01.003

[28] Yi, J. and Wang, S., Optimal contract design of reverse supply chain considering uncertain recycle price, International Conference on E-Business and E-Government, pp. 1-4, 2011.

[29] Amindoust, A., Ahmed, S., Ahmed, S., Saghafinia, A. and Bahreininejad, A., Sustainable supplier selection: A ranking model based on fuzzy inference system, Applied Soft Computing, 12(6), pp. 1668-1677, 2012. DOI: 10.1016/j.asoc.2012.01.023

[30] Lamming, R. and Hampson, J., The environment as a supply chain management issue, British Journal of Management, 7(1), pp. S45-S62, 1996. DOI: 10.1111/j.1467-8551.1996.tb00147.x

[31] Xiaoye, Z., Qingshan, Z., Miao, Z. and Xiaorong, L., Research on evaluation and development of green product design project in manufacturing industry, 4th International Conference on Wireless Communications, Networking and Mobile Computing (WiCOM), pp. 1-5. Shenyang, Liaoning, China, 2008.

[32] Chen,Y.S., The driver of green innovation and green image: Green core competence, Journal of Business Ethics, 81, pp. 531-543, 2008. DOI: 10.1007/s10551-007-9522-1

[33] Canal-Marques, A., Ortega-Vega, M.R., Cabrera J.M. and De Fraga-Malfatti, C., Alternative methods to attach components in printed circuit boards to improve their recyclability, DYNA, 81 (186), pp. 146-152, 2014. DOI: 10.15446/dyna.v81n186.39760

[34] Shrivastava, P., Environmental technologies and competitive advantage. Business Ethics and Strategy, 1, pp. 317-334, 2007.

[35] Bansal, P. and Hunter, T., Strategic explanations for the early adoption of ISO 14001, Journal of Business Ethics, 46(3), pp. 289-299, 2003. DOI: 10.1023/A:1025536731830

[36] Darnall, N., Why firms mandate ISO 14001 certification, Business and Society, 45(3), pp. 354-381, 2006. DOI: 10.1177/0007650306289387

[37] Coglianese, C. and Nash, J., Regulating from the inside: Can environmental management systems achieve policy goals? Routledge Publishing, New York, USA, 2001.

[38] Seijo-García, M.A., Filgueira-Vizoso, A. y Muñoz-Camacho, E., Consecuencias positivas de la implantación de la certificación ISO 14001 en las empresas gallegas (España), DYNA, 80 (177), pp. 13-21, 2013.

[39] Chiou, C.Y., Hsu, C.W.W. and Hwang, W.Y., Comparative investigation on green supplier selection of the American, Japanese and Taiwanese electronics industry in China, IEEE Industrial Engineering and Engineering Management (IE and EM), pp. 1909-1914, 2008.

[40] Tseng, M.L. and Chiu, A.S.F., Evaluating firm's green supply chain management in linguistic preferences, Journal of Cleaner Production, 40, pp. 22-31, 2013. DOI: 10.1016/j.jclepro.2010.08.007

[41] Ying-Tuo, P. and Yang, C., Iron and steel companies green suppliers' selection model based on vague sets group decision-making method, IEEE International Conference on Electronics Communication and Control, pp. 2702-2705, 2011. DOI: 10.1109/icecc.2011.6066284

[42] Zheng, W. and Zhao, L., Research on the selection of strategic supplier based on grey relation and multi-level fuzzy evaluation in the electronics industry, International Conference on Systems, Man and Cybernetics, pp.12-16, 2012. DOI: 10.1109/icsmc.2012.6377669

[43] Yang, Y.Z. and Wu, L.Y., Grey entropy method for green supplier selection, IEEE International Conference on Wireless Communications, Networking and Mobile Computing (WiCOM), pp. 4682-4685, 2007. DOI: 10.1109/wicom.2007.1150

[44] Li, X. and Zhao, C., Selection of suppliers of vehicle components based on green supply chain, 16th International Conference on

Industrial Engineering and Engineering Management, pp. 1588-1591, 2009.
[45] Bai, C. and Sarkis, J., Integrating sustainability into supplier selection with grey system and rough set methodologies, International Journal of Production Economics, 124(1), pp. 252-264, 2010. DOI: 10.1016/j.ijpe.2009.11.023
[46] Yan, G., Research on green suppliers' evaluation based on AHP and genetic algorithm, IEEE International Conference on Signal Processing System, pp. 615-619, 2009. DOI: 10.1109/icsps.2009.92
[47] Xu, W., Daoping, W. and Yan, W., Study on the vendor selection index system of iron and steel industry for green purchasing, International Conference on Management and Service Science (MASS), pp. 1-4, 2009.
[48] Thongchattu, C., and Siripokapirom, S., Green supplier selection consensus by neural network, 2nd International Conference on Mechanical and Electronics Engineering: VS313-VS316, Phayao, Thailand, 2010.
[49] Shaw, K., Shankar, R., Yadav, S. and Thakur, L.S., Supplier selection using fuzzy AHP and fuzzy multi-objective linear programming for developing low carbon supply chain, Expert Systems with Applications, 39(9), pp. 8182-8192, 2012. DOI: 10.1016/j.eswa.2012.01.149

R. Villanueva-Ponce, was born in Estado de México, México on June 17th 1978. He gained his BSc. in Electromechanical Engineering in 2001, from the Ciudad Juarez Institute of Technology, Juárez; México; his MSc. in Manufacturing Engineering in 2011 and his PhD. in Engineering Sciences in 2014 both from the Autonomous University of Ciudad Juarez, Juarez; México. His fields of interest include supplier selection criteria and multi-criteria decision making techniques within a supply chain.

L. Avelar-Sosa, was born in Durango, México on May 10th 1977. She received her BSc. in 2001, in Electronic Engineering from the Technological Institute of Durango, Durango., México; her M.Sc. in Industrial Engineering in 2005, from the Technological Institute of Ciudad Juarez, in Ciudad Juárez, México, and her PhD. in Engineering Sciences in 2014 from the Autonomous University of Ciudad Juarez, México. She is currently working as a full professor in the Industrial and Manufacturing Department, in the Institute of Engineering and Technology at the Autonomous University of Ciudad Juarez, Juárez, México. She has published papers in journals recognized by the Journal Citation Report, and participated in research in other universities outside Mexico. Her research interests include: supply chain, supply chain performance, logistics, structural equation modeling, and manufacturing processes.

A. Alvarado-Iniesta, is currently an assistant professor in the Department of Industrial and Manufacturing Engineering in the Autonomous University of Ciudad Juarez, Juarez, Mexico. He obtained his BSc. in Electronics Engineering, has a MSc. in Industrial Engineering, and a PhD. in Engineering, specializing in Industrial Engineering. His research interests are in the optimization and control of manufacturing processes such as plastic injection molding. His areas of research are focused on methodologies such as fuzzy logic, artificial neural networks employed as surrogate models, evaluative algorithms, and swarm intelligence.

V. Cruz-Sánchez, was born in Cárdenas, Tabasco, México, on September 14th 1978. She gained her BSc. in Computer Engineering in 2000, from the Instituto Tecnológico de Cerro Azul, México, her MSc. in Computer Science in 2004, from the Center of Research and Technological Development (CENIDET) and her PhD. in Computer Science in 2010 from CENIDET. She currently works as a professor at the Autonomous University of Ciudad Juarez, México. She is a member of the IEEE Computer Society. Her fields of interest include neuro-symbolic hybrid systems, digital image processing, knowledge representation, artificial neural networks, and augmented reality.

UNIVERSIDAD NACIONAL DE COLOMBIA
SEDE MEDELLÍN
FACULTAD DE MINAS

Área Curricular de Ingeniería Administrativa e Ingeniería Industrial

Oferta de Posgrados

Especialización en Gestión Empresarial
Especialización en Ingeniería Financiera
Maestría en Ingeniería Administrativa
Maestría en Ingeniería Industrial
Doctorado en Ingeniería - Industria y Organizaciones

Mayor información:

E-mail: acia_med@unal.edu.co
Teléfono: (57-4) 425 52 02

UNIVERSIDAD NACIONAL DE COLOMBIA
SEDE MEDELLÍN
FACULTAD DE MINAS



DYNA
http://dyna.medellin.unal.edu.co/

The effect of crosswinds on ride comfort in high speed trains running on curves

Miguel Aizpun-Navarro [a] & Ignacio Sesma-Gotor [b]

[a] *Escuela de Ingeniería Mecánica, Pontificia Universidad Católica de Valparaíso, Valparaíso, Chile. miguel.aizpun@ucv.cl*
[b] *Departamento de Mecánica Aplicada, CEIT, Donostia San Sebastián, España. nacho.sesma@me.com*

Received: July 25th, 2014. Received in revised form: March 15th, 2015. Accepted: November 8th, 2015

Abstract
The effect of crosswinds on the risk of railway vehicles overturning has been a major issue ever since manufacturers began to produce lighter vehicles that run at high speeds. However, ride comfort can also be influenced by crosswinds, and this effect has not been thoroughly analyzed. This article describes the effect of crosswinds on ride comfort in high speed trains when running on curves and for several wind velocities under a Chinese hat wind scenario, which is the scenario recommended by the standard. Simulation results show that the combination of crosswinds and the added stiffness of the lateral bumpstop on the secondary suspension can become a significant source of instability, leading to flange-to-flange contact and greatly jeopardizing ride comfort. Moreover, this comfort problem is an issue even when the wheel unloading ratio is well below the standard's limits and vehicle safety can be guaranteed.

Keywords: Rail vehicle models; crosswind stability; ride quality.

Influencia del viento lateral en el confort de vehículos ferroviarios de alta velocidad circulando en curvas

Resumen
La influencia del viento lateral en el descarrilamiento de los vehículos ferroviarios es un factor crítico desde que se comenzaron a producir vehículos ligeros que circulan a altas velocidades. Además, el confort del pasajero también puede verse afectado por el viento lateral. Sin embargo, este efecto todavía no ha sido investigado en profundidad en la literatura ferroviaria. Este artículo describe el efecto del viento lateral en el confort para trenes de alta velocidad que circulan en curvas para diferentes velocidades de viento, utilizando un escenario de viento tipo sombrero chino. Las simulaciones muestran que la combinación del viento lateral y la rigidez del tope de la suspensión secundaria pueden suponer una fuente importante de inestabilidad, produciendo contacto pestaña-pestaña y disminuyendo significativamente el confort. Además, este efecto se produce cuando el índice de descarrilamiento está muy por debajo del límite según la norma de seguridad ferroviaria.

Palabras clave: modelos de vehículos ferroviarios; estabilidad con viento lateral; confort.

1. Introduction

Nowadays, rolling stock manufacturers are reducing the weight of railway vehicles while progressively increasing vehicle speed. This tendency has promoted research into the effect of crosswinds on high-speed railway vehicles due to the risk of overturning and issues relating to ride comfort.

The study of crosswinds on railway vehicles can be divided into two separate but complementary issues: the effect of crosswinds on the dynamic behavior of the vehicle; and the aerodynamics, which requires the study of steady and unsteady aerodynamic forces and their interaction with the vehicle system [1].

One of the main concerns in crosswind research has been the study of the risk of overturning due to high wheel unloading. Andersson et al. [2] showed that crosswinds are the main cause of wheel unloading, with a relative importance of 64%. Moreover, several other authors have studied the effect of crosswinds from a safety point of view. Sesma et al. [3] showed how this process could be analyzed by using a simple 2D model,

© The author; licensee Universidad Nacional de Colombia.

whereas Carranini [4] focused instead on the parameters that should be included in car models to simulate crosswind effects on the vehicle. Thomas et al. made a major contribution to the state of the art in terms of vehicle dynamics when exposed to crosswinds. Their research in [5] compared different types of wind gusts in order to determine which one produces the highest wheel unloading value. Additionally, in [6] they compared on-track tests with 2D and 3D models of the real car, showing that although it is difficult to carry out on-track tests with high wind speed values, it is possible to reproduce those tests with computational models.

Even though safety is one of the most critical issues when studying crosswinds, it is also true that crosswinds are on most occasions a comfort issue rather than a safety issue. This is because once the safety standards are met there is a guarantee that those vehicles can run without being at risk of overturning. Some authors, such as Alfi et al. [7], Conde et al. [8] and Baker et al. [9] have approached this issue from this perspective. The first two articles deal with the improvement of ride comfort when using active secondary suspension, whereas the third article details a comfort test procedure in which a several kilometer track is simulated.

This article continues with the research on the effect of crosswinds on vehicle comfort by analyzing the behavior of a railway vehicle under a Chinese hat wind scenario [10] while running on a curve using a full multibody model. The aim of this work is to show the instability effects that can be caused by crosswinds, which directly influence passenger comfort. The lateral bumpstop effect of the secondary suspension is also analyzed in order to assess its importance on ride comfort.

The article is organized as follows. First the vehicle model, the wind and track scenarios, and the process of how vehicle comfort is analyzed are described. Then the main body of the article presents the analysis of vehicle comfort while running on a curve under the effects of the wind scenario. In addition, the influence that the lateral bumpstop has on curve ride comfort is presented in the last part of the article.

2 Definition of a multibody model and wind/track scenario for comfort analysis

Prior to analyzing ride comfort on a curved track, the multibody model of the vehicle and the chosen wind and track scenario must be described.

Analyzing a vehicle running on a curve requires the problem to be studied in 3D, so only a full multibody model can be used (see [11] for another example). The model has 23 bodies and 44 degrees of freedom. The aerodynamic forces, which are represented in Fig. 1, have been computed by taking into account the coefficients provided by the annex of standard EN 14067-6 for an ICE3 train. The carbody, bogies and wheelsets each have six degrees of freedom. The primary suspension consists of vertical and lateral linear springs and dampers. The secondary suspension was built in vertical, lateral and longitudinal directions, and linear and non-linear springs and dampers were taken into account. In addition, torsion springs were added to the full model. However, the model parameters were estimated in order to have a "generic high speed vehicle", and they do not correspond exactly to any existing train.

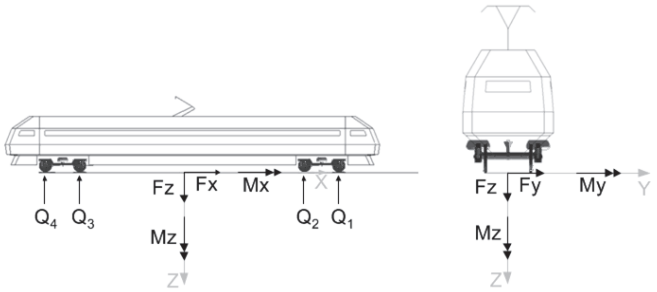


Figure 1. Multibody model. Description of Qi forces and aerodynamic loads Fx, Fy, Fz, Mx, My and Mz.
Source: The authors.

Table 1.
Track layout of the curved track.

Length of initial tangent track [m]	300	Total length [m]	6250
Length of transition tracks [m]	470	Curve radius [m]	5350
Length of circular arc [m]	3600	Track cant [mm]	140
Length of tangent track at the end [m]	1410		

Source: The authors.

The model includes the standard S1002 wheel profile, and the rail profile is UIC60 with an inclination of 1:40. The wheel-rail forces were calculated by means of Kalker's FASTSIM algorithm. Multibody simulations with a multibody model were run with the commercial MBS SIMPACK code [12].

The track used in the model is fully described in Table 1. The curve radius and the cant in the curve were chosen according to the regulation provided by the Spanish railway administrator ADIF. The values selected are the minimum established by ADIF for the case of a new line and have a nominal speed of 300 km/h, which is the vehicle velocity used to study vehicle dynamics.

The scenario begins and ends with a tangent track. In between, there is the curved track with a constant 5350 m radius and a cant height of 140 mm. The curved section is connected to the tangent tracks by a transition track, where both the cant and the radius increase linearly. In terms of wind direction, in order to create the most critical loading case the wind attack angle was set to 90 degrees along the whole scenario. Because wind forces act in the same direction of the centrifugal force, the effects of both the wind and the curve were added. Finally, the Chinese hat wind scenario begins and ends when the vehicle runs on the constant radius curve (see Fig. 2). The standard [10] defines this gust model as an input for multibody model simulations. The full wind scenario includes a linear rise to the base level of wind (18m/s in Fig. 2) when the train is loaded in steady state. The rise of the wind speed corresponds to the Chinese hat scenario that represents the wind gust. After reaching the maximum wind speed, it decreases again to the previous base level, also following the Chinese hat function. We then use another time period with constant wind loads. Lastly, we make a linear decrease to zero wind speed in order to complete the scenario.

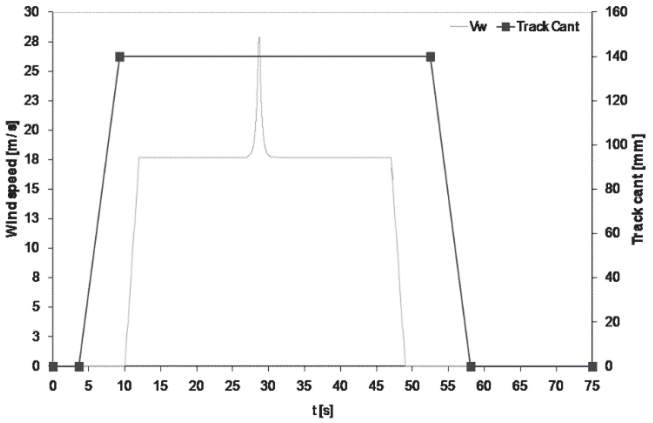


Figure 2. Example of one wind scenario and track cant used for the simulations on a curved track.
Source: The authors.

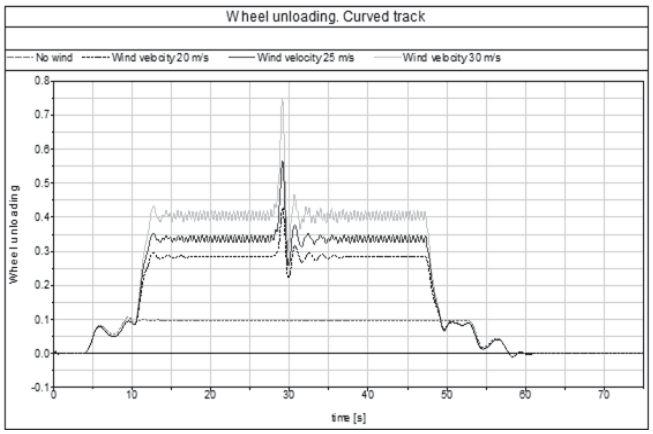


Figure 3. Wheel unloading ratio of the vehicle whilst running on a curved track under different crosswind conditions.
Source: The authors.

The wind scenario was considered a 'discrete event'. Time signals of the non-compensated acceleration were extracted from the simulations. Two sensors provided the signals; one was located at the front-end of the passenger compartment above the bogie, and the other was located in the geometric center of the same car. Time signals were filtered using a low-pass 2nd order Butterworth filter with an upper corner frequency of 2.52 Hz.

The results presented in the following sections compare three load cases created by three different wind velocities: 20 m/s, 25 m/s and 30 m/s. These wind scenarios are compared to a fourth scenario with no wind. The purpose of the experiment is to check the stability and comfort of the vehicle running on the curve with no wind and to show that the hunting oscillation does not appear until the crosswinds reach a certain speed.

3. Vehicle comfort while running on a curve when there are crosswinds

Although the aim of the article is to analyze the effects of crosswinds on vehicle comfort, it seems logical to first check the value of the wheel unloading ratio in order to dismiss the possibility of reaching the maximum value set by the safety standards.

Fig. 3 shows the time signal of the wheel unloading ratio. The value of this ratio was close to 0.1 when the vehicle ran with no wind. This measurement seems reasonable since the value of the curve radius was set to keep the vehicle stable, with low values for the wheel unloading ratio and the derailment factor. Obviously, wheel unloading increases with wind speed, with 0.75 being the maximum value; therefore, there is still certain margin until the limit value (0.9) is reached. The vehicle is stable with a wind speed of 20 m/s; however, it is somewhere near 22 m/s when the instability becomes noticeable (not represented in the figure). The time signal already indicates the instability with a wind speed of 25 m/s, which only increases when the speed is 30 m/s. A Fast Fourier Transform (FFT) of the signals reveals that the frequency matches the natural frequency of the vehicle's hunting oscillation.

Comfort is qualitatively assessed by using the information from the lateral non-compensated accelerations represented in Fig. 4, setting the no-wind scenario as a reference. Both the track layout and the vehicle satisfy the standards for maximum lateral accelerations since the restriction from the ride comfort standard is to keep accelerations below 0.6 m/s2 for high-speed vehicles when there is no wind scenario.

The 20 m/s wind speed case increases the acceleration value, but it is still within the limits, even though the maximum value is 0.9 m/s2 when the gust of wind hits the vehicle. However, this acceleration is not considered since instant values do not fall within the scope of comfort standards. The 25 m/s and 30 m/s wind speed cases cause the average value of the accelerations to be above the limits, and they also result in high peak-to-peak acceleration values. Leaving aside the influence of frequencies on comfort, peak-to-peak values are significant since passengers feel both the average value and the amplitude of accelerations. This means that the worst comfort indexes are reached, not only because of higher average values, but also as a result of having higher acceleration amplitudes. Since the peak-to-peak values increase by 0.3 m/s2 and 0.4 m/s2 in the 25 m/s and 30 m/s wind speed cases, the comfort index will be substantially worse in comparison with the 20 m/s wind speed case.

Thus, according to the results in Fig. 4, we can conclude that crosswinds can also become a source of instability that significantly reduces ride comfort. Fig. 5 and Fig. 6 provide more information about vehicle instability by analyzing the signals from two different vehicle points and the displacement of one wheel-rail contact point.

When the vehicle runs on tangent track, the sensor located in the front-end records the same acceleration level as the center sensor. However, on curved tracks, passengers located near the front-end of the compartment always have worse ride comfort (see Fig. 5). The reason for this behavior is that the leading bogie is always more unstable, which means that positions near the front-end lead to higher peak-to-peak values. Taking the 30 m/s wind speed scenario as an example, the peak-to-peak value at the front-end of the carbody

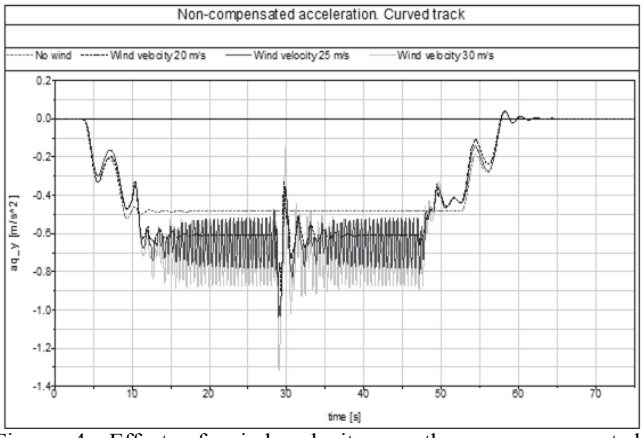


Figure 4. Effect of wind velocity on the non-compensated accelerations measured at the center of the carbody.
Source: The authors.

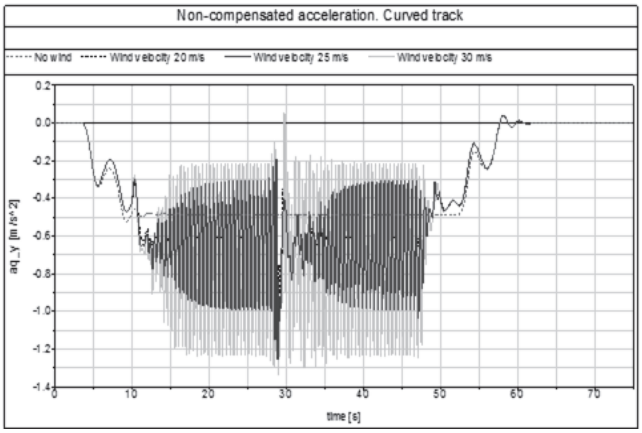


Figure 5. Effect of wind velocity on the non-compensated accelerations measured at the front-end of the carbody.
Source: The authors.

increases up to 1 m/s2, which is 0.6 m/s2 higher than the value measured at the center of the carbody. This means that the increase of the peak-to-peak acceleration value equals the limit value of the non-compensated acceleration given by the CEN standard. Nevertheless, as expected, the average acceleration value does not change between the front-end and the center of the carbody.

The increase in instability can be easily observed in Fig. 6, which represents the displacement of the contact point at the wheel's tread. The coordinate system is defined with the Y-axis pointing to the flange, i.e. positive values denote that the contact point is moving towards the flange.

The contact point moves towards the interior of the curve when there is no wind loading the vehicle. Once crosswinds begin to load the vehicle, the contact point changes direction, moving towards the flange. As previous figures showed, the 20 m/s wind speed case showed no hunting oscillation, and, in fact, the contact point describes a stable movement along the whole scenario. Fig. 6 shows that the larger the loads, the more unstable the contact point movement along the tread becomes, with amplitudes increasing as the wind loads increase.

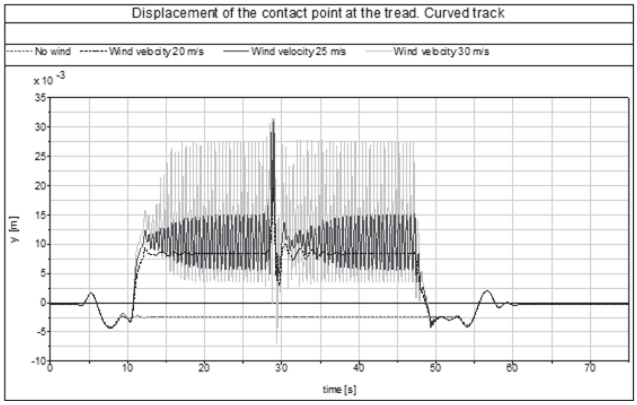


Figure 6. Displacement of the contact point on the tread under different wind load conditions (absolute measurements from static equilibrium point). Measurements were taken on the left wheel of the leading wheelset.
Source: The authors.

In the 30 m/s wind speed case, the contact point moves up to the limit of the thread, reaching flange contact in the instant when the gust of wind appears (around second 28). Since the wheel unloading ratio limit was not reached in any of the presented load cases, we expect to have severe flange contact during the times when wind loads are constant (between 12 s to 28 s and from 32 s to 47 s), if larger loads are introduced in the model. When the wind speed is 30 m/s, the contact point already reaches the limit of the wheel's tread, and since there is still room to increase the wind loads until the wheel unloading reaches 0.9; the instability of the vehicle will also increase. The leading wheelset will then describe an unstable movement in which the wheels' flanges at both sides will make contact with the rail.

Simulations showed that the vehicle instability explained above is caused by the effect of the added stiffness of the lateral bumpstops of the secondary suspension. These components have a non-linear stiffness characteristic, so the value of the stiffness depends on the lateral deformation of the suspension element. In addition, these bumpstops have a +/- 25 mm clearance (stiffness 0 N/m). The element begins to introduce stiffness to the model for displacements larger than 25 mm, and the bumpstop reaction force progressively increases until the suspension is blocked (limit of bumpstop deformation). The suspension cannot be deformed by more than 60 mm (lateral deformation from a centered position) since the lateral stiffness introduced by the element is very high (stiffness 230 000 N/m).

Fig. 7 shows that in the case of a vehicle running on a curve without wind, the lateral displacement of the bumpstop is 25 mm, which means that the element is not yet working. For low wind speeds, such as 20 m/s, the vehicle does not hunt even though the lateral deformation of the bumpstop is quite high (52 mm) and the bumpstop is already increasing the overall lateral stiffness of the vehicle. By increasing the wind speed up to 25 m/s, the vehicle is already hunting when the wind loads are constant and the lateral suspension is not blocked. For this wind speed, the bumpstop only gets blocked with the wind gust. However, the suspension is blocked during the whole wind scenario when the wind speed is 30 m/s.

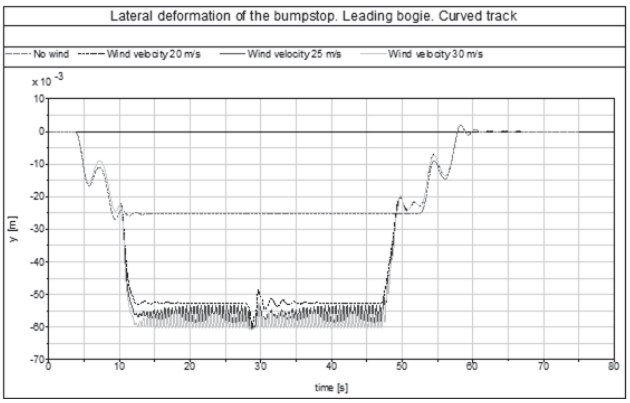


Figure 7. Lateral deformation of the bumpstop for the given crosswind velocities on a curved track.
Source: The authors.

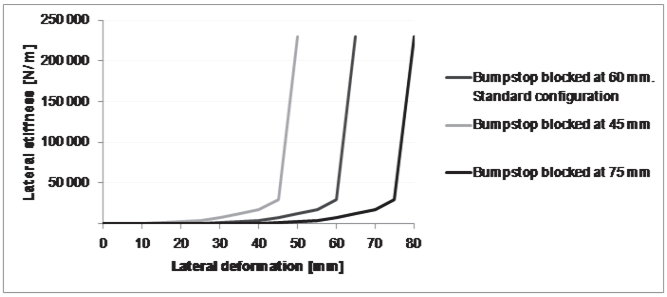


Figure 8. Stiffness of the bumpstop under three different hypotheses.
Source: The authors.

3.1. Influence of lateral bumpstop on vehicle comfort under crosswinds

This sub-section deals with the effect of one specific vehicle component, the lateral bumpstop of the secondary suspension on the vehicle comfort under different crosswinds scenarios.

The standard configuration of this component sets the maximum deformation of the vehicle's lateral bumpstop at 60 mm. If wind loads are high enough, the limit can be reached and cause passengers to feel unexpected discomfort. A suitable solution for this problem could be to increase the maximum deformation of this component. If this change is made, comfort improves but the downside is that the lateral displacement of the carbody increases and gauge problems can appear. Consequently, the solution should meet both gauge and bumpstop deformation requirements.

The multibody model had four lateral bumpstops: two on each bogie. The results presented here refer to the bumpstop located on the front bogie as simulations showed that it was the most critical. The sensitivity analysis discussed herein consisted of modifying the available lateral deformation and clearance but not modifying the stiffness of the bumpstop. This led to three different hypotheses, named by referring to the value of maximum deformation before blocking (see Fig. 8): the standard configuration (bumpstop blocked at 60 mm), bumpstop blocked at 45 mm and bumpstop blocked at 75 mm. By increasing the maximum lateral deformation of the element to 75 mm for example, the displacement where the lateral stiffness is zero (clearance) was also increased by 15 mm.

Fig. 9 shows a comparison of the non-compensated acceleration signals obtained when the vehicle runs on a curve. The chart compares the scenario where there are no crosswinds with the results of the scenario where the stiffness of the bumpstop was modified for the 30 m/s wind speed case. In the latter case, the accelerations obtained with the nominal value (suspension blocked at 60 mm of lateral deformation) are compared with the effect of reducing the maximum deformation to 45 mm, and also when the bumpstop blocks are at 75 mm.

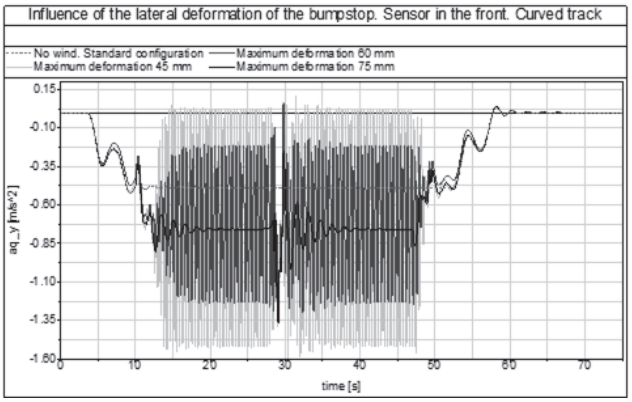


Figure 9. Influence of the lateral deformation of the bumpstop on the non-compensated acceleration measured on the front of the carbody
Source: The authors.

By decreasing the allowed deformation of the bumpstop, the element operates at deformations corresponding to higher stiffness values, which indirectly increases the overall lateral stiffness of the vehicle. Results show that comfort is drastically reduced when the bumpstop blocking is set to 45 mm, since the peak-to-peak acceleration values increase, with the maximum amplitude being almost 1.6 m/s2. In this case, the element operates with the suspension blocked during the whole scenario, increasing the amplitude of the hunting oscillation in comparison to the 'standard configuration' hypothesis. Conversely, by allowing the bumpstop to become deformed up to 75 mm, the bumpstop operates at deformation values where the lateral stiffness is lower and the vehicle stops describing the hunting oscillation.

Simulations were also performed in order to account for the variation of the wheel unloading ratio after modifying the maximum deformation of the bumpstop from its nominal value (60 mm). The variations are small for both the tangent track and the curved track. However, the wheel unloading ratio is slightly more sensitive to variations when the vehicle runs on tangent track, although the differences do not seem very important and can be considered irrelevant.

By increasing the maximum displacement of the bumpstop, the vehicle's behavior in crosswinds improves and the hunting oscillation is most likely avoided. Simulations showed that the maximum percentage of the lateral

displacement of the carbody's CoG is less than 10 per cent, which could be considered safe enough to avoid exceeding the gauge limits stated by the standards.

4. Conclusions

This article shows that crosswinds can have an effect on passenger comfort as well as on the risk of the vehicle overturning when running on curves. The lateral non-compensated accelerations were used to assess the vehicle comfort levels for the Chinese hat wind scenario for three different wind velocities—20m/s, 25m/s and 30m/s—which were then compared with the no-wind scenario. The vehicle shows stable behavior on curves at 20m/s, although for a 25m/s wind velocity value the vehicle is already unstable.

Results show that crosswinds can become a source of instability, which significantly reduces ride comfort, even when the wheel unloading ratio is well below the limits set by the safety standards. Thus, there can be comfort problems before there is any risk of overturning. Moreover, when running on curved tracks, positions near the leading end of the carbody always have worse ride comfort. Simulations confirm that this vehicle instability is also caused by the effect of adding the stiffness of the lateral bumpstop from the secondary suspension to the lateral stiffness of the whole vehicle, since the grouping effect of curve and crosswinds led to the activation of the most rigid part of the lateral bumpstop.

In addition, by changing the deformation/stiffness characteristics of the bumpstop the hunting oscillation can be avoided, although this might involve gauge problems. Thus, other options such as increasing the lateral stiffness of the secondary suspension, modifying the stiffness characteristics of the first part of the bumpstop curves, or including active secondary suspensions devices (centering systems), could be analyzed in order to deal with this drawback.

References

[1] Baker, C., The flow around high speed trains. J. Wind Eng. Ind. Aerodyn., 98, pp. 277-298, 2010. DOI: 10.1016/j.jweia.2009.11.002

[2] Andersson, E., Häggström, J., Sima, M. and Stichel, S., Assessment of train overturning risk due to strong cross-winds. Proc. IMechE, Part F: J. Rail and Rapid Transit, 218, pp. 213-223, 2004. DOI: 10.1243/0954409042389382

[3] Sesma, I., Vinolas, J., San Emeterio, A. and Gimenez, J.G., A comparison of crosswind calculations using a full vehicle and a simplified 2D model. Proc. IMechE, Part F: J. Rail and Rapid Transit, 226, pp. 305-317, 2012. DOI: 10.1177/0954409711424094

[4] Carrarini, A., Efficient models and techniques for the computational analysis of railway vehicles in crosswinds. Vehicle System Dynamics, 46, pp. 77-86, 2008. DOI: 10.1080/00423110701882322

[5] Thomas, D., Diedrichs, B., Berg, M. and Stichel, S., Dynamics of a high-speed rail vehicle negotiating curves at unsteady crosswind. Proc. IMechE, Part F: J. Rail and Rapid Transit, 224, pp. 567-579, 2010. DOI: 10.1243/09544097JRRT335

[6] Thomas, D., Berg, M. and Stichel, S., Measurements and simulations of rail vehicle dynamics with respect to overturning risk. Vehicle System Dynamics, 48, pp. 97-112, 2010. DOI: 10.1080/00423110903243216

[7] Alfi, S., Bruni, S., Diana, G., Facchinetti, A. and Mazzola, L., Active control of airspring secondary suspension to improve ride quality and safety against crosswinds. Proc. IMechE, Part F: J. Rail and Rapid Transit, 225, pp. 1-15, 2010. DOI: 10.1243/09544097JRRT392

[8] Conde-Mellado, A., Casanueva, C., Vinolas, J. and Gimenez, J.G., A lateral active suspension for conventional railway bogies. Vehicle System Dynamics, 47, pp. 1-14, 2009. DOI: 10.1080/00423110701877512

[9] Baker, C.J., Hemida, H., Iwnicki, S., Xie, G. and Ongaro, D., Integration of crosswind forces into train dynamic modelling. Proc. IMechE, Part F: J. Rail and Rapid Transit, 225, pp. 154-164, 2011. DOI: 10.1177/2041301710392476

[10] CEN. EN 14067-6 Railway Applications - Aerodynamics - Part 6: Requirements and test procedures for cross wind assessment, 2010.

[11] Lagos-Cereceda, R.F., Alvarez-C, K.L., Vinolas-Prat, J. and Alonso-Pazos, A., Rail vehicle passing through a turnout: Influence of the track elasticity. DYNA, 81(188), pp. 60-66, 2014. DOI: 10.15446/dyna.v81n188.40047

[12] SIMPACK AG. SIMPACK Reference Guide – SIMPACK, 2008. Available from: www.simpack.de.

M. Aizpun-Navarro, received his MSc. in Mechanical Engineering in 2009, and his PhD in Mechanical Engineering (railway dynamics) in 2013, both from Tecnun-University of Navarra, San Sebastian, Spain. From 2008 to 2013 he worked at both the CEIT research centre on European research projects and for the Spanish railway manufacturer CAF while carrying out his PhD. Currently, he is an associate professor in the School of Mechanical Engineering, Facultad de Ingeniería, Pontificia Universidad Católica de Valparaíso, Chile. His research interests include: simulation, modeling and experiments concerning railway vehicle dynamics; noise and vibration in mechanical systems; and optimization of railway vehicle testing.
ORCID: 0000-0003-1154-9659

I. Sesma-Gotor, received his MSc. in Mechanical Engineering in 2009, and his PhD in Mechanical Engineering (railway crosswinds) in 2013, both from Tecnun-University of Navarra, San Sebastian, Spain. From 2009 to 2013 he worked at the CEIT research centre on Spanish research projects while carrying out his PhD. Currently he is Operations Services Manager in Doppelmayr Cable Car. His research interests include: simulation and modeling concerning railway vehicle dynamics; simulation and modeling of railway vehicle aerodynamics; and analysis and design of railway wind fences.
ORCID: 0000-0002-1881-493X

UNIVERSIDAD NACIONAL DE COLOMBIA
SEDE MEDELLÍN
FACULTAD DE MINAS



DYNA
http://dyna.medellin.unal.edu.co/

Valorization of vinasse as binder modifier in asphalt mixtures

Mª José Martínez-Echevarría-Romero [a], Gema García-Travé [a], Mª Carmen Rubio-Gámez [a], Fernando Moreno-Navarro [a] & Domingo Pérez-Mira [b]

[a] *Laboratorio de Ingeniería de la Construcción, Universidad de Granada, Granada, España,. mjmartinez@ugr.es, labic@ugr.es, mcrubio@ugr.es, fmoreno@ugr.es*
[b] *Departamento I+D+i, Construcciones AZVI, Sevilla, España. dperez@construccionesazvi.es*

Received: July 15th, 2014. Received in revised form: July 29th, 2015. Accepted: October 22th, 2015.

Abstract
The reutilization of waste generated by industrial processes has become a majorenvironmental objective in scientific and technical research. In the construction sector, there is a broad range of techniques for the exploitation of different types of waste, which can then be used as a replacement for raw materials. This paper presents the results of a study of vinasse, a by-product of biomass ethanol, andanalyzes its viability as a bitumen modifier in asphalt mixes. For this purpose, four AC-16S asphalt mixes were evaluated for moisture sensitivity, plastic deformation, stiffness, and fatigue. The mix formulas were the following: (Mix 1) 50/70 bitumen; (Mix 2) 50/70 bitumen modified with 10% vinasse; (Mix 3) rubber bitumen; (Mix 4) rubber bitumen modified with 10% vinasse. The results of this study showed that bitumen modified with vinasse improved the mechanical performance of the AC-16S mix and also contributed to the valorization of vinasse waste.

Keywords: Asphalt mixture, binder modifier, mechanical behavior, vinasse.

Revalorización de la vinaza como modificador de betún para mezclas bituminosas

Resumen
La reutilización de los residuos derivados de los procesos industriales se ha convertido en uno de los objetivos prioritarios de carácter ambiental en la investigación científica y técnica. En el sector de la construcción, se pueden aprovechar materiales residuales de otros procesos en sustitución de materias primas. Este artículo presenta los resultados de un estudio desarrollado con el objetivo de valorizar la vinaza residual del proceso de fabricación de etanol a partir de biomasa, como material modificante del betún utilizado en las mezclas bituminosas. Se han fabricado cuatro mezclas bituminosas tipo AC-16S (1: Betún 50/70, 2: Betún 50/70 + 10%vinaza, 3: Betún-caucho, 4: Betún-caucho + 10%vinaza) y se han realizado ensayos de caracterización como son sensibilidad al agua, resistencia a las deformaciones plásticas, rigidez y fatiga.Los resultados muestran que las mezclas modificadas con vinaza mejoran el comportamiento mecánico de la mezcla AC-16 S y contribuye a la revalorización del residuo.

*Palabras clave:*Mezcla bituminosa, betún modificado, comportamiento mecánico, vinaza

1. Introduction

Vinasse is a by-product that remains in the distillation column when ethanol is produced from biomass. It is the main waste material generated in alcohol distilleries and its release without previous treatment has an extremely negative impact on the environment. The composition of vinasse can vary depending on the nature of the distillation process. However, vinasse typically has a low pH (3-5) and a high content of organic matter (35,000-50,000 mg O_2/L BOD),which makes it a toxic substance[1].

The uncontrolled discharge of vinasse into the soil can negatively affect soil quality by increasing thesalinity of the soil, thusdeteriorating its structure, porosity, and fertility[2]. Furthermore, since the production temperature ofvinasse is 50-80ºC, its release into aquatic environments without previous cooling can increase water temperature and lower the oxygen content to a level at which fish cannot survive[3,4]. In addition, the turbidity and color of vinasse can trigger processes of photosynthesis that also endanger aquatic life forms [5].

© The author; licensee Universidad Nacional de Colombia.

Currently, more and more countries are enacting stricter laws that regulate the discharge of waste from alcohol distilleries. For example, in 2005, the Indian government decided to rapidly transform distillation industries into zero-discharge industries [6]. Europe is also implementing similar measures to achieve the same objective by processing waste in waste treatment plants as well as by reusing and recycling it[7].

The anaerobic digestion of vinasse is an interesting way to reduce vinasse waste, because, in addition to promoting the stabilization of organic matter, it also enables energy generation from biogas, as Bruna S. Moraes reflects in her study[8].

Another way to reuse waste is by incorporating it into bituminous mixes. A wide range of studies have analyzed how the characteristics of these mixes can be enhanced with the addition of recycled waste material or by using this waste instead of one of the mix ingredients. This is an excellent way of reducing waste deposits and discharges. It is also more cost-effective since there is less need to use raw materials. Glass, steelworks slag, plastic, and rubber are examples of different types of waste material that have been used in asphalt mixes[9]. However, in recent years, the main focus has been on rubber from end-of-life tires and polymers [10-14].

In this study, vinasse was the waste used to manufacture bituminous mixes. The objective was to study the mechanical performance of these mixes when vinasse binder was added to modify the bitumen. For this purpose, we analyzed an AC 16 S bituminous mix, manufactured with 50/70 bitumen modified with 10% vinasse,as well as a rubber bitumen mix also modified with 10% vinasse. The performance of thevinassemixes was compared to that of the same mixes manufactured with unmodified bitumen and rubber bitumen.

2. Material and methods

For this study the asphalt mix used wasan AC-16S mix, which is commonly used in wearing courses in countries throughout the world. It is a dense asphalt concrete mix with an air voids percentage of 4-6%, a continuous coarse grain size (maximum particle size of 22 mm) and a bitumen content of 3.5-5% of the total mix weight. The mix is usually spread in layers of 5-8 centimetres.

Before beginning the battery of laboratory tests, four AC-16 S mixes were manufactured. The first two were regarded as the reference mixes. The first mix was manufactured with conventional penetration grade bitumen B 50/70 and the second with rubber bitumen. The third and fourth mixes were also manufactured with the same types of bitumen as the first two, but they were modified with biopolymers obtained from vinasse. In other words, the third mix was made from penetration grade bitumen B 50/70 modified with 10% vinasse and the fourth mix was made from rubber bitumen, also modified with 10% vinasse.

The bitumen was supplied by the University of Huelva in southern Spain where it was characterized and modified with the previously mentioned percentage of vinasse. The laboratory tests in this research study start with the design of the asphalt mixes by determining the optimal bitumen content for four mixes with the same mineral skeleton. This bitumen content was ascertained with the Marshall Test, as described in the Spanish Standard NLT 159/00 and in article 542 (guidelines for hot bituminous mixes) of the General Technical Specifications for Road and Bridge Works (PG3).

As previously mentioned, the substance used to modify the bitumen was vinasse, the liquid waste remaining after alcohol distillation. The phase separation of vinasse effluent (pH =4.58) is characterized by a precipitate with a higher concentration at the bottom and a supernatant with suspended solids on the surface. Before being mixed with the bitumen, the vinasse was first dehydrated at 70º in a convection oven. Its grain size was reduced with a laboratory blade mill (IKA, Werke model) as well as a sieve with a mesh size of 3.0 mm. The final product was then added to the bitumen in a proportion of 10%.

Ophite was used as an aggregate in the mix for the coarse fraction, and limestone was used for the fine fraction. The filler was CEM II /B-L 32,5 N cement. The materials in the mixes were first characterized as specified in article 542 (guidelines for hot bituminous mixes) of the General Technical Specifications for Road and Bridge Works (PG3).

The same set of tests was then applied to all four mixes in order to study their mechanical performance and to compare the mixes with modified bitumen withthe mixes made of unmodified bitumen. The tests performed were the following:

The moisture sensitivity test. Water action is one of the most common road pavement pathologies. The presence of moisture causes problems such as potholes, aggregate peeling or stripping which eventually lead to the structural failure of the pavement. There are numerous laboratory tests that analyze the susceptibility of bituminous mixes to moisture, providing a qualitative or quantitative evaluation [15]. In this work, the test performed was the moisture sensitivity test as described in the Spanish Standard UNE-EN 12697-12, which determines the response of mixes to water action.

The wheel-tracking. Rutting causes the loss of road surface regularity, so it is necessary to analyze this damage to avoid a negative impact on the quality of service to users. In this work, the test performed was the wheel-tracking test as described in the Spanish Standard UNE-EN 12697-22 [16]

Determination of the dynamic modulus according to the Spanish Standard UNE-EN 12697-26 to calculate the stiffness of the samples.The modulus is a parameter used in the mechanical design of asphalt mixes. For this reason, it was interesting to discover whether the modulus value changed when the bitumen was modified [17].

The fatigue test characterizes the performance of bituminous mixes when they are subjected to repeated loads at a constant mode of loading. A mix's fatigue resistance can be determined by different methods such as two, three, or four-point bending flexural tests on parallelepiped test specimens or the diametral compression test in which loads are applied to test cylinders. This test is described in Annex E of the Spanish Standard UNE-EN 12697-24 and was the one used in this research.

The experimental design is shown in Fig. 1:

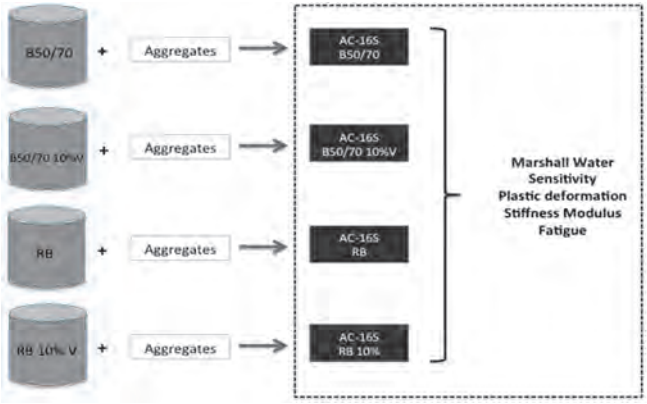


Figure 1. Experimental design diagram.
Source: The authors

Table 1
Percentages of aggregate fractions

Percentage of mix weight				
Fraction (mm)	Ophite 12/18	Ophite 6/12	Limestone 0/6	Cementfiller
AC-16 S	5%	50%	40%	5%

Source: The authors

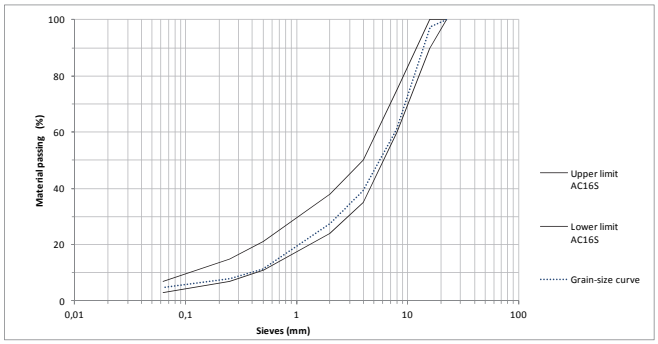


Figure 2.Particle size of the combined aggregate
Source: The authors

3. Results and Discussion

The mineral skeleton of the mix had the following composition: (i) 5% ophite aggregatewith a grain size of 12/18; (ii) 50% ophite aggregatewith a grain size of 6/12; (iii) 40% limestone aggregate with a grain size of 0/6 (sand); (iv) 5% cement filler. The composition of the mineral skeleton is shown in Table 1.

The aggregate was mixed in the percentages shown in Table 1, and the following grain size of the combined aggregate was obtained. When represented in a graph, (Fig.2), the grain-size curve of the mineral skeleton is a continuous line that falls within the envelope of an AC mix.

As previously mentioned, the mixes in this study all had the same mineral skeleton in which the combined aggregate fit within the grain-size envelope corresponding to that of an AC 16S mix.

The optimal binder content was determined by means of the Marshall Test as described in Spanish Technical Standard NLT 159/00. The parameters used for this purpose were the following:Design Marshall stability,Design Marshall deformation, Maximum Marshall stability, Maximum Marshall deformation, Density, Air voids and aggregate voids.

Regarding the first two mixes, Mix 1 was made from 50/70 bitumen, and Mix 2 was made from 50/70 bitumen modified with 10% vinasse. Both mixes had the mineral skeleton shown in Table 1. A set of test specimens were then manufactured, each with a different binder content (3.5%, 4 %, 4.5%,and 5% b/m). The manufacturing temperatures were 160ºC for the 50/70 bitumen mix (Mix 1) and 170-175ºC for the bituminous mix modified with vinasse (Mix 2). The compaction temperatures were 155-160ºC for the first mix and 165-170ºC for the second.

The specimens were compacted with 75 blows to each side by a Marshall hammer. The density of each specimen was determined according to Spanish Standard UNE-EN 12697-6 Procedure B, Dry Saturated Surface. Air voids were calculated by determining the maximum density (UNE-EN 12697-5.Procedure A: Volumetricof the mix for each of the specimens).

To obtain the stability and deformation values, the specimens were fractured in theMarshall stability breaking head. Based on the results of this test, the optimal bitumen content was 4.0 % of the mix weight. This same process was also followed to determine the bitumen content for the second mix with bitumen modified with 10% vinasse. In this case, the optimal bitumen content was 4.2% of the mix weight. Regarding the mixes made of rubber bitumen, and of rubber bitumen modified with 10% vinasse, the optimal binder contents were 4.5% and 4.6%, respectively.

As can be observed, the optimal bitumen content was slightly higher when the bitumen binder was modified with vinasse. This occurred because the addition of this biopolymer also increased binder viscosity. Consequently, more binder was needed to guarantee a good mixture of the aggregate.

After the optimal bitumen content was calculated, the moisture sensitivity of the mix was tested. Table 2 shows the values obtained:

Table 2.
Results of the Moisture Sensitivity Test

	AC-16 SBitumen 50/70 Ref. Mix	AC-16 S Bitumen 50/70 +10 % Vinasse	AC-16 SRubber Bitumen Ref. Mix	AC-16 S Rubber Bitumen +10 % Vinasse
Nº of specimens tested	6	6	6	6
Time elapsed between mixing and testing	4 days	4 days	4 days	4 days
Temperatureand immersion time of the wet specimens	40 °C 72 hours	40 °C 72 hours	40 °C 72 hours	40 °C 72 hours
Testing temperature	15 °C	15 °C	15 °C	15 °C
Subset of Dry Specimens				
Mean ITSd (KPa)	1679.4	2083.3	1786.0	1860.8
Subset of Wet Specimens				
Mean ITSd (KPa)	1526.3	1761.5	1431.8	1635.0
ITSR (%)	90.9	84.6	80.2	87.9

Source: The authors

Table 3.
Results of the Wheel-tracking Test

	AC-16 SRef. Bitumen 50/70	AC-16S B 50/70 + 10% Vin.	AC-16S Ref. Rubber Bitum.	AC-16S Rubber Bitumen+ 10 % Vin.
MeanWTS (mm/103 load cycles)	0.088	0.07	0.076	0.087
Test temperature(° C)		60		

Source: The authors

Table 4.
Stiffness results

Stiffness Modulus 20ºC (MPa)			
AC-16 S Ref. Bitumen 50/70	AC-16 S Bitumen 50/70 +10 % Vinasse	AC-16 SRef. Rubber Bitumen	AC-16S Rubber Bitumen +10 % Vinasse
4462	8807	4212	8237

Source: The authors

The results of the moisture sensitivity test for reference Mix 1 with bitumen 50/70 was very satisfactory with an ITSR valueof 90.6 %. When this bitumen was modified with vinasse (Mix 2), the ITSR value was somewhat less. This less satisfactory performance could be due to a slight reduction in aggregate-binder adhesion caused by the incorporation of the biopolymer. Reference Mix 3with rubber bitumen obtained an ITSR of 80.2%. However, in the case of Mix 4, rubber bitumen modified with vinasse, the addition of the biopolymer improved mix performance by 7.7% with an ITSR value of 87.9%.

Another result worth highlighting is the increase in indirect tensile strength in the four groups of test specimens, the dry specimens as well as the wet ones. This shows that the vinasse-modified binder improved mix cohesion.

Results obtained of the Wheel-Tracking Test are shown in Table 3.

It can be observed that the mix with vinasse-modified bitumen and the one with vinasse-modified rubber bitumen have a considerable increase in stiffness due to the impact of the biopolymer. This can be regarded as an advantage since it could enhance the bearing capacity of the mix.

In order to analyze the fatigue performance of the mixes, test cylinders specimens were manufactured for each of the four mixes, as specified in Spanish Standard UNE-EN 12697-24. For this purpose, the test cylinders specimens were first maintained at 20ºC for four hours. They were then subjected to repetitivesinusoidal loading until fracture occurred.

Each test cylinder specimen was subjected to repeated compression loads with haversine loading through the vertical diametric plane. This resulted in the application of a uniform stress perpendicular to the direction of the applied load and throughout the vertical diametric plane. This eventually led to the failure of the test cylinder specimen, which eventually splitalong the central sectionvertical diameter.

Fig.3 reflects the results of the fatigue tests with the data obtained from the test specimens manufactured with conventional bitumen B50/70 and bitumen B50/70+10% vinasse. They-axis shows the stress applied to the specimens and the x-axis, the number of loading cycles until fracture occurred.

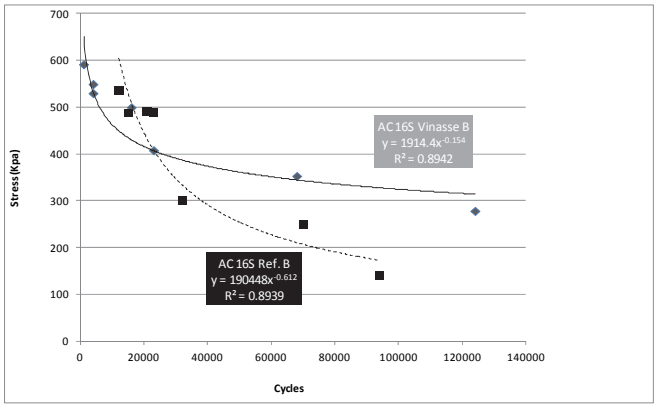


Figure 3. Fatigue laws for bitumen B 50/70, and vinasse-modified bitumen
Source: The authors

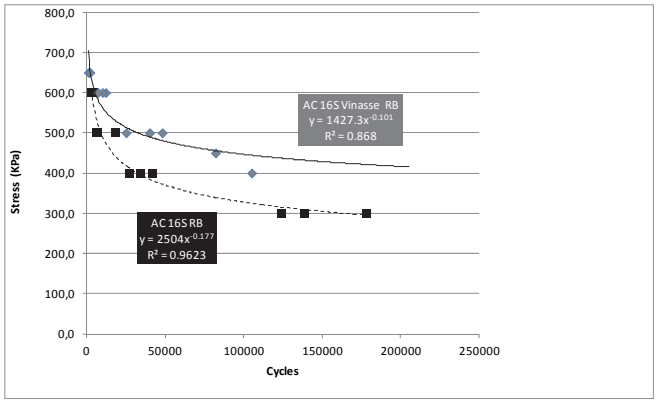


Figure 4. Fatigue laws for rubber bitumen and vinasse-modified rubber bitumen
Source: The authors

The analysis of the fatigue lines shows that in the initial cycles, the performance of the reference mix with bitumen B 50/70 wasmore satisfactory than that of the other mixes. However, at a stress less than 400 KPa, the vinasse-modified bitumen became more resistant to fatigue. As can be observed, the slope of the line representing the fatigue life of this mix becomes considerably gentler when compared to that of the reference mix.

In Fig. 4, the performance of the mixes manufactured with rubber bitumen and vinasse-modified rubber bitumen shows a similar tendency. At stresses less than 700KPa, the fatigue life of the vinasse-modified rubber bitumen mix was found to be more satisfactory.

4. Conclusions

Based on the results obtained, it was found that the use of vinasse-modified bitumen influenced the mechanical performance of the bituminous mix used in the study. Generally speaking, the modified bitumen had a positive impact since its addition produced an overall enhancement of the characteristics of the mix. The following conclusions can be derived from this study:

1. Vinasse enhances mix cohesion. This was evident in the increase in indirect tensile strength, as reflected in the values obtained in the fracture of the specimens with the Marshall stability breaking head as well as in the results of the indirect tensile test to perform the moisture sensitivity test.
2. The variations obtained in the permanent deformation tests were not very significant. Nevertheless, in one of the cases, there was a slight improvement in mix performance, possibly due to the lesser influence of the temperature on the mix manufactured with vinasse. These results complied with the requirements for the most demanding traffic loads. Furthermore, the deformation values obtained were lower than that of the reference mix.
3. Regarding the dynamic tests, the stiffness of the mix increased to almost double its value.
4. The expressions for the fatigue laws reflected an improvement in the performance of the mixes modified with 10% vinasse, when subjected to repeated loads.
5. The results obtained in this research study show that when vinasse was used to modify the bitumen in the AC-16 S bituminous mixes studied in this work, the addition of this biopolymer improved their mechanical performance and at the same time, revalued a highly-polluting industrial waste that is otherwise very difficult to eliminate.

Acknowledgments

The authors would like to thank the Spanish Ministry of Science and Innovation for the financial support provided to develop this research.

References

[1] Robles-González, V., Integrated treatment of mescal vinasses for depuration and discharge. Doctoral Thesis. ENCB del INP. México D.F. México, 2011.

[2] Tejada, M., Moreno, J.L., Hernández, M.T. and García, C., Application of two beet vinasse forms in soil restoration: Effects on soil properties and environment in southern Spain. Agric. Ecosyst. Environ., 119(3-4), pp. 289-298, 2007. DOI: 10.1016/j.agee.2006.07.019

[3] Jiménez, A.M., Borja, R., Martín, A. and Raposo, F., Mathematical modelling of aerobic degradation of vinasses with Penicilliumdecumbens. Process Biochem., 40(8), pp. 2805-2811, 2005. DOI: 10.1016/j.procbio.2004.12.011

[4] Mane, J.D., Modi, S., Nagawade, S., Phadnis, S.P. and Bhandari, V.M., Treatment of spentwash using chemically modified bagasse and colour removal studies. Bioresour, Technol., 97(14), pp. 1752-1755, 2006. DOI: 10.1016/j.biortech.2005.10.016

[5] Fitzgibbon, F.J., Nigam, P., Singh, D., Marchant, R., Biological treatment of distillery waste for pollution-remediation. J. Basic Microbiol., 35(5), pp. 293-301, 1995.

[6] Pant, D. and Adholeya, A., Biological approaches for treatment of distillery wastewater: a review. Bioresour Technology, 98(12), pp. 2321-2334, 2007. DOI: 10.1016/j.biortech.2006.09.027

[7] Asghar, N., Khan, S. and Mushtaq, S., Management of treated pulp and paper mill effluent to achieve zero discharge. J. Environ. Manage, 88(4), pp. 1285-1299, 2008. DOI: 10.1016/j.jenvman.2007.07.004

[8] Moraes, B.S., Junqueiraa, T.L., Pavanelloa, L.G., Cavaletta, O., Mantelattoa, P.E., Bonomia, A. and Zaiatb, M., Anaerobic digestion of vinasse from sugarcane biorefineries in Brazil from energy, environmental and economic perspectives: Profit or expense?, Applied Energy, 113, pp. 825-835, 2014. DOI: 10.1016/j.apenergy.2013.07.018

[9] Huang, Y., Bird, R.N., Heidrich, O., A review of the use of recycled solid waste materials in asphalt pavements. J. Resour. Conserv. Recy., 52(1), pp. 1065-1071, 2007. DOI: 10.1016/j.resconrec.2007.02.002

[10] Moreno, F., Rubio, M.C. and Martínez-Echevarría, M.J., The mechanical performance of dry-process crumb rubber modified hot bituminous mixes: The influence of digestion time and crumb rubber percentage. J. Cons. and Build. Materials, 26(1), pp. 466-474, 2011. DOI: 10.1016/j.conbuildmat.2011.06.046

[11] Arabani, M., Mirabdolazimi, S.M. and Sasani, A.R., The effect of waste tire thread mesh on the dynamic behaviour of asphalt mixtures. J. Cons. and Build. Materials, 24(6), pp. 1060-1068, 2010. DOI: 10.1016/j.conbuildmat.2009.11.011

[12] Katman, H.Y., Karim, M.R., Mahrez, A. and Ibrahim V.R., Performance of wet mix rubberized porous asphalt. Proc. Eastern Asia Soc. for Transport. Stud., 5, pp. 695-708, 2005.

[13] Casey, D., McNally, C., Gibney, A. and Gilchrist, M.D., Development of a recycled polymer modified binder for use in stone mastic asphalt. J. Reour. Conserv. Recy., 52(10), pp. 1167-1174, 2008. DOI: 10.1016/j.resconrec.2008.06.002

[14] Hinishoglu, S. and Agar, E., Use of waste high density polyethylene as bitumen modifier in asphalt concrete mix. J. Mater Lett., 58(3), pp. 267-271, 2004. DOI: 10.1016/S0167-577X(03)00458-0

[15] Moreno, F., García, G., Rubio, M.C. and Martínez-Echevarría, M.J. Analysis of the moisture susceptibility of hot bituminous mixes based on the comparison of two laboratory test methods. DYNA, 81(183), pp 49-59, 2013.

[16] García, G., Martínez-Echevarría, M.J., Rubio, M.C. and Moreno, F., Bituminous mix response to plastic deformations: Comparison of the Spanish NLT-173 and UNE-EN 12697-22 Wheel-Tracking test. DYNA, 79(174), pp 51-57, 2012.

[17] Del Río, M., Castro, D., Vega, A. and Sánchez, E., Effects of aggregate shape and size and surfactants on the resilient modulus of bituminous mixes. Canadian Journal of Civil Engineers, 38, pp. 893-899, 2011.

M.J. Martínez-Echevarría-Romero, is PhD. in Civil Engineering, is a professor in the Department of Construction Engineering and Engineering Projects and in charge of the Laboratory work in the Universidad de Granada, España. Her research interests include asphalt mixes, fatigue cracking, reuse of wastes in construction and concrete.
ORICD: 0000-0001-5799-1843

G. García-Travé, is PhD Degree in Chemistry, is a researcher in the Construction Engineering Laboratory research group at the Universidad de Granada, España. Her research interests include asphalt mixes, asphalt binders and reuse of wastes in construction.
ORCID: 0000-0002-5101-1610

M.C. Rubio-Gámez, is Ph.D. in Civil Engineering, is a professor in the Department of Construction Engineering and Engineering Projects and Head of the Construction Engineering Laboratory research group at the Universidad de Granada, España. Her research interests include asphalt mixes, fatigue cracking, reuse of wastes in construction.
ORCID: 0000-0002-1874-5129

F. Moreno-Navarro, is PhD. in Civil Engineering, is a lecturer in the Department of Construction Engineering and Engineering Projects and research coordinator of the Construction Engineering Laboratory research group at the Universidad de Granada, España. His research interests include asphalt mixes, fatigue cracking, reuse of wastes in construction, railway materials, and concrete.
ORCID: 0000-0001-6758-8695

D. Pérez-Mira, is an Industrial Engineer. He is in charge of the I+D+i Department in AZVI CNES, España, with ample experience in materials research in different fields.
ORCID: 0000-0002-2240-567X

UNIVERSIDAD NACIONAL DE COLOMBIA
SEDE MEDELLÍN
FACULTAD DE MINAS



DYNA
http://dyna.medellin.unal.edu.co/

Comparison of consistency assessment models for isolated horizontal curves in two-lane rural highways

Danilo Cárdenas-Aguilar [a] & Tomás Echaveguren [b]

[a] *Depatamento de Ingeniería Civil, Facultad de Ingeniería, Universidad de Concepción, Concepción, Chile. ercardenas@udec.cl*
[b] *Depatamento de Ingeniería Civil, Facultad de Ingeniería, Universidad de Concepción, Concepción, Chile. techaveg@udec.cl*

Received: July 17th, 2014. Received in revised form: May 29th, 2015. Accepted: October 22th, 2015.

Abstract
This consistency assessment of highways' geometrical design has the objective of providing safer roads. There are two types of models for consistency assessment: aggregated and disaggregated. The first one considers the difference between design and operating speed at the middle point of isolated horizontal curves. The second one considers the spatial variation of the operating speed profile along the horizontal curve. This paper compares the two types of consistency assessment models, using naturalistic speed and geometry data obtained in 34 horizontal curves of two-lane rural roads in Chile, using a 10 Hz GPS. Results obtained showed that in only 19 cases both methods are equivalent. This equivalence occurred only when operating speed profiles have the lowest spatial variance along the curves. If the operating speed profile has a high variance the consistency level obtained using both methods is different and the better option is combine it.

Keywords: consistency; design speed; operating speed; isolated horizontal curves.

Comparación de modelos de análisis de consistencia para curvas horizontales aisladas en carreteras de dos carriles

Resumen
El análisis de consistencia del diseño geométrico de carreteras tiene por objetivo contar con carreteras más seguras. Para analizar consistencia existen dos tipos de modelos: agregados y desagregados. Los primeros consideran diferencias de velocidades de diseño y operación en la mitad de la curva. Los segundos consideran la variación espacial del perfil de velocidad de operación. Este trabajo comparó los dos métodos usando datos empíricos de velocidad de operación obtenidos con un GPS de 10 Hz en 34 curvas horizontales simples de carreteras de dos carriles en Chile. Los resultados permitieron concluir que solo en 19 casos los métodos resultaron equivalentes entre sí. Esta compatibilidad sólo se da cuando el perfil de velocidad de operación posee poca varianza especial. Si el perfil de velocidad de operación es muy variable espacialmente, el nivel de consistencia obtenido usando los 2 métodos es diferente, caso en el cual resulta más conveniente combinarlos.

Palabras clave: consistencia; velocidad de diseño; velocidad de operación; curvas horizontales aisladas.

1. Introduction

The consistency of the geometrical design can be defined as the harmony between drivers' expectancy and the geometry of the road. If this harmony is high, drivers can guide their vehicles along the road alignment, minimizing the possibility of making a mistake and having an accident [1]. Consistency assessment provides a tool for highway engineers to discriminate between safer and less safe road designs, and to improve designs, including re-design or to use posted speed signs. There are various consistency assessment models (CAM) that, even though they all seek the same objective, the framework, procedures and indexes are different. A simple taxonomy of CAM makes two classifications: aggregate and disaggregates [2]. The disaggregated CAM allows isolated and "s" shaped horizontal curves to be analyzed and considers the operating speed at the middle point of each curve; the Lamm's model [3] is a good example. Another model is presented in Camacho – Torregrosa et al [4]. The aggregated CAM uses the operating speed profile along road segments to assess the consistency level. The Polus' model falls into this category

© The author; licensee Universidad Nacional de Colombia.

[5]. Each type of CAM estimates a consistency level of a certain road section, based on consistency indexes. Practical questions include, which model is more suitable for consistency studies, are the models case – dependent, and are the aggregated and disaggregated CAM equivalent? The state of the art does not provide answers to these questions.

The aim of this paper is to compare the Lamm's and Polus' models and to try to seek answers to the above questions. The paper begins with a description of Lamm's and Polus' models, including the algorithms for estimating the consistency index and the consistency levels provided by each one. After the data collection is described, including the road test section selection, the speed and geometry data collection procedure and the data processing are presented. The database used for the study is also included. This is followed by an estimation of the operating and design speed profiles, an estimation of consistency indexes and a description of their comparisons. Finally, a proposal for the integration of a consistency assessment model is presented, based on the findings of this research.

2. Models to be used for consistency assessment

2.1. The Lamm's model

The model postulates that the consistency of isolated horizontal curves is described by using the differences between the operating speed (V_{85}, in km/h) and the design speed (V_D, in km/h) at the middle point of the curve. This is shown in eq. (1). The IC is a consistency index (in km/h) for isolated horizontal curves. If the IC value is high, the difference between operating speeds is high, the consistency level is low and the accident risk increases.

$$IC = \left| V_D - V_{85} \right| \quad (1)$$

The design speed (V_D) can be obtained from project drawings or by back-calculating its value from in-field measurements of the curve geometry. The operating speed (V_{85}) is the 85th percentile of the cumulated frequency distribution of the speed obtained from in-field measurements of instantaneous speed, usually measured at the middle point of the curve. If the operating speed cannot be measured, for instance if there is a new design, it can be obtained by using speed-radius models that are locally calibrated. The Lamm's model grades consistency with the levels "good", "fair" and "poor", using the following thresholds for the IC [6]:

- "good" design: IC ≤ 10 km/h
- "fair" design: 10 km/h < IC ≤ 20 km/h
- "poor" design: IC > 20 km/h

Depending on the consistency level, the road improvements needs can be: do nothing, for "good" designs; limit speed signs, for "fair" or "poor" designs; and redesign, for "poor" designs. Some methods based on consistency levels for estimating speed limits in horizontal curves can be seen in [7,8].

2.2. The Polus' model

The model estimates the consistency index C of eq. (4), and considers the variability of the operating speed profile around the spatial mean of the operating speed along a road segment [9]. If the variability of the operating speed is high, its variance σ (eq. (3), in m/s) is high, the speed parameter R_a (eq. (2), in m/s) is high and the consistency index is low. Lower values of C mean a "poor" consistency level, and higher values mean a "good" consistency level. Therefore, in a consistent design of isolated horizontal curves, a flat speed profile is expected. However, it is not a guarantee that the operating speed will be similar to the design speed.

$$R_a = \frac{\sum_i |a_i|}{L} \quad (2)$$

$$\sigma = \frac{1}{3.6}\sqrt{\frac{(V_i - V_m)^2}{n}} \quad (3)$$

$$C = 2.808e^{(-0,278R_a\sigma)} \quad (4)$$

In eq. (2), Ra represents the relative area between the speed profile and the mean speed, normalized by the length of a road section. (See Fig. 1). The term $\Sigma \left| a_i \right|$ is the absolute sum of unitary areas, in m^2/s. The term L is the segment length, in m. In eq. (3) the term σ represents the standard deviation of the operating speeds, in m/s. V_i is the operating speed at the discrete element of length "i", in km/h. V_m is the spatial average operating speed along the segment of length L and n is the number of discrete elements of length along the segment L, which can be selected arbitrarily. The model rates the consistency level as "good", "fair" and "poor", using the following thresholds for C [9]:

- "good" design: C > 2 m/s
- "fair" design: 1 < C ≤ 2 m/s
- "poor" design: C ≤ 1 m/s

3. Field data collection

3.1. Test sections selection

In this research a test section is defined, which is an isolated horizontal curve with a tangent length of up to 400 m in length at the both sides of the curve. It ensures that the horizontal curve is isolated from the neighboring horizontal curves. The selection of test sections was performed in two

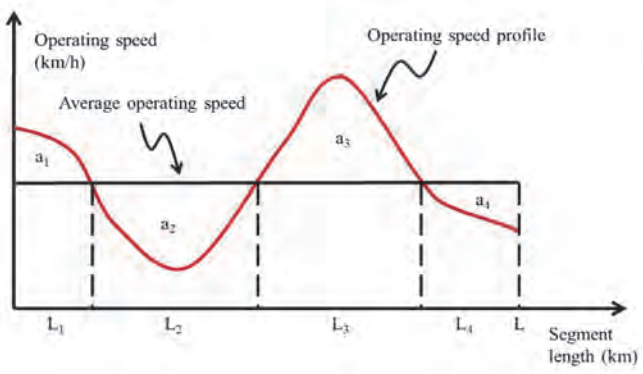


Figure 1. Speed profile used in the Polus' model, considering n = 4.
Source: adapted from [10]

stages. In the first stage, a preliminary set of test sections was obtained using satellite images, the road network stored in the GIS at the University of Concepcion's Transport Laboratory , the National Road Traffic Survey and the National Road Inventory both Chilean Ministry of Public Works [11-13]. Using this database and the following criteria, 67 test sections were selected.

- Location: only test sections near to Concepcion City were selected in order to reduce the operating costs of taking the measurements.
- Type of pavement surface: only paved surfaces.
- Traffic: annual average daily traffic lower than 5000 vehicles/day-year, according to [14].
- Access: without lateral access or intersections.
- Land use: outside urban areas and without a presence of houses, schools, and farms in the test section or near in order to avoid pedestrian, non-motorized and agricultural machine traffic.

In the second stage, each test section, selected using the previous criteria was inspected in-field. The criteria considered were the following:

- Good pavement condition.
- Test sections without road works.
- Test section with proper lateral clearance and without facilities in lateral areas that could interrupt traffic.
- Test sections in areas in which satellite signal could be destabilized were avoided, such as in areas with dense forest or that have high tension electric towers or electric stations.
- For safety, only test sections with enough clearance for vehicle maneuvers or parking of probe vehicles were selected.
- Test section with low roadside hazard index according to [15].

3.2. Speed and geometry measurements in the test sections

A 10 Hz GPS logger was used for speed measurements. The GPS obtained position data from eight satellites based on RTK (Real Time Kinematics) technology and speed was based on the Doppler Effect, which allows location and speed data to be obtained from a vehicle in motion. The device simultaneously measured position, time, distance, longitudinal speed and heading, as well as other parameters, every 0.1 s, with a precision of 0.2 km/h for speed, 0.05 % for distance and 0.1° for heading [16]. The device uses software for raw-data processing and to generate data reports, with which it is possible to build a speed and position data base. The device can be easily mounted and dis-mounted in a probe vehicle. The device was mounted in the interior part of the windshield of the car and then connected to the GPS antenna. It was placed on the roof and aligned to the longitudinal axis of the vehicle. This position is fixed during the speed measurements.

Speed measurements were obtained using the car following procedure in which the probe vehicle is the follower and the vehicle followed is the leader. The objective is to replicate the speed of the leader vehicle using a probe vehicle (the follower). While this is taking place the probe vehicle tries to keep a constant gap between both vehicles. Details of this measurement procedure can be seen in [17]. The measurement started with the probe vehicle being parked at the roadside with the GPS logger aligned and paused, waiting for a vehicle to enter the test section. Once the vehicle overtakes the probe, the driver turns on the GPS and the probe begins to follow the car and adjusts its speed until the distance between both vehicles is stable, by approximately 50 m. The stabilization of the speed is in the entrance tangent. If the probe vehicle confronts road or traffic conditions that force it to change speed, trajectory or abandon the pursuit, the measurement was discarded. The procedure was repeated between 20 and 30 times per test section, in order to obtain enough speed, position and heading data points.

3.3. Data processing

The data processing allows the horizontal curve geometry and the operating speed to be estimated. The process begins with the coupling and debugging of raw-data by using the Kalman filter implemented in the software of the GPS logger. Data coupling allows the speed-distance and heading-distance signals along the test section to be obtained. The depuration of data consisted in correcting data anomalies or data missing that was caused by dropouts (satellite signal disruption or degradation due to, for instance, the presence of dense forest or high voltage transmission towers). After this distance profiles were built for each run and test section heading: distance and speed –.

4. Geometry and speed profiles estimation

4.1. Geometry estimation

The geometry of the test section was obtained from the heading-distance profile. In these types of diagrams the slope changes allowed the starting and ending point of the curve (PK and FK respectively) to be detected. Once both points are identified, the middle point of the curve (MC) and the starting point (TE) of the entrance tangent were obtained. The TE was located 200 m from the starting point of the curve. After locating the characteristic point, the radius was estimated to be the inverse of the curvature and the curve length to be the distance between the PK and FK points. Fig. 2 shows a generic diagram of the test section.

4.2 Operating speed profile estimation

In each test section the speed-distance diagram of each run were organized in such way that the TE, PK, MC and FK points coincided as much as was possible. Because the trajectory of the probe vehicle is slightly different for each run, an exact coincidence of these points is not possible. Anomalous speed-distance data were erased from the database, and a total of 34 test sections with 20 runs were used in the remainder of the study. The speed-distance profiles were used to estimate operating speed at each characteristic point of the test section. The departure tangent was not considered as drivers usually accelerate and rapidly increase their speed when leaving the horizontal curve, which changes the distance from the probe vehicle. In this case

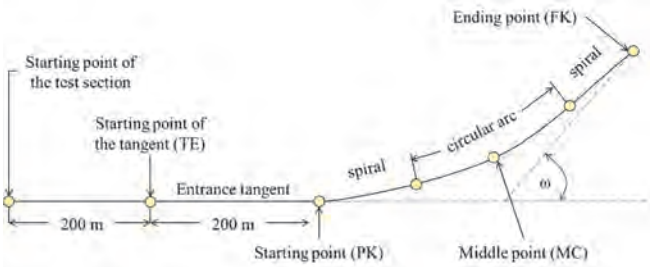


Figure 2. Configuration of a test section and its characteristics points.
Source: The authors

the car pursuit method loses accuracy and does not represent the speed of the leader vehicle. The operating speed was estimated at points TE, PK, MC, and FK as follows. Around each one of these points the 40 neighbor speed data points were grouped (20 data points per side). This procedure was repeated for each run. After the speed data points were grouped, a sample of between 820 and 1230 speed data points was obtained, depending on the number of runs. This sample was used to elaborate an empirical probability density function (pdf). It was fitted to a normal pdf to finally estimate the 85th speed percentile.

4.3. Design speed profile estimation

It was assumed that the design speed is constant along the test section. The design speed was estimated according to the design criterion of the Chilean Highways Manual, which recommends designing horizontal curves, assuming that the superelevation is twice the design friction [18]. Considering this criterion in the mass-point model for horizontal curves design, the design speed (V_D in km/h) can be obtained by using eq. (5), in which R is the radius (in m) and f is the design friction coefficient (decimal).

$$V_D = \sqrt{190.5\, fR} \tag{5}$$

4.4. Summary of data

The data obtained for each test section was summarized in an isolated database as is shown Table 1. It includes the geometrical radius, the design speed and the operating speed at each point of the test section.

Table 1.
Summary of geometric and speed data used to compare the consistency assessment methods.

# of Curve	Radius (R) (m)	Design speed (V_D) (km/h)	Operating speed (V_{85}) (km/h) at the			
			first point of the entrance tangent (TE)	starting point of the curve (PK)	middle point of the curve (MC)	ending point of the curve (FK)
4 - I	457	104.4	108.5	99.1	94.7	106.4
4 - II	457	104.4	118.2	106.8	109.7	113.2
7 - I	457	104.4	114.8	110.1	100.8	108.6
7 - II	457	104.4	115.0	113.4	106.9	106.7
11 - I	627	115.7	110.7	110.4	107.6	112.9
11 - II	509	108.4	120.6	112.0	108.8	110.8
12 - I	509	108.4	106.2	102.8	100.7	107.0
12 - II	627	115.7	112.6	108.5	105.6	105.0
19 - I	455	104.3	99.5	96.0	92.7	93.5
19 - II	222	77.4	106.3	96.6	92.4	98.0
20 - I	222	77.4	73.8	89.5	90.8	98.4
20 - II	455	104.3	105.3	95.1	93.5	97.3
21 - I	488	106.8	109.0	105.3	105.4	106.2
21 - II	466	105.1	106.3	103.7	98.5	98.2
22 - I	466	105.1	107.6	104.1	102.5	105.2
22 - II	488	106.8	114.6	108.3	102.5	107.1
37 - I	340	91.5	104.6	95.3	91.8	95.7
41 - I	312	88.0	108.5	102.0	93.1	96.0
44 - I	223	77.5	99.8	91.4	83.3	88.3
46 - I	330	90.0	83.9	84.4	79.4	77.2
47 - I	193	73.3	95.1	84.9	82.9	80.7
50 - I	190	72.9	84.2	78.0	72.3	74.6
52 - I	190	72.9	100.4	94.8	89.2	87.7
54 - I	687	119.2	102.1	104.9	106.0	106.5
55 - I	687	119.2	108.4	107.2	107.2	110.9
55 - II	687	119.2	109.5	107.4	108.9	105.3
60 - I	517	109.0	117.5	111.3	103.7	102.5
60 - II	676	118.6	104.0	103.6	101.9	102.3
61 - I	327	89.7	91.3	100.2	103.3	109.3
62 - I	402	100.1	110.4	104.5	98.8	103.3
63 - I	253	81.4	114.8	104.4	96.6	97.4
65 - I	296	86.2	93.6	93.7	90.9	92.0
66 - I	355	93.6	101.8	101.5	99.1	100.9
67 - I	192	73.2	95.2	94.3	88.3	93.3

Source: The authors

5. Comparison of Lamm's and Polus' models

5.1. Estimation of the consistency indexes

The consistency indexes were estimated using the data from Table 1. The operating speed at the middle point of the curve (MC) was used to estimate the IC of eq. (1). To estimate the C index of eq. (4) two sceneries were considered. In the first, the value of σ (eq. (3)) was obtained using the operating speed and the spatial average value of the operating speed from Table 1. In the second, the mean value of the operating speed was replaced by the design speed in eq. (3), consequently obtaining eq. (6) and eq. (7).

$$\sigma_D = \frac{1}{3.6}\sqrt{\frac{(V_i - V_D)^2}{n}} \quad (6)$$

$$C_D = 2.808e^{(-0,278R_a\sigma_D)} \quad (7)$$

The term Ra of eq. (6) remains the same, but the expression $\Sigma \mid a_i \mid$ is estimated in terms of the operating speed and design speed in each test section. It was assumed that the parameters of the models do not vary if the spatial average speed is replaced by the design speed.

5.2. Comparison of consistency indexes

The comparison considered four analyses: (a) comparison between the IC and C indexes for all the test sections (Fig. 3); (b) comparison between the IC and C indexes for all the test sections for 3 levels of radius (Fig. 4); (c) comparison between the IC and C indexes for all test sections, but replacing the spatial average of the operating speed by the design speed (Fig 5); and (d), comparison between the IC and C indexes for 3 levels of radius and replacing the spatial average of the operating speed by the design speed (Fig. 6). In Fig. 3 – 6 the quadrants 1 to 3 represents a "fair" consistency level and the quadrants 4 to 6 represents a "good" consistency level, both according to Lamm's model. Note that for the data analyzed none of the test sections was rated as "poor" according to Lamm's model. Similarly, according to the Polus' model, the quadrants 1 and 4 represent a "poor" consistency level, the quadrants 2 and 5 a "fair" consistency level and the quadrants 3 and 6 a "good" consistency level. Thereby, only in quadrants 2 and 6 are both models of consistency assessment equivalent.

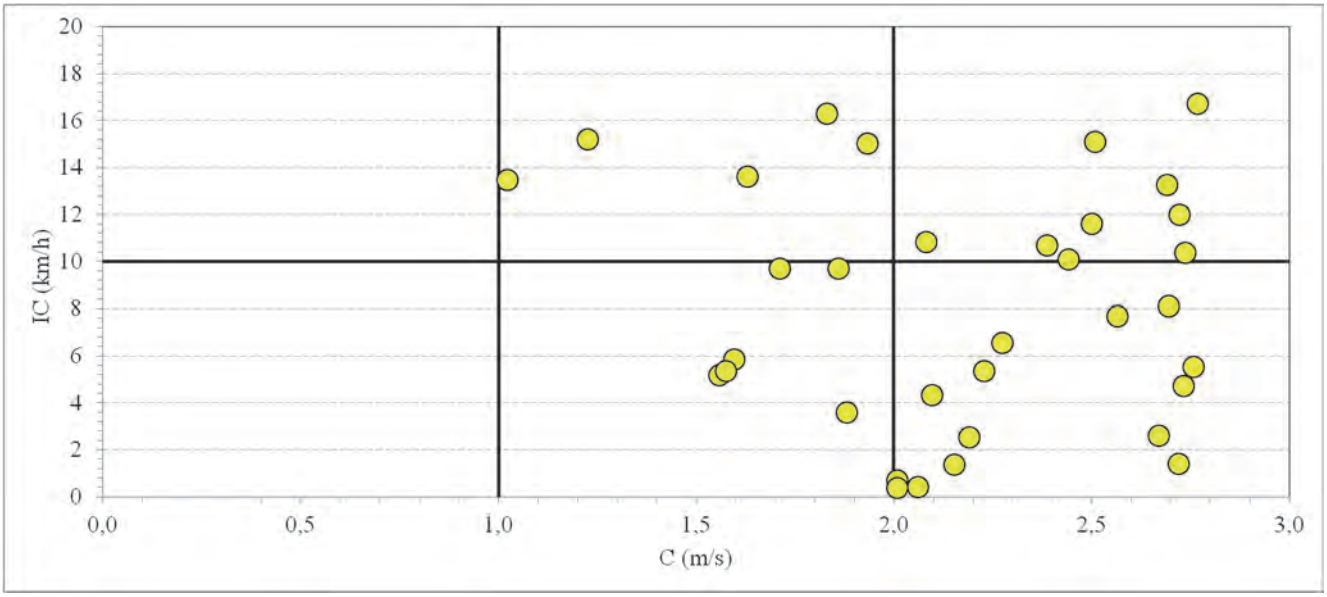


Figure 3. IC and C indexes plotted for all test sections.
Source: The authors

According to Fig. 3, 5 test sections were rated as having a "fair" design and 14 as having a "good" design by the two models (quadrants 2 and 6). However, 15 test sections were rated as having a different consistency level, depending on the method used (quadrants 3 and 5). This ambiguity shows that the actual consistency level cannot be obtained by separately using the CAM.

The test sections located in quadrant 3 of Fig. 3, have differences between the operating and design speeds that are higher than 10 km/h as the operating speed profiles of these curves are approximately uniform along the test sections and the variability of the speed is low. As a consequence, the value of Ra and σ are low and, therefore, the C index is high. The consistency level according Polus' model was "good" despite the consistency level according to Lamm's model being described as "fair". This means that if the operating speed profile is uniform, the consistency level will tend to be "good" when using Polus' method, but at the same time it will have a "poor" or "fair" consistency level according to Lamm's method, depending on the differences between the operating and design speeds.

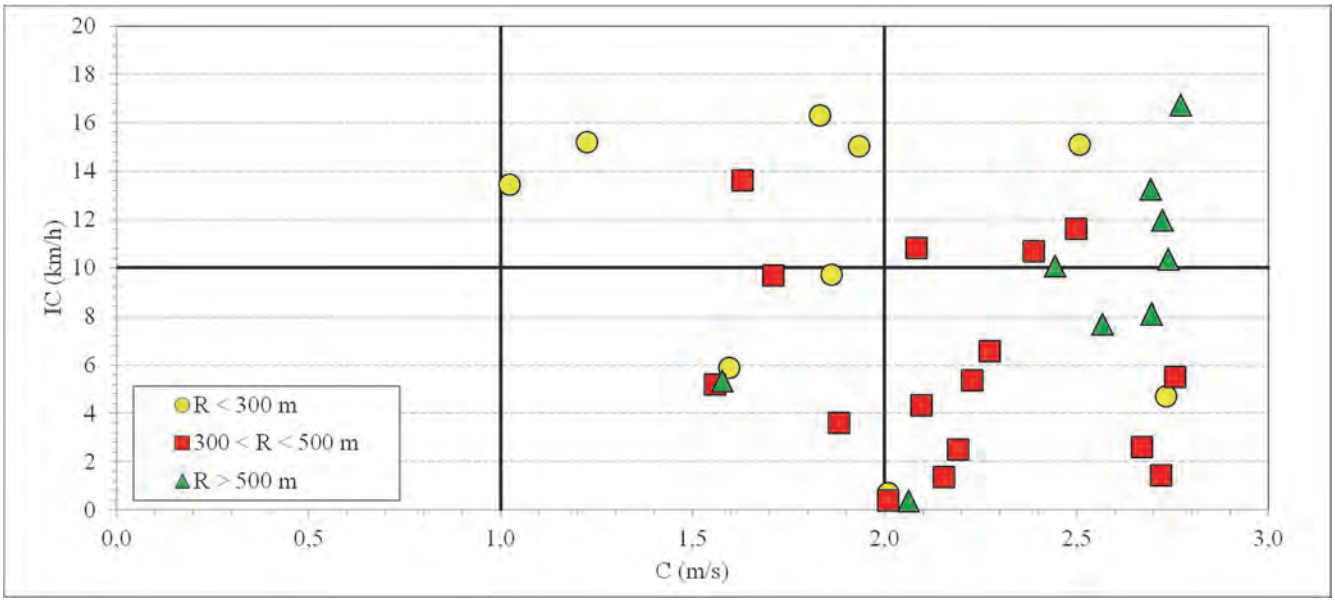


Figure 4. IC and C indexes are plotted for all test sections and classified in 3 levels of radius.
Source: The authors

The test sections located in quadrant 5 have a "good" consistency level according to Lamm's model, because the difference between the operating and design speed was lower than 10 km/h. Also, because the operating speed profiles in these test sections were not uniform the values of Ra and σ tended to be higher and consequently the C value tends to be low. This behavior is typical of horizontal curves in which the operating speed diminishes at the entrance tangent up to the design speed inside the curve. In this case, Polus' method detected high variability, but Lamm's method only detected harmony between operating and design speed at the middle point of the horizontal curve.

In a second analysis, the comparison of consistency models considered three levels of radius, as shown in Fig. 4. In test sections with a radius lower than 300 m, the consistency level obtained is similar for both models. In test sections with a radius between 300 and 500 m the variability of operating speeds tends to diminish, but the difference between operating speed and design speed do not follow a clear pattern. For this reason, in this segment of radius, the consistency level tends to be "good" when using Polus' model and "good" or "fair" when using Lamm's model. For a radius higher than 500 m, the speed profiles tend to be uniform and the C values tends to be higher. As a consequence, test sections can be located in quadrants 3 or 6 depending on the IC value. The variability of the IC index for higher radius is explained for the operating speed at the entrance tangent. Because the speed profiles are uniforms, if the operating speed at the entrance tangent is very different to the design speed, the CI values increase and the consistency level decrease. Conversely, if the radius is low, the variability of the speed profile increases, especially if the operating speed at the entrance tangent is high. In this case, the C value decreases but the IC value will depend on the difference of that speed with regards to the design speed.

Fig. 5 and 6 show the comparison between the IC index and the modified index of Polus' model (see eq. (7)). Following the same order of the previous analysis, Fig. 5 plots the consistency index for all the test sections and Fig. 6 for three radius levels. The consistency index's observed pattern is different to these observed in Fig. 3 and 4, because both consistency indexes are linked by design speed. In Fig. 5 the test sections that have a low consistency level using the IC index also have a low consistency level using the C index. This means that the test sections exhibit a speed profile that is highly variable that, at the same time, has an operating speed higher than 10 km/h (quadrant 1). Conversely, the test sections that have low IC values, also have higher C values, which means that they have a better consistency level. This is due to the low variability of operating speed profile and the low difference between the operating and design speed.

As Fig. 6 shows, this pattern is not only dependent on the radius of the horizontal curves. The pattern is not absolutely clear, but the general trend shows that the test sections with low radii tend to be less consistent than those with higher radii. Test sections with radii lower than 300 m (V_D < 85 km/h) simultaneously exhibit high IC values ("fair" design) and low C values ("poor" or "fair" design). This means that the gap between operating and design speed increases at the same time that the operating speed profile oscillates around the design speed. For radii between 300 and 500 m, the pattern is more attenuated. The gap between operating and design speed decreases but not necessarily the variability of the speed profile. However, the oscillation is sufficiently low to increase the consistency level, and according to Polus' model obtains more stable speed profiles.

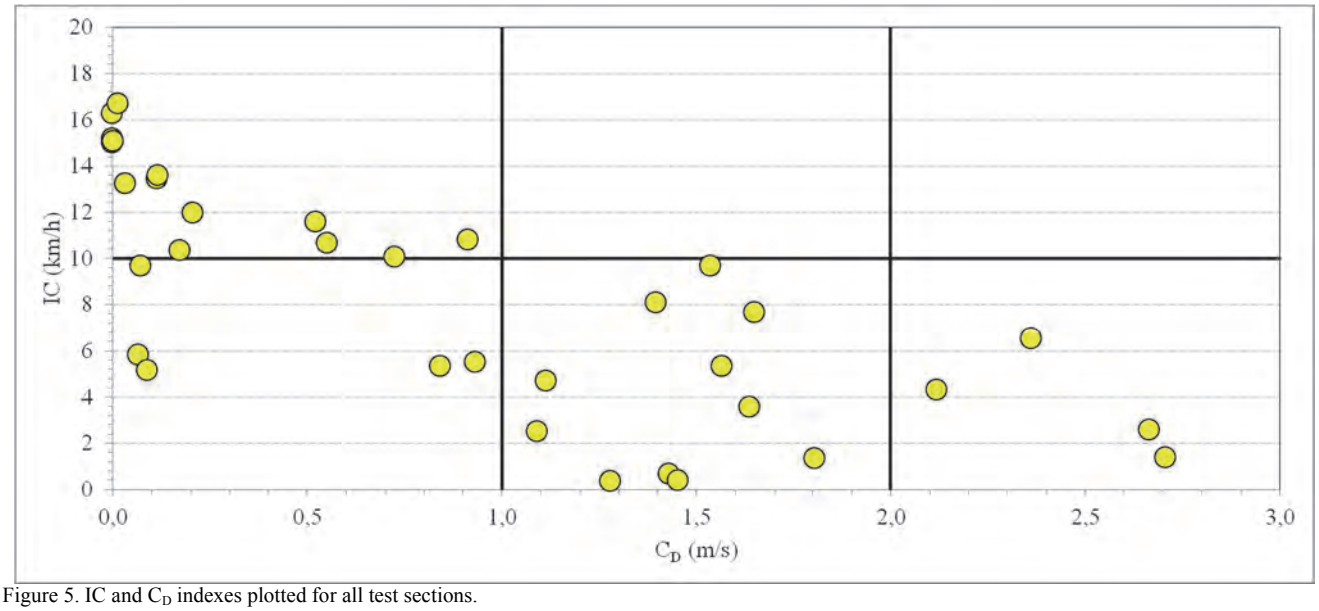


Figure 5. IC and C_D indexes plotted for all test sections.
Source: The authors

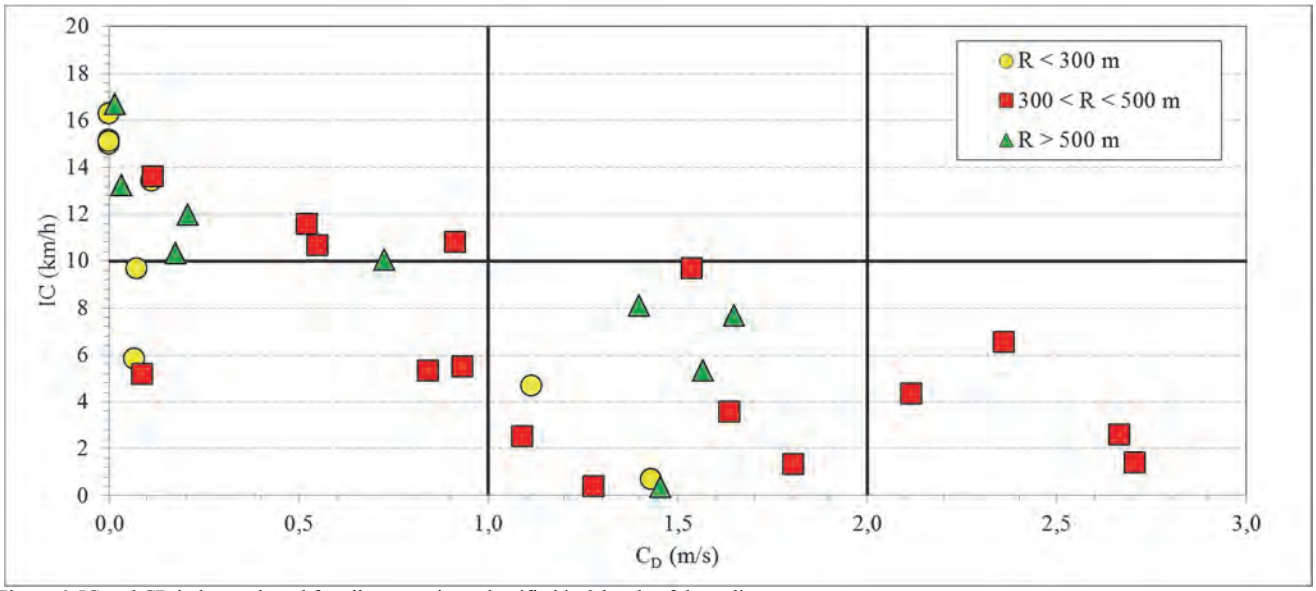


Figure 6. IC and CD indexes plotted for all test sections classified in 3 levels of the radius.
Source: The authors

5.3. Integrated Consistency assessment

From the previous discussion the following aspects can be highlighted:

- The Lam and Polus models are not equivalent but complimentary.
- The lack of equivalence is due to Lamm's model not considering the variability of the speed profile and Polus' model considering the spatial variability of the speed profile with a mean value of operating speed and not with the design speed.
- If complimentary, the consistency level obtained using both models at the same time, depends on the radius, operating speed at the entrance tangent and on the design speed.
- Although that the sample size is not enough to establishes a definitive pattern, when design speed is included in Polus' model, it is observed that both models tend to be correlated. Therefore if the consistency level is "good" according to Lamm's model, it will also be "good" according to Polus' model.

For purposes of geometrical design, the findings of this research are summarized in Fig. 7. This figure shows a generic shape of the speed profile in isolated horizontal curves and the gap between operating speed and design speed, assuming that the operating speed at the entrance

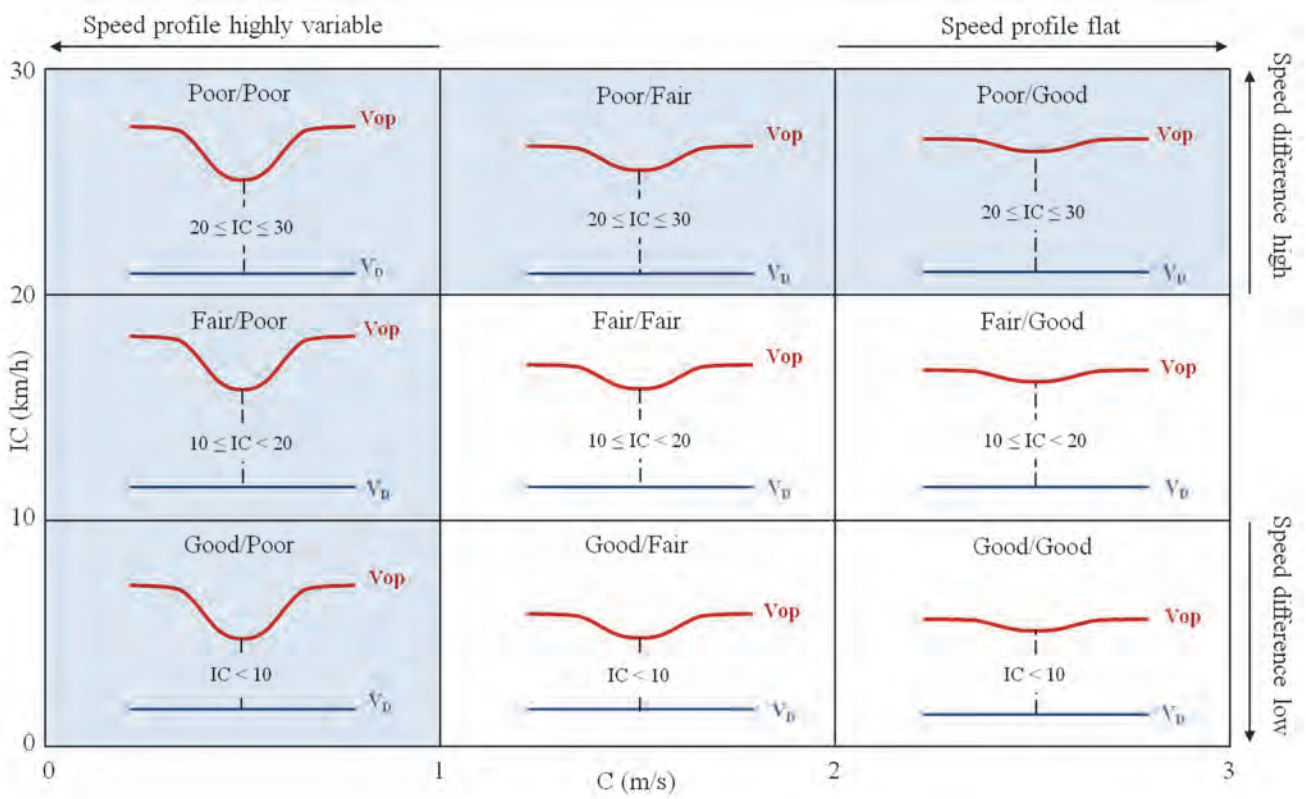


Figure 7. A generalization of operating speed profile and design speed for consistency assessment integrating Lamm's and Polus' models.
Source: The authors

tangent is high and that the driver always decelerates when entering the curve. In the figure, Vop represents the operating speed and V_D the design speed.

Fig. 7 shows that the better design (the more consistent one) is that in which the operating speed profile is flat and similar to the design speed (quadrant "Good/Good"). The worst design (least consistent) is that in which the operating speed profile is highly variable and the gap between operating speed and design speed is high (quadrant "Poor/Poor"). Other acceptable designs (slightly consistent) are those that obtain speed profiles such as the "Fair/Good", "Fair/Fair" and "Good/Fair" quadrants, in which the operating speed profile is relatively flat and the difference between operating and design speed is lower than 20 km/h. However it is recommended that in these cases the geometrical design included an advisory speed at the entrance tangent to inform drivers about the curve's lack of consistency. Other designs that promote speed profiles associated with the consistency levels "Poor/Poor", "Poor/Fair", "Poor/Good", "Fair/Poor" and "Good/Poor" are not desirable, because lack of consistency increases the risk of accident (The highlighted quadrants in Fig. 7).

6. Conclusions

This paper compared two models for consistency assessment: the Lamm's model, which estimates the consistency level using the difference between the operating and design speed; and the Polus' model, which estimates the consistency level by assessing the spatial variability of the speed profile along a road segment. The comparison was performed for 34 isolated horizontal curves on two-lane rural roads. Speed data, position and headings were obtained using a GPS device.

Lamm's model compares the operating speed with the design speed at the middle point of the curve, and this is not capable of detecting the spatial variability of the operating speed profile. On the other hand, Polus' model detects variability but is not capable of estimating the differences between operating speeds and design speeds. For this reason it was hypothesized that both models are not equivalent but complementary. The results obtained for the 34 horizontal curves studied show evidence of this assumption. Some horizontal curves were rated as "good" using Polus' model because the speed profile was flat, but at the same time were rated as "fair" using Lamm's model because the operating speeds were quite different to the design speed and vice versa.

The study also shows that if the spatial average of the operating speed is replaced by the design speed in Polus' model, coherence with Lamm's model increases. In fact, when the consistency level obtained using Polus' model is high, it is also high under Lamm's model. However, to improve Polus' model using the design speed, a recalibration of the coefficient of the C index could be necessary. As such, this finding should be studied in more detail.

The results obtained with empirical data allow us to propose a general guideline to promote consistent designs of

isolated horizontal curves, which was synthetized in a conceptual diagram that included the combination of operating speed profiles and design speed desirables associated to the geometrical design. In general, designs that promote flat operating speed profiles and are similar to designs speed are preferable to ensure that drivers can guide their vehicles along the road in an aligned manner, minimizing the possibility of making a mistake and suffering an accident. This is the essence of consistent geometrical design.

Acknowledgements

The authors thanks to the Chilean National Fund for Scientific and Technological Development (FONDECYT) for supporting the research project FONDECYT 11090029 for which this paper was written.

References

[1] Glennon, J. and Harwood, D., Highway design consistency and systematic design related to highway safety. Transportation Research Record, 682, pp. 77-88, 1978.
[2] Echaveguren, T., Altamira, A., Vargas-Tejeda, S. y Riveros, D., Criterios para el análisis de consistencia del diseño geométrico: Velocidad, fricción, visibilidad y criterios agregados, Proceedings of the Argentinean Conference on Highways and Traffic, pp. 66, 2009.
[3] Lamm, R., Choueiri, E., Hayward, J. and Paluri, A., Possible design procedure to promote design consistency in highway geometric design on two-lane rural roads. Transportation Research Record, 1195, pp. 111-122, 1988.
[4] Camacho-Torregrosa, F., Pérez-Zuriaga, A., Campoy-Ungría, J. and García, A., New geometric design consistency model based on operating speed profiles for road safety evaluation. Accident Analysis & Prevention, 61, pp. 32-42, 2013. DOI: 10.1016/j.aap.2012.10.001
[5] Polus, A. and Mattar-Habib, C., New consistency model for rural highways and its relationship to safety. Journal of Transportation Engineering, 130(3), pp. 286-293, 2004. DOI: 10.1061/(ASCE)0733-947X(2004)130:3(286)
[6] Lamm, R., Beck, A., Ruscher, T., Mailaneder, T., Cafiso, S. and La Cava, G., How to make two - lane rural roads safer. Boston: Wit Press, 2007.
[7] Echaveguren, T. and Vargas-Tejeda, S., A model for estimating advisory speeds for horizontal curves in two-lane rural roads. Canadian Journal of Civil Engineering, 40, pp. 1234-1243, 2013. DOI: 10.1139/cjce-2012-0549
[8] Echaveguren, T. and Piña, J., Determinación de límite de velocidad en curvas horizontales de caminos rurales bidireccionales, Proceedings of the Iberoamerican Conference on Road Safety, pp. 79, 2010.
[9] Polus, A., Pollatschek, M. and Mattar-Habib, C., An enhanced integrated design - consistency model for both mountainous highways and its relationship to safety. Road and Transportation Research, 14(4), pp. 13-26, 2005.
[10] Echaveguren, T., Two-lane rural highways consistency analysis using continuous operating speed measurements obtained with GPS. Revista Ingeniería de Construcción, 27(2), pp. 55-70, 2012. DOI: 10.4067/S0718-50732012000200004
[11] MOP., National highways network. Dimensions and characteristics. Chile: Ministry of Public Works, 2013.
[12] MOP., National traffic survey. Santiago, Chile, Ministry of Public Works, [Online]. 1994 – 2012. [Visited, 10th, may of 2013]. Available at: http://servicios.vialidad.cl/censo/index.htm.
[13] MOP., Proposal of maintenance operations and condition of traveled way and shoulders for paved road network. Chile: Ministry of Public Works, 2012.
[14] Echaveguren, T. and Sáez, J., Estudio de relaciones velocidad – geometría horizontal en vías de la VIII Región, Proceedings of the Congreso Chileno de Ingeniería de Transporte, pp. 341-350, 2001.
[15] Rivera, J.I. and Echaveguren, T., A hazard index for roadside of two-lane rural roads. DYNA, 81(184), pp 55-61, 2014. 10.15446/dyna.v81n184.38929
[16] Racelogic. VBOX Mini User Guide. United Kingdom: Racelogic, 2008.
[17] Arellano, D., Echaveguren, T. and Vargas-Tejeda, S., A model of truck speed profile in short upwards slopes. Proceedings of the ICE – Transport. 168(5), pp. 466-474, 2015. DOI: 10.1680/tran.13.00012.
[18] MOP. Instrucciones de Diseño. Chile: Ministerio de Obras Públicas, 1994.

D. Cárdenas-Aguilar, is a Civil Engineer from the Universidad Austral de Chile, Chile and obtained his MSc. in 2014 at the Universidad de Concepción, Chile. Since 2012 he has worked for the transport research team at the Universidad de Concepción. His field of research includes road geometrical design, GPS data analysis and road safety.
ORCID: 0000-0002-3372-9274

T. Echaveguren, is a Civil Engineer from the Universidad de Concepción and obtained his PhD in 2008 from the Pontificia Universidad Católica, Chile. From 1994 until today he has been a professor at the Universidad de Concepción in Chile. He teaches and researches in the following topics: highways geometric design, road safety and highway asset management, also in association with the Escuela de Ingeniería de Caminos de Montaña (EICAM) at the Universidad Nacional de San Juan, Argentina. He has also advised the Chilean Ministry of Public Works on their low volume road investment plan in Patagonia, and for the last four years has worked on public infrastructure concessions planning. He is currently associate professor in the Civil Engineering Department at the Universidad de Concepción, a member of the Chilean Society of Transportation Engineering, and a member of the Chilean Association of Highways and Transportation, in which is head of the road safety committee.
ORCID: 0000-0003-1632-5988

UNIVERSIDAD NACIONAL DE COLOMBIA
SEDE MEDELLÍN
FACULTAD DE MINAS



DYNA
http://dyna.medellin.unal.edu.co/

Competition between anisotropy and dipolar interaction in multicore nanoparticles: Monte Carlo simulation

Juanita Londoño-Navarro [a], Juan Carlos Riaño-Rojas [b] & Elisabeth Restrepo-Parra [c]

[a] *Facultad de Ciencias Exactas y Naturales Universidad Nacional de Colombia, Manizales, Colombia. jlondonon@unal.edu.co*
[b] *Facultad de Ciencias Exactas y Naturales Universidad Nacional de Colombia, Manizales, Colombia. jcrianoro@unal.edu.co*
[c] *Facultad de Ciencias Exactas y Naturales Universidad Nacional de Colombia, Manizales, Colombia. erestrepopa@unal.edu.co*

Received: July 5th, 2014. Received in revised form: March 1rd, 2015. Accepted: October 25th, 2015.

Abstract
Monte Carlo simulations combined with the Heisenberg model and Metropolis algorithm were used to study the equilibrium magnetic properties of magnetic multi-core nanoparticles of magnetite. Three effects were considered in this simulation: the Zeeman effect, magneto crystalline anisotropy, and dipolar interaction. Moreover, the influence of the size distribution (mean diameter and standard deviation) on the magnetization was analyzed. As an important result, a reduction of the equilibrium magnetization caused by the dipolar interaction and the magneto crystalline anisotropy was observed. On the other hand, the nanoparticle size increase produces an enhancement in the equilibrium magnetization, because of the lower influence of dipolar interaction. Cooling temperature effect was also observed, presenting a decrease in the equilibrium magnetization as the temperature was increased. The influence of the easy axis direction was studied.

Keywords: Magnetic multi-core nanoparticle, Monte Carlo, Magnetic dipolar interaction, Magneto crystalline anisotropy

Competición entre la anisotropía y la interacción dipolar en nanopartículas multi-núcleo: simulación Monte Carlo

Resumen
Se realizaron simulaciones computacionales empleando Monte Carlo combinado con el modelo de Heisenberg y el algoritmo de Metropolis con el fin de estudiar las propiedades de equilibrio magnético en nano partículas multi-núcleo de magnetita. Se consideraron tres tipos de efectos: Interacción Zeeman, anisotropía magneto cristalina e interacción dipolar. Se observó una reducción en la magnetización debido a la influencia de la interacción dipolar y la anisotropía. Se estudió el efecto de la distribución de tamaños (diámetro medio y desviación estándar) en la magnetización de las nano partículas, obteniéndose un mejor comportamiento magnético para tamaños grandes, ya que, en este caso se reduce la influencia del término de interacción dipolar. Se estudió además el efecto de la temperatura y de la dirección del eje fácil de magnetización sobre las propiedades magnéticas.

Palabras clave: Nanopartículas multi-núcleo, Monte Carlo, Interacción dipolar, Anisotropía magnetocristalina, magnetita.

1. Introduction

Nanostructures have been widely studied for several applications as semiconductors [1], cements [2] mechanics [3] and magnetics [4] among others. The use of magnetic nanoparticles in several technological applications has increased, making the experimental and theoretical investigations very important and even essential [5]. Over the past few years, the scientific community have studied the applications of nanoparticles in medicine and the most important applications have been those using nanoparticles as magnetic carriers in bio separation [6-8], drug delivery [9,10] and mediators for hyperthermia in cancer treatment [11-13]. Magnetic particles composed by several magnetic single domains, named multi-core nanoparticle (MCN), can be used in bio-medical applications [14], because of their higher particle magnetic moment compared to single-core particles containing only one or a few magnetic single domains [15]. The efficiency of the bio-medical applications based on magnetic MCN depends on the well-characterized

© The author; licensee Universidad Nacional de Colombia.

magnetic properties of these particles [8,16]. In the case of biomedical application, nanoparticles should be small in order to produce a super-paramagnetic behavior to avoid agglomeration and remain in circulation without being removed by the body's natural filters such as the liver or the immune system [15,17,18]. Magnetic multi-core nanoparticles typically have a hydrodynamic diameter of 50–200 nm containing a magnetic core consisting of a cluster of magnetite (Fe_3O_4) or magnetite (g-Fe_2O_3) single domains with a diameter of about 5–20 nm each, surrounded by a non-magnetic coating (e.g. dextranorstarch) [19,20].

There are a few theoretical works in MCN which have studied the magnetic properties of MCN [19,21-22]. Nevertheless, they have not studied the influence of different size distributions of MCN in the magnetic properties of these systems.

In this work, we carried out a numerical investigation in order to study the influence of the single-domain size distribution on the magnetic behavior of MCN systems. Monte Carlo simulation based on the Heisenberg model and Metropolis algorithm were carried out to study the MCN magnetic properties with different single-domain size distribution. The magnetic anisotropy of the single domains and the dipolar interactions between the single domains were considered and their influence on magnetization was studied. The influence of the temperature on magnetization behavior was also studied.

2. Simulations model

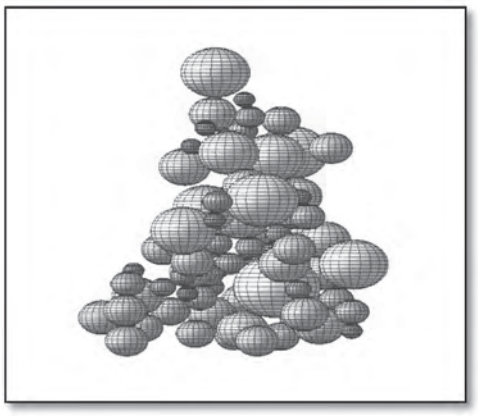
The geometry and model employed in these simulations of MCN are similar to those described by V. Schaller et al. [19]. The geometry consists in a three dimensional cluster of single domains where each domain is randomly located in a finite tree dimensional volume and is in contact with at least one neighbor in the cluster. The sizes of the single domains vary according to a log-normal distribution. Fig. 1 (a) shows a cluster of nanoparticles implemented in this work and Fig. 1(b) presents one of the log-normal distributions employed for the simulations. Each single-domain has a uniform magnetization due to the coherent rotation of the atomic moments within the single domain [23]. Hence, the magnetic moment of the single domain is represented by a classical vector with magnitude

$$|\boldsymbol{\mu_i}| = M_s V_i (1)$$

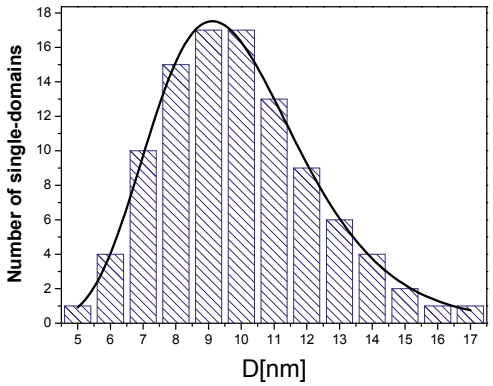
where, M_s is the intrinsic saturation magnetization and V_i is the volume of the *i-th* single domain.

The model is based on a three dimensional classical Heisenberg Hamiltonian which is described by

$$H = -\sum_i \boldsymbol{\mu_i}\cdot\boldsymbol{B} - \sum_i (K_a V_i)\left(\frac{\boldsymbol{\mu_i}}{|\boldsymbol{\mu_i}|}\cdot\boldsymbol{e_i}\right)^2 - \frac{\mu_o}{4\pi}\sum_i\left[\frac{3(\boldsymbol{\mu_i}\cdot\boldsymbol{r_{ij}})(\boldsymbol{\mu_j}\cdot\boldsymbol{r_{ij}})}{|\boldsymbol{r_{ij}}|^5} - \frac{(\boldsymbol{\mu_i}\cdot\boldsymbol{\mu_j})}{|\boldsymbol{r_{ij}}|^3}\right] \quad (2)$$



(a)



(b)

Figure 1(a). Simulated 3D cluster of 100 spherical single domains with log-normal size distribution and (b) Size distribution of 100 single domains of diameter *Dm* randomly sampled from a log-normal distribution function (solid line) with a mean diameter of 10 nm and standard deviation 2.5nm. Source: The authors

The first term describes the Zeeman energy with $\vec{B}$ as the external applied magnetic field. The second term corresponds to the anisotropy energy, where $\vec{e}_i$ as a unit is the vector along the magnetization easy axis of the single domain, and K_a is the anisotropy constant. The last term is the dipolar interaction, where μ_0 is the vacuum permeability and $\vec{r}_{ij} = \vec{r}_i - \vec{r}_j$ is a distance vector joining the centers of the two dipoles ($\vec{\mu}_i$ and $\vec{\mu}_j$). This interaction is taken into account if the distance between the single domains is less than or equal to five times the mean diameter. Further increases of the distance do not influence the simulation results for the particle [19].

Monte Carlo simulations with the standard Metropolis algorithm were used for calculating the cluster equilibrium magnetization. A first direction of $\vec{\mu}_i$ is chosen and H_1 is calculated. A random direction of $\vec{\mu}_i$ is chosen and H_2 is calculated. The difference ΔH is calculated and the new direction of $\vec{\mu}_i$ is accepted or rejected according to the Metropolis criterion [24] with the probability determined by the Boltzmann distribution factor *exp (-ΔH/K_BT)*, where K_B is

Table 1.
Values of size parameters used in the simulations.

Mean diameter (nm)	Standard deviation (nm)
6	1.7
8.8	3.5
10	2.5
19	4.5

Source: The authors

the Boltzmann constant and T is the absolute temperature. This procedure is undertaken for all the single domains. Because the MCN is in suspension in a liquid (non-magnetic coating), the rotation of the particle in the liquid must be considered in the algorithm. Then, the interaction energy between the applied magnetic field $\vec{B}$ and the total magnetic moment of the particle $\vec{\mu}_p$, defined as the vector sum of all the Nth single domains ($\vec{\mu}_p = \sum_{i=1}^{N} \vec{\mu}_i$), is calculated by

$$H_P = -\boldsymbol{\mu_p} \cdot \boldsymbol{B} \qquad (3)$$

Contrary toV. Schaller et al. [19], we calculated the energy difference ΔH_p changing the direction of $\vec{\mu}_p$. The direction of $\vec{\mu}_p$ obtained by the sum of all single domains is used to calculate H_{p1},$H_{p2}$is calculated choosing a random direction of $\vec{\mu}_p$. As explained above the new direction is accepted or rejected according to the metropolis criterion. This procedure is carried out at each Monte Carlo step (MCS).

The particle equilibrium magnetic properties are characterized by the projection of the particle magnetic moment in the direction of the applied field $\mu_B = \vec{\mu}_p \cdot \vec{B} / |\vec{B}|$ The magnetization is defined as $\langle \mu_B \rangle / V_{mag}$, where V_{mag} is the sum of the volume of all single domains and $\langle \mu_B \rangle$ is the average value [19].

Around 50000 MCS were considered in order to compute equilibrium averages. The parameter values used in our simulation were an absolute temperature $T$of 293K, an intrinsic saturation magnetization of Ms=350kA/m which is a typical value for magnetite single domains in the nanometer range at room temperature. The anisotropy constant used was $1.5x10^4 J/m^3$; these values were used by Vincent Schaller et al. [19].Three different cases of the easy axis direction were studied: random direction, the magnetic field direction and the single domain direction. All the simulations were carried out for 100 single domains and the sizes varied according to a log-normal distribution. The parameters needed to construct a log-normal distribution are the mean diameter Dm and the standard deviation σ of the single domains. In our simulations, we used different size distributions with similar values to those obtained in experimental works of magnetic nanoparticles [19, 2, 5]. These values are shown in Table 1.

3. Results and discussion

Fig. 2 presents magnetization curves for three different cases of the easy axis direction at a size distribution of Dm=6 nm and σ= 3.5 nm. An increase in the magnetization values was observed when the easy axis has the same direction of the external magnetic field. Both, magnetic field and the anisotropy produce an ordering effect in the single domains; therefore, magnetization in this case is higher than in the others. Anisotropy aligned randomly and in the single domain direction can reproduce the real behavior of MCN systems, where the easy axis of each single domain is oriented in different directions.

Figs. 3(a) and 3(b) show the influence of the anisotropy and the dipolar interaction on the magnetization depending on the applied field. Curves at room temperature (293K) for two cases of easy axis direction were obtained: at random and the external magnetic field directions.

Parameters used were Dm=8.8nm and a standard deviation σ=3.5nm; the external magnetic field direction remained constant in the x-axis. Fig. 3(a) shows the magnetic curves when the direction of the easy axis was randomly chosen. The signature of both, dipolar interaction and anisotropy effects on these systems is a reduction of equilibrium magnetization [19,22]. According to the reports [26], it must be stressed that the resulting magnetic structure depends upon the anisotropy and consequently magnetization is affected. Fig. 3(b) shows the magnetic curves when the easy axis was chosen in the magnetic field direction. In this case, the magnetic behavior is contrary to the random case, it is because the anisotropy generates an ordering in the system, and it aligns the single domains. This effect combined with the alignment generated by the magnetic field produces a higher magnetization. According to the literature, for the case of a nonzero anisotropy ($K_V \neq 0$), the magnitude of the average value of atomic spin projection onto the rotating total moment direction depends on the angle between the anisotropy axis and the direction of the total magnetic moment [27]. Regarding the dipolar interaction effect, it seems to have a poor influence on the magnetic properties. This interaction enlarges the disorder of the magnetic moments but not as simply as thermal fluctuations

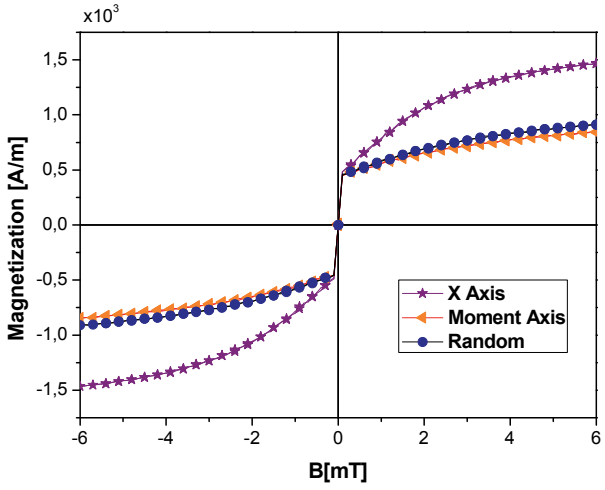


Figure 2. Magnetization curves obtained by Monte Carlo simulation for a cluster of 100 single domains, Dm 6nm, σ 1.7nm (293K), for three different easy axis directions: random, magnetic field direction and single domain direction.
Source: The authors

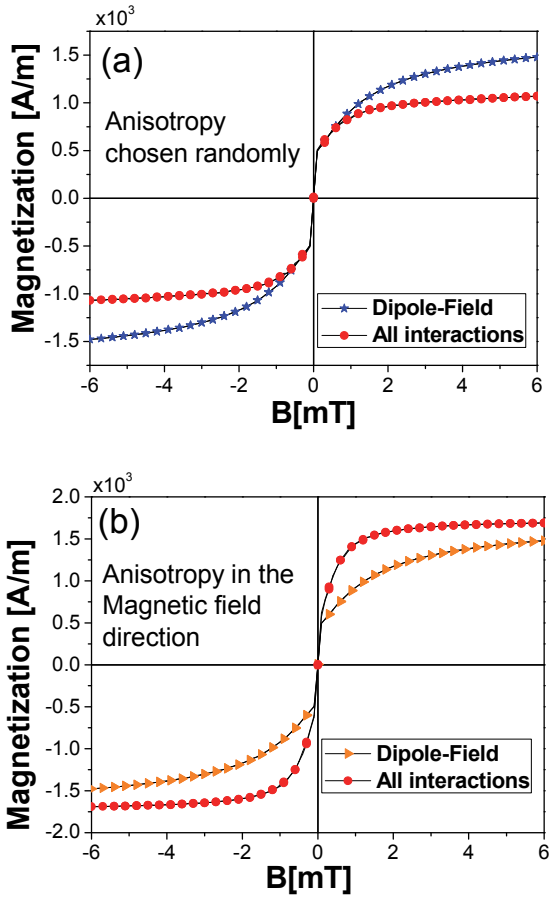


Figure 3.Magnetization curves obtained for a cluster of 100 single domains, *Dm* 8.8nm, σ 3.5nm (293K),taking in account only dipole-field interaction, and all three interactions. a) Directions of easy axes were chosen randomly. b) Directions of easy axes were chosen in the same direction as the applied magnetic field.
Source: The authors

do. Firstly, the structure of the systems—spatial arrangement and easy axis distribution—affects the energy barrier distribution and consequently affects the magnetization process; secondly, the dipolar interaction can also introduce a certain magnetic order which also gives rise to a large spread in the effective energy barrier distribution as the nanoparticles concentration increases [28].

In Fig. 4, the magnetization obtained for different size distribution is plotted as a function of the applied magnetic field. Random directions of easy axes were chosen to simulate real cases. These curve shows that the saturation magnetization decreases as the sizes of the single domains decrease. This behavior has been reported for magnetic nanoparticles in experimental works [29-31]; nevertheless it is attributed to a surface disorder in small nanoparticles due to the increased surface/volume ratio [30,32].

F. Tournus et al. [33] stated that the final moment of a nanoparticle assembly is proportional to its volume. In this work, we have represented MCN as a system composed by spherical particles with uniform magnetization, according to the Stoner and Wohlfarth model [32,34]. It means that all spins are collinear and rotate coherently without differentiating the core and surface nanoparticle components. This representation is valid for small particles and dense systems [32], hence the obtained results indicate that the reduction in the saturation magnetization is not only associated to surface disorder but also to the sizes of the single domains (MCN size). Thus, this could be due to dipolar interactions being dominant among small sized nanoparticles due to less separation between the magnetic particles. According to many experiments, substantial dipolar interactions between nanoparticles in a compacted sample (as presented here) were observed, finding evidence that the nanoparticles in dense samples are organized in a dipolar super spin-glass system [35]. Then, the super paramagnetic behavior is better observed in small particles (6nm and10nm), and when the particle size increases, the magnetic behavior tends to be ferromagnetic. The magnetite particles are ferromagnetic when they exceed the super paramagnetic limit, which is in the order of 26nm at room temperature [35]. Thus, it could be concluded that for different applications (i.e. medical interest), the nanoparticles size is highly relevant. If the nanoparticle size is lower than a critical value, the dipolar interaction increases, this being negative for the total magnetization (that decreases). On the other hand, if nanoparticle size is greater than the critical value, not only do the nanoparticle clusters tend to behave in a ferromagnetic way, but they are also difficult to transport into the body and to eliminate.

Figs. 5(a) and 5(b) show the magnetization as a function of the applied magnetic field of 100 single domains with *Dm*10nm and σ of 2.5 nm for different temperatures. Easy axes were chosen randomly. The obtained behavior in Fig. 5(a) is consistent with the expected; as the temperature increases, the magnetization exhibits a slight increment. The small reduction in the magnetization is due to the small disorder caused by the temperature in the orientation of the single-domain magnetic moments that presents a competition with the magnetic field. Given that one of the most important applications of these nanoparticles is in medicine—as they are inserted into biological organisms—Fig. 5(b) shows the magnetization curve for temperatures close to the human

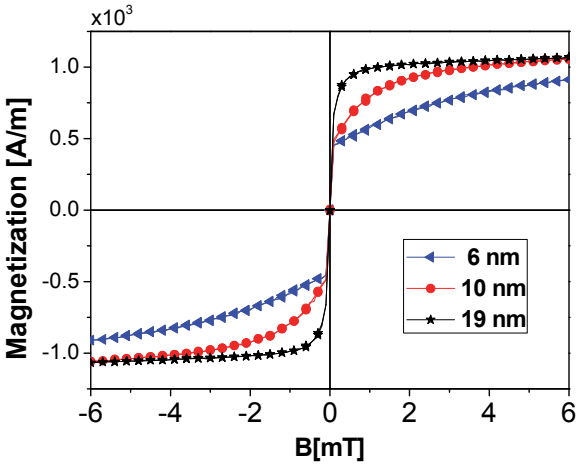


Figure 4.Magnetization curves of different size distributions. All curves were simulated at 293K, easy axes were chosen randomly.
Source: The authors

body temperature. This behavior allows us to observe that the multicore nanoparticles exhibit a super paramagnetic behavior presenting almost the same magnetization, this being a suitable characteristic for medical applications in the human body.

4. Conclusions

The magnetic properties of MCN were studied using Monte Carlo simulations combined with the Metropolis Algorithm. In agreement with previous works, a reduction in the equilibrium magnetization was observed as a consequence of dipolar interaction and anisotropy The magnetization behaviour of different size distributions was studied, observing that the reduction in size of the nanoparticles produces a decrease in the saturation magnetization, caused by the increase in the dipolar interaction. The influence of the temperature on the magnetization was also studied, finding that temperature generates a disorder in the system causing a reduction in the magnetization. It was also found that for temperatures close to the human body temperature, the magnetic behaviour of MCN does not change.

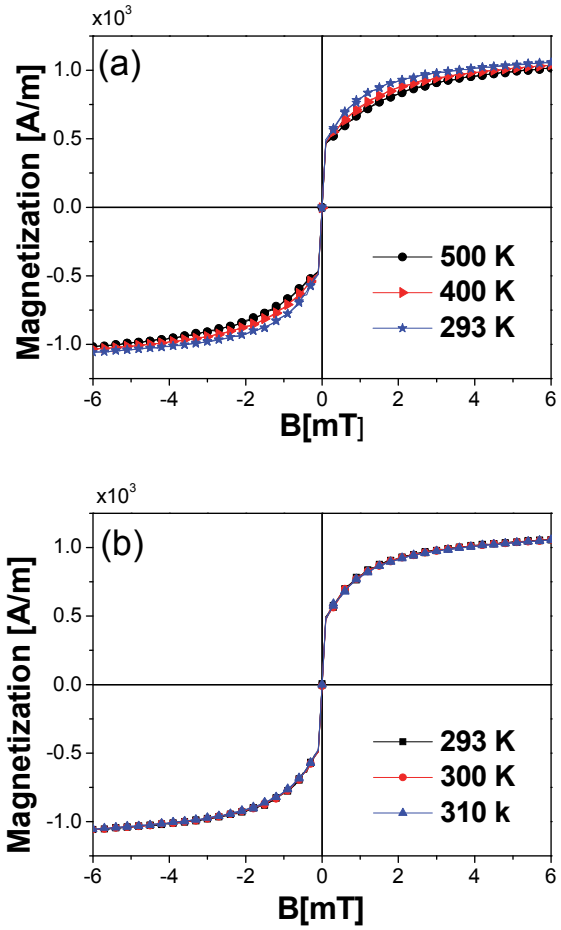


Figure 5 Magnetization curves of 100 singledomains with *Dm*10 nm and σ=2.5 nm for different temperatures a) 293K, 300K and 500K. b) Temperatures close to the human body temperature 293K, 300K and 310K. Source: The authors

The influence of the easy axis direction in the magnetization behaviour was studied, and it was found that the random direction decreases the magnetic behaviour generating a disorder in the system. The magnetization increased when the easy axis was chosen in the same direction as the applied magnetic field; in this case, the anisotropy increased the magnetic ordering in the system, in contrast to the random case.

Acknowledgments

The authors gratefully acknowledge the financial support of the Dirección Nacional de Investigaciones at Universidad Nacional de Colombia during the course of this research, under project 12920 “Desarrollo teórico-experimental de nanoestructuras basadas en Bismuto y materiales similares” approved by the Convocatoria Nacional de Investigación I Creación Artística de la Universidad Nacional de Colombia 2010-2012

References

[1] Raba-Paez, A.M., Suárez, D.N., Martínez, J.J., Rojas-Sarmiento, H.A. and Rincón-Joya, M., Pechini method used in the obtention of semiconductor nanoparticles based niobium, DYNA, 82(189), pp. 52-58, 2015. DOI: 10.15446/dyna.v82n189.42036

[2] Tobón, J.I, Restrepo-Baena, O.J. y Payá-Bernabeu, J.J., Adición de nanopartículas al cemento Portland, DYNA, 74(152), pp. 277-291, 2007.

[3] Gallego, J., Sierra-Gallego, G., Daza, C., Molina, R., Barrault, J., Batiot-Dupeyat, C. and Mondragón, F., Production of carbon nanotubes and hydrogen by catalytic ethanol decomposition, DYNA, 80(178), pp. 78-85, 2013.

[4] Jiménez-Pérez, J.L., Sánchez-Ramírez, J.F., Correa-Pacheco, Z.N., Cruz-Orea, A., Chigo-Anota, E. and Sánchez-Sinencio, F., Thermal characterization of solutions containing gold nanoparticles at different pH values. Int J Thermophys, 34, pp. 955-961, 2013. DOI: 10.1007/s10765-012-1372-0

[5] Lan, T.N. and Hai, T.H., Monte Carlo simulation of magnetic nanoparticle systems, Computational Materials Science, 49, pp. S287-S290, 2010. DOI: 10.1016/j.commatsci.2010.01.025

[6] Sieben, S., Bergemann, C., Lübbe, A., Brockmann, B. and Rescheleit D., Comparison of different particles and methods for magnetic isolation of circulating tumor cells, Journal of Magnetism and Magnetic Materials, 225, pp. 175-179, 2001. DOI: 10.1016/S0304-8853(00)01248-8

[7] Adolphi, N.L., Huber, D.L., Jaetao, J.E., Bryant, H.C., Lovato, D.M., Fegan, D.L., Venturini, E.L., Monson, T.C. and Tessier, T.E., Hathaway, H. J., Bergemann, C., Larson, R. S. and Flynn E. R. Characterization of magnetite nanoparticles for SQUID-relaxometry and Magnetic Needle Biopsy, Journal of Magnetism and Magnetic Materials, 321, pp. 1459-1464, 2009. DOI: 10.1016/j.jmmm.2009.02.067

[8] Schaller, V., Kräling, U., Rusu, C., Petersson, K., Wipenmyr, J., Krozer, A., Wahnström, G., Sanz-Velasco, A., Enoksson, P. and Johansson, C. Motion of nanometre sized magnetic particles in a magnetic field gradient, Journal of Applied Physic,. 104, pp. 093918-093932, 2008. DOI: 10.1063/1.3009686

[9] Steinfeld, U., Pauli, C., Kaltz, N., Bergemann, C. and Lee, H.H., T lymphocytes as potential therapeutic drug carrier for cancer treatment, International Journal of Pharmaceutics, 311, pp. 229-236, 2006. DOI: 10.1016/j.ijpharm.2005.12.040

[10] Yang, J., Lee, C.H., Park, J., Seo, S., Lim, E.K., Song, Y.J., Suh, J.S., Yoon, H.G., Huh, Y.M. and Haam S., Antibody conjugated magnetic PLGA nanoparticles for diagnosis and treatment of breast cancer, Journal of Materials Chemistry, 17, pp. 2695-2699, 2007. DOI: 10.1039/B702538F

[11] Kettering, M., Winter, J., Zeisberger, M., Bremer-Streck, S., Oehring, H., Bergemann, C., Alexiou, C., Hergt, R. and Halbhuber, K., Magnetic nanoparticles as bimodal tools in magnetically induced labelling and magnetic heating of tumor cells: An in vitro study, Nanotechnology, 18, pp. 175101, 2007. DOI: 10.1088/0957-4484/18/17/175101

[12] Dutz, S., Clement, J.H., Eberbeck, D., Gelbrich, T., Hergt, R., Muller, R., Wotschadio, J. and Zeisberger M., Ferrofluids of magnetic multicore nanoparticles for biomedical applications, Journal of Magnetism and Magnetic Materials, 321, pp. 1501-1504, 2009. DOI: 10.1016/j.jmmm.2009.02.073

[13] Kallumadil, M., Tada, M., Nakagawa, T., Abe, M., Southern, P. and Pankhurst, Q.A., Suitability of commercial colloids for magnetic hyperthermia, Journal of Magnetism and Magnetic Materials, 321, pp. 1509-1513, 2009. DOI: 10.1016/j.jmmm.2009.02.075

[14] Dutz, S., Kettering, M., Hilger, I., Müller, R., and Zeisberger, M., Magnetic multicore nanoparticles for hyperthermia –influence of particle immobilisation in tumour tissue on magnetic properties, Nanotechnology, 22, pp. 265102, 2011. DOI: 10.1088/0957-4484/22/26/265102

[15] Pankhurst, Q.A., Connoly, J., Jones, S.K. and Dobson, J., Applications of magnetic nanoparticles in biomedicine, Journal of Physics D: Applied Physics, 36, pp. R167-R181, 2003. DOI: 10.1007/978-0-387-85600-1_20

[16] Astalan, A.P., Johansson, C., Petersson, K., Blomgren, J., Ilver, D., Krozer, A. and Johansson, A., Magnetic response of thermally blocked nanoparticles in a pulsed magnetic field, Journal of Magnetism and Magnetic Materials, 311, pp. 166-170, 2007. DOI: 10.1016/j.jmmm.2006.10.1182

[17] Chomoucka, J., Drbohlavova, J., Huska, D., Adam, V., Kizek, R. and Hubalek, J. Magnetic nanoparticles and targeted drug delivering, Pharmacological Research, 62, pp. 144-149, 2010. DOI: 10.1016/j.phrs.2010.01.014

[18] Balakrishnan, S., Bonder, M.J. and Hadjipanayis, G.C., Particle size effect on phase and magnetic properties of polymer-coated magnetic nanoparticles, Journal of Magnetism and Magnetic Materials, 321, pp. 117-122, 2009. DOI: 10.1016/j.jmmm.2008.08.055

[19] Schaller, V., Wahnström, G., Sanz-Velasco, A., Enoksson, P. and Johansson, C., Monte Carlo simulation of magnetic multi-core nanoparticles, Journal of Magnetism and Magnetic Materials, 321, pp. 1400-1403, 2009. DOI: 10.1016/j.jmmm.2009.02.047

[20] Tartaj, P., del-Puerto-Morales, M., Veintemillas-Verdaguer S., Gonzales-Carreño, T. and Serna C.J., The preparation of magnetic nanoparticles for applications in biomedicine, Journal of Physics D: Applied Physics, 36, pp. R182-R197, 2003.

[21] Weddemann, A., Auge, A., Kappe, D., Wittbracht, F. and Hütten A., Dynamic simulations of the dipolar driven demagnetization process of magnetic multi-core nanoparticles, Journal of Magnetism and Magnetic Materials, 322, pp. 643-646, 2010. DOI: 10.1016/j.jmmm.2009.10.031

[22] Schaller, V., Wahnström. G., Sanz-Velasco, A., Gustafsson, S., Olsson, E., Enoksson, P. and Johansson, C., Effective magnetic moment of magnetic multicore nanoparticles, Physical Review B, 80, pp. 092406, 2009. DOI: 10.1103/PhysRevB.80.092406

[23] Bean, C.P. and Livingston, J.D., Superparamagntism, Journal of Applied Physics, 30, pp. 120S-129S, 1959. DOI: 10.1063/1.2185850

[24] Metropolis, N., Rosenbluth, A.W., Rosenbluth, M.N., Teller, A.H. and Teller, E., Equation of state calculations by fast computing machines, Journal of Chemical physics, 21, pp. 1087-1092, 1953. DOI: 10.1063/1.1699114

[25] Balakrishnan, S., Bonder, M.J. and Hadjipanayis G.C., Particle size effect on phase and magnetic properties of polymer-coated magnetic nanoparticles, Journal of Magnetism and Magnetic Materials, 321, pp. 117-122, 2009. DOI: 10.1016/j.jmmm.2008.08.055

[26] Mazo-Zuluaga, J., Restrepo, J. and Mejía-López, J., Surface anisotropy of a Fe3O4 nanoparticle: A simulation approach, Physica B, 398, pp. 187-190, 2007. DOI: 10.1016/j.physb.2007.04.070

[27] Kokorina, E.E. and Medvedev, M.V., Magnetization curves of nanoparticle with single-ion uniaxial anisotropy, Journal of Magnetism and Magnetic Materials, 310, pp. 2364-2366, 2007. DOI: 10.1016/j.jmmm.2006.11.107

[28] Mao, Z., Chen, D. and He Z., Equilibrium magnetic properties of dipolar interacting ferromagnetic nanoparticles, Journal of Magnetism and Magnetic Materials, 320, pp. 2335-2338, 2008. DOI: 10.1016/j.jmmm.2008.04.118

[29] Nishio, K., Ikeda, M., Gokon, N., Tsubouchi, S., Narimatsu, H., Mochizuki, Y., Sakamoto, S., Sandhu, A., Abe, M. and Handa, H., Preparation of size-controlled (30–100 nm) magnetite nanoparticles for biomedical applications, Journal of Magnetism and Magnetic Materials, 310, pp. 2408-2410, 2007. DOI: 10.1016/j.jmmm.2006.10.795

[30] Gonzalez-Fernandez, M.A., Torres, T.E., Andrés-Vergés, M., Costo, R., de-la-Presa, P., Serna, C.J., Morales, M.P., Marquina, C., Ibarra, M.R. and Goya, G.F., Magnetic nanoparticles for power absorption: Optimizing size, shape and magnetic properties, Journal of Solid State Chemestry, 182, pp. 2779-2784, 2009. DOI: 10.1016/j.jssc.2009.07.047

[31] Salado, J., Insausti, M., Gil-de-Muro, I., Lezama, L. and Rojo, T., Synthesis and magnetic properties of monodisperse Fe3O4 nanoparticles with controlled sizes, Journal of Non-Crystalline Solids, 354, pp. 5207-5209, 2008. DOI: 10.1016/j.jnoncrysol.2008.05.063

[32] Papaefthymiou G.C., Nanoparticle magnetism, Nano Today, 4, pp. 438-447, 2009. DOI: 10.1016/j.nantod.2009.08.006

[33] Tournus, F. and Tamion, A., Magnetic susceptibility curves of a nanoparticle assembly II. Simulation and analysis of ZFC/FC curves in the case of a magnetic anisotropy energy distribution, Journal of Magnetism and Magnetic Materials, 323, pp. 1118-1127, 2011. DOI: 10.1016/j.jmmm.2010.11.057

[34] Petracic, O., Superparamagnetic nanoparticle ensembles, Superlattices and Microstructures, 47, pp. 569-578, 2010. DOI: 10.1016/j.spmi.2010.01.009

[35] Nadeem, K., Krenn, H., Traussnig, T., Würschum, R., Szabo, D.V. and Letofsky-Papst, I., Effect of dipolar and exchange interactions on magnetic blocking of maghemite nanoparticles, Journal of Magnetism and Magnetic Materials, 323, pp. 1998-2004, 2011. DOI: 10.1016/j.jmmm.2011.02.041

E. Restrepo-Parra, completed her BSc. Eng in Electrical Engineering in 1990 at the Universidad Tecnológica de Pereira, her MSc. degree in Physics in 2000, and PhD. degree in Automation Engineering in 2009, both at Universidad Nacional de Colombia, Manizales, Colombia. From 1991 to 1995, she worked in the Colombian electrical sector and since 1996 for the Universidad Nacional de Colombia. Currently, she is a senior Professor in the Physics and Chemistry Department, Facultad de Ciencias Exactas y Naturales, Universidad Nacional de Colombia – Sede Manizales. Her research interests include: simulation and modeling of materials properties by several methods; Materials processing by plasma assisted technique and materials characterization. She is currently the director of the Laboratories at the Manizales campus of Universidad Nacional de Colombia.
ORCID 0000-0002-1734-1173

J. Riaño-Rojas, completed his BSc. in Mathematics in 1993, his MSc degree in Mathematics in 1998 and his PhD. in Automation Engineering in 2010 at Universidad Nacional de Colombia. Currently, he is a full professor in the Mathematics and Statistics Department, Facultad de Ciencias Exactas y Naturales, Universidad Nacional de Colombia, Manizales, Colombia. His research interests include: simulation and modeling of materials properties by several methods, among others. He is currently the director of PCM Computational Applications research group at Universidad Nacional de Colombia.
ORCID 0000-0002-5719-2854

J. Londoño-Navarro, completed hers BSc. Eng. in Physical Engineering in 2011 at Universidad Nacional de Colombia, Manizales, Colombia. She is currently finishing a MSc degree in Physics at the same university. Her research interests include: simulation and modeling of materials properties by several methods, among others.
ORCID 0000-0001-6165-0160

UNIVERSIDAD NACIONAL DE COLOMBIA
SEDE MEDELLÍN
FACULTAD DE MINAS



DYNA
http://dyna.medellin.unal.edu.co/

Broad-Range tunable optical wavelength converter for next generation optical superchannels

Andrés F. Betancur-Pérez [a], Ana Maria Cárdenas-Soto [b] & Neil Guerrero-González [c]

[a] *Facultad de Ingeniería, Universidad de Antioquia, Colombia. andresfbp@gmail.com*
[b] *Facultad de Ingeniería, Universidad de Antioquia, Colombia. ana.cardenas@udea.edu.co*
[c] *Photonic Systems Group, Tyndall National Institute, Ireland. neil.gonzalez@tyndall.ie*

Received: September 11th, 2014. Received in revised form: June 1rd, 2015. Accepted: July 8th, 2015.

Abstract
A broad-range tunable all optical wavelength conversion scheme that is based on a dual driven Mach-Zehnder modulator with an integrated microwave generator to tune the channel spacing along the entire C band, is proposed. Successful signal demodulation up to 8 wavelength conversions, in steps of 50-400 GHz of 100 Gbps Nyquist QPSK channels with configurable channel spacing is reported. The proposed wavelength conversion scheme enables flexible wavelength routing on gridless optical networks, as can be seen in the Superchannels with a BER lower than 10^{-13}.

Keywords: Comb generator; elastic networks; Nyquist QPSK; superchannels; wavelength conversion.

Conversor de longitud de onda óptico sintonizable de banda ancha para la siguiente generación de supercanales ópticos

Resumen
En esta investigación se propone un esquema de conversión de longitud de onda netamente óptico sintonizable y de banda ancha usando como dispositivo de conversión un modulador Mach-Zehnder junto con un generador de microondas para sintonizar el espaciamiento entre canales a lo largo de la banda C. Se reporta una demodulación exitosa de hasta 8 conversiones de longitud de onda, en pasos desde 50-400GHz de canales en formato Nyquist QPSK de 100Gbps con espaciamiento entre canal configurable. El esquema de conversión de longitud de onda propuesto habilita el enrutamiento flexible de longitudes de onda en redes ópticas con grilla espectral no fija, tal y como se puede observar en los Supercanales con una tasa de error de bit más baja que 10^{-13}.

Palabras clave: Conversion de longitud de onda; generador de Comb; Nyquist QPSK; redes elásticas; supercanales.

1. Introduction

With the increasing demand for information on the Internet, the next generation of optical high capacity telecommunication systems is expected to work with multiple sets of highly dense subcarriers in the frequency domain or "Superchannels", which are capable of transporting information in Terabits per second. A Superchannel is a set of several optical subcarriers combined to create a channel of desired capacity. Every subcarrier is modulated with advanced modulation formats that can be reconfigured according to the underlying demand on the network [1-4]. The capacity that will provide the optical Superchannels also presents new challenges to design and develop the next generation of optical telecommunication systems. Generally, these technological challenges can be summarized in two points: a) The optimal use of the telecommunication network resources to manage the available bandwidth in an efficient way (e.g. wavelength routing) and b) the upgrade of deployed networks (10G, 40G and recently 100G).

In order to enable devices, with a capability to correctly process the optical multicarrier signals, the emerging technology should lead to four main technologies for optical Superchannels [5-8]: a) Optical subcarrier generation spaced very close in the frequency domain (in the order of the transmission bitrate value), b) optical multilevel modulation of each subcarrier using advanced modulation, c) digital detection and demodulation employing the coherent detection techniques and d) reconfigurable optical devices that work with flexible spectral grids (*gridless spectrum*).

© The author; licensee Universidad Nacional de Colombia.

Among the optical devices that should be used for the Superchannels to function is the wavelength converter with the capability to work with a flexible spectral grid. This device is very important in making it possible for the wavelength to be reused and to prevent collisions among channels with common wavelengths. The wavelength converter should have the following characteristics: No modulation format dependence, C band operation, low signal distortion, low cost and processing must be all optical in order to decrease network latency. Several wavelength conversion techniques using SOAs (*semiconductor optical amplifiers*) and MZI (*Mach-Zehnder Interferometer*) have been demonstrated in the scientific literature [9-10], using intensity modulated signals with a 40Gbps bitrate. However, these techniques require continuous wave probe lasers to perform the conversion of each wavelength in the context of the Superchannels. On the other hand, the SOA by itself has a non-uniform gain and presents a polarization dependent gain, which results in an amplitude distortion of the pulses and Chirp, which limits the reach of the optical link. Nowadays, the wavelength conversion is performed before the modulation, obtaining the signal and using it to modulate the converted optical carrier provided by a tunable optical source (laser). This method of conversion requires optical-electrical-optical (*OEO*) transformations that add delays in the network and consume additional energy.

In this paper we propose a novel all-optical wavelength converter (AO*WC*) for advanced modulation signals along 32 nm of the C band. This proposed optical device is a critical component, which makes the easy reconfiguration of the optical network possible, taking into account the available resources such as bandwidth, wavelengths and routes. The presented wavelength converter avoids the need for OEO transformations and it can be employed as a subcarrier repeater (*e.g. broadcast transmission*). In order to configure the channel spacing, the proposed device makes use of a broad-range tunable microwave generator (TMWG) to change the spacing size. This TMWG has the advantage that, with only two optical sources, we can make a wavelength conversion for every optical subcarrier in the superchannel due to refractive index dependence with the electric field in the $LiNbO_3$, which allows the same RF tone generated on parallel Mach Zehnder modulators to be used. In this paper, we demonstrate a wavelength converter that works with different channel spacing (*until 400GHz*) for Nyquist-*Quadrature Phase Shift Keying* (QPSK) () signals for 100Gbps (*50GBaud/s*) transmission rates with maximum degradations of the *Bit Error Rate* (BER*)* in the order of 10^{-10}.

The working principle of the wavelength converter is presented in the first section of the paper. Later, the experimental setup and the simulation parameters are described in order to discuss the results analysis of the proposed wavelength converter, and, finally we present our conclusions. This proposed wavelength converter opens the doors to new flexible wavelength conversion techniques for the next generation of adaptive optical networks.

2. AOWC working principle

The proposed wavelength converter is based on the Optical Frequency Comb (OFC), a key system element, shown in Fig. 1. The OFC generation is designated in the literature as the optical mechanism that generates a set of carriers from only one laser with have characteristics such as: high coherence, low noise, stability, simple operation, and great spectral flatness (i.e. power fluctuations among optical subcarriers) [11]. The OFC output spectrum is a set of copies of the original modulated optical signal, but it is located in different wavelengths. The set of the modulated optical signals shifted in the wavelength domain, pass through a bandpass tunable optical filter that will allow the passage of the desired optical signal, as it is shown in Fig. 1. The result is the same input signal as the AOWC but it is located in the desired channel. The filtered optical signal is demodulated by the receiver by means of coherent detection, with an optical local oscillator tuned to the same wavelength as the converted signal.

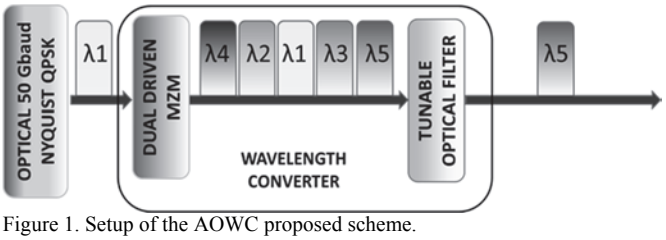


Figure 1. Setup of the AOWC proposed scheme.
Source: Author Andrés F. Betancur Pérez

Among the techniques used to generate multiple optical carriers from one single source are: The spectral slicing broadband light source [12], the FWM (Four Wave Mixing) technique [13,14], the ultrashort pulses generation technique [15] and the MZMs [16]. These techniques intend to reduce both the use of several optical sources in the telecommunication networks and reduce costs by using a single laser. The OFCG-MZM is attractive because it offers several characteristics described previously such as high coherence, stability, and simple operation. However, the characterization of the wavelength conversion of modulated optical signals based on MZMs has not been either proved or tested.

The OFCG with MZM, implemented according to Fig. 2a, obeys an electro-optic phase modulation with a RF tones, as can be seen in the equation 2. The expressions 1 and 2 show that the modulation index βi is adjusted if the amplitude of the RF signals (VRFi) are modified, and if the Vbiasi applied to the arms of the MZM is altered, the phase of each side band can be varied [17]. On the end side of the MZM, the spectrum of each arm is superposed and every side band is added constructively or destructively in certain quantity, depending on the phase of each side band. In this way, the spectral flatness can be improved if different amplitude and bias are applied to each arm of the MZM.

$$\beta_i = \pi \frac{V_{RFi}}{V_\pi} \tag{1}$$

$$E_o(t) = \frac{f(t)}{2} \sum_{k=-\infty}^{\infty} \begin{bmatrix} J_k(\beta_1) e^{-i(k\omega_m t + \theta_1(VBias_1)} \\ + J_k(\beta_2) e^{-i(k\omega_m t + \theta_2(VBias_2)} \end{bmatrix} \tag{2}$$

$$E_o(\omega_0) = \frac{1}{2} \sum_{k=-\infty}^{\infty} \begin{bmatrix} J_k(\beta_1) F(\omega_0 - k\omega_m) e^{-i\theta_1(VBias_1)} \\ + J_k(\beta_2) F(\omega_0 - k\omega_m) e^{-i\theta_2(VBias_2)} \end{bmatrix} \tag{3}$$

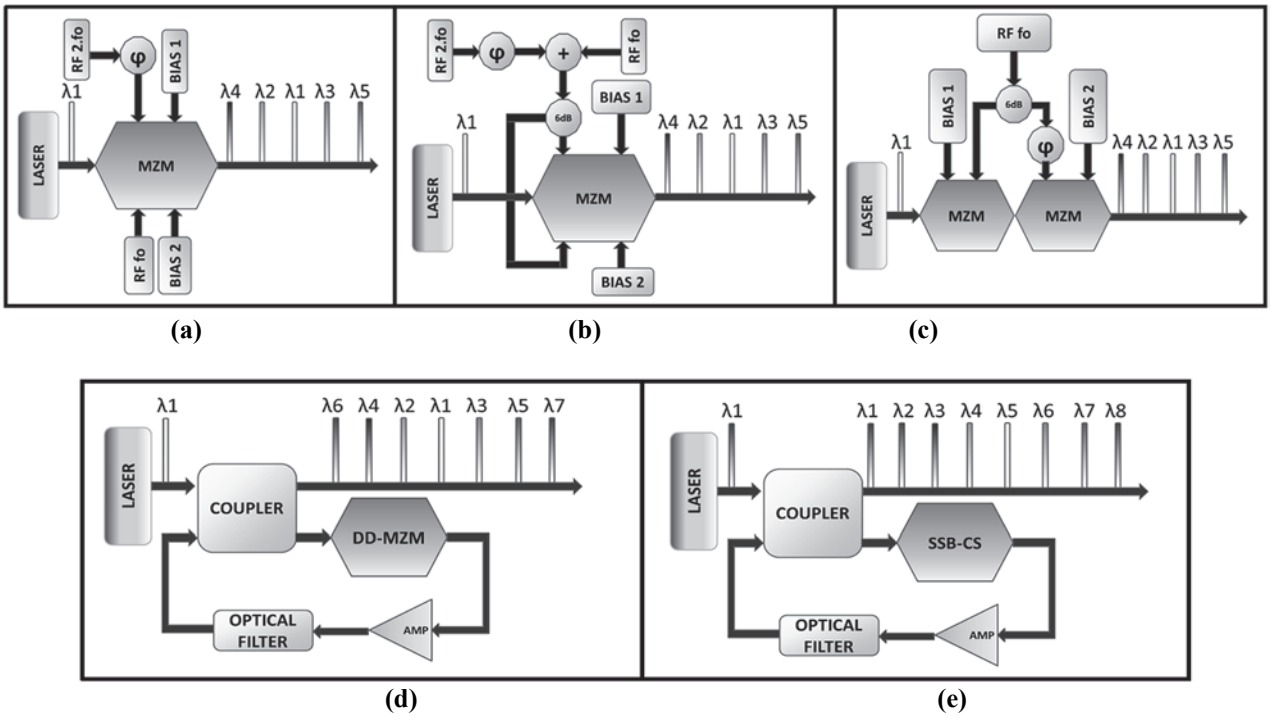


Figure 2. Comb generator techniques: (a) DD-MZM, (b) DD-MZM with Diplexer, (c) two cascaded MZM, (d) DD-MZM with fiber loop, (e) SSB-CS with fiber loop
Source: Andrés F. Betancur Pérez

Where:
f(t): Input modulated optical signal with center frequency ω_c.
V_π: Induced voltage in which the phase of the optical electric field in the MZM reaches 180°.
ω_m: Angular frequency of the RF tone.
θ_1: Phase induced by the polarization on arm 1.
θ_2: Phase induced by the polarization on arm 2.
β_1: Modulation Index related to RF tone amplitude on arm 1.
β_2: Modulation Index related to RF tone amplitude on arm 2.
F(ω): The Fourier transform of f(t).
k: Order of Bessel function

The Fourier transform in equation 2 can be appreciated in expression 3 where $\omega_0=\omega-\omega_c$. This equation shows that countless side bands are created according to the Bessel functions; however, the power decreases as the frequencies of the side bands go away from the central frequency.

There are several OFCG-MZM techniques with or without feedback, as can be seen in the Fig. 2 [17]. Fig. 2(a), 2(b), and 2(c) show some examples of open loop OFCG-MZM. In Fig. 2(a) a dual driven Comb generator (*DD-MZM*) is described and two Radio Frequency (RF) signals are used, the frequency of one being double that of the other. The phase and amplitude of the RF signals are different as is the bias of each arm of the MZM. In the Fig. 2(b), one similar configuration is appreciated with the difference being that each arm of the MZM is operated with two combined RF sinusoidal signals with frequencies of f_o and $2f_o$. This method adds the diplexer device to generate the comb. In Fig. 2(c) the setup of two cascaded MZMs can be visualized. In this method, the operation of each MZM is carried out with the same RF frequency; however, each one is separately biased. The amplitude and the phase of the RF signals that are used to operate each MZM are different.

Moreover, there are techniques to generate combs with MZMs using fiber loops. One of them uses the same DD-MZM setup and a fiber loop with an optical amplifier (Fig. 2(d)), and the other technique (Fig. 2(e)) uses the same optical loop and two parallel MZMs configured to make SSB-CS modulation (*Single Side Band Modulation with Carrier Suppression*). These methods add more complexity but can create more optical carriers by taking the generated components to the MZMs' input and repeating the process. The new spectral components create more optical carriers, and in every lap the new components interfere with each other adding or subtracting the amplitude, depending on each spectral component phase [18,19].

An implementation based on feedback loop techniques presents impairments as interference among channels is caused by the fiber loop. This is because, in every lap, the signals have conversions that also generate new ones, due to the interference between the incoming signals and the previous ones. The interference is possible because the RF tone produces the same channel spacing between each spectral component, increasing the symbol error rate with the number of laps. Even if the SSB-SC is used, the same problem still exists as there is no total side band suppression or carrier suppression. Hence, side bands remain with enough power spectral density to be a considerable noise, just as is illustrated in Fig. 3.

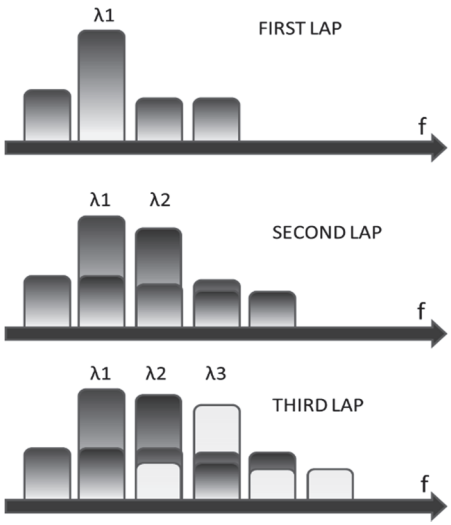


Figure 3. Problem experienced using Conversion based in Comb generation technique with SSB-CS and feedback loop
Source: Andrés F. Betancur Pérez

The OFCG scheme used is the configuration that can be seen in Fig. 2a. It is used because of its simple operation, low complexity, and its cost effectiveness. The other configurations add more complexity and generate just one or two more subcarriers, which result in a non-reliable cost-benefit ratio.

In order to generate new wavelength conversions to cover most of the C band, it is desirable to generate high RF tone frequencies up until 400 GHz in order to create the same channel spacing value between conversions. According to the state of the art for electronics there is no shown capacity shown to generate such frequencies; consequently, another approach should be taken into account in order to overcome this limitation. The proposed model to generate frequencies higher than 100 GHz is based on the schemes used in radio over fiber (*RoF*) systems [20] to generate millimeter wave signals using two optical sources in which one of them is tunable and the other has a fixed frequency. With the quadratic characteristic of the photodetector we could generate RF tones with a frequency equal to the difference of the two optical source frequencies. In the next section, we demonstrate our technique to generate RF tones in the range of 10 GHz to 400 GHz.

3. AOWC model setup

In Fig. 4, the general scheme of the back-to-back implementation carried out using VPI simulation software can be seen. It can be divided in three stages: The DD-MZM, the tunable optical filter and the coherent receiver.

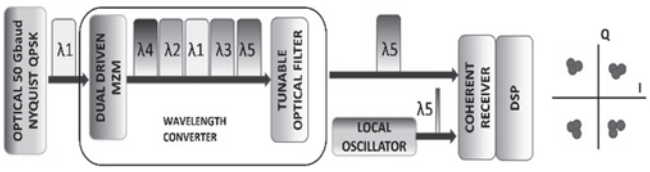


Figure 4. General simulation setup
Source: Andrés F. Betancur Pérez

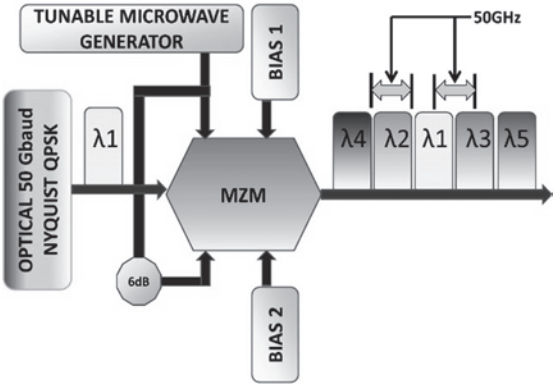


Figure 5. Setup dual driven MZM
Source: Andrés F. Betancur Pérez

3.1. DD-MZM based converter

The proposed system is based on the MZM setup in dual drive operation that is shown in Fig. 5. It has equal RF operation frequencies in both arms and different amplitudes (0.5V and 1V) on each arm, the modulation indexes of which are different because each arm is biased in different operating points.

The optical source is a 193.1THz optical carrier, with 20mW of power that is modulated externally by Nyquist. Its pulses are generated with a raised cosine filter with a roll off factor equal to 1, it has a QPSK format and a 100 Gbps bit rate (50GBaud/s). The MZM has values of $V\pi$ y V_{RF} equal to 1V [21] and an extinction ratio of 25dB. One arm of the MZM is operated with a RF tone with an amplitude equal to 0.5V and biased to 0.4V. The other arm is operated with an RF tone amplitude of 1V and biased with 0V. The RF tones are generated with a tunable microwave generator (TMWG).

The TMWG setup was configured according to the scheme illustrated in Fig. 6. The fixed Laser has a frequency of 193.1THz. Both lasers have linewidth of 1 KHz and a power of 20 mW to get a RF sine wave as pure as possible at the output of the TMWG. The optical carriers are injected to a coupler and the mixed wavelengths are detected by a photodiode APD with a 1A/W responsivity, 2nA dark current, 100 multiplicative factor, 1 ionization coefficient and a 10^{-12} A/Hz thermal noise of. The quadratic characteristic of the photodiode generates an electric current at a frequency equal to the difference between the frequencies of the optical sources. The detected electrical signal is filtered by a bandpass filter to reduce the noise, and it is then applied to the MZM. This method has great benefits such as: high integration (the AOWC can be made on a single chip), and it can be easily controlled by other systems with electric signals that can be useful in adaptive optical networks.

The MZM output signal is a set of channels where eight of them possess a low BER degradation and channel spacing equal to the generated frequency on the TMWG, as can be seen in the scheme illustrated in Fig. 5. Every channel has the same information as the original input signal.

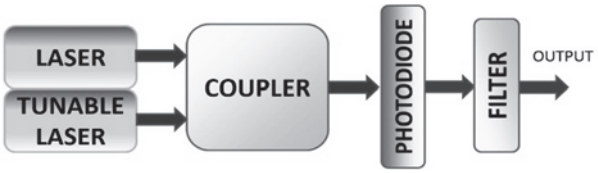


Figure 6. Setup tunable microwave generator
Source: Andrés F. Betancur Pérez

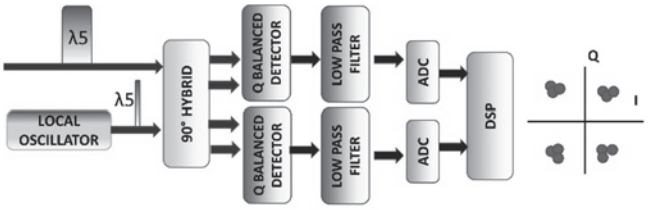


Figure 7. Coherent detection scheme
Source: Andrés F. Betancur Pérez

3.2. Tunable Optical Filter

The optical signal is then filtered by a tunable bandpass Gaussian optical filter, the central frequency of which is tuned to the central frequency of each generated channel, allowing the wavelength conversion process. In our tests, the filter was tuned every 50 GHz and 400 GHz around the original channel (193.1THz) depending on the frequency spacing caused by the wavelength conversion process. The bandwidth of the filter is 0.9 fold the baudrate and it has a Gaussian order equal to 9 in order to obtain the desired channel. Nowadays, an optical filter that has tunable bandwidth and central frequency without deformation of its frequency response at speeds in the order of microseconds functions as the liquid crystal filter. At this rate, the wavelength conversion process is limited to offline applications.

3.3. Coherent Receiver

In Fig. 7, the scheme of the coherent receiver is illustrated. The signal is detected with a coherent receiver with a local oscillator tuned to the central frequency of each detected channel and with a power equal to 1mW. The photodetectors in the balanced detectors are PIN with a responsivity of 1A/W and thermal noise equal to 10^{-11} A/Hz. The lowpass electrical filter of the receiver has a Bessel transfer function of order 4, with a bandwidth of 0.75 fold the baudrate (37.5GHz). In the DSP (*Digital Signal Processor*) a BER estimation is performed assuming a Gaussian probability density function with a mean and variance equal to that of the signal samples. For such purpose, the logical channels are used to obtain the bit sequence sent by the transmitter.

4. Analysis of results

The spectrum obtained at the output of the AOWC is illustrated in Fig. 8. The tunable microwave generator was tuned to get a RF tone with frequencies of 50 GHz and 400 GHz in order to obtain the respective channel spacing. In this way, the location of the converted channels, according to the variable channel spacing suggested by the elastic optical networks (channel spacing, multiples of 12.5GHz), can be configured.

The minimum obtained BER (see Table 1) was in the order of 10^{-150} for the channel located on 193 THz. This corresponded to channel 4 for a 50GHz channel spacing; however, the BER was related to the variable power among the channels, the more power the converted signal, the less

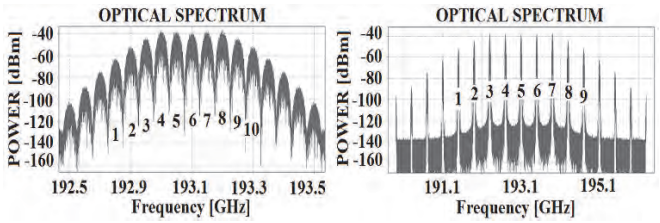


Figure 8. Optical spectrum: On the left 50 GHz spacing. On the Right 400 GHz spacing
Source: Andrés F. Betancur Pérez

the BER. This is due to the optical signal power decreasing when the digital signal is phase modulated and because the power of each channel follows the pattern imposed by the Bessel functions inducing intensity variations compared with the original signal. The power variations on every converted channel must be equalized and amplified in order to level all the Superchannels at the output. The advantage of the Nyquist pulse format is its reduced spectrum compared to the pulses with NRZ (Non Return to Zero) format [22]. Moreover, Nyquist pulses belong to the Superchannel systems because it is desired that every subcarrier is tightly separated with a minimum channel spacing equal to the bit rate. In each spectrum, the peak power reduction of each channel with respect to the average input power (20dBm) can be seen; this effect is caused by the power distribution of the main optical channel among the generated side bands. This is a product of the OFCG modulation process, which gives multiple converted frequency options. Table 1 contains a summary of the BER for every converted channel option of the AOWC that was implemented. The BER of the channel 10 for 50GHz channel spacing is the biggest, but it may be recovered with FEC techniques after propagation through optical fiber in an adaptive optical network.

The calculated constellation diagrams in the coherent receiver output can be seen in Fig. 9. How the acquired points deviate around the original decision point is shown on the left. The standard deviation is greater in 194.7THz than in the original operation frequency (i.e. 193.1THz) because the OSNR (Optical Signal to Noise Ratio) is reduced in this channel.

To visualize the wavelength conversion effect over the QPSK signal, Fig. 10 illustrates the optical eye diagram of the AOWC input signal and the optical eye diagram of channel 9 (194.7THz) when a 400 GHz RF tone is used. The result when there is a wavelength conversion by means MZM is reduced power on each channel compared to the input signal. This effect impacts the eye pattern, closing it. However, the information on the phase transitions can still be detected as the wavelength converter is transparent to this modulation format.

Table 1.
(a) BER for 400GHz channel spacing,

Channel #	Frequency [THz]	BER
1	191.5	5.337e-15
2	191.9	2.508e-55
3	192.3	1.04e-112
4	192.7	1.352e-106
5	193.1	3.737e-101
6	193.5	4.504e-108
7	193.9	1.529e-112
8	194.3	1.819e-55
9	194.7	5.472e-15

(b) BER for 50GHz channel spacing

Channel #	Frequency [THz]	BER
1	192.85	2.955e-13
2	192.9	1.876e-52
3	192.95	8.618e-104
4	193.0	4.581e-150
5	193.05	5.634e-83
6	193.1	1.327e-49
7	193.15	1.700e-136
8	193.2	6.584e-83
9	193.25	3.386e-22
10	193.3	5.438e-10

Source: Andrés F. Betancur Pérez

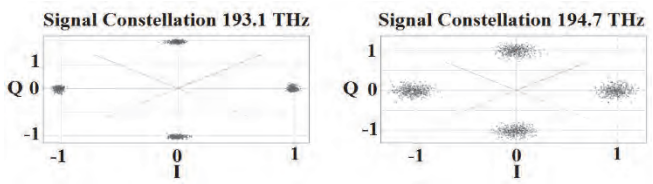
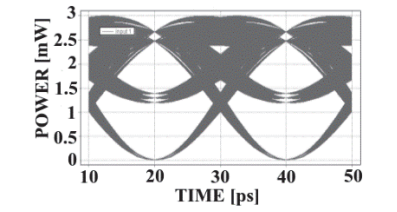
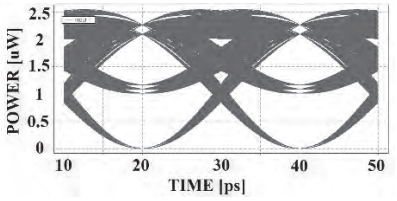


Figure 9. Constellations: On the left 193.1 THz. On the right 194.7 THz
Source: Andrés F. Betancur Pérez



(a)



(b)

Figure 10. Optical eye patterns: (a) Input of the WS. (b) Output of the WS on 194.7 THz
Source: Andrés F. Betancur Pérez

5. Conclusions

A method for wavelength conversion without OEO transformations that is based on the MZM comb generation scheme without feedback was presented. Eight copies or subchannels were generated and spaced according to the tunable microwave tone generator, with the same as the original modulated optical signal as a central frequency value. The BER was reduced as low as 10^{-150} (error free), and this is due to the low noise present in the simulated back-to-back system. However, to evade a link that is limited by transmission power or attenuation, the processed optical signal in the wavelength converter must be amplified and equalized to get enough power and a flat spectrum in order to launch the optical subcarriers over the optical link or lightpath.

A satisfactory demodulation scheme for each one of the converted optical signals in the spectrum was presented, demonstrating a good performance of the proposed converter. Covering almost the entire C band of the standard single mode fiber was possible thanks to the tunable microwave generator that can generate RF tones until 400GHz. This functional block has the advantage of being integrated in a single photonic chip. This conversion has the characteristic of being transparent to the Nyquist QPSK modulation format. The method for wavelength conversion of modulated optical signals opens doors to photonic routing research for future elastic networks.

Acknowledgments

We would like to thank to Antioquia University, and specifically, the CODI (Comite para el Desarrollo de la Investigación), which supported us in our research project with code MDC 11-1-04. Sostenibilidad 2014 Project.

References

[1] Klekamp, A., Dischler, R. and Buchali, F., Limits of spectral efficiency and transmission reach of optical-OFDM superchannels for adaptive networks. IEEE Photonics Technology Letters, 23(20), pp. 1526-1528, 2011. DOI: 10.1109/LPT.2011.2161979

[2] Bosco, G., Curri, V., Carena, A., Poggiolini, P. and Forghieri, F., On the performance of nyquist-WDM terabit superchannels based on PM-BPSK, PM-QPSK, PM-8QAM or PM-16QAM subcarriers. Journal of Lightwave Technology, 29(1), pp. 53-61, 2011. DOI:10.1109/JLT.2010.2091254

[3] INFINERA. Super-Channels DWDM transmission beyond 100Gb/s. White paper, [Online]. 2011. Available at: http://www.infinera.com/pdfs/whitepapers

[4] Dischler, R., Buchali, F., Klekamp, A., Idler, W., Lach, E., Schippel, A., Schneiders, M., Vorbeck, S. and Braun, R.-P., Terabit transmission of high capacity multiband OFDM superchannels on field deployed single mode fiber, ECOC, pp. 1-3, 2010. DOI: 10.1109/ECOC.2010.5621258

[5] Tomkos, I., Palkopoulou, E. and Angelou, M., A survey of recent developments on flexible/elastic optical networking, 14th International Conference on Transparent Optical Networks (ICTON), 2012, pp. 1-6. DOI: 10.1109/ICTON.2012.6254409

[6] Colavolpe, G., Foggi, T., Forestieri, E. and Prati, G., Robust multilevel coherent optical systems with linear processing at the receiver. Journal of Lightwave Technology, 27(13), pp. 2357-2369, 2009. DOI: 10.1109/JLT.2008.2008821

[7] Van den Borne, D., Alfiad, M., Jansen, S.L. and Wuth, T., 40G/100G long-haul optical transmission system design using digital coherent receivers, 14th OptoElectronics and Communications Conference OECC, 2009, pp.1-2. DOI: 10.1109/OECC.2009.5214277

[8] Gerstel, O., Jinno, M., Lord, A. and Yoo, S.JB., Elastic optical networking: A new dawn for the optical layer?. Communications Magazine, IEEE, 50(2), pp. s12-s20, 2012. DOI: 10.1109/MCOM.2012.6146481

[9] Cao, B., Shea, D.P. and Mitchell, J.E., Wavelength converting optical access network for 10Gbit/s PON, 15th International Conference on Optical Network Design and Modeling (ONDM), 2011, pp. 1-6.
[10] Nguyen, A., Porzi, C., Pinna, S., Contestabile, G. and Bogoni, A., 40Gb/s all-optical selective wavelength shifter, Conference on Lasers and Electro-Optic (CLEO), 2011, pp. 1-2.
[11] Apex Technologies. Ultra high resolution OSA/OCSA for characterizing and evaluating optical frequency comb sources. White paper [Online]. 2013. Available at: http://www.apex-t.com/optical-frequency-comb/
[12] Pendock, G.J. and Sampson, D.D., Transmission performance of high bit rate spectrum-sliced WDM systems. Journal of Lightwave Technology, 14(10), pp. 2141-2148, 1996. DOI: 10.1109/50.541201
[13] Sefler, G.A. and Kitayama, K.-I., Frequency comb generation by four-wave mixing and the role of fiber dispersion. Journal of Lightwave Technology, 16(9), pp. 1596-1605, 1998. DOI: 10.1109/50.712242
[14] Takahashi, M., Hiroishi, J., Tadakuma, M. and Yagi, T., FWM wavelength conversion with over 60nm of 0dB conversion bandwidth by SBS-suppressed HNLF, Optical Fiber Communication Conference, 2009, pp. 1-3.
[15] Avrutin, E.A., Ryvkin, B.S., Kostamovaara, J. and Portnoi, E.L., Analysis of symmetric and asymmetric broadened-mode laser structures for short and ultrashort optical pulse generation, ICTON, 2010, pp. 1-4. DOI: 10.1109/ICTON.2010.5549074
[16] Mishra, A.K., Nellas, I., Tomkos, I., Koos, C., Freud, W. and Leuthold, J., Comb generator for 100Gbit/s OFDM and low-loss comb-line combiner using the optical inverse Fourier Transform (IFFT). ICTON, 2011, pp. 1-5. DOI: 10.1109/ ICTON.2011.5971034
[17] Puerto-Leguizamón, G.A., Suarez-Fajardo, C.A., Analytical model of signal generation for radio over fiber systems, DYNA, 81(188), pp. 26-33, 2014.
[18] Kawanishi, T., Sakamoto, T., Shinada, S. and Izutsu, M., Optical frequency comb generator using optical fiber loops with single-sideband modulation. IEICE Electronics Express, 1(8), pp. 217-221. DOI: 10.1587/elex.1.217
[19] Morohashi, I., Sakamoto, T., Yamamoto, N., Kawanishi, T., Hosako, I. and Sotobayashi, H., Broadening of comb bandwidth by multiple modulation using feedback loop in Mach-Zehnder-Modulator-Based flat comb generator, Microwave Photonics MWP IEEE Topical Meeting, 2010, pp. 220-223. DOI: 10.1109/MWP.2010.5664165
[20] Zhang, W. and Yao, J., Photonic generation of milimeter-wave signals with tunable phase shift. IEEE Photonics Journal, 4(3), pp. 889-894, 2012. DOI: 10.1109/MWP.2012.6474049
[21] Ding, J., Chen, H., Yang, L., Zhang, L., Ruiqiang, J., Tian, Y., Zhu, W., Lu, Y., Zhou, P. and Min, R., Low-voltage, high-extinction-ratio, Mach-Zehnder silicon optical modulator for CMOS-compatible integration. Optics Express, 20(3), pp. 3209-3218, 2012. DOI: 10.1364/OE.20.003209
[22] Torres-Nova, J. M. y Paz-Penagos, H., Estudio y comparación en eficiencia espectral y probabilidad de error de los esquemas de modulación GMSK y DBPSK, Ingeniería e Investigación, 28(3), pp. 75-80, 2008.

A.F. Betancur-Pérez, is Electronic Engineer from the Universidad de Antioquia, Colombia. He received his MSc in Telecommunications Engineering in 2014from the Universidad de Antioquia, Colombia. Currently, he is professor of telecommunications engineering and gives courses such as digital signal processing and optical communications, and is an associated researcher in the Instituto Tecnológico Metropolitano - ITM, Medellín, Colombia.
ORCID: 0000-0002-4738-8052

A.M. Cárdenas-Soto, obtained her PhD. in 2003 from the Universidad Politécnica de Valencia, Spain. She worked in planning and design of telecommunication infrastructure in 1994-2005, at Empresas Públicas de Medellín – EPM, Medellín; Colombia, and as a professor in 2005-2009, at the Universidad Pontificia Bolivariana, Medellín, Colombia. She currently works at the Universidad de Antioquia, Medellín, Colombia. Her research interests are optical elastic networks and optical spectrum engineering.
ORCID: 0000-0001-9152-8246

N. Guerrero-Gonzalez, is a postdoctoral researcher, has a BSc. Electronic Engineer degree in 2005 and a MSc. in industrial automation in 2007, both from the Universidad Nacional de Colombia, Medellín, Colombia. He completed his PhD. degree in Photonics Engineering in 2011, from the Technical University of Denmark (DTU). During March and August 2011, Neil was associated as a postdoctoral researcher to DTU - Fotonik under the FP7 European framework project CHRON. He has been also associated with Huawei Technologies (Munich, Germany) in 2012 as an optical engineer and with CPqD (Campinas, Brazil) between 2013 and 2014 as manager of the division of optical communication systems. Currently he is associated as a postdoctoral researcher to the Photonic Systems Group at Tyndall National Institute. His research interests include coherent optical communication, digital signal processing and hybrid fiber-wireless communication systems.
ORCID: 0000-0002-8053-6280
ResearchID: E-7356-2015

UNIVERSIDAD NACIONAL DE COLOMBIA
SEDE MEDELLÍN
FACULTAD DE MINAS

Área Curricular de Ingeniería Eléctrica e Ingeniería de Control

Oferta de Posgrados

Maestría en Ingeniería - Ingeniería Eléctrica

Mayor información:

E-mail: ingelcontro_med@unal.edu.co
Teléfono: (57-4) 425 52 64

UNIVERSIDAD NACIONAL DE COLOMBIA
SEDE MEDELLÍN
FACULTAD DE MINAS



DYNA
http://dyna.medellin.unal.edu.co/

Numerical analysis of the influence of sample stiffness and plate shape in the Brazilian test

Martina Inmaculada Álvarez-Fernández [a], Celestino González-Nicieza [b], María Belén Prendes-Gero [c], José Ramón García-Menéndez [d], Juan Carlos Peñas-Espinosa [e] & Francisco José Suárez-Domínguez [f]

[a] *Departamento de Explotación y Prospección de Minas, Universidad de Oviedo, Oviedo, Asturias, España. inma@git.uniovi.es*
[b] *Departamento de Explotación y Prospección de Minas, Universidad de Oviedo, Oviedo, Asturias, España. celes@git.uniovi.es*
[c] *Departamento de Construcción e Ingeniería de Fabricación, Universidad de Oviedo, Gijón, Asturias, España. belen@git.uniovi.es*
[d] *Departamento de Explotación y Prospección de Minas, Universidad de Oviedo, Oviedo, Asturias, España. juan@git.uniovi.es*
[e] *Departamento de Explotación y Prospección de Minas, Universidad de Oviedo, Oviedo, Asturias, España. penasjc@ocacp.es*
[f] *Departamento de Construcción e Ingeniería de Fabricación, Universidad de Oviedo, Gijón, Asturias, España. paco@constru.uniovi.es*

Received: September 19th, 2014. Received in revised form: August 6th, 2015. Accepted: September 24th, 2015.

Abstract
Due to the heterogeneity of rocks, their tensile strength is around 10% of their compressive strength, which means that breakage is mainly caused by tensile stress. The measure of tensile stress is very difficult due to rock fragility, so it has usually been measured by indirect measurement methods , including the Brazilian test. However, recent works indicate that the tensile strength values obtained through the Brazilian test must be increased by almost 26%.
To understand this divergence, indirect tensile tests have been monitored. The aim is to know the material deformation and load increase by means of stepwise regression. Stress fields in slightly deformed samples are analyzed and modeled (3D finite differences) with loads applied on flat and curved plates and different Young's modulus. Finally, the results are analyzed and compared with strength values reported using Timoshenko theory and Hondros' approximation.

Keywords: Brazilian test; test monitoring; numerical simulation.

Análisis numérico de la influencia de la dureza de la muestra y la forma de placa en el ensayo Brasileño

Resumen
La heterogeneidad de las rocas hace que su fuerza tensora sea un 10% de su fuerza de compresión provocando roturas principalmente por tensión. Sin embargo la resistencia a tensión es muy dificil de medir debido a la fragilidad de la roca, por lo que normalmente se emplean métodos de medida indirecta entre los que destaca el ensayo Brasileño. Sin embargo trabajos recientes indican que este ensayo reduce en un 26% los valores de resistencia.
Para entender esta divergencia, se han monitorizado ensayos de tensión indirecta. El objetivo es conocer la deformación del material y la carga discontinua incrementada. Se han analizado y modelado los campos de tensión de muestras ligeramente deformadas mediante cargas aplicadas en platos curvos y planos y con diferentes Módulos de Young. Los resultados se analizan y comparan con los valores obtenidos con la Teoría de Timoshenko y la Aproximación de Hondros.

Palabras clave: Ensayo Brasileño; ensayo de monitorización; simulación numérica.

1. Introduction

Rocks and artificial materials are not generally homogeneous and contain numerous micro-cracks, show anisotropy and grain-matrix resistance differences, this meaning that the tensile strength is lower than the compressive strength. Most of the efforts have been focused in calculate the compression strength of the materials [1,2], but rock breakage is mainly due to its low tensile strength (approximately 10% of its compressive strength).

© The author; licensee Universidad Nacional de Colombia.

Great efforts have been focused on determining rock tensile strength. However, due to rock fragility, no direct tensile tests can be completed, so techniques developed until now have always been focused on the development of indirect measurement methods.

In 1971 Mellor & Hawkes [3] thoroughly researched the Brazilian test, also known as the diametrical compressive test. As a result, they presented a formula that allows rock tensile strength to be calculated. Several years later, the International Society of Rocks Mechanics (ISRM), proposed that the Brazilian test be made the standard method to determine rock tensile strength [4]. Due to the ease of its implementation, this method has been widely adopted in many fields and countries over the last 20 years. For instance, China included it among its engineering regulations in the 1980s [5], as well as in State regulations and specifications for water storage and hydroelectric power in 1999 and 2001 [6,7]. The Brazilian test, although with slight variations, is currently applied to measure tensile strength in concrete [8], rock materials [9], concrete and ceramic materials [10], pharmaceutical materials [11], and other fragile materials.

For the tensile test, a testing sample extracted from the material to be analyzed is used. This sample can be of either disc or cube-shaped; however, the disc-shaped type is more widely used since probes are easy to obtain and it demands almost no mechanizing. According to the literature [3-7], the disc diameter usually ranges from 48 to 54 mm, and the disc thickness-radius ratio ranges from 0.5 mm to 1 cm.

Some researchers have recently completed works on the Brazilian test [12], proposing new formulae to estimate tensile strength, starting with the formula contributed by Timoshenko & Goodier [13]. Yong et al. [14] and Yong et al. [15] completed their correction of the test by maximizing the initial expression with a coefficient which, in the first work, depends on disc shape and dimensions and, in the second, depends on the sample's Poisson coefficient. In both cases, the coefficient is obtained by numerical simulations with finite 3D elements. The result is increase of over 26% and 30%, respectively. Jonsen et al. [16] obtain 25% higher tensile results. These authors consider experimental methods and fracture energy in compressed materials (pressed metal powders). Other authors such as Jianhong et al. [17] make an estimate for the rock tensile elastic module and propose a formula based on the tensile strength in rocks obtained from the Brazilian test. Es-Saheb et al. [18] analyze, by means of finite elements, the influence of materials such as flat grounds and soft pads on stress distribution. It seems clear that the current trend considers a higher tensile strength value than that obtained with the Brazilian test.

To be able to understand variation in tensile strength values and, more precisely, the tendency that started last years to consider values over 20% of those obtained in Brazilian tests, numerous indirect tensile tests have been monitored. This monitoring is aimed at observing how materials deform throughout time and under increasing loading values. Once this behavior is analyzed, the values are calculated and modeled by means of 3D finite differences with loads applied on flat and curved plates and with varying Young's modulus. Finally, results are analyzed and compared to the strengths obtained with the Timoshenko theory and Hondros' approximation.

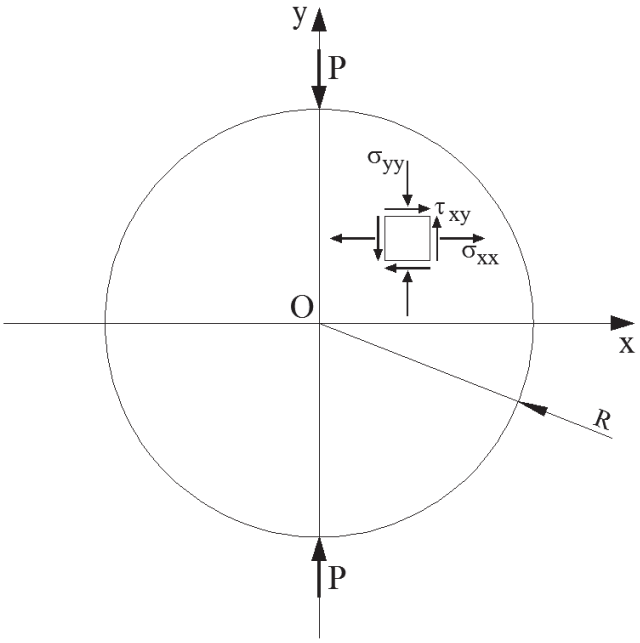


Figure 1. Test of diametrical compression by "points" loads.
Source: Álvarez Fernández et al.

2. Methods

2.1. Stress fields in diametrical compression by "points" loads

Diametrical compression by "points" loads involves a tensile stress perpendicularly to the compressed diameter which depending on the theory followed- holds sensitively constant in a wide-enough area of the disc center [8,11]. Under these conditions and applying Timoshenko theory, the stress fields at all points in a disc with radius R, thickness t, and subjected to actual loads of magnitude P in extreme points within the same diameter (Fig. 1) [13,19] are given by:

$$\begin{cases} \sigma_{xx}(x,y) = Q\left[\dfrac{1}{2R} - x^2\left(R_1^*(x,y) + R_2^*(x,y)\right)\right] \\ \sigma_{yy}(x,y) = Q\left[\dfrac{1}{2R} - \left(R-y\right)^2 R_1^*(x,y) - \left(R+y\right)^2 R_2^*(x,y)\right] \\ \tau_{xy}(x,y) = Qx\left[\left(R-y\right) R_1^*(x,y) - \left(R+y\right) R_2^*(x,y)\right] \end{cases} \quad (1)$$

Where:

$$Q = \frac{2P}{\pi t}$$

$$R_1^*(x,y) = \frac{R-y}{\left[x^2 + \left(R-y\right)^2\right]^2} \quad (2)$$

$$R_2^*(x,y) = \frac{R+y}{\left[x^2 + \left(R+y\right)^2\right]^2}$$

Eq. (1) allows for stresses to be obtained n along axes x eq. (3) and y eq. (4) by annulling variable y or x, respectively.

$$\begin{cases} \sigma_{xx}(x,0) = Q\left[\dfrac{1}{2R} - \dfrac{2x^2R}{\left(x^2+R^2\right)^2}\right] \\ \sigma_{yy}(x,0) = Q\left[\dfrac{1}{2R} - \dfrac{2R^3}{\left(x^2+R^2\right)^2}\right] \\ \tau_{xy}(x,0) = 0 \end{cases} \quad (3)$$

$$\begin{cases} \sigma_{xx}(0,y) = \dfrac{Q}{2R} = \dfrac{P}{\pi Rt} \\ \sigma_{yy}(0,y) = Q\left[\dfrac{1}{2R} - \dfrac{2R}{R^2-y^2}\right] \\ \tau_{xy}(0,y) = 0 \end{cases} \quad (4)$$

In eq. (4), the horizontal stress is deduced to be constant along the vertical diameter and vertical line to tend to infinite in the extreme points of the diameter. Likewise, in eq. (1), the strengths at the disc center can be deduced equaling variables x and y to zero:

$$\sigma_{xx}(0,0) = \frac{P}{\pi Rt};\ \sigma_{yy}(0,0) = -\frac{3P}{\pi Rt} = -3\sigma_{xx} \quad (5)$$

Disc center stresses eq. (5) show that upon breakage, vertical compressive stress is three times higher than horizontal tensile stress. If the Mohr's circle corresponding to this stress state is drawn, and considering that breakage occurs at the point of the circle tangent which is on the envelope of Fig. 2, an error in estimating the tensile strength would be made. This error would be around 40%, but yes, the side of safety.

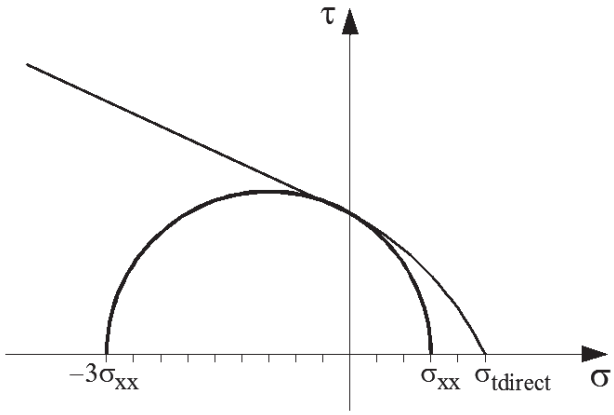


Figure 2. Tensile breakage in the Brazilian test.
Source: Álvarez Fernández et al.

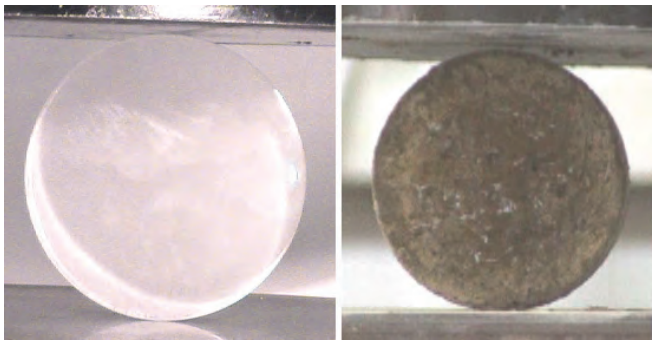


Figure 3. Tensile test monitoring: onset.
Source: Álvarez Fernández et al.

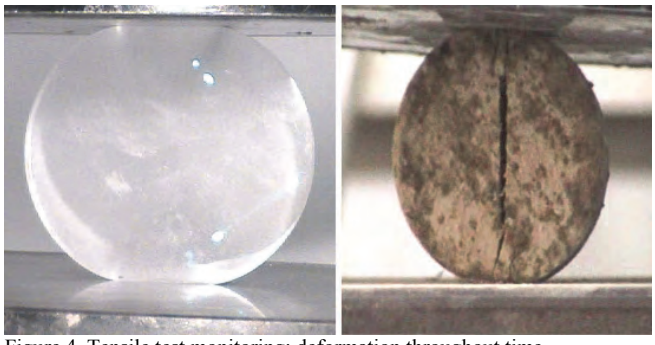


Figure 4. Tensile test monitoring: deformation throughout time.
Source: Álvarez Fernández et al.

To understand what happens in an indirect stepwise tensile test, numerous indirect tensile tests have been monitored. 50 mm diameter samples with approximately the same thickness as the sample radius were used in all tests and tensile stresses was applied at a speed of approximately 200 N/s [20].

Fig. 3 shows the onset of a test on methacrylate (left-hand) and concrete (right-hand) samples, while Fig. 4 shows deformation throughout time. The methacrylate test is not exactly a Brazilian test since it changes from tensile to simple compressive, yet this work is reported because it allows clear observation of the deformation process throughout time. These tests allow for it to be deduced that in the earliest moments of the test (Fig. 3), samples present linear contact with the machine's clamps along a generatrix. However, an increased applied load leads to sample deformation and transforms initially linear contact into superficial contact, that is until breakage occurs (Fig. 4).

Therefore, the initial linear diameter compressive defined by Timoshenko [11] occurs, and as time goes by and load increases, compression is applied on horizontal strips, similar to yet slightly different from Hondros' approximation [8]. This considers that contact occurs on 2α amplitude curved areas.

2.2. Field of compressive stresses by loads on diametrically opposed arches

The application of Hondros' theory gives rise to stress fields along the horizontal and vertical diameters, defined by eq. (6), (7), respectively Fig. 5.

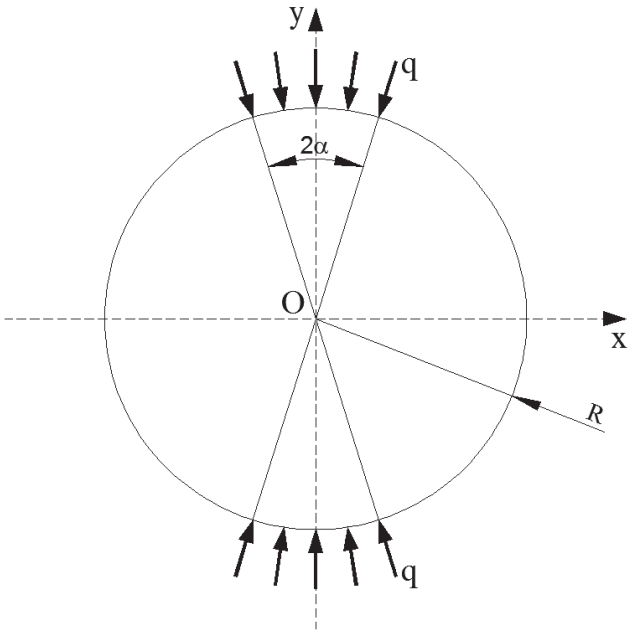


Figure 5. Compression on diametrically opposed arches.
Source: Álvarez Fernández et al.

$$\begin{cases} \sigma_{xx}(x,0) = \dfrac{2q}{\pi}\left[\dfrac{\left(1-\dfrac{x^2}{R^2}\right)\cdot\sin 2\alpha}{1+\dfrac{2x^2}{R^2}\cos 2\alpha+\dfrac{x^4}{R^4}} - arctg\left(\dfrac{1-\dfrac{x^2}{R^2}}{1+\dfrac{x^2}{R^2}}\cdot tg\alpha\right)\right] \\ \sigma_{yy}(x,0) = -\dfrac{2q}{\pi}\left[\dfrac{\left(1-\dfrac{x^2}{R^2}\right)\cdot\sin 2\alpha}{1+\dfrac{2x^2}{R^2}\cos 2\alpha+\dfrac{x^4}{R^4}} + arctg\left(\dfrac{1-\dfrac{x^2}{R^2}}{1+\dfrac{x^2}{R^2}}\cdot tg\alpha\right)\right] \\ \tau_{xy}(x,0) = 0 \end{cases} \quad (6)$$

$$\begin{cases} \sigma_{xx}(0,y) = \dfrac{2q}{\pi}\left[\dfrac{\left(1-\dfrac{y^2}{R^2}\right)\cdot\sin 2\alpha}{1-\dfrac{2y^2}{R^2}\cos 2\alpha+\dfrac{y^4}{R^4}} - arctg\left(\dfrac{1+\dfrac{y^2}{R^2}}{1-\dfrac{y^2}{R^2}}\cdot tg\alpha\right)\right] \\ \sigma_{yy}(0,y) = -\dfrac{2q}{\pi}\left[\dfrac{\left(1-\dfrac{y^2}{R^2}\right)\cdot\sin 2\alpha}{1-\dfrac{2y^2}{R^2}\cos 2\alpha+\dfrac{y^4}{R^4}} + arctg\left(\dfrac{1+\dfrac{y^2}{R^2}}{1-\dfrac{y^2}{R^2}}\cdot tg\alpha\right)\right] \\ \tau_{xy}(0,y) = 0 \end{cases} \quad (7)$$

In this case, compressive stress in the extreme points on the vertical axis is not infinite, as is true in the case of actual loads, yet and similarly, maximum tensile stress is found at disc center, eq. 8.

$$\sigma_{xx}(0,0) = \frac{2q}{\pi}\left(\sin 2\alpha - \alpha\right) \quad (8)$$

The applied force P can be expressed as P=q 2Rt and, small α values with maximum fracture strength coincide with what was obtained applying Timoshenko theory. Therefore, at the disc center, both Timoshenko's and Hondros' theories are equivalent. Strength calculation is completed on a non-deformed sample in both theories. However, tensile test monitoring Fig. 3 shows that the sample progressively deforms as time goes by and the load increases. Therefore, this load is not applied on a curved surface but on a slightly flat surface due to deformation.

2.3. Stress Fields in compression by loads on deformed surfaces

Analysis of the stress fields in compression on slightly curved surfaces was completed by means of numeric simulation by applying explicit finite differences using the Flac3D software package.

Studies were completed with flat and curved plates (Fig. 6) using a 50 mm diameter cylinder, thickness equal to radius, 2500 kg/m3 density, and 104N applied force. Young's modulus values that were applied ranged from a minimum of 0.3375 GPa up to maximum of 67.5 GPa, which allows the influence of rock stiffness on sample strengths to be analyzed.

Model geometry was divided into 36351 nodes, and 33920 areas, and each element was assigned a linear elastic behavior model. Sample press plate contact was simulated by means of the interface logic with a 10º friction (Fig. 7). The stress-deformational estate of the model was solved by consecutive approximations, by recalculating the distribution of stresses and deformations in each calculation stage. In each stage, the unbalanced forces in each node produced acceleration and displacement. These were limited by the adjoining nodes, thus force redistribution was produced.

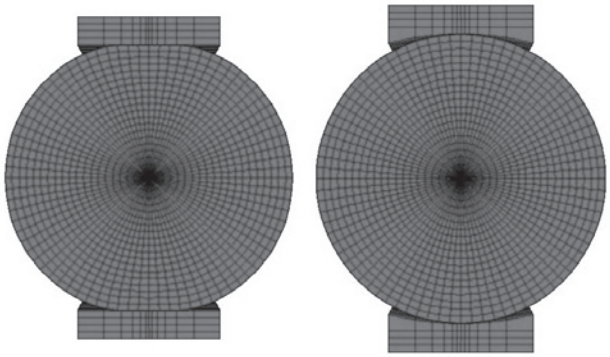


Figure 6. Plate shapes that were used.
Source: Álvarez Fernández et al.

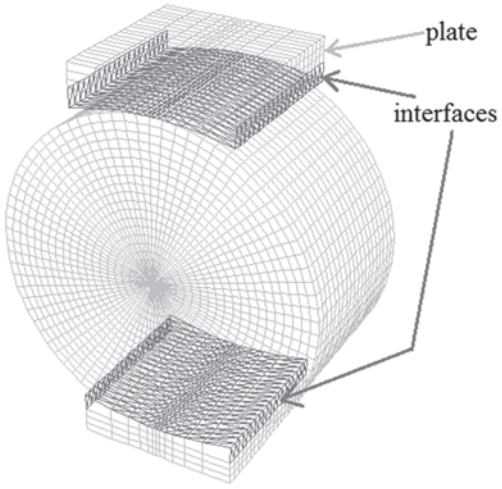


Figure 7. Geometry of calculus.
Source: Álvarez Fernández et al.

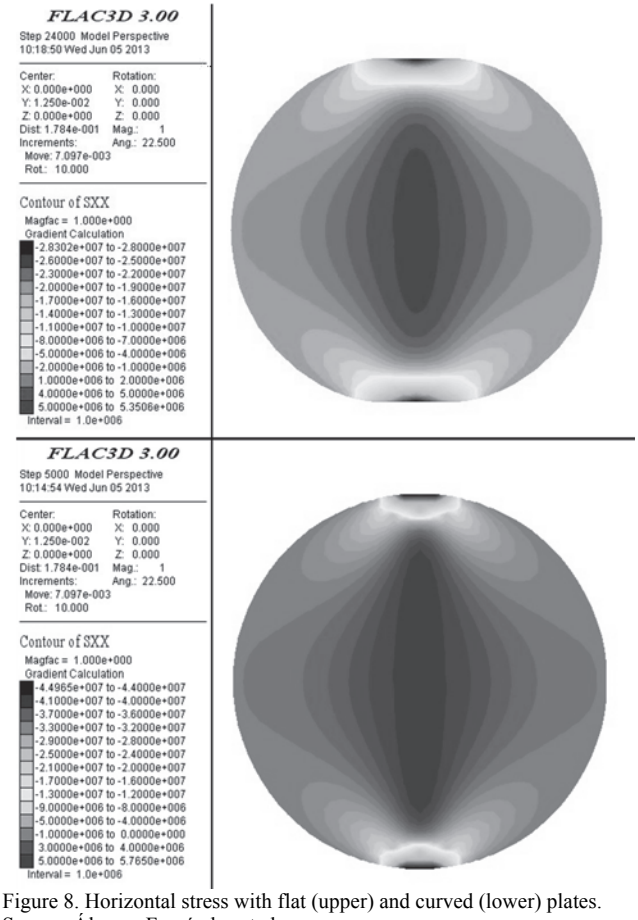


Figure 8. Horizontal stress with flat (upper) and curved (lower) plates.
Source: Álvarez Fernández et al.

The representation of the field of horizontal stresses for a sample of 6.75 GPa of stiffness (Fig. 8) shows very similar stress distributions for both plate types. However, the values in the extremes of the sample, that are in contact with the plates, are higher for the curved than for the flat plate.

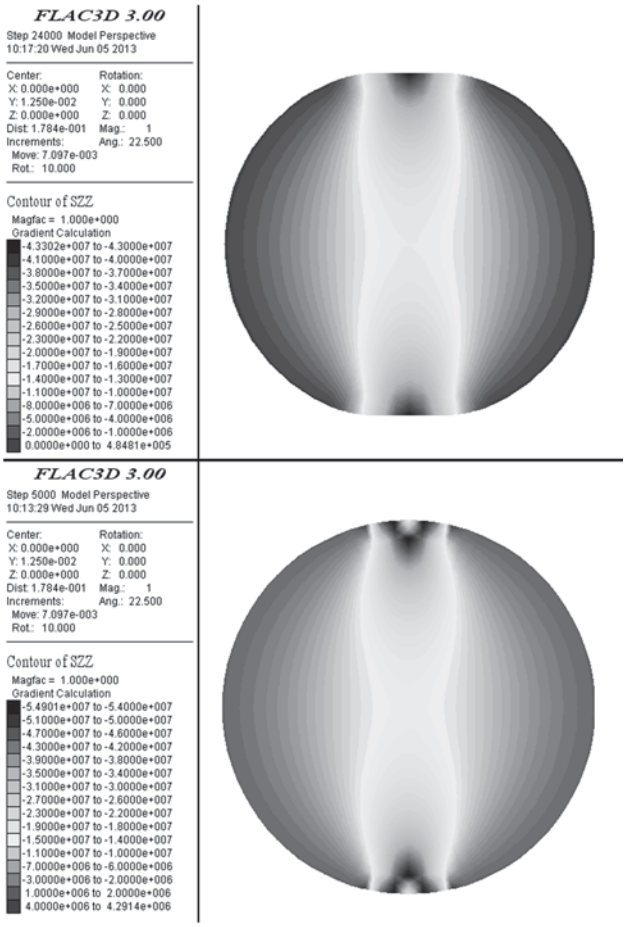


Figure 9. Vertical stress with flat (upper) and curved (lower) plates.
Source: Álvarez Fernández et al.

The same behavior was observed for a similar sample to that in Fig. 8 for vertical stresses (Fig. 9). Again, the curved plate shows higher stress values around plate-contact. However, the maximum point in this case is not in the extremes, as with the flat plate, but in its environment.

Tables 1 and 2 (flat and curved plates, respectively) report the numeric values obtained from the completed tests. They show Δr or radius shortening in mm due to deformation, α or deformation angle in sexagesimal degrees, and horizontal and vertical stress obtained by means of 3D numerical simulation (σFxx, σFzz) as well as through the application of the approximation developed by Hondros (σHxx, σHzz) (8). This is according to the load-application angle, which is considered equal to the deformation angle.

For low stiffness values below 13.5 GPa, the values of both horizontal and vertical stress, obtained in numerical simulation and flat plate (Table 1), are higher than those obtained with curved plate (Table 2). However, for stiffer samples, strengths do not depend on plate shape. The same occurs when stress is calculated with Hondros' approximation. However, in this case, low stiffness values give rise to higher stress with a curved plate, compared to with a flat plate; this is unlike what occurs with numerical simulation.

The value of horizontal and vertical stress calculated from Timoshenko's formulation (5) are 5.093 and 15.28 MPa,

respectively. Both values are slightly higher than the highest values obtained with both numerical simulation and Hondros' approximation.

Moreover, with stiffness values below 13.5GPa, increased sample stiffness leads to reduced sample deformation, thus giving rise to lower shortening and deformation angle values. In this case, the values obtained with flat plate are below those obtained with curved plate. However, for high stiffness values, deformation is similar regardless of plate shape.

Table 3 reports the values of average deviations among the strength values calculated with the three approximations that were considered. The lowest deviations for the flat plate occur between the strengths calculated according to Timoshenko's theory and those provided by the numerical simulation, while for the curved plate, the lowest deviations are observed with Hondros' approximation and the numerical simulation.

3 Conclusions

- Monitoring numerous tests allowed us to become more informed of sample behavior over time. Deformation is observed to cause surface sample-testing machine contact.

Table 1.
Numerical results of strengths for flat plates.

test	E (GPa)	Δr (mm)	α (º)	σ_{Fxx} (MPa)	σ_{Hxx} (MPa)	σ_{Fzz} (MPa)	σ_{Hzz} (MPa)
1	0.34	1.712	21.51	4.91	4.17	14.71	14.34
2	0.67	1.006	16.31	5.12	4.54	15.45	14.72
3	3.37	0.259	8.25	4.94	4.94	15.07	15.11
4	6.75	0.152	6.32	4.97	4.99	15.13	15.17
5	13.50	0.080	4.57	4.97	5.04	15.15	15.21
6	20.25	0.053	3.73	4.97	5.05	15.14	15.22
7	67.50	0.016	2.04	4.96	5.07	15.12	15.24

Source: Álvarez Fernández et al.

Table 2.
Numerical results of strengths for curved plates.

test	E (GPa)	Δr (mm)	α (º)	σ_{Fxx} (MPa)	σ_{Hxx} (MPa)	σ_{Fzz} (MPa)	σ_{Hzz} (MPa)
1	0.33	1.516	20.05	4.70	4.27	14.54	14.45
2	0.67	0.871	15.17	4.77	4.61	14.66	14.79
3	3.37	0.023	7.85	4.91	4.95	15.01	15.13
4	6.75	0.134	5.94	4.93	5.01	15.06	15.18
5	13.50	0.080	4.57	4.97	5.04	15.15	15.21
6	20.25	0.053	3.73	4.97	5.05	15.14	15.22
7	67.50	0.016	2.04	4.96	5.07	15.12	15.24

Source: Álvarez Fernández et al.

Table 3.
Average deviations between strengths values.

Plate	Horizontal strengths		
	Timoshenko - simulation	Hondros - Timoshenko	Hondros - simulation
flat	0.12	0.26	0.23
curved	0.21	0.23	0.14
Plate	Vertical strengths		
	Timoshenko - simulation	Hondros - Timoshenko	Hondros - simulation
flat	0.21	0.28	0.21
curved	0.32	0.25	0.10

Source: Álvarez Fernández et al.

- The deformation observed in samples causes sample lengthening along the OX axis and sample shortening along the OZ axis.
- The relationship between tensile and compressive stresses in numerical simulation has a theoretical value of around 3.
- Sample strengths and deformations depend on the sample material's stiffness.
  - Low stiffness values lead to large deformations and therefore greater vertical-axis shortening and greater deformation angles. Also, they give rise to lower strength values for both vertical and horizontal ones.
  - Conversely, stiffer materials show very small deformations, and have strength values approximate to the values obtained with Timoshenko's formulation, which do not depend on the sample's material.
- Strengths and deformations with flat plates are higher than those obtained with curved plates for materials with low stiffness values. However, for stiffness values over 13.5 GPa, plate shape has no impact on results.
- The strengths obtained according to Timoshenko theory are greater than those obtained by using numerical simulation.
- Finally, the strengths obtained from both 3D numeric simulation and Hondros' formulation in slightly deformed samples are lower than those obtained by using Timoshenko's formulation.

References

[1] Lizarazo-Marriaga, J.M. and Claisse, P., Compressive strength and rheology of environmentally-friendly binders. Revista Ingeniería e Investigación, 29(2), pp. 5-9, 2009.

[2] Valderrama, C.P., Torres-Agredo, J.and Mejía de Gutiérrez, R., A high unburned carbon fly ash concrete's performance characteristics. Revista Ingeniería e Investigación, 31(1), pp. 39-46, 2011.

[3] Mellor, M. and Hawkes, I., Measurement of tensile strength by diametral compression of discs and annuli. Engineering Geology, 5(3), pp. 173-225, 1971. DOI: 10.1016/0013-7952(71)90001-9

[4] SRM., Suggested methods for determining tensile strength of rock materials. International Journal of Rock Mechanics and Mining Sciences Geomechanics Abstracts, 1978, pp. 99-103.

[5] The Professional Standards Compilation Group of People's Republic of China. Specifications for rock tests in water conservancy and hydroelectric engineering (SLJ2-81). Beijing: China Waterpower Press, 1981.

[6] National Standards Compilation Group of People's Republic of China. Standard for tests methods of engineering rock masses (GB/T50266-99). Beijing: China Plan Press, 1999.

[7] The Professionals Standards Compilation Group of People's Republic of China. Specifications for rock tests in water conservancy and hydroelectric engineering (SL-264-2001). Beijing: China Waterpower Press, 2001.

[8] Hondros, G., The evaluation of Poisson's ratio and the modulus materials of a low tensile resistance by the Brazilian (indirect tensile) test with particular reference to concrete. Australian Journal of Applied Science, 10(3), pp. 243-268, 1959.

[9] Hudson, J.A., Brown, E.T. and Rummel, F., The controlled failure of rock disk and rings loaded in diametral compression. International Journal of Rock Mechanics and Mining Science, 9(2), pp. 241-248, 1972. DOI: 10.1016/0148-9062(73)90034-X

[10] García-Leiva, M.C., Ocaña, J., Martin-Meizoso, A. and Martínez-Esnaola, J.M., Fracture mechanics of sigma sm1140+ fibre. Engineering Mechanics. 69(9), pp. 1007-1013, 2002. DOI: 10.1016/S0013-7944(01)00117-5

[11] Fell, J.T. and Newton, J.M., Determination of tablet strength by the diametral compression test. Journal of Pharmaceutical Sciences, 39(5), pp. 688 - 691, 1970. DOI: 10.1002/jps.2600590523
[12] Yu, Y., Question the validity of the Brazilian test for determining tensile strength of rock. Chinese Journal of Rock Mechanical Engineering, 24(7), pp.1150-1157, 2005. [in Chinese].
[13] Timoshenko, S.P. and Goodier, J.N., Theory of Elasticity. 3rd Edition, Mc Graw-Hill, New York, 1970.
[14] Yong, Y., Jianmin, Y. and Zouwu, Z., Shape effects in the Brazilian tensile strength test and a 3D FEM correction. International Journal of Rock Mechanics and Mining Science, 43(4), pp. 623-627, 2006. DOI: 10.1016/j.ijrmms.2005.09.005
[15] Yong, Y., Jianxun, Z. and Jichun, Z., A modified Brazilian disk tension test International Journal of Rock Mechanics and Mining Science, 46(2), pp. 421-425, 2009. DOI: 10.1016/j.ijrmms.2008.04.008
[16] Jonsen, P., Häggblad, H. and Sommer, K., Tensile strength and fracture energy of pressed metal powder by diametral compression test. Powder Technology, 176(2-3), pp. 148-155, 2007. DOI: 10.1016/J.POWTEC.2007.02.030
[17] Jianhong, Y., Wu, F.Q. and Sun, J.Z., Estimation of the tensile elastic modulus using Brazilian disc by applying diametrically opposed concentrated loads. International Journal of Rock Mechanics and Mining Science, 46(3), pp. 568 - 576, 2008. DOI: 10.1016/j.ijrmms.2008.08.004
[18] Es-Saheb, M.H., Albedah, A. and Benyahia, F., Diametral compression test: Validation using finite element analysis. International Journal of Advanced Manufacturing Technology, 57(5-8), pp. 501-509, 2011. DOI: 10.1007/s00170-011-3328-0
[19] Frocht, M.M., Photoelasticty, Vol. 2, John Wiley & Sons Inc, New York, 1948.
[20] UNE 22950-2. 1990., Mechanical properties of rocks. Strength determination tests. Part 2: Tensile strength. Indirect determination (Brazilian test). Madrid: AENOR, 1990. 4 p.

M.I. Álvarez-Fernández, is a BSc. in Mining Engineering and Dr in Mining Engineering from the University of Oviedo, Spain. In 1997, she started her career as a lecturer at the University of Oviedo in the Department of Mining and Prospective Mines. Her teaching experience is focused on rock mechanics and soils, and mine design and monitoring. She has been a member of the Ground Engineering Research Group for more than 15 years. During this time she has collaborated on several European Projects and worked with prestigious companies in the mining and civil engineering fields. Over her professional career she has highlighted patents concessions and published many research papers in important international journals.
ORCID: 0000-0002-5681-6530

C. González-Nicieza, is BSc. in Industrial and Mining Engineer from the University of Oviedo, Spain. After he received his PhD in Mining Studies, in 1986, he started working as a professor at the University of Oviedo (Dept. of Exploitation and Prospecting Mines). He focused on rock mechanics and soils, and mine design and monitoring. He has been the chief of the Ground Engineering research Group for more than 20 years and has collaborated on many European Projects. He has also worked with prestigious companies in the mining and civil engineering fields. Over her professional career she has highlighted patents concessions and published many research papers in important international journals.
ORCID: 0000-0002-2575-9676

M.B. Prendes-Gero, received her PhD in Mining Studies in 2002. From 1997 she taught at the University of Oviedo in Spain, and has worked as a full professor since 2002. She is also an honorary visiting researcher at Sherbrooke University in Canada. She has published widely on genetic algorithms, on stability of roofs and on the mining area. She has received two research recognitions from the Spanish Government. Throughout her career she has coordinated a European Project and has been member of research groups in several projects at the Spanish National Research Program. In 2009 she was sub-director of the Polytechnic School of Mieres and she has participated in the elaboration of the new Mines studies at the European Space of Superior Education.
ORCID: 0000-0001-9125-4863

J.R. García-Menéndez, is BSc. in Industrial Engineer. He has been a member of the Ground Engineering Research Group team of the University of Oviedo, Spain, since 1999. In this team he has collaborated on many projects for prestigious companies in the mining and civil engineering sectors. He has a wide experience in instrumentation applied to ground engineering (use, maintenance and repair) both in the laboratory and outside.
ORCID: 0000-0001-9551-0617

J.C. Peñas-Espinosa, PhD in Mining Studies. He is the chief of OCA Constructions and Projects, an important enterprise in the civil engineering field. He has extensive experience in this sector due to the projects he has worked in throughout his career.

F.J. Suárez-Domínguez, received his PhD in Industrial Engineering studies in 1996. From 1994 he has taught at the University of Oviedo in Spain, working as a full professor since 2002. He has received two research recognitions from the Spanish Government. He has been member of research groups working on several projects at the Spanish National Research Program. He is also a member of the Research Group on Sustainable Construction, Simulation and Testing (GICONSIME). He has published 24 papers in national and international magazines.
ORCID: 0000-0002-4630-1218

UNIVERSIDAD NACIONAL DE COLOMBIA
SEDE MEDELLÍN
FACULTAD DE MINAS

Área Curricular de Ingeniería
Geológica e Ingeniería de Minas y Metalurgia

Oferta de Posgrados

Especialización en Materiales y Procesos
Maestría en Ingeniería - Materiales y Procesos
Maestría en Ingeniería - Recursos Minerales
Doctorado en Ingeniería - Ciencia y Tecnología de Materiales

Mayor información:

E-mail: acgeomin_med@unal.edu.co
Teléfono: (57-4) 425 53 68

UNIVERSIDAD NACIONAL DE COLOMBIA
SEDE MEDELLÍN
FACULTAD DE MINAS



DYNA
http://dyna.medellin.unal.edu.co/

Validating the University of Delaware's precipitation and temperature database for northern South America

Juan Sebastián Fontalvo-García [a], José David Santos-Gómez [a b] & Juan Diego Giraldo-Osorio [a]

[a]. *Facultad de Ingeniería, Pontificia Universidad Javeriana, Bogotá, Colombia. fontalvoj@javeriana.edu.co, j.giraldoo@javeriana.edu.co.*
[b]. *Facultad de Ingeniería, Universidad de los Andes, Bogotá, Colombia. jd.santos10@uniandes.edu.co.*

Received: October 14th, 2014. Received in revised form: July 29th, 2015. Accepted: August 4th, 2015.

Abstract
Vast sections of the planet face either a dearth of ground-based weather stations or are hampered by the poor quality of those in service. In response, researchers are forced to turn to climate field databases, as they constitute a source of reliable information for local studies. Insofar as the Amazon region, these databases prove to be valuable given their open-access platform and the fact that this expansive region possesses few quality stations (coupled with insufficient temporal coverage). However, before basing research on such archives, this information should be compared against *in situ* station measurements. Then, the present study assesses the validity of temperature and precipitation information furnished by University of Delaware's database (UD-ATP) by means of a comparison with the open-access information available from Climate Explorer project (CLIMEXP). Results show that UD-ATP database offers better precipitation data representation, especially on Brazil, which is perhaps the effect of higher-quality and larger-quantity observed data.

Keywords: time series of interpolated climate fields; precipitation; temperature; South America; Amazon region.

Validación de la precipitación y temperatura de la base de datos de la Universidad de Delaware en el norte de Suramérica

Resumen
Debido a la carencia de estaciones en tierra, o a la mala calidad de éstas, en amplias regiones del planeta, las bases de datos de campos climáticos emergen como fuentes de información confiable para realizar estudios locales. En el caso específico de la Amazonía, estas bases de datos son valiosas porque son de libre acceso, y porque este vasto territorio cuenta con pocas estaciones de calidad y suficiente longitud. Sin embargo, previo a su utilización, es necesario comparar estos datos con la información disponible de las estaciones. Se verificó la validez de la información de precipitación y temperatura contenida en la base de datos de la Universidad de Delaware (UD-ATP), contrastándola con la información de libre acceso disponible en el *Climate Explorer* (CLIMEXP). Se encontró que la precipitación es mejor representada por la base de datos UD-ATP, y que los resultados son mejores sobre el territorio brasilero, posiblemente por la mejor calidad de los registros observados.

Palabras clave: Series temporales de campos climáticos interpolados; precipitación; temperatura; Suramérica; región de la Amazonía.

1. Introduction

For regions as massive as the one occupied by the Amazon Rainforest, climate variables are notorious for being incomplete, fragmented and outdated. Together, these inconveniences comprise the primary limitations faced by climatologists. In general, meteorological station data for the Amazon is not uniform in spatial or temporal terms. The construction of evenly distributed grids is crucial to climate analysis, seeing as these are the principal sources for variables in regions removed from measuring stations; in addition, they facilitate local studies in inaccessible regions which lacking information [1-3]. Disciplines benefitting from these interpolated grids are as diverse as: agriculture, biological sciences, hydrology, water resources management, and climate change studies [1,4-6].

On a global scale, high-resolution fields of climate variables are found for long-term monthly averages. For example, Hijmans et al. [4] built monthly average grids for

© The author; licensee Universidad Nacional de Colombia.

the years 1950-2000 that take into account precipitation and temperature with 30" (~1 km) spatial resolution; New et al. [5] laid out monthly averages for eight climate variables and a wide range of statistics extracted from data for 1960-1990 with 10' (~20 km) spatial resolution. Yet, while time series have been constructed to cover the entire planet, spatial resolution has turned out to be much harder to achieve, possibly due to the spatial and temporal gaps plaguing the data. For the most part, global databases rely on interpolation with a spatial resolution of 0.5° (~50 km); one of the most well-known is that developed by the Climate Research Unit (CRU) at the University of East Anglia, most recently updated to encompass the period spanning 1900-2012 [6-8]. These climate field time-series databases often stem from the direct interpolation of station data, which grants the highest spatial resolution and greatest length of time [9-11]. Likewise, there is the inclusion of satellite-based observations to assist in the process of interpolation, providing information ranging from 1970 to today [12]. Another method is the reanalysis of observed data in climate models, although this method only covers relatively short periods [13-15].

Nevertheless, interpolated climate-variable maps for specific areas are assembled with extremely high spatio-temporal resolution. From these sets of quasi-continental databases, we highlight the work of (i) Jeffrey et al. [16] for Australia, which depicts precipitation, maximum and minimum temperature, evaporation, solar radiation and vapor pressure information all at 10' spatial resolution, and daily temporal resolution (1890-2000 or 1957-2000, depending on the variable in question); (ii) interpolated precipitation and temperature grids constructed for Europe on a daily basis (1950-2006) at 25 km spatial resolution [1]; (iii) the precipitation and temperature database built by Hutchinson et al. [17] for Canada on a daily basis (1961-2003), and 5' spatial resolution. Database resolution can be even better, at least in spatial terms, when the study is restricted to a smaller area and the information required to carry out the interpolation is of high quality: Perry and Hollys [18] built monthly fields (1961-2000) for 36 variables for the United Kingdom, with 5 km spatial resolution. In the case of Spain, Herrera et al. [19] made daily precipitation and temperature fields (1950-2003) with a spatial resolution of close to 20 km. Additionally, Hurtado-Montoya and Mesa-Sánchez [20] provide invaluable information for Latin America, insofar as it provides monthly historical precipitation grids for Colombia with high spatial resolution by virtue of an optimal integration of updated information and distributed grids (satellite images and re-analysis). Here, the downside is that the interpolated period only runs from 1975 to 2006, and, at the time of writing the present document, restrictions regarding access to this information were in effect.

Ground station information for the Amazon region, located in the northern part of South America is not complete. Most stations in the territory are concentrated in the mountainous region of the Andes range, or near the Brazilian coast. In effect, this concentration leaves large tracts of open jungle plains void of either quality information or with sufficient temporal length. As a way of tackling this information scarcity, researchers look to interpolated databases. Precisely here is where databases like the University of Delaware's Air Temperature and Precipitation database (UD-ATP) comes into play. The database's key features include: open access, more than 100 years of information from across the entire planet with 0.5° spatial resolution, and monthly temporal resolution. Database assessment is indispensable, and the present study has taken on this task, through the validation of UD-ATP precipitation and temperature variable for northern South America. For the purposes of the present study, validation means comparing the UD-ATP data to ground station data obtained via the Climate Explorer (CLIMEXP) webpage using a set of statistical analyses (the Pearson correlation coefficient –*R*–; and the Kolmogorov-Smirnov –KS– test), in order to verify the fit of probability distributions from station-collected data to those of interpolated grids. Finally, annual cycles from observed data against interpolated grid data were compared, using the normalized root-mean-square error (NRMSE).

2. Study area and data

2.1. Study area

The study area spans 20ºS to 15ºN and 85ºW to 35ºW (see Fig. 1), which corresponds to the northern portion of South America, where the Amazon basin is located. For this region, the CLIMEXP ground-station data, and precipitation and temperature grids from the UD-ATP database, were employed.

2.2. UD-ATP interpolated grids

The UD-ATP information consists of monthly grids of total precipitation and average temperature values for 1901 to 2010 (version V3.01), with 0.5º spatial resolution (approximately 50 km close to the equator) and grid-points centered at 0.25º. These archives encompass all emerged surfaces on Earth (read: dry land areas), relying on 720 x 360 x 1332 pixilation.

The interpolation process, as it pertains to the construction of monthly fields, is explained by Matsuura and Willmott [10,11]. In broad terms, their study collects a myriad of pieces of data from the ground stations that form part of the Global Historical Climatology Network (GHCN2) and gleans data from local agencies supporting the project.

2.3. Climate Explorer (CLIMEXP) ground stations

The ground-based data utilized for this study's comparison of grid data come from the CIMEXP (CLIMEXP; [21]), which belongs to the *Koninklijk Nederlands Meteorologisch* Instituut (KNMI; known in English as the Royal Netherlands Meteorological Institute). Without any sort of financial expectation, CLIMEXP gathers precipitation and temperature variables, among others. The provenance of these variables is global, in line with the project's goal of sharing this invaluable information globally and free of charge. The webpage was selected because it contains current research and boasts the most precipitation and temperature weather stations with monthly registries in

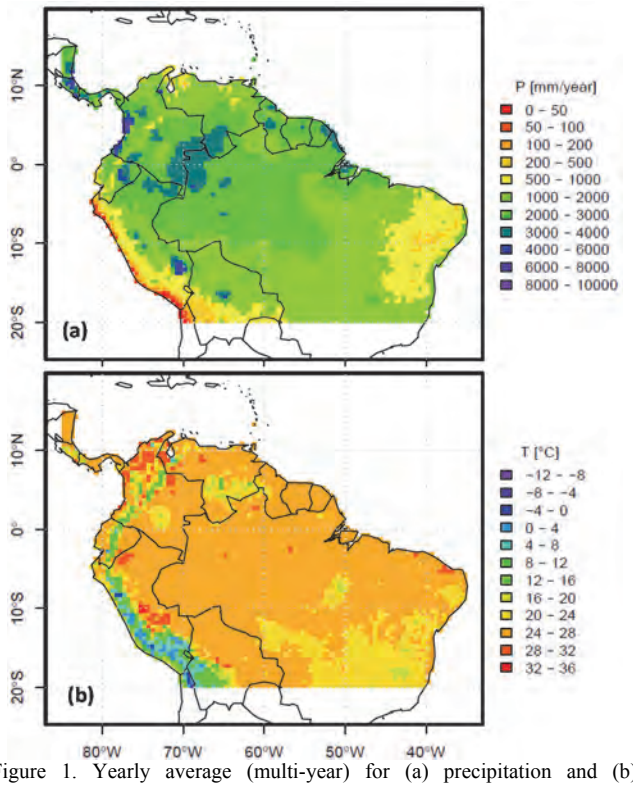


Figure 1. Yearly average (multi-year) for (a) precipitation and (b) temperature in the Amazon region, calculated using UD-ATP data (1950-2010 period).
Source: Authors' own compilation.

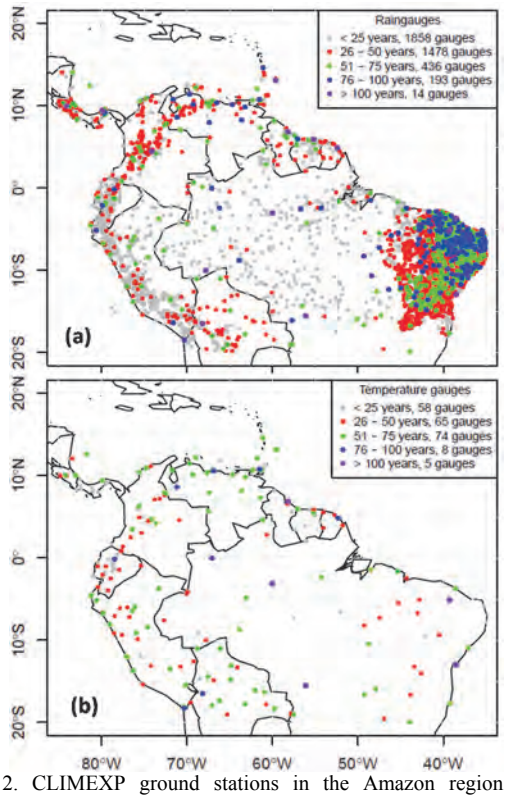


Figure 2. CLIMEXP ground stations in the Amazon region for (a) precipitation and (b) temperature data.
Source: Authors' own compilation.

the study area. Ground-based station location and record length can be observed in Fig.2. It is important to bear in mind that the record length is that reported on CLIMEXP, without removing years missing registry data. This situation was seen to occur with some frequency.

3. Preliminary data treatment

3.1. Trimming the UD-ATP interpolated grid

Interpolated grids provide information for the entire planet with 0.5º spatial resolution. In order to trim the grid down for the appropriate study area, NCO (*netCDF Operators*; [22]) commands were utilized. This procedure creates an archive with nothing more than the data pertaining to the study area. Once the archive was fine-tuned, *R software*, in tandem with a number of support libraries (notably, the library *ncdf* makes it easier to manage netcdf files; [23]), allowed us to verify the proper selection of information. As seen in Fig. 1., average yearly (multi-year) precipitation and temperature maps were developed based on time series for monthly interpolated grids from the UD-ATP.

3.2. Selecting and filling gaps in CLIMEXP data

The CLIMEXP registry possesses a variety of *in situ* measurement stations located across Earth. In order to focus the validation procedure on the study zone, the stations within the aforementioned area were extracted from the CLIMEXP database. Fig. 2 includes maps representing where precipitation and temperature data information are found in the region, showing not only the temporal irregularity of the registries, but also that of the spatial coverage of the stations.

In the relevant study area, we identified 3979 rain gauges. Of these, not all were deemed appropriate for analysis, given that some stations do not meet the criteria established for this study. With regard to these criteria for station selection, the first criterion is of a temporal nature: all those dating back less than 25 years were discarded. It is worth mentioning that great care was taken to fill the missing data for years with gaps of 3 months or less, as per the normal ratio method described by Subramanya ([24], p. 26). Nonetheless, it was quite common to stumble across completely data-free years, a fact which ineluctably forced us to opt for either trimming or abandoning certain time series. The second criterion was geographic: for interpolated grids with 50x50 km^2 pixels size, each one suffers from high variability in terms of precipitation and temperature data, especially in mountainous regions. In the case of precipitation, those pixels with at least two ground-based measurement stations were employed. A grand total of 280 precipitation stations spread out over 105 pixels in the study zone were chosen, and temporal coverage runs from 25 to 80 years. Fig. 3(a) portrays the spatial location of the selected pixels along with their temporal registry. Readers are reminded that the amount of time in the figure implies that all stations within the pixel report complete data for the same temporal window.

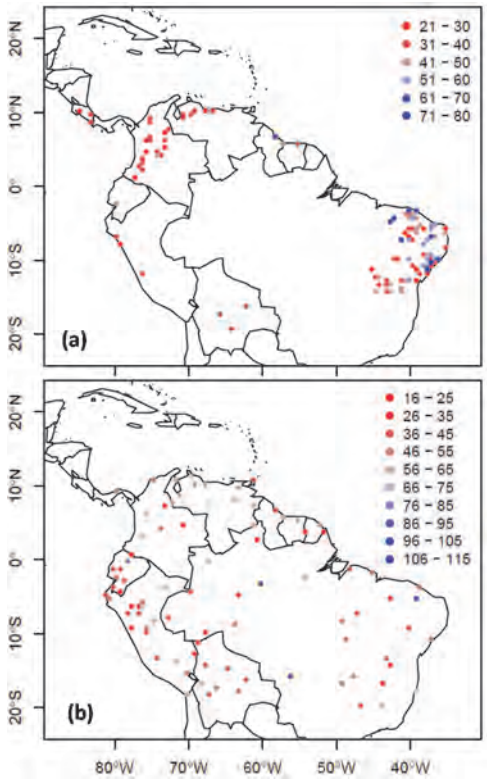


Figure 3. Pixel location for (a) precipitation and (b) temperature —color scale indicates the amount of time covered by a selected registry (in years). Source: Authors' own compilation.

Having outlined the precipitation station selection process, our attention turned to temperature stations. There is a noticeable lack of quantity—not to mention quality—with respect to this aspect. So, to discern the best data sites from the 210 stations found (as compared to 3979 for precipitation) within the study area, less stringent requirements were enforced. Only one temperature station within each pixel was chosen, and the temporal registries start at a minimum of 17 years. In this way, 87 temperature stations provide the relevant data, spread throughout the same number of pixels, with temporal spans from 17 to 110 years. 3(b) shows the results of this search, plus each pixel's temporal registry.

To fill missing precipitation data for the CLIMEXP series within each pixel, the previously mentioned normal ratio method was employed, as expressed by the equation below [24]:

$$P_{x-Y} = \frac{\overline{P_x}}{n} \cdot \left(\frac{P_{1-Y}}{\overline{P_1}} + \frac{P_{2-Y}}{\overline{P_2}} + \cdots + \frac{P_{n-Y}}{\overline{P_n}} \right) \quad (1)$$

where

P_{x-Y} = Missing precipitation for month Y in problem station x.

$\overline{P_x}$ = Yearly average precipitation (multi-year) for problematic station x.

$\overline{P_1}, \overline{P_2}, \ldots, \overline{P_n}$ = Yearly average precipitation (multi-year) for n support stations.

$P_{1-Y}, P_{2-Y}, \ldots, P_{n-Y}$ = Precipitation/temperature during month Y for n support stations.

This method establishes the neighbor relations among stations located near one another in order to fill out the missing data. For this study "near" was taken to signify that the problem and all support stations fall within the same pixel. Each station was then equally weighted as part of the calculation of missing values.

4. Methodology and results

To reiterate, this paper verifies the UD-ATP interpolated grid data by comparing said dataset with the ground-based weather stations reported in CLIMEXP. With an eye towards ensuring the independence hypothesis of the data, in-situ station data were averaged on a monthly basis for all CLIMEXP stations inside each pixel, resulting in two time series for each pixel studied. While the first time series represents the average of station data, the second represents the UD-ATP grid data in each pixel. Finally, both series were trimmed using the same time window.

An example of the time series obtained for each pixel (analyzed in accordance with the procedure outlined in the previous section) is presented in Fig. 4, with the center placed at 76°15'W-3°15'N. From here on out, this pixel will be discussed as the "pixel-example." This "pixel-example" encompasses part of Southwest Colombia, ranging in elevation from 950 m above mean sea level (amsl; the Cauca River Valley) to 4250 m amsl (the peaks of the Central Colombian Andes), close to the Huila Summit. The pixel's center, however, is situated at roughly 1050 m amsl.

For rainfall, three gauge stations were counted on to arrive at the series for observed data (between 1953 and 1989); however, for temperature, there was only one reliable station (1951-2010). The dispersion diagram included in Fig. 4(d) evinces a systematic positive deviation from the interpolated temperature grids when compared to the station data. Nevertheless, this deviation is not seen in the pixel's constructed precipitation series (Fig. 4c).

To objectively measure the deviations between observed and UD-ATP series, a handful of analytical tools were used: a) deviation calculation between yearly cycles calculated for each series, b) comparison of empirical probability distributions constructed for both datasets (yearly and seasonally) and c) a correlation test to confirm temporal coherence among the data. All of these steps are explored in further detail below.

4.1. Yearly cycle analysis

Yearly cycle analysis allows us to check whether the UD-ATP adequately mimics the intra-yearly variability of the variables, a situation of particular importance because, for example, temperature abides by seasonal cycles in areas located far from the equator. Yet, for tropical zones, rainfall displays two peaks associated with the Intertropical Convergence Zone (ITCZ) passing over these regions.

Averages for observed and UD-ATP series for each variable and each month, including a 95% confidence interval (95% CI), where computed. Confidence intervals were calculated assuming normality—per Eq. (2)—in spite of the fact that the short registry time span of some pixels potentially complicates this assumption:

$$\bar{x} - z_{\alpha/2} \cdot \frac{s_x}{\sqrt{n}} \leq \mu \leq \bar{x} + z_{\alpha/2} \cdot \frac{s_x}{\sqrt{n}} \quad (2)$$

where

$\bar{x}$= Average value of x for each month, calculated with the observed data.

$z_{\alpha/2}$= Normal significance value $\alpha/2$. If significance is 0.05, then $z_{\alpha/2} \approx 1.96$.

s_x= Standard deviation for x each month, calculated with the observed data.

n = Number of data used to calculate $\bar{x}$ and s_x.

μ = Expected value of x.

Yearly precipitation and temperature cycles can be consulted in Fig. 5 for the pixel-example. As expected, the UD-ATP better reflects the annual rainfall cycle than the annual temperature cycle, reinforcing the systematic deviation of the latter dataset for the UD-ATP database versus its representation by CLIMEXP (observed data).

To calculate the degree of deviance between the interpolated and observed yearly cycles, the Mean-Squared Error was used, normalized to fit within the variable's range, which is known as the Normalized Root-Mean-Square Error (NRMSE); the NMRSE helped determine an independent metric of variable magnitude. (i.e. a way to compare deviations in rainy Amazonian regions and arid Peruvian coastal regions, was sought). NRMSE, though, requires the prior calculation of the Root-Mean-Square Error (RMSE; [25]), which is expressed below:

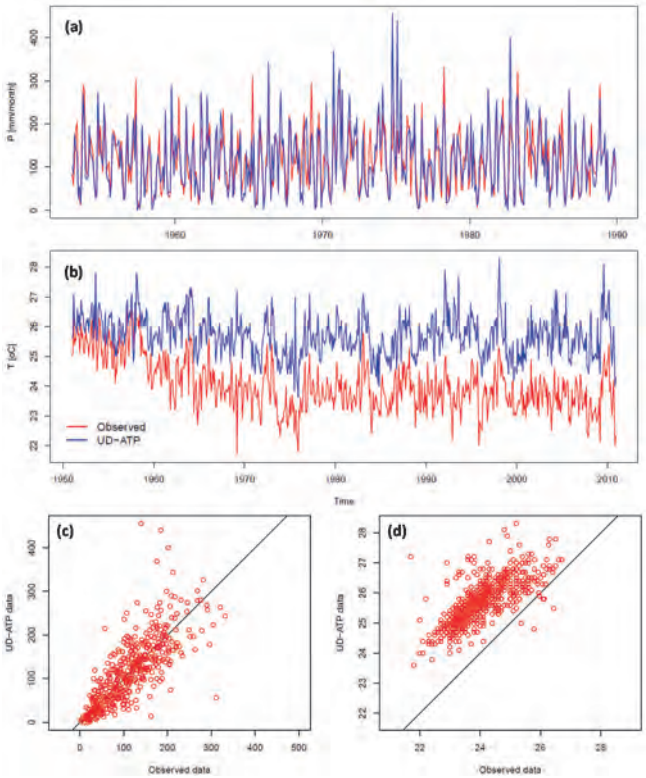


Figure 4. Precipitation (a) and temperature (b) time series obtained in pixel-example (Center 76°15'W-3°15'N). The dispersion plot depicting observed data vs. UD-ATP data for precipitation (c) and temperature (d), with the black unit-slope line representing observed data = UD-ATP data.
Source: Authors' own compilation.

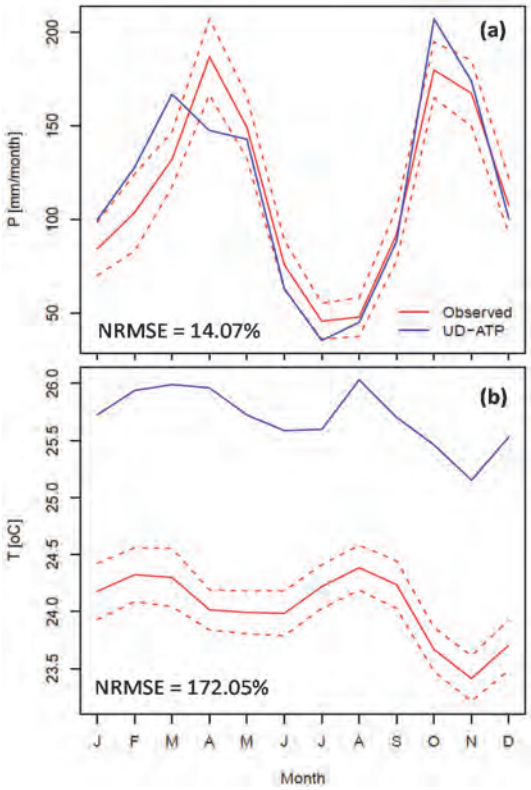


Figure 5. Yearly cycle for precipitation (a) and temperature (b) per pixel-example calculations—the dotted lines represent 95% confidence interval for average monthly values calculated with the observed data; the figure also displays NRMSE.
Source: Authors' own compilation.

$$RMSE = \sqrt{\sum_{i=1}^{12} \frac{\left(\bar{x}_{obs-i} - \bar{x}_{udatp-i}\right)^2}{12}} \quad (3)$$

where

$\bar{x}_{obs-i}$= Average variable value for month i, calculated with CLIMEXP data.

$\bar{x}_{udatp-i}$= Average variable value for month i, calculated with UD-ATP data.

Completing this step leads us to the NRMSE -Eq. (4)-:

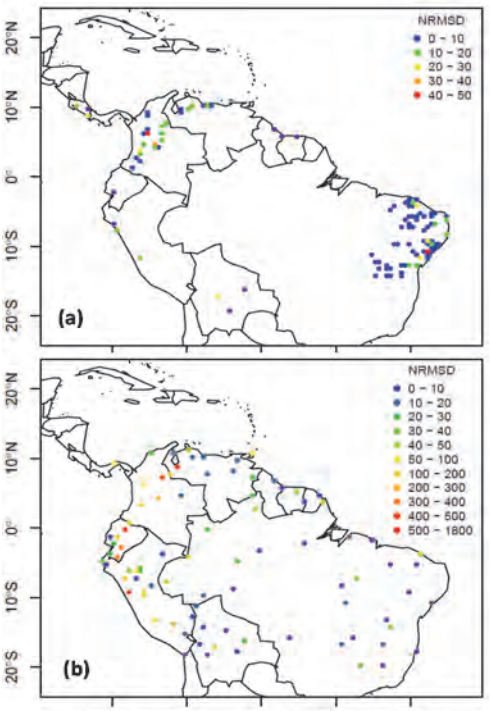
$$NRMSE = \frac{RMSE}{x_{MAX} - x_{MIN}} \quad (4)$$

where

x_{MAX} = Maximum value of monthly average (multi-year) for the variable (i.e. rainiest month of the year or highest average temperature).

x_{MIN} = Minimum value of monthly average (multi-year) for the variable (i.e. driest month of the year or lowest average temperature).

After computing NRMSE for both variables and all pixels analyzed, the maps shown in Fig. 6 were created. On one hand, precipitation saw the gauges exhibiting the lowest NRMSE clustered in Brazil; for the country, 67 pixels were studied, of which 56 had an NRMSE below 10%. Overall, gauges in other countries performed in a more hit-or-miss fashion: from a group of 38 pixels, only 20 had an NRMSE value less than 10%. But,



(c)

NRMSE	Precipitation		Temperature	
0 - 10	76	72,4%	26	29,9%
10 - 20	20	19,0%	18	20,7%
20 - 30	6	5,7%	10	11,5%
30 - 40	1	1,0%	6	6,9%
40 - 50	2	1,9%	6	6,9%
50 -100			5	5,7%
>100			16	18,4%

Figure 6. NRMSE values for precipitation (a) and temperature (b) (expressed as percentages)—the table (c) briefly summarizes the number of pixels for NRMSE ranges. Source: Authors' own compilation.

temperature errors were greater still—only 26 of the 87 pixels possess NRMSE values of less than 10%, with 16 presenting values greater than 100%.

4.2. Goodness-of-fit test for comparing data distribution

The present study employs the Kolmogorov-Smirnov (KS) goodness-of-fit test for two samples. This test allows us to evaluate the fit of any distribution to a dataset by way of comparing the reference's cumulative distribution function (CDF) to the data's empirical CDF. One of the primary benefits of the KS test is that it compares the probability distributions for both datasets without needing to estimate the theoretical distributions for either a priori. It is precisely this strength that makes it well-suited to the present study. The test was used to find out the fit of precipitation and temperature distributions for in situ weather stations (CLIMEXP database taken as reference distribution) and distributions for the same variables in the corresponding pixel using the UD-ATP database.

4.2.1. Computing empirical non-exceedance probabilities

To carry out the KS goodness-of-fit test, empirical non-exceedance probabilities must be assigned to the data (both observed and UD-ATP), ordering them in ascending order. Said probabilities were calculated using probability plotting positioning, which plots yearly time series and estimates a variable's probability of exceeding each value [26], [27]. The general equation reads as follows:

$$\mathrm{P}[X < x_i] = \frac{i-a}{n+1-2a} \tag{5}$$

where

$\mathrm{P}[X<x_i]$ = Empirical probability of no exceedance for the i-th datum x_i.

i = Data order within the series (ascending).

n = Sample size.

a = Parameter of the plot position, which depends on the distribution to which it will be adjusted.

This study employed Weibull's formula to calculate the non-exceedance probabilities, a formula applicable to any distribution. In this case, a = 0, which in turn translates into a simplified version of Eq. (5):

$$\mathrm{P}[X < x_i] = \frac{i}{n+1} \tag{6}$$

4.2.2. Goodness-of-fit test p-value

As mentioned above, the KS goodness-of-fit test for two samples is a non-parametric test that assesses the "equality" of two probability functions for two independent samples, determining the maximum distance between the CDF based on the samples. Doing so implies that the precipitation/temperature time series should be obtained from the CLIMEXP database, and those corresponding to the UD-ATP database. The two-tailed KS goodness-of-fit test is as follows:

$$D_{m,n} = \mathrm{MAX}|S_m(x) - S_n(x)| \tag{7}$$

where

$S_m(x)$, $S_n(\mathrm{x})$ = Empirical CDF of the independent samples calculated with Eq. (6).

m, n = Sample size (even though the present study always saw m=n; inside each pixel, both the CLIMEXP and the UD-ATP series, share the same time span).

It has been shown that asymptotic distribution meets the following standards [28]:

$$\lim_{m,n\to+\infty} \mathrm{P}\left[\sqrt{\frac{m\cdot n}{m+n}}\cdot D_{m,n} \le d\right] = L(d) \tag{8}$$

where $L(d) = 1 - 2\cdot\sum_{i=1}^{+\infty}(-1)^{i-1}\cdot \mathrm{e}^{-2\cdot i^2\cdot d^2}$.

Finally, the p-value of the test is calculated thusly:

$$p(d) = 1 - L(d) = 2\cdot\sum_{i=1}^{+\infty}(-1)^{i-1}\cdot \mathrm{e}^{-2\cdot i^2\cdot d^2} \tag{9}$$

Generally speaking, if the p-value is greater than α (the statistical significance level), the null hypothesis is accepted, thus $S_m(x) = S_n(x)$. Well known significance values are 0.01 and 0.05, which are frequently used in several statistical tests.

4.2.3. Results for the goodness-of-fit test

The KS goodness-of-fit test was undertaken for each pixel studied. The time series were split into yearly and seasonal periods, according to seasons occurring in the northern hemisphere: winter (December-January-February); spring (March-April-May); summer (June-July-August); and, autumn (September-October-November). For the sake of clarity, precipitation is defined as the depth of rainfall in each analyzed period (yearly or seasonal), for each year in the registry, while temperature is defined as the average air temperature computed for each analyzed period.

Pixel-example results obtained are visually represented in Fig. 7, where the cumulative empirical probability distributions calculated for precipitation are graphed. The p-value proved to be greater than the significance value ($\alpha = 0.05$) in every case; this fact leads us to conclude that the distribution of UD-ATP data does indeed adjust to the observed data, though the p-value calculated for temperature in the pixel-example is virtually zero for all tests (not shown), in and of itself an expected situation in light of the previously run tests. Armed with results for each pixel, the maps seen in Fig. 8 were developed; these maps differentiate p-values according to varying significance values (p-value < 0.001 being the worst fit, and p-value > 0.05 indicating that the distributions equal using a good significance value).

Overall, precipitation results were good (see Table 1), even for the Andean region. This implies that the UD-ATP precipitation data reproduces the data observed by ground-based weather stations. Thus, it is possible to rely upon the UD-ATP for areas lacking high-quality data. When looking at the figures, readers should not forget that "summer" was the most deficient season with respect to the number of properly adjusted pixels, which can be chalked up to a concentration of pixels analyzed in Brazilian territory; that is, a territory for which the boreal summer (June-July-August) exhibits low rainfall values. That notwithstanding, the rest of the periods analyzed saw 80% of their pixels well-adjusted, especially true for the Andean countries (Colombia, Ecuador, Peru and Venezuela), where, despite the fact that some pixels have less than stellar performance, the majority have a p-value greater than 0.05. Perhaps this is due to the effect of the Andes on the variables studied. In other words, this geographical feature may cause problems in the interpolation, in addition to the widely recognized precarious nature of weather stations located on mountain ranges.

Temperature, on the other hand, produced poor results (see Fig. 9). As Table 1 evinces, more than half of the pixels had p-values of less than 0.01 for all periods investigated. Though detection of spatial behavior is no easy task with these results, on the whole, the fit for the Amazon Basin and the Brazilian Highlands are better than for the stations located in Andean countries. The latter group ended up demonstrating undesirable adjustments, no doubt attributable to the bulwark known as the Andes Mountain Range, with the concomitant topographical challenges imposed on variable interpolation (mentioned in the previous paragraph). When discussing the results, it is essential to be forthright about the risks of imposing the temperature characterization for a vast area (50x50km^2) on only one station. Is very likely that the temperature station is not located close to the pixel center, and if so, it does not represent the temperature variability within the pixel.

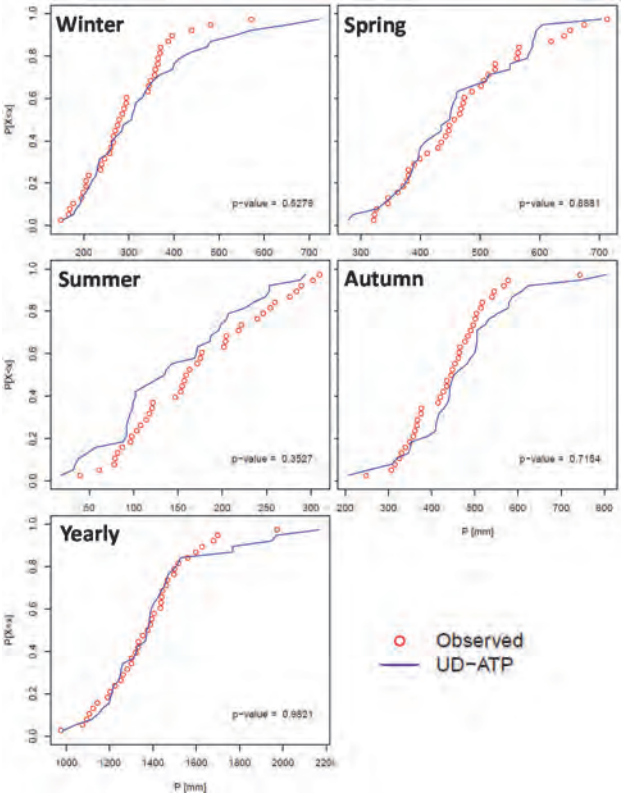


Figure 7. Goodness-of-fit results for precipitation in the pixel-example. Yearly division according with northern hemisphere seasons.
Source: Authors' own compilation.

4.3. Pearson correlation coefficient

The covariance measures the tandem change of two random variables, which implies that if large values for one of the variables correspond to large values for the other, with the same situation playing out for low values, then covariance is said to be positive. If this is not the case, and low values for one variable match high values for the other, then the covariance is said to be negative. Consequently, covariance indicates the linear relation trend among variables. Nevertheless, sometimes it is hard to explain or interpret the covariance, because it depends on both the magnitude and the units of measurement of the variable. This difficulty can be overcome using the Pearson correlation coefficient (denoted by R) calculated between series. The Pearson correlation coefficient could be interpreted as the normalized version of covariance. The correlation coefficient is distinguished by the fact that it is always comprised between -1 and +1, where +1 is a perfect positive correlation [28].

The project at hand expected, and saw, observed data to be strongly positively correlated to the UD-ATP data (i.e. R values near +1). Furthermore, negative correlations were not expected to be encountered as correlations of this sort would indicate temporal inconsistencies between observed and interpolated grid data. The Pearson correlation results for each pixel can be found inFig. 10. Both variables have more than 70% of their analyzed pixels with R values above 0.8, but the proportion of pixels for temperature that are poorly correlated (that is, $R < 0.5$) is smaller than the proportion of the precipitation pixel.

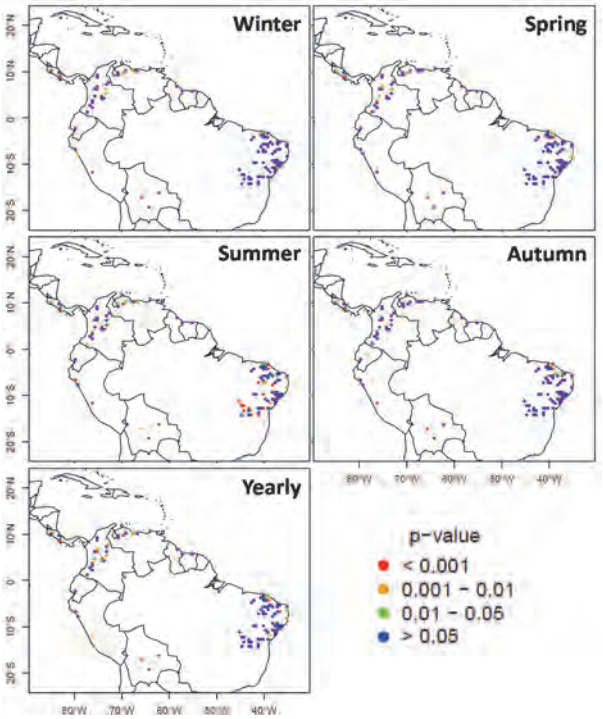


Figure 8. Maps of goodness-of-fit test results for precipitation, in seasonal and yearly terms, for pixels analyzed. Yearly division according with northern hemisphere seasons.
Source: Authors' own compilation.

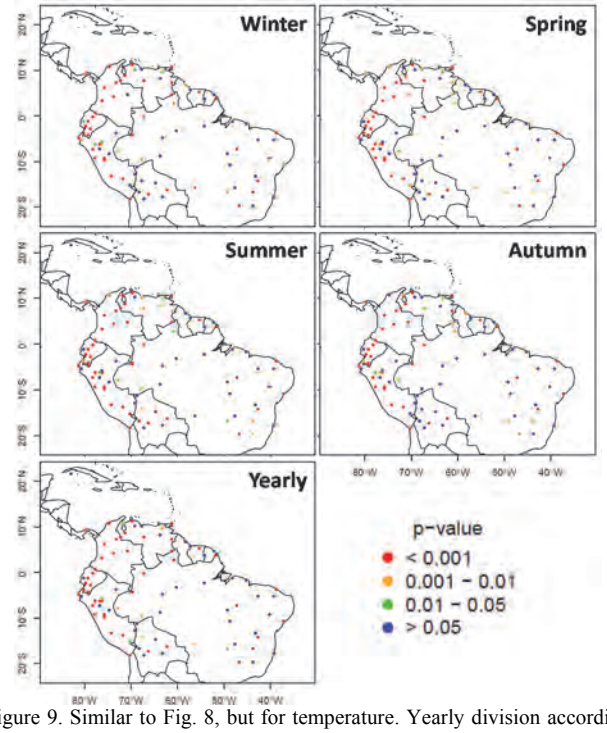


Figure 9. Similar to Fig. 8, but for temperature. Yearly division according with northern hemisphere seasons.
Source: Authors' own compilation.

Insofar as the correlation coefficient's spatial distribution, neither variable led to identify any discernible spatial pattern

Table 1.
Summary of results for goodness-of-fit test, with pixel count for each p-value range. Yearly division according with northern hemisphere seasons.

	p-value	Winter		Spring		Summer		Autumn		Yearly	
Precipitation	< 0,001	7	6,7%	6	5,7%	23	21,9%	10	9,5%	10	9,5%
	0,001 - 0,01	2	1,9%	1	1,0%	8	7,6%	3	2,9%	6	5,7%
	0,01 - 0,05	6	5,7%	9	8,6%	7	6,7%	3	2,9%	8	7,6%
	> 0,05	90	85,7%	89	84,8%	67	63,8%	89	84,8%	81	77,1%
	p-value	**Winter**		**Spring**		**Summer**		**Autumn**		**Yearly**	
Temperature	< 0,001	41	47,1%	36	41,4%	41	47,1%	35	40,2%	45	51,7%
	0,001 - 0,01	6	6,9%	9	10,3%	7	8,0%	9	10,3%	5	5,7%
	0,01 - 0,05	7	8,0%	6	6,9%	8	9,2%	5	5,7%	4	4,6%
	> 0,05	33	37,9%	36	41,4%	31	35,6%	38	43,7%	33	37,9%

Source: Authors' own compilation.

This conclusion is based on the sprinkling of high and low correlation values from pixel to pixel. This is especially evident for Brazilian pixels in terms of precipitation data.

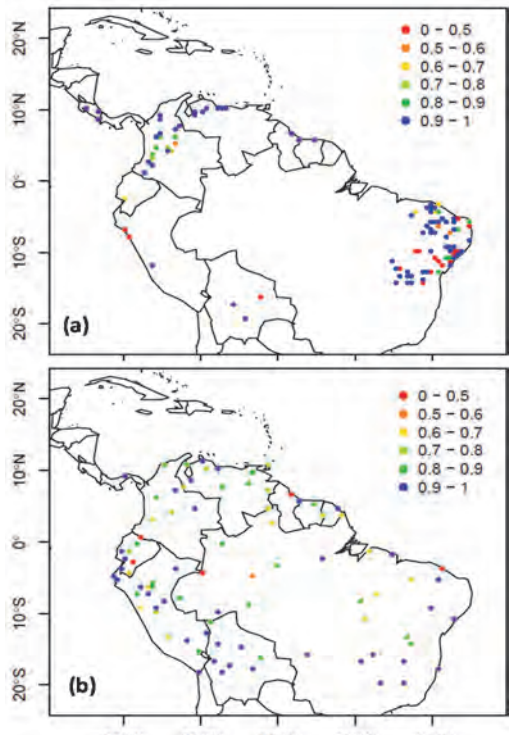
Colombian-based data for precipitation ranged from adequate to good. Correlations from the northern Peruvian coast provide evidence of an area whose rainfall is difficult to represent for the UD-ATP database. As far as the distribution of the correlation coefficient for temperature is concerned, no overarching spatial behavior stands out, given that low *R* values are spread throughout the entire study area without regard for a region's topography, whether this is mountainous or open plain.

5. Conclusions

On balance, the UD-ATP database contributes to hydrological research by virtue of its useful information for areas with few reliable ground-based weather stations. However, there are valid concerns about the database's representation of precipitation and temperature variables. Undoubtedly complicated by the nature of measuring these variables, the proper construction of an interpolated grid is sensitive to a number of complex relations inside a geographical zone, especially regional topography (e.g. the Andean mountain range).

The benefits proffered by the UD-ATP really come to the forefront when discussing macro-level hydrological studies, for they cover vast areas with relatively dependable and temporally-adequate information. Its value is amplified when the scientists turn their attention to areas lacking in climate variables, as is the case for much of the Amazon region. However, micro-level studies should be wary of the spatial resolution employed by these databases, which may restrict quality and fail to provide information that is any more worthwhile than that provided by in situ stations (often achieving better spatial interpolation and resolution).

On the whole, UD-ATP precipitation data present better results than temperature, as has been shown throughout the present analysis. The difference in the quality of the two becomes salient from the perspective of yearly cycles, where the interpolated temperature data in many pixels are systematically deviated from the observed data. Not surprisingly, the majority of these deviations popped up around the Andean mountain range.



(c)

R	Precipitation		Temperature	
0,0 - 0,5	17	16,2%	5	5,7%
0,5 - 0,6	3	2,9%	1	1,1%
0,6 - 0,7	5	4,8%	8	9,2%
0,7 - 0,8	2	1,9%	12	13,8%
0,8 - 0,9	10	9,5%	21	24,1%
0,9 - 1,0	68	64,8%	40	46,0%

Figure 10. *R* values calculated for precipitation (a) and temperature (b). The table (c) summarizes number of pixels for different *R* values.
Source: Authors' own compilation.

Results stemming from the goodness-of-fit test reinforce the notion of interpolated precipitation data reliability. Here, pixels for the Andean chain are good, even if they are available in lesser quantity than for the relatively flat regions found in Brazil. The value of such data does not speak for temperature: results for temperature reflect the poor approximation of UD-ATP database for the entire area studied as regards this variable, nowhere more than areas pertaining to mountainous regions.

Cross-correlation analysis led to good results for both variables. Precipitation saw its worst results concentrated in the northern Peruvian coast, a very dry zone, and in Brazilian territory, where result quality fluctuated from pixel to pixel. As has been the case, UD-ATP temperature performance was not strong in this facet. Additionally, it behoves us to point out that spatial distribution does not define any sort of pattern for temperature data.

Lastly, the authors urge that further attention needs to be paid to developing climate databases with high spatial resolution. Such databases are indispensable for the study of areas with strong climate gradients, although we stress the fact that high resolution does not necessarily translate into better data.

Acknowledgments

Interpolated precipitation and air temperature grids from the University of Delaware (UD-ATP) were provided by the National Oceanic and Atmospheric Administration (NOAA) and Office of Oceanic and Atmospheric Research (OAR), as well as the Earth System Research Laboratory (ESRL) and Physical Science Division (PSD) located in Boulder, Colorado, United States of America. This information can be accessed at http://www.esrl.noaa.gov/psd/.

Data of precipitation and air temperature from ground stations were provided by KNMI (*Koninklijk Nederlands Meteorologisch Instituut* - Royal Netherlands Meteorological Institute) through the Climate Explorer (CLIMEXP) website http://climexp.knmi.nl/.

References

[1] Haylock, M.R., Hofstra, N., Klein-Tank, A.M.G., Klok, E.J., Jones, P.D. and New, M., A European daily high-resolution gridded data set of surface temperature and precipitation for 1950–2006, J. Geophys. Res., 113(D20), pp. D20119, 2008. DOI: 10.1029/2008JD010201.

[2] León-Hernández, J.G., Domínguez-Calle, E.A. y Duque-Nivia, G., Avances más recientes sobre la aplicación de la altimetría radar por satélite en hidrología. Caso de la cuenca amazónica, Ingeniería e Investigación, 28(3), pp. 126-131, 2008.

[3] León-Hernández, J.G., Rubiano-Mejía, J. and Vargas, V., Series temporales de niveles de agua en estaciones virtuales de la Cuenca Amazónica a partir de altimetría radar por satélite, Ingeniería e Investigación, 29(1), pp. 109-114, 2010.

[4] Hijmans, R.J., Cameron, S.E., Parra, J.L., Jones, P.G. and Jarvis, A., Very high resolution interpolated climate surfaces for global land areas, Int. J. Climatol., 25(15), pp. 1965-1978, 2005. DOI: 10.1002/joc.1276.

[5] New, M., Lister, D., Hulme, M. and Makin, I., A high-resolution data set of surface climate over global land areas, Clim. Res., 21(1), pp. 1-25, 2002. DOI: 10.3354/cr021001.

[6] New, M., Hulme, M. and Jones, P., Representing twentieth-century space–time climate variability. Part II: Development of 1901–96 Monthly grids of terrestrial surface climate, J. Climate, 13(13), pp. 2217-2238, 2000. DOI: 10.1175/1520-0442(2000)013<2217:RTCSTC>2.0.CO;2.

[7] Harris, I., Jones, P.D., Osborn, T.J. and Lister, D.H., Updated high-resolution grids of monthly climatic observations – the CRU TS3.10 Dataset, Int. J. Climatol., 34(3), pp. 623-642, 2014. DOI:10.1002/joc.3711.

[8] Mitchell, T.D. and Jones, P.D., An improved method of constructing a database of monthly climate observations and associated high-resolution grids, Int. J. Climatol., 25(6), pp. 693-712, 2005. DOI:10.1002/joc.1181.

[9] Fan, Y. and van den Dool, H., A global monthly land surface air temperature analysis for 1948–present, J. Geophys. Res., 113(D1), pp. D01103, 2008, DOI: 10.1029/2007JD008470.

[10] Matsuura, K. and Willmott, C., Terrestrial air temperature: 1900-2010 gridded monthly time series, version V3.01, Global air temperature archive. National Oceanic and Atmospheric Administration (NOAA), Earth System Research Laboratory (ESRL) Physical Science Division (PSD)., [Online]. Jun-2012. [Date of reference July 15th, 2014] Available at: http://climate.geog.udel.edu/~climate/html_pages/Global2011/README.GlobalTsT2011.html.

[11] Matsuura, K. and Willmott, C., Terrestrial precipitation: 1900-2010 gridded monthly time series, version V3.01, Global precipitation archive. National Oceanic and Atmospheric Administration (NOAA), Earth System Research Laboratory (ESRL) Physical Science Division (PSD)., [Online]. Jun-2012. [Date of reference July 15th, 2014], Available at:

http://climate.geog.udel.edu/~climate/html_pages/Global2011/README.GlobalTsP2011.html.
[12] Adler, R.F., Huffman, G.J., Chang, A., Ferraro, R., Xie, P.-P., Janowiak, J., Rudolf, B., Schneider, U., Curtis, S., Bolvin, D., Gruber, A., Susskind, J., Arkin, P. and Nelkin, E., The version-2 global precipitation climatology project (GPCP) monthly precipitation analysis (1979–Present). J. Hydrometeor, 4(6), pp. 1147-1167, 2003, DOI: 10.1175/1525-7541(2003)004<1147:TVGPCP>2.0.CO;2.
[13] Kalnay, E., Kanamitsu, M., Kistler, R., Collins, W., Deaven, D., Gandin, L., Iredell, M., Saha, S., White, G., Woollen, J., Zhu, Y., Leetmaa, A., Reynolds, R., Chelliah, M., Ebisuzaki, W., Higgins, W., Janowiak, J., Mo, K. C., Ropelewski, C., Wang, J., Jenne, R. and Joseph, D., The NCEP/NCAR 40-Year reanalysis project, Bull. Amer. Meteor. Soc., 77(3), pp. 437-471, 1996. DOI: 10.1175/1520-0477(1996)077<0437:TNYRP>2.0.CO;2.
[14] Xie, P. and Arkin, P.A., Global precipitation: A 17-year monthly analysis based on gauge observations, satellite estimates and numerical model outputs, Bull. Amer. Meteor. Soc., 78(11), pp. 2539-2558, 1997. DOI: 10.1175/1520-0477(1997)078<2539:GPAYMA>2.0.CO;2.
[15] Kanamitsu, M., Ebisuzaki, W., Woollen, J., Yang, S.-K., Hnilo, J.J., Fiorino, M. and Potter, G.L., NCEP–DOE AMIP-II reanalysis (R-2), Bull. Amer. Meteor. Soc., 83(11), pp. 1631-1643, 2002. DOI: 10.1175/BAMS-83-11-1631.
[16] Jeffrey, S.J., Carter, J.O., Moodie, K. B. and Beswick, A.R., Using spatial interpolation to construct a comprehensive archive of Australian climate data, Environmental Modelling & Software, 16(4), pp. 309-330, 2001. DOI: 10.1016/S1364-8152(01)00008-1.
[17] Hutchinson, M.F., McKenney, D.W., Lawrence, K., Pedlar, J. H., Hopkinson, R.F., Milewska, E. and Papadopol, P., Development and testing of Canada-wide interpolated spatial models of daily minimum–maximum temperature and precipitation for 1961–2003, J. Appl. Meteor. Climatol., 48(4), pp. 725-741, 2009. DOI: 10.1175/2008JAMC1979.1.
[18] Perry, M. and Hollis, D., The generation of monthly gridded datasets for a range of climatic variables over the UK, Int. J. Climatol., 25(8), pp. 1041–1054, 2005. DOI: 10.1002/joc.1161.
[19] Herrera, S., Gutiérrez, J.M., Ancell, R., Pons, M.R., Frías, M. D. and Fernández, J., Development and analysis of a 50-year high-resolution daily gridded precipitation dataset over Spain (Spain02), Int. J. Climatol., 32(1), pp. 74-85, 2012, DOI: 10.1002/joc.2256.
[20] Hurtado-Montoya, A.F. and Mesa-Sánchez, Ó.J., Reanalysis of monthly precipitation fields in Colombian territory, DYNA, 81(186), pp. 251-258, 2014. DOI: 10.15446/dyna.v81n186.40419.
[21] van Oldenborgh, G.J., KNMI Climate Explorer, KNMI Climate Explorer, [Online] 1999. [Date of reference July 18th, 2014], Available at: http://climexp.knmi.nl/.
[22] Zender, C.S., Analysis of self-describing gridded geoscience data with netCDF Operators (NCO), Environmental Modelling & Software, 23(10–11), pp. 1338-1342, 2008. DOI: 10.1016/j.envsoft.2008.03.004.
[23] Pierce, D., ncdf: Interface to Unidata netCDF data files. 2014.
[24] Subramanya, K., Engineering Hydrology, 3rd edition. Singapore: McGraw-Hill Education, 2009.
[25] Hyndman, R.J. and Koehler, A.B., Another look at measures of forecast accuracy, International Journal of Forecasting, 22(4), pp. 679-688, 2006. DOI: 10.1016/j.ijforecast.2006.03.001.
[26] De, M., A new unbiased plotting position formula for Gumbel distribution, Stochastic Environmental Research and Risk Assessment, 14(1), pp. 1-7, 2000. DOI: 10.1007/s004770050001.
[27] Shabri, A., A Comparison of plotting formulas for the pearson type III distribution, Jurnal Teknologi C, [Online]. 36C, pp. 61-74, 2002, Available at: http://www.penerbit.utm.my/onlinejournal/36/C/JT36C5.pdf.
[28] Gibbons, J.D. and Chakraborti, S., Nonparametric Statistical inference, 5 ed. Boca Raton: Chapman and Hall/CRC, 2010.

J.S. Fontalvo García, BSc. in Civil Engineeringin 2014 from Pontificia Universidad Javeriana, Colombia. Currently studying a MSc. in Civil Engineering at Pontificia Universidad Javeriana., Bogotá, Colombia.
ORCID: 0000-0003-1041-8286

J.D. Santos Gómez, BSc. in Civil Engineering in 2014 from Pontificia Universidad Javeriana, Colombia. Currently studying a MSc. in Civil Engineering at Universidad de los Andes, Bogotá, Colombia.
ORCID: 0000-0002-9641-3082

J.D. Giraldo Osorio, BSc. in Civil Engineering in 2001 from Universidad Nacional de Colombia, Colombia. Is MSc. in Civil Engineering, in 2003, focused on water resources management, from Universidad de los Andes, Colombia. PhD. in water resources in 2012, from Universidad Politécnica de Cartagena, Spain. He is currently a full professor at the Civil Engineering Department, School of Engineering, Pontificia Universidad Javeriana, Bogotá D.C., Colombia.
ORCID: 0000-0001-6205-3341.

UNIVERSIDAD NACIONAL DE COLOMBIA
SEDE MEDELLÍN
FACULTAD DE MINAS

Área Curricular de Medio Ambiente

Oferta de Posgrados

Especialización en Aprovechamiento de Recursos Hidráulicos
Especialización en Gestión Ambiental
Maestría en Ingeniería Recursos Hidráulicos
Maestría en Medio Ambiente y Desarrollo
Doctorado en Ingeniería - Recursos Hidráulicos
Doctorado Interinstitucional en Ciencias del Mar

Mayor información:

E-mail: acia_med@unal.edu.co
Teléfono: (57-4) 425 5105

UNIVERSIDAD NACIONAL DE COLOMBIA
SEDE MEDELLÍN
FACULTAD DE MINAS



DYNA
http://dyna.medellin.unal.edu.co/

Experimental behavior of a masonry wall supported on a RC two-way slab

Alonso Gómez-Bernal [a], Daniel A. Manzanares-Ponce [b], Omar Vargas-Arguello [c], Eduardo Arellano-Méndez [d], Hugón Juárez-García [e], & Oscar M. González-Cuevas [f]

[a] *Departamento de Materiales, Universidad Autónoma Metropolitana Azcapotzalco, México, D.F., México. agb@correo.azc.uam.mx*
[b] *Posgrado Ing. Estructural División de CBI, Universidad Autónoma Metropolitana Azcapotzalco, México, D.F., México. dmanzanares@anivip.org.mx*
[c] *Posgrado Ing. Estructural División de CBI, Universidad Autónoma Metropolitana Azcapotzalco, México, D.F., México. omanem_9@hotmail.com*
[d] *Departamento de Materiales, Universidad Autónoma Metropolitana Azcapotzalco, México, D.F., México. eam@correo.azc.uam.mx*
[e] *Departamento de Materiales, Universidad Autónoma Metropolitana Azcapotzalco, México, D.F., México. hjg@correo.azc.uam.mx*
[f] *Departamento de Materiales, Universidad Autónoma Metropolitana Azcapotzalco, México, D.F., México. omgc@correo.azc.uam.mx*

Received: October 17th, 2014. Received in revised form: March 29th, 2015. Accepted: October 22th, 2015

Abstract
This paper discusses the experimental results of a prototype slab-wall that is subjected to vertical and horizontal cyclic loading. The key aspects under discussion are: (a) the differences between the capacity resistance of a wall supported on a slab vs. a wall supported on a fixed base, (b) the implications when shear walls are placed directly on transfer concrete slabs, and (c) the effects that these walls cause on the slabs. The most important results presented herein are the change on lateral stiffness and resistance capacity of the load-bearing wall supported on a slab versus the wall supported on a fixed base. Analytical finite element slab-wall models were built using ANSYS. During the experimental test process of horizontal loading, we detected that the stiffness of the slab-wall system decreased by a third compared to the one on the fixed base wall; a result that supported by the numerical models.

Keywords: transfer slab; masonry wall test; concrete slab test; finite element.

Comportamiento experimental de un muro de mampostería apoyado sobre una losa de concreto reforzado

Resumen
Este trabajo analiza los resultados experimentales de un prototipo losa-muro sometido a cargas verticales y horizontales cíclicas. Los aspectos claves en estudio son: (a) las diferencias entre la capacidad resistente de un muro apoyado sobre una losa contra la de otro apoyado sobre base rígida, (b) las implicaciones cuando un muro de carga se desplanta sobre losas de transferencia y (c) los efectos que causan estos muros en las losas de concreto reforzado. Los resultados más importantes encontrados son las diferencias de rigidez lateral y de capacidad resistente del muro apoyada sobre la losa, respecto al empotrado en su base. Para apoyar los resultados del estudio, varios modelos de elementos finitos losa-muro fueron estudiados usando ANSYS. Durante el proceso de prueba con carga horizontal, se detectó que la rigidez de la losa-muro del sistema disminuye a la tercera parte, respecto de la pared fija, este resultado es apoyado por el estudio numérico.

Palabras clave: losas de transferencia; ensaye de muros; muros de mampostería; ensaye losas de concreto; elemento finito.

1. Introduction

In Mexican cities the construction of medium-rise buildings with a structural floor system called "transfer slabs" have been popularized over recent years. Researchers [1] evaluated a set of new buildings constructed in a sector of Mexico City called Colonia Roma, which was severely damaged during the 1985 earthquake. They detected a high percentage of buildings that were designed with discontinuous walls, a structural configuration that induced soft story in some buildings. Furthermore, many of them are projected with transfer floor systems. This situation is worrying because it is known that buildings with discontinuity in elevation are vulnerable to seismic loads. This situation is critical when load-bearing walls,

© The author; licensee Universidad Nacional de Colombia.

especially on the first floor, are not aligned with the vertical forces, therefore increasing seismic vulnerability increased.

These structures have a floor system (transfer slab or transfer floor) supported on one rigid level, which is used as a parking lot. On top of this transfer slab, a four-story shear wall super-structure is constructed. A large percentage of these walls are interrupted at the transfer floor level, and they are not continuous through the foundation. However, a few walls are continuous in height over the edges of the structure, but a significant percentage of walls in the upper stories are not aligned with the axes of the frames of the first floor. This structural configuration causes a significant increase in the shear stress in these walls, as is observed and discussed in detail in the following references [2,3]. This can be explained due to the excessive deflections that walls induce to the slab. The shear forces calculated are two to three times larger than those that these walls would have if they were continuous throughout all their height. In addition, the transfer slab is exposed to additional stresses and high deformations.

The transfer floor system requires further investigation, and in this work the fundamental objective is to analyze, using an experimental model, the interaction between the wall and the slab on which is supported. There are significant differences in behavior between these systems and the traditional ones that do not have discontinuities. Several slab-wall numerical models were also analyzed using ANSYS in order to characterize the behavior of a transfer slab system. In the experimental phase a full-scale slab-wall specimen was designed, built and tested by cyclic loads in the Laboratory of Structures at UAM-Azcapotzalco. The prototype slab-wall was subjected to three load patterns: 1) gravitational load; 2) horizontal load only; and 3) a combination of gravitational and lateral loads.

Mexico and other countries have conducted experimental research on the behavior of load-bearing walls subjected to lateral forces in order to characterize the seismic effects. Walls that have different characteristics, in terms of materials, reinforcement, load conditions and other properties have been tested [4-7], and some of the most notable results were documented [8]. Moreover, in terms of the experimental behavior of concrete slabs, there is less information due to the limited number of tests performed [9,10]. In the limited research the slabs were subjected to distributed or concentrated loads; however, there was no specific linear loads information directly applied on the slabs (walls supported on the slabs).

2. Experimental model

The experimental test included three load protocols: (1) gravitational loads with less than 8 Tons, which is the vertical loading observed in buildings that have the stated floor system, (2) horizontal cyclic loads with a relatively low value that are used in order to study the linear response, and (3) gravitational constant loads with less than 8 Tons that are combined with horizontal increased loading cycles until the failure of the system is reached.

2.1 Geometry and reinforcement

The specimen consists of a masonry wall placed on top of a squared two-way slab of 4.25 m in width, and 12 cm thick, with four reinforced concrete beams (25 x 77) cm along the perimeter. The slab and beams were monolithically casted. The concrete strength was f'_c=250 kg/cm². The details and steel reinforcement in the slab were designed using conventional procedures, such as the ones used in real buildings in Mexico City. On the outer strips, the spacing of the bottom re-bars was set to 40 cm. On the central strip, the spacing was set to 20 cm in both directions. In the top of the slab, the reinforcement spacing was also set to 20 cm. Fig. 1 shows details of the reinforcement used in the slab specimen.

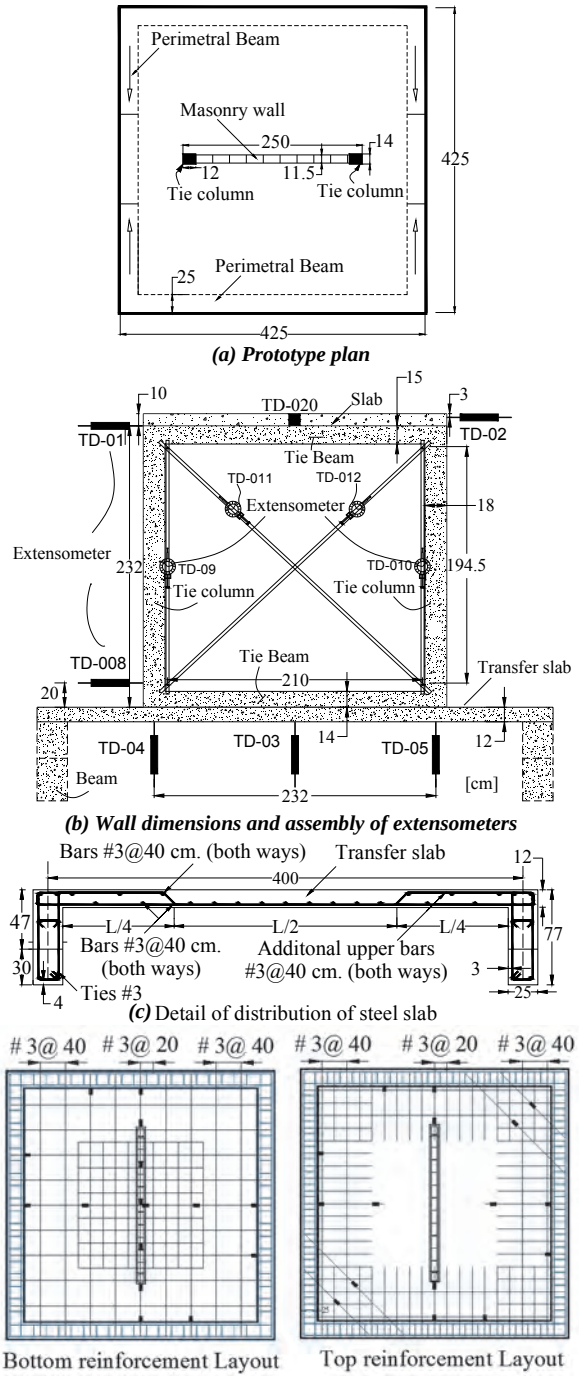


Figure1. Geometry and details of Slab-Wall specimen.
Source: The Authors

The masonry wall that is 2.50 m wide by 2.41m high, was placed on the slab's central strip. The wall is confined with two tie-columns, 14 cm x 18 cm, and with a tie-beam, 14 cm x 14 cm. The bottom tie-beam was integrated with the slab. The concrete resistance of the tie-columns was f'_c=150 kg/cm^2, with four re-bars in the corners. The re-bars complied with the minimum steel requirements of the Mexico City code for masonry structures [11].

2.2. Setup, devices, and instrumentation

We designed and built three mechanical steel devices that helped with the experimental protocol of the specimen: one for attachment purposes, the second one for using in vertical loading, and the third one for horizontal loading. The attachment device prevented the slab-wall specimen from moving in a horizontal or vertical way during the test whenever the loads were applied to the wall. This anchor system consists of a set of steel girders that are fixed in the Laboratory's reaction slab. The gravitational load device was constituted by a system of steel beams, eight tensors and their anchorages (see Fig. 2). The main girders have a box section that is made out of two I sections welded together by its flanges, and reinforced with stiffeners. At the top of the girders there are four vertical actuators (each with a 25 ton capacity), supported on a base plate, which keeps them in an upright position and prevents them from slippage. At the ends, there are re-bars that connect down to the perimeter reinforced concrete beams. The third device was designed for the incremental cyclic horizontal loading. We used a double-action hydraulic actuator with a 25 ton push capacity, and a 12 ton pull capacity. We estimated that the lateral capacity of the wall would reach 12 tons. The corresponding LVDT's were attached to each actuator (four verticals and one horizontal).

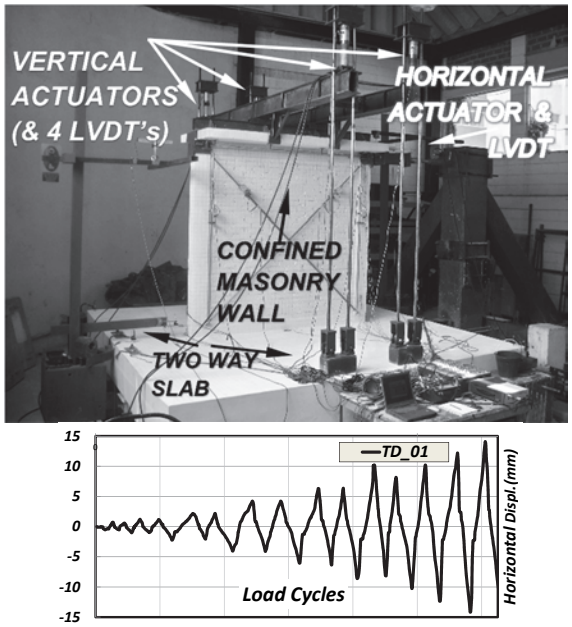


Figure 2. Test set up and typical displacement time history.
Source: The Authors

Table 1.
Numerical models of slab-wall studied in ANSYS [13]

Concrete wall model	Masonry wall model	Wall width (m)	Slab depth (cm)
M1_C2.5_12V	M2_M2.5_12V	2.50	12
M3_C3_12V	M4_M3_12V	3.00	12
M7_C3_13V	M7_M3_13V	3.00	13
M9_C2.5_12VL	M10_M2.5_12VL	2.50	12
M11_C3_12VL	M12_M3_12VL	3.00	12
M15_C3_13VL	M16_M3_13VL	3.00	13

Source: The Authors

The measurement of the strains in the model was possible due to a set of strain gages (SGs) that were installed in the reinforcement of the concrete elements. The slabs had 16 SGs in the bottom and 16 SGs in the top of the slab. The tie-columns of the masonry wall had 20 SGs in the longitudinal re-bars. And finally, there were 10 SGs in the concrete slab and the tie-columns [12]. In order to record the displacements of the slab and the wall, twenty extensometers (TD) were also installed at strategic points, Fig. 1.

3. Numerical models

In the literature, several experimental and theoretical research studies assumed that shear walls are supported on a non-deformable base. In this research, we considered that the walls are supported on a flexible base, and that the performance of the wall-slab system might be different to the one observed for rigid base supports. Our interest is in the definition of the deformation relationship of the wall-slab system; for example, the determination of the relationship between the slab deformation and the wall crack pattern will define the serviceability conditions for these types of structures. These results are important because they will clarify the reasons for the occurrence of a particular crack pattern on the first story walls in buildings with transfer-slabs.

Detailed numerical non-linear models for the slab-wall system were analyzed [13] using ANSYS software [14]. Several geometries were studied, and two materials were used for the wall: masonry and reinforced concrete. Table 1 shows the geometric characteristics of six studied models: four wall lengths and two slab thicknesses. The model was divided in two sections for reducing computational time in analysis. The support conditions of the slab is supposedly restricted on all edges. The M10_M2.5_12V and M10_M2.5_12VL models are similar to the tested specimen.

One of the main goals was the definition of capacity curves for the slab-wall models subjected firstly to incremental vertical loading and secondly to a constant gravitational load combined with incremental cyclic horizontal loading. In the vertical loading models group an additional model subjected to uniform loading without any wall was included for the purposes of comparison. For the lateral loading group, a non-linear model with wall on a rigid base was used for the purposes of comparison (wall on flexible base).

4. Definition of specimen response

Different configurations, or deformation modes, of the slab-wall model in each of the three loading protocols

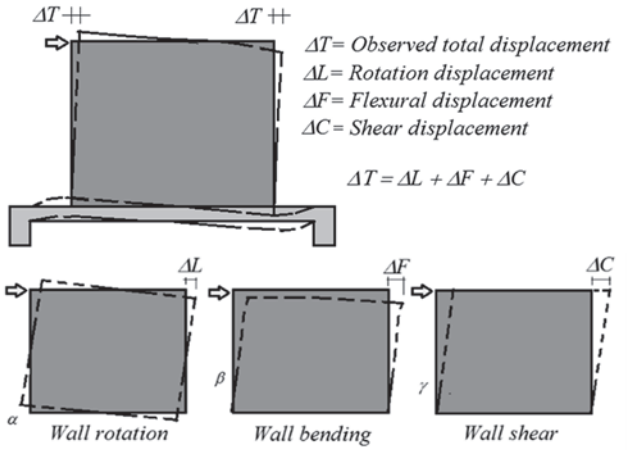


Figure 3. Total deformation (above), and principal deformations modes.
Source: The Authors

(vertical, horizontal, and combined), define the structural behavior and the failure of the system (Fig. 2). Thus, the failure in the tested wall will depend on the bending (ΔF) and shear (ΔC) deformations induced by lateral loading. However, in this case, since the wall is supported by a slab, the lateral displacement due to the wall rotation (ΔL), induced by the slab deformation, has to be considered. Total displacement at the top of the wall ΔT is then induced and presented in Fig. 3.

Shear deformations in the wall can be obtained from the records of displacement transducers that are installed in diagonal directions. Based on the strength of materials theory, the unitary angular deformation, **γ**, is due to the shear stress acting on the wall element [4]. In general the reversible cyclic load is defined by the following expression:

$$\gamma = \frac{\delta_2 L_2 - \delta_1 L_1}{2 l_m h_m} \quad (1)$$

where:

γ = angular deformation of wall,

δ_1, δ_2 = shortening or elongation measured on the diagonals,

L_1, L_2= initial length of diagonals

l_m, h_m _ are the width and height of the wall respectively.

And the total distortion (R_{tot}) or effective distortion (R_{Eff}) is calculated as:

$$R = \Delta E / H \quad (2)$$

$$\Delta E = \Delta F + \Delta C - \Delta L \quad (3)$$

$$\Delta L = (\Delta I - \Delta D) * H / L \quad (4)$$

where:

R= effective drift of the wall.

ΔE= effective lateral displacement at top of the wall,

ΔL, ΔF, and ΔC _are defined in Fig. 3.

ΔI, ΔD _ are vertical displacements at ends in wall-slab joint,

H= distance between TD-01 y TD-08 (Fig 1 (b))

L= distance between TD-04 y TD-05 (Fig 1 (b))

5. Experimental and numerical results

5.1. Response to gravitational loading, experimental vs. analytical results

The code in the analytical models (Table 1) is defined as: M#_Mat#_#V. The M# indicates the model number. The Mat# indicates the material and length of the wall, for example M2.5 indicates that the wall is made out of masonry and has a length of 2.5 m, C indicates that the wall is made out of Concrete. The #V indicates the thickness of the slab, for example 12V indicates that the slab is 12 cm thick.

The capacity curve obtained from the experimental (Exp) specimen is compared with that of the numerical model (M2_M2.5_12V). The experimental system produced a minor stiffness value, as is shown in the curve. This can be explained due to the perfect fixed ends on the perimeter of the slab in the numerical model. However, in both curves the first cracking of the slab occurred at the same time. This happened at an approximate load value of 5.5 tons (Fig. 4). The numerical model was taken to failure mode, the first slab cracking occurred at 5.5 tons; the whole system exhibited linear behavior until the ultimate load of 25 ton was reached. From this point an almost elastic-perfectly-plastic "non-linear" behavior was observed (Fig. 4).

The numerical models M1_C2.5_V12 and M2_M2.5_12V differ in the wall material, _C#_ refers to concrete and _M#_ refers to masonry, as was previously explained. When their capacity curves are compared, they look very similar. This indicates that under vertical loading, no matter what material the wall is made of, the capacity of the whole structural system will almost remain the same. This is confirmed with the curves of the other two pairs of models shown in Fig. 4, which also portrayed the same behavior. Furthermore, whenever the wall is larger, for example 3 m (M3_C3_V12 and M4_M3_V12), both the capacity and the stiffness of the system were increased. Similarly, when the slab thickness was increased to 13 cm (M7_C2.5_V13 and M8_M2.5_V13), the ultimate capacity was also increased.

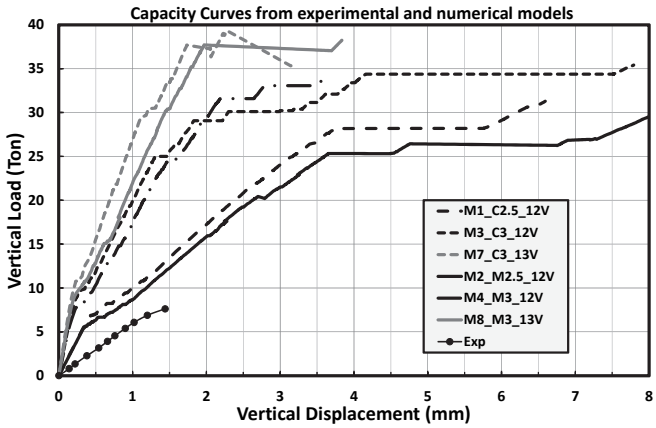


Figure 4. Capacity curves obtained from numerical and experimental models, subjected to vertical loading.
Source: The Authors

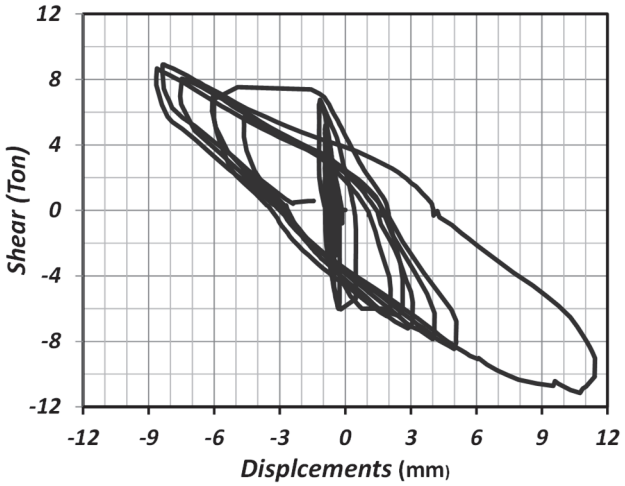


Figure 5. Shear displacement, ΔC, of the wall.
Source: The Authors

The stiffness is the same for loads less than 10 Tons. One of the results that we would like to highlight from the numerical analysis is that, for slab-wall models with a varied slab thicknesses, the ultimate capacity in the system was increased. The stiffness that was observed during the service conditions was also very similar, and, therefore a thicker slab does not guarantee a greater stiffness value while in service conditions.

5.2. Response to gravitational and lateral loading

The tested specimen was subject to a constant vertical load of 8 tons and 16 cycles of monotonic and cyclic horizontal loading. The load was applied with a hydraulic jack with the capacity to perform push and pull actions. The loading was controlled by the horizontal displacement at the top of the wall. The 16 cycles were applied in pairs (push and pull actions), from 0.5 mm to 12 mm; the last two cycles were asymmetric (14 mm and 27 mm), due to the limitation of the hydraulic jack in performing pull actions. The corresponding applied loads were above 11 Tons and 8.9 Tons in push and pull actions.

5.2.1. Displacement and rotation of the wall

Three locations - vertical displacements - under the specimen slab were measured during the test. These are the points TD05, TD03, TD04, which are along the centerline and right under the wall (Fig. 1). Due to the effect of horizontal loading, whenever the right transducer (TD05) climbed above the original reference line it generated rigid-body rotation of the wall (Fig. 3). The vertical displacement increased with every cycle from the beginning of the load. This indicated that due to vertical load intensity on the slab the overall structural behavior observed was non-linear. In every cycle, the slab suffered a displacement of 0.5 mm without returning to its initial position. This represented an approximate accumulated displacement of 9.5 mm at the end of the test.

5.2.2. Shear strains

Rotation, γ, of the wall due to shear deformation is calculated according to the strength of materials theory. Micrometers on wall diagonals did not record any deformation during the first six loading cycles; therefore, it can be concluded that the wall did not have any shear deformations in the first part of the loading process. It only suffered bending and rotation at the base due to slab rotation. However, during the seventh cycle, the diagonal micrometers (TD011 and TD012) began recording shear strains. Until the tenth cycle, the masonry wall exhibited linear behavior, after which the wall experienced non-linear deformations. Fig. 5 shows the hysteresis cycles of shear deformations on the wall.

5.2.3. Global and relative horizontal drifts

Fig. 6 shows the total distortions, R_{tot}, of the specimen, and the relative drift, R_{Ef}, which was calculated during the process of the combined load. In addition, it shows the envelopes of the hysteresis cycles, which are defined by a bilinear trend in the curves. The stiffness was calculated from the slopes of the curves; the stiffness of the slab-wall system was estimated as 11.25 Ton/cm, while the stiffness of the isolated wall (we removed the effect of the rotation as a rigid body) was computed to be 40.0 Tons/cm. This is 3.5 times larger than the wall supported on a flexible base, which is the case whenever the wall is placed in the middle of a two-way slab.

Fig. 7 compares the capacity curves of numerical models M10_M2.5_12VL (wall on flexible base) withMBR_M2.5 (wall on rigid base). We observed significant differences in the curves; even though the load capacity was close to 8 Tons, it is evident that the slopes are different. Stiffness values are also different, for a wall on a flexible base 14 Tons/cm was reached and the one on rigid base was computed as 40 Tons/cm. Numerical and experimental curves were compared, the slopes are very similar for all the models, and the stiffness values obtained in the tested specimen slab-walls were quite similar to those from numerical analysis.

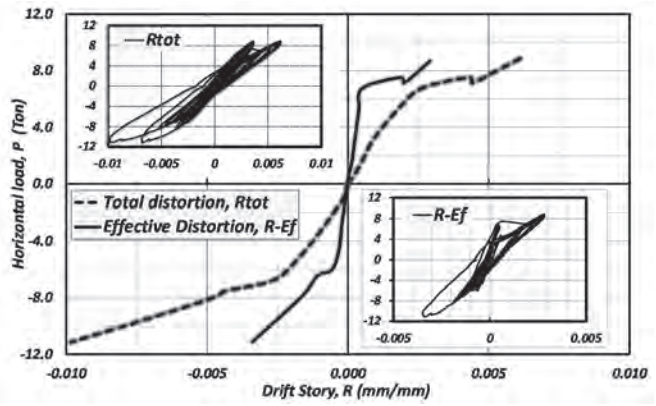


Figure 6. Global (R_{tot}) and effective (R_{eff}) distortions of specimen during the combined load, as well as their respective envelopes.
Source: The Authors

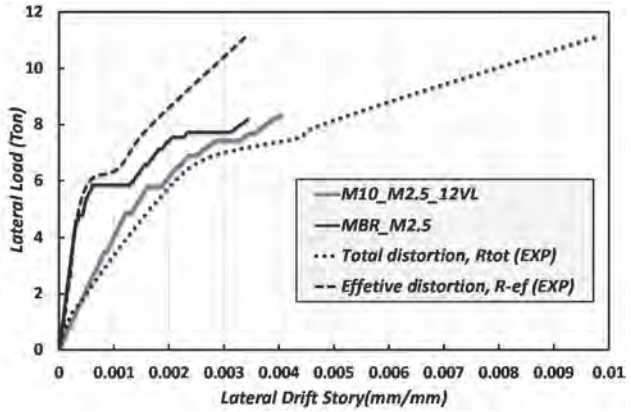


Figure 7. Comparison of numerical and analytical models. Experimental flexible base (*total*) and rigid base (*effective*) versus numerical behavior.
Source: The Authors

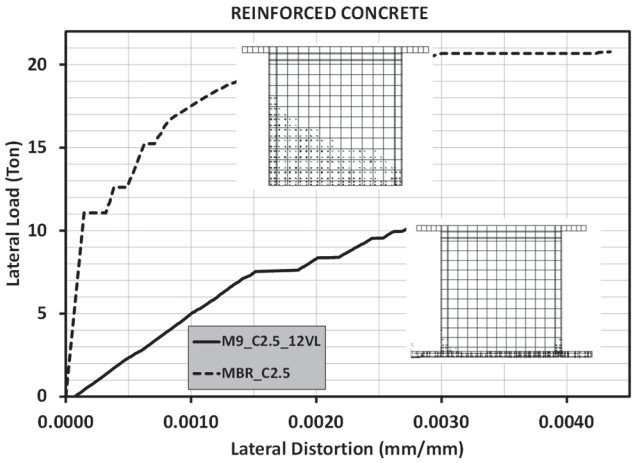


Figure 8. Load-distortion curves for M9_C2.5_12VL and MBR_C2.5 (fixed) models of the concrete wall, including crack patterns.
Source: The Authors

Results from numerical models that consider concrete walls (Fig. 8) show that the behavior is significantly different from the one observed in the masonry wall models. The capacity curves from numerical models M9_C2.5_12VL and MBR_C2.5 (fixed base), show a difference in the linear slopes for as many as 15 times; we computed 14.06 Tons/cm and 210 Tons/cm. However, the stiffness values for the masonry and concrete flexible models M10_M2.5_12VL and M9_C2.5_12VL are very similar, (14.06 Ton/cm vs. 11.25 Ton/cm). The flexibility of the slab does not allow the concrete wall to develop its full capacity and stiffness. This is one result that we would like to draw great attention to.

5.3. Analysis of crack patterns

The crack patterns of numerical models with masonry walls is very similar in both cases, regardless of how the wall is supported (flexible or fixed). This distribution of cracks is typical in confined masonry walls where the cracks are located in the diagonals of the wall. The numerical model cracks are very similar as the ones observed in the slab-wall prototype experimental test (Fig. 9).

We also studied the pattern and distribution of cracking in the numerical models. In the case of concrete walls (Fig. 8), the crack pattern was quite different. The wall on the slab only had a few cracks, and the crack pattern observed on the wall supported on a rigid base was located in the tension zone (lower left corner) of the wall. The concrete wall on a rigid base developed its full shear capacity, while the wall on the transfer slab developed few shear deformation. This phenomenon was attributed to the rotations in the slab, which provoked a large decrease in the stiffness capacity of the whole system, Fig. 8. This condition is very critical for the slab, specifically in the areas located at the ends of the wall. In this area the slab had large cracks on its down side and sustained concrete crushing on the up side. This situation significantly reduces the slab capacity Fig. 10 shows the crack pattern on the up side of the slab(top left) and the crack pattern on the down side of the slab(top right).

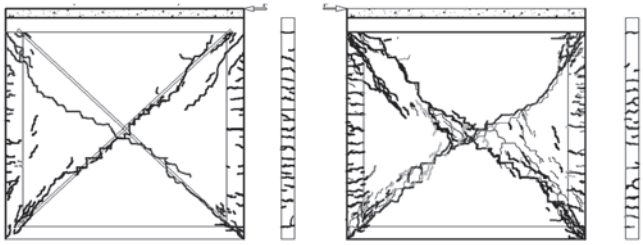


Figure 9. Cracking on the masonry wall after applying the complete load cycles. *Left*: wall cracking on the left side of the wall. *Right*: wall cracking on the right side of the wall.
Source: The Authors

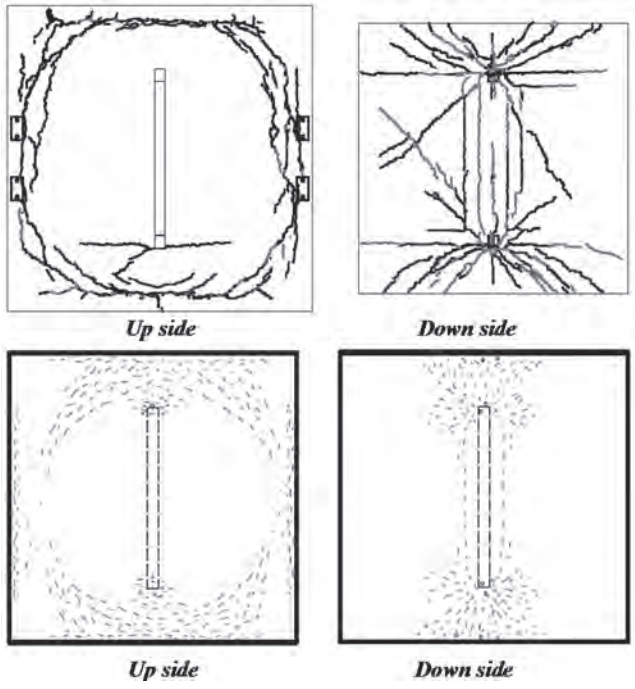


Figure 10. *Top*: Cracking in the concrete slab after applying the complete load cycles in the wall-slab prototype. *Bottom*: status of cracking of the slab in the corresponding ANSYS model under vertical load.
Source: The Authors



Figure 11. Cracking on the masonry wall the day after.
Source: The Authors

5.3.1. Cracking in the slab

When a vertical load was applied to the specimen, the first cracks were observed at the edges of the slab, near the adjacent beams, and normal to the wall. However, at the end of the test, crack patterns at both sides of the slab was observed (Fig. 10 Top). Cracks in the up side of the slab were concentrated on the perimeter edges, and some cracks were observed at the edges of the wall (Fig. 10 Top-left). However, in the down side of the slab, concentrated cracks were observed along the line of the wall in horizontal and radial position. All the cracks had a common origin, which were the unions between the tie-columns and the slab. As a reference, Fig. 10 (bottom) shows the results of the numerical model in ANSYS with vertical loading.

6. Conclusions

In the first stage the specimen was subjected to a process of semi-cycles of increased vertical loading. We observed the first cracking of the concrete slab when the vertical load reached 5.8 Tons. The recorded deflection was 0.5 mm at the centerline of the slab; the load was very close to the design load. After the first stage, the specimen regained its elastic behavior. The numerical model of ANSYS also predicted the onset of cracking at the same load value.

Whenever a low horizontal load was applied, we observed that the stiffness of the slab-wall system was a third of the one observed for a wall on a fixed base. The wall had horizontal displacement mainly because of the slab bending (66%) and the wall bending (33%). The shear deformations were not measured.

During the combined loads process, we observed that the slab sustained deformation in such a way that, after each cycle, a residual deformation in the center line of the slab was growing bigger. The rate was 0.5 mm per cycle without returning to its initial position, due to the intensity of the constant vertical load and the increasing horizontal load.

In the combined loads process, the wall did not suffer shear strains during the first six loading cycles, and was only deformed by bending and rotation of the base, due to the bending of the slab. However, from the seventh cycle, the shear deformation started. Up to the tenth load cycle the behavior was elastic, and after that cycle we consider that the behavior was non-linear.

When the curves from the experimental model are compared to those from the numerical model with ANSYS, we observed an excellent correlation between the two analyzed conditions. The initial stiffness of the isolated wall is 3.5 times greater than the one in the slab-wall model. The concrete wall stiffness supported on a slab decreases by 15 due to the flexibility of the slab.

Acknowledgements

The authors would like to thank the partial support provided by the Secretaría de Obras del Gobierno del Distrito Federal (GDF, Mexico City) through conventions 212015 and 22611040.

References

[1] Gómez-Soberón, C., Gómez-Bernal, A., González-Cuevas, O., Terán, A. y Ruiz-Sandoval, M., Evaluación del diseño sísmico de estructuras nuevas ubicadas en la Colonia Roma del Distrito Federal. Proc. XVII Congreso Nacional de Ing. Sísmica, SMIS, Puebla, Méx. Nov. 2009.

[2] Gomez-Bernal, A., Manzanares, D.A. y Juarez-Garcia, H. Interaction between shear walls and transfer-slabs, subjected to lateral and vertical loading Proc. Vienna Congress on Recent Advances in Earthquake Engineering and Struc. Dynamics. 447, pp. 28-30. Viena, Aut. Aug. 2013

[3] Gómez-Bernal, A., Manzanares, D. y Juárez-García, H., Comportamiento de edificios discontinuos en altura y con pisos de transferencia. Proc. XVIII Congreso Nacional de Ingeniería Sísmica, SMIS, Veracruz, Ver. 2013.

[4] Carrillo, J., Alcocer, S. y González, G., Deformation analysis of concrete walls under shaking table excitations. Revista DYNA, 79(174), pp. 145-155, 2012. ISSN 0012-7353. Medellín.

[5] Gouveia, J.P. and Lourenço, P.B., Masonry shear walls subjected to cyclic loading: influence of confinement and horizontal reinforcement. Proc. Tenth North American Masonry Conference, St. Louis M. USA. Junio 2007.

[6] Astroza, M. y Schmidt, M., Capacidad de deformación de muros de albañilería confinada para distintos niveles de desempeño, Revista de Ingeniería Sísmica, 70, pp. 59-75, 2002.

[7] Preti, M., Migliorati, L. and Giuriani, E., Experimental testing of engineered masonry infill walls for post-earthquake structural damage control, Bulletin of Earthquake Engineering, 13(7), pp 2029-2049, 2015. DOI 10.1007/s10518-014-9701-2.

[8] Meli, R., Mampostería estructural, la práctica, la investigación y el comportamiento sísmico observado en México. CENAPRED Reporte Seguridad sísmica de la vivienda económica, n17 julio, México, 1994.

[9] Park, R. and Gamble, W.L., Reinforced Concrete Slabs, 2nd. Ed., John Wiley & Sons, Inc. 2000.

[10] Vecchio, F. and Tang, K., Membrane action in reinforced concrete slab. Can. J. Civ. Eng. 17, pp. 686-697, 1990. DOI: 10.1139/l90-082

[11] Reglamento de Construcciones del Distrito Federal. NTC de Mampostería. Gaceta Oficial del Gobierno del D.F. México, 2004.

[12] Vargas-Arguello, O.S., Diseño, construcción y ensaye ante carga cíclica de un prototipo losa-muro a escala natural. Tesis de Maestría. Posgrado en Ing. Estructural, CBI – Universidad Autónoma de Mexico, Mexico, 2014.

[13] Manzanares-Ponce, D.A., Comportamiento de edificios estructurados con losa de transferencia. Tesis de Maestría. Posgrado en Ing. Estructural, CBI - Universidad Autónoma de Mexico, Mexico, 2013.

[14] Tickoo, S. and Singh, V., ANSYS 11.0 for Designers, CADCIM Technologies, 2009.

A. Gómez-Bernal, received his BSc. in Civil Engineering in 1984 from the Universidad Autónoma Metropolitana-Azcapotzalco, Mexico, his MSc. in 1989 and his PhD. in 1989, both in Structural Engineering from the Universidad Nacional Autónoma de México, Mexico. From 1984 to 1994, he worked for consulting companies within the structural engineering sector in Mexico City. From 1992 up until the present he has worked for consulting companies and higher education research programs in Mexico. Currently, he is a professor in the structures area at the Materials Department in the Universidad Autónoma Metropolitana - Azcapotzalco. His research interests include: structural behavior in steel structures and their connections, vulnerability and seismic hazard, post-earthquake damage assessment of masonry and concrete structures, post-earthquake evaluation and damage recognition.
ORCID: 000-0002-7131-1688.

D.A. Manzanares-Ponce, received his BSc. in Civil Engineering in 2006 from the Universidad Nacional Autonoma de Honduras and his MSc. in Structural Engineering from the Universidad Autonoma Metropolitana in Mexico City, MExico. From 2006 to 2010 he worked in the design, supervision and construction of roads and edifications. He has developed several pieces of research related to concrete precast slabs, prestressed concrete, the use of recycled concrete and sustainability in construction. Currently he works in Mexico at the Asociacion Nacional de Industriales de Vigueta Pretensada as the Technical Manager and is a structural engineering advisor in several companies.
ORCID: 0000-0001-8534-8724

O.S. Vargas-Arguello, received his BSc. in Civil Engineering in 2011 and his MSc. in Structural Engineering all of them from the Universidad Autonoma Metropolitana in Mexico City, Mexico.
ORCID: 0000-0002-1230-7865

E. Arellano-Méndez, received his BSc. in Civil Engineering in 2000 from the Universidad Autónoma Metropolitana - Azcapotzalco, Mexico his MSc. in Structural Engineering in 2005 from the Universidad Nacional Autónoma de México, and his PhD. in Structural Engineering in 2013 from the Universidad Autónoma Metropolitana – Azcapotzalco.
ORCID: 0000-0001-7790-1104

H. Juárez-García, received his BSc. in Civil Engineering in 1986 from the Universidad Autónoma Metropolitana-Azcapotzalco (UAM-A), Mexico, his MSc. in Structural Engineering in 1990 from the Universidad Nacional Autónoma de México, and his PhD in Earthquake Engineering (Civil Engineering) in 2010 from the University of British Columbia, Canada. From 1986 to 1994, he worked for consulting companies within the structural engineering sector in Mexico City. From 1992 up until the present he has worked for consulting companies and higher education research programs in Mexico, Canada and the USA. Currently, he is a Professor in the Structures Area in the Materials Department in UAM-A. His research interests include: structural behavior due to earthquake loading, multi-risk hazard assessment, vulnerability and seismic hazard, post-earthquake damage assessment of masonry and concrete structures, post-earthquake evaluation and damage recognition.
ORCID: 0000-0002-0432-6476

O.M. González-Cuevas, is a BSc. in Civil Engineer from the Universidad de Yucatán, Mexico. He undertook his masters' degree as well as his PhD in Structural Engineering at the Universidad Nacional Autónoma de México (UNAM), Mexico. Since 1974 he has been a Research-Professor at the Universidad Autónoma Metropolitana (UAM), Mexico. He was also President of this university from 1985 to 1989. Among other appointments he is a former President of the Academy of Engineering of Mexico and of the Mexican Society of Structural Engineering. He has written several textbooks related to "Fundamentals of Reinforced Concrete" and "Structural Analysis". His field of research is mainly reinforced and prestressed concrete structures.
ORCID: 0000-0001-9214-042X

UNIVERSIDAD NACIONAL DE COLOMBIA
SEDE MEDELLÍN
FACULTAD DE MINAS

Área Curricular de Ingeniería Civil

Oferta de Posgrados

Especialización en Vías y Transportes
Especialización en Estructuras
Maestría en Ingeniería - Infraestructura y Sistemas de Transporte
Maestría en Ingeniería – Geotecnia
Doctorado en Ingeniería - Ingeniería Civil

Mayor información:

E-mail: asisacic_med@unal.edu.co
Teléfono: (57-4) 425 5172

UNIVERSIDAD NACIONAL DE COLOMBIA
SEDE MEDELLÍN
FACULTAD DE MINAS



DYNA
http://dyna.medellin.unal.edu.co/

Synthesis of ternary geopolymers based on metakaolin, boiler slag and rice husk ash

Mónica Alejandra Villaquirán-Caicedo [a] & Ruby Mejía-de Gutiérrez [b]

[a] *Composite Materials Group, Faculty of Engineering, CENM, Universidad del Valle, Cali, Colombia, monica.villaquiran@correounivalle.edu.co*
[b] *Composite Materials Group, Faculty of Engineering, CENM, Universidad del Valle, Cali, Colombia, ruby.mejia@correounivalle.edu.co*

Received: October 18th, 2014. Received in revised form: March 29th, 2015. Accepted: October 22th, 2015.

Abstract
Ternary mixtures of geopolymers obtained from the alkaline activation of metakaolin (MK), boiler slag (BS), and rice husk ash (RHA) using a solution of potassium hydroxide were mechanically, thermally, and microstructurally characterized. The geopolymer properties and final microstructures indicate that the addition of BS, despite containing large amounts of unburned material (16.36%), allows for greater densification and greater homogeneity of the geopolymeric gel, which results in greater stability in strength at long curing ages. Substitution of 30% of MK by BS results in an increase in compressive strength of up to 21% and 122% after 28 and 180 days of curing, respectively. These results demonstrate the possibility of the construction sector using geopolymers based on MK and adding BS and RHA to obtain cementitious materials with a lower environmental impact.

Keywords: Geopolymer; metakaolin; boiler slag; rice husk ash.

Síntesis de geopolímeros ternarios basados en metakaolin, escoria de parrilla y ceniza de cascarilla de arroz

Resumen
Mezclas ternarias de geopolímeros fueron obtenidas a partir de la activación alcalina de metacaolín (MK), ceniza de parrilla (BS) usando como activador alcalino una mezcla de hidróxido de potasio con ceniza de cascarilla de arroz (RHA). Los materiales producidos fueron caracterizados mecánica, térmica y microestructuralmente. Las propiedades de los geopolímeros y microestructura final indica que la adición de la escoria de parrilla (con grandes cantidades de material sin quemar, 16.36%), permite un mayor grado densificación y una mayor homogeneidad del geopolímero, resultando en una mayor estabilidad de la resistencia para largas edades. La sustitución del 30% del MK por BS genera un incremento de la resistencia a compresión hasta del 21% y 122% después de 28 y 180 días de curado respectivamente. Los resultados aquí obtenidos demuestran la posibilidad de usar geopolímeros basados en MK son adición de BS y RHA en el sector de la construcción para obtener materiales cementicios con bajo impacto ambiental.

Palabras claves: geopolímero, metacaolín, escoria de parrilla, ceniza de cascarilla de arroz.

1. Introduction

Portland cement is the most widely used construction material due to its physicochemical and mechanical properties; however, its production process demands high energy consumption and emits large amounts of CO_2, primarily due to the consumption of limestone as raw material and the use of fossil fuels during the clinkering process. Environmental demands in the global industry have led to the development of alternative cementitious materials with lower environmental impacts; among these, alkali-activated cements and geopolymers have emerged. Geopolymers are a diverse group of ceramic materials created by the geosynthesis reaction of an aluminosilicate-type material with an alkaline solution at low temperatures (<100 °C). Thus, the geopolymerization process involves a chemical reaction that results in a network-type tridimensional structure. Geopolymers are known as eco-friendly materials because in addition to the fact that they can use industrial residues and sub-products as raw materials,

© The author; licensee Universidad Nacional de Colombia.

they require less energy during their synthesis process and acquire great hardness and strength at ambient temperature and at early ages, as early as the first few hours of being produced [1-3]. Geopolymers are non-combustible materials, resistant to high temperatures, and stable against chemical attack [4,5]; in particular, when they are subjected to elevated temperatures, geopolymers undergo a process similar to the sintering of ceramic materials, where the pore sizes are reduced, which densifies the structure and increases the compressive strength. These properties support the potential for widespread implementation of these materials in engineering applications [6,7].

In general, primary-type materials are used as raw materials, i.e., the material is taken directly from natural sources, such as kaolin-type clays or volcanic tuffs. Secondary-type materials are also used, such as waste (ceramic products waste) or industrials sub-products, which also include Fluid Catalytic Cracking [8], fly ash, and slag obtained from different metallurgic processes [9-12]. The function of alkaline activators is to accelerate the dilution of the aluminosilicate source. Alkaline activators include hydroxides, silicates, and carbonates.

Geopolymer synthesis is affected by different parameters, among which, the size and morphology of the precursor particles influence the viscosity of the fresh-state mixture [13]. Thus, geopolymers based on metakaolin (MK) require greater amounts of mixing water due to the laminar morphology and the greater surface area of MK particles [14]; in contrast, the spherical morphology of fly ash (FA) particles means that less mixing water is required, which reduces cracking at elevated temperatures. Other parameters that can affect the synthesis are related to the chemical composition and microstructure of the raw material; thus, it is affirmed that when FA is used, iron and crystalline phases, such as quartz, are unwanted because at temperatures >500°C, cracking by expansion occurs [15,16].

The combination of precursors in geopolymers results in better final properties; in the case of geopolymers based on MK, mixtures of MK and FA [17-21], and MK and blast furnace slag (GBFS) [22] have been investigated. In several cases, reports contradict each other, particularly in the definition of the optimum mixture percentages [12]. Yunsheng [17] studied the durability of MK geopolymeric mortar fibers reinforced with substitutions of up to 50% FA and concluded that with 10% FA, a material with lower porosity, greater impact strength, and a greater tenacity can be obtained; larger percentages adversely affect the properties due to the lower reactivity of FA compared with that of MK. However, in a later study, the same researcher [19] suggested using mixtures of up to 30% FA to obtain acceptable strengths and to immobilize heavy metals. Zhang [20] evaluated percentages of up to 66.7% FA and reported increases in fluidity, setting time, and compressive strength for mixtures with 35.5% FA in MK geopolymers reinforced with polypropylene fibers. In a later study, the same author [18] recommends the substitution of MK for FA in the order of 10%, and attributes the loss of mechanical properties to the increase in porosity of the geopolymeric paste when using higher percentages. Aguilar [21] produced lightweight geopolymeric concretes based on MK enhanced with 25% FA with acceptable properties. It is worth noting that the physicochemical properties of the raw materials in these studies were different. In this sense, the goal in selecting the raw materials for binary and/or ternary mixtures for geopolymeric materials is to seek the best combination of properties, which depends on the application of the final product.

Table 1.
Chemical composition of the raw materials (wt.%).

Compound, (wt, %)	MK	BS	RHA
SiO_2	51.52	49.24	92.33
Al_2O_3	44.53	25.39	0.18
Fe_2O_3	0.48	7.65	0.17
CaO	0.02	0.77	0.63
MgO	0.19	0.53	0.49
Na_2O	0.29	-	0.07
K_2O	0.16	-	0.15
TiO_2	1.71	-	-
LOI[a]	1.09	16.36	2.57

[a]LOI: Loss on ignition at 1000°C

Source: Authors' own.

The present study analyzes the mechanical performance of geopolymeric mixtures based on MK and incorporates a sub-product of coal combustion obtained from industrial boilers, which contains a high content of unburned material (boiler slag). It is noteworthy that there is no literature on the use of this material as a partial substitution for MK in the synthesis of geopolymeric materials. In addition, agro-industrial waste is used, i.e., rice husk ash mixed with potassium hydroxide as the alkaline activator. The mechanical compressive strength is evaluated, and techniques, such as thermogravimetric analysis, Fourier transform infrared spectroscopy and scanning electron microscopy, are applied to analyze the microstructure of the developed materials.

2. Experimentation

2.1. Materials

Metakaolin (MK, supplied by the BASF Corporation) and boiler slag (BS, collected from a boiler of PROPAL S.A.) were used as precursor materials. Table 1 shows the chemical composition of the materials determined by X-ray fluorescence (XRF). An X-ray fluorescent spectrometer, MagixPro (PW–2440 Philips) equipped with a Rhodium tube with a maximum power of 4 kW was used. Fig. 1 shows the results of the X-ray diffraction test for the raw materials, where it can be observed that MK is a highly amorphous material; the small crystalline phase signals are attributed to impurities, such as anatase (TiO_2, Inorganic Crystal Structure Database, ICSD 154604) and quartz (SiO_2,). The BS contained large amounts of quartz, mullite, hematite and in addition, it was possible to identify a slight increase in the base line for the 2θ angles between 20°-30°, which suggests the presence of amorphous-state material.

The BS was conditioned by milling in a hammer mill and then in a ball mill for 1 hour until an average particle size of 19.143 μm was obtained. The MK particle size was 7.8 μm.

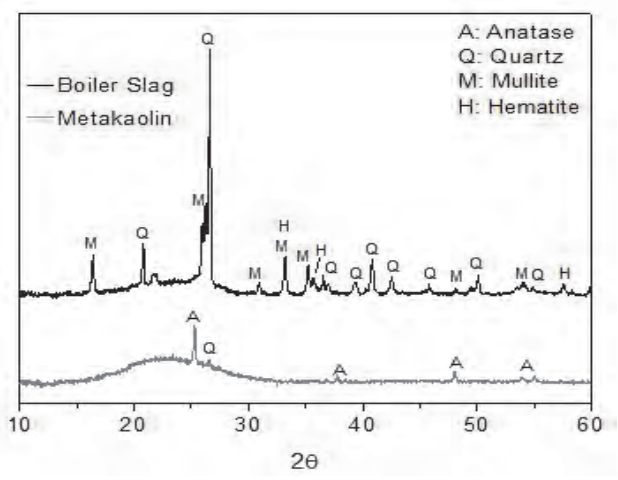


Figure 1. XRD patterns for the raw materials.
Source: Authors' own.

In both cases, the laser granulometry technique was performed using Mastersizer 2000 equipment. Rice husk ash (RHA) was used as the silica source to prepare the activator. The RHA was obtained via a thermal treatment of the rice husk at 700°C for 2 hours in an electric oven; the amorphous SiO2 content in the RHA was 92%.

2.2. Preparation of the geopolymers

Three geopolymeric systems were studied: E0 (100% MK), E20 (80% MK and 20% BS by weight), and E30 (70% MK and 30% BS). The alkaline solution used as the activating agent was prepared from the RHA mixture with potassium hydroxide pellets in the presence of water. In the E0 mixture, a SiO_2/Al_2O_3 molar ratio of 2.5 and a liquid/solid ratio of 0.4 were used; in the remaining mixtures, the molar ratios were 3.0 and 0.35, respectively; the K_2O/SiO_2 molar ratio was 0.28 for all mixtures. The specimens were cured at a temperature of 70°C for 20 hours at a relative humidity >90%. Afterwards, they were demolded, wrapped in plastic film to avoid water evaporation, and placed in a chamber at a relative humidity of ~60%; then, the compressive strengths at different curing ages were determined.

2.3. Test

The compressive strength was determined for each of the geopolymeric systems up to an age of 180 curing days using cubic specimens with dimensions of 20 x 20 mm; the test was performed in a universal testing machine, Instron® 3369, at a displacement rate of 1 mm/min. The performance index (P.I) was determined following the eq. (1), where *Ex* corresponds to E20 and E30

$$P.I(\%) = \frac{Strength(Ex) - Strength(E0).}{InitialStrength(E0).} x100 \quad (1)$$

The following instrumental techniques were used for the mineralogical and microstructural analysis of the specimens: X-ray diffraction (XRD) using wide angle diffraction equipment (RINT2000) with a Cu-Kα1 signal at 45 kV and 40 mA with a step of 0.02° in a 2θ range of 10°- 60° at a scan speed of 5°/min; Fourier transform infrared spectroscopy analysis (FTIR) was performed with a Perkin Elmer spectrum 100 spectrometer in the transmittance mode in a frequency range of between 450 cm^{-1} and 4000 cm^{-1}, where the samples were prepared by the KBr compression method; the thermogravimetric analysis (TGA/DTG) of the samples was performed in a nitrogen atmosphere using TA Instruments STD Q-600 equipment at a heating rate of 10 °C/min and up to a temperature of 1250ºC. The collected data were analyzed with *Universal Analysis* software, version 4.4A from TA Instruments. The scanning electron microscopy (SEM) images were obtained using JEOL JSM-6490LV equipment, which has an INCAPentaFETx3 detector (OXFORD INSTRUMENTS, model 7573).

3. Results and discussion

Fig. 2a shows the results of the compressive strength obtained for the mixtures evaluated up to an age of 180 curing days. Fig. 2b shows that the P.I can be observed when substituting MK by 20 and 30% of BS in the geopolymer; this index represents the strength increment with the added percentage. The average compressive strength at 7 curing days for E20 and E30 was 6.5 and 1.6% better than that of E0, respectively. It can be observed that in general, a decrease in strength occurs at long curing ages (greater than 90 days). This effect is attributed to the curing temperature and time used in the geopolymer synthesis during the initial hardening phase at 70°C for 20 hours [12]. Rovnanik [23] performed a study on the curing temperature (10-80°C) effect on the strength development of the geopolymer based on MK and also reported a decrease in strength as the temperature and time increased, which is associated with a less densified and less compact structure. The author claims that when subjecting the specimen to thermal curing, in particular, at temperatures above 60°C, the polymerization degree increases, which contributes to increased strength during the early ages. However, with rapid setting and hardening, the formation of a lower quality structure with greater porosity is obtained, which is detrimental to the mechanical properties at greater ages [23]. This conclusion coincided with those expressed by other authors [24]. It is noted that the open porosity (ASTM C642) of the geopolymers based only on MK (E0) is 13.7% and 28.9% higher than the open porosity of the E30 and E20 respectively. The addition of BS stabilizes this effect and reduces the porosity, which is seen in the smaller decrease in strength for E20 and E30 at ages of 90 and 180 days. This result is reflected in the performance indexes calculated for E20 and E30 at an age of 180 days, which were 87 and 121%, respectively. Based on compressive strength results of the geopolymer pastes, the samples E0 and E30 were selected. These geopolymer were characterized by FTIR, TGA/DTG and SEM.

Fig. 3 shows the FTIR analyses of the aluminosilicate precursors (MK and BS) and the silica source used in the preparation of the alkaline activator. The RHA spectrum exhibited a broad band centered at 1100 cm^{-1}, which is

associated with the asymmetric stretching vibrational band of the Si-O-Si bonds, and similarly, a vibrational mode at 802 cm^{-1}, which is attributed to the symmetric stretching of Si-O-Si. The MK spectrum contains a broad asymmetric stretching band centered at 1089 cm^{-1}, which is associated with the presence of amorphous structures and with the Si-O-Al/Si bond. A vibrational mode is also observed at 814 cm^{-1}, which is associated with the Al-O bond of Al^{IV}, and at 472 cm^{-1}, which is associated with the Si-O-Si and O-Si-O bond-bending vibrations [25].

The BS spectrum revealed an absorption band between 900-1200°C, which is centered at 1103 cm^{-1} and associated with the asymmetric stretching vibrations of the Si/Al-O bonds that correspond to quartz, mullite, and minerals found in the XRD spectra of the BS. The signals at 471 cm^{-1} and 799.5 cm^{-1} are associated with symmetric stretching vibrations of the Si-O-Si and O-Si-O bonds due to the presence of quartz in the raw material [26]. The signal at 561.2 cm^{-1} is attributed to the symmetric stretching vibrations of the Al-O-Si-type bonds [27], which is associated with the octahedral aluminum (Al^{VI}) present in the mullite phase, previously identified in the XRD of the material. The signal located at approximately 1630 cm^{-1} in RHA and MK is associated with the vibration of the O-H bond, which is characteristic of water molecules being weakly adsorbed on the surface by the samples during their preparation.

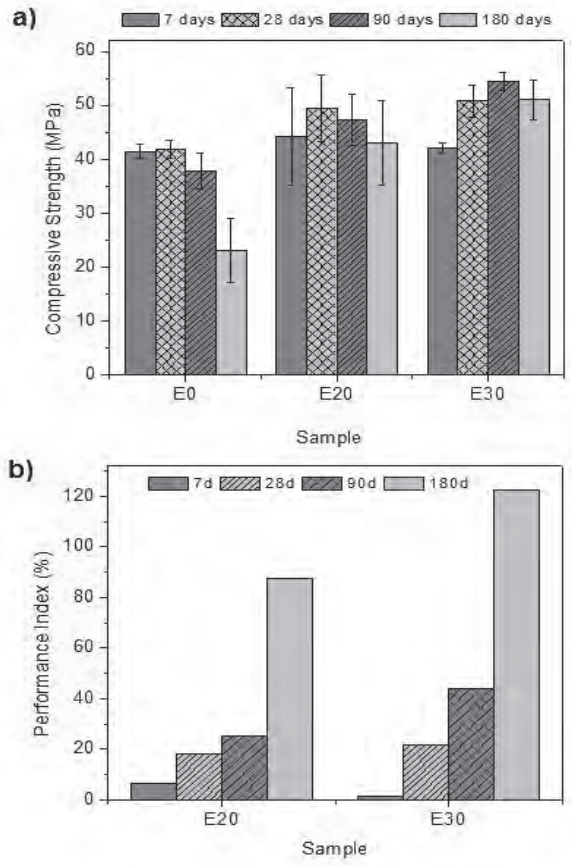


Figure 2. Compressive strength and performance index of the geopolymer pastes at different curing ages.
Source: Authors' own.

In the FTIR spectra of E0 and E30 (Fig. 4), a broad band of great intensity was identified between 1200 and 800 cm^{-1}, which corresponds to the asymmetric stretching vibration of the Si-O-T bonds (where T corresponds to Si or Al) [14,24]. Generally, this band can be associated with the polymerization degree [29]. Compared with those corresponding to the precursors, this band shifted to lower wavelengths by approximately 50 cm^{-1} in the geopolymer, as shown in Fig.4. The E0 signal is at slightly higher wavelengths (1047.4 cm^{-1}) compared with that exhibited by E30 (whose signal is located at 1036 cm^{-1}) after 28 curing days (Fig. 4a). The signals corresponding to the bending vibrations of the Si-O-Si bonds are approximately between 463 and 473 cm^{-1} in both geopolymers. The signals between 591-616 cm^{-1} are attributed to the symmetric stretching vibrations of Si-O-Al [30].

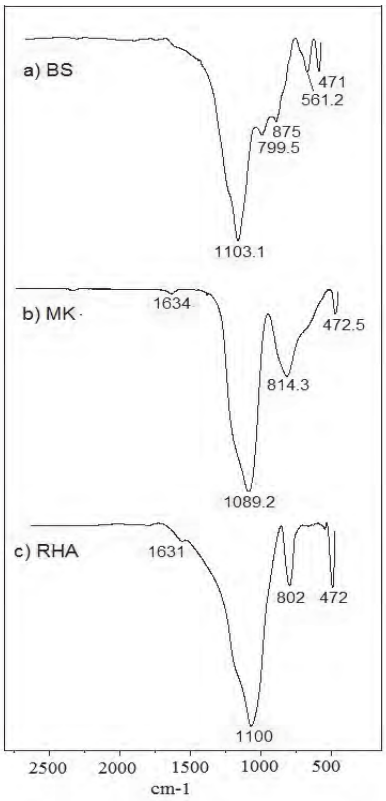


Figure 3. FTIR analysis for the raw materials.
Source: Authors' own.

The signal identified at ~858 cm^{-1} corresponds to the asymmetric stretching vibration of the tetrahedrally coordinated Al present in the formed gel, which corroborates the presence of structures composed by tetrahedrons of SiO_4 and AlO_4 distributed in different configurations, characteristic in these types of materials [14]. The signal at 875 cm^{-1} identified for geopolymer E30 corresponds to the asymmetric stretching vibration of Al^{V}, associated with mullite from the raw material; this result is an indication that this phase is inactive during the geopolymerization process and remains unaltered. The signals identified at ~697-713 cm^{-1} correspond to the stretching of the Si-O-Si(Al) bonds, whose intensity indicates the elevated substitution degree of

Al in the Si-rich gel, which is characteristic of the formation of amorphous polymers [17,25,31]. This signal is more intense in geopolymer E0.

Likewise, a band located at ~1650-1658 cm^{-1} is observed, which corresponds to the stretching vibration of the H-OH in molecules of water for reaction products and determines whether they are weakly bound at the surface level or trapped in the structure cavities [32]. The signal at 1430.6 cm^{-1} is attributed to CO-type bonds associated with stretching vibrations of CO_3^{-2} compounds, in particular, alkaline carbonates generated by the reaction with CO_2 in the atmosphere (K_2CO_3) [33-35] and calcite ($CaCO_3$) generated by the reaction between CO_2 in the atmosphere and Ca^{+2} from BS. Similarly, for the case of E0, the signal is associated with organic matter present in BS.

For both the E0 and E30 samples, the shift of the primary T-O-T band at lower wavelengths (1007 cm^{-1}) in the samples at 180 days can be attributed to a greater substitution of SiO_4 tetrahedrons by AlO_4 tetrahedrons in the geopolymeric gel, which is a result of a decrease in the SiO_2/Al_2O_3 ratio in the geopolymer matrix with time. The shifts to lower values are due to the lower strength of the Al-O bond, which vibrates at lower frequencies compared with that of the Si-O bond [36,37].

Fig. 5 shows the thermograms for samples E0 and E30 at the age of 180 curing days. The TGA shows that a greater mass loss occurs at temperatures below 400°C, where the mass loss was ~8.70 and 5.99% for E0 and E30, respectively. This loss is attributed to the evaporation of the free water contained in the larger pores (<100 ºC), to the water adsorbed in the gel pores, and to the water bound to the K-A-S-H structure [1]. The decay in the mechanical properties of the sample E0 could be related to the greater content of water weakly bound in this matrix, which was observed in the TGA. In addition, a second weight loss is detected in the DTG for sample E30 in the temperature range of 600-800°C, which is associated to the slag residual coal identified in the XRF test (Table 1), and to the decomposition of the carbonate

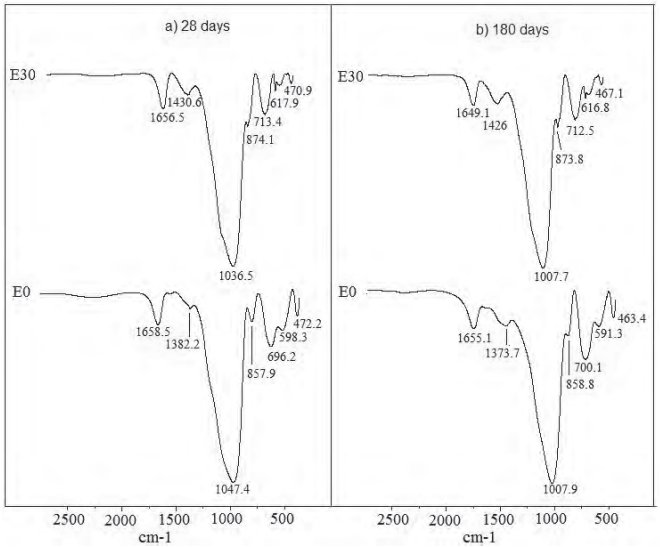


Figure 4. FTIR spectra of the geopolymers at different curing ages. Source: Authors' own.

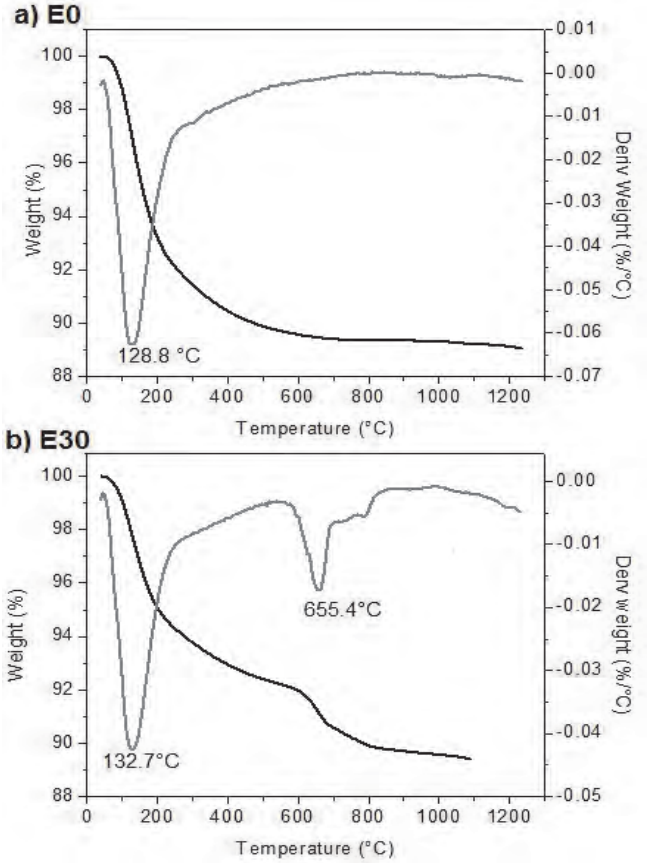


Figure 5. TGA and DTG curves of the geopolymers at 180 curing days. Source: Authors' own.

species previously identified in the FTIR test (Fig. 4), which can be in the form of potassium carbonate or bicarbonate (K_2CO_3 or $KHCO_3$) [34, 35]. The loss in total weight of up to 1200°C was 9.93% for E0 and 9.44% for E30.

The microstructure of the raw materials and of the geopolymers produced can be observed in the SEM micrographs shown in Fig. 6. Here, a hexagonal laminar morphology is identified for MK in contrast with BS, which contains particles of angular morphology, greater size, and with porous characteristics due to the content of unburned coal (Figs.6a, 6b, respectively). On the surface of geopolymer E0, at a curing age of 28 days, it is possible to observe small particles of unreacted residual MK (**O**) embedded in the gel, and in E30, particles of unreacted BS (◊) (Figs 6c, 6d). After 180 days (Fig.6e), a similar morphology is observed for geopolymer E0, with the presence of pores (Δ) and particles of unreacted MK. In contrast, in E30 (Fig. 6f), the surface is more homogenous, soft, and compact, with less porosity and less proportion of unreacted BS or MK particles. The greater porosity in E0 can be attributed to the effect of curing at 70°C, and the greater amount of water in the mixture (liq./sol. ratio of 0.4). Although higher water contents are necessary for workability and mobilization of the alkaline ions during the mixing process, and in the fresh state, at a greater age, this contributes to contraction and cracking and increases porosity in the microstructure of the hardened gel [12,24].

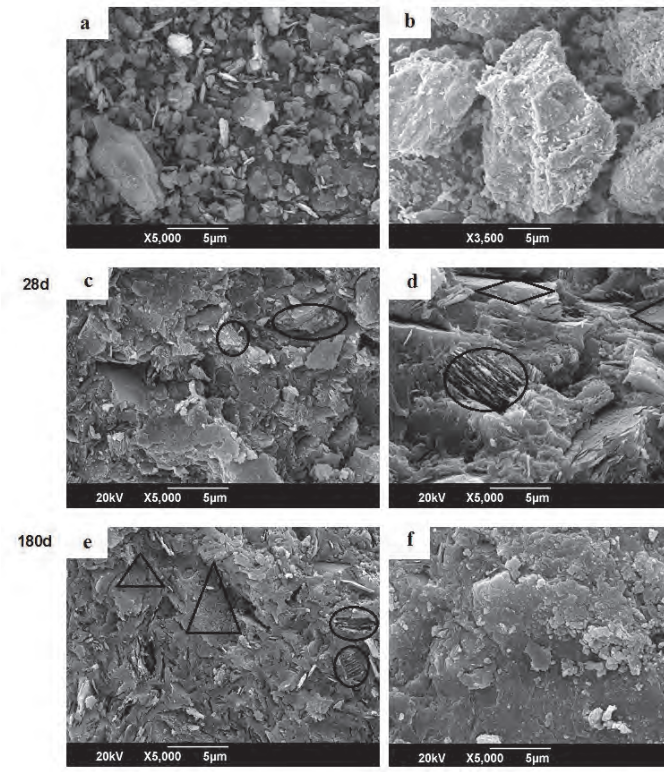


Figure 6. SEM images for the raw materials (a) MK, (b) BS; (c) E0 and (d) E30 geopolymers pastes at 28 curing days; (e) E0 and (f) E30 geopolymer pastes at 180 curing days.
Source: Authors' own.

The presence of the BS decreases the water mixing requirements, producing a less porous material, with a more densified and compact structure, which keeps its compressive strength stable for long ages.

4. Conclusions

The geopolymerization of ternary mixtures based on MK, BS, and RHA was successfully performed. The materials produced were mechanically tested and their microstructural characterization was followed up to 180 days of aging. From the results of this investigation, it can be concluded that two industrial sub-products, BS and RHA, can be used along with MK as starting materials in the preparation of ternary geopolymeric mixtures. The high contents of unburned material and crystalline phases, such as quartz and mullite in BS, do not affect the geopolymerization process. The ternary mixture with 30% BS exhibited better mechanical strength for greater ages in comparison with the reference mixture, which indicates that the partial substitution of MK by 30% BS contributes positively to the stabilization of the matrix; strength increments of 121% were obtained after 180 days. In time, the ternary geopolymer showed a greater degree of geopolymerization, a more homogenous surface, and a lower content of unreacted material, which maintains a high strength for long curing times (51 MPa). These materials present properties of interest for their application in the construction sector, in particular, in the production of structural elements, while simultaneously contributing to the reutilization of two industrial residues, BS and RHA, and to a lower environmental impact.

Acknowledgements

The authors would like to thank the Colombian Institute for the Development of Science, Technology, and Innovation (Colciencias) and Universidad del Valle (Centre of Excellence for Novel Materials - CENM) (Cali, Colombia) for their financial support provided for this study.

References

[1] Duxson, P., Lukey, G.C. and van Deventer, J.S.J., Physical evolution of Na-geopolymer derived from metakaolin up to 1000 C. J. Mater. Sci., 42(9), pp. 3044-3054, 2007. DOI: 10.1007/s10853-006-0535-4

[2] Al-Bakri, M.M., Mohammed, H., Kamarudin, H., Niza, I.K., and Zarina, Y., Review on fly ash-based geopolymer concrete without Portland Cement. J. Eng. Technol. Res., 3(1), pp. 1-4, 2011.

[3] Zhang, Z., Yao, X. and Zhu, H., Potential application of geopolymers as protection coatings for marine concrete I. Basic properties. Appl. Clay Sci., 49(1–2), pp. 1-6, 2010. DOI: 10.1016/j.clay.2010.01.014

[4] Nicholson, C., Fletcher, R., Miller, N., Stirling, C., Morris, J., Hodges, S., Mackenzie, K. and Schmucker, M., Building innovation through geopolymer technology. Chem. New Zel., 69(3), pp. 10-13, 2005.

[5] Lloyd, R.R., Provis, J.L. and van Deventer, J.S.J., Acid resistance of inorganic polymer binders. I. Corrosion rate. Mater. Struct., 45(1–2), pp. 1-14, 2011. DOI:10.1617/s11527-011-9744-7

[6] Duxson, P., Fernández-Jiménez, A., Provis, J.L., Lukey, G.C., Palomo, A. and van Deventer, J.S.J., Geopolymer technology: The current state of the art. J. Mater. Sci., 42(9), pp. 2917-2933, 2006. DOI: 10.1007/s10853-006-0637-z

[7] Komnitsas, K. and Zaharaki, D., Geopolymerisation: A review and prospects for the minerals industry. Miner. Eng., 20(14), pp. 1261-1277, 2007. DOI: 10.1016/j.mineng.2007.07.011

[8] Martínez-López, C., Mejía-Arcila, J.M., Torres-Agredo, J. y Mejía-de Gutiérrez, R. Evaluación de las características de toxicidad de dos residuos industriales valorizados mediante procesos de geopolimerización. DYNA, 82(190), pp 74-81, 2015. DOI: 10.15446/dyna.v82n189.43136

[9] Buchwald, A., Weli, M. and Dombrowski, K., Evaluation of primary and secondary materials under technical, ecological and economic aspects for the use as raw materials in geopolymeric binders, Proceedings of the 2nd International Symposium of Non-Traditional Cement and Concrete, 2005. pp. 32-40. ISBN: 80-214-2853-8

[10] Duxson, P. and Provis, J.L., Designing precursors for geopolymer cements. J. Am. Ceram. Soc., 91(12), pp. 3864-3869, 2008. DOI: 10.1111/j.1551-2916.2008.02787.x

[11] Kovalchuk, G., Fernández-Jiménez, A. and Palomo, A., Alkali-activated fly ash. Relationship between mechanical strength gains and initial ash chemistry. Mater. Constr., 58(291), pp. 35-52, 2008. eISSN: 1988-3226

[12] Rashad, A.M., Alkali-activated metakaolin: A short guide for civil Engineer – An overview. Constr. Build. Mater., 41, pp. 751-765, 2013. DOI: 10.1016/j.conbuildmat.2012.12.030

[13] Steveson, M. and Sagoe-Crentsil, K., Relationships between composition, structure and strength of inorganic polymers. J. Mater. Sci., 40(16), pp. 4247-4259, 2005.

[14] Granizo, M.L., Blanco-Varela, M.T. and Martínez-Ramírez, S., Alkali activation of metakaolins: Parameters affecting mechanical, structural and microstructural properties. J. Mater. Sci., 42(9), pp. 2934-2943, 2007. DOI: 10.1007/s10853-006-0565-y

[15] Rickard, W.D.A., Williams, R., Temuujin, J. and van Riessen, A. Assessing the suitability of three Australian fly ashes as an aluminosilicate source for geopolymers in high temperature applications. Mater. Sci. Eng. A, 528(9), pp. 3390-3397, 2011. DOI: 10.1016/j.msea.2011.01.005

[16] Rickard, W.D.A., van Riessen, A. and Walls, P., Thermal character of geopolymers synthesized from class F fly ash containing high concentrations of iron and α-quartz. Int. J. Appl. Ceram. Technol., 7(1), pp. 81-88, 2010. DOI: 10.1111/j.1744-7402.2008.02328.x
[17] Yunsheng, Z., Wei, S. and Zongjin, L., Impact behavior and microstructural characteristics of PVA fiber reinforced fly ash-geopolymer boards prepared by extrusion technique. J. Mater. Sci., 41(10), pp. 2787-2794, 2006. DOI: 10.1007/s10853-006-6293-5
[18] Zhang, Z., Wang, H., Zhu, Y., Reid, A., Provis, J. and Bullena, F., Using fly ash to partially substitute metakaolin in geopolymer synthesis. Appl. Clay Sci., 88–89, pp. 194-201, 2014. DOI: 10.1016/j.clay.2013.12.025
[19] Yunsheng, Z., Wei, S., Wei, S. and Guowei, S., Synthesis and heavy metal immobilization behaviors of fly ash based gepolymer. J Wuhan Univ Technol– Mater Sci., 24(5), pp. 819-825, 2009. DOI: 1007/s11595-009-5819-5
[20] Zhang, Z-H,, Yao, X., Zhu, H. J., Hua, S-D. and Chen, Y., Preparation and mechanical properties of polypropylene fiber reinforced calcined kaolin fly ash based geopolymer. J Cent South Univ Technol., 16, pp. 49-52, 2009. DOI: 10.1007/s11771-009-0008-4
[21] Arellano-Aguilar, R, Burciaga-Diaz, O. and Escalante-Garcia, J.I., Lightweight concretes of activated metakaolin-fly ash binders, with blast furnace slag aggregates. Constr. Build. Mater. 24, pp.1166-1175, 2010. DOI: 10.1016/j.conbuildmat.2009.12.024
[22] Bernal, S.A, Rodriguez, E.D, Mejía-de Gutierrez, R., Gordillo, M.I. and Provis, J.L., Mechanical and thermal characterisation of geopolymers based on silicate-activated metakaolin/slag blends. J. Mater. Sci. 46, pp. 5477-5486, 2011. DOI: 10.1007/s10853-011-5490-z
[23] Rovnaník, P., Effect of curing temperature on the development of hard structure of metakaolin-based geopolymer. Construction and Building Materials, 24, pp. 1176-1183, 2010. DOI: 10.1016/j.conbuildmat.2009.12.023
[24] Arellano-Aguilar, R., Burciaga-Díaz, O., Gorokhovsky A. and Escalante-García, J.I., Geopolymer mortars based on a low grade metakaolin: Effects of the chemical composition, temperature and aggregate: Binder ratio. Constr. Build. Mater., 50, pp. 642-648, 2014. DOI: 10.1016/j.conbuildmat.2013.10.023
[25] Bernal, S., Rodríguez, E., Mejía-de Gutierrez, R., Provis, J. and Delvasto, S., Activation of metakaolin/slag blends using alkaline solutions based on chemically modified silica fume and rice husk ash. Waste and Biomass Valorization, 3(1), pp. 99-108, 2012. DOI: 10.1007/s12649-011-9093-3
[26] Lee, W.K.W. and van Deventer, J.S.J., Structural reorganisation of class F fly ash in alkaline silicate solutions. Colloids Surfaces A Physicochem. Eng. Asp., 211(1), pp. 49-66, 2002. DOI: 10.1016/S0927-7757(02)00237-6
[27] Criado, M., Fernández-Jiménez, A. and Palomo, A., Alkali activation of fly ash: Effect of the SiO_2/Na_2O ratio: Part 1: FTIR study. Microporous Mesoporous Mater., 106(1–3), pp. 180-191, 2007. DOI: 10.1016/j.micromeso.2007.02.055
[28] Heah, C.Y., Kamarudin, H., Mustafa-Al Bakri, A.M., Bnhussain, M., Luqman, M., Khairul-Nizar I., Ruzaidi, C.M. and Liew, Y.M., Kaolin-based geopolymers with various NaOH concentrations. Int. J. Miner. Metall. Mater., 20(3), pp. 313-322, 2013. DOI: 10.1007/s12613-013-0729-0
[29] Chindaprasirt, P., Jaturapitakkul, C., Chalee, W. and Rattanasak, U., Comparative study on the characteristics of fly ash and bottom ash geopolymers. Waste Manag., 29(2), pp. 539-543, 2009. DOI: 10.1016/j.wasman.2008.06.023.
[30] Panagiotopoulou, C., Kontori, E., Perraki, T. and Kakali, G., Dissolution of aluminosilicate minerals and by-products in alkaline media. J. Mater. Sci., 42(9), pp. 2967-2973, 2006. DOI: 10.1007/s10853-006-0531-8
[31] Zuhua, Z., Xiao, Y., Huajun, Z. and Yue, C., Role of water in the synthesis of calcined kaolin-based geopolymer. Appl. Clay Sci., 43(2), pp. 218-223, 2009. DOI: 10.1016/j.clay.2008.09.003
[32] Elimbi, A., Tchakoute, H.K. and Njopwouo, D., Effects of calcination temperature of kaolinite clays on the properties of geopolymer cements. Constr. Build. Mater., 25(6), pp. 2805-2812, 2011. DOI: 10.1016/j.conbuildmat.2010.12.055
[33] Hounsi, A.D., Lecomte-Nana, G.L., Djétéli, G. and Blanchart, P., Kaolin-based geopolymers: Effect of mechanical activation and curing process. Constr. Build. Mater., 42, pp. 105-113, 2013. DOI: 10.1016/j.conbuildmat.2012.12.069
[34] Onori, R., Alkaline activation of incinerator bottom ash for use in structural applications, PhD. dissertation, Course in Environmental Engineering, Sapienza University of Rome XIII, Italy, 2011.
[35] Prud'homme, E., Michaud P., Joussein E., Peyratout C., Smith A., Arrii-Clacens S., Clacens J.M. and Rossignol S., Silica fume as porogent agent in geo-materials at low temperature. J. Eur. Ceram. Soc., 30(7), pp. 1641-1648, 2010. DOI: 10.1016/j.jeurceramsoc.2010.01.014
[36] Duxson, P., Lukey, G.C. and van Deventer, J.S.J., Evolution of gel structure during thermal processing of Na-geopolymer gels. langmuir, 22, pp. 8750-8757, 2006. DOI: 10.1021/la0604026
[37] Wei, Z.Y.S. and Zongjin, L. Preparation and Microstructure of Na-PSDS Geopolymeric Matrix. Ceramics-Silikáty, 53(2), pp. 88-97, 2009.

M.A Villaquirán-Caicedo, has a BSc. in Materials Engineering from Universidad del Valle, Cali, Colombia and a MSc. in Engineering with emphasis in Materials Engineering from the same institution. She is an active member of the Composite Materials Group, category A1-2014 Colciencias, in which she works as a young researcher and research assistant participating in various projects related to the utilization of industrial solid waste. She has been a teaching assistant in courses on composite materials and materials properties in the materials engineering academic program. She is currently a Doctoral candidate in Engineering, with the support of Colciencias Doctoral Scholarship.
ORCID: 0000-0001-5145-0472

R. Mejía-de Gutiérrez, has a BSc. in Chemistry, a MSc. degree in Chemical Sciences all of them from Universidad del Valle, Cali, Colombia, and a PhD in Chemical Science (Materials) from the Universidad Complutense de Madrid, Spain. She has extensive experience in the implementation, development and management of research projects related to construction materials (cement, additions, concrete high performance), production of materials from industrial wastes, alkaline activation processes and geopolymerization, composites, ceramic aggregates, and studies on materials durability and corrosion. She has been the director of the GMC since its foundation (1986) and has directed more than 30 research projects. She was the director of the School of Materials Engineering program of the Universidad del Valle, during 2000 and 2006. She is currently the coordinator of the graduate program in the same academic unit.
ORCID: 0000-0002-5404-2738

UNIVERSIDAD NACIONAL DE COLOMBIA
SEDE MEDELLÍN
FACULTAD DE MINAS



DYNA
http://dyna.medellin.unal.edu.co/

New tuning rules for PID controllers based on IMC with minimum IAE for inverse response processes

Duby Castellanos-Cárdenas [a] & Fabio Castrillón-Hernández [b]

[a] *Facultad de Ingeniería, Universidad de Medellín, Medellín, Colombia. dcastellanos@udem.edu.co*
[b] *Escuela de Ingeniería, Universidad Pontificia Bolivariana, Medellín, Colombia. fabio.castrillon@upb.edu.co*

Received: October 23th, 2014. Received in revised form: March 13th, 2015. Accepted: October 10th, 2015.

Abstract
In this paper new tuning rules for Proportional Integral Derivative (PID) are presented, which are based on Internal Model Control (IMC). This set of equations minimizes the performance index, in this case, the Integral Absolute Error (IAE). Furthermore, a correlation is proposed in order to calculate the tuning parameter of the method, where a holding oscillation response is obtained regarding changes in the set point. This value represents a stability limit for the IMC method. The overall development is then applied to an Inverse Response System of second order and with dead time.

Keywords: Inverse Response, PID Controller, Internal Model Control, IAE, Experimental Design.

Nuevas reglas de sintonía basadas en IMC para un controlador PID con IAE mínimo en procesos con respuesta inversa

Resumen
En este artículo se presentan nuevas reglas de sintonía para un controlador PID (Proporcional Integral Derivativo) basado en IMC (por sus siglas en inglés *Internal Model Control*). Este conjunto de ecuaciones minimiza un índice de desempeño óptimo, para este caso la Integral del Error Absoluto (IAE por sus siglas en inglés, *Integral Absolute Error*). Adicionalmente se presenta una correlación para calcular el valor crítico del parámetro de sintonía del método, τ_C, donde se obtiene una respuesta de oscilación sostenida frente a cambios en el punto de control. Este valor representa un límite de estabilidad para el método IMC. Todo este desarrollo es aplicado a un Sistema con Respuesta Inversa (SRI) de segundo orden y con tiempo muerto.

Palabras clave: Respuesta Inversa, controlador PID, Control por Modelo Interno, Integral del Error Absoluto, Diseño de Experimentos.

1. Introducción

El comportamiento de los sistemas con respuesta inversa (SRI) ha sido de interés en muchos trabajos académicos ya que a nivel industrial se pueden encontrar sistemas que exhiben este tipo de dinámica [1]. Algunos ejemplos de procesos con respuesta inversa son: el nivel en una caldera de vapor y en la sección del rehervidor de una columna de destilación, la temperatura tanto en reactores catalíticos exotérmicos como en reactores tubulares adiabáticos [1-3], el caudal de silicio en reactores para la producción de silicio de metal [4] y el caudal de vapor en plantas de incineración de residuos [5].

En este tipo de procesos aparecen problemas asociados con el comportamiento dinámico que dificultan su control y que generan limitaciones importantes en el rendimiento y robustez del sistema. Por este motivo las técnicas de control tradicional presentan un bajo desempeño cuando son aplicadas a este tipo de plantas. Estos inconvenientes se hacen más notorios cuando el proceso también presenta tiempo muerto [2,6].

Aunque son varios los métodos de control de SRI que se reportan en la literatura, estos pueden agruparse básicamente en dos tipos de estructuras de control: compensadores de respuesta inversa, que generalmente utilizan el concepto del predictor de Smith para sus diseños; y controladores PID en los que se han utilizado muchas técnicas de sintonía [7].

En general, los compensadores basados en el predictor de Smith eliminan el tiempo muerto de la ecuación característica del sistema, colocan los ceros de fase no mínima fuera del

© The author; licensee Universidad Nacional de Colombia.

lazo de realimentación, arrojan controladores con una alta sensibilidad a errores en los parámetros del modelo y se consideran útiles en procesos que presentan un tiempo muerto significativo [7,8].

Con relación a los controladores PID aplicados a procesos con respuesta inversa y tiempo muerto, se han obtenido muy buenos resultados, inclusive en uno de los primeros trabajos realizados sobre el tema se compararon las ventajas poco significativas de las estructuras de control para compensar la presencia de polos y ceros complejos frente al control PID convencional propuesto por Ziegler y Nichols [9]. Una de las razones del éxito del controlador PID reside en la acción derivativa que logra anticipar la dirección errónea en la respuesta inicial del sistema [7]. Además, gracias al desarrollo de los componentes de hardware y software necesarios para su implementación, el control PID es el más utilizado a nivel industrial [10,11].

En este trabajo se introduce un conjunto de reglas de sintonía para un controlador PID sintonizado ante cambios tipo escalón en la perturbación para SRI de segundo orden más tiempo muerto, ya que son sistemas que no se analizan comúnmente en la literatura por su complejidad, debido al orden del sistema y la inclusión del tiempo muerto. Las correlaciones obtenidas minimizan el índice de desempeño IAE lo que se traduce en un beneficio para los usuarios de este tipo de sistemas.

En la primera parte del artículo se explican las características de los SRI, luego se presenta tanto la técnica de sintonía como la metodología utilizada para el desarrollo de las reglas propuestas. A continuación se introducen las correlaciones halladas y, con el fin de verificar la validez de estas, se compara un controlador sintonizado con el método propuesto con otros controladores sintonizados con algunas reglas reportadas por la literatura. Finalmente se presentan las conclusiones del trabajo realizado.

2. Sistemas con respuesta inversa

Un SRI se caracteriza por tener uno o más ceros de fase no mínima. Cuando este tipo de proceso es excitado con una entrada tipo escalón, la respuesta inicial del sistema es opuesta al valor final de estado estable. Este efecto se debe a que en el proceso se ponen en marcha dos fenómenos físicos con dinámicas opuestas. Un primer fenómeno al que se le asocia una función de transferencia con ganancia pequeña y de respuesta rápida, responsable de que el sistema responda en forma inversa inicialmente; y un fenómeno más lento, con una ganancia mayor que la anterior y cuyo efecto finalmente predomina sobre el inicial [3,12,13].

La función de transferencia de un sistema con respuesta inversa de segundo orden con un retardo θ, que es el sistema que se analiza en este trabajo, puede considerarse como:

$$G(s) = \frac{K(1-\eta s)e^{-\theta s}}{(\tau_1 s+1)(\tau_2 s+1)} \quad (1)$$

Donde Kes la ganancia del proceso, η determina el cero de fase no mínima, θ corresponde al tiempo muerto y τ_1, τ_2 son las constantes de tiempo.

En este tipo de procesos la pendiente de la respuesta en el origen es de signo opuesto a la ganancia y a medida que la magnitud del parámetro η se incrementa el comportamiento de inversión que aparece en la respuesta transitoria es mucho más pronunciado y las dificultades asociadas al control de este proceso aumentan. El valor de estado estable de un sistema con respuesta inversa es igual su ganancia [3,14,15].

En este tipo de procesos es común tener problemas de estabilidad y, cuando el SRI posee tiempo muerto, se puede presentar una salida no acotada para una excitación tipo escalón en la perturbación; adicionalmente aparecen limitaciones en el ajuste del controlador a bajas frecuencias [6,16].

3. Método de sintonía

En la literatura se han presentado algunos trabajos que estudian el problema del control de sistemas de primer o segundo orden con respuesta inversa, pero pocos autores han analizado SRI que además incluyan tiempo muerto. Como el fenómeno de la respuesta inversa presenta algunas similitudes con la respuesta de sistemas con tiempo muerto, es común encontrar técnicas de sintonía que utilizan la estructura del predictor de Smith [17]. Otras técnicas modelan el efecto del cero de fase no mínima como un tiempo muerto, con el fin de utilizar alguna técnica de sintonía tradicional para este tipo de procesos, aunque esto origina controladores mucho más conservativos [7,16,18]. Adicionalmente, estas aproximaciones introducen un error adicional en el modelo, el cual se ve reflejado en una disminución del ancho de banda del sistema [19]. Otra forma de abordar el problema de la respuesta inversa consiste en reducir el orden del sistema, aproximándolo a uno de primer orden, lo que permite hallar un controlador PI. La respuesta de este último controlador es mucho más lenta cuando se compara con la respuesta que generan las técnicas descritas anteriormente [6].

En cuanto al diseño de controladores PID utilizando las técnicas de análisis de la respuesta en frecuencia para sistemas con respuesta inversa, este fue abordado por Luyben [20] pero las expresiones que obtuvo fueron muy complejas. Por otra parte, el método de síntesis directa ante cambios en la perturbación fue estudiado por Chen y Seborg [21] aunque no abordaron el tratamiento de los sistemas con respuesta inversa así que para hacer uso de sus ecuaciones se tendría que utilizar la aproximación de Padé o de Taylor con el fin de reemplazar el cero de fase no mínima, generando los problemas antes mencionados.

Otro de los métodos más utilizados para la sintonía de controladores PID es el IMC. Este método ha resultado de interés a nivel industrial porque, al igual que el método de síntesis directa, utiliza un único parámetro de sintonía (τ_C). Las ecuaciones del controlador IMC son función de los parámetros de la función de transferencia del sistema y de τ_C. Este último parámetro está relacionado con la velocidad de la respuesta de lazo cerrado del sistema y a medida que se incrementa su magnitud también lo hace la robustez del lazo de control. Por otra parte, a nivel experimental, se ha encontrado que este controlador mejora el comportamiento del sistema ante perturbaciones y minimiza las interacciones

del controlador. Además, la correcta selección del filtro pasa bajo que utiliza el método, evita que la respuesta de lazo cerrado sea oscilatoria y con sobreimpulso; estas características reducen los efectos de la perturbación [22]. Por estos motivos, en este trabajo se utilizó el IMC ya que es una técnica que le brinda al diseñador del controlador la posibilidad de especificar el comportamiento del sistema en lazo cerrado y de obtener un controlador con un único parámetro de sintonía. En el trabajo presentado por Chien y Fruehauf (1990) se proponen un conjunto de reglas de sintonía para sistemas de segundo orden con respuesta inversa que tienen la ventaja de no contener términos negativos, por lo que no se hace necesario resolver inecuaciones que finalmente se traducen en limitaciones en el rango útil del parámetro τ_C [23].

El IMC factoriza la función de transferencia de la planta como:

$$G_M = G_{M+}G_{M-} \tag{2}$$

Tal que G_{M+} es una función que contiene todos los ceros de fase no mínima y el tiempo muerto, mientras que G_{M-} contiene los polos de la función de transferencia. El controlador IMC se define en términos del inverso de la función G_{M-} y un filtro pasabajo en serie. La ecuación para el controlador es:

$$G_{IMC} = G_{M-}^{-1} f \tag{3}$$

Donde f es la función del filtro pasa bajo especificado por el usuario. La estructura del controlador IMC puede ser reducida a la clásica estructura de control al definir la función del controlador como:

$$G_C = \frac{G_{IMC}}{1 - G_{IMC}G_M}, \tag{4}$$

De manera que se puede utilizar la estructura del controlador IMC para obtener los parámetros de un controlador PID clásico [24]. Los autores utilizan la aproximación de Padé, o la de Taylor, para reemplazar la expresión del tiempo muerto en la función de transferencia y sugieren definir la función del filtro para sistemas de primer y segundo orden, sin integrador, de la siguiente forma:

$$f = \frac{1}{\tau_c s + 1} \tag{5}$$

A continuación se utilizan las ecuaciones (2) y (4) para hallar la función de transferencia del controlador G_C y el resultado se compara con la estructura de un controlador PID, serie o paralelo, con el fin de obtener la relación para los parámetros del controlador. Para un sistema con respuesta inversa de segundo orden más tiempo muerto la estructura del controlador PID ideal y las ecuaciones de sus parámetros son:

$$G_C = K_C\left(1 + \frac{1}{T_I s} + T_d s\right) \tag{6}$$

$$K_C = \frac{\tau_1 + \tau_2 + \dfrac{\eta\theta}{\tau_C + \eta + \theta}}{K(\tau_C + \eta + \theta)} \tag{7}$$

$$T_i = \tau_1 + \tau_2 + \frac{\eta\theta}{\tau_C + \eta + \theta} \tag{8}$$

$$T_d = \frac{\eta\theta}{\tau_C + \eta + \theta} + \frac{\tau_1\tau_2}{\tau_1 + \tau_2 + \dfrac{\eta\theta}{\tau_C + \eta + \theta}} \tag{9}$$

Como se observa, los parámetros PID del controlador dependen del valor de los parámetros de la función de transferencia del SRI y de τ_C, que es el parámetro de sintonía del método.

4. Metodología para generar las reglas de sintonía

El primer paso consistió en elaborar con la herramienta Simulink de Matlab®, un programa para simular la respuesta del lazo cerrado del sistema con un controlador IMC. A continuación se utilizaron técnicas de análisis dimensional, tanto en la ecuación que describe la función de transferencia del sistema (6) como en las del controlador (7)-(9); lo que hizo posible la reducción de la cantidad de parámetros involucrados. Las ecuaciones adimensionalizadas para el sistema de interés son:

$$\hat{G}(\hat{s}) = \frac{K(1 - \hat{\eta}\hat{s})e^{-\hat{\theta}\hat{s}}}{(\hat{s} + 1)(\hat{\tau}_2\hat{s} + 1)} \tag{10}$$

$$K_C K = \frac{(1 + \hat{\tau}_2)\left(\hat{\tau}_C + \hat{\eta} + \hat{\theta}\right) + \hat{\eta}\hat{\theta}}{(\hat{\tau}_C + \hat{\eta} + \hat{\theta})^2} \tag{11}$$

$$\hat{T}_i = \frac{(1 + \hat{\tau}_2)\left(\hat{\tau}_C + \hat{\eta} + \hat{\theta}\right) + \hat{\eta}\hat{\theta}}{(\hat{\tau}_C + \hat{\eta} + \hat{\theta})} \tag{12}$$

$$\hat{T}_d = \frac{\hat{\eta}\hat{\theta}}{(\hat{\tau}_C + \hat{\eta} + \hat{\theta})} + \frac{\hat{\tau}_2(\hat{\tau}_C + \hat{\eta} + \hat{\theta})}{(1 + \hat{\tau}_2)\left(\hat{\tau}_C + \hat{\eta} + \hat{\theta}\right) + \hat{\eta}\hat{\theta}} \tag{13}$$

Donde $\hat{\eta} = \frac{\eta}{\tau_1}$, $\hat{\tau}_2 = \frac{\tau_2}{\tau_1}$, $\hat{\theta} = \frac{\theta}{\tau_1}$ y $\hat{s} = \tau_1 s$, lo que puede interpretarse como un escalamiento en el tiempo o en la frecuencia. Los rangos típicos de los valores de cada uno de los parámetros de la planta reportados en la literatura [16, 25], son:

$$0.1 \leq \hat{\tau}_2 \leq 0.9 \tag{14}$$

$$0.1 \leq \hat{\eta} \leq 4 \tag{15}$$

$$0.01 \leq \hat{\theta} \leq 1 \tag{16}$$

Se diseñó un experimento factorial de tipo central compuesto circunscrito y uniforme que suministró los conjuntos de valores más apropiados para cada corrida de simulación. Posteriormente se elaboró una regresión para

evaluar diferentes modelos de ajuste y, para definir la forma exacta de la correlación de interés, se desarrolló un análisis de varianza (ANOVA) utilizando el software Statgraphics. Adicionalmente, esta aplicación suministró diferentes estadísticos que con el fin de medir la calidad del ajuste. Finalmente, se procedió a evaluar el comportamiento del sistema con un controlador sintonizado con las correlaciones obtenidas.

5. Correlación para el límite de estabilidad

El parámetro de sintonía del IMC es denominado τ_C y, como se mencionó anteriormente, este se encuentra asociado con la velocidad de respuesta de lazo cerrado. A medida que τ_C toma valores más pequeños el sistema responde más rápidamente, característica deseable para un lazo de control; sin embargo tendrá como consecuencia una respuesta cada vez más oscilatoria, al punto que la estabilidad del sistema puede afectarse drásticamente.

Ninguno de los artículos revisados han usado el IMC o la técnica de síntesis directa, que también utiliza este parámetro para la sintonía del controlador, entregan un límite o al menos una sugerencia, para el valor mínimo que puede tomar sin que se lleve el sistema a la inestabilidad. Por este motivo, la primera tarea a desarrollar en este trabajo consistió en encontrar una expresión que entregara el valor crítico de τ_C, para un proceso de segundo orden con respuesta inversa y tiempo muerto, en el cual la respuesta del sistema fuera una oscilación sostenida. Esta expresión resulta de mucha utilidad para cualquier usuario del método de sintonía, pues le permite conocer una aproximación del valor que le garantizará la respuesta de lazo cerrado más rápida sin llevar el sistema a la inestabilidad.

La forma de la correlación para el parámetro de sintonía, considerando que se realizó un proceso de adimensionalización de la función de transferencia y de las ecuaciones del controlador (*10*)-(*13*), es:

$$\hat{\tau}_{Cult} = f(\hat{\tau}_2, \hat{\eta}, \hat{\theta}) \tag{17}$$

De esta expresión se observa que $\hat{\tau}_{Cult}$ es función de tres variables, por lo que se diseñó un diseño central compuesto de tres factores y se realizó una regresión no lineal. La correlación que se halló fue:

$$\begin{aligned}\hat{\tau}_{cult} = {} & -0.14856 + 0.90336\hat{\tau}_2 + 0.33166\hat{\eta} \\ & + 0.39094\hat{\tau}_2\hat{\eta} - 0.19992\hat{\tau}_2\hat{\theta} \\ & + 0.38428\hat{\eta}\hat{\theta} - 0.30502\hat{\tau}_2^2 \\ & - 0.01572\hat{\eta}^2 - 0.20783\hat{\theta}^2\end{aligned} \tag{18}$$

Para analizar la influencia de un factor en la variable de salida se hace uso de diferentes estadísticos para medir el grado de influencia de un factor en la correlación, en el caso de la ANOVA se utiliza el estadístico p [26]. Se acepta que una variable tiene influencia sobre la respuesta si el estadístico p es inferior a 0.05. Este valor está asociado con el nivel de significancia prefijado de la prueba que típicamente es del 95% y entre más pequeña sea su magnitud mayor será la influencia del factor asociado [27]. Después de optimizar el modelo en Statgraphics el factor $\hat{\theta}$ fue eliminado de la correlación final debido a que su influencia no era significativa.

Tabla 1.
ANOVA para $\hat{\tau}_{Cult}$.

Parámetro	Valor estimado	Error	Estadístico	Valor p
Constante	-0.1901	0.0846	-2.2472	0.0484
$\hat{\tau}_2$	0.9429	0.1879	5.0193	0.0005
$\hat{\eta}$	0.3385	0.0366	9.2386	0.0000
$\hat{\theta}$	0.1065	0.1433	0.7434	0.4743
$\hat{\tau}_2\hat{\eta}$	0.3909	0.0399	9.7931	0.0000
$\hat{\tau}_2\hat{\theta}$	-0.2641	0.1573	-1.6793	0.1240
$\hat{\eta}\hat{\theta}$	0.3732	0.0323	11.5692	0.0000
${\tau_2}^2$	-0.3122	0.1450	-2.1529	0.0568
$\hat{\eta}^2$	-0.0160	0.0061	-2.6267	0.0253
$\hat{\theta}^2$	-0.2548	0.0947	-2.6913	0.0227

Fuente: Elaboración propia.

Tabla 2.
Estadísticos de interés para $\hat{\tau}_{Cult}$

Estadístico	Valor
R^2	99.9005%
$R^2_{adjustado}$	99.8110%
Durbin-Watson	1.7829

Fuente: Elaboración propia.

Tabla 3.
Valores de los parámetros del proceso

Parámetros	$\hat{\tau}_2$	$\hat{\eta}$	$\hat{\theta}$
P1	0.2622	3.2095	0.7993
P2	0.7378	3.2095	0.7993
P3	0.5000	2.0500	1.0000
P4	0.7378	0.8905	0.7993
P5	0.9000	2.0500	0.5050
P6	0.5000	2.0500	0.0100

Fuente: Elaboración propia.

Adicionalmente, se utilizan otros estadísticos, según el tipo de regresión que se realice, con el fin de verificar las suposiciones hechas sobre el polinomio ajustado. Para este caso al tratarse de una regresión no lineal se usaron los estadísticos: R-cuadrado (R^2), R-cuadrado-ajustado ($R^2_{ajustado}$) y el Durbin-Watson (DW). Para todas las correlaciones presentadas en este trabajo se consideró que los polinomios ajustados explicaban la variabilidad de los datos si los valores para R^2 y $R^2_{ajustado}$ eran superiores al 95% y que no existía una correlación serial entre los residuos si el estadístico DW estaba en el rango $1.5 \leq DB \leq 2.5$. En las Tablas 1 y 2 se presentan los resultados de la ANOVA y los estadísticos analizados.

En la Fig. 1. se muestra la respuesta del sistema ante una entrada tipo escalón unitario, con un controlador sintonizado con las ecs. (11)-(13) y (18); para tres conjuntos de parámetros diferentes de la función de transferencia del proceso seleccionados en la Tabla 3.

En la Fig. 2 se observa como la respuesta del sistema es oscilatoria cuando se sintoniza el controlador con un valor del parámetro de sintonía calculado con (18) y para diferentes valores de los parámetros de la planta. En caso de sintonizar

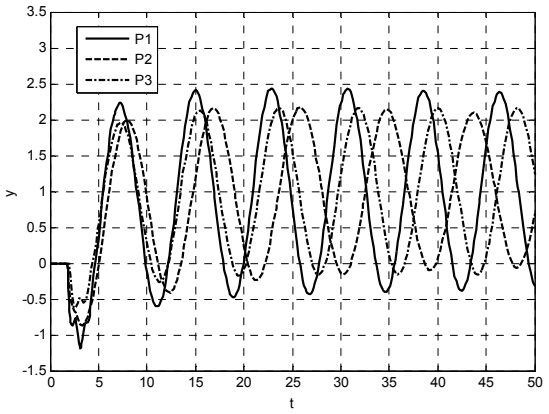


Figura 1. Ejemplos aplicación de la correlación $\hat{\tau}_{cult}$ para valores diferentes del parámetro de sintonía.
Fuente: Elaboración propia.

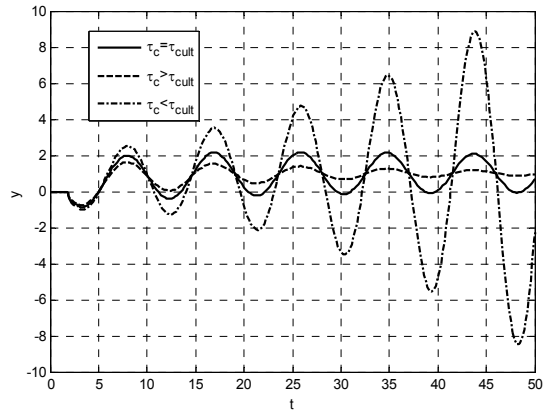


Figura 2. Respuesta del sistema con valores mayores y menores que $\hat{\tau}_{cult}$ para el conjunto de parámetros P2.
Fuente: Elaboración propia.

el controlador con valores superiores a $\hat{\tau}_{Cult}$ el sistema es inestable, mientras que para valores inferiores no; luego la correlación hallada permite encontrar el límite de estabilidad del sistema ante una entrada tipo escalón.

6. Correlación para $\hat{\tau}_C$ que minimiza el IAE

En este caso se encontró una correlación para calcular el valor de $\hat{\tau}_C$ que minimiza el índice de desempeño IAE. Para todas las corridas experimentales se utilizó como estímulo una perturbación tipo escalón unitario, es decir, las pruebas realizadas se enfocaron en un control regulatorio.

Ya que $\hat{\tau}_{C-IAE}$ es función de los parámetros del modelo, tal como en el caso anterior, se utilizó el mismo diseño de experimentos y la forma de la correlación propuesta también es igual. A continuación se elaboró un algoritmo para variar el valor del parámetro $\hat{\tau}_C$ manteniendo fijos los parámetros del proceso, de manera que con cada cambio de $\hat{\tau}_C$ se afectaban únicamente los parámetros del controlador. El valor de partida de $\hat{\tau}_C$ se obtuvo de (18), por lo tanto, el valor

Tabla 4.
ANOVA para $\hat{\tau}_{C-IAE}$.

Parámetro	Valor estimado	Error	Estadístico	Valor p
Constante	-0.5764	0.1609	-0.9350	-0.2178
$\hat{\tau}_2$	2.1858	0.3574	1.3894	2.9823
$\hat{\eta}$	0.7350	0.0697	0.5797	0.8904
$\hat{\theta}$	1.7129	0.2726	1.1056	2.3204
$\hat{\tau}_2\hat{\eta}$	0.6400	0.0759	0.4707	0.8093
$\hat{\tau}_2\hat{\theta}$	-0.1418	0.2992	-0.8086	0.5250
$\hat{\eta}\hat{\theta}$	0.3412	0.0614	0.2044	0.4779
${\tau_2}^2$	-1.6608	0.2759	-2.2755	-1.0459
$\hat{\eta}^2$	-0.0295	0.0116	-0.0553	-0.0036
$\hat{\theta}^2$	-0.9626	0.1802	-1.3641	-0.5612

Fuente: Elaboración propia.

Tabla 5
Estadísticos de interés para $\hat{\tau}_{C-IAE}$

Estadístico	Valor
R^2	99.8733%
$R^2_{adjustado}$	99.7593%
Durbin-Watson	2.2056

Fuente: Elaboración propia.

mínimo que se le asignó a este parámetro correspondía con el valor del límite de estabilidad del sistema. El resultado final del procedimiento de simulación fue una tabla de datos que contenía el valor de $\hat{\tau}_C$ que hacía mínimo el IAE para cada conjunto de parámetros. Con base en esta información y en el conjunto de valores de parámetros del proceso se llevó a cabo el ajuste de los datos. La correlación hallada se presenta a continuación:

$$\begin{aligned}\hat{\tau}_{c-IAE} = -0.54026 + 2.11424\hat{\tau}_2 + 0.73504\hat{\eta} \\ + 1.64210\hat{\theta} + 0.64002\hat{\tau}_2\hat{\eta} \\ + 0.34115\hat{\eta}\hat{\theta} - 1.66075\hat{\tau}_2^2 \\ - 0.02945\hat{\eta}^2 - 0.96263\hat{\theta}^2\end{aligned} \quad (19)$$

Los estadísticos utilizados para evaluar esta correlación y los resultados de la ANOVA aparecen en las Tablas 4 y 5.

Según los resultados de las tablas anteriores se puede afirmar que la correlación que se encontró explica en alto grado el comportamiento de los datos.

7. Evaluación de desempeño

Para los ejemplos que se presentan a continuación se seleccionaron tres conjuntos de valores para los parámetros del proceso, ver Tabla ; luego se sintonizó un controlador utilizando las correlaciones propuestas en este trabajo (CD-CF), ver ecs. (11)-(13) y (19); y se obtuvo la respuesta del sistema ante una entrada tipo escalón unitario. Las pruebas se realizaron tanto para operación servo como regulatoria. En la operación servo la señal de entrada se ingresa como un cambio en la referencia mientras que en la operación regulatoria la señal de excitación del sistema ingresa como una perturbación. En la Tabla se presenta una comparación entre el valor obtenido para $\hat{\tau}_{C-IAE}$ con (19) y el que se calcula con $\hat{\tau}_{Cult}$, esto con el fin de mostrar que siempre el

Tabla 6.
Comparación valores para $\hat{\tau}_{C-IAE}$ y $\hat{\tau}_{Cult}$

Conjunto de parámetros	$\hat{\tau}_{C-IAE}$	$\hat{\tau}_{Cult}$
P4	2.1073	0.9145
P5	3.5178	2.0065
P6	2.1637	1.2483

Fuente: Elaboración propia.

valor del parámetro de sintonía del método debe ser mayor que $\hat{\tau}_{Cult}$ para evitar la inestabilidad del lazo de control.

A continuación se comparó el desempeño del sistema tanto con un controlador en el que se utilizó el método de sintonía PID tradicional propuesto por Ziegler y Nichols (ZN) [9], como con un controlador PID sintonizado con las ecuaciones de Tyreus y Luyben (TL) [28]. El método de sintonía de ZN se utiliza como punto de referencia para establecer comparaciones en muchos estudios, por otra parte, la técnica TL es similar a la ZN pero esta ofrece la ventaja de que el coeficiente de amortiguación de lazo cerrado presenta un valor mucho mayor al de ZN, por lo que la respuesta es más suave. En las Figuras 3 - 8 se presentan las respuestas del sistema, tanto en operación servo como regulatoria, para tres conjuntos diferentes de parámetros del proceso y con los tres controladores estudiados.

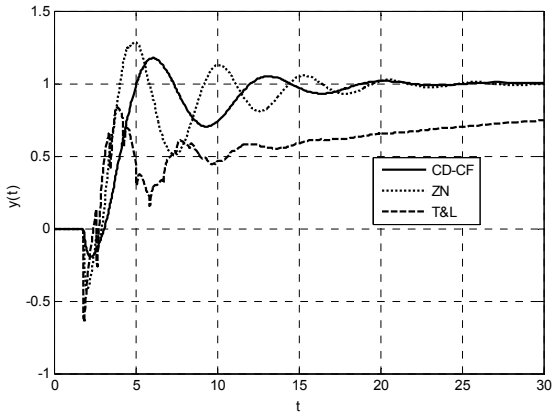


Figura 3. Respuesta del sistema en operación servo para P4
Fuente: Elaboración propia.

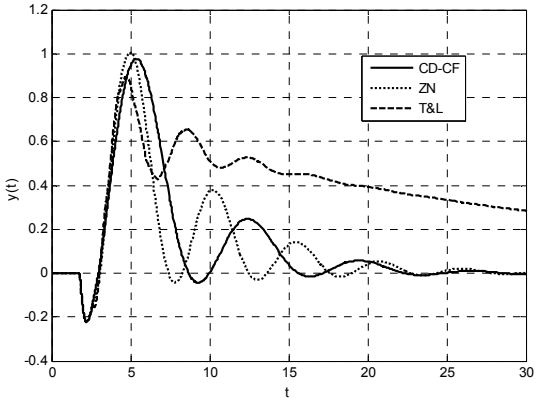


Figura 4. Respuesta del sistema en operación regulatoria para P4
Fuente: Elaboración propia.

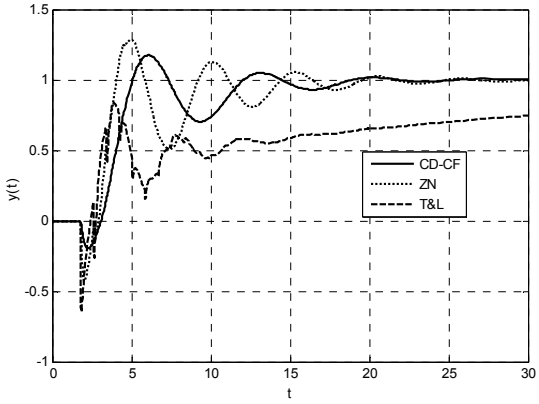


Figura 5. Respuesta del sistema en operación servo para P5
Fuente: Elaboración propia.

Tabla 7.
Índices de desempeño para operación servo

	P1		P2		P3	
Controlador	**IAE**	**TVM**	**IAE**	**TVM**	**IAE**	**TVM**
CD-CF	4.696	3.872	6.436	2.942	4.517	2.844
ZN	4.937	17.810	6.810	11.410	4.176	7.096
TYL	16.510	268.300	17.150	255.100	19.450	105.900
	Mejor resultado					

Fuente: Elaboración propia.

Tabla 8.
Índices de desempeño para operación regulatoria

	P1		P2		P3	
Controlador	**IAE**	**TVM**	**IAE**	**TVM**	**IAE**	**TVM**
CD-CF	4.416	2.663	8.135	3.111	7.027	3.749
ZN	4.181	4.513	8.540	5.259	7.062	4.398
TYL	16.400	6.259	17.2700	15.600	20.690	12.400
	Mejor resultado					

Fuente: Elaboración propia.

Para cada uno de los ejemplos se calcularon dos indicadores de desempeño: el IAE y el Trabajo de la Variable Manipulada (TVM). Este último se define como la integral del valor absoluto del cambio de la variable manipulada. En las Tablas 7 y 8 se presentan los valores de estos índices tanto para operación servo como regulatoria.

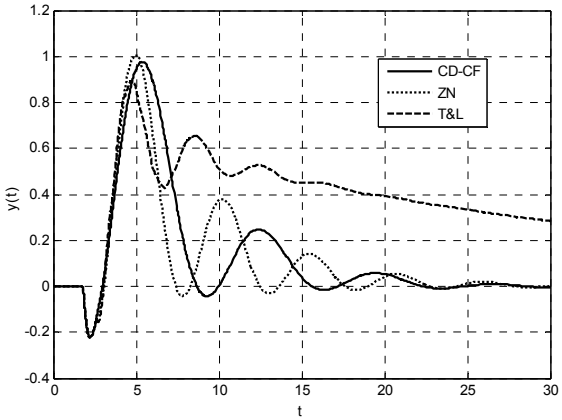


Figura 6. Respuesta del sistema en operación regulatoria para P5
Fuente: Elaboración propia.

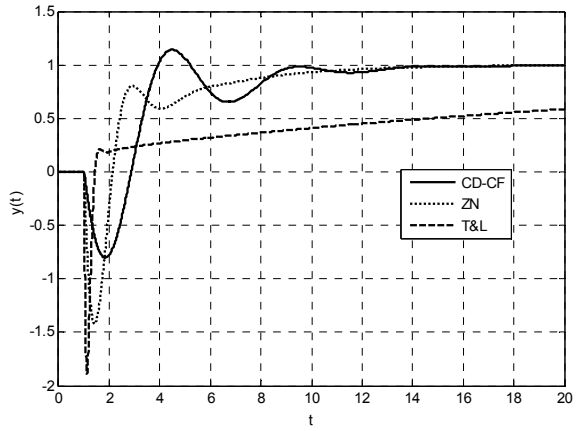


Figura 7. Respuesta del sistema en operación servo para P6
Fuente: Elaboración propia.

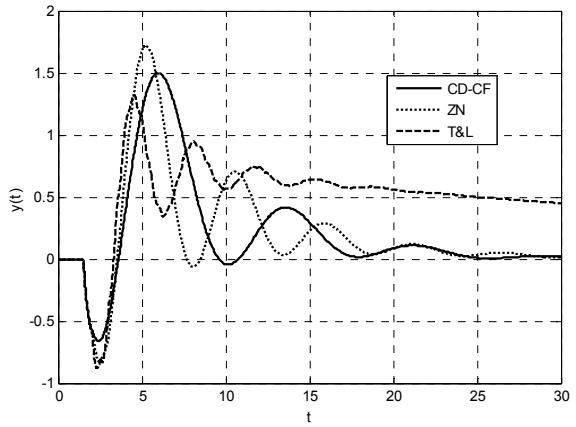


Figura 8. Respuesta del sistema en operación regulatoria para P6
Fuente: Elaboración propia.

En general, para los diferentes parámetros de la función de transferencia estudiados, el controlador CD-CF presenta los mejores resultados tanto para el índice de desempeño IAE como para TVM. Aunque los valores obtenidos para el IAE con el controlador ZN en algunos casos son cercanos a los del controlador CD-CF, es notorio el esfuerzo que realiza el elemento final de control con ZN. Respecto al controlador TYL, este se caracterizó por presentar un menor sobre impulso en la respuesta transitoria con la desventaja de que generar siempre el mayor tiempo de estabilización.

8. Conclusiones

En este trabajo se propone un método de sintonía para ajustar un controlador PID para un sistema de segundo orden y tiempo muerto con respuesta inversa basado en el método IMC para lo que se presenta una correlación que permite calcular el valor de $\hat{\tau}_C$ que minimiza el IAE. La correlación que se obtuvo es de tipo polinómica y es función de los parámetros del proceso.

En este trabajo se presenta una correlación que permite calcular el valor límite que se le puede asignar al parámetro de sintonía del controlador de manera que la respuesta del sistema sea lo más rápida posible, pero sin llegar a la inestabilidad. Esta expresión resulta de interés para cualquier usuario del método. La literatura no reporta hasta el momento una correlación o método para calcular el valor de $\hat{\tau}_{Cult}$ a partir de los datos del modelo.

Se resalta el buen desempeño del controlador CD-CF para un rango variado de los parámetros del proceso y tanto para operación servo como regulatoria del lazo de control. Adicionalmente, se observa una disminución del efecto de respuesta inversa en el sistema con este controlador.

Un sistema con un controlador sintonizado con las reglas de sintonía propuestas alarga la vida útil del elemento final de control.

Para la generación de datos se realizó un diseño estadístico de experimentos de tipo central compuesto, uniforme y circunscrito; que permitió una reducción considerable del número de corridas de simulación y un mejor ajuste de los datos al polinomio propuesto.

References

[1] Luyben, W.L., Tuning proportional-Integral controllers for processes with both inverse response and deadtime. Industrial Engineering Chemical Research, 39, pp. 973-976, 2000. DOI: 10.1021/ie9906114

[2] Chien, I., Chung, Y., Chen, B. and Chuang, C., Simple PID controller tuning method for processes with inverse response plus dead time or large overshoot response plus dead time. Industrial Engineering Chemical Research, 42, pp. 4461-4477, 2003. DOI: 10.1021/ie020726z

[3] Ogunnaike, B. and Harmon, W., Process dynamics and modeling and control. USA. Oxford University Press, 1994.

[4] Lund, B.F., Foss, B.A. and Løvåsen, K.R., Analysis and characterization of complex reactor behaviour: A case study. Journal of Process Control, 16, pp. 711-718, 2006. DOI: 10.1016/j.jprocont.2006.01.005

[5] Manca, D., Rovaglio M., Pazzaglia G. and Serafini G., Inverse response compensation and control optimization of incineration plants with energy. Computers & Chemical Engineering. 22(12), pp.1879-1896, 1998. DOI: 10.1016/S0098-1354(98)00239-7

[6] Ocampo, J.E. y Castrillón, F., Control de sistemas con respuesta inversa. Madrid. Ingeniería química, 42(486), pp. 76-85, 2010.

[7] Jeng, J. and Lin, S., PID controller tuning based on smith-type compensator for second-order process with inverse response and time delay. Proceedings of 2011 8th Asian Control Conference (ASCC), 56, pp. 15-18, 2011.

[8] Barberà, E., Predictor de Smith + PI en el control de procesos con tiempo muerto dominante. Revista de Ingeniería Química, 43(491), pp. 46-50, 2011.

[9] Ziegler, J.G. and Nichols, N.B., Optimum setting for automatic controllers. Transactions ASME, 64, pp. 759-768, 1942.

[10] Alfaro, V.M., Ecuaciones para controladores PID universales. San José de Costa Rica. Revista Ingeniería de Costa Rica, 12(1,2), pp. 11-20, 2002.

[11] Yu, C.C., Autotuning of PID Controllers: A relay feedback approach. Springer, 2006.

[12] De Castro, P. y Fernández, E., Control e instrumentación de procesos químicos. Madrid. Editorial Síntesis, 2006.

[13] Stephanopoulos, G., Chemical process control. An introduction to theory and practice. New Jersey, Prentice Hall, 1984.

[14] Alcántara, S., Pedret, C., Vilanova, R. and Zhang, W.D., Analytical H^{∞} design for a Smith-type inverse-response compensator. American Control Conference, Hyatt Regency Riverfront, St. Louis, MO, USA; pp. 10-12, 2009. DOI: 10.1109/ACC.2009.5160324

[15] Scali, C. and Rachid, A., Analytical design of proportional-integral-derivative controllers for inverse response process. Industrial

Engineering Chemistry, 37(4), pp. 1372-1379, 1998. DOI: 10.1021/ie970558o
[16] Pai, N.S., Changb, S.C. and Huangb, C.T., Tuning PI/PID controllers for integrating processes with deadtime and inverseresponse by simple calculations. Journal of Process Control 20, pp.726-733, 2010. DOI: 10.1016/j.jprocont.2010.04.003
[17] Romagnoli, J. and Palazoglu, A., Introduction to process control. Taylor & Francis Group, 2006.
[18] Castellanos, D. y Castrillón, F., Controladores PI/PID en procesos con respuesta inversa evaluación de la robustez. Ingeniería Química, 502, pp. 48-52, 2012.
[19] Rivera, D., Morari, M. y Skogestad, S., Internal model control: PID controller design. Ind. Eng. Chem. Process, 25(1), pp. 252-265, 1986. DOI: 10.1021/i200032a041
[20] Luyben, W., Identication and tuning of integrating processes with deadtime and inverse response. Industrial Engineering Chemical Research, 42, pp. 3030-3035, 2003. DOI: 10.1021/ie020935j
[21] Chen, D. and Seborg, D.E., PI/PID Controller design based on direct synthesis and disturbance rejection. Industrial Engineering Chemical Research, 41, pp. 4807-4822, 2002. DOI: 10.1021/ie010756m
[22] Chien, I. and Fruehauf ,P., Consider IMC tuning to improve controller performance. Chemical Engineering Progress, 86, pp. 33-41, 1990.
[23] Castellanos, D. y Castrillón, F., Propuesta de nuevas reglas de sintonía para el ajuste de controladores PI/PID para sistemas con respuesta inversa. Tesis MSc., Escuela de Ingenierías, Universidad Pontificia Bolivariana, Medellín, Colombia, 2013.
[24] García, Y. y Lobo, I., Control PID integrado por la estructura de control de modelo interno (IMC) y lógica difusa. Revista Ciencia e Ingeniería, 30, pp. 29-40, 2009.
[25] Balaguer, P., Alfaro, V. y Arrieta, O., Second order inverse response process identification from transient step response. ISA Transactions, 50, pp. 231-238, 2011. DOI: 10.1016/j.isatra.2010.11.005
[26] Morales, H., Claudio, A., Adam, M. and Mina, J., An improved measurement strategy based on statistical design of experiments for a boost Converter. Revista DYNA, 78(166), pp. 7-16, 2011.
[27] Gutiérrez H. y De la Vara, R., Análisis y diseño de experimentos. McGraw Hill, 2008.
[28] Tyreus, B.D. and Luyben, W.L., Tuning PI controllers for integrator/dead time process. Industrial Engineering Chemistry Research. 31(11), pp. 2625-2628, 1992. DOI: 10.1021/ie00011a029

D. Castellanos-Cárdenas, es Ing. Electrónica en 2006, de la Universidad de Antioquia, Colombia, Sp. en Automática en 2010 y MSc. en Ingeniería en 2013 ambos de la Universidad Pontificia Bolivariana, Colombia. Es profesora de tiempo completo de la Universidad de Medellín, Colombia y pertenece al grupo de investigación ARKADIUS. Sus áreas de interés son: control e instrumentación de procesos, sintonía de controladores PID.
ORCID: 0000-0003-1496-9958

F. Catrillón-Hernández, es Ing. Químico en 1996, de la Universidad Pontificia Bolivariana, Colombia, Sp. en Automática en 2000 y MSc. en Ingeniería en 2007, de la misma institución. Es profesor titular de la Facultad de Ingeniería Química, de la Universidad Pontificia Bolivariana, Colombia; investigador asociado según Colciencias y pertenece al Grupo de Investigación en Automática y Diseño A+D. Sus áreas de interés son: control de procesos, sintonía de controladores PID y educación en ingeniería.
ORCID: 0000-0003-3906-4610

UNIVERSIDAD NACIONAL DE COLOMBIA
SEDE MEDELLÍN
FACULTAD DE MINAS

Área Curricular de Ingeniería
Eléctrica e Ingeniería de Control

Oferta de Posgrados

Maestría en Ingeniería - Ingeniería Eléctrica

Mayor información:

E-mail: ingelcontro_med@unal.edu.co
Teléfono: (57-4) 425 52 64

UNIVERSIDAD NACIONAL DE COLOMBIA
SEDE MEDELLÍN
FACULTAD DE MINAS



DYNA
http://dyna.medellin.unal.edu.co/

Low-cost platform for the evaluation of single phase electromagnetic phenomena of power quality according to the IEEE 1159 standard

Jorge Luis Díaz-Rodríguez [a], Luis David Pabón-Fernández [b] & Jorge Luis Contreras-Peña [c]

[a]*Facultad de Ingenierías y Arquitectura, Universidad de Pamplona, Pamplona, Colombia. jdiazcu@unipamplona.edu.co*
[b]*Facultad de Ingenierías y Arquitectura, Universidad de Pamplona, Pamplona, Colombia. davidpabon@unipamplona.edu.co*
[c]*Facultad de Ingenierías y Arquitectura, Universidad de Pamplona, Pamplona, Colombia. luisjp88@hotmail.com*

Received: October 30th, 2014. Received in revised form: May 6th, 2015. Accepted: September 24th, 2015.

Abstract
This paper presents the development of a data acquisition system and the evaluation of the electromagnetic phenomena associated with power quality according to the IEEE Standard 1159-1992 and applied to the particular case of single-phase electrical power systems. The evaluation software is implemented in the Labview® professional software using a NI 6009 USB board of the National Instrument® as acquisition device. The hardware implementation of the sensors was shown. Also the development of the algorithm and the design of a graphical user interface for viewing of the voltage and current waveforms, spectra, frequency and the power quality disturbances such as sags, swells, undervoltage, overvoltage, so on. Likewise, at the end a concise analysis of costs is presented to show that the developed system has a lower price to current solutions that are available in the market. Finally a study case was shown.

Keywords: Power quality; acquisition system; electromagnetic phenomena; Labview; evaluation software.

Plataforma de bajo costo para la evaluación de fenómenos electromagnéticos monofásicos de calidad de la energía según el estándar IEEE 1159

Resumen
Este artículo presenta la implementación de un sistema de adquisición y evaluación de fenómenos electromagnéticos asociados con la calidad de la energía según el Estándar IEEE 1159-1992 y aplicado al caso particular de sistemas eléctricos monofásicos. El software de evaluación se implementa en el software profesional Labview®, utilizando como dispositivo de adquisición una tarjeta NI USB 6009 de la National Instrument®. Se muestra la implementación del hardware de la sensórica, también el desarrollo del algoritmo y el diseño de una interfaz gráfica de usuario que permiten visualizar las formas de onda de tensión y de corriente, espectros, frecuencia, potencia y los disturbios de calidad de la energía tales como *sag*, *swell*, *undervoltage*, *overvoltage,* etc. De igual forma al final se realiza un conciso análisis de costos para demostrar que el sistema desarrollado presenta un precio inferior a las soluciones actuales que se consiguen en el mercado, por último se muestra un estudio de caso.

Palabras clave: Calidad de la energía; sistema de adquisición; fenómenos electromagnéticos; Labview; software de evaluación.

1. Introducción

Como consecuencia de la generalización de las actividades agrícolas, industriales y domésticas, la demanda de energía se ha incrementado notablemente [1]; y sobre todo en los países emergentes; presentándose una necesidad, por parte de los usuarios, de tener un suministro permanente.

Pese a esto, históricamente en los sistemas eléctricos de potencia no se ha tenido en cuenta la problemática asociada a calidad de la energía, ya que se tenía la concepción de que al no existir interrupciones se contaba con un óptimo suministro, sin embargo como se menciona, hasta hace muy poco tiempo el único factor que se consideraba importante era la continuidad del servicio, que para la mayoría de usuarios podría ser considerado como satisfactorio [2].

Llegándose a considerar como aspecto de mayor peso la

© The author; licensee Universidad Nacional de Colombia.

eficiencia eléctrica, como indicativo de una buena calidad de la energía en el área industrial [3].

Sin embargo, el incremento masivo que ha tenido la utilización de equipo basado en electrónica de potencia ha sido fuente de contaminantes en la red y causa de diferentes problemas para los usuarios residenciales e industriales, al igual que para las compañías electrificadoras [4].

Es entonces donde el estudio de la calidad de la energía eléctrica se constituye como el primer y más importante paso para identificar y solucionar problemas de los sistemas de potencia, problemas eléctricos que pueden dañar los equipos, reducir su confiabilidad, disminuir la productividad, la rentabilidad e incluso puede poner en peligro la seguridad del personal, si permanece sin corregirse [5].

El surgimiento de la necesidad del estudio de la calidad de la energía, en los últimos años, ha disparado las investigaciones en cuanto a evaluación de calidad de la energía, desde la utilización de técnicas inteligentes [6,7], nuevos métodos para calcular ciertos fenómenos como el total de distorsión armónica [8-10] métodos para mitigar los disturbios específicos [11], hasta el campo de las mediciones [12]. Este último de consideración puesto que las mediciones juegan un papel primordial en casi cualquier problema de calidad de la energía eléctrica, ya que estos se constituyen en el principal método de caracterización del problema [13]. La monitorización de la calidad de energía eléctrica es la mejor manera de detectar y diagnosticar problemas en sistemas de energía eléctrica. Sin embargo, los equipos utilizados son generalmente muy costosos [14].

Equipos como los analizadores de red Fluke, especializados en el área de medición de calidad de la energía, pueden llegar a costar más de 8.000 €, lo que ha motivado a los investigadores a nivel nacional a generar opciones de bajo costo que permitan obtener los mismos resultados [14-16].

Sin embargo, no todos presentan soluciones completas para la evaluación de los fenómenos asociados a calidad de la energía, es por esto que este trabajo busca presentar una solución completa de bajo costo para la monitorización y evaluación de los fenómenos más importantes asociados calidad de la energía eléctrica y análisis de potencias, con el ánimo de dotar de una herramienta versátil que pueda fácilmente dar un panorama de la calidad de la energía de un punto en particular.

En repuesta a esto, el este trabajo presenta el desarrollo de una plataforma para evaluar fenómenos de calidad de la energía, que incluye el hardware de la sensórica, el software de evaluación y el sistema de adquisición aprovechando las herramientas computacionales en la solución de problemas de ingeniería eléctrica [17]; profundizando en los conceptos previos establecidos por los autores en el trabajo [18]. Incluyendo un estudio de caso, en el cual se establece un comparativo entre la alimentación de cargas lineales y cargas no lineales, siendo estas últimas generadoras de contaminantes en la red, provocando la aparición de fenómenos electromagnéticos [13].

2. Sistema de evaluación de calidad de la energía

El estándar IEEE 1159-1995 [19] clasifica los fenómenos electromagnéticos que describen los problemas de la calidad de energía de la forma como se muestra en la Tabla 1, fenómenos presentes en sistemas eléctricos como: *sags*, *swells*, sobretensiones, bajos voltajes, interrupciones, *offset* de CD (corriente directa), armónicos, *Flicker*, y variaciones de frecuencia [5], quedan caracterizados en esta tabla.

Tabla 1.
Categorías y características de fenómenos electromagnéticos (IEEE 1159 - 1995).

Categoría	Contenido Típico Espectral	Duración Típica	Magnitud Típica del Voltaje
1.0 Transitorios			
1.1 Impulsos			
1.1.1 Nanosegundos	5ns de elevación	<50 ns	
1.1.2 Microsegundos	1 ms de elevación	50ns-1ms	
1.1.3 Milisegundos	0.1ms elevación	>1ms	
1.2 Oscilatorios			
1.2.1 Baja Frecuencia	< 5kHz	0.3-50ms	0-4 pu
1.2.2 Frecuencia Media	5-500 kHz	20us	0-8 pu
1.2.3 Alta Frecuencia	0.5 - 5MHz	5us	0-4 pu
2.0 Variaciones de corta duración			
2.1 Instantáneas			
2.1.1 Sag		.5-30 ciclos	0.1-0.9 pu
2.1.2 Swell		.5-30 ciclos	1.1-1.8 pu
2.2 Momentáneas			
2.2.1 Interrupción		.5 ciclos -3s	< 0.1 pu
2.2.2 Sag		30 ciclos-3s	0.1-0.9 pu
2.2.3 Swell		30 ciclos-3s	1.1-1.4 pu
2.3 Temporal			
2.3.1 Interrupción		3 seg-1 min	< 0.1 pu
2.3.2 Sag		3 seg-1 min	0.1-0.9 pu
2.3.3 Swell		3 seg-1 min	1.1-1.2 pu
3.0 Variaciones de larga duración			
3.1 Interrup. sostenida		>1 min	0.0 pu
3.2 Bajo voltaje		>1 min	0.8-0.9 pu
3.3 Sobrevoltaje		>1 min	1.1-1.2 pu
4.0 Desbalance de V		Estado Estable	0.5-2%
5.0 Distorsión de Forma de Onda			
5.1 Componente de CD		Estado Estable	0-0.1%
5.2 Contenido armónico	0-100th H	Estado Estable	0-20%
5.3 Interarmónicas	0-6 kHz	Estado Estable	0-2%
5.4 Muescas en el voltaje		Estado Estable	
5.5 Ruido Banda amplia		Estado Estable	0-1%
6.0 Fluctuaciones de Voltaje			
	<25 Hz	Intermitente	0.1-7%
7.0 Variaciones de Frecuencia			
		<10 seg	

Fuente: Adaptado de [13].

En el sistema de evaluación desarrollado en este trabajo sólo se incluyen los fenómenos relacionados en la Tabla 2. Fenómenos que involucran magnitudes medio cuadráticas (*Root-Mean Square* - RMS) y duración de tiempo, al igual que variaciones de frecuencia, distorsión armónica y fluctuaciones de voltaje como el *Flicker*. Se dejan afuera los fenómenos transitorios por la dificultad de la medición y la falta de instrumentación para esto, en cuanto a la capacidad de sobretensión y de muestreo para la determinación de fenómenos oscilatorios de media y alta frecuencia. Al igual que no se determinan los fenómenos de los sistemas trifásicos, como los desbalances de tensión.

Tabla 2
Fenómenos electromagnéticos.

Fenómenos	Duración típica	Magnitud de voltaje típica
Interrupción Instantáneas.	0.5 - 30 ciclos	< 0.1 pu
Interrupción momentáneas.	30 ciclos – 3 s	< 0.1 pu
Interrupción Temporal.	3 seg - 1 min	< 0.1 pu
Interrupción sostenida.	> 1 min	0.0 pu
Elevación (*Swell*).	0.5 - 1 min	0.1 - 0.9 pu
Depresión (*Sag*, *dip*).	0.5 - 1 min	1.1 - 1.8 pu
Bajos voltajes.	> 1 min	0.8 - 0.9 pu
Sobrevoltajes.	> 1 min	1.1 - 1.2 pu
Variaciones de frecuencia.	< 10s	
Distorsión armónica.		
Parpadeo (*Flicker*).		

Fuente: Autores.

2.1. Hardware

El núcleo del sistema es la adquisición de datos, esta se realiza mediante una tarjeta de adquisición (DAQ) NI USB-6009 que cuenta con 8 entradas análogas, con niveles de voltaje recomendados de hasta 10 V y con una corriente máxima de 1 mA. Esta tarjeta permite muestrear señales a una tasa de 48 kS/s. Las señales muestreadas de tensión y de corriente las proveen dos sensores, el primero, un sensor de corriente ACS714 de efecto Hall de 0 a 30 Amperios, para ser utilizado en aplicaciones que requiere aislamiento eléctrico sin el uso de aisladores ópticos u otras técnicas de aislamiento costosas. El segundo un sensor de voltaje basado resistores con circuito de protección incluido con el fin de replicar las ondas de tensión a baja escala de una forma segura en tensión y corriente para las entradas de la tarjeta, sin perturbar las formas de las ondas.

Para completar el Hardware se incluye una fuente de 5 Vdc para alimentar el sensor de corriente; y los respectivos circuitos de protección contra sobre corrientes basados en fusibles extra-rápidos.

Este hardware de medición y adquisición se conecta mediante cable USB a un computador que debe tener instalado Labview® 2012 para ejecutar el software de evaluación y si es posible Excel para poder visualizar los registros históricos de las mediciones. En la Fig. 1 se muestran los componentes del hardware.

En la Fig. 2 se muestra el diagrama en bloques del sistema desarrollado, involucrando tanto el hardware antes mencionado, como el software, explicado en la siguiente sección.

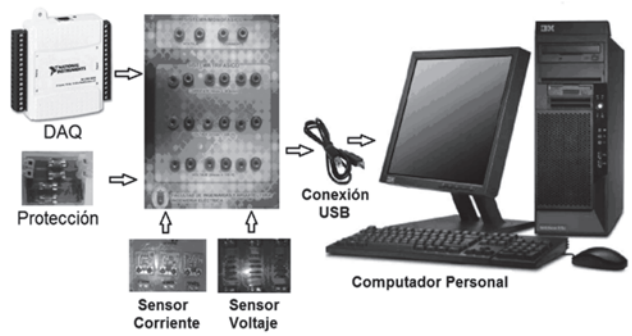


Figura.1. Hardware del sistema.
Fuente: Autores.

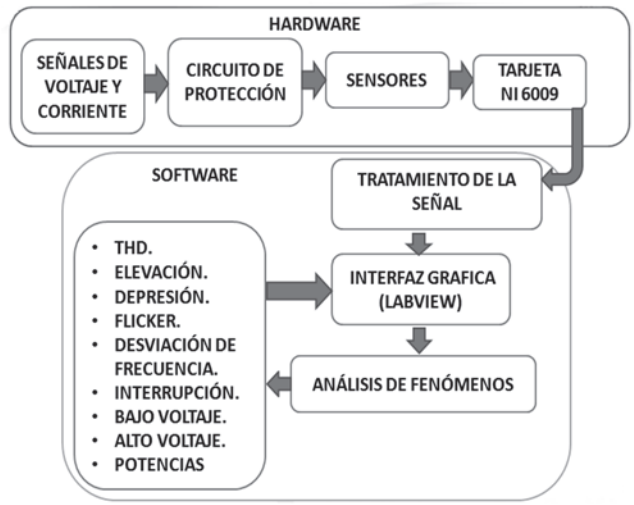


Figura. 2. Estructura del sistema.
Fuente: Autores.



Figura. 3. Procesamiento del software
Fuente: Autores.

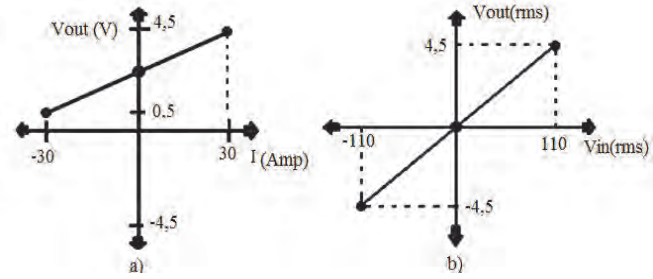


Figura.4 Escalonamiento de las señales.
Fuente: Autores.

2.2. Software

En la Fig. 3. se muestra la lógica el procesamiento que debe realizar el software.

A continuación se describen cada una de las etapas que componen el procesamiento.

2.2.1. Escalonamiento de las señales

Las señales provenientes de los sensores se acondicionan mediante un filtrado pasa baja <20 kHz, realizado por software, para limitar la evaluación a bajas frecuencias que son las requeridas para las perturbaciones relacionadas en la Tabla 2, además las señales se escalan con el fin de que la visualización en la interfaz gráfica corresponda con los valores medidos y no

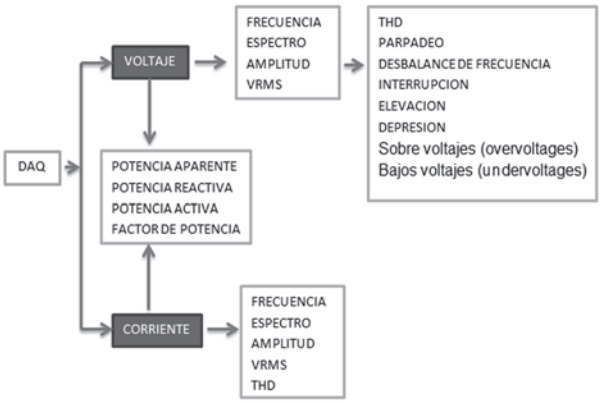


Figura. 5. Proceso de evaluación.
Fuente: Autores.

con los valores de las pequeñas señales provenientes de los sensores; estos escalonamientos se muestran en la Fig. 4.

2.2.2. Análisis de los fenómenos electromagnéticos

En la Fig. 5 se muestra el proceso de evaluación del software en términos de las dos señales que provienen de los sensores y que son previamente acondicionadas. El algoritmo, como primer paso en esta etapa, visualiza en la interfaz gráfica de usuario (GUI) las formas de onda y calcula su valor RMS, amplitud y la frecuencia. Se evalúan los disturbios de acuerdo con estos datos y según las características de cada fenómeno electromagnético.

A continuación se describe brevemente como se analizan cada uno de los fenómenos evaluados.

- Interrupciones

Con la señal escalada del sensor de tensión se calcula su valor eficaz, se compara con el valor RMS nominal para el voltaje del sistema en p.u. y se establece si existe o no una interrupción, si existe se contabiliza el tiempo y se visualiza con un indicador en la interfaz gráfica de que interrupción se trata y se genera el respectivo reporte histórico mediante una exportación de datos hacia un archivo de *Excel*. En la Fig. 6 se muestra el algoritmo *Labview*® de evaluación de interrupciones.

- Depresión y bajo voltaje

Los fenómenos de depresión y bajo voltaje tienen la misma caracterización en valores de magnitud sólo se diferencian entre sí por su duración.

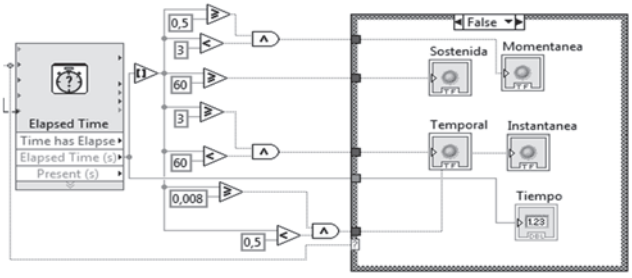


Figura. 6. Algoritmo de evaluación de interrupciones.
Fuente: Autores.

El proceso de evaluación de este fenómeno consiste en comparar la tensión nominal del sistema con el valor RMS de la señal medida en p.u. y se establece si existe o no un disturbio de esta categoría, si existe se contabiliza el tiempo y se visualiza con un indicador en la interfaz gráfica si se trata de una depresión (*Sag* IEC61000-2-2) [20] o un bajo voltaje dependiendo de la duración. Se genera el respectivo reporte histórico mediante una exportación de datos hacia un archivo de Excel.

- Elevación y sobre voltaje

Esta parte del algoritmo de evaluación es idéntica a la descrita para depresiones y bajos voltajes, lo único que cambia son las caracterizaciones en valores por unidad que tienen los fenómenos de elevación (*Swell* IEC61000-4-30) [21] y sobre voltaje.

- Desviación de la frecuencia

La desviación de la frecuencia se evaluó, como una regulación de frecuencia (Rf), mediante la siguiente ec. (1):

$$\%Rf = \left|\frac{f_{sensada} - f_{nominal}}{f_{nominal}}\right| * 100\% \quad (1)$$

Con la señal proveniente del sensor de voltaje un bloque se encarga de determinar la frecuencia de dicha señal ($f_{sensada}$) y otro bloque opera la ecuación anterior, teniendo en cuenta el valor nominal de frecuencia ingresado por teclado.

- Fluctuaciones del voltaje o Flicker

Los niveles de referencia para fluctuaciones de tensión, se establecen mediante el índice de severidad del *Flicker* de corta duración (*Pst*), o de larga duración (*Plt*), el *Pst* se define para intervalos de observación base de 10 minutos. La forma de calcular los índices de parpadeo se define en el estándar IEC-61000-4-15 [22] y sus límites en la norma IEC 61000-3-3 [23]. En base a estos estándares el algoritmo de evaluación calcula el *Pst*, como primer paso se determina Variación Relativa de Tensión, mediante la ec. (2):

$$\frac{\Delta V}{V} * 100\% \quad (2)$$

Donde V es la tensión cuando no hay perturbaciones y ΔV es la variación de las fluctuaciones. Esto se ilustra en la Fig. 7.

Para medir la severidad del *Pst* se debe calcular la anterior expresión con muestras de cada tres segundos durante 10 minutos, al terminar este intervalo de tiempo con los datos recopilados, se realiza una distribución de frecuencias, que permite calcular el índice de parpadeo de corta duración mediante la expresión:

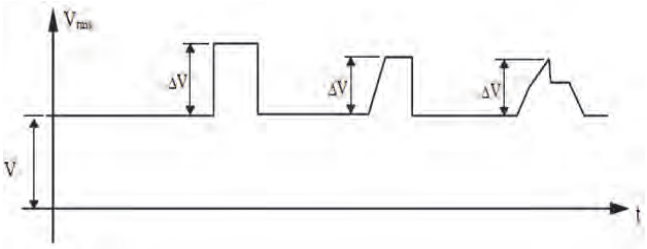


Figura. 7. Fluctuaciones en el valor eficaz de la tensión**.**
Fuente: Autores.

$$P_{st} = \sqrt{K_{0.1}P_{0.1} + K_1P_1 + K_3P_3 + K_{10}P_{10} + K_{50}P_{50}} \quad (3)$$

Dónde:

P_{st}	Severidad de parpadeo de período corto.
$P_{0.1}$, P_1, P_3, P_{10} y P_{50}	Percentiles del 0.1%, 1%, 3%, 10% y 50%
$K_{0.1}$, K_1, K_3, K_{10} y K_{50}	Constantes definidas por la IEC61000-4-15 [19] y sus valores son respectivamente: 0.0314, 0.0525, 0.0657, 0.28 y 0.08.

Este análisis es realizado en una hoja de cálculo en *Excel*, mediante un enlace en tiempo real con *Labview*® en donde se calcula el valor de la variación relativa de tensión y cada 3 segundo se van guardando en una data las muestras que al final de los diez minutos se exporta a una hoja de *Excel* que calcula la estadística y la expresión *Pst* y devuelve el valor a *Labview*® para ser visualizado. En la Fig. 8 se observa el algoritmo de comunicación de los dos programas.

- Distorsión armónica

Para evaluar este fenómeno el algoritmo determina, mediante una Transformada Rápida de Fourier (FFT) de Labview®, el espectro armónico, que se calcula hasta el armónico 100, sin embargo, las magnitudes de los armónicos mostradas en pantalla sólo son las primeras 25 componentes y calcula la Distorsión Armónica Total (THD) tanto para la señal de voltaje como para la de corriente (IEEE 519) [24]. Se seleccionó el THD como de medida de la distorsión, por ser el factor medición más conocido, por lo que es recomendable para medir la distorsión en parámetros individuales [25], la expresión del cálculo del THD es la siguiente:

$$THD_I = \frac{\sqrt{\sum_{h=2}^{hmax} {I_h}^2}}{I_1} * 100 \quad (4)$$

$$THD_V = \frac{\sqrt{\sum_{h=2}^{hmax} {V_h}^2}}{V_1} * 100 \quad (5)$$

Dónde:

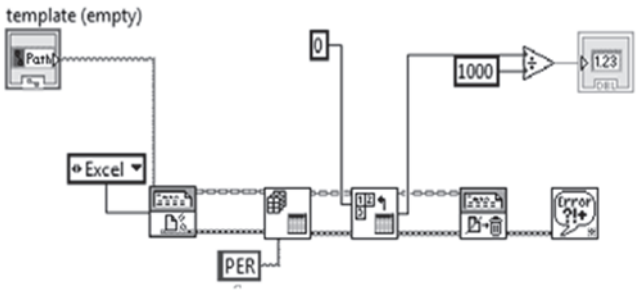


Figura. 8. Algoritmo de comunicación Excel-Labview.
Fuente: Autores.

I_h, V_h: Magnitud de la armónica individual de orden h.
I_1, V_1: Magnitud de la armónica fundamental de corriente y voltaje.

- Potencias y factor de potencia

Con las señales escaladas de voltaje y de corriente mediante bloques en Labview® y determinando los desfases entre las dos señales se puede calcular el factor de potencia y las potencias del sistema según las expresiones Ec. (6) - Ec. (9):

$$S = V_{eff} * I_{eff} \quad (6)$$

$$FP = \frac{P}{S} = \cos(\theta - \Phi) \quad (7)$$

$$P = S * FP \quad (8)$$

$$Q = S * \sin(\cos^{-1}(FP)) \quad (9)$$

En donde FP es el factor de potencia, θ el ángulo del desfase del voltaje, ϕ el ángulo de desfase de la corriente, P la potencia activa, Q la potencia reactiva y S la potencia aparente.

Sin embargo, estas relaciones corresponden al factor de potencia de desplazamiento [13], para estimar de una manera más exacta las relaciones de potencias, incluyendo los aportes dados por las distorsiones armónicas, se deben aplicar las ecuaciones:

$$U_{rms} = \sqrt{\frac{1}{T}\int_0^T \left(U_0 + \sum_{n=1}^{\infty} U_m \sin nwt + \theta_n\right)^2} \quad (10)$$

$$I_{rms} = \sqrt{\frac{1}{T}\int_0^T \left(I_0 + \sum_{n=1}^{\infty} I_m \sin nwt + \theta_n\right)^2} \quad (11)$$

$$S = U_{rms} * I_{rms} \quad (12)$$

$$P = \frac{1}{T}\int_0^T \left(U_0 + \sum_{n=1}^{\infty} U_m \sin nwt + \theta_n\right) * \frac{1}{T}\int_0^T \left(I_0 + \sum_{n=1}^{\infty} I_m \sin nwt + \theta_n\right) \quad (13)$$

$$Q = \sqrt{S^2 - P^2} \quad (14)$$

Donde n, hace referencia a la componente de orden n de la serie de Fourier, T es el periodo de las ondas de corriente o de tensión dependiendo del caso [26]. Estos valores calculados con las ec. (10) – ec. (24), corresponderían a las relaciones del factor de potencia real.

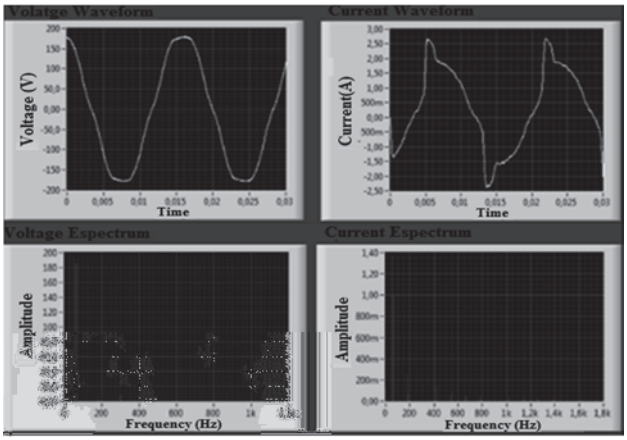


Figura. 9. GUI de formas de onda y espectros armónicos.
Fuente: Autores.

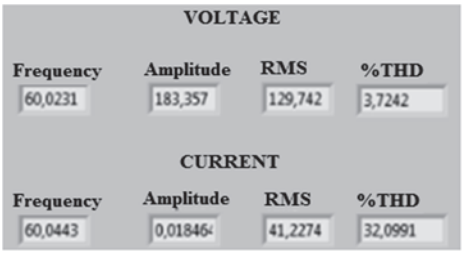


Figura. 10. GUI de formas de onda y espectros armónicos.
Fuente: Autores.

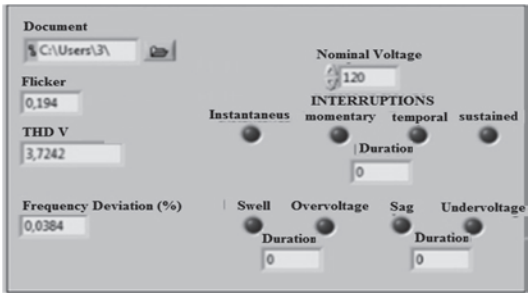


Figura. 11. GUI de fenómenos evaluados
Fuente: Autores.

2.3. Interfaz Gráfica de Usuario

En Labview® se desarrolló una interfaz gráfica en la cual se visualizan las formas ondas de corriente y de tensión junto con sus espectros armónicos (ver Fig. 9)

Los valores RMS, frecuencia, amplitud, y THD, para la corriente y el voltaje se visualizan en un GUI como el mostrado en la Fig. 10.

Los indicadores de *Sag*, *Swell*, interrupciones, bajos voltajes, sobrevoltajes, desviación de frecuencia, Flicker, junto con el espacio para el ingreso de la tensión nominal del sistema evaluado se observan en la interfaz que se muestra en la Fig. 11.

De igual forma se realizo una interfaz para de visualizar las potencias y el factor de potencia junto con las magnitudes de los primeros 25 armónicos tanto en valores pico como en RMS. El GUI completo se muestra en la Fig. 12.

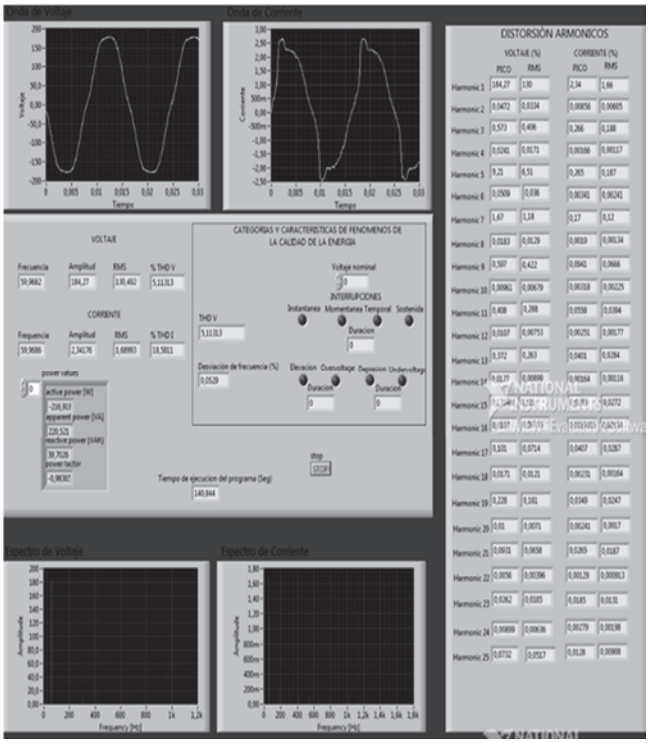


Figura. 12. Interfaz gráfica completa**.**
Fuente: Autores.

3. Validación

Para validar los datos del sistema de evaluación se hicieron pruebas y se compararon los resultados con equipos de medida como la pinza amperimétrica MS2205, osciloscopio, multímetro FLUKE 122, etc. La Fig. 13 muestra una fotografía de una prueba de validación con carga resistiva.

La Fig. 14 muestra datos de validación de las potencias, se muestra los valores capturados por el sistema y las fotografías de la pinza amperimétrica.

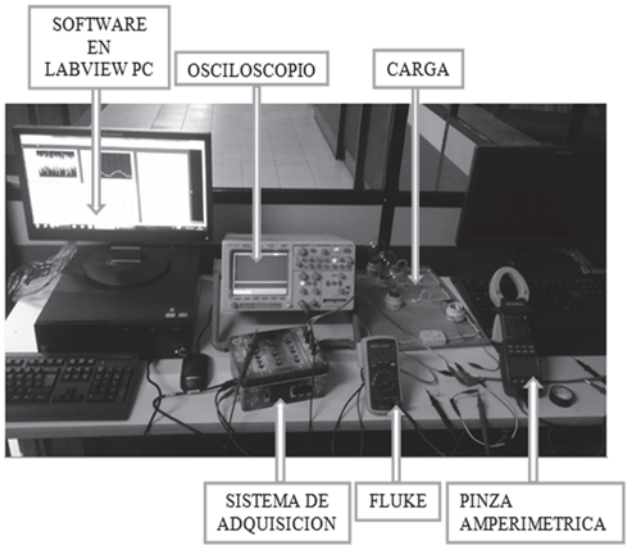


Figura. 13. Fotografía prueba de validación.
Fuente: Autores.



Figura. 14. Comparación valores de potencias.
Fuente: Autores.

Tabla 3
Resumen de valores de potencia.

Variable eléctrica	Sistema diseñado	Harmonic Power Clamp
Potencia Activa (W).	237.9	238
Potencia Aparente (VA).	239.14	238.45
Factor de potencia (FP).	0.995	0.995

Fuente: autores.

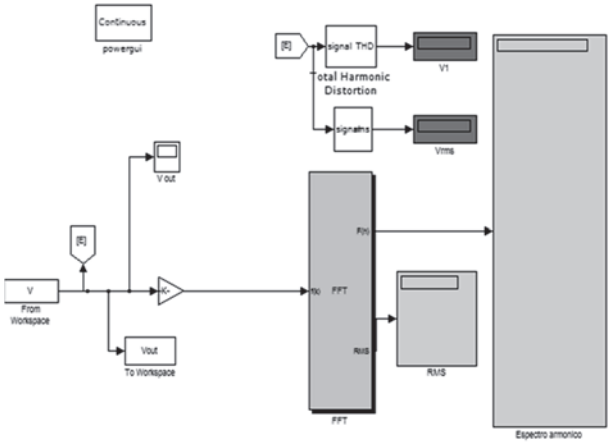


Figura 15. Programa en *simulink* para evaluar espectros y valores RMS.
Fuente: Autores.

Los valores se resumen en la Tabla3.

Con este mismo procedimiento se validaron los demás valores evaluados, excepto los espectros armónicos que se validaros adquiriendo las datas y evaluándolas en un FFT de Matlab®, en la Fig. 15 se muestra el esquema en *Simulink* de este programa; la entrada es la data adquirida por Labview®, guardada en los históricos de Excel he importada de matlab, la salida son los analisis dados por el bloque FFT del simulink, junto con los valores RMS.

La Fig. 16 muestra las formas de onda y los espectros armónicos en Matlab® y en Labview® para la onda de tensión de una prueba con una carga compuesta de lámparas ahorradoras y lámparas incandescentes, caso de estudio que se presentará en una sección posterior de este artículo.

4. Análisis de costos

En cuanto a costos, en el mercado se encuentran equipos que permiten analizar la calidad de la energía de sistemas

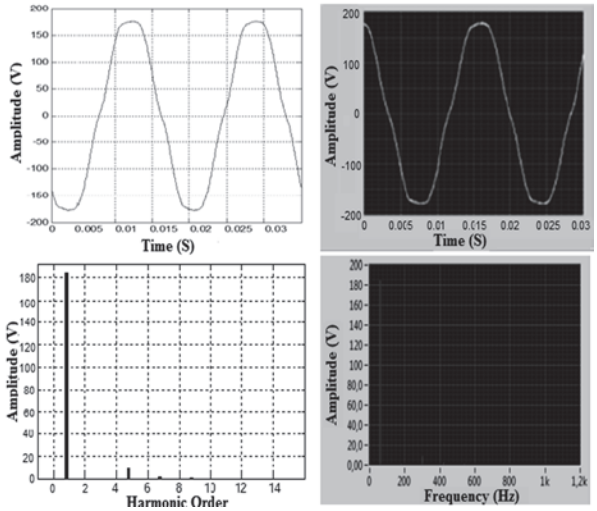


Figura. 16. Forma de onda y espectro en Matlab y Labview.
Fuente: Autores.

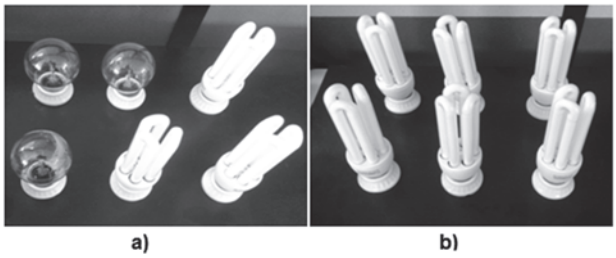


Figura 17. a) Carga mixta. b) Carga no lineal.
Fuente: Autores.

electricos monofásicos como trifásicos, sin embargo presentan costos elevados.

Se realizó una comparación del costo del sistema diseñado, que fue de 1170 €, con algunos equipos de medición y evaluación de calidad de la energía disponibles en el mercado como por ejemplo: el equipo Fluke 43B/001 Power Quality Analyzer (single-phase) con costo de 3493€, o Fluke 43 Basic Analizador de calidad de la energia eléctrica (monofásico) de 2396€, el equipo Fluke 435-II/BASIC Analizador de calidad eléctrica con costo 5025€ o el Fluke 435-II Analizador trifásico de calidad eléctrica 5634€ o el Fluke 434-II/BASIC. Esta comparación permite establecer que el sistema implementado se puede catalogar como un sistema de bajo costo.

5. Estudio de caso

Por último, se realizó un pequeño estudio de caso, evaluando la calidad de la energía presente en la alimentación de una carga no lineal (compuesta por lámparas ahorradoras de la marca LEELITE®) y una carga mixta (compuesta por bombillas incandescentes marca Philips y lámparas ahorradoras LEELITE®), la Fig. 17 muestra el arreglo de las cargas. El montaje de la prueba se muestra en la Fig. 13.

Debido a que la alimentación se dispuso mediante la red eléctrica convencional a cargo de Centrales Eléctricas de

Norte de Santander (CENS), fenómenos como depresiones, elevaciones, parpadeo e interrupciones, no se visualizaron a causa de que el suministro eléctrico en cuanto al valor RMS de la onda de tensión es bueno, sin embargo, fenómenos como la distorsión armónica si se pudieron evidenciar y cuantificar. A continuación se presentan los resultados:

5.1. Carga no lineal

La Fig. 18, muestra una fotografía de los resultados del software de evaluación.

La forma de onda de la tensión se muestra en la Fig. 19, la forma de onda de la corriente se muestra en la Fig. 20

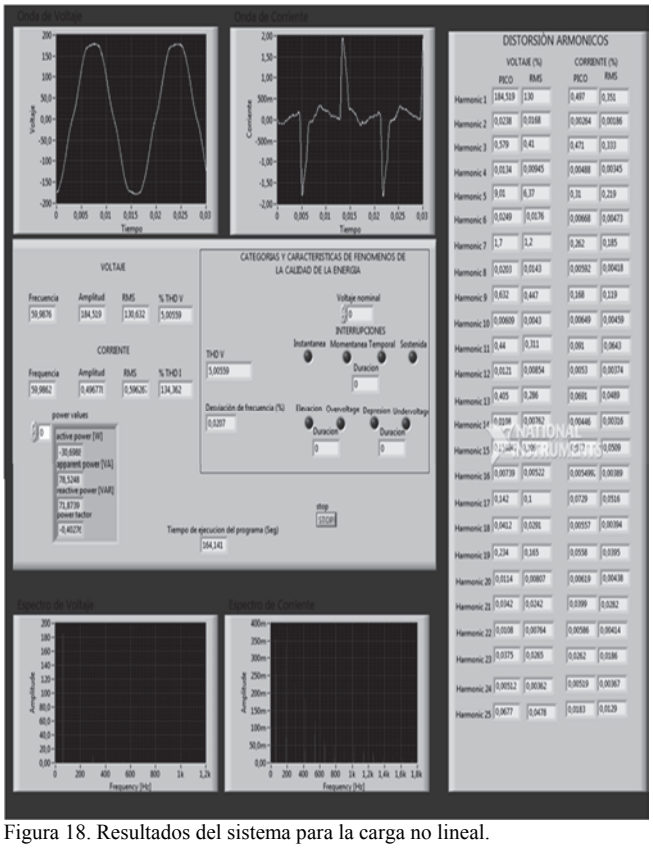


Figura 18. Resultados del sistema para la carga no lineal.
Fuente: Autores.

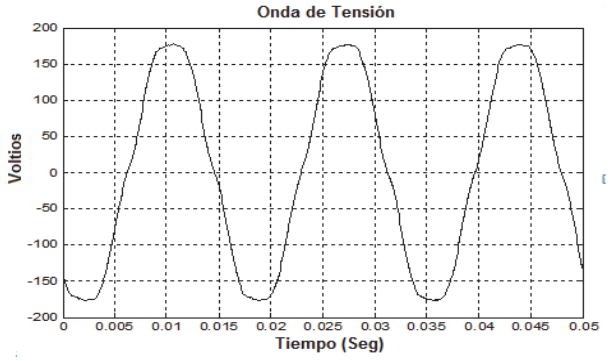


Figura 19. Forma de onda de tensión con la carga no lineal.
Fuente: Autores.

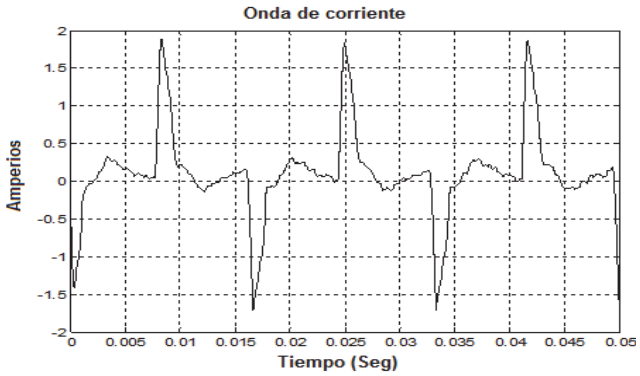


Figura 20. Forma de onda de corriente de la carga no lineal.
Fuente: Autores.

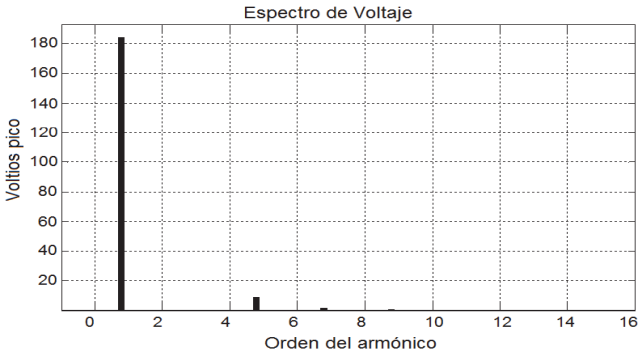


Figura 21. Espectro de la onda de tensión.
Fuente: Autores.

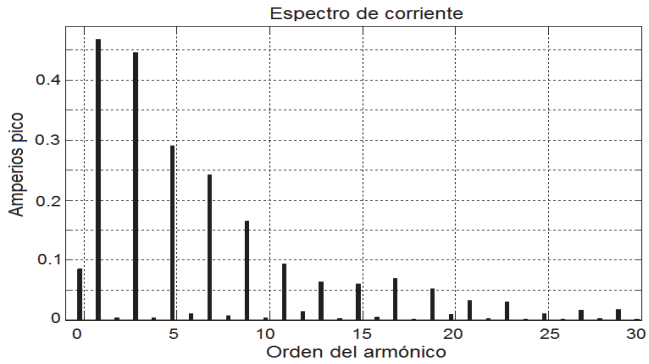


Figura 22. Espectro de la onda de corriente.
Fuente: Autores.

De igual forma los espectros para cada una de las formas ondas se muestran en la Fig. 21 y en la Fig. 22.

Los valores del total de distorsión armónica se muestran en la Tabla 4.

Tabla 4
Consolidado de THD para la prueba con carga no lineal.

Medio de evaluación	***THD de corriente (%)***	***THD de tensión (%)***
Sistema desarrollado	134.3	4.9

Fuente: Autores.

Los resultados de esta prueba evidencian que la distorsión armónica en la corriente es muy alta, debido a que los dispositivos semiconductores (que constituyen las lámparas ahorradoras) recortan la onda de corriente. Sin embargo, el contenido armónico de la tensión cumple con los estándares vigentes, al estar por debajo del 5% de THD. De igual forma la presencia de contenido armónico de orden 5 en la onda de voltaje, evidencia un problema de calidad de la energía, si esta forma de onda alimentara motores, el armónico 5 y 7 provocarían la aparición de pares opuestos parásitos, contribuyendo al calentamiento de la máquina [27].

5.2. Carga mixta

Al igual que en la prueba anterior, se alimentó el arreglo con la red convencional y se tomaron los resultados del sistema de evaluación, la Fig. 23 muestra la forma de onda de voltaje.

La forma de onda de la corriente se muestra en la Fig. 24.

La presencia de las lámparas incandescentes, mejoran la forma de onda de la corriente, con respecto a la prueba anterior. Al ser la corriente total la superposición de las corrientes demandadas por las cargas lineales y no lineales, la forma de onda se aproxima a la forma sinusoidal (presente en la carga lineal), pero se deforma debido a las discontinuidades de las corrientes de las cargas no lineales.

Los espectros mostrados en las Figs. 25 y 26 evidencian la mejora en la calidad de la energía. Los valores del total de distorsión armónica se resumen en la Tabla 5.

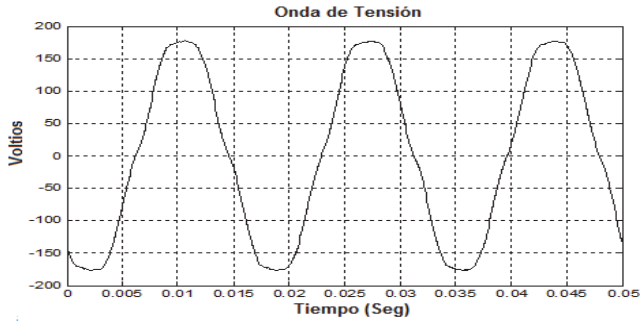


Figura 23. Forma de onda de tensión con la carga mixta.
Fuente: Autores.

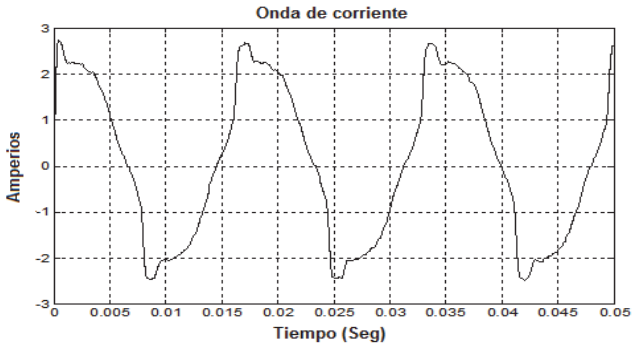


Figura 24. Forma de onda de corriente.
Fuente: Autores.

Tabla 5
Consolidado de THD para la prueba con carga mixta.

Medio de evaluación	*THD de corriente (%)*	*THD de tensión (%)*
Sistema desarrollado	19.1	4.9

Fuente: Autores.

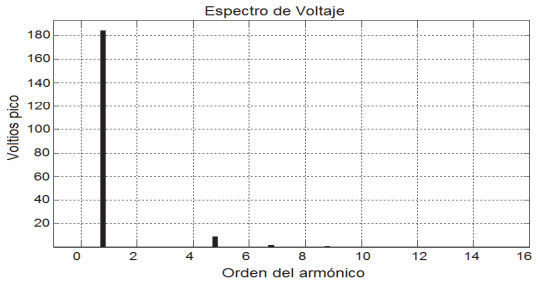


Figura 25. Espectro de la onda de tensión.
Fuente: Autores.

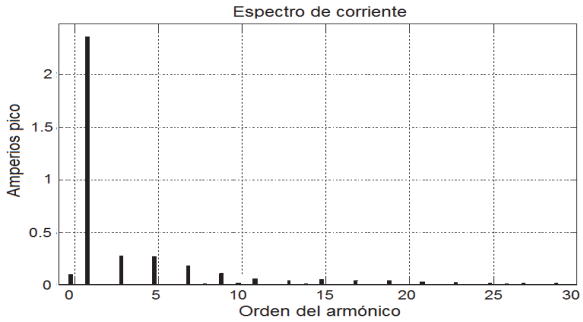


Figura 26. Espectro de la onda de corriente.
Fuente: Autores.

La disminución en el contenido armónico de la corriente es bastante grande, sin embargo, aún el THD es muy elevado, evidenciando la contaminación que las cargas no lineales le imprimen a la red. La tensión permanece con un contenido armónico casi invariante, cumpliendo los estándares vigentes al estar por debajo del 5%. El hecho de que la potencia demandada de la carga es baja causa que la onda de tensión no se deforme de manera significativa.

Las pruebas muestran que las lámparas ahorradoras presentan una impedancia variante durante el ciclo de tensión, lo que conlleva a que se presenten deformaciones en las ondas de corriente, generando perjuicios para la red.

6. Conclusiones

El sistema desarrollado presenta excelentes resultados en cuanto a la evaluación de la calidad de la energía en sistemas monofásicos; y debido al bajo costo de los elementos que lo componen, en comparación con las soluciones actuales del mercado, este constituye una alternativa para tener mediciones de buena calidad a bajo costo.

El contenido armónico se puede cuantificar mediante el total de distorsión armónica, sin embargo, es de suma importancia poder visualizar este tipo de distorsión mediante

los espectros armónicos y cuantificar el valor de cada armónico, ya que esto da un panorama claro de los efectos indeseados que se pueden presentar y cuáles pueden ser las técnicas de mitigación más eficientes.

Las ventajas más importantes que se tienen al trabajar con instrumentación virtual, como en este trabajo, es que al estar basadas en un computador, las aplicaciones crecen de manera significativa, pues se aprovechan todas sus bondades como memoria, velocidad de procesamiento, despliegue de la información, etc. Además de que las características y funcionalidad que tendrá el instrumento son definidas por el usuario y existe la posibilidad de incorporar nuevas tecnologías.

La principal desventaja de la instrumentación virtual, es que al inicio requiere una fuerte inversión por la compra de las tarjetas DAQ, pero esta se puede compensar debido a la reutilización que se le puede dar al equipo.

El fenómeno más difícil de caracterizar en cuanto a calidad de la energía según la normativa vigente, y bajo nuestro criterio es el *Flicker*, pues requiere preparación de las señales, análisis estadístico y cálculos matemáticos.

La validación de las variables comparándolas con instrumentos comerciales, verificó que se puede implementar un instrumento que permita analizar la calidad de la energía de una red eléctrica, utilizando instrumentación virtual de bajo costo.

Del estudio de caso presentado se puede concluir que las lámparas ahorradoras LEELITE® se comportan como cargas no lineales y generan gran cantidad de contaminantes a la red, causadas por las discontinuidades de las corrientes demandadas.

Referencias

[1] Banos, R., Manzano-Agugliaro, F., Montoya, F.G., Gil, C., Alcayde, A. and Gómez, J., Optimization methods applied to renewable and sustainable energy: A review. Renewable and Sustainable Energy Reviews, 15(4), pp. 1753-1766, 2011. DOI: 10.1016/j.rser.2010.12.008.

[2] Montoya, F.G., Manzano-Agugliaro, F., Gómez, J. and Sánchez-Alguacil, P., Power quality research techniques: Advantages and disadvantages DYNA, 79(173), pp. 66-74, 2012.

[3] Carrillo-Rojas, G., Andrade-Rodas, J. Barragán-Escandón, A., and Astudillo-Alemán, A., Impact of electrical energy efficiency programs, case study: Food processing companies in Cuenca, Ecuador. DYNA, 81(184), pp. 41-48, 2014. DOI: 10.15446/dyna.v81n184.40821.

[4] Enriquez, G., El ABC de la calidad de la energía eléctrica. Ed. Limusa, Noriega Editores, México, 2004.

[5] Dugan, R.C., McGranaghan, M.F., Santoso S. and Beaty, W.H., Electrical Power Systems Quality, 2ª Ed., McGraw-Hill, USA, 2004.

[6] Ze-jun, D., Yuan, J., Huang, R. and Sen, O., Research of fuzzy synthetic evaluation method of power quality based on improved membership function. IEEE Proc. for Power Engineering and Automation Conference (PEAM), Hangzhou, pp.1-4, 2012. DOI: 10.1109/PEAM.2012. 6612484.

[7] Zhai, X.L, Lin, Z., Wen, F.S. and Huang, J.S., Power quality comprehensive evaluation based on combination weighting method. Proc. for Sustainable Power Generation and Supply (SUPERGEN 2012), IEEE Int. Conf., Hangzhou, pp.1-5, 2012. DOI: 10.1049/ cp.2012.1838.

[8] Leng, S., Edrington, C.S. and Cartes, D.A., A new harmonic distortion measurement algorithm for power quality evaluation and compensation. Proceedings for Power and Energy Society General Meeting, IEEE, San Diego, California, pp.1-8, 2011. DOI 10.1109/PES.2011.6039131.

[9] Sánchez, P. and Montoya, F.G., Manzano-Agugliaro,F., Consolación, G., Genetic algorithm for S-transform optimization in the analysis and classification of electrical signal perturbations, Expert Systems with Applications, 40(17), pp. 6766-6777, 2013. DOI: 10.1016/j.eswa.2013.06.055.

[10] López, D.J., Camacho, G.A., Díaz, O., Gaviria, C.A. and Bolaños G., A novel hybrid PWM algorithm having superior harmonic performance. Revista Ingeniería e Investigación, 29(1), pp. 82-89, 2009.

[11] Francess, G., Sumpera, A., Díaz, F. and Galceran, A.S., Flicker mitigation by reactive power control in wind farm with doubly fed induction generators. International Journal of Electrical Power & Energy Systems, 55, pp. 285-296 2013. DOI: 10.1016/j.ijepes.2013.09.016.

[12] Kilter, J., Meyer, J., Howe, B. and Zavoda, F., Current practice and future challenges for power quality monitoring perspective Harmonics and Quality of Power (ICHQP). IEEE Proceedings 15th Int., Conference on, Hong Kong, pp. 390-397, 2012. DOI: 10.1109/ICHQP.2012.6381311.

[13] Sánchez, M.A., Calidad de la energía eléctrica. Instituto Tecnológico de Puebla, México, 2009.

[14] Joao, L., Batista A.J., Sepúlveda, M.J., Low cost digital system for power quality monitoring. Información Tecnológica, 18(4), pp. 15-23, 2003. DOI: 10.4067/S0718-07642007000400004.

[15] Ángel, Á. y Ordóñez, P., Calidad de la energía eléctrica: Diseño y construcción de un prototipo como alternativa para la monitorización de interrupciones y caídas de tensión. UIS Ingenierías, 4(2), pp. 75-84, 2005.

[16] Pinzón, A.O., Useche, G. and Rodriguez., G., Diseño e implementación de un equipo analizador de calidad de energía eléctrica, Revista Colombiana de Tecnologías de Avanzada, 2(18), pp. 46-52, 2011.

[17] Mago, M.G., Valles, L. and Olaya, J.J., An analysis of distribution transformer failure using the statistical package for the social sciences (SPSS) software. Ingeniería e investigación, 32(2), pp. 40-45, 2012.

[18] Pabón, L.D., Diaz, J.L. and Contreras, J.L., Low cost system for power quality evaluation of single-phase electric power systems. Proceedings for Congreso Internacional de Ingeniería Eléctrica, Electrónica y Computación, INTERCON 2014, IEEE, pp. 13-18, 2014.

[19] IEEE Standard 1159. Recommended practice for monitoring electric power quality a status update, IEEE, 1995. DOI: 10.1109/IEEESTD. 2009.5154067.

[20] IEC61000-2-2. Electromagnetic Compatibility (EMC) - Part 2-2: Environment compatibility levels for low-frequency conducted disturb and signaling in public low-voltage power supply systems, 2002.

[21] IEC61000-4-30 Electromagnetic compatibility (EMC) –Part: Testing and measurement techniques Power quality measurement methods, 2002.

[22] IEC61000-4-15. Compatibilidad electromagnética (CEM) – Parte 4 Técnicas de ensayo y medida, Sección 15, Medidor de Flicker, 2003.

[23] IEC 61000-3-3. Electromagnetic compatibility (EMC) - Part 3-3: Limits - Limitation of voltage changes, voltage fluctuations and flicker in public low-voltage supply systems, for equipment with rated current ≤16 A per phase and not subject to conditional connection, 2003.

[24] IEEE Std. 519-1992 IEEE Recommended practices and requirements for harmonic control in electrical power systems, IEEE, 1992. DOI: 10.1109/IEEESTD.1993.114370.

[25] Pabón-Fernandez, L.D., Andres-Caicedo, E. and Diaz-Rodriguez, J.L., Comparative analysis of 9 levels cascade multilevel converters with selective harmonic elimination, in Power Electronics and Power Quality Applications (PEPQA), 2015 IEEE Workshop on, 2-4 June, 2015, pp.1-6. DOI: 10.1109/PEPQA.2015.7168244.

[26] *Edminister, J.A. y Nahvi, M. Circuitos Eléctricos. McGraw-Hill, 3ra. Ed., 1999.*

[27] *Mora, J.F. Máquinas eléctricas. McGraw-Hill, 5ta Edición, 2003.*

J.L. Díaz-Rodríguez, nació en Camagüey, Cuba. Es graduado *Summa Cum Laude* de Ingeniero Electricista en 1996 de la Universidad de Camagüey, Cuba. MSc. en Automática en 2000 de la Universidad Central "Marta Abreu" de Las Villas, Cuba. Actualmente es profesor titular del Departamento de Ingeniería Eléctrica, Electrónica, Sistemas y Telecomunicaciones de la Universidad de Pamplona, Colombia. Imparte la materia de Máquinas Eléctricas.
ORCID: 0000-0001-7661-8665.

L.D. Pabón-Fernández, nació en Pamplona, Norte de Santander, Colombia. Es graduado como Ingeniero Eléctrico en 2011 de la Universidad de Pamplona, Colombia. Candidato a MSc. en Controles Industriales de la Universidad de Pamplona, Colombia. Joven investigador del Programa "Jóvenes Investigadores e Innovadores" de Colciencias en año 2012 y 2014. Actualmente docente del programa de Ingeniería Eléctrica de la Facultad de Ingenierías y Arquitectura. Imparte las materias de Máquinas Eléctricas y de Suministro Eléctrico.
ORCID: 0000-0003-1788-4781.

J.L. Contreras-Peña, nació en Arauca departamento de Arauca, Colombia. Es graduado como Ingeniero Eléctrico en 2014 de la Universidad de Pamplona, Colombia, actualmente desempeña el cargo de apoyo profesional a la dirección TOPMA en la Empresa Enelar E.S.P.
ORCID: 0000-0003-4536-8506.

UNIVERSIDAD NACIONAL DE COLOMBIA
SEDE MEDELLÍN
FACULTAD DE MINAS

Área Curricular de Ingeniería
Eléctrica e Ingeniería de Control

Oferta de Posgrados

Maestría en Ingeniería - Ingeniería Eléctrica

Mayor información:

E-mail: ingelcontro_med@unal.edu.co
Teléfono: (57-4) 425 52 64

UNIVERSIDAD NACIONAL DE COLOMBIA
SEDE MEDELLÍN
FACULTAD DE MINAS



DYNA
http://dyna.medellin.unal.edu.co/

Self-assessment: A critical competence for Industrial Engineering

Domingo Verano-Tacoronte [a], Alicia Bolívar-Cruz [b] & Sara M. González-Betancor [c]

[a] *Facultad de Economía, Empresa y Turismo, Universidad de Las Palmas de Gran Canaria, España. domingo.verano@ulpgc.es*
[b] *Facultad de Economía, Empresa y Turismo, Universidad de Las Palmas de Gran Canaria, España. alicia.bolivar@ulpgc.es*
[c] *Facultad de Economía, Empresa y Turismo, Universidad de Las Palmas de Gran Canaria, España. sara.gonzalez@ulpgc.es*

Received: November 6th, 2014. Received in revised form: May 14th, 2015. Accepted: October 22th, 2015.

Abstract
Assess one's own abilities realistically and critically is the key for a continuous adaptation to the changing labor market conditions. The university system must train the future engineers to rate their own performance accurately, reducing biases as self-benevolence. This paper analyzes, with a sample of students of Industrial Engineering, the accuracy of self-assessment in oral presentations, using a scoring rubric. The results of several statistical tests indicate that students are good assessors of others work, but benevolent with their own work. In addition, men evaluate themselves significantly higher than women do. Finally, self-assessment tend to compensate for others assessments, mainly in the case of students considered worse by teachers. These results point to the need of including self-assessment activities in an increasing number to improve students' performance.

Keywords: self-assessment; higher education; engineering; transversal competences; employability; scoring rubrics.

Autoevaluación: Una competencia crítica para la Ingeniería Industrial

Resumen
Valorar de manera realista y crítica las propias capacidades es clave para una adaptación continua a las cambiantes condiciones del mercado de trabajo. El sistema universitario debe preparar a los futuros ingenieros para que puedan juzgar su propio trabajo de manera precisa, reduciendo los sesgos como la auto-benevolencia. Este trabajo analiza, con una muestra de estudiantes de Ingeniería Industrial, la precisión de la autoevaluación en presentaciones orales, utilizando una rúbrica. Los resultados, fruto de varias pruebas estadísticas, indican que los estudiantes son buenos valoradores del trabajo de otros, pero benevolentes consigo mismos. Además, los hombres se autoevalúan de manera significativamente superior que las mujeres. Finalmente, las autoevaluaciones tienden a compensar las valoraciones efectuadas por otros valoradores, fundamentalmente en el caso de los estudiantes peor considerados por los profesores. Estos resultados sugieren la necesidad de incluir actividades de autoevaluación en un número creciente que mejoren el desempeño de los estudiantes.

Palabras clave: autoevaluación; educación superior; ingeniería; competencias transversales; empleabilidad; rúbricas.

1. Introducción

Como consecuencia de la situación económica por la que atraviesa España, la tasa de paro no ha dejado de aumentar en los últimos años. En el campo de la ingeniería, un estudio encargado por el Consejo General de Ingenieros Industriales de España y que se basa en una encuesta que se realizó en 2013 al colectivo de ingenieros industriales colegiados de España pone de manifiesto que la tasa global de desempleo asciende al 15,5% de los encuestados, alcanzando el 27,1% en el colectivo que tiene una experiencia entre 1 y 5 años [1]. A pesar de estos datos tan desalentadores, hay que tener en cuenta que la crisis es coyuntural y que a medida que la economía se recupere, estos titulados volverán al mercado laboral. De cara a facilitar ese retorno y, por tanto, fomentar la empleabilidad es vital poseer, además de conocimientos técnicos, una serie de competencias de carácter transversal, también denominadas habilidades blandas o *soft-skills*. Estas competencias transversales incluyen el trabajo en equipo, la presentación oral, la resolución de problemas, el aprendizaje y trabajo autónomos y el razonamiento crítico. La Universidad asume, dentro del Espacio Europeo de

© The author; licensee Universidad Nacional de Colombia.

Educación Superior, la responsabilidad de capacitar a sus estudiantes para que puedan desarrollar de manera efectiva una actividad profesional. Esto es así dados los nuevos retos profesionales y los desafíos del mercado actual debidos a las nuevas formas de trabajo multicultural e interdisciplinar. Por ello se hace necesario potenciar las competencias que desarrollen la capacidad de los estudiantes de integrarse en el mercado de trabajo y permanecer en él a lo largo del tiempo, e incluso poder volver a él si lo abandonan temporalmente.

Este trabajo se centra en la autoevaluación, que está íntimamente relacionada con las competencias de aprendizaje y trabajo autónomos y de razonamiento crítico por cuanto la autonomía requiere la capacidad para evaluar el propio trabajo y, por definición, esta evaluación debe ser crítica para reconocer las limitaciones que tiene la persona respecto a su preparación y sus resultados laborales e intelectuales [2-6]. Asimismo, la autoevaluación es fundamental para la mejora y la innovación en el ámbito empresarial a través de los procesos de I+D+i en los que se involucran los ingenieros [7]. Estas competencias son de gran importancia para potenciar la empleabilidad de los ingenieros, tal y como se reconoce en el Libro Blanco de las titulaciones de Ingeniería rama industrial (propuesta de las Escuelas Técnicas Superiores de Ingenieros Industriales) [8], en el que las citadas competencias reciben valoraciones de 7 y 8 puntos, respectivamente, en una escala de 1 a 10.

Por otra parte, si se consigue garantizar que la autoevaluación sea precisa, en cuanto a que exista coincidencia entre las puntuaciones de un valorador y las de otras fuentes de valoración consideradas como referencia [6,9-11] se está contribuyendo a desarrollar el espíritu crítico del estudiante con su propio trabajo y, por tanto, a estimular el aprendizaje continuo del mismo, tanto en el plano académico como profesional.

El enfoque sobre la precisión de la autoevaluación ya ha sido tratado en estudios previos [e.g., 12-14], sin embargo son pocos los que se han centrado en el campo de la Ingeniería Industrial o los que han realizado el estudio segmentando su muestra atendiendo al género del estudiante o a las diferencias de rendimiento en la competencia objeto de evaluación. Así pues, el objetivo principal de este trabajo es determinar si el estudiante de Ingeniería Industrial es preciso a la hora de autoevaluarse en un contexto de evaluación sumativa y si aspectos como el género o su rendimiento valorado por otros evaluadores influyen en su propia evaluación.

Tras esta introducción, se presentan los fundamentos teóricos de la cuestión. Seguidamente, se describe el diseño metodológico que ha guiado la investigación. A continuación se analizan los resultados del trabajo empírico. Por último, se discuten los principales resultados y se exponen las conclusiones alcanzadas, así como las limitaciones del estudio y las líneas futuras de trabajo.

2. Marco teórico

En el ámbito educativo, la autoevaluación se refiere a la capacidad de los estudiantes para enjuiciar su propio aprendizaje, particularmente sus logros y resultados [15]. La participación de los estudiantes en su propia evaluación presenta una serie de ventajas para el estudiante [16-18] que se pueden sintetizar en ayudar a desarrollar competencias de gran valor en el mercado de trabajo, como el espíritu crítico con el propio trabajo, y aumentar la involucración de los estudiantes en su propio aprendizaje. Específicamente, en el ámbito de la ingeniería, se defiende la autoevaluación como mecanismo de estimulación de las capacidades para la reflexión continua y la resolución de problemas [2].

Son estas ventajas las que conducen a que la literatura se muestre favorable a la implantación de herramientas docentes orientadas al desarrollo de la autoevaluación, aunque su precisión sea inferior a la deseable [15,19,20]. Para ser competitivo, cualquier profesional debe ser capaz de evaluar de manera crítica su preparación y su trabajo, con el fin de poder mejorarlo y adaptarse a las necesidades del mercado laboral y de los clientes. Esto ocurre especialmente en el ámbito de la ingeniería, donde es habitual el ejercicio libre de la misma. Como resultado de esta percepción favorable, se puede observar un creciente número de metodologías docentes innovadoras en el ámbito de la educación que emplean la autoevaluación en diferentes tipos de actividades, fundamentalmente orientadas a la evaluación formativa (i.e., centrada en la mejora de las capacidades de los estudiantes).

Sin embargo, no es frecuente que se presente en la evaluación sumativa (i.e., orientada a obtener la calificación de los estudiantes), ya que los profesores suelen pensar que los estudiantes no son suficientemente precisos a la hora de evaluarse, tal y como refleja la literatura en el ámbito de la educación. Se han identificado dos tipos de sesgos especialmente relevantes para la autoevaluación [4], como son la auto-indulgencia (i.e., la tendencia a valorarse por encima de las valoraciones dadas por otros) y la comparación descendente (i.e., la tendencia general a puntuarse positivamente a uno mismo y más negativamente a los demás). A este respecto, al comparar las puntuaciones de autoevaluación con las de los profesores, las primeras resultan ser superiores [3].

De cara a mejorar la precisión de la autoevaluación se recomienda tomar una serie de medidas. En primer lugar se recomienda combinar la autoevaluación, con otro tipo de indicadores, como las calificaciones de los profesores, preferentemente más de uno, por su carácter integrador [21]. Asimismo es conveniente tener en cuenta a los pares pues su evaluación es más precisa que la autoevaluación [12,13,16].

En segundo lugar, se hace necesario proporcionar al evaluador formatos de evaluación fáciles de utilizar, fiables y con alta validez de contenido, lo cual se puede conseguir a través de la utilización de rúbricas. Las rúbricas constituyen herramientas de evaluación que posibilitan valorar la calidad de las aportaciones de los estudiantes en distintos ámbitos, así como su nivel de ejecución, especificando, antes de la realización de la actividad evaluada, los factores o variables que se van a analizar y los niveles de cumplimiento en cada uno de ellos [22-24].

En tercer lugar, se debe proveer de formación y experiencia en la utilización de los formatos de evaluación, en este caso de las rúbricas, a los evaluadores, sean estos estudiantes o profesores [14, 23].

Por último, es recomendable tener en cuenta la diferencia entre los evaluadores, los cuales pueden actuar de diferente forma atendiendo a su género o sus habilidades en la competencia analizada.

Tabla 1.
Número de evaluaciones por tipo de evaluador

Fuente de evaluación	Número
Autoevaluación	63
Profesores	126
Pares	3.843

Fuente: Elaboración propia

Con el fin de dar cumplimiento al objetivo formulado, se llevó a cabo un estudio en una asignatura troncal de 13,5 créditos, correspondiente al cuarto curso de la titulación de Ingeniero Industrial y que se imparte en el primer semestre. Este estudio, a su vez, tiene como objetivos específicos:

- Analizar si la autoevaluación del estudiante de Ingeniería Industrial es precisa. Para ello, se compara con la proporcionada por profesores y pares.
- Verificar si la precisión de las autoevaluaciones guarda relación con el género del estudiante, teniendo en cuenta que se trata de unos estudios con mayoritaria presencia masculina.
- Comprobar si, al clasificar a los estudiantes en función de la valoración de los profesores, distinguiendo entre los que mejor valoración obtienen en la presentación oral y los que resultan peor valorados, se detectan diferencias en la precisión de sus autoevaluaciones.

3. Metodología

Durante el primer semestre del curso se explicó a los estudiantes que debían realizar un trabajo y exponer el mismo en equipos de dos miembros. Una parte de la valoración de este trabajo consistiría en la presentación oral del mismo, que debía realizarse bajo unas condiciones específicas de formato y tiempo. Cada presentación sería valorada por dos profesores (el responsable de la asignatura y otro profesor ajeno a la misma, ambos con amplia experiencia en la evaluación de presentaciones orales), el resto de compañeros y los propios ponentes. Por lo que, a partir del total de participantes (47 hombres y 16 mujeres) se obtuvo un total de 4.032 evaluaciones, conforme al detalle que se muestra en la Tabla 1.

Se ha de tener en cuenta que la competencia de presentación oral es otra de las competencias que se requiere a los ingenieros industriales y que recibe una valoración de 7 puntos sobre 10 en el Libro Blanco anteriormente citado [8]. Específicamente, con respecto a la capacidad de presentación oral, se indica que la autoevaluación mejora su aprendizaje y desarrollo [12].

Para proporcionar criterios de evaluación homogéneos y así mejorar la precisión de la autoevaluación y generar buenas prácticas en el desarrollo de esta competencia se facilitó con antelación a los evaluadores (estudiantes y profesores) la rúbrica que figura en el anexo. Ésta fue elaborada por profesores con amplia experiencia en la valoración de presentaciones orales en el contexto universitario y fue diseñada y validada a través del proceso que se detalla en un estudio previo [25]. La rúbrica está compuesta por diez criterios, que reflejan las principales dimensiones de la competencia analizada. Cada uno de los criterios es evaluable según una escala de tres niveles (1-deficiente, 2-aceptable, 3-excelente), en función del nivel de consecución de los estándares previamente definidos en cada uno de ellos. Se optó por una rúbrica de 3 niveles, con el fin de hacer identificable a los usuarios de la misma qué patrones de comportamiento debían tener en cuenta para poder asignar una determinada puntuación en cada uno de los criterios. A medida que se incrementa el tamaño de la escala resulta más difícil poder identificar estándares diferenciados para cada uno de los niveles. De hecho, en el caso extremo de una escala Likert en la que no se identifican estándares sino tan sólo los extremos, ante un mismo comportamiento, dos evaluadores pueden dar puntuaciones totalmente diferentes, pues interviene la subjetividad del evaluador.

La calificación obtenida en la presentación oral se vinculó a la calificación final de la asignatura (evaluación sumativa), con el fin de lograr una mayor implicación de los estudiantes. Con relación al diseño metodológico hubiera sido deseable poder trabajar con un grupo de control. Sin embargo, esto hubiese implicado que una parte de los estudiantes no dispusiera de parte de su calificación final, por lo que se descartó esta posibilidad.

El contenido y funcionamiento de la rúbrica se explicó pormenorizadamente a todos los evaluadores, resolviendo antes de su aplicación las posibles dudas que pudieran surgir. Una vez recogidas las evaluaciones de las presentaciones, se valoró la fiabilidad de la rúbrica a través de la consistencia intra-valorador [26], considerando los tres grupos de valoradores.

La variable que se analiza a lo largo de este artículo para responder a los objetivos planteados es la puntuación global, obtenida mediante la agregación de las puntuaciones otorgadas por los evaluadores en cada criterio de la rúbrica. De esta forma, se generan las variables puntuación total de los profesores, puntuación total de los pares y autoevaluación. En las dos primeras, al tratarse de varios evaluadores, se utiliza el promedio de la puntuación otorgada por cada uno de los mismos, es decir, la media de los profesores o la media de los pares. Para facilitar la comparativa entre ellas, se redondean los promedios calculados al primer número entero, puesto que la autoevaluación sólo puede dar lugar a números enteros.

Respecto al primer objetivo específico, analizar si la autoevaluación del estudiante de Ingeniería Industrial es precisa, se analiza gráficamente el nivel de coincidencia en la puntuación otorgada a cada una de las presentaciones por las tres fuentes de evaluación disponibles (profesores, pares y autoevaluación), así como los principales estadísticos descriptivos, comprobando en cada caso su significatividad estadística a través de los contrastes de igualdad de medias.

El análisis para el segundo objetivo específico se realiza diferenciando por el género del estudiante. Se parte de los histogramas de frecuencias, así como de los estadísticos descriptivos básicos, para posteriormente buscar una relación lineal entre las puntuaciones a través del coeficiente de correlación lineal simple y, en caso de no detectarla, se procede a determinar su posible independencia a través del coeficiente de Spearman.

Por último, el análisis para el tercer objetivo específico se realiza a través la interpretación gráfica para las submuestras de estudiantes que reciben mayor y menor puntuación por

parte de los profesores. Para seleccionar a estos dos grupos de alumnos se determina el intervalo de confianza para la puntuación media otorgada por los profesores, de forma que los alumnos que caigan fuera del intervalo (construido como la puntuación media más/menos una desviación típica) serán los que se clasifiquen como estudiantes "con competencia de comunicación alta/baja".

4. Resultados

La fiabilidad de la rúbrica se analizó a través del cálculo del Alpha de Cronbach, obteniendo los resultados que muestra la Tabla 2. Como se puede observar, existe una buena consistencia interna en los tres colectivos en ambas titulaciones, pues todas son superiores al 75%, por lo que se consideró que la rúbrica era fiable [27].

Una primera aproximación al nivel de consenso logrado entre los tres colectivos implicados (precisión de las evaluaciones) se deduce de la Fig. 1. Se observa cómo la valoración de los profesores coincide en mayor medida con la de los pares que con la autoevaluación. De hecho, esta última suele ser en muchos casos superior a las otras dos. En líneas generales, se aprecia cómo la senda trazada por la puntuación de profesores es muy similar a la de los pares, aunque esta última presenta menores oscilaciones y, por tanto, discrimina menos.

El rango entre las puntuaciones mínima y máxima de los profesores es superior al rango de los pares, mientras que la horquilla de la autoevaluación se sitúa siempre por encima del mínimo y del máximo del resto de evaluadores (Tabla 3). Por tanto, así como entre compañeros parece más habitual poner puntuaciones intermedias, mientras que el profesorado utiliza un mayor rango de puntuación, la autoevaluación parece otorgar mayoritariamente puntuaciones más elevadas. Por su parte, y ahondando en el nivel de consenso entre evaluadores, se comprueba que no hay diferencias significativas entre la media de las evaluaciones de profesores y pares, mientras que las diferencias entre cualquiera de estos dos y la autoevaluación sí resultan estadísticamente significativas. Una vez más, se observa que profesores y pares puntúan de forma similar, mientras que la autoevaluación se desvía de ellos.

Tabla 2.
Fiabilidad de la rúbrica medida a través del Alpha de Cronbach

Fuente de evaluación	Alpha de Cronbach
Profesores	0,8578
Pares	0,8003
Autoevaluación	0,7520

Fuente: Elaboración propia

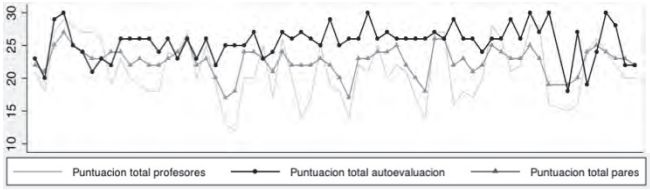


Figura 1. Puntuaciones otorgadas a los estudiantes por tipo de evaluador.
Fuente: Elaboración propia

Tabla 3.
Estadísticos descriptivos de las puntuaciones otorgadas a las presentaciones

Mín. – Máx.	Profesores	12 – 29
	Pares	17 – 27
	Autoevaluación	18 – 30
Media	Profesores	21,29
	Pares	22,62
	Autoevaluación	25,39***
Desviación típica	Profesores	4,41
	Pares	2,14
	Autoevaluación	2,94

*** = Diferencia de medias significativa al 1%
Fuente: Elaboración propia

A continuación se desagrega la información en función del género del estudiante, para comprobar si este comportamiento diferenciado de la autoevaluación se mantiene independientemente de si se trata de un hombre o de una mujer (segundo objetivo específico). Con esta finalidad, se presenta la Fig. 2, en donde se muestra el histograma de frecuencias de la puntuación total otorgada por cada uno de los sujetos evaluadores, diferenciando por género del estudiante. Al haber utilizado una rúbrica de 10 criterios y una escala de 3 valores para obtener la puntuación total, la distribución de dicha puntuación podrá oscilar entre un mínimo de 10 y un máximo de 30 puntos. Se observa una tendencia generalizada a que la distribución se desplace hacia la derecha a medida que se cambia de evaluador (profesores, pares, autoevaluación), para ambos sexos, aunque esta tendencia parece más acusada cuando la autoevaluación es de hombres que cuando es de mujeres. En términos generales,

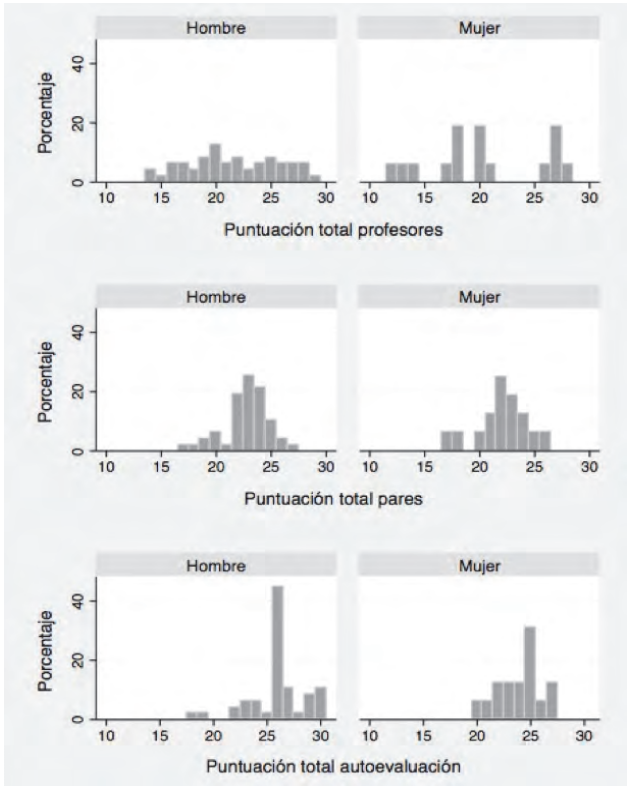


Figura 2. Histograma de frecuencias para la puntuación total según género del estudiante y tipo de evaluador.
Fuente: Elaboración propia

Tabla 4.
Estadísticos descriptivos de las puntuaciones otorgadas a las presentaciones según el género del estudiante

		Hombres	Mujeres
Porcentaje		74,6%	25,4%
Mín. – Máx.	Profesores	14 – 29	12 – 28
	Pares	17 – 27	17 – 26
	Autoevaluación	18 – 30	20 – 27
Media	Profesores	21,60	20,38
	Pares	22,81	22,06
	Autoevaluación	26,00***	23,86***
Desv. típica	Profesores	4,11	5,26
	Pares	2,06	2,35
	Autoevaluación	3,02	2,14

*** = Diferencia de medias significativa por género del estudiante al 1%
Fuente: Elaboración propia

los pares puntúan más alto la habilidad comunicativa de sus iguales que el profesorado, independientemente del sexo del estudiante. Asimismo la propia percepción de dicha habilidad es, en términos generales, superior a la percepción de los compañeros. Además, esta última diferencia parece superior en los hombres que en las mujeres.

Estas diferencias gráficas en función del género del estudiante deben ser verificadas en términos estadísticos, por lo que se realizan contrastes de diferencias de medias y se analiza la tendencia de las puntuaciones por grupo valorador (Tabla 4). En primer lugar, y sin entrar en la significatividad de las diferencias, destaca que todos han otorgado una mayor puntación a los hombres que a las mujeres. Sin embargo, al contrastar la significatividad estadística de dicha diferencia, resulta que sólo es significativa en el caso de la autoevaluación. Por tanto, profesores y pares no muestran apenas diferencias en función del género del estudiante evaluado, mientras que la autoevaluación sí. De hecho, los datos manifiestan que, en promedio, la autoevaluación de los hombres es sistemáticamente más alta que la de las mujeres, siendo esta diferencia significativa.

A partir de los datos de la Tabla 4 se puede intuir una cierta correlación entre las valoraciones de pares y profesores, no así entre éstas y la autoevaluación. No obstante, antes de poder aseverarlo, se hace necesario cuantificar dicha relación (Tabla 5).

Tal y como era de esperar, se detecta una alta correlación lineal entre la valoración de pares y profesores (83% para hombres y mujeres). Sin embargo, la correlación lineal entre la autoevaluación y el resto de fuentes no resulta estadísticamente significativa. No obstante, dado que todos los evaluadores habían visto la misma presentación y además habían utilizado la misma rúbrica, se consideró la posibilidad de que la relación entre la puntuación total otorgada por los diferentes evaluadores fuera diferente a la lineal, por lo que también se calculó la correlación a través de los rangos de Spearman, sin que se modificaran los resultados.

Tabla 5.
Correlación lineal entre fuentes de evaluación según el género del estudiante

	Hombres			**Mujeres**		
	Profesores	Pares	Autoev.	Profesores	Pares	Autoev.
Profesores	1			1		
Pares	0,8351***	1		0,8327***	1	
Autoevaluación	0,1981	0,2438	1	-0,0939	0,3163	1

*** = Coeficiente de correlación estadísticamente significativo al 1%
Fuente: Elaboración propia

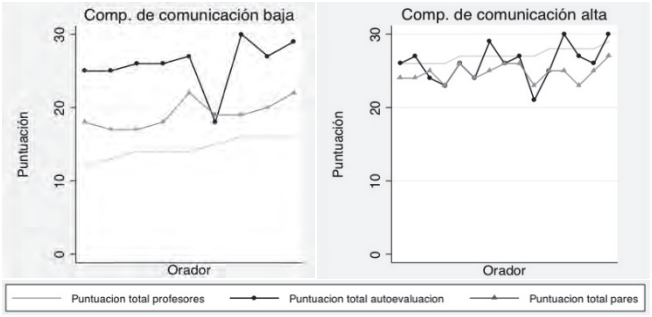


Figura 3. Puntuación otorgada por los evaluadores a los estudiantes con alta/baja competencia de presentación oral.
Fuente: Elaboración propia

El análisis del tercer objetivo específico se realiza sin diferenciar por género del estudiante, puesto que la diferencia de puntuación otorgada por los profesores no resulta estadísticamente significativa por este motivo. La Fig. 3 muestra la puntuación otorgada por cada una de las tres fuentes de valoración para el colectivo de estudiantes peor/mejor valorado por el profesorado (con competencia de comunicación baja/alta) según los intervalos de confianza creados previamente.

En el caso de las presentaciones de aquellos estudiantes peor valorados por el profesorado se observa mayor disparidad en la valoración de las tres fuentes, mientras que entre los alumnos con mayor valoración es donde se aprecia mayor consenso entre las puntuaciones.

En cualquier caso el comportamiento de profesores y pares parece mantener un mismo patrón, de forma que en las presentaciones de los estudiantes con competencia baja el profesor es más estricto que los pares. En cambio, en las de aquellos con competencia alta el profesor es más benévolo que los pares. De la misma forma se detecta un patrón claro en la autoevaluación cuando se trata de presentaciones de estudiantes con baja competencia. En éstas, la autoevaluación es sistemáticamente mayor a la de las otras dos fuentes de evaluación.

5. Conclusiones

Saber autoevaluarse es una competencia clave en una profesión como la ingeniería sometida a constantes cambios y que requieren una permanente actualización. La importancia de la autoevaluación adquiere aún más valor en una situación como la que se vive en España, con elevadas tasas de paro.

Un buen desempeño en la autoevaluación implica que el individuo sea capaz de desarrollar la tarea con precisión. Ello se debe potenciar desde la Universidad a través de la implicación del estudiante en actividades en las que tenga que valorar su propio trabajo. Para mejorar la precisión de la autoevaluación, la literatura recomienda tomar una serie de medidas como la formación de los valoradores o la utilización de rúbricas. Este trabajo ha determinado el grado de precisión de un grupo de estudiantes de Ingeniería Industrial teniendo en cuenta sus estímulos a la hora de autoevaluarse (i.e, evaluación sumativa) y las diferencias entre los evaluadores debidas al género y a su capacidad como oradores, valorada por los profesores.

Los resultados alcanzados muestran que la rúbrica

posibilita un alto nivel de precisión, dado que los profesores y los pares puntúan de manera similar. Sin embargo, el efecto no es el mismo en la autoevaluación, tal y como señala la literatura [11,14,28,29]. Por tanto, el estudiante es capaz de evaluar de manera precisa (i.e., de forma similar a los profesores) cuando dispone de criterios claros; el problema surge cuando se evalúa a sí mismo. Esto se puede justificar con varios argumentos. En primer lugar, la repercusión en la nota de la autoevaluación puede influir en el resultado de la misma, sobrevalorándola respecto a otras fuentes de evaluación, dejando sin efecto a la rúbrica. La falta de hábito de autoevaluación y la no implicación de los estudiantes en la identificación de los criterios son otras posibles explicaciones. Por último, cabría pensar que las diferencias entre profesores y autoevaluaciones pueden deberse a la mayor experiencia de los profesores al juzgar las presentaciones orales [12]. No obstante, hay que considerar que los propios estudiantes sí fueron capaces de valorar con precisión a sus compañeros, cuando actuaban como pares, lo que parece dar más peso a la motivación de los estudiantes para mejorar su calificación a la hora de autoevaluarse.

Respecto al segundo objetivo específico, se puede concluir, a partir de los datos analizados, que la autoevaluación guarda relación con el género. Al separar a los estudiantes en dos grupos atendiendo a esta característica, se observa que tanto hombres como mujeres se autoevalúan por encima de los pares y profesores en línea con lo descrito en la literatura revisada [15,30]. Además, en general, y también consistente con los estudios previos, los hombres presentan una autoevaluación estadísticamente más alta que las mujeres [11,31,32]. Habría que indagar en cuáles son las causas que justifican este comportamiento de los hombres que sistemáticamente se puntúan por encima de lo que lo hacen las mujeres. La literatura señala como causa la menor percepción de auto-eficacia de las mujeres y, por tanto, un menor nivel de confianza en su propio desempeño [33].

En relación con el tercer objetivo específico, la rúbrica hace más precisas las puntuaciones cuando el estudiante que se autoevalúa es un orador con alta competencia de presentación oral según el criterio de los profesores. En el caso de los estudiantes con bajo nivel de competencia, desde el punto de vista del profesorado, su autoevaluación es sistemáticamente mayor que la de los pares y la del profesorado. Este resultado apoya la afirmación de que especialmente los estudiantes brillantes son muy buenos juzgando su propio desempeño, mientras que los estudiantes con menos habilidades son menos precisos [6,34,35].

Por tanto, como conclusión general, la mejora de la precisión en la competencia de autoevaluación requiere atender las características individuales diferenciadoras de cada estudiante. El trabajo presentado evidencia que los estudiantes, a la hora de autoevaluarse, no actúan de forma homogénea, por lo que hay que actuar en consecuencia.

Para mejorar la precisión de la autoevaluación en el ámbito educativo y, como consecuencia, en el profesional se proponen una serie de líneas de actuación: (1) incrementar la formación de los estudiantes en autoevaluación, haciendo hincapié en la indulgencia a la hora de valorar el propio trabajo, así como en la mayor severidad de las mujeres al evaluarse; (2) aumentar las experiencias de autoevaluación, dado que mejoran la capacidad de los estudiantes para autoevaluarse [15]; (3) involucrar al estudiante en el diseño de las escalas de evaluación [18], puesto que aumenta su compromiso con el sistema y (4) advertir a los estudiantes de que, de cara a la evaluación sumativa, el profesor podrá aplicar factores correctores [17], en la medida en que su autoevaluación difiera significativamente de las evaluaciones de los referentes.

A pesar de las contribuciones realizadas, este estudio presenta una serie de limitaciones. En primer lugar, hay que tener en cuenta que los resultados se han obtenido en unas condiciones determinadas entre las que se encuentra el hecho de que la autoevaluación estaba ligada a la calificación del estudiante (i.e., evaluación sumativa). De cara a valorar el efecto que tiene en la precisión de la autoevaluación su carácter sumativo, hubiese sido deseable contar con un grupo de control de estudiantes para los que la autoevaluación no tuviese repercusiones en su calificación. Así, sería posible analizar si los resultados se mantienen cuando la autoevaluación no tiene efecto en la nota final. No obstante, y puesto que en este trabajo los mismos estudiantes han evaluado con la misma rúbrica a los pares, y ahí se ha observado un grado significativo de precisión entre la evaluación de pares y profesores, esta limitación podría quedar, en cierta medida, solventada. Dado que la evaluación de los pares sí presenta un grado significativo de precisión respecto a los profesores, podría considerarse como una forma de controlar que los estudiantes conocen la rúbrica y saben aplicarla con criterios similares a los profesores y que lo hacen cuando no existe un estímulo.

La segunda limitación se relaciona con la muestra. A pesar del elevado número de evaluaciones obtenidas (más de 4.000), sería deseable poder aumentar la muestra, tanto en número como en diversidad, incorporando a estudiantes de otras universidades e incluso a egresados. Asimismo se pondría incrementar la muestra con individuos de otros países al objeto de valorar la incidencia de los factores culturales.

En tercer lugar, no se tiene información sobre la opinión del estudiante sobre la utilidad de la autoevaluación para mejorar sus habilidades y competencias. Sería conveniente conocer cómo esta opinión influye en la precisión de la autoevaluación.

Por último, aunque se ha estudiado la influencia del género en la precisión de la autoevaluación, no se ha profundizado en las causas que motivan estas diferencias de comportamiento entre hombres y mujeres, lo que se debería hacer en futuros estudios.

La baja precisión de la autoevaluación no debe desalentar su utilización pues no sólo tiene utilidad cuando se emplea con fines sumativos, sino que se puede utilizar para desarrollar la capacidad de autocrítica de la persona. La incorporación de la autoevaluación ofrece ventajas [12,36,37], por lo que hay que integrar estas formas de evaluación en los planes de estudio [17], vinculándolas a la calidad del aprendizaje [36]. La autoevaluación es una herramienta efectiva en aras de capacitar a los estudiantes para unir varios aspectos de su aprendizaje, reflejar sus logros y examinar las implicaciones en su formación posterior. Por tanto, la gran utilidad de la autoevaluación estaría en su dimensión de evaluación formativa, esto es, para mejorar las habilidades y capacidades del estudiante de Ingeniería Industrial, lo cual redundará en su mejor empleabilidad.

Anexo

VALORACIÓN DEL GRUPO

UNIFORMIDAD DE LOS MEDIOS DE APOYO VISUALES

Nivel	Definición	Ejemplos
Deficiente	Existen diferencias ostensibles de diseño entre las diferentes diapositivas utilizadas	Diferentes tipos de letras, tamaño, estilos, fondos….entre los ponentes
Aceptable	La mayor parte de las diapositivas utilizadas responden al mismo diseño	Solo cambian gráficos y tablas
Excelente	El formato utilizado a lo largo de la presentación es homogéneo	No existe ninguna variación entre las diapositivas

COORDINACIÓN DE LA EXPOSICIÓN

Nivel	Definición	Ejemplos
Deficiente	No se ha efectuado un reparto adecuado de tiempos y cometidos para la presentación	No queda claro quién tiene que hacer cada parte de la exposición. Se expresan con vocabulario diferente.
Aceptable	El reparto de trabajo para la exposición es homogéneo	El contenido expuesto es similar en envergadura, así como el tiempo utilizado para hacerlo
Excelente	Además de lo anterior, la sincronización entre los participantes es correcta	Se da la palabra el uno al otro y hace referencia cada uno a las partes expuestas por los demás.

CALIDAD DE LAS DIAPOSITIVAS UTILIZADAS

Nivel	Definición	Ejemplos
Deficiente	Hay varios errores en las diapositivas en cuanto a nitidez, tipografía, ortografía y diseño	Las imágenes no son nítidas, están mal enfocadas, alineadas o no identificables. El color elegido dificulta la lectura del texto.
Aceptable	Pequeños errores de formato, sin faltas de ortografía	Se admite algún error puntual en la justificación de párrafos, alineación de imágenes o tipografías diferentes entre diapositivas
Excelente	No hay errores de formato y el diseño es especialmente atractivo	Gráficos, imágenes y texto se ven con precisión. La elección de colores y formatos es atractiva visualmente. Se diferencia en tamaño entre encabezados y texto

ORDEN Y CLARIDAD EN LA PRESENTACIÓN

Nivel	Definición	Ejemplos
Deficiente	Las ideas están pobremente organizadas.	Idea principal no entendida o no existe. No abre la presentación con un esquema de contenidos. Repite los contenidos en diferentes apartados. No agrupa contenidos en un orden lógico. No se presenta ni introduce el objetivo de la charla. Utiliza términos no comunes y no los explica.
Aceptable	Se sigue un orden coherente en la exposición, si bien faltan algunos elementos de ayuda	Explica las ideas principales, pero no expone un esquema de contenidos y/o conclusiones principales
Excelente	Mantiene una secuencia lógica y ordenada entre cada una de las partes. Concluye con las ideas principales	La audiencia no se he perdido en toda la exposición y sabía de qué estaba hablando en cada momento

VALORACIÓN INDIVIDUAL

RELACIÓN DEL DISCURSO CON LAS IMÁGENES

Nivel	Definición	Ejemplos
Deficiente	Las imágenes no están relacionadas con el contenido del trabajo	La imagen es graciosa o impactante, pero no aporta nada a la explicación
Aceptable	Las imágenes tienen relación con el trabajo presentado, pero no aportan información esencial, solo repiten el contenido del discurso	La imagen es básicamente el discurso, pero proyectado en grande
Excelente	Las imágenes apoyan claramente el contenido del discurso. El estudiante "interactúa" con las imágenes	Las imágenes han hecho que el discurso sea más interesante y lo enriquecen

APOYO EN EL MATERIAL ESCRITO

Nivel	Definición	Ejemplos
Deficiente	Siempre lee el material escrito (diapositivas, guión o similar)	No mira al resto; sin guión le sería imposible exponer.
Aceptable	Lee el material en ocasiones puntuales, como apoyo a su discurso	Se lee una definición para dar precisión
Excelente	Nunca lee el material	No se lo sabe de memoria, sino que domina la exposición

TONALIDAD Y MODULACIÓN DE LA VOZ

Nivel	Definición	Ejemplos
Deficiente	Tono monótono, sin inflexiones en la voz	No se le escucha. No destaca aspectos concretos de la presentación a través del tono de voz
Aceptable	Tono adecuado , aunque no enfatiza lo importante	Se le oye bien, pero no siempre refuerza con su tono o volumen el mensaje
Excelente	Utiliza los tonos y volúmenes de la voz para reforzar el mensaje	Hace pausas dramáticas después de lanzar una pregunta o un comentario, con el fin de generar atención

CLARIDAD AL HABLAR / VOCALIZACIÓN

Nivel	Definición	Ejemplos
Deficiente	No vocaliza adecuadamente	No se le entiende
Aceptable	Habla bien y con naturalidad.	Se le entienden las palabras. Pequeños problemas de entendimiento por vocalización.
Excelente	Se esfuerza por hablar con claridad suficiente para que lo entienda la audiencia	No se atropella con las palabras

DOMINIO DEL ESPACIO		
Nivel	**Definición**	**Ejemplos**
Deficiente	No mira al público o se concentra en una parte muy reducida de la audiencia	Mira al techo, mira por la ventana, mira al suelo, mira al infinito del aula…
Aceptable	Reparte su mirada por el público, pero de manera irregular	Mira más tiempo al profesor que a los compañeros
Excelente	Distribuye la mirada uniformemente por el público asistente	Incluye a todos en el discurso, alguna vez
EXPRESIÓN CORPORAL		
Nivel	**Definición**	**Ejemplos**
Deficiente	Muestra grandes gestos de nerviosismo durante la exposición. La postura corporal no está en consonancia con la exposición.	Manos en los bolsillos, tics, temblores. Se apoya en el pupitre o la pared. Mastica chicle durante la exposición.
Aceptable	Mantiene una postura adecuada durante la exposición	No se apoya en el pupitre o pizarra. Se mueve por la zona de presentación de manera pausada
Excelente	Además de lo anterior, refuerza con sus gestos el contenido de la presentación	Además del nivel anterior, utiliza las manos para señalar aspectos concretos de las diapositivas

Referencias

[1] Díaz-Lucas, A., La empleabilidad de los ingenieros industriales españoles. DYNA, 88(6), pp.614-615, 2013.

[2] Beyerlein, S., Davis, D., Trevisan, M., Thompson, P. and Harrison, K. Assessment framework for capstone design courses, en Annual ASEE Conference and Exposition (113th, 2006, Chicago). Proceedings of the American Society for Engineering Education. Chicago: ASEE, 2006.

[3] Ryan, G.J., Marshall, L.L., Porter, K. and Jia, H., Peer, professor and self-evaluation of class participation. Active Learning in Higher Education, 8(1), pp. 49-61, 2007. DOI: 10.1177/1469787407074049

[4] Van Duzer, E. and McMartin, F., Methods to improve the validity and sensitivity of a self/peer assessment instrument. IEEE Transactions on Education, 43(2), pp.153-158, 2000. DOI: 10.1109/13.848067

[5] Rychen, D.S. and Salganick, L.H., A holistic model of competence, en D.S. Rychen, and Salganick, L.H., (Ed.). Key Competencies for a successful life and a well-functioning society, Cambridge, MA: Hogrefe & Huber, 2003, pp. 41-62.

[6] Brown, G.T.L. and Harris, L.R., Student self-assessment, en J.H. McMillan, (Ed.), The SAGE handbook of research on classroom assessment, Thousand Oaks, CA: Sage, 2013, pp.367-393.

[7] Vicente-Oliva, S., Martínez-Sánchez, A. y Berges-Muro, L., Buenas prácticas en la gestión de proyectos de I+D+i, capacidad de absorción de conocimiento y éxito. DYNA-Colombia 82(191), pp. 109-117, 2015. DOI: 10.15446/dyna.v82n191.42558.

[8] ANECA. Libro Blanco. Titulaciones de ingeniería rama industrial (Propuesta de las Escuelas Técnicas Superiores de Ingenieros Industriales). Madrid: Agencia Nacional de Evaluación y Certificación de la Calidad, 2006, pp. 163-167.

[9] Brown, G.T.L. and Harris, L.R., The future of self-assessment in classroom practice: reframing self-assessment as a core competency. Frontline Learning Research, 2(1), pp. 22-30, 2014. DOI: 10.14786/flr.v2i1.24

[10] Boud, D., The role of self-assessment in student grading. Assessment and Evaluation in Higher Education, 14(1), pp. 20-30, 1989. DOI: 10.1080/0260293890140103

[11] Panadero, E. and Romero, M., To rubric or not to rubric? The effects of self-assessment on self-regulation, performance and self-efficacy. Assessment in Education: Principles, Policy & Practice, 21(2), pp. 133-148, 2014. DOI: 10.1080/0969594X.2013.877872

[12] De Grez, L., Valcke, M. and Roozen, I., How effective are self- and peer assessment of oral presentation skills compared with teachers' assessments?. Active Learning in Higher Education, 13(2), pp.129-142, 2012. DOI: 10.1177/1469787412441284

[13] Langan, A.M., Shuker, D.M., Cullen, W.R., Penney, D., Preziosi, R.F. and Wheater, C.P., Relationships between student characteristics and self-, peer and tutor evaluations of oral presentations, Assessment and Evaluation in Higher Education, 33(2), pp.179-190, 2008. DOI: 10.1080/02602930701292498

[14] Marín-García, J.A., Los alumnos y los profesores como evaluadores. Aplicación a la calificación de presentaciones orales, Revista Española de Pedagogía, 67(242), pp.79-98, 2009.

[15] Boud, D. and Falchikov, N., Quantitative studies of student self-assessment in higher education: a critical analysis of findings. Higher Education, 18(5), pp. 529-549, 1989. DOI: 10.1007/BF00138746

[16] Campbell, K.S., Mothersbaugh, D.L., Brammer, C. and Taylor, T., Peer- versus self-assessment of oral business presentation performance. Business Communication Quarterly, 64(3), pp.23-42, 2001. DOI: 10.1177/108056990106400303

[17] Dochy, F, Segers, M. and Sluijsmans, D., The use of self-, peer and co-assessment in Higher Education: A review. Studies in Higher Education, 24(3), pp.331-350, 1999. DOI: 10.1080/03075079912331379935

[18] Falchikov, N., Improving assessment through student involvement: Practical solutions for aiding learning in Higher and Further Education. Nueva York: Routledge Farmer, 2005, pp. 128.

[19] Boud, D., The role of self-assessment in student grading. Assessment and Evaluation in Higher Education, 14(1), pp. 20-30, 1989. DOI: 10.1080/0260293890140103

[20] Taras, M., Student self-assessment: Processes and consequences. Teaching in Higher Education, 15(2), pp.199-209, 2010. DOI: 10.1080/13562511003620027

[21] Fagerholm, F and Vihavainen, A., Peer assessment in experiential learning, en Frontiers in Education Conference (2013, Oklahoma City) IEEE Proceedings, 2013.

[22] Andrade, H. and Du, Y., Student perspectives on rubric-referenced assessment, Practical Assessment, Research & Evaluation, 10(3), pp.1-11, 2005.

[23] Jonsson, A. and Svingby, G., The use of scoring rubrics: reliability, validity and educational consequences, Educational Research Review, 2(2), pp. 130-144, 2007. DOI:10.1016/j.edurev.2007.05.002

[24] Panadero, E. and Jonsson, A., The use of scoring rubrics for formative assessment purposes revisited. A review, Educational Research Review, 9, pp.129-144, 2013. DOI: 10.1016/j.edurev.2013.01.002

[25] Bolívar-Cruz, A., Verano-Tacoronte, D., y González-Betancor, S.M., Is university students' self-assessment accurate? En: Peris-Ortiz, M. y Merigó-Lindahl (Eds). Sustainable Learning in Higher Education, Netherlands: Springer, 2015: pp., 21-35. DOI: 10.1007/978-3-319-10804-9

[26] García-Ros, R., Análisis y validación de una rúbrica para evaluar habilidades de presentación oral en contextos universitarios. Electronic Journal of Research in Educational Psychology, 9(25), pp.1043-1062, 2011.

[27] Cortina, J.M., What is coefficient alpha? An examination of theory and applications, Journal of Applied Psychology, 78(1), pp.98-104, 1993. DOI: 10.1037/0021-9010.78.1.98

[28] Kwan, K.P. and Leung, RW., Tutor versus peer group assessment of student performance in a simulation training exercise, Assessment & Evaluation in Higher Education, 21(3), pp.205-214, 1996. DOI: 10.1080/0260293960210301

[29] Magin, D. and Helmore, P., Peer and teacher assessments of oral presentation skills: How reliable are they? Studies in Higher Education, 26(3), pp.287-298, 2001. DOI: 10.1080/03075070120076264

[30] Das, M., Self and tutor evaluations in problem based learning tutorials: is there a relationship? Medical Education, 32(4), pp 411-418, 2001.

DOI: 10.1046/j.1365-2923.1998.00217.x
[31] Acker, D. and Duck, N.W., Cross-cultural overconfidence and biased self-attribution, The Journal of Socio-Economics, 37, pp. 1815-1824, 2008. DOI: 10.1016/j.socec.2007.12.003
[32] Blackwood, T., Business undergraduates' knowledge monitoring accuracy: How much do they know about how much they know? Teaching in Higher Education, 18(1), pp. 65-77, 2013. DOI: 10.1080/13562517.2012.694100
[33] Pallier, G., Gender differences in the self-assessment of accuracy on cognitive tasks, Sex Roles, 48(5-6), pp. 265-276, 2003. DOI: 10.1023/A:1022877405718
[34] Dinsmore, D.L. and Parkinson, M.M., What are confidence judgements made of? Students' explanations for their confidence ratings and what that means for calibration, Learning and Instruction, 24, pp. 4-14, 2013. DOI: 10.1016/j.learninstruc.2012.06.001
[35] Hattie, J., Calibration and confidence: Where to next? Learning and Instruction, 24, pp. 62-66, 2013. DOI: 10.1016/j.learninstruc.2012.05.009
[36] Boud ,D., Reframing assessment as if learning were important", en Boud, D. and Falchikov, N., (Ed.), Rethinking assessment in higher education: Learning for the longer term. Londres: Routledge, 2007, pp.14-28.
[37] Langan, A.M., Wheater, C.P., Shaw, E.M., Haines, B.J., Cullen, W.R., Boyle, J.C., Penney, D., Oldekop, J.A., Ashcroft, C., Lockey, L. and Preziosi, R.F., Peer assessment of oral presentations: effects of student gender, university affiliation and participation in the development of assessment criteria. Assessment and Evaluation in Higher Education, 30(1), pp.21-34, 2005. DOI: 10.1080/0260293042003243878

D. Verano-Tacoronte, es Lic. en Ciencias Económicas y Empresariales y Dr. en Economía y Dirección de Empresas por la Universidad de Las Palmas de Gran Canaria, España. Actualmente es profesor de Dirección de Recursos Humanos en dicha Universidad, donde ha impartido docencia desde el año 1993 en el Departamento de Economía y Dirección de Empresas en diferentes Facultades y escuelas universitarias, incluyendo Ingeniería Industrial e Ingeniería Informática. Sus líneas de trabajo a nivel investigador son la evaluación del rendimiento, la precisión en los procesos de evaluación del desempeño profesional y académico y la influencia que los sistemas de recompensas tienen en el desempeño profesional y académico. Asimismo, estudia aspectos personales y contextuales relacionados con los procesos de adquisición y mejora de competencias académicas y profesionales.
ORCID: 0000-0001-7612-4147

A. Bolívar-Cruz, es Lic. en Ciencias Económicas y Empresariales y Dra. en Economía y Dirección de Empresas por la Universidad de Las Palmas de Gran Canaria, España. En la actualidad es profesora de Organización de Empresas en dicha Universidad, donde imparte docencia desde el año 1994 en el Departamento de Economía y Dirección de Empresas en diferentes centros universitarios, como la Escuela de Ingenierías Industriales y Civiles y la Facultad de Economía, Empresa y Turismo. Sus intereses de investigación se centran en el emprendimiento, los procesos de autoevaluación y en el estudio de las competencias para la empleabilidad.
ORCID: 0000-0003-2765-527X

S.M. González-Betancor, es Lic. en Ciencias Económicas y Empresariales y Dra. en Economía por la Universidad de Las Palmas de Gran Canaria, España. Es profesora en dicha Universidad desde 1998, impartiendo Estadística y Econometría en diferentes titulaciones de la Facultad de Economía, Empresa y Turismo así como de Ciencias Jurídicas. Sus principales líneas de investigación son la Economía de la educación (funciones de producción educativa, evaluación educativa, determinantes del rendimiento educativo, inserción laboral, indicadores educativos, evaluación de competencias), las Investigaciones bibliométricas (bibliometría, factores de impacto, bases de datos bibliométricas) y la Economía de la pobreza.
ORCID: 0000-0002-2209-1922

UNIVERSIDAD NACIONAL DE COLOMBIA
SEDE MEDELLÍN
FACULTAD DE MINAS

Área Curricular de Ingeniería Administrativa e Ingeniería Industrial

Oferta de Posgrados

Especialización en Gestión Empresarial
Especialización en Ingeniería Financiera
Maestría en Ingeniería Administrativa
Maestría en Ingeniería Industrial
Doctorado en Ingeniería - Industria y Organizaciones

Mayor información:

E-mail: acia_med@unal.edu.co
Teléfono: (57-4) 425 52 02

UNIVERSIDAD NACIONAL DE COLOMBIA
SEDE MEDELLÍN
FACULTAD DE MINAS



DYNA
http://dyna.medellin.unal.edu.co/

Maintenance management program through the implementation of predictive tools and TPM as a contribution to improving energy efficiency in power plants

Milton Fonseca-Junior [a], Ubiratan Holanda-Bezerra [b], Jandecy Cabral-Leite [c] & Tirso L. Reyes-Carvajal [d]

[a]*Instituto de Tecnología y Educación Galileo de la Amazonía, Brasil. milton.fonseca@eletrobrasamazonas.com*
[b]*Departamento de Ingeniería Eléctrica - CEAMAZON, Universidad Federal de Pará, Belém, Brasil. bira@ufpa.br*
[e]*Instituto de Tecnología y Educación Galileo de la Amazonía, Brasil. jandecy.cabral@itegam.org.br*
[d]*Instituto de Tecnología y Educación Galileo de la Amazonía, Brasil. tirsolrca@gmail.com*

Received: December 02nd, 2014. Received in revised form: October 26th, 2015. Accepted: November 3rd, 2015.

Abstract
This paper presents an application method of a Maintenance Management Program through the implementation of predictive tools and the Total Productivity Maintenance (TPM) methodology as a contribution for the energy efficiency improvement in thermoelectric power plants. The results of the vibration analysis, lubricating oil condition and of the thermograph analysis are registered as diagnostic methods. The innovative advance in this paper was the application of four pillars from the TPM methodology at the control of the internal combustion engines efficiency at a thermoelectric power plant. This research has the objective to provide a more reliable maintenance process through the implementation of the measurement and control of the operating parameters of the plant resulting in a better management by reducing the stops due unforeseen problems. Some results of the methodology application were shown like: annual maintenance cost reduction due corrective maintenance, increase of the mean time between failure (MTBF) and reduction of the mean time to repair (MTTR) in all applied areas. These results reflected in a more reliable power generation without putting the facilities of the plant at risk with an annual cost reduction for the company.

Keywords: Management Maintenance Program, Maintenance Preditive, TPM and Thermal Plants.

Programa de gestión de mantenimiento a través de la implementación de herramientas predictivas y de TPM como contribución a la mejora de la eficiencia energética en plantas termoeléctricas

Resumen
En el presente trabajo se presenta un Programa de Gestión de Mantenimiento a través de la implementación de herramientas predictivas y de TPM como contribución a la mejora de la eficiencia energética en plantas termoeléctricas. Se registran los resultados de análisis de vibraciones, de aceite lubricante y la termografía como métodos de diagnostico, por otra parte se aplican cuatro de los pilares del TPM, todo lo cual resulta novedoso en el entorno de las plantas termoeléctricas con el uso de motores de combustión interna. Este estudio tiene como objetivo proporcionar un proceso de mantenimiento más fiable a través de la implementación de la medición, el control y de parámetros de funcionamiento de la planta, lo que redunda en una mejor gestión al reducirse el número de paradas por averías imprevistas. Son mostrados algunos resultados de la aplicación de la metodología, tales como: reducción del coste anual de mantenimiento por reducción del mantenimiento correctivo, aumento del tiempo medio entre fallos (MTBF) y menor tiempo medio de reparación (MTTR) en todas las áreas. Estos resultados se reflejan en la generación de energía más confiable sin poner en peligro la seguridad de las instalaciones, a un costo de menos gasto anual para la empresa.

Palabras clave: Metodología de gestión de mantenimiento, mantenimiento predictivo, TPM, Plantas termoeléctricas.

© The author; licensee Universidad Nacional de Colombia.
DYNA 82 (194), pp. 139-149. December, 2015 Medellín. ISSN 0012-7353 Printed, ISSN 2346-2183 Online
DOI: http://dx.doi.org/10.15446/dyna.v82n194.47642

1. Introducción

En el presenta trabajo se incluye, la propuesta de implementación de técnicas de mantenimiento predictivo, (análisis de vibraciones, análisis del aceite lubricante en el monitoreo y control de las fallas y la implementación de cuatro pilares básicos del TPM teniendo como objetivo el incremento de la eficiencia energética

Los esquemas de reposición más antiguos son por edad del componente o instalación y política de sustitución en masa [1,2]. En el primer caso un componente es sustituido después de un determinado tiempo de explotación o cuando el mismo falla, lo que generalmente ocurre primero. En el segundo caso, todos los dispositivos de una determinada clase son sustituidos en determinados intervalos o cuando estos fallan.

Lo antes expuesto resulta en una mejor administración, pues el tiempo de explotación de los equipos generalmente no es conocido y resulta más económico que una política basada en la sustitución individual. Esquemas de sustitución más recientes en muchos casos están basados en modelos probabilísticos (por ejemplo, [3,4] lo que si bien puede aportar buenos resultados requiere del historial de las instalaciones y equipos lo que puede resultar bastante complejo en mucho de los casos. En la mayoría de los casos en las concesionarias de energía eléctrica a pesar de estar presenta la actividad de mantenimiento no goza de buena efectividad. A su vez, el concepto de la simplicidad en una empresa está asociada generalmente con procesos y soluciones de tecnología, cuyas características y procedimientos son estrictamente necesarios para satisfacer las necesidades especificas de requisitos que son fáciles de implementar, mantener y utilizar [5].

Para una evaluación completa de los efectos de una política de mantenimiento se tiene que saber cómo su aplicación extendería la vida útil de un componente medido en, por ejemplo, el tiempo medio hasta el fallo o entre fallos. Para descubrir eso, es necesario un modelo matemático del proceso de deterioro de los componentes que describa los efectos del mantenimiento. En los últimos diez años o más han sido propuestos varios de esos modelos [6,7].

La situación es bien diferente para los procesos de deterioro, donde algunas veces la nueva condición de fallo no es exponencialmente distribuida igualmente los tiempos entre etapas sucesivas de deterioro [8]. En un proceso de este tipo la función de riesgo aumenta y el mantenimiento traerá mejorías independientes de los tipos de distribución entre las etapas sucesivas [9].

Es así, que algún tipo de monitoreo (por ejemplo, la inspección) debe ser parte del modelo [10]. Otras características deseables se enumeran en el estudio de la siguiente manera. Identificación del sistema y la lista de componentes críticos y sus funciones.

Modo de falla y análisis de efectos y criticidad para cada componente seleccionado, la determinación del historial de fallos y el cálculo del tiempo medio entre fallos, categorización de los efectos de la falla (utilizando flujogramas apropiados) y determinación de posibles tareas de mantenimiento [11-13], la atribución de tareas de mantenimiento y la evaluación del programa, incluyendo el análisis de costos. [14].

PREMO - Optimización del Mantenimiento Preventivo, se basa en un amplio análisis de las tareas, en lugar del análisis de sistemas, con una capacidad para reducir drásticamente el número tareas de mantenimiento en una planta [15-17]. Programas como PREMO han sido muy útiles para garantizar la operación económica de centrales eléctricas. Sin embargo estos programas no ofrecen todos los beneficios y flexibilidad de los programas en basa a modelos matemáticos [18].

En otros enfoques desarrollados; de ellos, al menos dos están interesados en las aplicaciones de sistemas de potencia [19,20]. En [19], un modelo de mantenimiento que se deriva de ramas paralelas de componentes en serie, como frecuentemente encontramos en subestaciones, en [20], el mantenimiento y la confiabilidad de los dispositivos en espera son estudiados. Ambos son, en esencia, los modelos de sustitución, donde la reparación y mantenimiento son asumidos "como nuevas" condiciones.

Una planta de energía térmica consiste en conjunto de sistemas mecánicos y eléctricos que requieren una vigilancia constante para la producción de energía. Se necesitan los datos obtenidos a través de las acciones de monitoreo en la evaluación de la operación, el mantenimiento y el rendimiento de las plantas. Para este propósito, se utilizan las llamados *Distributed Control Systems*– DCS.

La obsolescencia de estos dispositivos (DCS) aumenta el riesgo de falta de disponibilidad de unidades de generación, principalmente en centrales térmicas, que tienen un alto grado de desgaste mecánico debido a las altas temperaturas y productos químicos utilizados para la producción de energía eléctrica [21].

La gestión en mantenimiento procura reducir costos asociados al mantenimiento, en particular horas/hombre, y costos de reparación. Varias metodologías han sido empleadas para el logro de estos objetivos, tales como TPM (Total Productive Maintenance), RCA (Root Cause Analysis), mantenimiento preventivo, entre otras otros. [22].

El sector eléctrico mundial ha venido afrontando una serie de reformas estructurales muy importantes desde hace más de 20 años. En términos generales, tales reformas tienen como objetivo fundamental el incremento en la eficiencia de la producción de energía aumentando la calidad en el servicio a precios cada vez más competitivos. [23].

Tal renovación / actualización ofrece la posibilidad de utilizar nuevos sistemas DCS basado, principalmente en el libre flujo de datos en tiempo real sin la necesidad de integrar cualquier interface en las arquitecturas de software propietarias como ha sido la práctica hasta ahora [24].

2. Etapas en la realización de la investigación

La investigación se llevó a cabo en cuatro etapas, comenzando con un estudio a fondo de la literatura nacional e internacional sobre el tema objeto de la investigación, para conocer y profundizar en las causas que pueden conducir al fracaso y el tiempo de inactividad inesperado de los equipos, así como sobre los métodos y las técnicas que se pueden aplicar para cumplir con los objetivos propuestos.

Un requisito inicial para el desarrollo de estas etapas es la comprensión general del sistema de producción y los datos de consumo de energía y la producción [25].

La segunda fase tuvo lugar la semana siguiente con la entrevista al líder de la actividad de mantenimiento en la empresa, el diagnóstico de dificultades para controlar los fallos del equipo. También se realiza en esta etapa, el estudio documental de las carpetas y las reglas rutinas de mantenimiento, informes de mantenimiento preventivo registro para obtener la base fundamental en la preparación de la lista de verificación (*checklist),* que se aplicó posteriormente para satisfacer el cumplimiento de las cuestiones expuestas en el ámbito nacional e internacional y detectar las causas de posibles ocurrencias de hechos indeseables.

El tercer paso consistió en la aplicación de la técnica de observación simple directa, realizada durante la tercera semana de investigación de los motores, los equipos auxiliares y generadores, junto con la observación del medio ambiente bajo estudio, que dio cuenta de la realidad expresada en el momento.

En el cuarto paso fueron propuestas las medidas que permitieron el seguimiento de los equipos elegidos para el análisis de vibración, análisis de aceite y la termografía.

- **Las aplicaciones se realizaron en cuatro etapas**

Etapa 1 - Diagnóstico: Realizado, por el consultor en las áreas de operación donde se implementará el programa, con el objetivo de obtener los datos de operación, entrevistas y análisis de documentos que son la base del Plan Maestro Estratégico de la segunda etapa. Después de realizar los diagnósticos, se presentó a la Directoria y la Administración de la empresa, un informe de los datos recogidos, oportunidades y recomendaciones para el análisis, la discusión y aprobación de las adaptaciones.

Etapa 2 - Plan Maestro Estratégico: El Plan Maestro Estratégico contempla las oportunidades y los objetivos definidos y aprobados en el informe de diagnóstico presentado en la Etapa 1 Preparado por el Consultor, para la presentación, el análisis, la adaptación y la aprobación por los directivos y la Gerencia de la empresa y las personas involucradas en el programa para determinar las necesidades y objetivos específicos de las áreas en las que se ejecutará el programa.

Etapa 3 - Formación: Necesario para nivelar el conocimiento de los participantes, que serán los responsables de la elaboración del programa interno, funciones líderes, coordinadores y miembros del Comité de Dirección.

Etapa 4 -Seguimiento: El programa de seguimiento fue realizado por el consultor de conjunto con el Coordinador General del Programa, incluyendo reuniones con los coordinadores de Pilar, auditorías durante las etapas y orientación de las actividades de aplicación, conceptos, hipótesis y metodología del Plan Maestro Estratégico aprobado. Las actividades previstas y recomendadas para cada pilar se desarrollarán internamente por los Coordinadores y los grupos de trabajo, siendo el consultor el responsabilizado por las auditorias y recomendaciones necesarias durante el período especificado en el contrato.

3. Estudio de caso

El estudio de caso describe los problemas de mantenimiento correctivo que estaban ocurriendo constantemente en equipos de la planta. Por lo tanto, se realizó una investigación con el fin de identificar la causa raíz de paradas de la unidad generadora, siendo necesario obtener alguna información técnica durante el período hasta que se produjo el daño: Análisis de las alarmas y eventos / temperatura del aceite lubricante / Contenido de agua en el aceite lubricante / contenido de metales en el aceite lubricante. A partir de las observaciones derivadas del estudio de caso, que diagnosticó un problema constante en la operación de un motor de Eletrobras Amazonas Energia, la metodología considerada en este trabajo se aplicó en dos etapas, la primera, la implementación de un mantenimiento predictivo y la segunda la aplicación del TPM. Los resultados de la aplicación de la metodología en el estudio de caso se presentan a continuación. La generación es con motores diesel (Wartsila), compuesto por 10 máquinas, que operan a 13,8 kV, teniendo como valores nominales, una potencia aparente de 20.795 MVA.

4. Resultados de la aplicación de GPM

El mantenimiento predictivo y los dispositivos usados en la mayoría de las veces para establecer la necesidad de mantenimiento fue la inspección periódica. Los intervalos de inspección varían en gran medida y también son diferentes para diferentes tareas. Por ejemplo, fueron reportados intervalos que van desde 1 semana a 5 años con entradas más frecuentes de 1 mes. Lo mismo para la parte C**.** En la parte A, las inspecciones anuales fueron más frecuentes. Otra vía de detección de necesidades de mantenimiento es el monitoreo continuo. Esto fue mencionado con más frecuencia en la parte A (fugas de aceite, la vibración, la temperatura del cojinete) y en menor medida para equipos menos relevantes (condición de conmutación, la corrosión, alta tensión). Se encontró que las herramientas de diagnóstico más eficaces para ser aplicadas en la parte A son el análisis de aceite, pruebas de sobretensión, monitoreo de vibración; en la Parte B, el factor de análisis de imágenes por el poder las pruebas, ensayos térmicos, pruebas dieléctricas; En la Parte C, pruebas de resistencia.

4.1. Análisis de vibraciones

Analizador de vibraciones mod. CMVA60; celerómetro CMSS787A 100 mV / g de la SKF número de serie 13259; Software Prisma 4, versión 1.35, de la SKF.

Esta práctica se aplica periódicamente y se utiliza para evaluar la vibración de motores y equipos dinámicos, siendo capaz de detectar si el equipo necesita alineación, equilibrio o intercambio de cojinete o partes. La clasificación adoptada para la severidad de la vibración es una función de la potencia de accionamiento, la velocidad de rotación de la máquina, así como el nivel crítico para la producción. Cada conjunto se evaluó cuidadosamente para que los niveles de vibración fueran compatibles y registrados con la máxima fidelidad en el Software Prisma 4, con el objetivo de gerenciar y controlar los valores para el análisis de los puntos de acuerdo con la Fig. 1.

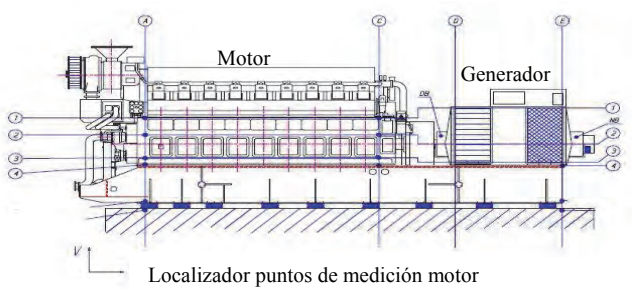


Figura. 1 Análisis de vibraciones. Puntos de medición.
Fuente: Empresa Eletrobras Amazonas Energía aplicación de GPM 2014.

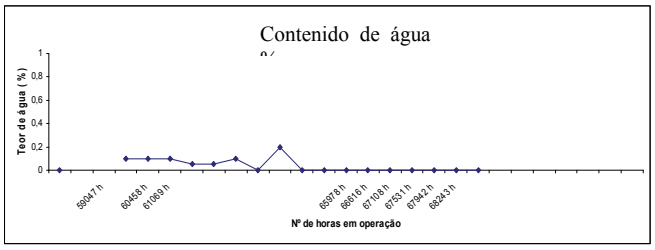


Figura 2. Contenido de agua en el aceite lubricante.
Fuente: Propia.

De acuerdo a las normas ISO 10816-6 e ISO 8528-9, podemos clasificar los motores y generadores instalados en la planta Mauá, pertenecientes al grupo 3 de la tabla estándar ISO 10816-6. Siguiendo esta tabla, encontramos que los niveles de vibración deben ser inferiores a 18 mm/ s (rms) lo que resulta satisfactorio para el funcionamiento sin restricciones durante largos períodos. En el análisis de los valores de la tabla, se observa que ninguno de los puntos de medición supera el límite de 18 mm/s (rms), por lo que podemos decir que los generadores están en buen estado, siendo clasificados como SATISFACTORIO para el funcionamiento y uso.

4.2. Análisis del contenido de agua en el aceite lubricante

Los resultados de los análisis del contenido de agua (Fig. 2), tomadas periódicamente, como mantenimiento predictivo, muestran niveles normales debido a que valores inferiores a 0,3% son tolerables.

Para este análisis con solo 100 ml de muestra del aceite lubricante del Carter es suficiente, el que se vierte en un frasco de 150 ml. El exceso de lubricante después de la recolección se debe eliminar de inmediato para evitar que las partículas se precipiten. El espacio de 50 ml que representa un 1/3 del mismo se deja vacio lo que permite la posterior agitación de la muestra. La determinación de la presencia de agua en el aceite lubricante puede ser determinada a través de los métodos de control de turbidez en aceites ligeros, crepitación en placa caliente. El método que se utilizó en este estudio es la destilación, que evalúa las características de la volatilidad del aceite de lubricante.

La prueba se hace tomando 100 ml de producto de la muestra que se colocan en un matraz que después se somete a calor para la destilación en condiciones controladas. El calentamiento de los productos provoca la evaporación colectándose el condensado en una probeta de vidrio que se sumerge en un baño de hielo. Después de esta operación las temperaturas registradas son corregidas teniendo en cuenta las pérdidas que se producen en la evaporación de pequeñas partes del producto.

4.3. Análisis de contenido de metal en el aceite lubricante

Los métodos describen el análisis de fluoruro - Metodología de análisis de metales en aceites y grasas para la determinación de metales en el aceite lubricante. Los análisis se realizaron por ferrografía para la lectura directa (hierro y cobre), basado en la extracción de partículas contaminantes magnetizables contenidas en el lubricante, a través de la acción de un campo magnético. El equipo utilizado distribuye las partículas de acuerdo a su tamaño, mientras menor es, menor será la distancia recorrida dentro del campo magnético. Las partículas no magnéticas son "fijas" a una distancia mayor, este patrón se refiere a partículas mayores de 2,5 a 15 micras en un volumen de 100 ml de partículas. El número de partículas mayores a de 2 a 5 micras se utiliza como punto de referencia para las partículas sedimentadas. Las partículas mayores de 15 micras, contribuyen en gran medida a un posible fallo catastrófico de algún componente. Después del análisis, fueron obtenidas las Figs. 3 y 4.

4.4. Termografía

Medición en sistemas eléctricos de baja o alta tensión: las variaciones de temperatura provocadas por el exceso de corriente eléctrica en sistemas de baja tensión pueden ser detectadas por la cámara termográfica. El desequilibrio eléctrico puede ser provocado por diferentes causas: problema de suministro, baja tensión en una fase o falla en la resistencia de aislamiento dentro del bobinado del motor.

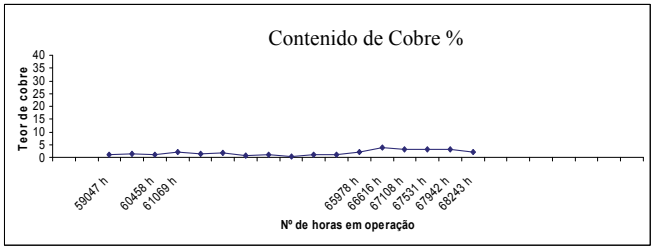


Figura 3.Contenido de cobre en el aceite lubricante.
Fuente: Propia

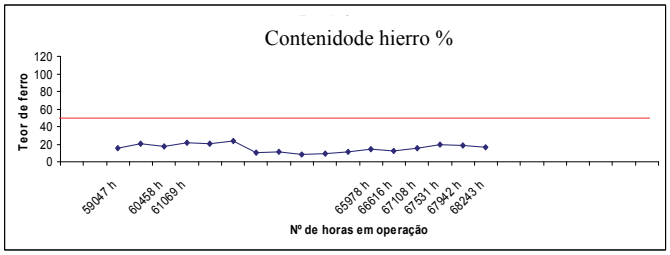


Figura 4. Contenido de hierro en el aceite lubricante.
Fuente: Propia.

Este artículo analiza las causas de sobrecalentamiento en nuestra planta termoeléctrica, así como las pruebas y las herramientas utilizadas con mayor frecuencia para revelar problemas de sobrecalentamiento. Se realizaron pruebas en un sistema eléctrico de baja tensión.

5. Resultados de la ejecución de TPM

El seguimiento de los indicadores se llevó a cabo durante un período de 12 meses, lo que permitió analizar las ventajas de la aplicación de las herramientas del TPM en la empresa. El análisis de los resultados de cada pilar que se describe en la metodología, demostraron los avances significativos logrados con la adopción del TPM, como se describe a continuación.

- **Pilar de Educación y Formación**

Todos los empleados que participan en el programa se sienten identificados para recibir la Formación Básica en TPM, impartido por los Coordinadores Pilares. Materiales didácticos para la formación básica, aprobados por el comité de la directoria y puestos a disposición de las entidades aseguradoras de los Pilares del TPM. Una planificación más rigurosa de los entrenamientos con el calendario actualizado que se llevó a cabo con los datos relativos a los empleadosa ser entrenados, con fechas definidas e instructores capacitados. Divulgación actualizada constantemente, cantidad de personal y las horas de formación de capacitación realizada. Habilidades de cálculo y clasificación de operadores y equipos de mantenimiento actualizados por el departamento de recursos humanos, indicaciones de la formación básica y específica necesaria para la empresa. La planificación de la capacitación indicada en el párrafo anterior, incluyendo conferencias. Reuniones celebradas sobre TPM dentro de los estándares aprobados, con actas, con el tiempo, temas de la agenda, etc. Tabla de Gestión de TPM aprobado y actualizado, con la información con el personal involucrado incluido en el programa.

- **Pilar de mejorías específicas**

Grupo de Trabajo formado, Flujo Operacional de una manera clara y didáctica, los equipos, las prioridades y los principales riesgos identificados son conocidos por todos los participantes. Motores, equipos auxiliares y peraciones identificadas por sus capacidades nominales y reales. Criterio para analizar e identificar las principales pérdidas de operación, la estratificación de Pareto (como muestran las Figs. (9, 10 11 y 12). En espina de pescado (Fig. 5). La metodología a utilizar para investigar y eliminar las pérdidas. Plan de acción (de acuerdo con la Tabla 1 Muestra secuencial del control de etiquetas y Tabla 2. El Plan de acción y control de ejecución de la tarea.), preparado por las acciones del grupo de trabajo, responsables, plazos y avance de las actividades. Poner en marcha el Plan de Acción y comparar los resultados antes y después. Completar el Estándar operacional a ser utilizado por los operadores en cada motor y los equipos auxiliares. Rendimiento de operación /Motor y equipos auxiliares que se evalúa a través de la comparación de los indicadores y los objetivos establecidos para cada motor / Planta. La información sobre los informes de operaciones que se presentan con calidad y supervisados por los Gerentes, Supervisores y Operadores. Los resultados fueron evaluados continuamente por los Gerentes, Supervisores y Operadores. El antes y el después, incluyendo la ganancia de materiales y financiera, etc. Operadores capaces de identificar cualquier distorsión en de los indicadores operacionales. Normas de operación supervisadas por los gerentes, supervisores y operadores.

Operación monitoreada continuamente por los operadores y actuando dentro de las especificaciones de causa y efecto, diagrama de Ishikawa, como se muestra en la Fig. 5, y la Fig. 6 muestra el modelo de etiquetas. Procedimiento adoptado para la colocación del etiquetado, como muestra la Tabla 1 y las acciones y procedimientos a ser adoptados para la retirada del etiquetado como se muestra en la Tabla 2. Es explicado el procedimiento y el control secuencial de etiquetas y el control de la ejecución del Plan de Acción, Figs. 7 y 8.

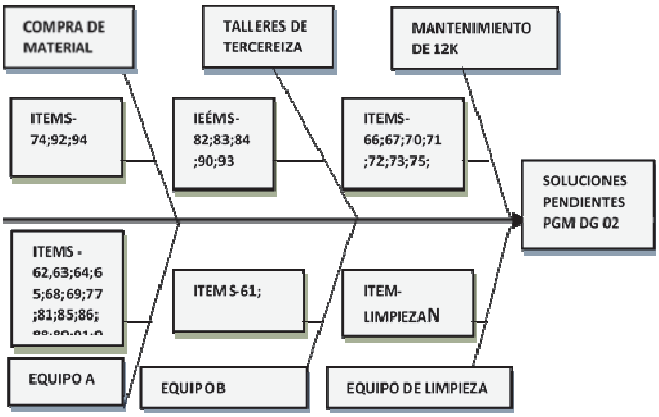


Figura 5. Diagrama de causa y efecto (ishikawa) - pilar de mantenimiento autónomo.
Fuente: ropia.



Figura 6. Modelo de etiquetas (Válvulas de aire, lados: A e B).
Fuente: Propia.

Tabla 1.

N° Etiqueta	Local motivo DG#02 MUUGD10	Responsable	Colocación	Retirada
62	Fugas en la base del filtro de lodo O.L	Paulo	27/06/13	30/06/13
63	Red flexible de retorno OC con vibración	Marcelo	04/07/13	10/07/13
64	Válvula globo de entrada de LFO con la base suelta	Jeam	06/07/13	10/07/13
65	Protección de entrada y salido de O.C. suelta	Paulo	12/07/2013	12/07/13

Fuente: Propia.

Tabla 2.

N.º RN	Descripción	Que es? (Acción correctiva)	Quien?	Cuando? (Hasta)
62	Fugas en la base del filtro de lodo O.L	Paulo	27/06/13	30/06/13
63	Red flexible de retorno OC con vibración	Marcelo	04/07/13	10/07/13
64	Válvula globo de entrada de LFO con la base suelta	Jeam	06/07/13	10/07/13
65	Protección de entrada y salido de O.C. suelta	Paulo	12/07/13	12/07/13

Fuente: Propia.

FLUXOGRAMA	RESPONSÁVEL	DETALHAMENTO
Inicioc Identificación deanomalias Llenado de la etiqueta Aplicación de la etiqueta Registrar A	• Supervisores, Técnicos o Auxiliar de Planta. • Colaborador que identifico la anomalia. • Colaborador que identifico la anomalia. • Supervisor.	- Constatando la existencia de cualquier anomalía, desvío o irregularidad El buen funcionamiento del equipamiento, sistemas, ambientes y necesidades de entrenamientos. Seguir secuencia numérica de las etiquetas. - Llenar todos los ítems de las etiqueta. - Describir los detalles de las anomalías en los espacios en Blanco (al dorso de la etiqueta). - Colocar La etiqueta e la instalación o equipo bien visible - Abrir libros de REGISTRO - Registrar las etiquetas de forma secuenciada - Lleve a una hoja electrónica el control secuencial de las tarjetas.

Figura 7. Aacciones adoptadas para la colocación de las etiquetas
Fuente: Propia.

A		
	• Supervisor o Gerente.	- Generando acciones en conjunto con el coordinador de pilar en cuestión
Retirada da etiqueta	• Supervisor	- Concluyendo un plan de acción, hacer la retirada de las etiquetas del local y hacer el registro de retirada.
Generar control estadístico	•Coordinador de Pilar	- GráficoPareto
Final		

Figura 8. Acciones adoptadas para la retirada de las etiquetas.
Fuente: Propia.

- **Pilar Mantenimiento Autónomo**

En la limpieza inicial los operadores deben ser entrenados e involucrados para identificar anomalías en Pilar Mantenimiento Autónomo. En la limpieza inicial los operadores deben ser entrenados e involucrados para identificar anomalías en los motores, equipos auxiliares, las instalaciones y el lugar de trabajo a través de las etiquetas como se muestra en la Fig. 6. Áreas, motores, equipos e instalaciones auxiliares deberán estar limpias y mantenerse en estas condiciones, no tolerar ninguna señal de desorganización y falta de higiene. Uso de las 5S. Los sitios que no cumplen con este requisito, al menos, se indicarán con las etiquetas y la reparación futura debe ser incluida en un plan de acción con el tiempo y la responsabilidad como se indica en los cuadros 1 y 2**.** Después de la colocación de Etiquetas, debe ser creado un controle indicando: El tipo de problema, el número de etiquetas colocadas y removidas y las áreas involucradas en las anomalías, tales como: mantenimiento, operación, seguridad y medio ambiente. Los operadores tienen la obligación de comprobar siempre las condiciones ideales de los motores y equipos auxiliares, el personal siempre debe inspeccionar los locales y zonas de trabajo, siempre se marcan con los colores de la seguridad industrial, placas de identificación, la iluminación y la limpieza. Indicadores de etiquetas actualizados, lo que indica el volumen de etiquetas retirado y colocado en el mes. Todas las actividades antes mencionadas se llevan a cabo con la correcta identificación de zonas de difícil acceso, la eliminación de las fuentes de suciedad y la preparación de los Estándares Provisionales de limpieza, lubricación, inspección, seguridad y medio ambiente.

- **Plan Maestro de Mantenimiento Autónomo.**

Estructuración del Pilar Mantenimiento Autónomo que aparece en el organigrama de la planta. Determinar cómo identificar anomalías (Identificación por etiquetas). Formación del grupo de trabajo en el procedimiento de etiquetado. Determinar la forma de hacer la limpieza inicial. Establecer la forma de controlar las etiquetas. Iniciar el proceso de etiquetado. INFORME de KPI (número de etiquetas utilizadas). Iniciar proceso de retirada de las etiquetas. Informar a través e KPI el número de etiquetas retiradas. Realizar auditorías internas para asegurar el éxito del programa.

- **Pilar de Mantenimiento Programado.**

Hoja de Trabajo con las prioridades que contenga las preguntas pertinentes sobre las áreas involucradas con la operación (Operación, Mantenimiento, Ingeniería y Medio Ambiente). Reunión para evaluar y clasificar en A, B y C, todos los motores, equipos e instalaciones auxiliares de la empresa, que se llevan cabo con todas las áreas involucradas. Todos los motores, equipos e instalaciones auxiliares, que se clasifican como A, B y C (Gerenciamiento de Inventario según clasificación), (A) es más importante que no puede faltar en la acción, (B) intermedia, que debe contener al inventario (C) inventario mínimo.El equipo de mantenimiento debe llevar a cabo la inspección de la planificación de la operación en todos los equipos catalogados, el mantenimiento debe realizar una revisión de los motores y el equipamiento de las instalaciones para verificar el cumplimiento con las normas de mantenimiento de acuerdo a como lo define el fabricante para restituirle las condiciones de funcionamiento deseadas. Plan de acción conteniendo lo siguiente: Actividades, materiales, plazos, previstos en cada actividad de reparación y mantenimiento, equipo de mantenimiento en las instalaciones de acuerdo a su clasificación A, B y C y el tipo de mantenimiento recomendado en el plan de mantenimiento. Realizar la planificación y cronograma de las actividades de mantenimiento a realizar para los motores, equipamientos auxiliares y motores. Realizar el informe de las actividades concluidas e iniciadas. Ingeniería debe realizar un análisis crítico de los diagramas de Pareto

referido a las fallas como muestran las Figs. 9, 10, 11 y 12 los nuevos informes indicando MTBF y MTTR (de acuerdo con las Tablas 6 y 7 y en la Fig. 12) por motor.

5.1. Análisis de los indicadores

Para facilitar se utilizó el análisis de la evolución de los resultados como las Tablas 3, 4, y 5 (de acuerdo con las Figs. 1a 18 lasTablas (3, 4, 5, y 8) presentan los valores consolidados de cada uno de los indicadores utilizados, centrándose en los resultados antes y después de la implementación de TPM y la aplicación de MP

Tabla 3.
Fallas del motor, frec.y el tiempo de inactividad para el cálculo de MTBF y MTTR, comparación (enero 2013 hasta enero 2014).

Fallas en el mes de enero 2013	Frec.	Tempo de parada
1-Bbomba inyectora	2	6,88
2- Mangueraflexible	1	2,72
3- Transmisor de presión	1	91,81
4-Mmanguera flexible	1	0,80
5- Válvula de control de presión	3	6,93
6- Disyuntor de 69 kv	4	3,45
7- Válvula reguladora depres.	1	3,15
8- Válvulaecualizadora de presión	1	1,24
9- Cabezal	3	2,69
10-Inyector	1	2,17
11- Abrazadera en la red de retorno	1	0,20
12- Tubo de alta presión	1	1,30
13-Red de salida del filtro de lodo	1	1,24
Fallas en el mes de enero 2014	**Frec.**	**Tempo de parada**
01-bomba inyectora	1	1,24
9-cabezal	3	2,69
10-inyector	2	2,17
11- abrazadera en la red de retorno	1	0,20
12- tubo de alta presión	1	1,30
11- abrazadera en la red de retorno d\	1	0,20
12- tubo de alta presión	1	1,30
13-red de salida del filtro de lodo	1	1,24

Fuente: Propia.

Tabla 4.
Presenta las fallas del motor, tiempo e porcentaje para el cálculo de MTBF y MTTR, comparación (Enero 2013 y enero 2014).

Fallas en el mes de enero 2013	Ffrec.	Tiempo de parada
1- Abrazadera en la red de retorno turbina	1	4,55%
2-Ttubo de alta presión	1	4,55%
3- Válvulaecualizadora de presión	1	4,55%
4-Mmangueraflexible	1	4,55%
5- Válvulas reguladora de presión	1	4,55%
6-Trasmisor de presión	1	4,55%
7- Valvula de alivio	1	4,55%
8-Rred de salida del filtro de lodo	1	4,55%
9-Bomba inyectora	2	9,09%
10-Inyector	2	9,09%
11- Válvula de control de presión	3	13,64%
12- Cabezal	3	13,64%
13-Disyuntor de 69kv	4	18,18%
Total	**22**	**100,00%**
Fallas en el mes de enero 2014	**freq**	**Tempo de parada**
01-Bomba inyectora	1	10,00%
9-Vabezal	1	10,00%
10-Inyector	1	10,00%
11- Abrazara retorno de la turbina	1	10,00%
12- Tubo de alta presión	1	10,00%
11- Abrazadera en la red de retorno	1	10,00%
12- Tubo de alta presión	4	40,00%

Fuente: Propia.

Tabla 5.
Presenta las fallas del motor, tiempo y porcentaje para el cálculo de MTBF y MTTR, comparación (Enero 2013 y enero 2014).

Falhas no mês janeiro 2013	Tempo	%
1- Abrazadera en la red de retorno de la turbina	0,20	0,16%
2-Valvula de alivio	0,80	0,64%
3-Rred de salida del filtro de lodo	1,24	1,00%
4- Válvula ecualizadora de presión	1,24	1,00%
5-Tubo de alta presión	1,30	1,04%
6-Inyector	2,17	1,74%
7-Cabezal	2,69	2,16%
8-Mmanguera flexible	2,72	2,18%
9-Válvula reguladora de presión	3,15	2,53%
10-Disyuntor de 69kv	3,45	2,77%
11-Bomba inyectora	6,88	5,52%
12-Válvula de controle de presión	6,93	5,56%
13-Transmisor de presión	91,81	73,70%
Total	**124,58**	**100,00%**
Fallas em el mês de enero 2010	**Tempo**	**%**
1- Mangueraflexible	0,08	0,42%
2-Red de desaeración	0,60	3,15%
3-Tubo de alta presión	0,98	5,14%
4-Inyector	1,42	7,45%
5-Tapa del soporte del eje de manivela	2,85	14,95%
6- Tubo de retorno de la turbina	2,93	15,37%
7-Bomba inyectora	10,20	53,52%
Total	**19,06**	**1000%**

Fuente: Propia.

Por consiguiente, se ha tratado de demostrar las mejoras obtenidas en el área de mantenimiento de acuerdo a los resultados de MTBF y MTTR.

MTBF es un valor asignado a un dispositivo o aparato para describir su fiabilidad en particular. Este valor asignado indica cuándo se puede producir un fallo en el dispositivo en cuestión. Cuanto mayor sea este indicador, mayor fiabilidad de los equipos y, en consecuencia, el mantenimiento será evaluado en términos de eficiencia.

MTTR es una medida básica del mantenimiento de elementos reparables. Representa el tiempo medio necesario para reparar un componente que ha fallado en las Tablas 6 y 7.

5.2. Formulaciónmatemática

- Cálc. porcentaje de fallas enero de 2013 (Tab.5 y Fig. 10).

$$POCENTAGEM = \frac{\text{TEMPO}}{\sum \text{DE LOS TIEMPO DE FALHA}} \times 100 \quad \text{Ec. (1)}$$

$$(0{,}20 \div 124{,}58) \times 100 = 0{,}16\,\%$$
$$(0{,}8 \div 124{,}58) \times 100 = 0{,}64\,\%$$
$$(1{,}24 \div 124{,}58) \times 100 = 1{,}00\,\%$$
$$(1{,}24 \div 124{,}58) \times 100 = 1.00\,\%$$
$$(1{,}30 \div 124{,}58) \times 100 = 1{,}04\,\%$$
$$(2{,}17 \div 124{,}58) \times 100 = 1{,}74\,\%$$
$$(2{,}69 \div 124{,}58) \times 100 = 2{,}16\,\%$$
$$(2{,}72 \div 124{,}58) \times 100 = 2{,}18\,\%$$
$$(3{,}15 \div 124{,}58) \times 100 = 2{,}53\,\%$$
$$(3{,}45 \div 124{,}58) \times 100 = 2{,}77\,\%$$
$$(6{,}88 \div 124{,}58) \times 100 = 5{,}52\,\%$$
$$(6{,}93 \div 124{,}58) \times 100 = 5{,}56\,\%$$
$$(91{,}81 \div 124{,}58) \times 100 = 73{,}70\,\%$$

- Cálculo del porc.de fallas enero, (Tabla 5 y Fig. 11).

$$PORCENTAGE = \frac{\text{TEMPO}}{\sum \text{DE LOS TIEMPO DE FALHA}}$$

Ec.(2)

$$(0,60 + 0,80 + 0,6 + 0,98 + 1,42 + 2,85 + 2,93 + 10,20) = 3,15\%$$
$$(0,98 + 0,80 + 0,6 + 0,98 + 1,42 + 2,85 + 2,93 + 10,20) = 5,14\%$$
$$(1,42 + 0,80 + 0,6 + 0,98 + 1,42 + 2,85 + 2,93 + 10,20) = 7,45\%$$
$$(2,85 + 0,80 + 0,6 + 0,98 + 1,42 + 2,85 + 2,93 + 10,2) = 14,95\%$$
$$(2,93 + 0,80 + 0,6 + 0,98 + 1,42 + 2,85 + 2,93 + 10,2) = 15,37\%$$
$$(10,2 + 0,80 + 0,6 + 0,98 + 1,42 + 2,85 + 2,93 + 10,2) = 53,52\%$$

- Cálc.total de ocurr.de fallas ene de 2013 (Tab. 4 y fig. 8).

$$\sum de\ las\ frecuencia\ de\ fallas \qquad Ec.\ (3)$$

$$1+1+1+1+1+1+1+2+2+3+3+4=22$$

- Cál.total de ocurr.de fallas ene de 2014(Tab.4 y Fig. 9).

$$\sum de\ las\ frecuencia\ de\ fallas \qquad \text{Ec.(4)}$$
$$1+1+1+1+1+1+4=10$$

- Cálc.totaltiemp.de parada ene de 2013(Tab. 5 y Fig. 10).

$$\sum de\ tiempo\ de\ parada \qquad \text{Ec.(5)}$$
$$0,20 + 0,80 + 1,24 + 1,30 + 2,17 + 2,69 + 2.72 + 3,15 + 3,45 + 6,88 + 6,93 + 91,81 = 124,58$$

- Cálc. Total tiemp.de parada enero de 2014 (Tab.5 y Fig. 11).

$$\sum de\ tiempo\ de\ parada \qquad \text{Ec.(6)}$$
$$0,88 + 0,60 + 0,98 + 1,42 + 2,85 + 2,93 + 10,20 = 19,06$$

- Cálculo del MTBF 2013 (Cuadro 6)

$$MTBF = \frac{(24\ x\ 9\ x\ \sum \text{Total de dias}) - \sum \text{Total de temp.de parada}}{\sum \text{Total de ocurrencias}} \quad \text{Ec. (7)}$$

$$MTBF = \frac{(24\ x\ 9\ x\ 29) - 124,28}{22} \qquad MTBF = 279,06$$

- Cálculo del MTTR 2013 (Cuadro 6).

$$MTTR = \frac{\sum \text{Total de temp.de parada}}{\sum \text{Total de ocurrencias}} \quad \text{Ec. (8)}$$

$$MTTR = \frac{124,28}{22} \qquad MTTR = 5,66$$

- Cálculo del MTBF 2014 (Cuadro 7)

$$MTBF = \frac{(24\ x\ 9\ x\ \sum \text{Total de dias}) - \sum \text{Total de temp.de parada}}{\sum \text{Total de ocurrencias}}$$

$$MTBF = \frac{(24\ x\ 9\ x\ 15) - 19,06}{10} \qquad MTBF = 322,09 \quad \text{Ec. (9)}$$

- Cálculo do MTTR 2014 (Cuadro7).

$$MTTR = \frac{\sum \text{Total de tiemp.de parada}}{\sum \text{Total de ocurrencias}} \quad \text{Ec.(10)}$$

$$MTTR = \frac{124,28}{22} \qquad MTTR = 1,99$$

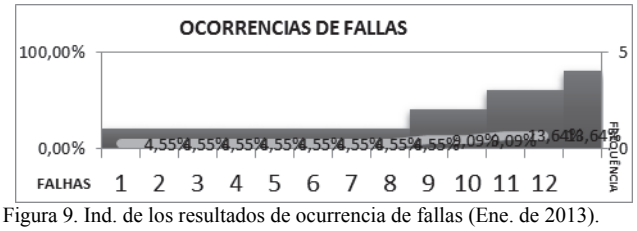


Figura 9. Ind. de los resultados de ocurrencia de fallas (Ene. de 2013).
Fuente: Propia.

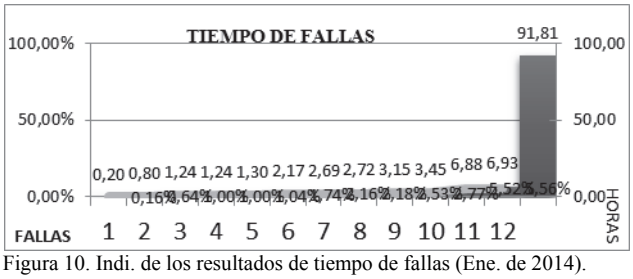


Figura 10. Indi. de los resultados de tiempo de fallas (Ene. de 2014).
Fuente: Propia.

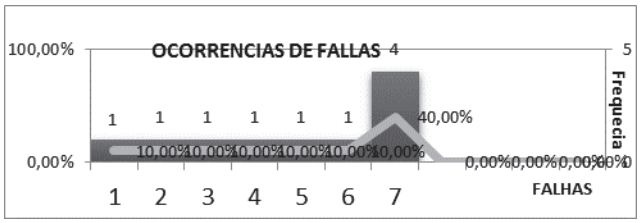


Figura 11. Ind. de los resultados de tiempo de fallas (Ene. de 2013).
Fuente: Propia.

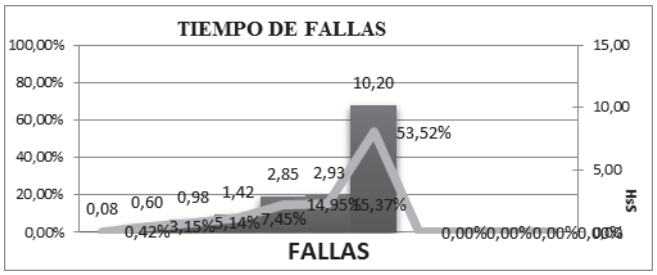


Figura 12.Ind. de los resultados de tiempo de fallas (Ene. de 2014).
Fuente: : Propia.

Tabla 6.
Resultado de MTBF y MTTR comparación Enero 2013.

Total de ocurrencias Ene/13	22
Total de tiempo de paradas	124,58
Fecha inicial	01/01/2013
Fecha inicial	31/01/2013
Total de dias	29

Fuente: Propia.

- Cálculo de MTBF ENERO 2013 – 279,06
  - ✓ Cálculo de MTTR ENERO 2013 – 5,66
  - ✓ Cálculo de MTBF Enero 2014 – 322,09
  - ✓ Cálculo de MTTR Enero 2014 – 1,99

Tabla 7.
Resultado dE MTBF Y MTTR comparación Enero 2014.

Total de ocurrencias Ene/14	10
Total de tiempo de paradas	19,06
Fecha inicial	01/01/2014
Fechaa inicial	31/01/2014
Total de diasTotal de tiempo de paradas	15

Fuente: Propia.

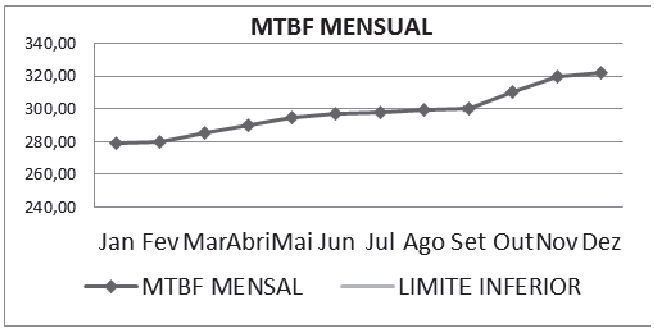


Figura 13. MTBF Mensual de Enero de 2013 hasta Diciembre 2013.
Fuente: Propia.

Tabla 8:
Información del tiempo y la frecuencia de fallos de motor del mes de enero a diciembre de 2013 para el cálculo del tiempo de indisponibilidad debido a fallas del año 2013.

motor	frecuencia de fallasen 2013	tempo indisponible en razon de fallas ano 2013
9	6	12,83
10	7	12,82
11	0	0,00
12	7	13,47
13	5	3,88
14	5	6,46
15	10	25,31
16	5	25,53
17	3	8,13
18	11	65,61

Fuente: Propia.

Se encontró la ganancia real del MTBF, 322.9 después de la implantación del MP y el TPM como muestran los valores de enero 2014 en comparación con enero de 2013. La Disminución de MTTR, 1,99 después de la aplicación de MP y programa de TPM como se muestra por los valores de enero 2014 en comparación con enero de 2013, Fig.. 13.

- Cálculo del porcentaje de fallas, 2013 para la elaboración de (Fig. 17).

$$POCENTAGE = \frac{\text{TEMPO}}{\sum \text{DE LOS TIEMPO DE FALHA}} \times 10 \qquad \text{Ec. (11)}$$

$$\sum de\ las\ frec.de\ fallas \qquad \text{Ec. (12)}$$

12,83 + 12,82 + 0 + 13,47 + 3,88 + 6,46 + 25,31 + 25,53 + 8,13 + 65,

Motor 9 $(12{,}83 \div 174{,}04) \times 100 = 7{,}36\%$

Motor 10 $(12{,}83 \div 174{,}04) \times 100 = 7{,}36\%$

Motor 11 Motor parado com averiadelárbol de manivela

Motor 12 $(12{,}47 \div 174{,}04) \times 100 = 7{,}73\%$

Motor 13 $(3{,}88 \div 174{,}04) \times 100 = 2{,}22\%$

Motor 14 $(6{,}46 \div 174{,}04) \times 100 = 3{,}71\%$

Motor 15 $(25{,}31 \div 174{,}04) \times 100 = 14{,}54\%$

Motor 16 $(25{,}53 \div 174{,}04) \times 100 = 14{,}66\%$

Motor 17 $(8{,}13 \div 174{,}04) \times 100 = 4{,}67\%$

Motor 18 $(65{,}61 \div 174{,}04) \times 100 = 37{,}69\%$

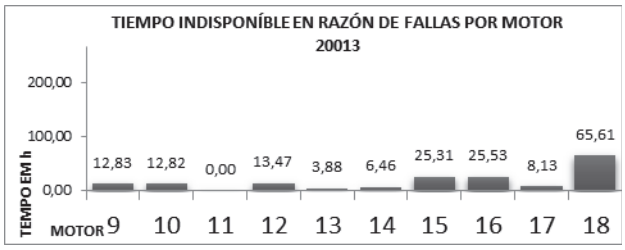


Figura 14. Ind. de los result. de tiempo disp. razón de fallas del (2013).
Fuente: Propia.

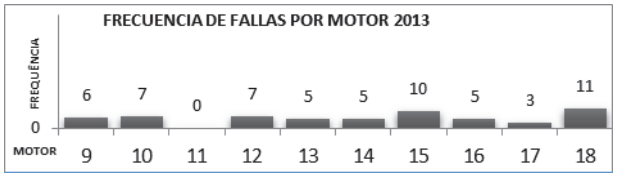


Figura 15. Ind. de los resultados frecuencia de fallas del motor (2013).
Fuente: Propia.

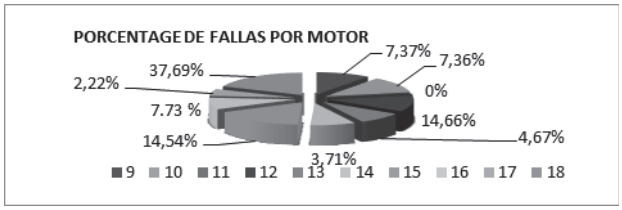


Figura 16. Ind. de los resultados, porcentaje de fallas del motor (2013).
Fuente: Propia.

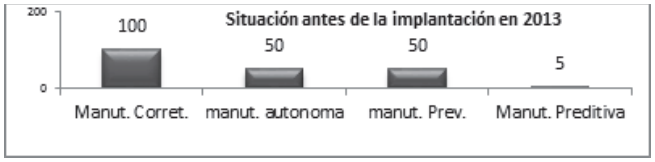


Figura 17. Ind.de los Resultados del mant. antes de La implan.(2013).
Fuente: Propia.

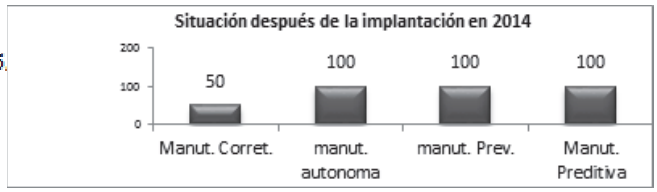


Figura 18. Indicadores de los Resul.del mant. después de la implantación 2014.
Fuente: Propia.

Con el análisis de los resultados y discusión de los hechos fue verificado que La implantación del TPM y MP

Tabla 9.
Costo de aplicación de los mantenimiento

Motores de la planta	Máquinas paradas	Potencia parada MW	Tiempo de Mntmto en h	Precio de la energia R$/MWh	Costo de la máq. parada U$
9	9	16	12,83	43,1	5.978,08
10	10	16	12,82	43,1	5.973,42
11	11	16	0	43,1	0
12	12	16	13,47	43,1	1.807,86
13	13	16	3,88	43,1	1.807,86
14	14	16	6,46	43,1	3.010,01
15	15	16	25,31	43,1	11.793,08
16	16	16	25,53	43,1	11.895,59
17	17	16	8,13	43,1	3.788,13
18	18	16	65,61	43,1	30.570,71
Costo anual de los mantenim. en h 174,04					**U$ 81.093,21**

Fuente: Propia.

Tabla 10.
Costo de combustible para la generación térmica por año.

Precio del combustible fosil	Potencia sustituir aproximada	Tiempo de generación térmica	Consumo específico	Costo del combustible
[U$/l]	[MW]	[h]	[l/MWh]	[U$]
822,07	150	174,04	280	828.648,64
			Costo del combustible por año	**U$ 6.009.083,78**

Fuente: Propia.

Tabla 11.
Costo de generación térmica para reponer las pérdidas

Cantidad de motores	Potencia a sustituir aproximada [MW]	Tiempo de generación térmica	Costo de La energia térmica con diésel oil [U$]	Costo del combustible [U$]
10	150	174,04	67,56	243.243,24
			Costo del combustible por año	**U$ 1.763.918,18**
COSTO TOTAL POR AÑO U$: 7.854.095,91				

Fuente: Propia.

es viable económicamente como muestra el aumento del MTBF y la disminución del MTTR. Además fue verificado un aumento del mantenimiento autónomo realizado por los operadores, un aumento de las actividades predictivas y disminución del mantenimiento correctivo, las Figs. 17 y 18.

6. Costos ligados a los mantenimientos en la planta termoeléctrica de MauáManaus-Amazonas-Brasil.

Tablas 9, 10 y 11 presentan un estudio de los costes directos de mantenimiento correctivo de los diez motores y generadores de la central eléctrica de Mauá, incluidos los costos de sustituir la energía generada por las centrales termoeléctricas en Manaus - AM.

7. Conclusiones

Con base en la información del estudio de caso de Eletrobras Amazonas Energía, fue posible identificar las posibles causas de parada de los equipos. Se dio solución a un problema real de la empresa, lo que reporto ganancias. Una vez detectado los problemas el área de mantenimiento de la empresa propuso la aplicación, primero, de un programa de mantenimiento predictivo; y en una segunda etapa, la aplicación de un programa de mantenimiento productivo total. Después de las implementaciones de los programas, se ha demostrado, a través de la mejora de los indicadores de mantenimiento, la solución de un problema en una situación real con la continua disminución de mantenimiento correctivo en un año en la empresa Eletrobras Amazonas Energía.

Con poca inversión, podemos resolver el problema del mantenimiento correctivo en nuestra planta sin afectar la producción de energía eléctrica de la planta de forma segura y eficaz, sin causar más daños al medio ambiente, manteniendo al mismo tiempo la fiabilidad del sistema eléctrico de Manaus, sin comprometer la seguridad de las instalaciones, a un costo menor de U$ 7,854.095,91 gastados anualmente.

Agradecimientos

ITEGAM, FAPEAM y ELETROBRAS

Referencias

[1] Barlow, R.E. and Proschan, F., Statistical Theory of reliability and life testing. New York: Holt, Rinehart and Winston, Inc., 1975.

[2] Anders, G.J., Probability concepts in electric power systems. New York: J. Wiley & Sons, 1990.

[3] Zheng, X. and Fard, N., A maintenance policy for repairable systems based on opportunistic failure-rate tolerance, IEEE Trans. Reliability, 40(2), pp. 237-244, 1991. DOI: 10.1109/24.87134..

[4] Ebrahimi, N., Two new replacement policies, IEEE Trans. Reliability, 42(1), pp. 141-147, 1993.

[5] Arango-Serna, M.D., Enterprise arquitecture as tool for managing operational complexidy in organizations. DYNA, 81(185), pp. 219-226, 2014. DOI: 10.15446/dyna.v81n185.41928

[6] Canfield, R.V., Cost optimization of periodic preventive maintenance, IEEE Trans. Reliability, 35(1), pp. 78-81, 1986. DOI: 10.1009/TR1986.4335355

[7] Endrenyi, J. and Sim, S.H., Availability optimization for continuously operating equipment with maintenance and repair, in Proceedings of the Second PMAPS Symposium, Sept. 1988, Nov. 1989, EPRI Publication EL-6555.

[8] Anders, G.J. et al., Maintenance planning based on probabilistic modeling of aging in rotating machines, in CIGRE Conference, Paris, 1992, Paper No. 11-309.

[9] Reichman, B. et al., Application of a maintenance planning model for rotating machines, in CIGRE Conference, Paris, 1994, Paper No. 11-204.

[10] Jardine, A.K.S., Maintenance, replacement and reliability. London: Pitman Publishing, 1973.

[11] Reliability Centered Maintenance Seminar. New York: A publication of the Consolidated Edison Company, 1988.

[12] Smith, A.M., Reliability-centered maintenance. New York: McGraw-Hill, Inc., 1993.

[13] Moubray, J., Reliability-centered maintenance. New York: Industrial Press Inc., 1992.

[14] Wisconsin Public Service Corp., PM optimization boosts reliability at small cost, Utility Best Practices, 157 P., 1995.

[15] Ascher, H. and Feingold, H., Repairable systems reliability. NewYork: Marcel Dekker, Inc., 1984.

[16] Valdez-Flores, C. and Feldman, R.M., A survey of preventive maintenance models for stochastically deteriorating single-unit systems, Naval Research Logistics Quarterly, 36, pp. 419-446, 1989.

[17] EPRI, Probabilistic model to estimate the remaining life of generator station components, Report RP-2577-1, 1993.
[18] Endrenyi, J., Anders, G.J. and Leite da Silva, A.M., Probabilistic evaluation of the effect of maintenance on reliability—An application, IEEE Trans. Power Systems, 13(2), pp. 576-583, 1998. DOI: 10.1109/59.667385.
[19] Billinton, R. and Pan, J., Optimal maintenance scheduling in a parallel redundant system of series components in each branch, IEEE Trans. Power Systems, to be published, 1999. DOI: 10.1109/61.772336.
[20] Dialynas, E.N. and Michos, D.G., Time-dependent unavailability analysis of standby components incorporating arbitrary failure distributions and three inspection/maintenance policies, Reliability Engineering and System Safety, 39, pp. 35-54, 1993. DOI: 10.1016/0951-8320(93)90146-P
[21] Decker, D.L., What is in store for DCS systems? Where are they headed? Pulp and Paper Industry Technical Conference, 2001 Conference Record of. pp.17-20, 2001.
[22] Quiroga-Méndez, J. and Oviedo-Castillo, S. Implementing condition- Implementing condition-based maintenance using modeling and simulation: A case study of a permanent magnet synchronous motor. Ingeniería e Investigación. 31(2), pp. 18-28, 2011.
[23] Gallego-Vega L.E. and Duarte-Velasco, O.G., The effect of electric transmission constraints on how power generation companies bid in the Colombian electrical power market. Ingeniería e Investigación, 30(2), pp. 62-77, 2010.
[24] Chen, L., A framework of a web-based distributed control system. Master of Science Thesis, Department of Electrical and Computer Engineering, University of Calgary, Calgary, Canada, 2003, 113 P. DOI: 10.1109/CCECE.2003.1226150
[25] Castrillón, R,P., González, A.J. y Quispe, E.C., Mejoramiento de la eficiencia energética en la industria del cemento por proceso húmedo a través de la implementación del sistema de gestión integral de la energia, DYNA, 80(177), pp. 115-123, 2013.

M. Fonseca-Junior, es MSc. en Ingeniería Eléctrica en 2012, de la Universidad Federal de Pará (UFPA), Brasil. Eng. de la empresa de Ingeniería Eléctrica Eletrobras. Cursa el Doctorado en Ingeniería Eléctrica (UFPA).
ORCID: 0000/0001/6001/3098

U. Holanda-Berzerra, es Dr. en Ingeniería Eléctrica en 1988, de la Universidad Federal de Rio de Janeiro (COPPE / UFRJ), Brasil. Es profesor en el Departamento de Ingeniería Eléctrica e Informática UFPA desde 1977. ORCID: 0000/0002/2853/8676.

J. Cabral-Leite, es Dr. en Ingeniería Eléctrica en 2013 de la Universidad Federal de Pará (UFPA), Brasil. Profesor e Investigador de ITEGAM. Manaus. Amazonas. Brasil.
ORCID: 0000/0002/1337/3549.

T.L. Reyes-Carvajal, es Dr. en Ingeniería Mecánica en 1997 de la Universidad Central de las Villas, Cuba. Profesor e Investigador de ITEGAM.
ORCID: 0000/0003/4699/0719.

UNIVERSIDAD NACIONAL DE COLOMBIA
SEDE MEDELLÍN
FACULTAD DE MINAS

Área Curricular de Ingeniería
de Sistemas e Informática

Oferta de Posgrados

Especialización en Sistemas
Especialización en Mercados de Energía
Maestría en Ingeniería - Ingeniería de Sistemas
Doctorado en Ingeniería- Sistema e Informática

Mayor información:

E-mail: acsei_med@unal.edu.co
Teléfono: (57-4) 425 5365

UNIVERSIDAD NACIONAL DE COLOMBIA
SEDE MEDELLÍN
FACULTAD DE MINAS



DYNA
http://dyna.medellin.unal.edu.co/

Numerical modelling of Alto Verde landslide using the material point method

Marcelo Alejandro Llano-Serna [a], Márcio Muniz-de Farias [b] & Hernán Eduardo Martínez-Carvajal [c]

[a] *Faculty of Technology, University of Brasilia, Brasilia, Brazil. mallano@unb.br*
[b] *Faculty of Technology, University of Brasilia, Brasilia, Brazil. muniz@unb.br*
[c] *Faculty of Technology, University of Brasilia, Brasilia, Brazil. carvajal@unb.br*
[c] *Facultad de Minas, Universidad Nacional de Colombia, Medellín, Colombia. hemartinezca@unal.edu.co*

Received: January 13th, 2015. Received in revised form: May 7th, 2015. Accepted: September 25th, 2015.

Abstract
A huge landslide took place at Alto Verde residential complex at the end of 2008 in the city of Medellin, Colombia, claiming the lives of twelve people and destroying six houses. Landslides are characterized by large deformations in the soil mass. This study used the material point method (MPM), a particle-based method that takes advantage of a double Lagrangian-Eulerian discretization. This approach provides a robust framework that enables the numerical simulation of large strains, without mesh entanglement issues that are common with the Finite Element Method. The numerical model proposed here assumes simplifications of the geotechnical, morphological and structural buildings conditions on the site. Nevertheless, the final numerical deformed configuration described the geometric features observed in the field successfully. The result allows applications such as the design of barriers, risk assessment or determination of a minimum safe distance for a building from a slope susceptible to landslides.

Keywords: Alto Verde; material point method; debris flow; large strains.

Modelamiento numérico del deslizamiento Alto Verde usando el método del punto material

Resumen
Finalizando el año 2008 en la ciudad de Medellín, Colombia, ocurrió un deslizamiento de tierra en la urbanización Alto Verde provocando la muerte de doce personas y la destrucción de seis viviendas. Los deslizamientos se destacan por el elevado nivel de deformaciones en una masa de suelo. El presente trabajo utilizó el método del punto material (MPM), método basado en partículas que utiliza una doble discretización Lagrangiano-Euleriana. La doble discretización genera un marco numérico robusto que permite la simulación de grandes distorsiones. El modelo numérico planteó una simplificación de las condiciones geotécnicas, morfológicas y estructurales de las edificaciones envueltas en Alto Verde. El estado de deformación final de la simulación se acomodó satisfactoriamente a las características geométricas finales observadas en campo. Los resultados obtenidos generan aplicaciones como el diseño de barreras, análisis de riesgo o la determinación de la distancia mínima de retiro a una ladera susceptible de deslizamiento.

Palabras clave: Alto Verde; método del punto material; flujo de escombros; grandes deformaciones.

1. Introducción

La historia de un movimiento en masa según Skempton y Hutchinson [1] está compuesta por tres etapas: (i) deformaciones previas a la ruptura, (ii) la ruptura como tal y (iii) los desplazamientos posteriores a la ruptura. Adicionalmente, la pérdida de resistencia al esfuerzo cortante durante la ruptura determinará la velocidad del movimiento, la cual involucra cambios cinemáticos del deslizamiento a flujo o caída. Esto es relevante porque definirá el comportamiento y destructividad del evento [2].

Los deslizamientos urbanos son detonados principalmente por cambios hidrológicos, ambientales y principalmente antropogénicos, tales como lluvias fuertes,

© The author; licensee Universidad Nacional de Colombia.

terremotos y actividades humanas. Los efectos adversos de los deslizamientos urbanos se han hecho más severos debido al crecimiento poblacional incontrolado en regiones de ladera. Consecuentemente, los riesgos que surgen de estos desarrollos urbanos en áreas susceptibles a deslizamientos están aumentando a pesar de los progresos en la aplicación de medidas de mitigación.

El análisis de la estabilidad del talud y el inicio del deslizamiento puede ser abordado mediante el uso de métodos clásicos en la ingeniería geotécnica, tales como el método de equilibrio límite o el ampliamente conocido método de los elementos finitos (MEF). Sin embargo para modelar el comportamiento del suelo durante un deslizamiento se debe utilizar un método numérico capaz de manejar grandes deformaciones [3].

Actualmente el MEF es el método más utilizado para el cálculo de deformaciones en problemas de geotecnia. A pesar de esto el método presenta fuertes limitaciones cuando la solución involucra grandes distoriones. Para extender el MEF a la simulación de grandes desplazamientos es necesario el uso de tensores de grandes deformaciones y la actualización de la discretización del sólido deformado. Este proceso de mapeamiento y relocalización de variables de estado produce pérdidas de información generando imprecisiones en la solución final [4].

Como respuesta a las limitaciones del MEF surgió el método del punto material (MPM) [5–7]. En este método se discretiza el dominio físico del problema en un número de puntos sobre los cuales se almacenan las propiedades del medio y las variables de estado. La interacción entre los diferentes puntos y el desarrollo de las tensiones y deformaciones se obtienen al rastrear éstas gracias a una malla computacional de fondo donde se resuelven las ecuaciones de movimiento. Al mismo tiempo la información se almacena en los puntos materiales (PM), la malla de cálculo es indeformable y se puede utilizar durante todo el análisis.

El MPM ha sido utilizado con éxito en la simulación de problemas relacionados a estabilidad de laderas y taludes. Entre ellos se destacan: El cálculo de estados de tensión [8], análisis multifásicos de taludes sometidos a cargas cíclicas [9], estudio paramétrico considerando la interacción entre deslizamientos con estructuras rígidas [10], problemas de flujos de detritos (*Debris-flows*) en tres dimensiones incorporando obstáculos en su trayectoria [11,12] y determinación de superficies de ruptura y análisis acoplados [13–15]. El único caso real simulado del que se tiene conocimiento corresponde a un deslizamiento cerca al pueblo de Lønstrup, Dinamarca, en el año de 2008 [3].

El 16 de noviembre de 2008 se presentó la falla de un talud en el barrio Alto Verde en la ciudad de Medellín, Colombia, con un volumen estimado entre 13000 m³ y 25000 m³. El mecanismo inicial, probablemente de tipo rotacional, evolucionó a un mecanismo de tipo *Debris-flow* con alto poder destructivo. El talud se había construido en una unidad superficial geológicamente conocida en el ambiente local como Suelo Residual de Dunita. El deslizamiento y flujo destruyeron a su paso seis casas, dejando un saldo de doce personas muertas y cuantiosas pérdidas económicas [16,17].

En este artículo se presenta la simulación del deslizamiento de Alto Verde utilizando el MPM, incluyendo la visualización y reproducción fiel de los cambios en la geometría del sitio durante y después del evento, además del cálculo de variables como la velocidad del movimiento en masa, lo que constituye un avance pionero en este tipo de análisis. Finalmente, la estimación de la velocidad y la energía cinética abre la posibilidad de resolver problemas relacionados con la cuantificación de la vulnerabilidad de estructuras y personas sometidas al impacto de deslizamientos.

2. Método del punto material

Durante este trabajo se utilizó como referencia la formulación presentada por Buzzi et al. [18]. La notación tensorial es definida de la siguiente forma: los tensores son representados por una letra y su orden es demarcado por la cantidad de líneas (-), un punto (·) simboliza una contracción simple, dos puntos (:) simbolizan una contracción doble y el símbolo (⊗) es el producto diádico o tensorial.

2.1. Formulación

La ecuación de campo que gobierna el balance de momento lineal en un medio continuo para satisfacer las condiciones de equilibrio dinámico se pueden representar utilizando notación tensorial así:

$$\frac{d\underline{\underline{\sigma}}}{d\underline{x}}:\underline{\underline{I}}+\rho\underline{b}=\rho\underline{a} \tag{1}$$

en la ec. (1) $\underline{\underline{\boldsymbol{\sigma}}}$ representa el tensor de tensiones de segundo orden, $\underline{\boldsymbol{x}}$ es el vector de posición de un punto, $\underline{\underline{\boldsymbol{I}}}$ se refiere al tensor identidad de segunda orden, ρ el campo de densidad escalar, $\underline{\boldsymbol{b}}$ tensor de primer orden con las fuerzas de cuerpo y externas actuantes y $\underline{\boldsymbol{a}}$ es el vector de aceleración.

Para obtener la forma débil del balance de momento lineal, la ec. (1) se multiplica por funciones de prueba arbitrarias de la forma $\underline{w}(\underline{x})$ que por medio del método de residuos ponderados es integrado sobre todo su dominio (V) y se obtiene:

$$\int_A \underline{w}\cdot\underline{t}dA+\int_V \rho\underline{w}\cdot\underline{b}dV-\int_V \frac{d\underline{w}}{d\underline{x}}:\underline{\underline{\sigma}}dV=\int_V \rho\underline{w}\cdot\underline{a}dV \tag{2}$$

donde $\underline{t}$ define las fuerzas de tracción en la superficie de una región A.

El campo de densidades, tensiones y aceleraciones de cada PM se discretiza por medio de funciones de característica aplicadas en la partícula de la siguiente forma:

$$\rho(\underline{x})=\sum_p \frac{m_p\chi_p(\underline{x})}{V_p} \tag{3}$$

$$\underline{\underline{\sigma}}(\underline{x})=\sum_p \underline{\underline{\sigma_p}}\chi_p(\underline{x}) \tag{4}$$

$$\rho(\underline{x})\underline{a}(\underline{x})=\sum_p \frac{\dot{q}_p\chi_p(\underline{x})}{V_p} \tag{5}$$

aquí el subíndice p se refiere a cada punto material donde m_p es la masa, $\underline{q_p}$ su momento lineal, $\underline{a}$ la aceleración y $\chi_p(\underline{x})$ es la función de característica en la partícula. Estas funciones se requieren para dividir la unidad referente a la configuración inicial, como se puede ver en la siguiente ecuación.

$$\sum_p \chi_p^i(\underline{x}) = 1 \quad \forall \quad x \tag{6}$$

Las funciones de peso y sus derivadas respecto a la posición son discretizadas de acuerdo a la malla computacional mediante las siguientes expresiones:

$$\underline{w}(\underline{x}) = \sum_n S_n(\underline{x})\underline{w}_n \tag{7}$$

y

$$\frac{d\underline{w}(\underline{x})}{d\underline{x}} = \sum_n \underline{w}_n \otimes \frac{dS_n(\underline{x})}{d\underline{x}} = \sum_n \underline{w}_n \otimes \underline{G}_n(\underline{x}) \tag{8}$$

Reemplazando las ecs. (3)-(8) en la ec. (2) se obtiene la ecuación de gobierno discreta:

$$\underline{f}_n^{ext} - \underline{f}_n^{int} = \underline{\dot{q}}_n \tag{9}$$

donde los vectores de fuerzas externas son:

$$\underline{f}_n^{ext} = \int_A S_n \underline{t} dA + \sum_p m_p \underline{b} \overline{S}_{np} \tag{10}$$

y el vector de fuerzas internas en término de las tensiones de Kirchhoff es:

$$\underline{f}_n^{int} = \sum_p m_p \frac{\underline{\underline{\tau}}}{\rho_i} \cdot \overline{\underline{G}}_{np} \tag{11}$$

Como fue discutido por Nairn y Guilkey [19] la forma de la ec. (11) es conveniente porque evita tener que calcular la densidad o el volumen de cada partícula en cada intervalo de tiempo.

Los términos $\overline{S}_{np}$ y $\overline{\underline{G}}_{np}$ en las ecs. (10)-(11) representan la influencia de las funciones de forma y sus gradientes respectivamente, estos pueden ser calculados a partir de:

$$\overline{S}_{np}(\underline{x}) = \frac{1}{V_p}\int_{V^*} S_n(\underline{x})\chi_p(\underline{x})dV \tag{12}$$

y

$$\overline{\underline{G}}_{np}(\underline{x}) = \frac{1}{V_p}\int_{V^*} \underline{G}_n(\underline{x})\chi_p(\underline{x})dV \tag{13}$$

donde el dominio de integración $\boldsymbol{V^* = V \cap V_p}$ es el volumen que soporta las funciones características. Las cuales son uno de los avances más relevantes que ha sufrido el MPM desde su formulación inicial [7].

2.2. Procedimiento de cálculo

El problema es integrado dinámicamente en el tiempo por medio de un esquema de diferencias finitas en avance donde la información es almacenada en los PMs. Después que el sólido en análisis es discretizado por un conjunto de puntos materiales, p, la masa de la malla de fondo, m_n, y su momento lineal, $\boldsymbol{\underline{q}_n}$, son inicializados por medio de las funciones de forma,

$$m_n = \sum_p \overline{S}_{np} m_p \tag{14}$$

y

$$\underline{q}_n = \sum_p \overline{S}_{np} m_p \underline{v}_n \tag{15}$$

El incremento de deformaciones es calculado para cada vértice al inicio y al final de cada intervalo de tiempo utilizando el gradiente de velocidades y la media ponderada de los volúmenes de las partículas contribuyentes así:

$$\Delta\underline{\underline{\varepsilon}}_p = \Delta t \sum_n \frac{1}{4}\left(\underline{v}_n \otimes \overline{\underline{G}}_{np} + \overline{\underline{G}}_{np} \otimes \underline{v}_n\right) \tag{16}$$

donde la matriz $\boldsymbol{\overline{\underline{G}}_{np}}$ se calcula con base en la ec. (13) y el incremento de las tensiones se obtiene por medio del modelo constitutivo adoptado para cada partícula. Para actualizar la posición y velocidades a partir de los vértices de la malla se utilizan las siguientes expresiones:

$$\underline{x}_p^{t+\Delta t} = \underline{x}_p^t + \Delta t \sum_n \frac{\overline{S}_{np}\underline{q}_n}{m_n} \tag{17}$$

y

$$\underline{v}_p^{t+\Delta t} = \underline{v}_p^t + \Delta t \sum_n \frac{\overline{S}_{np}\underline{\dot{q}}_n}{m_n} \tag{18}$$

El algoritmo completo para resolver el método adoptado puede ser consultad en Buzzi et al. [18].

2.3. Algoritmo de contacto

Para modelar la interacción entre dos materiales, el flujo de detritos y la topografía del terreno por ejemplo, es necesaria la implementación de un algoritmo de contacto. Las bases del algoritmo presentado aquí fueron establecidas por Bardenhagen et al. [20] y mejoradas por Lemiale et al. [21] y Nairn [22]. Para explicar el mecanismo se asume la existencia de dos materiales a y b que interactúan en un determinado nodo n de la malla. Las velocidades de cada material en el nodo son $\underline{v}_n^a$ y $\underline{v}_n^b$ respectivamente. También se define un vector normal, $\hat{n}$, positivo cuando el material a se dirige hacia el material b. El cálculo de este vector es el punto crucial del algoritmo de contacto [22]. Posteriormente, el momento lineal debe ser ajustado mediante la implementación de las características del contacto.

Una vez que la dirección del vector normal es determinada, se debe detectar la existencia del contacto, como es descrito en [20-22].

Para un caso de contacto friccional simple se emplean fuerzas normales y tangenciales descritas en las siguientes expresiones.

$$f_n^{norm} = -\frac{\Delta \underline{q}_n^a \hat{n}}{\Delta t} \tag{19}$$

y

$$f_n^{tan} = -\min\left\{\frac{\Delta \underline{q}_n^a \underline{t}_n}{|\underline{t}_n|\Delta t}; \mu f_n^{norm}\right\} \tag{20}$$

donde Δt es el intervalo de tiempo, $\underline{t}_n$ es un vector tangente al vector normal $\hat{n}$ en la dirección de deslizamiento y μ es el coeficiente de fricción de Coulomb.

3. Caso de análisis: Deslizamiento de Alto Verde

El deslizamiento de Alto Verde ocurrió en la región suroccidental del municipio de Medellín- Colombia, durante el mes de noviembre de 2008. El evento afectó una urbanización residencial que lleva el mismo nombre, compuesta por 16 viviendas unifamilares construidas a lo largo de un trecho de vía central.

El evento se produjo durante una época de alta pluviosidad, la cual fue calificada como la más crítica de los últimos sesenta años [17]. Entre las causas que originaron el deslizamiento fueron citadas: (i) el aumento de los niveles freáticos sobre la vertiente del talud, (ii) infiltración superficial originada por la presencia de un tanque de tratamiento de agua cerca de la corona, (iii) la construcción inadecuada del talud y (iv) intervención antrópica en la parte alta de la ladera [16]. De acuerdo con AMVA [16] los registros de precipitación indicaron un acumulado de 110 mm en los 15 días anteriores al evento.

En la

Figura 1 se observa una imagen del complejo residencial Alto Verde en mayo de 2008, seis meses antes de la ocurrencia del deslizamiento. Por otra parte, al lado derecho de la misma figura se muestra la situación en 2011, después de la ejecución de obras de estabilización. La comparación entre ambas imágenes da una idea clara del tamaño del deslizamiento y de su relación con las estructuras afectadas.

El lado izquierdo de la Figura 2 muestra la situación del evento el mismo día de su ocurrencia. En contraste, el lado derecho muestra la situación dos años después, ya ejecutados trabajos de estabilización.

3.1. Características geométricas y ambiente geológico-geotécnico

Los taludes que conformaban el costado posterior de la unidad residencial tenían alturas variables que alcanzaban hasta 18 m. Las condiciones que desencadenaron la tragedia corresponden al talud de máxima altura y 60° de inclinación como ha sido reconocido en trabajos técnicos previos [16,17].

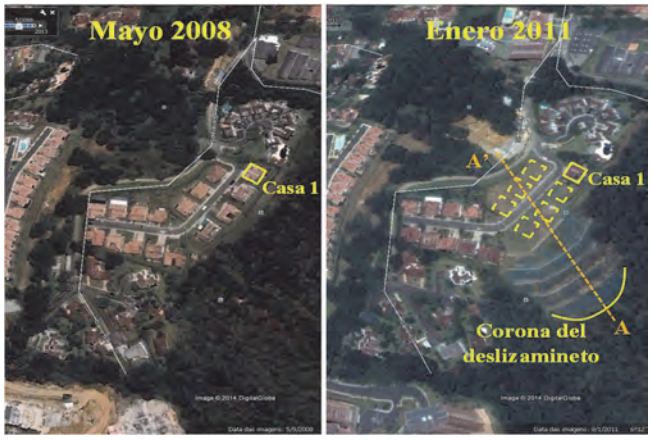


Figura 1. Imágenes satelitales del conjunto residencial Alto Verde.
Fuente: Adaptado de [23]

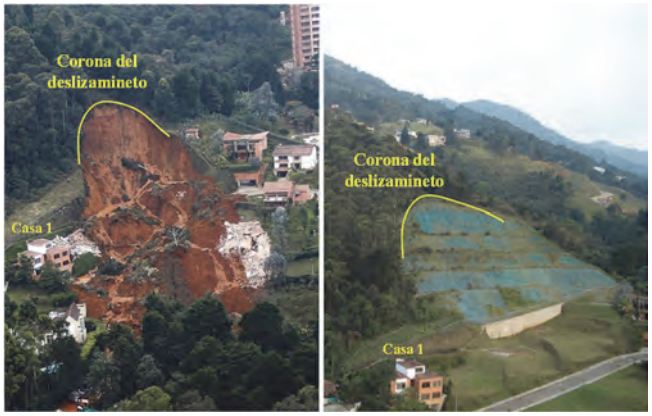


Figura 2. Situación global antes y después de ejecutar las obras de estabilización.
Fuente: Adaptado de [23, 24]

El perfil de suelo del sitio está compuesto por una capa de andosol (ceniza volcánica intemperizada) de un espesor aproximado de 2 metros sobreyaciendo a una capa de suelo residual de Dunita (probablemente fallada, por lo cual fue llamado de Brecha de Dunita) de 15 metros de espesor. El basamento de esta secuencia simple está conformado por la roca brechoide en condición sana. El deslizamiento afectó los horizontes de andosol y de suelo residual superiores, por lo que se resalta su carácter superficial.

Igualmente, el mecanismo observado fue de tipo rotacional tal como se puede verificar en la fotografía de la Figura 3.

La profundidad a la que se encontró el nivel de aguas freáticas fue de 14 metros cerca de la corona del talud y de 7 metros en la región de acumulación [16,17]. Las condiciones aquí descritas y la configuración general de la urbanización en el eje A'-A mostrado en la

Figura 1 se encuentran esquematizadas en la Figura 4.

3.2 Modelo numérico

El modelo numérico consideró algunas simplificaciones buscando reducir el tiempo computacional a valores razonables.

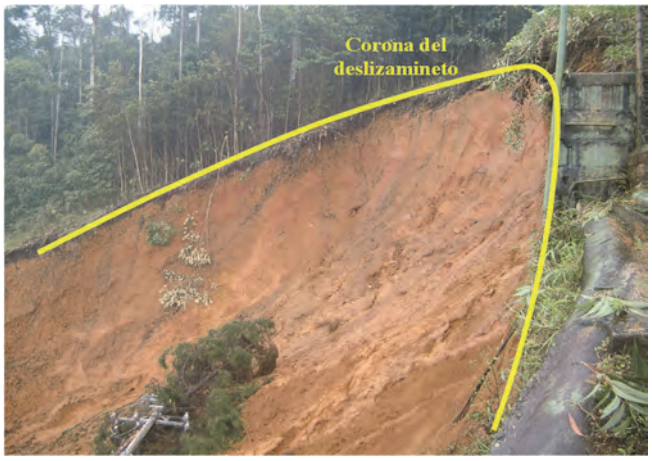


Figura 3. Vista de la corona del deslizamiento.
Fuente: Los autores

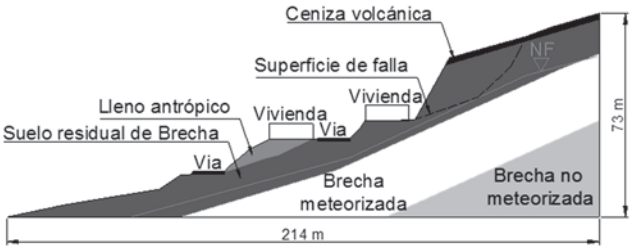


Figura 4. Perfil geológico-geotécnico previo al deslizamiento.
Fuente: Adaptado de: [17]

En primer lugar la representación bidimensional en un estado plano de deformaciones de un problema que efectivamente ocurrió bajo condiciones tridimensionales. La segunda y más importante simplificación se basa en el hecho de que como se mencionó anteriormente este trabajo se centra en la reproducción del fenómeno de flujo de escombros y no en la reproducción del mecanismo inicial de falla. Dicho mecanismo ya fue publicado [17] y verificado por los autores en análisis independientes con técnicas convencionales de equilibrio límite y mediante la observación de levantamientos topográficos posteriores a la ocurrencia del deslizamiento. Procedimientos similares al aquí descrito fueron usados y reportados por Sawada et al. [25].

En la Figura 5. El estrato rígido representa la masa de suelo que no se movilizó durante el incidente, mientras que el talud movilizado representa la masa de suelo que se desplaza ladera abajo. La última simplificación geométrica se refiere a la estructura de las viviendas. En primer lugar la profundidad de las fundaciones se asumió arbitrariamente ya que se espera una falla por tensión cortante directa y su longitud no tiene efecto. En segundo lugar la superestructura se simplificó buscando reducir el tiempo computacional. Esta es una suposición razonable considerando que el objeto de análisis en este trabajo se centra sobre la evolución geométrica del movimiento en masa desde el punto de vista geotécnico.

Las principales características geométricas del modelo se encuentran resumidas en la Tabla 1.

Para resolver el modelo numérico se utilizó el código abierto NairnMPM 8.1.0 [26]. Como fue mencionado anteriormente el estrato subyacente se consideró como un único material indeformable, es decir de rigidez infinita. Sin embargo este material puede interactuar con los demás materiales por medio de las leyes friccionales de contacto descritas en el capítulo anterior. Por otro lado la masa de suelo que se desliza y las estructuras fueron modeladas como materiales elásticos perfectamente plásticos con criterio de ruptura von Mises.

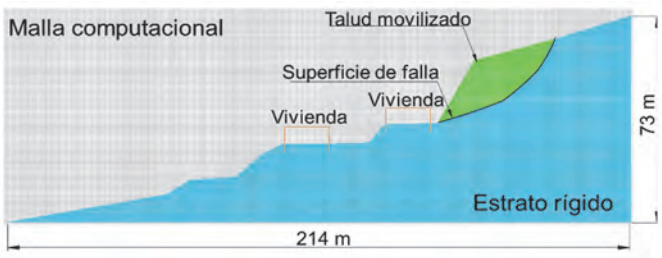


Figura 5. Modelo Numérico.
Fuente: Los autores

Tabla 1.
Características del modelo numérico en MPM

Tamaño de la célula (m)	0.6
Tamaño de los puntos materiales (m)	0.3
Tipo de célula	Cuadrada
Puntos materiales por célula	4
Puntos materiales representando el estrato rígido	68627
Puntos materiales representando el talud	5232
Puntos materiales representando las estructuras	218
Número de nodos en la malla de fondo	45824

Fuente: Los autores

Tabla 2.
Parámetros mecánicos

Parámetro	Suelo	Estructura
γ (kN/m³)	15.0	16.0
E (MPa)	271.0	2000.0
s_u (kPa)	7.2	-
σ_y (MPa)	-	25.0

Fuente: Los autores

El análisis se lleva a cabo en términos de tensiones totales en lugar de efectivas porque el deslizamiento se asume que ocurre bajo condiciones no drenadas debido a la velocidad con que se producen las deformaciones.

Una de las limitaciones que surgen en los modelos de grandes deformaciones es que los parámetros constitutivos referente a los materiales que se usan y reportan usualmente en la ingeniería civil se refieren a ensayos sometidos a pequeñas deformaciones. Esto se justifica porque las obras que se diseñan normalmente operan bajo estas condiciones. Teniendo esto en cuenta se reportan en la Tabla 2. los parámetros utilizados para los materiales considerados en la simulación.

Los valores de los parámetros usados se determinaron con base en los resultados reportados por Gómez et al. [17], los cuales fueron ajustados por medio de retroanálisis, buscando una semejanza en la configuración final observada y el modelo numérico aquí usado.

El coeficiente (μ) que gobierna la ley de contacto friccional entre el material que compone el deslizamiento y el estrato rígido es obtenido mediante la expresión propuesta por Davies [27].

$$\frac{H_{max}}{L_{max}} = \mu \tag{21}$$

donde H_{max} y L_{max} son la distancia vertical y horizontal entre la corona del deslizamiento y su lóbulo frontal. La ec. (21)fue calculada de acuerdo a los datos reportados por Gómez et al [17] y el resultado se encuentra reportado en la Tabla 3.

Por otro lado, debido a que no se contó con información sobre las fundaciones se asumió un coeficiente elevado entre la estructura y el suelo de fundación para evitar una falla de tipo arrancamiento. Entre las partículas del deslizamiento y las estructuras se consideró la inexistencia de fricción. Ver Tabla 3.

Tabla 3.
Coeficientes de fricción

Materiales	μ
Suelo de fundación / masa movilizada	0.4
Suelo de fundación / estructura	4.0
Masa movilizada / estructura	0

Fuente: Los autores

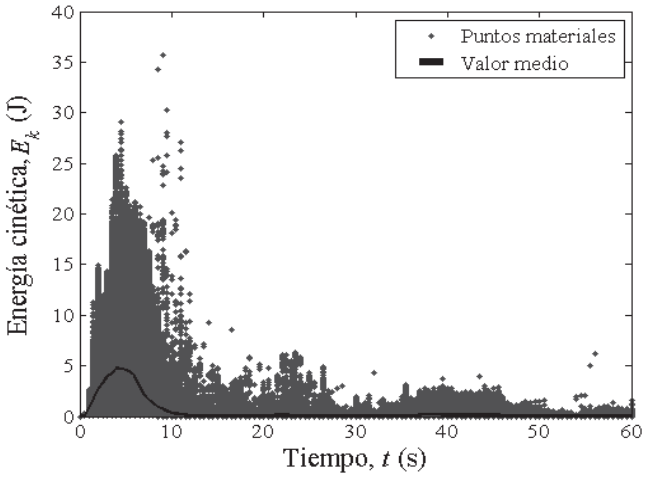


Figura 6. Energía cinética liberada durante el deslizamiento.
Fuente: Los autores

4. Resultados

Para la simulación de este trabajo se utilizó un computador de escritorio con 4 procesadores Intel i7-2600k, y CPU@3.4GHz. El intervalo de tiempo adoptado para la simulación fue de $\Delta t = 2.94.10^{-4}$ s con lo cual el tiempo total de simulación fue de 40 horas. Este tiempo de análisis puede ser disminuido a 10 horas por medio de la paralelización del código y el uso de un cluster computacional de 9 nodos intel i7-870 2.93 GHz CPU, 16 GB de memoria RAM y 1 TB de disco duro.

La simulación del deslizamiento comienza a partir del mecanismo de falla indicado t=0 s, instante en el cual se aplica la aceleración de la gravedad al sistema. La simulación del deslizamiento reproduce los primeros 60 segundos de evolución del movimiento en los cuales es posible acompañar, entre otras variables, la energía cinética de cada uno de los puntos. En la

Figura 6 se presenta gráficamente la energía cinética calculada para todos los puntos movilizados (color verde en la Figura 7) durante el tiempo simulado.

De acuerdo a los resultados de energía cinética (Ver

Figura 6), es posible notar que el momento más crítico se presentó a los 4 s aproximadamente en donde se observa claramente un pico de energía a partir del cual hay disminución de la misma. En la Figura 7 se observa que para el tiempo t=4 s el frente de avance impacta la segunda estructura (nivel topográfico inferior) después de haber pasado por encima de la primera casa (nivel topográfico superior), la cual colapsa.

El valor de energía cinética promedio máximo estimado es de aproximadamente 5.0 J correspondiente a una velocidad de 8.5 m/s. En la misma Figura 7 se muestran diferentes momentos de la simulación en los cuales se puede observar la evolución del flujo. Pasados 10 s la energía cinética se reduce drásticamente, justo después del colapso del segundo nivel de casas las cuales contienen en gran medida el avance del movimiento (Ver Figura 7). A partir de este punto la velocidad del movimiento es baja con algunos picos a los 25 y 40 s atribuidos al efecto de aceleración impuesto apenas por los escalones topográficos del terraceo del terreno.

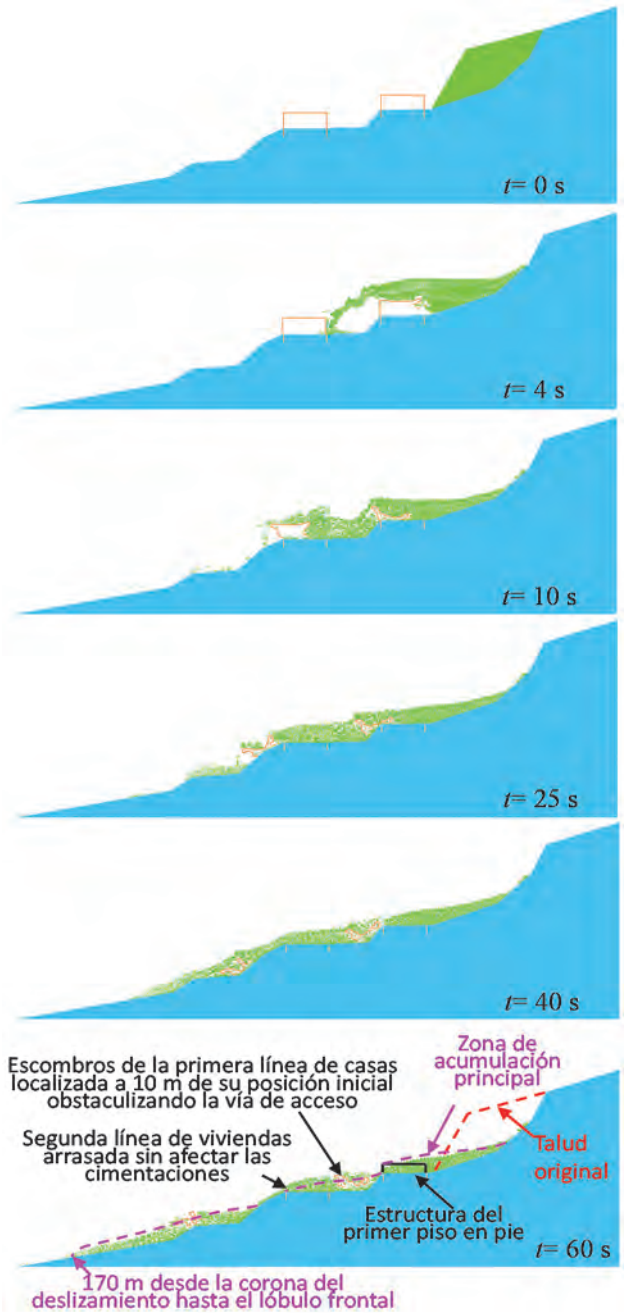


Figura 7. Evolución del movimiento en masa con el tiempo.
Fuente: Los autores

5. Discusión

La simulación realizada se ejecutó a partir de un retroanálisis del mecanismo de falla inicial para ajuste de las propiedades geotécnicas del deslizamiento en masa. Los valores de estos parámetros son compatibles con los que han sido publicados en la literartura para el mismo caso analizado (Ver Tabla 2.). Con la información topográfica disponible fue posible reproducir la trayectoria del *debris-flow* en una distancia de 170 metros desde la corona hasta el lóbulo

frontal que alcanzó el deslizamiento real [17].

De la misma forma es posible resaltar que la simulación reprodujo bien la configuración real del flujo, coincidiendo con las descripciones encontradas en los trabajos técnicos previos y en las fotografías sobre los sitios referentes a las zonas de acumulación.

En la etapa final, 60 s, en la Figura 7 fueron esquematizadas las descripciones encontradas en la literatura [16, 17] en donde la zona de acumulación, la localización de escombros de la primera línea de casas alcanzada por el deslizamiento que obstaculizó la vía de acceso, el arrancamiento de la superestructura de las casas en el nivel topográfico inferior y la distancia máxima desde la corona del talud hasta el lóbulo frontal fueron reproducidas exitosamente. Sin embargo, las descripciones técnicas también relatan que la superestructura del primer piso de las casas en el nivel superior permaneció de pie, fenómeno que no presenta el modelo aquí descrito.

Desde un punto de vista cualitativo se determinó que la ruptura tajante del talud suponía un movimiento extremadamente rápido con velocidades en términos de metros por segundo, AMVA [16]. Esta información fue validada al calcularse una velocidad máxima media del movimiento de 8.5 m/s.

Todas las estructuras impactadas por el deslizamiento sufrieron una pérdida de servicio total, con excepción de una caseta de vigilancia, cuyos daños fueron parciales (Figura 8). De acuerdo con el glosario de la sociedad internacional de mecánica de suelos e ingeniería geotécnica [28], la vulnerabilidad es el grado de pérdida de un elemento dado o conjunto de elementos dentro del área afectada por un deslizamiento, y se expresa en una escala de 0 (sin pérdidas) a 1 (pérdida total).

Para propiedades, la pérdida se estima como el costo de los daños en relación al valor de la propiedad. La estimación de la vulnerabilidad de estructuras y personas amenazadas por deslizamientos es generalmente cualitativa, altamente subjetiva y en muchos casos basada únicamente en registros históricos [29]. Trabajos recientes [30–33] han propuesto marcos teóricos para la evaluación cuantitativa de la vulnerabilidad física de estructuras en función de la intensidad del deslizamiento y de la resistencia estructural de los edificios expuestos.

El modelo propuesto por Li et al. [30] para el cálculo de la Vulnerabilidad, *V*, se basa en la aplicación de la siguiente expresión:

$$V = f(I,R) = \begin{cases} 2\frac{I^2}{R^2} & \frac{I}{R} \leq 0.5 \\ 1 - \frac{2(R-I)^2}{R^2} & 0.5 < \frac{I}{R} > 1 \\ 1 & \frac{I}{R} > 1 \end{cases} \quad (22)$$

en la cual *I* es la intensidad del deslizamiento y *R* es la resistencia del elemento en riesgo. Ambas variables son adimensionales. La intensidad del deslizamiento puede expresarse de diversas maneras mediante alguna de las siguientes variables, o combinación de ellas: velocidad, energía, volumen y/o espesor del material movilizado.

Según Li et al. [30] en las estructuras impactadas por deslizamientos la intensidad del evento puede ser cuantificada en función de la intensidad dinámica que depende de la velocidad del flujo y de su profundidad, de acuerdo con las siguientes ecuaciones:



Figura 8. Caseta de vigilancia en la urbanización Alto Verde.
Fuente: Los autores

$$I = I_{dyn} \cdot I_{dpt} \quad (23)$$

$$I_{dyn} = \begin{cases} 0 & C \leq 5 \times 10^{-7} mm/s \\ 1/36 \, (\log C + 6.3) & C > 5 \times 10^{-7} mm/s \end{cases} \quad (24)$$

$$I_{dpt} = 0.1 \cdot D_{dpt} \quad (25)$$

con: I_{dyn}=Factor de intensidad dinámica; I_{dpt}=Factor de espesura de detritos; *C*=Velocidad promedio del flujo de detritos (en mm/s) y D_{dpt}=Espesor del flujo de detritos (en metros) en el punto de impacto con la estructura.

Los mismos autores proponen que la resistencia física estructural (R_{str}) depende de cuatro factores: Profundidad de la fundación (ξ_{sfd}), tipología estructural (ξ_{sty}), grado de mantenimiento de la estructura (ξ_{smn}) y su altura (ξ_{sht}); de acuerdo con:

$$R_{str} = \left(\xi_{sfd} \cdot \xi_{sty} \cdot \xi_{smn} \cdot \xi_{sht}\right)^{1/4} \quad (26)$$

en donde:

$$\xi_{sfd} = \left(D_{fod}/10\right)^{1/3} + 0.05 \quad (27)$$

Los tres factores restantes dependen de la tipología estructural (ξ_{sty}), estado de mantenimiento de la estructura (ξ_{smn}) y de un factor de resistencia dependiente de la altura de la estructura (ξ_{sht}). Los valores de estos factores se encuentran tabulados por Li et al. [34] y para el caso específico de este trabajo asumen: ξ_{sty}= 1.3, ξ_{smn}= 1.5 y ξ_{sht}= 0.9.

Considerando entonces el modelo de vulnerabilidad y los valores presentados, se estimó la resistencia física de las

estructuras impactadas. La estimativa de la vulnerabilidad para estas estructuras dependerá entonces del espesor de la capa de detritos y de la velocidad del flujo. La Figura 9 presenta la relación entre la vulnerabilidad y el espesor de la capa de detritos para diferentes velocidades. La velocidad de referencia usada fue de 8.5 m/s, que corresponde a la máxima velocidad promedio estimada en la simulación numérica.

Valores adicionales de velocidades fueron usados para visualizar el efecto de esta variable en el comportamiento de la vulnerabilidad. Los valores adicionales usados son: 1 m/s, 0.1 m/s y 0.01m/s. A partir de las observaciones fotográficas y de la propia simulación se estima en 4 m el espesor promedio máximo del deslizamiento, es decir, el espesor calculado a lo largo de la sección más crítica. De esta forma, el punto A en la Figura 9 representa la vulnerabilidad de las casas impactadas por el deslizamiento. El valor estimado de la vulnerabilidad es 1 indicando, tal como realmente ocurrió, destrucción total de la estructura.

Por otra parte, estimativas realizadas para la caseta de vigilancia mostrada en la Figura 8 indican un valor de vulnerabilidad de 0.2. Esto con base en la suposición de una velocidad media de 1 m/s, la cual es justificable si se tiene en cuenta que la caseta se localiza en el flanco derecho del deslizamiento donde las velocidades de flujo y espesor de detritos son menores (estimada en 1.5 m. Figura 8). El punto B en la Figura 9 representa la vulnerabilidad de la caseta, indicando un grado de pérdida de 20% en su funcionalidad estructural, lo cual corresponde a las observaciones de campo.

Ragozin and Tikhvinsky [35] analizaron la vulnerabilidad de personas dentro de edificios expuestos a amenaza por deslizamientos. La Figura 10 presenta la probabilidad de que una persona (PoP) dentro de un edificio sufra lesiones de diferentes niveles, dependiendo de la vulnerabilidad física del edificio. Según los mismos autores, para una vulnerabilidad física estructural de 0.8, serias lesiones pueden esperarse en las personas dentro de la estructura. Para lesiones leves (heridas temporales) la vulnerabilidad estructural recomendada debe ser del orden de 0.2.

En la Figura 9 se han representado los límites de 0.2 y 0.8 para las vulnerabilidades estructurales, definiendo como aceptable V< 0.2, tolerable el intervalo 0.2< V< 0.8 e inaceptable V> 0.8.

De esta forma, es posible deducir que para el caso de Alto Verde, todas las estructuras que sufrieron el impacto del flujo con más de 2.5m de altura de detritos, están dentro de la clasificación de vulnerabilidad inaceptable, lo cual fue verificado para las seis casas que fueron destruidas. Solamente las zonas del deslizamiento que tuvieron velocidades muy bajas (0.1 m/s o menores) indicarían valores de vulnerabilidad tolerables para los espesores de detritos que realmente ocurrieron (entre 2 y 4 m).

Zonas con velocidades moderadas (del orden de 1 m/s), como es el caso de la caseta de vigilancia, producen vulnerabilidades cerca de un intervalo aceptable con espesores de detritos del orden de 1.5 m o menores.

Finalmente, los autores gustaríamos de enfatizar que las tragedias por deslizamientos en la ciudad de Medellín han sido tradicionalmente asociadas a la ocurrencia de épocas lluviosas intensas. No obstante, tal como fue observado por Muñoz et al. [36] en taludes de carreteras en los alrededores de Medellín, aunque existe una gran propensión natural de las laderas de la ciudad a presentar deslizamientos, no es apenas la lluvia la responsable por el gran número de estos eventos, sino la práctica

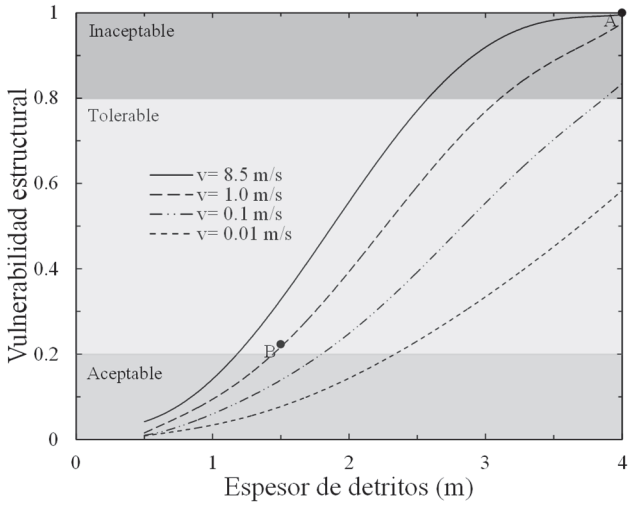


Figura 9. Relación entra la vulnerabilidad física de estructuras y el espesor de detritos para diferentes velocidades de flujo
Fuente: Los autores

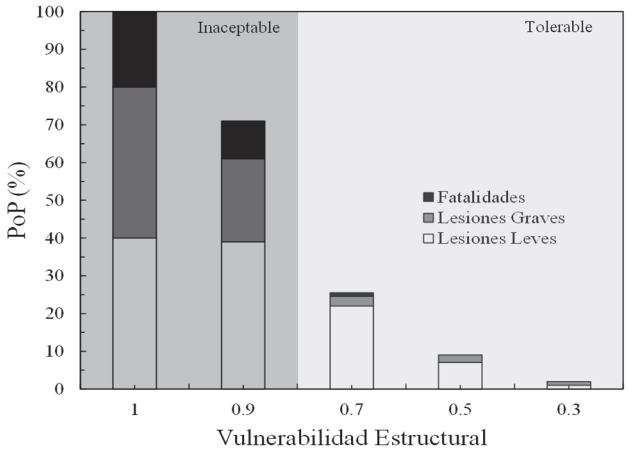


Figura 10. Vulnerabilidad de personas dentro de edificios expuestos a amenazas por deslizamientos.
Fuente: Modificado de: [35]

geotécnica local. Los referidos autores observaron que una gran cantidad de pequeños y moderados deslizamientos son deflagrados claramente por acciones antrópicas.

6. Conclusiones

El objetivo de este trabajo fue verificar la posibilidad de utilizar el MPM como una herramienta para describir los fenómenos asociados a deslizamientos de tierra. Para tal fin se definió un caso de estudio bien documentado que permitió el retro-análisis de las características de grandes deformaciones aquí detalladas.

A pesar de las simplificaciones respecto a modelos constitutivos y geometría fue posible establecer que las descripciones encontradas en la literatura sobre el estado

final del deslizamiento, zonas de acumulación y condiciones de las estructuras describieron adecuadamente el flujo de tierra que ocurrió en Alto Verde.

El MPM permitió calcular la velocidad, energía cinética y alcance del deslizamiento. Este tipo de información es fundamental y permite el análisis de riesgo en taludes en zonas urbanas, el diseño de estructuras de barrera ante flujos de escombros, o determinar distancias de retiro a taludes con probabilidad de ruptura alta. El modelo de análisis cuantitativo de la vulnerabilidad física usado mostró valores compatibles con las observaciones de campo.

Curvas como las presentadas en la Figura 9 pueden ser usadas por las autoridades encargadas de la administración de ciudades susceptibles a deslizamientos, para definir criterios de aceptabilidad de proyectos urbanísticos en laderas. Esta metodología, combinada con análisis de confiabilidad de taludes y laderas, se muestra como una herramienta prometedora para evolucionar eficientemente en los proceso de análisis, evaluación y gestión de riesgos asociados a deslizamientos.

La forma como se abordan actualmente las metodologías de diseño de taludes en la práctica local y, más importante aún, la forma como dichas metodologías están involucrando el factor de la vulnerabilidad estructural y la confiabilidad en el marco de la normativa vigente debe ser revisada.

Es responsabilidad de los administradores locales establecer códigos modernos que lleven en cuenta criterios de aceptabilidad basados en análisis de riesgo y no apenas en estimativas de la amenaza.

Agradecimientos

Los autores de este trabajo gustarían de agradecer a la Coordinación de Perfeccionamiento de Personal de Nivel Superior (CAPES) y el Consejo Nacional de Investigación (CNPq) del gobierno Brasileño por el apoyo económico para la ejecución de este trabajo.

Referencias

[1] Skempton, A.W. and Hutchinson, J., Stability of natural slopes and embankment foundations, Proc. 7th Int. Conf. on Soil Mech. and Found. Eng. Mexico. State-of-art Vol. P, pp. 3-35, 1969.

[2] Hungr, O., Leroueil, S. and Picarelli, L., The Varnes classification of landslide types, an update, Landslides, 11(2), pp. 167-194, 2013. DOI: 10.1007/s10346-013-0436-y

[3] Andersen, S. and Andersen, L., Material-point-method analysis of collapsing slopes, Proceedings of the 1st International Symposium on Computational Geomechanics (COMGEO I), pp. 817-828, 2009.

[4] Al-Kafaji, I.K.J., Formulation of a dynamic material point method (MPM) for geomechanical problems, PhD. Thesis, Stuttgart University, Stuttgart, Germany, 2013.

[5] Sulsky, D., Chenb, Z. and Schreyer, H.L., A particle method for history-dependent materials, Comput. Methods Appl. Mech. Eng., 118, pp. 179-186, 1994. DOI: 10.1016/0045-7825(94)00033-6

[6] Sulsky, D., Zhou, S.J. and Schreyer, H.L., Application of a particle-in-cell method to solid mechanics, Comput. Phys. Commun., 87, pp. 23-252, 1995.DOI: 10.1016/0010-4655(94)00170-7

[7] Bardenhagen, S.G. and Kober, E.M., The generalized interpolation material point method, Tech Sci. Press, 5(6), pp. 477-495, 2004. DOOI: 10.3970/cmes.2004.005.477

[8] Beuth, L., Wieckowski, Z. and Vermeer, P.A., Solution of quasi-static large-strain problems by the material point method, Int. J. Numer. Anal. Meth. Geomech., 35, pp. 1451-1465, 2011. DOI: 10.1002/nag.965

[9] Jassim, I., Stolle, D. and Vermeer, P., Two-phase dynamic analysis by material point method, Int. J. Numer. Anal. Meth. Geomech., 37 , pp. 2502-2522, 2013. DOI: 10.1002/nag.2146

[10] Andersen, S. and Andersen, L., Modelling of landslides with the material-point method, Comput. Geosci., 14, pp. 137-147, 2010. DOI: 10.1007/s10596-009-9137-y

[11] Numada, M., Konagai, K., Ito, H. and Johansson, J., Material point method for run-out analysis of earthquake-induced long-traveling soil flows, JSCE J. Earthq. Eng., 27, pp. 3-6, 2003. DOI: 10.11532/proee2003.27.227

[12] Shin, W., Miller, G.R., Arduino, P. and Mackenzie-Helnwein, P., Dynamic meshing for material point method computations, Eng. Technol., 48(9), pp. 84-92, 2010.

[13] Alonso, E.E., Pinyol, N.M. and Yerro, A., Mathematical modelling of slopes, Procedia Earth Planet. Sci., 9, pp. 64-73, 2014.

[14] Abe, K., Soga, K. and Bandara, S., Material point method for coupled hydromechanical problems, J. Geotech. Geoenviron. Eng., 1, pp. 1-16, 2013. DOI: 10.1061/(ASCE)GT.1943-5606.0001011

[15] Bandara, S. and Soga, K., Coupling of soil deformation and pore fluid flow using material point method, Computers and Geotechnics, 63, pp. 199-214, 2015. DOI: 10.1016/j.compgeo.2014.09.009

[16] Aristizabal-Giraldo, E.V., Informe técnico movimiento en masa barrio El Poblado, sector Cola del Zorro, AMVA, pp.1-3, 2008.

[17] Gómez, E.L. and Giraldo, V.M., Evaluación del deslizamiento en la Urbanización Alto Verde de la ciudad de Medellín, XV Jornadas Geotécnicas de la Ingeniería Colombiana, pp. 141-146, 2009.

[18] Buzzi, O., Pedroso, D.M. and Giacomini, A., Caveats on the implementation of the generalized material point method, Tech Sci. Press, 31(2), pp. 85-106, 2008.

[19] Nairn, J.A. and Guilkey, J.E., Axisymmetric form of the generalized interpolation material point method, Int. J. Numer. Methods Eng., vol. submited, pp. 1-25, 2014. DOI: 10.1002/nme.4792

[20] Bardenhagen, S.G., Guilkey, J.E., Roessig, K.M., Brackbill, J.U., Witzel,W.M. and Foster, J.C., An improved contact algorithm for the material point method and application to stress propagation in granular material, Tech Sci. Press, 2(4), pp. 209-522, 2001. DOI: 10.3970/cmes.2001.002.509

[21] Lemiale, V., Nairn, J. and Hurmane, A., Material point method simulation of equal channel angular pressing involving large plastic strain and contact through sharp corners, Tech Sci. Press, 70(1), pp. 41-66, 2010. DOI: 10.3970/cmes.2010.070.041

[22] Nairn, J.A., Modeling imperfect interfaces in the material point method using multimaterial methods, Comput. Model. Eng. Sci., 1(1), pp. 1-15, 2013.

[23] Google, Google Earth 7.1.2.2041, [Online] 2013, [visitado en: 13/01/2015].

[24] Martínez- Arango, R., En la unidad residencial Alto Verde florece la esperanza, Periodico El Colombiano, publicado: 13/10/2013.

[25] Sawada, K., Moriguchi, S., Yashima, A., Zhang, F. and Uzuoka, R., Large deformation analysis in geomechanics using CIP method, JSME Int. J., 47(4), pp. 735-743, 2004. DOI: 10.1299/jsmeb.47.735

[26] Nairn, J.A., Open-Source MPM and FEA Software – NairnMPM and NairnFEA. [Online]. [13/01/2015]. Disponible en: http://osupdocs.forestry.oregonstate.edu/index.php/Main_Page.

[27] Davies, T.R.H., Spreading of rock avalanche debris by mechanical fluidization, Rock Mech., 15, pp. 9-24, 1982. DO: 10.1007/BF01239474

[28] Davis, T., Geotechnical testing, observation, and documentation. Reston, American Society of Civil Engineers, 2008.

[29] Dai, F., Lee, C. and Ngai, Y.Y., Landslide risk assessment and management: an overview, Eng. Geol., 64(1), pp. 65-87, 2002.

[30] Uzielli, M., Nadim, F., Lacasse, S. and Kaynia, A.M., A conceptual framework for quantitative estimation of physical vulnerability to landslides, Eng. Geol., 102(3–4), pp. 251-256, 2008. DOI: 10.1016/j.enggeo.2008.03.011

[31] Kaynia, A., Papathomakohle, M., Neuhauser, B., Ratzinger, K., Wenzel, H. and Medinacetina, Z., Probabilistic assessment of vulnerability to landslide: Application to the village of Lichtenstein, Baden-Württemberg, Germany, Eng. Geol., 101(1–2), pp. 33-48, 2008. DOI: 10.1016/j.enggeo.2008.03.008

[32] Li, Z., Nadim, F., Huang, H., Uzielli, M. and Lacasse, S., Quantitative vulnerability estimation for scenario-based landslide hazards, Landslides, 7(2), pp. 125-134, 2010. DOI: 10.1007/s10346-009-0190-3
[33] Uzielli, M., Catani, F., Tofani, V. and Casagli, N., Risk analysis for the Ancona landslide—II: Estimation of risk to buildings, Landslides, January, pp. 1-14, 2014. DOI: 10.1007/s10346-014-0477-x
[34] Li, Z., Nadim, F. Huang, H., Uzielli, M. and Lacasse, S., Quantitative vulnerability estimation for scenario-based landslide hazards, Landslides, 7(2) pp. 125-134, 2010. DOI: 10.1007/s10346-009-0190-3
[35] Ragozin, A.L. and Tikhvinsky, I.O., Landslide hazard, vulnerability and risk assessment, Proceedings of the 8th International Symposium on Landslides, pp. 1257-1262, 2000.
[36] Muñoz, E., Martínez-Carvajal, H., Arévalo, J. and Alvira, D., Quantification of the effect of precipitation as a triggering factor for landslides on the surroundings of Medellín – Colombia, DYNA, 81(187), pp. 115-121, 2014. DOI: 10.15446/dyna.v81n187.40640

M.A. Llano-Sena, es estudiante de doctorado en el Programa de Posgrado en Geotecnia de la Universidad de Brasilia, Brasil; actualmente se encuentra realizando una pasantía en la Universidad de Queensland, Australia. Trabaja problemas de grandes deformaciones en geotecnia como penetración y deslizamientos y sus aplicaciones usando el método del punto material (MPM). Maestro en Geotecnia formado en la Universidad de Brasília (2012). Ingeniero Civil graduado en la Facultad de Minas adscrita a la Universidad Nacional de Colombia, Sede Medellín (2010).
ORCID: 0000-0002-4395-8636

M.M. Farias, recibió el título de Ingeniero Civil en 1983 en la Universidad Federal de Ceará, Brasil, el grado de MSc. en Geotecnia en 1986 por parte de la Pontificia Universidad de Rio de Janeiro, Brasil y su PhD en Métodos Numéricos en 1993 en la Universidad de Gales, Reino Unido. PhD. en 1998 formado en el Instituto Tecnológico de Nagoya –NIT, Japón. Es profesor de la Universidad de Brasilia desde 1986 e investigador del Consejo Nacional de Investigación (CNPq) del gobierno Brasileño. Sus principales áreas de acción se enmarcan en temas relacionados al modelamiento constitutivo y numérico aplicado a presas, túneles y diseño mecanístico de pavimentos. Link para información completa acerca del autor: http://lattes.cnpq.br/5345279954551868
ORCID: 0000-0002-5257-911X.

H.E. Martínez-Carvajal, se recibió de Ingeniero Geólogo en 1995 por la Universidad Nacional de Colombia, Medellín, Colombia; es MSc en Mecánica de Suelos, en 1999 de la Universidad Nacional Autónoma de México – UNAM, México y Dr. en Geotecnia, en 2006 en la Universidad de Brasilia, Brasil. Desde 1993 hasta 1999 trabajó para compañías consultoras en el área de Ingeniería Civil como geólogo de campo y exploración. Actualmente se desempeña como profesor asociado del Departamento de Ingeniería Civil y Ambiental en la Universidad de Brasilia, Brasil y Profesor de Cátedra en la Facultad de Minas de la Universidad Nacional de Colombia, Medellín, Colombia. Link para información completa acerca del autor: http://lattes.cnpq.br/2409917419986324
ORCID: 0000-0001-7966-1466.

UNIVERSIDAD NACIONAL DE COLOMBIA
SEDE MEDELLÍN
FACULTAD DE MINAS

Área Curricular de Ingeniería
Geológica e Ingeniería de Minas y Metalurgia

Oferta de Posgrados

Especialización en Materiales y Procesos
Maestría en Ingeniería - Materiales y Procesos
Maestría en Ingeniería - Recursos Minerales
Doctorado en Ingeniería - Ciencia y Tecnología de Materiales

Mayor información:

E-mail: acgeomin_med@unal.edu.co
Teléfono: (57-4) 425 53 68

UNIVERSIDAD NACIONAL DE COLOMBIA
SEDE MEDELLÍN
FACULTAD DE MINAS



DYNA
http://dyna.medellin.unal.edu.co/

The energy trilemma in the policy design of the electricity market

Carlos Jaime Franco-Cardona [a], Mónica Castañeda-Riascos [b], Alejandro Valencia-Arias[c] & Jonathan Bermúdez-Hernández [d]

[a] *Facultad de Minas, Universidad Nacional de Colombia, Medellín, Colombia. cjfranco@unal.edu.co*
[a] *Facultad de Minas, Universidad Nacional de Colombia, Medellín, Colombia. mcastanr@unal.edu.co*
[c] *Facultad de Ciencias Económicas y Administrativas, Instituto Tecnológico Metropolitano, Medellín, Colombia. jhoanyvalencia@itm.edu.co*
[d] *Facultad de Ciencias Económicas y Administrativas, Instituto Tecnológico Metropolitano, Medellín, Colombia. jonathanbermudez@itm.edu.co*

Received: January 23th, 2015. Received in revised form: September 4rd, 2015. Accepted: September 8th, 2015.

Abstract
The energy "Trilemma" seeks to develop an electricity market which simultaneously ensures environmental quality, security of supply, and economic sustainability. The objective of this paper is to present the "Trilemma" energy as the latest trend in the design of energy policy. For this, a theoretical framework is presented in sections 2 and 3, in section 4 and 5 the importance of security of supply and economic sustainability are discussed, respectively. In section 6 the energy "trilemma" is presented, in section 7 a brief state of the art is showed. Finally in section 8, it is approached three different electricity markets. It is concluded that the regulator has passed in recent years from encouraging a liberalized market scheme, to promote a scheme based on intervention through policies that affect the market competitiveness but allow achieving its environmental goals.

Keywords: electricity market; security of supply; environmental quality; economic sustainability.

El trilema energético en el diseño de políticas del mercado eléctrico

Resumen
El "Trilema" energético busca desarrollar un mercado eléctrico donde se garantice de manera simultánea la calidad ambiental, la seguridad de suministro y la sostenibilidad económica. El objetivo de este artículo es presentar el "Trilema" como la última tendencia en el diseño de política energética. Para esto se presenta un marco teórico en las secciones 2 y 3, en la sección 4 y 5 se discute la importancia de la seguridad de suministro y sostenibilidad económica, respectivamente. En la sección 6 y 7 se presenta el "Trilema" energético y un breve estado del arte, respectivamente. Finalmente, en la sección 8 se abordan tres mercados eléctricos diferentes. Se concluye que el regulador ha pasado en los últimos años de promover un esquema de mercado liberalizado, a promover un esquema basado en el intervencionismo a través de políticas que afectan la competitividad del mismo pero que le permiten alcanzar sus objetivos ambientales.

Palabras clave: mercado eléctrico; seguridad de suministro; calidad ambiental; sostenibilidad económica.

1. Introducción

Varios países alrededor del mundo han adoptado políticas ambientalmente amigables con el objetivo de cambiar los sistemas convencionales de energía a sistemas bajos en carbono [1], estas políticas están enfocadas en la reducción de emisiones del sector eléctrico el cual es responsable de un porcentaje importante de gases efecto invernadero a nivel mundial. Se pueden tomar varias medidas para lograr la reducción de emisiones, como la implementación de políticas de promoción de energías renovables, políticas de gestión de la demanda de electricidad o políticas directas como el impuesto al carbono [2,3]

El objetivo de este artículo es presentar el "Trilema" energético como la nueva tendencia en el diseño de política energética; el "Trilema" energético busca compatibilizar los objetivos ambientales, de seguridad de suministro y sostenibilidad económica. Para lograr los objetivos de calidad ambiental y seguridad de suministro en el mercado eléctrico puede implementarse una serie de políticas diferentes desde el lado de la oferta y la demanda del mercado de electricidad; aunque este artículo se enfoca de manera

© The author; licensee Universidad Nacional de Colombia.

especial en las políticas desde el lado de la oferta. Igualmente se presenta una pequeña revisión del estado del arte y un análisis general de las políticas de calidad ambiental y de seguridad de suministro en tres mercados eléctricos diferentes.

2. Esquemas de apoyo a las energías renovables y de reducción de emisiones

En esta sección se describen las políticas de calidad ambiental aplicables a la oferta de electricidad como los esquemas de apoyo a las energías renovables y de reducción de emisiones.

Las políticas de promoción de energías renovables, también llamados esquemas de apoyo de energías renovables establecen incentivos para ayudar a este tipo de energías a superar las barreras de entrada al mercado, facilitando su expansión, el avance en la curva de aprendizaje y por ende la reducción de sus costos; este tipo de políticas pueden ser evaluadas según su eficiencia, costo-efectividad y la capacidad de estas para incentivar mejoras tecnológicas y reducir costos [4,5].

Los instrumentos que apoyan la operación de las energías renovables son instrumentos de mercado que comprenden instrumentos de cantidad e instrumentos de precio; los instrumentos de cantidad fijan una cantidad de energía renovable que debe ser producida mediante un mecanismo de mercado como una subasta, mientras que los instrumentos de precio determinan el precio al cual debe ser remunerada la energía renovable. Algunos ejemplos de instrumentos basados en cantidad son: las licitaciones, los mercados de certificados verdes y las obligaciones renovables; entre los instrumentos basados en precio se encuentran feed-in tariff, feed-in premium e incentivos fiscales [6].

En la Obligación Renovable o Cuota Renovable el regulador establece sobre los suministradores de electricidad un mínimo porcentaje de energía renovable que deben suplir, la Obligación Renovable también es conocida como Portafolio Estándar [7].

En cuanto al Mercado de Certificados Verdes, en este es asignado un certificado verde por cada MWh de electricidad renovable, puede ser combinado con una obligación renovable, es decir los suministradores de electricidad deben comprar certificados verdes en la cantidad equivalente a su obligación o pagar una multa según sea su déficit; de este modo los generadores renovables son remunerados a través del precio de electricidad y del certificado verde [5].

Un feed-in tariff es una tarifa fija que reciben los generadores renovables por cada MWh renovable inyectado a la red, un feed-in premium es una prima recibida por los generadores de electricidad de forma adicional al precio de electricidad [8]. Bajo el esquema feed-in premium las alzas en el precio de electricidad pueden conllevar a "windfall profits" –beneficios inmerecidos–, es por eso que se han implementado sistemas "cap and floor" junto al feed-in premium bajo los cuales se define un límite superior e inferior, el límite superior limita el ingreso recibido por los generadores al igual que la carga monetaria asumida por los consumidores, mientras que el límite inferior asegura que el feed-in premium otorgado a los generadores permitirá remunerar la inversión renovable reduciendo los riesgos de los inversores [9,10]. Otro tipo de feed-in tariff es el feed-in tariff contrato por diferencias, en este los generadores venden su electricidad en el mercado mayorista recibiendo el precio de electricidad, posteriormente podrán reclamar o devolver la diferencia entre el precio de electricidad del mercado y el precio fijado en el contrato de largo plazo según esta diferencia sea negativa o positiva, respectivamente [11].

Aquellas medidas para lograr la reducción de emisiones como el mercado de carbono e impuesto al carbono tienen como objetivo transmitir los costos sociales asociados a la contaminación ambiental o externalidad negativa a los generadores fósiles; en teoría la internalización del precio de carbono en los precios de oferta de los generadores fósiles aumenta el precio de electricidad y encarece la generación fósil [12]. Las medidas de reducción de emisiones al igual que los esquemas de apoyo de energías renovables también se dividen en medidas basadas en precio y en cantidad, las medidas basadas en precio como el impuesto al carbono establecen el precio de las emisiones en tanto las medidas basadas en cantidad como un mercado de carbono determinan el precio del derecho de emisión mediante un mecanismo competitivo de oferta y demanda, donde cada generador fósil puede emitir una cantidad máxima de emisiones o "cap", cada tonelada de carbono emitida a la atmósfera debe ser compensada por un derecho de emisión, por lo cual se recurre al mercado de carbono para comprar o vender derechos de emisión según se presente déficit o superávit de estos [6,10]

3. Gestión de la demanda

Desde el lado de la demanda del mercado eléctrico pueden implementarse políticas dirigidas a reducir la demanda de electricidad e indirectamente las emisiones, por ejemplo políticas de Eficiencia Energética, Conservación Energética y Respuesta a la Demanda [3,13,14]. Estas políticas pueden ser agrupadas dentro de un concepto mayor que es la Gestión de la Demanda, esta se define como todas las tecnologías, acciones y programas aplicables a la demanda que reducen el consumo de energía permitiendo la reducción de los costos de energía del sistema, y contribuyendo a la reducción de emisiones y seguridad de suministro [15].

Como se mencionó previamente las políticas de Eficiencia Energética están orientadas a reducir la demanda de electricidad y por lo tanto las emisiones del sector eléctrico [2]. Algunas medidas para mejorar la eficiencia energética son la adopción de estándares de emisión, el uso de redes inteligentes, el empleo de vehículos híbridos y combustibles más eficientes, el uso de equipos ahorradores, la mejora de sistemas de enfriamiento y aislamiento térmico, entre otros [13].

La Conservación Energética se refiere a la reducción del consumo de electricidad debido a cambios de comportamiento del consumidor, en tanto la Eficiencia Energética permite la disminución del consumo energético a través de la adopción de tecnologías más eficientes [16]

La Respuesta a la Demanda es el cambio del consumo de electricidad del consumidor final como respuesta a cambios

en el precio de electricidad, supone que la demanda del consumidor es elástica, esto significa que se producirá una reducción de la demanda del consumidor cuando los precios de electricidad son altos [15].

La microgeneración o autogeneración, es decir la producción de electricidad por parte de los consumidores también se relaciona con la gestión de la demanda, en el corto plazo esta contribuye con la seguridad de suministro aunque en el largo plazo puede distorsionar las señales de inversión del mercado [1].

4. Importancia de la seguridad de suministro asociada a la expansión de energías renovables

Las energías renovables son recursos sostenibles no contaminantes que reducen la dependencia de los combustibles fósiles importados los cuales se han caracterizado por precios volátiles en los últimos años. Sin embargo, la intermitencia de energías renovables como eólica y solar fotovoltaica puede afectar la continuidad en el suministro de electricidad; en este caso la intermitencia se define como la indisponibilidad del recurso por condiciones climáticas [17]. Las **energías renovables intermitentes** son limitadas para cubrir la demanda pico por lo que se requieren otras tecnologías flexibles; es decir que puedan reaccionar rápidamente a cambios de consumo o producción, no obstante la presencia de energías renovables puede afectar las tecnologías más flexibles al reducir su eficiencia [18]. Aunque, existen otras energías renovables no intermitentes como biomasa y geotermia.

Así una de las principales restricciones que enfrenta la producción a partir de fuentes renovables como eólica y solar es su naturaleza intermitente, por lo cual su despliegue representa un desafío para la seguridad de suministro y crea la necesidad de aumentar la confiabilidad del sistema [19]. En cuanto a la inversión en capacidad en el largo plazo el regulador puede adoptar dos estrategias: "hacer algo" implementando un mecanismo de capacidad para garantizar la seguridad de suministro, o "no hacer nada". En el primer caso "hacer algo" implica la implementación de un mecanismo de capacidad ya sea un pago por capacidad, un mercado de capacidad o una reserva estratégica; el pago por capacidad consiste en un pago fijado por el regulador y otorgado a los generadores por su disponibilidad, en tanto en el mercado de capacidad este pago es otorgado mediante subasta y en la reserva estratégica las centrales viejas reciben una contribución por su disponibilidad en lugar de ser cerradas. En el segundo caso "no hacer nada" implica confiar en que el mercado por si sólo proveerá los incentivos de inversión en el largo plazo, este enfoque también es conocido como "mercado de sólo energía"[20, 21]. En un mercado de "sólo energía" se asume un mercado perfectamente competitivo, donde las ofertas de los generadores reflejan sus costos reales, la demanda refleja la necesidad de compra, el precio de equilibrio equivale al precio marginal del sistema y es igual al costo de producción marginal del sistema [22]. No obstante, algunos argumentan fallas de mercado dado que el mercado no provee los incentivos suficientes para garantizar la seguridad de suministro [21,24].

Para que se invierta en energías renovables estas deben ser subsidiadas, a su vez la expansión de energías renovables genera la necesidad de disponer de tecnologías flexibles que sirvan de back-up, al mismo tiempo el despliegue de energías renovables reduce los precios pico de electricidad que remuneran la inversión de aquellas centrales más costosas que pueden garantizar el cubrimiento de la demanda en condiciones de escasez, este fenómeno es conocido como "missing money" [17,23]. Por lo cual la expansión de energías renovables requiere la aplicación complementaria de un mecanismo de capacidad o de una política de gestión de la demanda, o incluso la presencia de tecnologías de almacenamiento sin olvidar el papel de las interconexiones internacionales de electricidad del país [24]. Igualmente, es necesario el desarrollo de nuevas redes de transmisión y distribución más flexibles aptas para facilitar el despliegue de energías renovables [25].

5. Importancia de la sostenibilidad económica asociada a la expansión de energías renovables

La implementación de las políticas para promover las energías renovables, reducir emisiones y garantizar la seguridad de suministro implica un costo para el sistema que es transmitido a la tarifa de electricidad pagada por el consumidor. Aunque las inversiones en energías renovables no son atractivas y necesitan ser subsidiadas, a medida que aumente su participación en el mercado se producirá una reducción de costos haciéndolas más atractivas para los inversionistas, reduciendo la carga tarifaria asumida por el consumidor [10,17]

En el caso de los subsidios a las energías renovables estos pueden ser financiados a través de la tarifa de electricidad cobrada al consumidor o distribuyéndose en el cobro de impuestos entre los contribuyentes [26].

Aunque un parque de generación 100% renovable es teóricamente posible, garantizar la seguridad de suministro requeriría una gran cantidad de capacidad instalada, que generaría un excedente de capacidad ocioso en períodos de alta disponibilidad renovable implicando altos costos para el sistema [27].

A favor del despliegue renovable algunos argumentan la reducción del precio de generación, es decir al tener costos variables insignificantes las tecnologías renovables permiten abastecer la demanda de electricidad con tecnologías menos costosas desplazando la curva de oferta de electricidad [28].

6. El "Trilema" energético

Dado que el cambio climático es acelerado por las emisiones de carbono, la descarbonización es el principal ingrediente en la concepción de políticas energéticas. Igualmente, los costos económicos de la descarbonización deben ser considerados para determinar el nivel óptimo de inversión que se requiere. La descarbonización puede presentarse a través de la expansión de energías de naturaleza intermitente lo cual puede arriesgar la seguridad de suministro. Por estas razones al diseñar una política energética deben considerarse tres elementos: la calidad ambiental, la seguridad de suministro y todos los costos asociados; estos tres elementos constituyen el "trilema"

energético, y pueden presentarse incompatibilidades entre los mismos al considerar que algunas tecnologías renovables son intermitentes aportando poco a la seguridad de suministro, y además requieren de subsidios lo cual incrementa los costos del sistema [29, 30]. En la Fig. 1 se presentan estos tres elementos en negrita; la calidad ambiental es representada por el despliegue renovable y la reducción de emisiones, los costos asociados son representados por el precio de electricidad. En la Fig. 1 las políticas de gestión de la demanda reducen la demanda de electricidad y contribuyen de forma indirecta a garantizar la seguridad de suministro, el despliegue de energía renovable y la reducción de emisiones; los esquemas de apoyo a las energías renovables y de reducción de emisiones fomentan la calidad ambiental y afectan el precio de electricidad, por último los mecanismos de capacidad garantizan la seguridad de suministro, son un complemento para las energías renovables y su valor es cargado al precio de electricidad.

7. Revisión del estado del arte

La revisión del estado del arte se ha dirigido a identificar las investigaciones donde se estudien los elementos del "trilema" energético. Por el momento, los resultados de la búsqueda sugieren que la mayoría de investigaciones se han dirigido a estudiar la coexistencia de políticas de apoyo a las energías renovables y de reducción de emisiones, los demás políticas han sido estudiadas para el sector eléctrico de manera aislada. Por lo tanto, escasas investigaciones se han enfocado en estudiar la coexistencia del portafolio de políticas derivadas del "trilema" energético.

En Del Río [12] se estudian la interacción entre el mercado de carbono europeo y los esquemas de apoyo a las energías renovables, se afirma que la sinergia entre estas políticas puede verse afectada por diferentes objetivos y alcances territoriales; además la coexistencia del mercado de carbono y otros esquemas puede ser justificada si estos últimos generan un beneficio social o son eficientes dinámicamente, es decir si producen un avance en la curva de aprendizaje. Adicionalmente, la reducción de emisiones a partir del despliegue de energías renovables no es económicamente eficiente; por otro lado, promover las energías renovables desde el mercado de carbono es improbable si el precio de los derechos de emisión es inferior al costo de inversión de estas tecnologías.

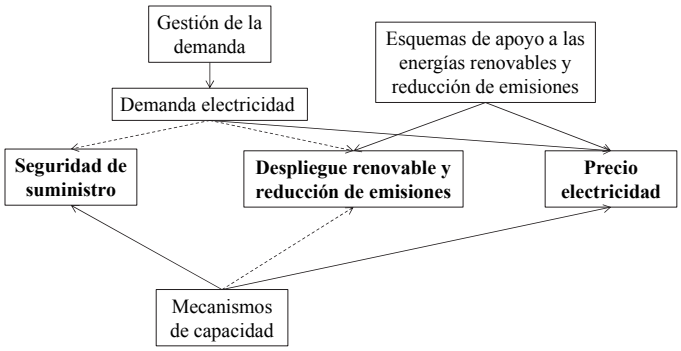


Figura 1. El "trilema" energético.
Fuente: Los autores

En Lehmann & Gawel [31] se analiza la coexistencia de esquemas de apoyo a las energías renovables y el mercado de carbono; en este artículo se afirma que el mercado de carbono no es el instrumento más eficaz para lograr un cambio tecnológico, sin embargo comparado con los esquemas de apoyo de las energías renovables es un medio más eficaz para reducir emisiones; además los esquemas de apoyo a las energías renovables reducen las emisiones y por lo tanto la demanda de derechos de emisión lo cual disminuye el precio del derecho de emisión.

Skytte [32] estudia el "trilema" energético realizando un análisis de las sinergias entre los instrumentos políticos empleados, resalta la dificultad que surge al intentar lograr de forma simultanea las metas planteadas en el "trilema" energético debido a las diferencias en los ámbitos de aplicación de los instrumentos políticos y metas entre sectores.

Sáenz de Miera et al. [10] emplean un modelo de regresión para estudiar el efecto de los incentivos de las energías renovables sobre el precio de electricidad del mercado eléctrico español, concluyen que la expansión renovable tras la implementación del feed-in tariff reduce el precio de electricidad, y esta reducción es mayor que el aumento del precio de electricidad final cobrado a los consumidores.

La interacción entre el mercado de carbono y el comercio de certificados verdes al igual que su influencia sobre el precio del consumidor es estudiada por Hindsberger et al. [33] para la región de Países Bálticos, ellos emplean un modelo de equilibrio parcial. Concluyen que dicha interacción induce a

patrones de inversión en el sector eléctrico y que los incentivos a las energías renovables afectan la inversión en tecnologías no renovables que aportan más a la seguridad de suministro.

Además Unger y Ahlgren [34] analizan la interacción entre un mercado de carbono y de certificados verdes en el Mercado de Electricidad Nórdico, mediante un modelo de optimización que emplea programación lineal. Concluyen que la cuota renovable establecida en el mercado de certificados verdes reduce el precio de electricidad mayorista y el precio de los derechos de emisión, el efecto sobre el precio de electricidad minorista depende de si la reducción del precio de electricidad mayorista compensa el precio del certificado verde y la magnitud de la cuota renovable.

Para analizar la interacción del mercado de carbono y de certificados verdes en el Reino Unido Nelson [35] emplea un modelo de equilibrio parcial; concluye que alcanzar las metas de reducción de emisiones y generación renovable requiere la coexistencia de un mercado de carbono y de certificados verdes.

El efecto de un mercado de certificados verdes, feed-in tariff y mercado de carbono es estudiado por De Jonghe et al.[6] mediante un modelo de optimización que considera tres países Francia, Alemania y Bélgica; ellos concluyen que en países con alto desarrollo de energía nuclear los incentivos de reducción de emisiones favorecen más la energía nuclear que la renovable.

Palmer et al. [36] presentan un modelo de simulación determinístico para evaluar la interacción de políticas de

certificados verdes y del mercado de carbono en Estados Unidos; el modelo simula el mercado eléctrico empleando un algoritmo iterativo de convergencia para encontrar el equilibrio del mercado eléctrico.

Rathmann [37] emplea un modelo de simulación para evaluar el efecto de los esquemas de apoyo a las energías renovables y el mercado de carbono en el mercado eléctrico alemán, en el artículo se afirma que los esquemas de apoyo a las energías renovables provocan un desplazamiento de las tecnologías convencionales reduciendo el precio de electricidad, aunque el precio de electricidad final cobrado a los consumidores es aumentado por los subsidios.

Empleando un modelo de equilibrio general multi-sectorial y multi-regional Böhringer et al. [38] estudian el mercado eléctrico y de carbono de la Unión Europea al igual que los subsidios a las renovables; ellos concluyen que la segmentación sectorial del mercado de carbono y la doble regulación de los países conlleva a una reducción de emisiones excesivamente costosa.

Ford [39] desarrolló un modelo de dinámica de sistemas para estudiar la influencia de un mercado de carbono sobre el sector eléctrico en Estados Unidos. El mercado de certificados verdes desde la dinámica de sistemas ha sido estudiado por Hasani-Marzooni & Hosseini [40] quienes realizaron un modelo para estudiar la inversión en capacidad eólica en presencia de un mercado de certificados verdes. También, Vogstad [41] construyó un modelo de dinámica de sistemas para estudiar el mercado de certificados verdes en el sistema Eléctrico Nórdico. Finalmente, Dyner [42] evaluó el efecto que tienen los incentivos de las energías renovables en el mercado eléctrico colombiano empleando dinámica de sistemas.

Por último, Fagiani et al. [43] desarrolla un modelo del mercado eléctrico español en matlab, que emplea elementos de dinámica de sistemas y de simulación basada en agentes para estudiar los efectos y causalidades derivados de la coexistencia de una política de mercado con piso al precio de carbono, Feed-in Tariff y mercado de certificados verdes.

Otros modelos desde dinámica de sistemas han sido desarrollados por Hsu [44] y Alishahi et al. [45] para evaluar los efectos del Feed-in Tariff sobre la energía solar y eólica respectivamente; así mismo, Assili et al. [46] y Hasani & Hosseini [47] han modelado un pago por capacidad y mercado de capacidad, respectivamente. Adicionalmente, Weigt et al. [48] desarrollaron un modelo genérico de dinámica de sistemas para estudiar el pago por capacidad.

8. Casos mercado eléctrico de España, UK y Colombia

En esta sección se presentan los elementos que componen el "trilema" energético desde la perspectiva del mercado eléctrico de tres países diferentes: España, Reino Unido y Colombia. En cuanto al desarrollo de energía eólica y solar, el mercado eléctrico español es uno de los más importantes de Europa; y su gran despliegue renovable está asociado a problemas de sostenibilidad económica [8]; por otro lado Reino Unido ha sido pionero en el proceso de liberalización del mercado eléctrico, desde entonces el mercado eléctrico británico ha atravesado una serie de reformas, la última es una reforma radical del sector enfocada en garantizar la calidad ambiental, seguridad de suministro y sostenibilidad económica [49, 50]. Finalmente, Colombia es un mercado dominado por generación hidráulica, esto crea una alta dependencia hacia las fuentes fósiles en épocas de escasez hidráulica, además el gobierno estudia la posibilidad de promover el despliegue de energías renovables [51].

8.1. España

En España el instrumento de mercado predominante para el apoyo de energías renovables es el feed-in tariff, el cual ha sido aplicado desde 1994 [52]. Mediante el Real Decreto 661 de 2007, los generadores renovables podían escoger entre un sistema feed-in tariff y feed-in premium, excepto para solar fotovoltaica que sólo recibía feed-in tariff. La opción de feed-in premium establece que los generadores renovables reciben el precio de electricidad más una prima [8]. Aunque estos sean los incentivos actuales existentes en España, a partir del Real Decreto-ley 1 de 2012 se suspendieron los incentivos económicos para las nuevas instalaciones renovables; debido a que las ayudas a las renovables encarecían el precio de electricidad cobrado a los consumidores y aumentaban el déficit tarifario [53].

En Ciarreta et al. [29] se argumenta que en las etapas iniciales del despliegue renovable cuando la capacidad renovable era baja (año 2008 a 2009), los incentivos a las energías renovables eran cubiertos; sin embargo, desde el año 2010 la producción renovable alcanzó un alto porcentaje imponiendo altos costos para el sistema, además algunas tecnologías más maduras como la eólica representaban un menor costo para el sistema mientras la solar fotovoltaica era la más costosa. A partir de la nueva regulación los incentivos a las energías renovables fueron cancelados en 2013, aunque el objetivo de esta nueva regulación era cubrir los costos de los productores y generar una rentabilidad razonable, la falta de incentivos y el cambio regulatorio han estancado la inversión en nueva capacidad renovable.

La ventaja del feed-in Premium es que depende del precio de electricidad y por lo tanto de las señales de mercado que este refleja, es decir el sistema basado en un feed-in premium refleja el comportamiento de la demanda y promueve el generación renovable durante horas pico, aunque puede generar ingresos excesivos o wind fall profits como se mencionó anteriormente, es por ello que en 2007 se introdujo un sistema "cap and floor" al feed-in premium. El feed-in premium es una opción orientada a generar mayores ingresos para los inversores, mientras que el feed-in tariff representa una menor carga para los consumidores y provee una mayor seguridad para la inversión en tecnologías [8].

En cuanto a la seguridad de suministro, los mecanismos de capacidad desarrollados en España han sido mecanismos de precio, es decir a partir de un precio se busca obtener cierto nivel de energía firme, el problema es fijar el precio adecuado para obtener la cantidad requerida. Desde el año 1998 se realizaba un pago de capacidad extra basado en la disponibilidad promedio de las térmicas y en la producción histórica promedio para las hidroeléctricas [20]. En el año 2007 este mecanismo cambio según la ORDEN ITC/2794/2007, dividiéndose en dos servicios:

El primero es el servicio de disponibilidad, cuyo objetivo

es permitir que el operador del sistema celebre contratos bilaterales, con una duración no superior a un año; este mecanismo promueve la seguridad de suministro en el mediano plazo. El segundo es el Incentivo a la Inversión (II), a partir de este las plantas de generación nuevas y de más de 50 MW reciben durante sus primeros 10 años de operación un pago anual que es función de un Índice de Cobertura; este mecanismo promueve la seguridad de suministro en el largo plazo [54].

Por otro lado, en el mercado eléctrico español la variabilidad eólica planteaba una pregunta crítica: ¿Cómo abastecer la demanda cuando no se presenten vientos?, el despliegue de térmicas a gas facilitó la expansión eólica, aunque otras tecnologías como la hidráulica también ofrecían un "back-up" para la expansión solar y eólica. Si bien la expansión renovable intermitente requería la complementariedad de otras tecnologías, en el mercado eléctrico español se han observado durante los últimos años un aumento en el factor de capacidad superior al 20% de las tecnologías renovables solar y eólica, al igual que una reducción del factor de capacidad de gas a niveles inferiores al 10% [53,55].

Otro aspecto interesante del mercado eléctrico español es que los altos subsidios recibidos por solar fotovoltaica provocaron un crecimiento excesivo de esta tecnología durante el año 2008, en dicho año solar fotovoltaica alcanzó los 3400 MW instalados aunque la meta el gobierno para el año 2010 eran 400 MW, en ese entonces la capacidad instalada solar fotovoltaica era superior a la capacidad instalada eólica. Esta burbuja de capacidad se vio reflejada en el aumento de la tarifa de electricidad final [53, 56].En este punto es evidente la relevancia de la curva de aprendizaje de las tecnologías renovables a nivel global y local a la hora de fijar los subsidios que reciben los generadores renovables. El crecimiento de la capacidad instalada eólica en España también fue importante gracias a los esquemas feed-in tariff, las metas de expansión de capacidad del gobierno y la promoción de la participación eólica en el pool de electricidad; es decir la combinación del ambiente institucional y de las capacidades de las firmas conllevaron a altos niveles de difusión eólica en España [7].

8.2. Reino Unido

Con el fin de fomentar la competitividad del mercado eléctrico británico se produjo la liberalización de este mercado en el año de 1989, en este nuevo mercado se promovía la competencia en las actividades de generación y comercialización, en tanto las actividades de generación, transmisión y distribución fueron segmentadas; igualmente se creó el mercado de electricidad mayorista o pool de electricidad [57].

El pool de electricidad funcionaba mediante un sistema marginalista de precios, durante la década de los 90's se presentaron alzas en los precios de electricidad aunque los generadores habían reducido sus costos de generación debido a que eran más eficientes, bajo estas circunstancias se sospechaba una manipulación de los precios del mercado por parte de los generadores [58]. Esta situación conllevo a una nueva reforma de mercado en 2001, en esta reforma el pool de electricidad fue reemplazado por un sistema de contratos, el nuevo mercado fue llamado NETA (New Electricity Trading Arrangement) e incluía a Gales e Inglaterra. Posteriormente, el mercado fue reformado de nuevo al incluir también Escocia pasando a llamarse BETTA (British Electricity Trading and Arrangement) [59].

Actualmente, el gobierno británico planea implementar una nueva reforma estructural del mercado eléctrico que implicará un cambio radical en el negocio de la electricidad en este país.

En 2011 el gobierno británico publico el libro blanco donde planteaba las medidas que contienen la nueva reforma, desde entonces sucesivas aclaraciones han sido publicadas para la implementación de la reforma, el objetivo del gobierno con esta reforma es transformar el sector eléctrico británico garantizando la seguridad de suministro, al igual que la sostenibilidad económica y ambiental [60].

El primer mecanismo para incentivar las energías renovables en el mercado eléctrico británico fue el esquema de Obligación de Combustibles no Fósiles, este fue introducido en el año 1990 y funcionaba como una subasta en la cual los proyectos ganaban contratos de largo plazo; sólo un 17% de los proyectos ganadores de la subasta fueron construidos y entraron en operación; únicamente tres de las más grandes empresas del mercado participaban en este mecanismo. Con la entrada en vigencia en el año 2000 de la Obligación Renovable las seis empresas más importantes del mercado o "big six" comenzaron a participar en este mecanismo, el cual impone a los suministradores de electricidad una obligación según la cual un porcentaje de la electricidad suministrada debe provenir de fuentes renovables, esta obligación debe ser soportada mediante certificados verdes los cuales son asignados por Ofgem (el regulador del mercado) por cada MWh renovable. Los suministradores de electricidad pueden comerciar con estos certificados para cumplir con su obligación, las compañías que no cumplen con su obligación asumen una multa. Aunque a partir del año 2009 se introdujo el "banding" según el cual se asigna diferentes cantidades de certificados verdes dependiendo del tipo de tecnología renovable. El mercado de certificados verdes funciona de forma separada del mercado de electricidad, esta separación implicaba altos costos de transacciones por lo cual las empresas verticalmente integradas eran más beneficiadas que los nuevos proyectos renovables, es decir este mecanismo favorecía más a las grandes compañías, además la incertidumbre regulatoria a partir del año 2010 frenó la financiación y por ende el desarrollo de nuevos proyectos [7,28,61]. Algunas fallas internas y externas presentes en el esquema de la Obligación Renovable no han permitido lograr las metas renovables establecidas por el gobierno, fallas internas como el exceso de competencia para reducir el precio, el riesgo financiero y de precio, el excesivo enfoque en reducción de costos y la incertidumbre regulatoria. Algunas de estas fallas también se presentaron en los esquemas de Obligaciones de Combustibles No Fósiles [62]

En el caso de Reino Unido la falta de competencia y de presión regulatoria llevo a que las empresas únicamente a cumplir con la regulación sin incentivar la difusión y adopción de la tecnología a nivel empresarial y de mercado.

El ambiente regulatorio de Reino Unido conllevó a que más del 80% de los proyectos eólicos fueran desarrollados por las seis más grandes compañías del mercado, además el marco regulatorio promovía un incremento anual de la capacidad renovable de sólo un 1% [7].

En cuanto al mecanismo de capacidad, Reino Unido tuvo un pago por capacidad desde el año 1990 hasta el año 2001, este era pagado cada media hora a todas las plantas que declaraban su disponibilidad. Este mecanismo fue fuertemente criticado por importantes personajes del sector, finalmente este mecanismo desapareció en el año 2001 con la introducción de NETA [20].

La reforma del mercado el eléctrico de Gran Bretaña consiste en la aplicación de dos instrumentos: el feed-in tariff contrato por diferencias y el mercado de capacidad, otras medidas complementarias están siendo aplicadas entre ellas el estándar de emisión y el piso al precio de carbono [60]. Similar al caso de España, en años recientes el feed-in tariff contrato por diferencias se ha asociado a una considerable expansión solar fotovoltaica conllevando a replantear el papel de este instrumento político en el mercado eléctrico británico.

El piso al precio del carbono establece un límite inferior para el precio del carbono, el aumento del precio del carbono incrementaría el precio de la electricidad reduciendo el valor de los subsidios a las renovables. El estándar de emisión exige que los nuevos generadores a carbón sean construidos con al menos 300 MW con captura y almacenamiento de carbono, pero esto no afecta las nuevas plantas a gas que son más eficientes en términos de emisiones [60].

Adicionalmente en España y Reino Unido se aplica el mercado de carbono de la Unión Europea –European Union Trading System EU ETS– el cual constituye un referente internacional en materia de comercio de emisiones, este mercado se ha desarrollado en tres fases y en este participan diferentes sectores contaminantes de Europa entre ellos el sector eléctrico. Sin embargo, la recesión económica, el gran número de derechos de emisión expedidos al igual que la superposición de políticas energéticas ha provocado un excedente de oferta de derechos de emisión y un bajo precio del carbono. Debido a los bajos precio de carbono Reino Unido ha implementado en su reforma el piso al precio de carbono [63].

8.3. Colombia

La "economía verde" constituye una tendencia de desarrollo económico y tecnológico, el uso de fuentes no convencionales de energía ha cobrado especial importancia incluso para los países de economías emergentes como Colombia. Donde recientemente se aprobó La Ley 1715 de 2014 "Por medio de la cual se regula la integración de las energías renovables no convencionales al Sistema Energético Nacional". La promulgación de la Ley 1715 de 2014, constituye un paso importante para Colombia en la promoción de energías no convencionales, esta Ley ha generado gran expectativa entre los agentes del mercado [64].

En Colombia la relación entre la generación hidráulica y térmica es aproximadamente de 64% contra el 31% [51], por lo que se puede afirmar que la matriz energética de Colombia es "limpia". Sin embargo, esta alta participación de la generación hidráulica representa un riesgo si se considera el continuo crecimiento de la demanda y la posibilidad de desabastecimiento de energía debido a las sequías producidas por el fenómeno del niño; la dependencia hidráulica crea una alta dependencia de la generación a partir de combustibles fósiles. Adicionalmente, los combustibles fósiles están sujetos a la volatilidad de precios de los hidrocarburos por lo cual encaren los costos del mercado. Por otro lado, Colombia tiene un gran potencial en materia de fuentes no convencionales de energía como solar fotovoltaica y eólica, sin mencionar la complementariedad existente entre la energía eólica e hidráulica [65]. El potencial de energía eólica en La Guajira es de 18GW; en el caso del recurso solar la irradiación promedio en territorio colombiano es de 4.5 kWh/m^2/día adicionalmente ya se presenta paridad de red de la energía solar fotovoltaica en diferentes ciudades de Colombia como lo demuestra Jiménez [66], por último el potencial de las pequeñas centrales hidroeléctricas es de 25000MW [67].

Respecto a la seguridad de suministro desde el año 1994 hasta diciembre de 1996 se aplicó el cargo por potencia y respaldo; luego desde 1997 hasta el año 2006 se aplicó en Colombia el "cargo por capacidad", el cual fue muy criticado desde sus comienzos hasta que fue cambiado en el año 2006 por un mecanismo de cantidad llamado "cargo por confiabilidad". El cargo por potencia se basaba en un cobro a los comercializadores por la energía comprada en bolsa que excediera a la energía contratada, y a los generadores por las compras en bolsa cuando la disponibilidad declarada de las plantas era menor a los contratos, el cobro era proporcional al excedente de la generación real respecto de la contratada; el cargo por respaldo remuneraba sólo a las plantas que operaban bajo niveles de hidrología extremas, eran retribuidas aquellas plantas no necesarias para atender la demanda a un nivel de confiabilidad del 95%.

En tanto el cargo capacidad remuneraba a los generadores de acuerdo a la capacidad remunerable teórica, una de sus fallas es que no garantizaba la remuneración de todos los generadores que aportaban a la confiabilidad del sistema. Por último el cargo por confiabilidad funciona como una opción "call" en donde si el precio de electricidad es mayor que el precio de escasez los generadores deben vender la electricidad comprometida al precio acordado o precio strike, a cambio los generadores reciben un pago fijo con el fin de que estén disponibles para generar durante periodos de escasez, la capacidad requerida es obtenida a través de una subasta de capacidad la cual permite aumentar la competencia en el mercado y considera la proyección de la demanda de electricidad. El cargo por confiabilidad fue introducido en el año 2006, la primera subasta se realizó en el año 2008; el regulador ha definido diferentes duraciones del contrato según el tipo de tecnología [20,68]. El cargo por confiabilidad no ha sido adecuado para promover la participación de energías renovables o de la demanda, actualmente es apropiado para las tecnologías hidráulica y térmica.

9. Conclusiones

Los objetivos ambientales han cobrado gran relevancia en los mercados de electricidad, por lo cual la nueva tendencia en materia de diseño de política energética en el mercado

eléctrico está enfocada a garantizar el "trilema" energético; este busca compatibilizar tres aspectos: calidad ambiental, seguridad de suministro y sostenibilidad económica. Es por ello que el regulador ha pasado en los últimos años de promover un esquema liberalizado de mercado, a incentivar un esquema completamente diferente basado en el intervencionismo a través de políticas que afectan la competitividad del mismo pero que le permiten alcanzar sus objetivos ambientales.

Es claro que una política no es suficiente para alcanzar el "trilema" energético, para ello es necesario considerar un portafolio diverso de políticas, la complementariedad tecnológica, los avances en la curva de aprendizaje a nivel local y global. Las políticas para garantizar la calidad ambiental y seguridad de suministro son políticas complementarias, buscan sobrepasar las barreras de mercado que afrontan las tecnologías no convencionales y al mismo tiempo garantizar la seguridad de suministro cuando el despliegue de tecnologías no convencionales afecta la inversión en tecnologías convencionales al reducir su eficiencia o distorsionar las señales de inversión.

Para estudiar el efecto económico del despliegue de tecnologías no convencionales en la tarifa final es necesario comparar el efecto de la reducción del precio de electricidad con el aumento total de la tarifa debido a los subsidios que reciben estas tecnologías; igualmente, se debe considerar el costo de las políticas para garantizar la seguridad de suministro que deben ser implementadas para lidiar con los efectos colaterales asociados a la expansión de energías no convencionales. Por último, diferentes políticas pueden ser implementadas para reducir emisiones de carbono, aumentar las energías renovables y garantizar la seguridad de suministro desde el lado de la oferta y la demanda del mercado eléctrico.

El mercado eléctrico español es un caso exitoso de despliegue renovable, aunque insostenible; esto es evidente si se estudia el despliegue de energía solar fotovoltaica ocasionado por los altos subsidios recibidos durante 2008, lo cual sugiere la importancia de lograr un equilibrio entre los subsidios y los costos que dependen de la curva de aprendizaje de la tecnología. En cuanto al mercado británico este no logró en los últimos años el despliegue renovable deseado debido a falta de competencia y de presión regulatoria. Por último, incluso Colombia se unió a la nueva tendencia en política energética ambientalmente amigable, si bien el panorama en cuanto a disponibilidad de recursos renovables es alentador aún es necesario esperar si se conservará o no el "status quo" del mercado eléctrico colombiano, dominado por centrales hidroeléctricas y respaldado por centrales térmicas.

Referencias

[1] Vogel, P., Efficient investment signals for distributed generation, Energy Policy, 37(9), pp. 3665-3672, 2009. DOI: 10.1016/j.enpol.2009.04.053

[2] Thema, J., Suerkemper, F., Grave, K. and Amelung, A., The impact of electricity demand reduction policies on the EU-ETS: Modelling electricity and carbon prices and the effect on industrial competitiveness, Energy Policy, 60, pp. 656-666, 2013. DOI: 10.1016/j.enpol.2013.04.028

[3] O'Connell, N., Pinson, P., Madsen, H. and O'Malley, M., Benefits and challenges of electrical demand response: A critical review, Renewable and Sustainable Energy Reviews, 39, pp. 686-699, 2014. DOI: 10.1016/j.rser.2014.07.098

[4] del Río, P., The dynamic efficiency of feed-in tariffs: The impact of different design elements, Energy Policy, 41, pp. 139-151, 2012. DOI: 10.1016/j.enpol.2011.08.029

[5] del Río, P., Analysing the interactions between renewable energy promotion and energy efficiency support schemes: The impact of different instruments and design elements, Energy Policy, 38(9), pp. 4978-4989, 2010. DOI: 10.1016/j.enpol.2010.04.003

[6] De Jonghe, C., Delarue, E., Belmans, R. and D'haeseleer, W., Interactions between measures for the support of electricity from renewable energy sources and CO_2 mitigation. Energy Policy, 37(11), pp. 4743-4752, 2009. DOI: 10.1016/j.enpol.2009.06.033

[7] Stenzel, T. and Frenzel, A., Regulating technological change—The strategic reactions of utility companies towards subsidy policies in the German, Spanish and UK electricity markets, Energy Policy, 36(7), pp. 2645-2657, 2008. DOI: 10.1016/j.enpol.2008.03.007

[8] Schallenberg-Rodriguez, J. and Haas, R., Fixed feed-in tariff versus premium: A review of the current Spanish system, Renewewable and Sustainable Energy Reviews, 16(1), pp. 293-305, 2012. DOI: 10.1016/j.rser.2011.07.155

[9] Couture, T. and Gagnon, Y., An analysis of feed-in tariff remuneration models: Implications for renewable energy investment, Energy Policy, 38(2), pp. 955-965, 2010. DOI: 10.1016/j.enpol.2009.10.047

[10] Sáenz de Miera, G., del Río-González, P. and Vizcaíno, I., Analysing the impact of renewable electricity support schemes on power prices: The case of wind electricity in Spain, Energy Policy, 36(9), pp. 3345-3359, 2008. DOI: 10.1016/j.enpol.2008.04.022

[11] Oak, N., Lawson, D. and Champneys, A., Performance comparison of renewable incentive schemes using optimal control, Energy, 64, pp. 44-57, 2014. DOI: 10.1016/j.energy.2013.11.038

[12] del Río, P., Interactions between climate and energy policies: The case of Spain, Climate Policy, 9(2), pp. 119-138, 2009. DOI: 10.3763/cpol.2007.0424

[13] Eyraud, L., Clements, B. and Wane, A., Green investment: Trends and determinants, Energy Policy, 60, pp. 852-865, 2013. DOI: 10.1016/j.enpol.2013.04.039

[14] Bradley, P., Leach, M. and Torriti, J., A review of the costs and benefits of demand response for electricity in the UK, Energy Policy, 52, pp. 312-327, 2013. DOI: 10.1016/j.enpol.2012.09.039

[15] Warren, P., A review of demand-side management policy in the UK, Renewable and Sustainable Energy Reviews, 29, pp. 941-951, 2014. DOI: 10.1016/j.rser.2013.09.009

[16] Shen, M., Cui, Q. and Fu, L., Personality traits and energy conservation, Energy Policy, 85, pp. 322-334, 2015. DOI: 10.1016/j.enpol.2015.05.025

[17] Wu, J.-H. and Huang, Y.-H., Electricity portfolio planning model incorporating renewable energy characteristics, Applied Energy, 119, pp. 278-287, 2014. DOI: 10.1016/j.apenergy.2014.01.001

[18] Brouwer, A.S., van den Broek, M., Seebregts, A. and Faaij, A., Impacts of large-scale intermittent renewable energy Sources on electricity systems, and how these can be modeled, Renewable and Sustainable Energy Reviews, 33, pp. 443-466, 2014. DOI: 10.1016/j.rser.2014.01.076

[19] Johansson, B., Security aspects of future renewable energy systems–A short overview, Energy, 61, pp. 598-605, 2013. DOI: 10.1016/j.energy.2013.09.023

[20] Batlle, C. and Rodilla, P., A critical assessment of the different approaches aimed to secure electricity generation supply, Energy Policy, 38(11), pp. 7169-7179, 2010. DOI: /10.1016/j.enpol.2010.07.039

[21] Neuhoff, K. and De Vries, L., Insufficient incentives for investment in electricity generations, Utilities Policy, 12(4), pp. 253-267, 2004. DOI: 10.1016/j.jup.2004.06.002

[22] Rodilla, P. and Batlle, C., Security of electricity supply at the generation level: Problem analysis, Energy Policy, 40, pp. 177-185, 2012. DOI: 10.1016/j.enpol.2011.09.030

[23] Cepeda, M. and Finon, D., How to correct for long-term externalities of large-scale wind power development by a capacity mechanism?,

Energy Policy, 61, pp. 671-685, 2013. DOI: 10.1016/j.enpol.2013.06.046

[24] Gouveia, J.P., Dias, L., Martins, I. and Seixas, J., Effects of renewables penetration on the security of Portuguese electricity supply, Applied Energy, 123, pp. 438-447, 2014. DOI: 10.1016/j.apenergy.2014.01.038

[25] Richter. M.. Utilities' business models for renewable energy: A review, Renewable and Sustainable Energy Reviews, 16(5), pp. 2483-2493, 2012. DOI: 10.1016/j.rser.2012.01.072

[26] Lehmann, P., Supplementing an emissions tax by a feed-in tariff for renewable electricity to address learning spillovers, Energy Policy, 61, pp. 635-641, 2013. DOI: 10.1016/j.enpol.2013.06.072

[27] Fernandes, L. and Ferreira, P., Renewable energy scenarios in the Portuguese electricity system, Energy, 69, pp. 51-57, 2014. DOI: 10.1016/j.energy.2014.02.098

[28] Klessmann,C., Nabe, C. and Burges, K., Pros and cons of exposing renewables to electricity market risks—A comparison of the market integration approaches in Germany, Spain, and the UK, Energy Policy, 36(10), pp. 3646-3661, 2008. DOI: 10.1016/j.enpol.2008.06.022

[29] Ciarreta, A., Espinosa, M.P. and Pizarro-Irizar, C., Is green energy expensive? Empirical evidence from the Spanish electricity market, Energy Policy, 69, pp. 205-215, 2014. DOI.: 10.1016/j.enpol.2014.02.025

[30] Boston, A., Delivering a secure electricity supply on a low carbon pathway, Energy Policy, 52, pp. 55-59, 2013. DOI: 10.1016/j.enpol.2012.02.004

[31] Lehmann, P. and Gawel, E., Why should support schemes for renewable electricity complement the EU emissions trading scheme?, Energy Policy, 52, pp. 597-607, 2013. DOI: 10.1016/j.enpol.2012.10.018

[32] Skytte, K., Interplay between Environmental Regulation and Power Markets [en línea], EUI Work Paper, 2006. [Consulta 1 de enero de 2015]. Disponible en: econpapers.repec.org/RePEc:erp:euirsc:p0169

[33] Hindsberger, M., Nybroe, M.H., Ravn, H.F. and Schmidt, R., Co-existence of electricity, TEP, and TGC markets in the Baltic Sea Region, Energy Policy, 31(1), pp. 85-96, 2003. DOI: 10.1016/S0301-4215(02)00120-9

[34] Unger, T. and Ahlgren, E.O., Impacts of a common green certificate market on electricity and CO_2-emission markets in the Nordic countries, Energy Policy, 33(16), pp. 2152-2163, 2005. DOI: 10.1016/j.enpol.2004.04.013

[35] Nelson, H.T., Planning implications from the interactions between renewable energy programs and carbon regulation. Journal of Environmental Planning and Management, 51(4), pp. 581-596, 2008. DOI: 10.1080/09640560802117101

[36] Palmer, K., Paul, A. Woerman, M. and Steinberg, D.C., Federal policies for renewable electricity: Impacts and interactions, Energy Policy, 39(7), pp. 3975-3991, 2011. DOI: 10.1016/j.enpol.2011.01.035

[37] Rathmann, M., Do support systems for RES-E reduce EU-ETS-driven electricity prices?, Energy Policy, 35(1), pp. 342-349, 2007. DOI: 10.1016/j.enpol.2005.11.029

[38] Böhringer, C., Löschel, A., Moslener, U. and Rutherford, T., EU climate policy up to 2020: An economic impact assessment, Energy Economics, 31, pp. S295-S305, 2009. DOI: 10.1016/j.eneco.2009.09.009

[39] Ford, A., Simulation scenarios for rapid reduction in carbon dioxide emissions in the western electricity system, Energy Policy, 36(1), pp. 443-455, 2008. DOI: 10.1016/j.enpol.2007.09.023

[40] Hasani-Marzooni, M. and Hosseini, S.H., Dynamic interactions of TGC and electricity markets to promote wind capacity investment, IEEE Systems Journal, 6(1), pp. 46-57, 2012. DOI: 10.1109/JSYST.2011.2162891

[41] Vogstad, K., A system dynamics analysis of the Nordic electricity market : The transition from fossil fuelled toward a renewable supply within a liberalised electricity market [en línea], 2004. [Consultado 5 de enero de 2015] Disponible en: http://www.researchgate.net/profile/Klaus_Vogstad/publication/234165778_A_system_dynamics_analysis_of_the_Nordic_electricity_market_The_transition_from_fossil_fuelled_toward_a_renewable_supply_within_a_liberalised_electricity_market/links/09e4150fb0eca7f9ed000000.pdf

[42] Zuluaga, M.M. and Dyner, I., Incentives for renewable energy in reformed Latin-American electricity markets: The Colombian case, Journal of Cleaner Production, 15(2), pp 153-162, 2007. DOI: 10.1016/j.jclepro.2005.12.014

[43] Fagiani, R., Richstein, J.C., Hakvoort, R. and De Vries, L., The dynamic impact of carbon reduction and renewable support policies on the electricity sector, Utilities Policy, 28, pp. 28-41, 2014. DOI: 10.1016/j.jup.2013.11.004

[44] Hsu, C.-W., Using a system dynamics model to assess the effects of capital subsidies and feed-in tariffs on solar PV installations, Applied Energy, 100, pp. 205-217, 2012. DOI: 10.1016/j.apenergy.2012.02.039

[45] Alishahi, E., Moghaddam, M.P. and Sheikh-El-Eslami, M.K., A system dynamics approach for investigating impacts of incentive mechanisms on wind power investment, Renewable Energy, 37(1), pp. 310-317, 2012. DOI: 10.1016/j.renene.2011.06.026

[46] Assili, M., Javidi, M.H., and Ghazi, R., An improved mechanism for capacity payment based on system dynamics modeling for investment planning in competitive electricity environment, Energy Policy, 36 (10), pp. 3703-3713, 2008. DOI: 10.1016/j.enpol.2008.06.034

[47] Hasani, M. and Hosseini, S.H., Dynamic assessment of capacity investment in electricity market considering complementary capacity mechanisms, Energy, 36(1), pp. 277-293, 2011. DOI: 10.1016/j.energy.2010.10.041

[48] Weigt, H., Ellerman, D. and Delarue, E., CO_2 abatement from renewables in the German electricity sector: Does a CO_2 price help?, Energy Economics, 40(1), pp. S149-S158, 2013. DOI: 10.1016/j.eneco.2013.09.013

[49] Sioshansi, F.P., Electricity market reform: What has the experience taught us thus far?, Utilities Policy, 14(2), pp. 63-75, 2006. DOI: 10.1016/j.jup.2005.12.002

[50] Foxon. T.J.. Transition pathways for a UK low carbon electricity future, Energy Policy, 52, pp. 10–24, 2013. DOI: 10.1016/j.enpol.2012.04.001.

[51] UPME., Plan de Expansión de Referencia Generación - Transmisión 2014 - 2028 [en línea], 2014 [consulta 11 enero de 2015]. Disponible en: http://www.upme.gov.co/Docs/Plan_Expansion/2015/Plan_GT_2014-2028.pdf

[52] Haas, R., Panzer, C., Resch, G., Ragwitz, M., Reece, G. and Held, A., A historical review of promotion strategies for electricity from renewable energy sources in EU countries, Renewable and Sustainable Energy Reviews, 15(2), pp. 1003-1034, 2011. DOI: 10.1016/j.rser.2010.11.015

[53] Moreno, F. and Martínez-Val., J.M., Collateral effects of renewable energies deployment in Spain: Impact on thermal power plants performance and management, Energy Policy, 39(10), pp. 6561-6574, 2011. DOI: 10.1016/j.enpol.2011.07.061

[54] MITyC., ORDEN ITC/2794/2007, de 27 septiembre, por la que se revisan las tarifas eléctricas a partir del 1 de octubre de 2007 [en línea] 2007 [consulta 11 enero de 2015]. Disponible en: https://www.boe.es/boe/dias/2007/09/29/pdfs/A39690-39698.pdf

[55] Urbina, A., Solar electricity in a changing environment: The case of Spain, Renewable Energy, 68, pp. 264-269, 2014. DOI: 10.1016/j.renene.2014.02.005

[56] de la Hoz, J., Martín, H., Ballart, J. and Monjo, L., Evaluating the approach to reduce the overrun cost of grid connected PV systems for the Spanish electricity sector: Performance analysis of the period 2010–2012, Applied Energy, 121, pp. 159-173, 2014. DOI: 10.1016/j.apenergy.2014.01.083

[57] Alikhanzadeh, A. and Irving, M., Combined oligopoly and oligopsony bilateral electricity market model using CV equilibria, IEEE, pp. 1-8, 2012. DOI: 10.1109/PESGM.2012.6345293

[58] Nielsen, S., Sorknæs, P. and Østergaard, P.A., Electricity market auction settings in a future Danish electricity system with a high penetration of renewable energy sources – A comparison of marginal pricing and pay-as-bid, Energy, 36(7), pp. 4434-4444, 2011. DOI: 10.1016/j.energy.2011.03.079

[59] Prandini, A., Good, BETTA, best ? The role of industry structure in electricity reform in Scotland. Energy Policy, 35(3), pp. 1628-1642, 2007. DOI: 10.1016/j.enpol.2006.05.004

[60] DECC., Implementing Electricity Market Reform (EMR) [en línea], London, 2014 [Consulta 12 de enero de 2015]. Disponible en: https://www.gov.uk/government/uploads/system/uploads/attachment_data/file/324176/Implementing_Electricity_Market_Reform.pdf
[61] Mitchell, C. and Connor, P., Renewable energy policy in the UK 1990–2003, Energy Policy, 32(17), pp. 1935-1947, 2004. DOI: 10.1016/j.enpol.2004.03.016
[62] Wood, G. and Dow, S., What lessons have been learned in reforming the Renewables Obligation? An analysis of internal and external failures in UK renewable energy policy, Energy Policy, 39(5), pp. 2228-2244, 2011. DOI: 10.1016/j.enpol.2010.11.012
[63] Helm, D., EMR and The Energy Bill: A Critique [en línea], pp. 1-17, 2012 [Consulta 12 de enero de 2015]. Disponible en: http://www.dieterhelm.co.uk/node/1330
[64] MinMinas., Ley 1715 del 13 de Mayo de 2014 Por medio de la cual se regula la integración de las energías renovables no convencionales al Sistema Energético Nacional [en línea], 2014 [Consulta 12 de enero de 2015]. Disponible en: http://www.upme.gov.co/Normatividad/Nacional/2014/LEY_1715_2014.pdf
[65] Vergara, P., Deeb, W., Cramton, A., Toba, P., Leino, N. and Benoit, I., Wind energy in Colombia: A framework for market entry, World Bank Publication [en línea]., 2010 [Consulta 12 de enero de 2015]. Disponible en: http://www.cramton.umd.edu/papers2010-2014/vergara-deep-toba-cramton-leino-wind-energy-in-colombia.pdf
[66] Jiménez, M., Cadavid, L. and Franco, C., Scenarios of photovoltaic grid parity in Colombia, DYNA, (81)188, pp. 237-245, 2014. DOI: 10.15446/dyna.v81n188.42165
[67] Corpoema., Formulación de un plan de desarrollo para las fuentes no convencionales de energía en Colombia (PDFNCE). [En línea] Bogotá, 2010 [consulta 12 enero de 2015]. Disponible en: http://www.upme.gov.co/Sigic/DocumentosF/Vol_2_Diagnostico_FNCE.pdf
[68] Rodilla, P., Batlle, C., Salazar, J. and Sánchez, J.J., Modeling generation expansion in the context of a security of supply mechanism based on long-term auctions. Application to the Colombian case, Energy Policy, 39(1), pp. 176-186, 2011. DOI: 10.1016/j.enpol.2010.09.027

C.J. Franco-Cardona, es Ing. Civil, MSc. en Aprovechamiento de los Recursos Hidráulicos y Dr. en Ingeniería, todos ellos de la Universidad Nacional de Colombia Sede Medellín, Colombia, actualmente es profesor investigador de dedicación exclusiva de la Escuela de Sistemas en la misma universidad. Su área de investigación comprende los mercados energéticos, la energía, la complejidad y el modelado de sistemas. Es miembro de System Dynamics Society. En el ámbito profesional laboró en Interconexión Electrica S.A ESP, como Especialista en Planeación de la Operación del Mercado Mayorista de Energía. Ha publicado artículos en revistas de alto impacto científico en el área de gestión de sistemas energéticos. ORCID: ORCID: 0000-0002-7750-857X

M. Castañeda-Riascos, es Ing. Administradora y MSc. en Ingeniería de Sistemas, todos de la Universidad Nacional de Colombia sede Medellín, Colombia, actualmente es estudiante de doctorado de la misma universidad. Sus intereses de investigación son política y regulación energética, los mercados de energía, el modelado y simulación de sistemas. Ha participado en el desarrollo de proyectos de investigación para importantes entidades como Colciencias, Interconexión Eléctrica S.A. E.S.P y EPM S.A. E.S.P. Igualmente, ha trabajado como analista de intercambios de energía en XM SA ESP empresa administradora del mercado eléctrico colombiano.
ORCID: 0000-0002-3137-3059

A. Valencia-Arias, es Ing. Administrador y MSc. en Ingeniería de Sistemas de la Universidad Nacional de Colombia Sede Medellín, Colombia. Docente del Departamento de Ciencias Administrativas del Instituto Tecnológico Metropolitano ITM de Medellín, Colombia, en el área de Investigación de Mercados, igualmente tiene experiencia en el área de simulación basada en agentes y dinámica de sistemas, especializándose en la elaboración de modelos sociales y económicos.
ORCID: 0000-0001-9434-6923

J. Bermúdez-Hernández, es Ing. Administrador de la Universidad Nacional de Colombia Sede Medellín y MSc en Administración de la Sede Bogotá de la Universidad Nacional de Colombia. Docente del Departamento de Ciencias Administrativas del Instituto Tecnológico Metropolitano ITM de Medellín, Colombia, en el área de Sistemas de Gestión de la Calidad, con experiencia en procesos de Certificación y Acreditación en Alta Calidad. Integrante del Grupo de Investigación en Ciencias Administrativas del ITM. ORCID: 0000-0002-1475-153X

UNIVERSIDAD NACIONAL DE COLOMBIA
SEDE MEDELLÍN
FACULTAD DE MINAS

Área Curricular de Ingeniería
de Sistemas e Informática

Oferta de Posgrados

Especialización en Sistemas
Especialización en Mercados de Energía
Maestría en Ingeniería - Ingeniería de Sistemas
Doctorado en Ingeniería- Sistema e Informática

Mayor información:

E-mail: acsei_med@unal.edu.co
Teléfono: (57-4) 425 5365

UNIVERSIDAD NACIONAL DE COLOMBIA
SEDE MEDELLÍN
FACULTAD DE MINAS



DYNA
http://dyna.medellin.unal.edu.co/

Influence of seawater immersion in low energy impact behavior of a novel colombian fique fiber reinforced bio-resin laminate

Fabuer Ramón-Valencia [a], Alberto Lopez-Arraiza [a], Joseba I. Múgica [b], Jon Aurrekoetxea [b], Juan Carlos Suarez [c] & Bladimir Ramón-Valencia [d]

[a] *Dpto. Ciencias y Técnicas de la Navegación, Máquinas y Construcciones Navales, Universidad del País Vasco (UPV/EHU), Lejona, España. fabuer@hotmail.com; alberto.lopeza@ehu.es*
[b] *Dpto de Mecánica y Producción Industrial, Mondragon Goi Eskola Politeknikoa (MGEP), Mondragon Unibertsitatea, Mondragoe, España. jimugica@mondragon.edu; jaurrekoetxea@mondragon.edu*
[c] *Escuela Técnica Superior de Ingenieros Navales. Universidad Politécnica de Madrid, Madrid, España. juancarlos.suarez@upm.es*
[d] *Facultad de Ingenierías y Arquitectura, Universidad de Pamplona, Colombia. hbladimir@unipamplona.edu.co*

Received: January 26th, 2015. Received in revised form: July 21th, 2015. Accepted: July 28th, 2015.

Abstract
This experimental work is aimed at the influence of seawater immersion in low impact energy behavior of a novel Colombian fique fiber reinforced bio-resin laminate. Such material was manufactured by vacuum infusion. The specimens were immersed in seawater during a bioactivity period of six months. Low energy impact tests were performed in order to obtain the penetration and perforation threshold according to energy profiles. The damage extent was characterized by means of Ultrasonics. Tensile stress tests were also performed and the breaking surfaces were analyzed by Scanning Electron Microscopy. The results revealed that the new biocomposite, after seawater immersion, has higher penetration and perforation thresholds than the biocomposite without immersion. Tensile test results show stiffness lost and increase of elongation at break. This behavior of the immersed biocomposite is due to a plasticization process of the material.

Keywords: Biocomposite, Fique fiber, Impact resistance, Ultrasonics.

Influencia del agua de mar en el comportamiento frente a impacto de baja energía de un nuevo laminado de resina natural reforzada con fibra de fique colombiano

Resumen
Este trabajo estudia el efecto del agua de mar en el comportamiento a impacto de baja energía de un nuevo laminado de resina natural reforzado con fibra de fique colombiano fabricado mediante infusión en vacío. Las probetas fueron sumergidas en agua de mar durante un periodo de bioactividad de seis meses. Posteriormente, fueron sometidas a impactos de baja energía para determinar el diagrama de perfil de energías. El daño se inspeccionó mediante la técnica de ultrasonidos. También se realizaron ensayos de tracción y se analizaron las superficies de rotura mediante microscopía electrónica. Los resultados muestran que el biocomposite, tras su inmersión en agua de mar, presenta unos umbrales de penetración y perforación más altos que el material sin sumergir. Los ensayos de tracción indican que la inmersión causa una pérdida de rigidez y un aumento del alargamiento a rotura. Este comportamiento del biocomposite sumergido es debido a un proceso de plastificación del material.

Palabras clave: Biocomposite, Fibra de fique, Resistencia a impacto, Ultrasonidos.

1 Introducción

En los últimos años, los materiales compuestos de matriz polimérica reforzada con fibras como el vidrio o el carbono, se están utilizando cada vez más en sectores como el aeronáutico, el de automoción, el eólico o el naval. Este hecho se debe fundamentalmente a las ventajas que presentan en cuanto a resistencia mecánica específica, bajo peso y posibilidad de realizar piezas de distintos tamaños y diseños a medida [1-4].

© The author; licensee Universidad Nacional de Colombia.

Sin embargo, presentan una doble problemática, por un lado, su elevada dependencia del petróleo, y por otro, la gestión de los residuos tras su fin de vida. En consecuencia la comunidad científica se está centrando en el desarrollo de nuevas resinas de origen renovable [5] reforzadas con fibras naturales como el yute, el kenaf, el lino o el cáñamo [3,6,7].

Entre las características que hacen atractivas las fibras naturales, destacan sus elevadas propiedades específicas de rigidez y resistencia a impacto [8-11]. Igualmente, proporcionan aislamiento térmico, acústico y ligereza estructural, lo que da lugar a una reducción de peso y por lo tanto, menor consumo de combustible y menores emisiones contaminantes. En consecuencia, en la última década, los composites de matriz polimérica reforzada con fibras naturales, se están introduciendo cada vez más en sectores como el de automoción, el ocio y el mobiliario [1,12-14].

En Colombia una de las fibras naturales que más se producen es el fique, cuyo uso en forma de tejido se limita a la fabricación de costales, calzado, bolsos y otros artículos de uso cotidiano. Sin embargo el tejido de fique se puede utilizar también como refuerzo estructural en piezas de materiales compuestos de matriz polimérica [15,16].

En este trabajo se ha desarrollado un nuevo laminado de resina natural reforzada con fibra de fique Colombiano. Posteriormente, se estudió su comportamiento a impacto de baja energía antes y después de su inmersión en agua de mar durante un periodo de seis meses. El daño generado en las pruebas de impacto se inspeccionó mediante técnicas no destructivas de ultrasonidos. Igualmente se realizaron ensayos normalizados de tracción analizando las superficies de rotura mediante microscopia electrónica de barrido.

2. Material y técnicas experimentales

2.1. Material

La resina utilizada como matriz ha sido la SuperSap®, resina epoxídica procedente de materiales renovables y suministrada por Entropy Resins. El porcentaje de resina:catalizador fue de 100:33 en peso. Como refuerzos se utilizaron fibras naturales fique trenzado bidireccional 0/90 no equilibrado 2:1, con un gramaje de 530 g/m^2 suministrado por la empresa Coohilados del Fonce LTDA. Los laminados se obtuvieron mediante el proceso de infusión en vacío con 3 capas de fibra natural como refuerzo. Las dimensiones de los laminados de biocomposite fueron 350mm x 350mm x 4mm, con un porcentaje de fibra del 44 % en peso. Después de 6 meses de inmersión en el agua de mar, el porcentaje de absorción de humedad del biocomposite se calculó por diferencia de pesos entre las muestras sumergidas en agua de mar y las muestras sin inmersión. El porcentaje de humedad obtenido fue del 8%.

2.2. Diagrama de perfil de energías

La energía absorbida (E_a) es un parámetro representativo del comportamiento frente a impacto de los materiales compuestos. Representando dicha energía en función de la energía de impacto (E_0) se construye el denominado diagrama de perfil de energías Fig 1. La línea discontinua

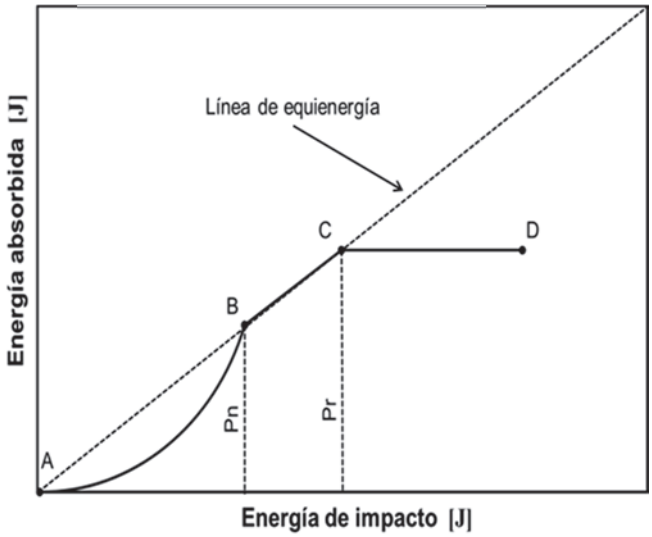


Figura 1. Diagrama del perfil energético típico de un material compuesto ensayado a impacto biaxial.
Fuente: Los autores

diagonal en el diagrama representa la línea de equienergías entre la energía de impacto y la energía absorbida.

En la Fig 1 se muestra el diagrama de perfil energético típico para un laminado de material compuesto. En el diagrama se pueden diferenciar tres regiones AB, BC, CD. En la región AB la probeta permanece sin penetración. La cantidad de daño que sufre la probeta y la superficie total de área dañada depende de la energía de impacto. En esta región la curva se encuentra por debajo de la curva de equienergía, lo que implica que la probeta no es capaz de absorber toda la energía (la diferencia entre la curva y la línea de equienergía). El exceso de energía se acumula en el impactor y produce el rebote del impactor tras el impacto [17].

A la región BC se le denomina como región de penetración, en esta región probablemente el total de la energía de impacto es absorbida por la probeta. Por último la región CD se denomina como región de perforación. Además, el punto B y C representan el umbral de penetración (P_n) y perforación (P_r), respectivamente. El umbral de penetración se puede definir como el punto donde la energía absorbida iguala a la energía de impacto por primera vez. Al alcanzar el umbral de penetración, el impactor se queda adherido dentro del laminado y no rebota [18]. A partir del umbral de perforación, la energía absorbida permanece más o menos constante. Esto implica que el impactor no produce más daño en la probeta ni siquiera aumentando la energía de impacto [17].

2.3. Ensayos de impacto de baja energía

Los ensayos de impacto biaxial de baja energía se han llevado a cabo en una máquina de caída de dardo instrumentado comercial Fractovis Plus. La máquina básicamente consta de dos partes: la cruceta móvil o impactor y la base. El impactor está compuesto por el portamasas y el indentador instrumentado.

El impactor utilizado ha sido instrumentado con una célula de carga de 20 kN, junto con el indentador de cabeza

semiesférica y 20 mm diámetro. El utillaje utilizado ha sido una base plana con forma de cilindro que presenta un agujero pasante de 40 mm de diámetro.

El ensayo de impacto biaxial consiste en dejar caer desde una altura variable un impactador de cabeza semiesférica, que colisionará en el centro de una probeta amordazada sobre el utillaje con una energía de impacto (E_0) determinada.

De los laminados fabricados se mecanizaron 15 probetas de dimensiones: 70 mm x 70 mm, tanto del biocomposite sin inmersión, como tras su inmersión en agua de mar. En ambos casos los ensayos se llevaron a cabo a temperatura ambiente.

El material sin sumergir y tras inmersión en agua de mar, se han ensayado subiendo la energía de impacto hasta llegar a la perforación. Se han realizado ensayos de impacto desde E_0=1J hasta E_0=50J, para lo que se han combinado diferentes masas y alturas.

2.4. Inspección del daño por ultrasonidos

Una vez impactadas las probetas tanto sin sumergir como las sumergidas en agua de mar a diferentes niveles de daño, se inspeccionaron mediante la técnica de ultrasonidos por inmersión. Este ensayo utiliza el agua como medio de acoplamiento acústico entre el palpador de 1 MHz y la pieza a examinar. Las probetas seleccionadas para este ensayo son aquellas cuyas energías de impacto están por debajo del umbral de perforación.

Para este ensayo el palpador y la pieza son sumergidos total o parcialmente en una piscina con agua de tal manera que no se requiere tener contacto entre ellos, ya que la onda de ultrasonido viaja a través del agua, utilizando la misma como medio acústico entre el palpador y la probeta.

Para esta práctica se utilizó un equipo de inspección por ultrasonidos marca TECNITEST C-SCAN, utilizado para inspecciones automáticas por inmersión total o inmersión local.

El TECNITEST C-SCAN sirve para detectar y evaluar defectos mediante la técnica no destructiva de ultrasonidos. Este sistema permite encontrar y determinar el tamaño y la posición de defectos típicos de materiales compuestos.

Como resultado de este ensayo se obtienen imágenes en una escala de 25 colores que varían de decibelio en decibelio empezando en 0 Db de atenuación.

2.5. Ensayo de tracción

La máquina utilizada para realizar los ensayos de tracción es una INSTRON equipada con una célula de carga de 5 kN. Se ha utilizado como sistema de medida de deformación un extensómetro por contacto. De los laminados secos y tras su inmersión en agua de mar se mecanizaron 5 probetas normalizadas (ASTM D3039). Los ensayos de tracción se llevan a cabo a temperatura ambiente T=20-23ºC y a una velocidad de deformación de 2 mm/min. El objetivo de este ensayo es comparar las propiedades a tracción del biocomposite antes y después de su inmersión en agua de mar.

2.6. Microscopía electrónica de barrido

Las probetas ensayadas a tracción fueron observadas mediante un Microscopio Electrónico de Barrido (SEM) marca Joel modelo JSM-6400. Previamente las muestras se metalizaron para mejorar la conductividad.

El objetivo de esta práctica es poder visualizar las superficies de rotura y analizar la adhesión matriz-refuerzo, de los biocomposites sin sumergir y tras su inmersión en agua de mar.

3. Resultados y discusión

3.1. Perfil energético

Con el objetivo de identificar las regiones representativas del comportamiento del material frente al daño, se traza la curva que relaciona la energía disipada por el material E_d frente a la energía de impacto inducida E_0.

En la Fig 2 se muestra el perfil energético para el nuevo biocomposite reforzado con fibra de fique sin inmersión en agua de mar, en el que se pueden apreciar claramente las regiones características del material sometido a impacto.

En la región AB, la curva se encuentra por debajo de la línea de equienergía, y comprende los valores de energías de impacto desde E_0=0J hasta E_0=19,02J ya que las probetas no disipan toda la energía de impacto. El exceso de energía se acumula en la probeta en forma de energía potencial de deformación produciendo un rebote del impactor [23,24].

La zona BC pertenece a la región de penetración, estos valores de impacto se encuentran sobre la línea de equienergía, lo que quiere decir que la energía de disipación es igual a la energía incidente. Al alcanzar esta región el impactor se queda adherido al laminado y no rebota [18,25]. El punto B es el umbral de penetración P_n=19,02J, a partir de este valor la energía absorbida por el material iguala a la energía incidente E_0 hasta alcanzar el punto C que es el umbral de perforación P_r=22,76J.

Por último, se encuentra la región CD o región de perforación. En esta zona la probeta es perforada por el impactor de tal manera que ya no puede generar más daño, ni siquiera aumentando la energía de impacto. A partir del umbral de perforación P_r=22,76J, la energía absorbida permanece más o menos constante.

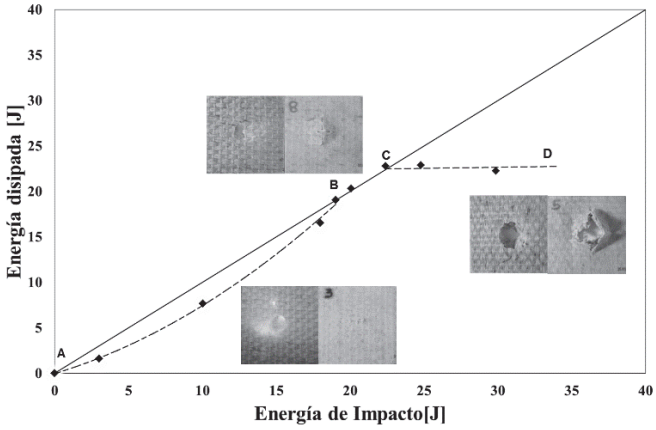


Figura 2. Diagrama de perfil energético para biocomposite reforzado con fibra de fique sin inmersión en agua de mar.
Fuente: Los autores

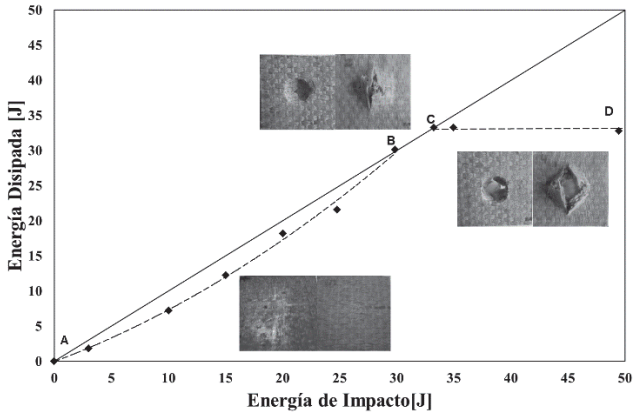


Figura 3. Diagrama de perfil energético para biocomposite reforzado con fibra de fique tras inmersión en agua de mar
Fuente: Los autores

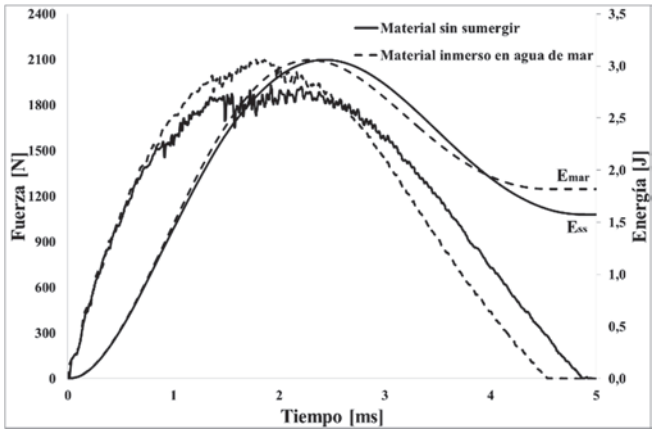


Figura 4. Curvas de F-t y E-t correspondiente a impactos de biocomposite reforzado con fibra fique para energía de impacto E_0=3J.
Fuente: Los autores

De igual forma se obtiene el perfil energético del material tras inmersión en agua de mar Fig 3. En donde se aprecian las regiones características del comportamiento del material tras inmersión en agua de mar.

La región AB comprende los valores de impacto entre E_0=0J hasta E_0=30,64J, es decir, el material sumergido en agua de mar presenta un mayor rango en el cual el impacto va a rebotar por la energía elástica devuelta por el laminado. Respecto a la zona BC, que pertenece a la región de penetración, tanto el umbral de penetración (P_n=30,64J) como el umbral de perforación (P_r=33,28J) son significativamente superiores en comparación con el material sin sumergir en agua de mar.

Las variaciones entre los perfiles energéticos pueden explicarse por el efecto plastificante que produce el agua de mar en el material, es decir, la absorción de humedad debido al carácter hidrofílico de la fibra de fique [24], lo cual conlleva a un retardo en la generación del daño durante los impactos. Este retardo se debe a que la respuesta estructural del material tras inmersión en agua de mar, es mayor provocando picos más altos de fuerza y por consiguiente permite al material disipar más energía antes de alcanzar los umbrales de penetración y de perforación.

3.1. Ensayos de impacto de baja energía

La Fig 4 representa las curvas fuerza-tiempo (F-t) y energía-tiempo (E-t) para ensayos de impacto con energía incidente de E_0=3J. Se observa que las curvas de fuerza siguen un patrón inicial similar para ambos casos hasta presentar una pérdida de simetría cuando la fuerza alcanza un valor aproximado de F_d=1500N para el material sin inmersión y de F_d=2000N para el material tras inmersión en agua de mar.

Este cambio de pendiente indica una generación de daño sobre el material y está relacionado con la fuerza del umbral crítico para el inicio de la delaminación, que es independiente de la energía de impacto [19-21]

Durante el ensayo de impacto el biocomposite tras inmersión en agua de mar opone más resistencia al impactor lo cual produce una delaminación más tardía que la generada

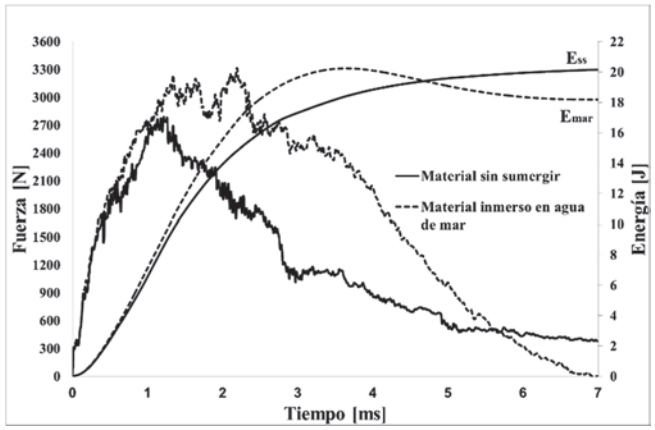


Figura 5. Curvas de F-t y E-t correspondiente a impactos de biocomposite reforzado con fibra fique para energía de impacto E_0=20J.
Fuente: Los autores

en el material sin sumergir y consecuentemente picos de fuerza más altos. Este comportamiento se debe a la generación de un estado plástico en el nuevo biocomposite, provocado por la absorción de humedad tras la inmersión en agua de mar.

Respecto a las curvas de E-t Fig 4 se observa el mismo patrón en ambos casos. La energía máxima corresponde con la energía que el impactor trasmite a la probeta (E_0=3J). A continuación la energía disminuye hasta E_{ss}=1,57J para la probeta sin sumergir y E_{mar}=1,87J para la probeta tras inmersion en agua de mar, siendo E_a la energía absorbida por cada material. El resto de la energía es la energía elástica que devuelve la probeta al impactor, es decir, que la probeta puede soportar más daño.

Con el aumento de la energía de impacto varían los valores de fuerza pico en ambos casos. La Fig 5 representa las curvas de F-t y E-t para un ensayo de impacto con energía incidente E_0=20J, correspondientes a ensayos que generan delaminación y rotura de fibras [19,20,22].

Los umbrales para el inicio de daño son iguales que el caso anterior puesto que no dependen de la energía de impacto [19-21]. El efecto plastificante que produce el agua

de mar aumenta la flexibilidad de la probeta cuando es impactada, lo cual le permite alcanzar un aumento del 15,89% en la fuerza pico (F_{pmar}=3314,18N) frente al material sin inmersión (F_{pss}=2787,38N).

El comportamiento post-pico, muestra una caída progresiva de la carga en el material sin inmersión hasta un valor aproximado (F=1200N), relacionado con la perdida de rigidez trasversal de la probeta. En el caso del material tras inmersión en agua de mar el comportamiento post-pico se genera una zona de reposo hasta que la carga desciende a un valor aproximado de (F=2700N). Por último, para ambos casos la carga disminuye progresivamente debido a la perdida de rigidez de la probeta.

Respecto a las curvas de E-t Fig 5, el comportamiento es distinto en el material sin inmersión y tras inmersión en agua de mar. El biocomposite sin sumergir absorbió la totalidad de la energía de impacto $E_{ss}=E_0$=20J lo que quiere decir que la probeta está saturada. En cambio, el material sumergido en agua de mar aún produce energía elástica lo cual quiere decir que la probeta esta insaturada y puede soportar más energía de daño.

La Fig 6 representa las curvas de F-t y E-t para un ensayo de impacto con energía incidente E_0=25J, correspondientes a ensayos que generan delaminación, rotura de fibras y perforación [19, 20, 22].

El comportamiento de la fuerza post-pico del material sin sumergir sufre un cambio significativo al producirse una caída brusca, debido a la pérdida total de rigidez trasversal de la probeta. Este comportamiento es típico de un ensayo de perforación [19,20]. En el caso del material tras inmersión en agua de mar no se observa dicha caída brusca, sin embargo, si presenta un mayor umbral de daño por delaminación.

Las curvas de E-t Fig 6 muestran que el material sin sumergir no es capaz de disipar la totalidad de la energía de impacto E_0=25J, y solamente puede dispar E_{ss}=22,89J lo que quiere decir que la probeta esta perforada o dañada totalmente como se ve en la Fig 7a. En cambio, el material tras inmersión en agua de mar aún devuelve energía elástica al impactor lo que quiere decir que aguanta más energía de daño debido a la plastificación generada por el agua de mar Fig 7b.

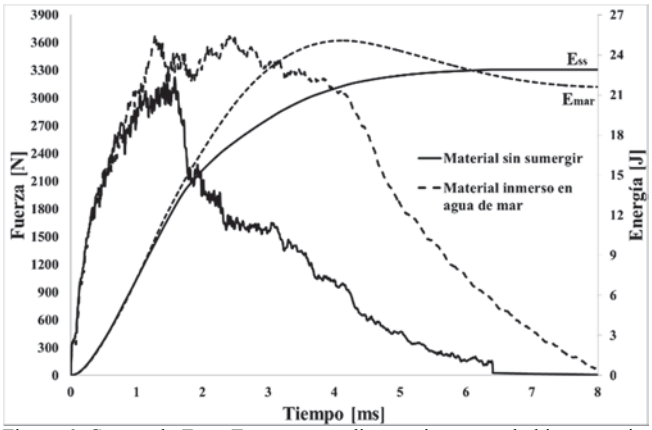


Figura 6. Curvas de F-t y E-t correspondiente a impactos de biocomposite reforzado con fibra fique para energía de impacto E_0=25J
Fuente: Los autores

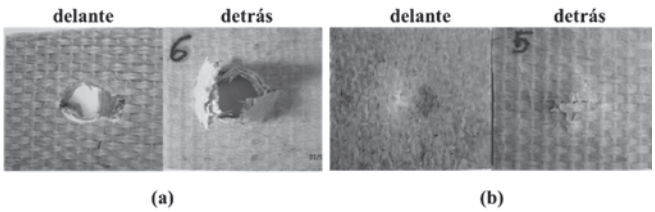


Figura 7. Probetas de biocomposite reforzado con fibra de Fique sin inmersión (a) y tras inmersión en agua de mar (b) a energía de impacto E_0=25J.
Fuente: Los autores

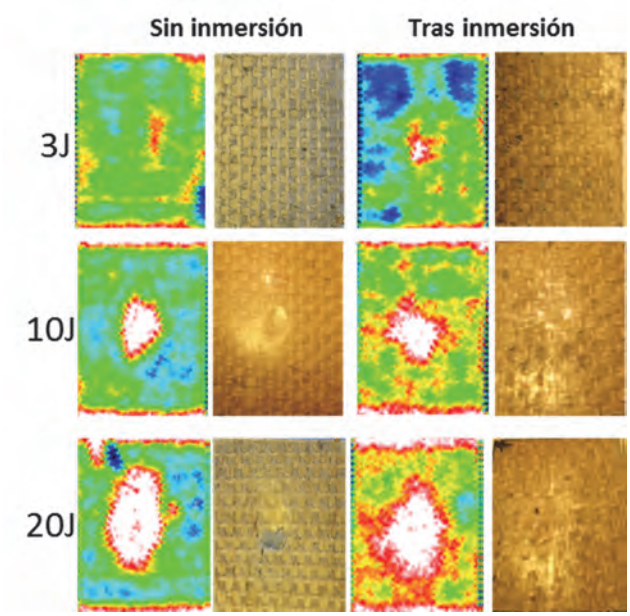


Figura 8. Imágenes de C-Scan de zonas de impacto de material sin inmersión y tras inmersión en agua de mar.
Fuente: Los autores

3.3. Inspección del daño por ultrasonidos

En la Fig 8 se observan las imágenes del C-Scan con su correspondiente fotografía, para distintas energías de daño aplicadas al nuevo laminado de matriz bioepoxi reforzado con fibra natural de fique. Estas imágenes representan la evolución del área dañada en las zonas donde el impactor hace contacto con la probeta a medida que aumenta la energía de impacto.

Para una energía de impacto de E_0=3J, valor de energía comprendido entre la delaminación y el inicio de rotura de fibras, el C-Scan detecta una mayor área de del daño en la probeta tras inmersion en agua de mar (zona blanca) con respecto a la probeta sin sumergir en agua de mar. En los impactos por encima del umbral de rotura de fibras, E_0=10J y E_0=20J, también se observa mayor área dañada en las probetas inmersas en agua de mar en comparación con las sin sumergir.

Además el daño provocado en el material sin inmersión se encuentra restringido justo a la zona de interacción entre el impactor y la pieza, mientras que en el material sumergido,

el daño por el impactor se extiende a una zona más amplia

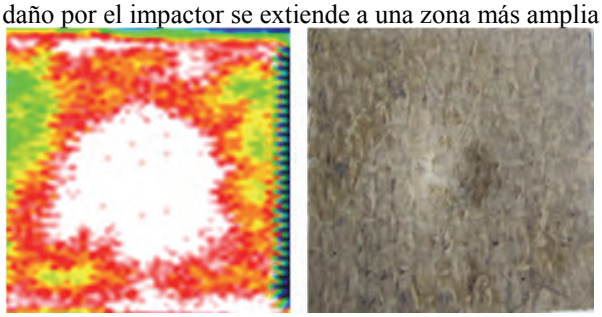


Figura 9. C-Scan para probeta tras inmersión en agua de mar con energía de impacto E_0=25J
Fuente: Los autores

Tabla 1.
Resultados de los ensayos a tracción del biocomposite seco y tras inmersión en agua de mar

Propiedad	Biocomposite Sin inmersión	Biocomposite Tras inmersión
E (MPa)	5723,1±94,7	4334,4±4,2
σr (MPa)	64,2±1,6	63,0±1,7
εr (%)	1,7±0,1	2,7±0,1

Fuente: Los autores

creando un gradiente de daño en el material a medida que aumenta la energía de impacto.

En la Fig 9 se observa el impacto a E_0=25J en el material sumergido. Para esta energía incidente el material sin inmersión ya ha perforado, mientras que en el material sumergido se observa penetración con un amplio espectro de daño representado por área blanca y roja.

En definitiva, el material sumergido presenta una respuesta estructural más global y por consiguiente, la extensión del daño es mayor y menos localizada que en el material sin sumergir

3.4. Ensayo de tracción

En la Tabla 1 se pueden observar los valores de: módulo elástico (E), tensión de rotura (σ_r) y deformación de rotura (ε_r), de las probetas ensayadas a tracción de biocomposite sin sumergir y tras inmersión en agua de mar.

La característica general del nuevo biocomposite es un comportamiento elasto-plástico con una pequeña deformación plástica antes de la rotura, típico de compuestos con matriz termoestable tipo epoxi reforzada con fibras [26].

La rigidez del material tras inmersión, es decir, el módulo elástico o de Young, disminuye un 24% en comparación con el biocomposite sin sumergir. La tensión de rotura permanece prácticamente igual, pero hay un incremento del 36% en la deformación a rotura en el material sumergido en agua de mar. Este hecho corrobora la hipótesis de plastificación por absorción de humedad del biocomposite tras su inmersión en agua de mar.

3.5. Microscopía electrónica de barrido

En la Fig 10 se observan las micrografías al SEM con una resolución de X200, de las superficies de fractura tras el ensayo de tracción para el biocomposite sin inmersión y tras su inmersión en agua de mar.

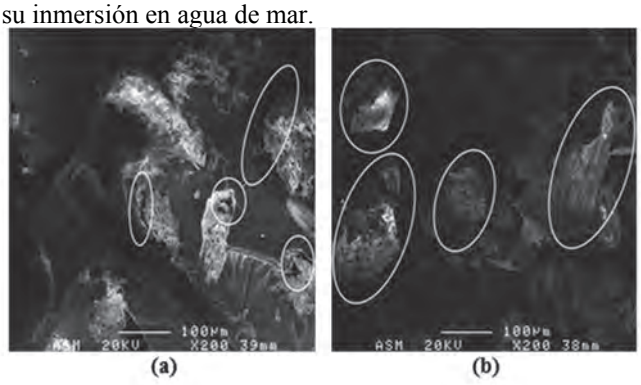


Figura 10. Microscopía electrónica de barrido de los bicomposites reforzados con fibras de fique. a) fique sin inmersión, b) fique después de inmersión en agua de mar.
Fuente: los autores

En la Fig 10a se puede ver una falta de adherencia entre la fibra y la matriz con una rotura frágil sin elongación apreciable. En cambio, en la Fig 10b, la rotura de la fibra presenta una mayor elongación tal y como se observó en los resultados de los ensayos de tracción

4. Conclusiones

Se fabricaron laminados de un nuevo biocomposite de resina natural reforzados con fibras naturales de fique trenzado. La mitad de dichos laminados se sumergieron en agua de mar durante un periodo de bioactividad marina de seis meses. Luego se caracterizaron a impacto biaxial de baja energía obteniendo sus correspondientes perfiles energéticos. Posteriormente se inspeccionaron por ultrasonidos las zonas de impacto. Además se realizaron ensayos de tracción y las superficies de rotura fueron observadas en un Microscopio Electrónico de Barrido. Las conclusiones que se han obtenido son las siguientes:

Durante el ensayo de impacto el biocomposite sumergido en agua de mar opone más resistencia al impactor lo cual produce una delaminación más tardía que la generada en el material sin inmersión y consecuentemente picos de fuerza más altos.

La absorción de humedad del material tras su inmersión en agua de mar, fundamentalmente debido al carácter hidrofílico de la fibra de fique, genera un efecto plastificante que permite al laminado disipar más energía antes de alcanzar los umbrales de penetración y de perforación.

Las pruebas de ultrasonidos muestran que los impactos en el material sin sumergir, se encuentran restringidos justo a la zona de interacción entre el impactor y la pieza, mientras que en el material sumergido, el daño por el impactor se extiende a una zona más amplia creando un gradiente de daño en el material a medida que aumenta la energía de impacto.

Tras la caracterización a tracción, se puede concluir que el biocomposite sumergido pierde rigidez debido a la degradación de la matriz. Sin embargo, aumenta ligeramente su elongación a rotura debido a la comentada absorción de humedad.

En el microscopio electrónico se corrobora la plastificación del laminado tras su inmersión en agua de mar, observándose una mayor elongación a rotura de las fibras.

Agradecimientos

Se agradece a la Estación Marina de Biología y Biotecnología Experimentales de Plentzia (Plentziako Itsas-Estazioa – PIE) perteneciente a la Universidad del País Vasco (UPV/EHU) por la disposición de sus instalaciones para la realización del presente trabajo de investigación.

Referencias

[1] AL-Oqla, F.M. and Sapuan, S.M., Natural fiber reinforced polymer composites in industrial applications: Feasibility of date palm fibers for sustainable automotive industry, J.Clean.Prod, 66(3), pp. 347-354, 2014. DOI: 10.1016/j.mseb.2006.02.034

[2] Kelkar, A.D. Tate, J.S. and Chaphalkar, P., Performance evaluation of VARTM manufactured textile composites for the aerospace and defense applications, Materials Science and Engineering: B, 132(7), pp. 126-128, 2006. DOI: 10.1016/S0266-3538(02)00265-8

[3] Corum, J.M. Battiste, R.L. and Ruggles-Wrenn, M.B., Low-energy impact effects on candidate automotive structural composites, Composites Sci.Technol., 63(6), pp. 755-769, 2003.

[4] John, M.J, and Thomas, S., Biofibres and biocomposites, Carbohydr. Polym., 71(3), pp. 343-364, 2008. DOI: 10.1016/j.carbpol.2007.05.040

[5] Marrot, L., Bourmaud, A., Bono, P. and Baley, C., Multi-scale study of the adhesion between flax fibers and biobased thermoset matrices, Materials & Desing, 62(10), pp. 47-56, 2014. DOI: 10.1016/j.carbpol.2007.05.040

[6] Dai, D. and Fan, M., Natural fibre composites: Materials, processes and properties, UK, Woodhead Publishing, 2013. ISBN: 978-0-85709-524-4

[7] Corradi, S., Isidori, T., Corradi, M., Soleri, F. and Olivari, L., Composite boat hulls with bamboo natural fibres, International Journal of Materials & Product Technology, 36(4), pp. 73-89, 2009. DOI: 10.1504/IJMPT.2009.027821

[8] Joshi, S.V., Drzal, L.T., Mohanty, A.K. and Arora, S., Are natural fiber composites environmentally superior to glass fiber reinforced composites?, Composites Part A: Applied Science and Manufacturing, 35(3), pp. 371-376, 2004. 10.1016/j.compositesa.2003.09.016

[9] Eichhorn, S.J., Baillie, C., Zafeiropoulos, N., Mwaikambo, L., Ansell, M., Dufresne, A., Entwistle, K., Herrera-Franco, P., Escamilla, G. and Groom, L., Review: Current international research into cellulosic fibres and composites, Journal of Materials Science, 36(9), pp. 2107-2131, 2001. DOI: 10.1023/A:1017512029696

[10] Nikolaos, E.Z., Interface engineering of natural fibre composites for maximum performance, Grece, Woodhead Publishing, 2011. ISBN: 978-1-84569-742-6

[11] Jacob, M., Thomas, S. and Varughese, K.T., Mechanical properties of sisal/oil palm hybrid fiber reinforced natural rubber composites, Composites Science and Technology, 64(7), pp. 955-965, 2004. DOI: 10.1016/S0266-3538(03)00261-6

[12] Koronis, G., Silva, A. and Fontul, M., Green composites: A review of adequate materials for automotive applications, Composites Part B: Engineering, 44(1), pp. 120-127, 2013. DOI: 10.1016/j.compositesb.2012.07.004

[13] La Mantia, F.P. and Morreale, M., Green composites: A brief review Composites Part A, 42(6), pp. 579-588, 2011. DOI: 10.1016/j.compositesa.2011.01.017

[14] Dicker, M.P.M., Peter, F.D., Anna, B.B., Guillaume, F., Mark K.H. and Paul M.W., Green composites: A review of material attributes and complementary applications, Composites Part A, 56(1), pp. 280-289, 2014. DOI: 10.1016/j.compositesa.2013.10.014

[15] Gómez-Hoyos. C. and Vázquez, A., Flexural properties loss of unidirectional epoxy/fique composites immersed in water and alkaline medium for construction application, Composites Part B: Engineering, 43(8), pp. 3120-3130, 2012. DOI: 10.1016/j.compositesb.2012.04.027

[16] Luna, G., Villada, H. y Velasco, R., Almidón termoplástico de yuca reforzado con fibra de fique: Preliminares, DYNA, 76(159), pp.145-151, 2009.

[17] Aktaş, M. Atas, C., İçten, B.M. and Karakuzu, R., An experimental investigation of the impact response of composite laminates, Composite Structures, 87(4), pp. 307-313, 2009. DOI: 0.1016/j.compstruct.2008.02.003

[18] Feraboli, P. and Kedward, K.T., A new composite structure impact performance assessment program, Composites Science and Technology, 66(10), pp. 1336-1347, 2006. DOI:

[19] Cartié, D.D.R. and Irving, P.E., Effect of resin and fibre properties on impact and compression after impact performance of CFRP Composites Part A: Applied Science and Manufacturing, 33(44), pp. 483-493, 2002. DOI: 10.1016/S1359-835X(01)00141-5

[20] Belingardi, G. and Vadori, R., Low velocity impact tests of laminate glass-fiber-epoxy matrix composite material plates, International Journal of Impact Engineering, 27(2), pp. 213-229, 2002. DOI: 10.1016/S0734-743X(01)00040-9

[21] González, E.V., Maimí, P., Camanho, P.P., Lopes, C.S. and Blanco, N., Effects of ply clustering in laminated composite plates under low-velocity impact loading, Composites Science and Technology, 71(6), pp. 805-817, 2011. DOI: 10.1016/j.compscitech.2010.12.018

[22] Lopes, C.S. Seresta, O., Coquet, Y., Gürdal, Z., Camanho, P.P. and Thuis, B., Low-velocity impact damage on dispersed stacking sequence laminates. Part I: Experiments, Composites Science and Technology, 69(7), pp. 926-936, 2009. DOI: 10.1016/j.compscitech.2009.02.009

[23] Agirregomezkorta, A., Martínez, A.B., Sánchez-Soto, G., Aretxaga, M.S. and Aurrekoetxea, J., Impact behaviour of carbon fibre reinforced epoxy and non-isothermal cyclic butylene terephthalate composites manufactured by vacuum infusion, Composites Part B: Engineering, 43(5), pp. 2249-2256, 2012. DOI: 10.1016/j.compositesb.2012.01.091

[24] Cuéllar, A. y Muñoz, I., Fibra de guadua como refuerzo de matrices poliméricas, DYNA, 77(162), pp. 137-142, 2010.

[25] Atas, C. and Liu, D., Impact response of woven composites with small weaving angles, International Journal of Impact Engineering, 35(2), pp. 80-97, 2008. DOI: 10.1016/j.ijimpeng.2006.12.004

[26] Fombuena, V., Bernardi, L., Fenollar, O., Boronat, T. and Balart, R., Characterization of green composites from biobased epoxy matrices and bio-fillers derived from seashell wastes, Materials Desing, 57(5), pp. 168-174.5, 2014.

F. Ramón-Valencia, es Ing. Mecánico en 2007 por la universidad de Antioquia, Colombia y MSc. en Diseño y Fabricación de alto rendimiento en 2009 por la Universidad de País Vasco (UPV/EHU) España, ha trabajado en el laboratorio de diseño de producto PDL, perteneciente a la escuela técnica superior de ingeniería ETSI de la Universidad de País Vasco, España, en áreas de digitalización tridimensional sin contacto y prototipado rápido (2009-2010). Actualmente es alumno del Programa de Doctorado Dirección de Proyectos – EURO MPM de la Universidad de País Vasco (UPV/EHU) España. Sus áreas de interés son principalmente caracterización físico-mecánica de materiales compuestos de matriz polimérica, procesos de fabricación de materiales compuestos reforzados con fibras naturales e ingeniería inversa.

A. Lopez-Arraiza, es Ing. Industrial en 2000 y Dr. en Ingeniería de Materiales en 2008, ambos por la Universidad del País Vasco (UPV/EHU) España. Ha desarrollado su carrera investigadora (2007-2009) en el área de materiales de matriz polimérica tanto para uso médico como industrial en la Universidad de Mondragón, España y en el Centro Tecnológico IDEKO-IK4 (2009-2011). Actualmente, es docente investigador en la Escuela Náutica de la Universidad del País Vasco (UPV/EHU), España. Ha participado en más de 10 proyectos de investigación correspondientes a convocatorias competitivas y en cuanto a publicaciones, es autor/coautor de 13 artículos en revistas de impacto JCR y ha participado en 11 congresos nacionales/internacionales.
ORCID: 0000-0002-3258-1888

J.I. Múgica, recibió el título de Ing. Industrial, especializado en Mécanica, en 2012 por la Escuela Politécnica Superior de Mondragón (Mondragon

University), España. Tras haber trabajado como becario colaborador a lo largo de la carrera, comienza en 2012 su tesis doctoral en la misma universidad. Simultáneamente, comenzó el Máster de Comportamiento Mecánico de Materiales en la misma universidad, que finalizó en 2013, así como el Máster de Métodos Numéricos para Cálculo y Diseño en Ingeniería (a distancia) en el International Center for Numerical Methods in Engineering (CIMNE) de Barcelona. Actualmente, se encuentra haciendo la tesis de fin de máster, del anteriormente citado, y en su cuarto y último año de tesis doctoral, pendiente de la defensa de la misma.

J. Aurrekoetxea, es Ing. Mecánico y Dr. en Ingeniería de Materiales por la Universidad de Mondragón, España. Desde el año 2009 es responsable de la línea de investigación en tecnología de materiales de la Escuela Politécnica Superior de Mondragón, España. Ha participado en más de 20 proyectos de investigación correspondientes a convocatorias competitivas nacionales y europeas y en cuanto a publicaciones, es autor/coautor de 23 artículos en revistas de impacto JCR y ha participado en 21 congresos nacionales/internacionales. Igualmente ha sido miembro del comité organizador X Congreso Nacional de Materiales (2008).

J.C. Suárez-Bermejo, es Ing. en Metalurgia en 1985 por la Universidad Complutense, España, esMSc. en Ciencia de los Materiales en 1987 en la Universidad Politécnica, España, Dr. en Ciencia de los Materiales en 1990 por la Universidad Complutense, España y Diplomado en Física en 2005 en la UNED, todos ellos en Madrid, España. De 1987 a 1990, trabajó en Airbus (Madrid, España) en el departamento de desarrollo de ingeniería de compuestos. En 1995 y 1996 fue investigador invitado por la Universidad de Osaka, con las comunidades europeas S & T programa de becas en Japón. Actualmente es profesor titular del Departamento de Ciencia de Materiales y director del Centro de Investigación de Materiales Estructurales (CIME) de la Universidad Politécnica de Madrid, España. Sus intereses de investigación incluyen: la mecánica de fractura, ensayos no destructivos, y la integridad estructural de materiales híbridos.
ORCID: 0000-0001-7789-2164

B.A Ramón-Valencia, Ingeniero Metalúrgico en 2002 de la Universidad Industrial de Santander, Colombia. Dr. en Ingeniería de Materiales en 2010 en la Universidad del País Vasco, España. Vinculado desde el 2003 hasta 2013 como profesor de tiempo completo ocasional en el Dpto de Mecánica, Mecatrónica e Industrial de la Facultad de Ingenierías y Arquitectura de la Universidad de Pamplona, Colombia. Actualmente, es profesor titular del programa de Ingeniería Mecánica en la misma Universidad. Coordinador de la línea de investigación en Materiales y Procesos en el Grupo de Investigación en Ingeniería Mecánica de la Universidad de Pamplona, Colombia. Sus áreas de interés son principalmente los materiales compuestos reforzados con fibras naturales y el desarrollo de materiales sostenibles medio-ambientalmente a partir de residuos agro-industriales.

UNIVERSIDAD NACIONAL DE COLOMBIA
SEDE MEDELLÍN
FACULTAD DE MINAS

Área Curricular de Ingeniería
Geológica e Ingeniería de Minas y Metalurgia

Oferta de Posgrados

Especialización en Materiales y Procesos
Maestría en Ingeniería - Materiales y Procesos
Maestría en Ingeniería - Recursos Minerales
Doctorado en Ingeniería - Ciencia y Tecnología de Materiales

Mayor información:

E-mail: acgeomin_med@unal.edu.co
Teléfono: (57-4) 425 53 68

UNIVERSIDAD NACIONAL DE COLOMBIA
SEDE MEDELLÍN
FACULTAD DE MINAS



DYNA
http://dyna.medellin.unal.edu.co/

Effect of V addition on the hardness, adherence and friction coefficient of VC coatings produced by thermo-reactive diffusion deposition

Fredy Alejandro Orjuela-Guerrero [a], José Edgar Alfonso-Orjuela [b] & Jhon Jairo Olaya-Flórez [c]

[a] *Facultad de Ingeniería, Fundación Universitaria Los Libertadores. Bogotá, Colombia. faorjuelag@libertadores.edu.co*
[b] *Departamento de Física, Grupo de Ciencia de Materiales y Superficies, Universidad Nacional de Colombia. Bogotá, Colombia. jealfonsoo@unal.edu.co*
[c] *Departamento de Ingeniería Mecánica y Mecatrónica, Universidad Nacional de Colombia. Bogotá Colombia. jjolayaf@unal.edu.co*

Received: February17th, 2015. Received in revised form: May 29th, 2015. Accepted: October 22th, 2015.

Abstract
Vanadium carbide (VC) coatings were deposited on AISI H13 and AISI D2 steel substrates via thermo-reactive deposition/diffusion (TRD) in order to evaluate their mechanical properties as a function of the vanadium content. The coatings were produced with different percentages of ferrovanadium in the reactive mixture. The chemical composition of the coatings was determined through X-ray fluorescence (XRF), the crystal structure was analyzed using X-ray diffraction (XRD), the morphology was characterized using scanning electron microscopy (SEM), the hardness was measured with nanoindention, and the tribological behavior was studied using the ball-on-disc test. The XRF analysis indicated that the coatings grown on D2 steel decreased the atomic percentage of vanadium when the coating was made with 20% ferrovanadium. The XRD analysis established that the coatings were polycrystalline, with a cubic structure. The SEM images revealed that the coatings grown on D2 steel were more compact than those grown on H13 steel. Finally, the wear tests established that the friction coefficient decreased with an increase of vanadium in the coating.

Keywords: Coatings, Thermo-reactive deposition, crystal structure, Mechanical properties

Efecto de la adición de V en la dureza, adherencia y el coeficiente de fricción de recubrimientos de VC producidos mediante deposito termo-reactiva/difusión

Resumen
Se produjeron recubrimientos de carburo de vanadio (VC) sobre sustratos de acero AISI H13 y acero AISI D2 mediante deposito termo-reactiva/difusión (TRD) con el fin de evaluar sus propiedades mecánicas como una función del contenido de vanadio. Los recubrimientos se producen con diferentes porcentajes de concentración de ferrovanadio. La composición química de los recubrimientos se determinó mediante fluorescencia de rayos X (XRF), la estructura cristalina se analizó utilizando difracción de rayos X (XRD), la morfología se caracterizó usando microscopía electrónica de barrido (SEM), la dureza se midió a través de nanoindentaciòn, y las propiedades tribológicas mediante la prueba de bola sobre disco. El análisis XRF indicó que los recubrimientos crecidos en acero D2 disminuyó el porcentaje atómico de vanadio cuando el recubrimiento se produce con 20% de ferrovanadio. El análisis XRD estableció que los recubrimientos eran policristalinos, con una estructura cúbica. Las imágenes de SEM revelaron que los recubrimientos crecidos en acero D2 eran más compactos que los crecidos en el acero H13. Finalmente, las pruebas de desgaste establecieron que el coeficiente de fricción disminuyó con un aumento de vanadio en el recubrimiento.

Palabras clave: Recubrimientos, deposito Termo-reactivo, estructura cristalina, propiedades mechanics

1. Introduction

Typical protective coatings applied by the steel industry to reduce the effect of wear on equipment exposed to mechanically aggressive environments are hard layers of carbides, nitrides, borides, and oxides. These coatings are deposited using techniques such as physical vapor deposition (PVD), chemical vapor deposition (CVD), thermal spray, and

© The author; licensee Universidad Nacional de Colombia.

thermo-reactive deposition/diffusion (TRD). TRD has the advantage that it can deposit dense and homogenous layers that can be applied to steels containing carbon that has percentages higher than 0.3% [1]. TRD is also used for coating surfaces with hard materials in fluidized beds, molten salt baths, or powder. In addition, TRD is a simple and economical alternative for the production of layers of binary carbides such as VC, NbC, TiC, or Cr_7C_3, which are formed by the reaction between the carbon atoms of the substrate and the atoms of the carbide-forming elements (CFE). These elements are dissolved in molten borax and are then added to a mixture of ferroalloy and aluminum [1,2]. The properties of carbide coatings deposited on steels are: excellent adhesion, and wear and corrosion resistance. Because the layer growth depends on the diffusion of carbon, the process requires high temperatures, ranging from 800 to 1250°C, in order to maintain an adequate deposition rate. Carbide coating thicknesses ranging from 4 to 15 microns are obtained with processing times between 10 minutes and 8 hours, depending on the bath temperature and steel type [1-2].

Vanadium is an excellent CFE because it has a lower free energy of carbide formation and its free energy of formation of oxides is higher than that of B2O3 [3]. Vanadium carbide (VC) is a chemically stable compound with a cubic crystalline structure; it melts at high temperatures and has a high degree of hardness [4-6]. The study and characterization of the effect of the addition of vanadium on mechanical properties such as hardness, friction coefficient, and adherence of vanadium carbides deposited via TRD has not been explored sufficiently, but it has great potential in industrial applications such as sheet forming, machine elements subject to wear, and sliding tools for machining and molding [6-9]. The wear resistance and hardness of layers containing carbides obtained via TRD have been studied [10-14], and the layers have been reported to have good tribological properties. Fan et al. [5-7] recently studied the mechanism of growth and the microstructure of carbides prepared using TRD, analyzed the effect of the carbon activity on the preparation of these coatings on AISI H13 and AISI 9Cr18 steel, and developed a mathematical model to explain this effect. The aim of the present paper is to study the effect of the atomic percentage of vanadium on the growth of vanadium carbide coatings on two kinds of steel with different atomic carbon contents and to study the hardness, friction coefficient, and adherence of these coatings.

2. Experimental Procedure

2.1. Preparation of the substrates

VC coatings were deposited onto substrates of AISI H13 and AISI D2 tool steel using the TRD technique. These substrates were prepared with a 16 mm diameter and a 3 mm thickness, were subsequently polished with 600 grit sandpaper, and then washed in an acetone solution for five minutes in an ultrasound device. The hardness of the annealed AISI D2 and the annealed AISI H13 were 223 HB and 200 HB, respectively. The vanadium ferroalloy had a high content of Si (2.5%), V (60%), Al (1.5%), and C (0.45%).

2.2. Growth of the coatings

The TRD treatment was carried out at a temperature of 1050°C for 4 hours. The reaction mixture is formed by 4 wt% aluminum, and various weight percentages of ferrovanadium concentration with the same chemical composition, from 8 to 20 wt%, combined with borax pentahydrated ($Na_2B_4O_7 \cdot 5H_2O$) to complete the mixture. The samples were quenched in water without agitation. The time and temperature conditions ensured the complete austenitization of the steel used in this study without excessive distortion or abnormal grain growth, which produces mechanical changes.

2.3. Chemical and structural characterizations

The chemical composition of the layers was evaluated using a MagixPro Philips PW-2440 XRF spectrometer equipped with a rhodium tube with 4 kW maximum power. This device has a sensitivity of 200 ppm (0.02%) for heavy metals. Semi-quantitative analysis was performed using IQ software. The specimens were ultrasonically washed in an acetone solution for 5 minutes before each measurement.

The microstructure of the coatings was determined using a PANalytical X'Pert PRO diffractometer using Bragg Brentano geometry with Cu Kα radiation (λ=1.5405Å) between 10° and 90° with steps of 0.02°, a current of 40 mA, and a potential difference of 45 kV.

Analysis of the morphology and thickness of the coatings was performed using a JEOL 7600F electron microscope and a FEI Quanta 200 electron microscope. The images were obtained using secondary and backscattered electrons that were accelerated with 15 kV at 5.000X. The samples were polished so they had a mirror finish and were attacked with Villela to reagent their surface microstructure.

2.4. Wear resistance

The friction coefficient of the coatings was measured on a CETR-UMC-2 ball-on-disk tribometer using an Al2O3 ball (6 mm in diameter) as a sliding counterpart in air at room temperature. The sliding speed was 100 mm/s, and the load was fixed at 4 N. At the beginning of the test, the maximum Hertzian contact pressure was 1.5 Pa and the radius of the contact circle was 1.5 × 10−3 m, assuming a Young's modulus (E) of 380 GPa and a Poisson's ratio (v) of 0.23 for Al2O3, as well as E = 380.4 GPa and v = 0.23 for the VC coating, obtained using the nano-indentation test. The maximum shear stress was 165 MPa, located at a depth of ~1 μm below the coating surface.

2.5. Adherence and hardness

Taking into account the loss of carbon on the surface of the substrate due to the process of outward diffusion, and with the aim of determining how much the D2 and H13 steels support the layer of vanadium carbide, the degree of adhesion of the carbide layer formed on the two steels was determined using scratch tests, in order to determine the critical load where the first phenomenon of cohesive and interfacial failure at the edges of the scratch test appeared, as specified

Table 1.
Vanadium content determined by XRF, layer thickness, and lattice parameter for both steel and various amounts of ferroalloy in the reactive mixture.

Experimental Setup				
STEEL	Ferro-Vanadium (wt %)	Vanadium content (wt %)	Lattice Parameter (Å)	Thickness (μm)
AISI H13	8	7.264	4.161	2.25
AISI H13	12	21.158	4.171	6.90
AISI H13	16	40.480	4.167	7.96
AISI H13	20	61.507	4.179	9.536
AISI D2	8	16.007	4.169	6.43
AISI D2	12	57.142	4.169	7.86
AISI D2	16	58.462	4.167	8.81
AISI D2	20	52.166	4.167	8.71

Source: The authors'.

by the standard DIN-EN 1071-3 [15]. The average lengths of the defects were taken from the beginning of the scratch to the first spallation defect, and the critical load was determined taking into account that a graduated load was used, from 0 to 90 N, along the length of the 9 mm scratch and with an indenter velocity of 10 mm/min.

The hardness of the coatings was determined in accordance with ISO standard 14577 by using an NTH2 nanoindenter from CSM Instruments that was outfitted with a Berkovich indenter tip. A linear load was used with an approximate speed of 2000 nm/min, loading rate of 60 mN/min, maximum load of 30 mN, and loading dwell time of 15 s. The hardness was measured on the surface of the coatings and was measured in five different zones for each sample.

3. Results and discussion

3.1. Chemical composition and structural characterization

Table 1 shows the XRF, thickness, and lattice parameter results of the coatings deposited on the two steels. It shows the vanadium percentages in the coatings as a function of the ferrovanadium used in the coating process. In the chemical analysis, it is possible to observe that the vanadium increases lineally with the ferrovanadium concentration on the H13 substrate, while in the D2 substrate the vanadium percentage exhibits very different behavior. Initially it increases from 15% to 60% wt at low concentrations of ferrovanadium in the reactive mixture. There is no change from between 12% to 16%, and it slightly decreases at a 20% ferrovanadium concentration. The behavior at high concentrations of ferrovanadium is related to the carbon activity, which will be explained below. Table 1 also shows the thickness of the coatings as a function of the concentration of ferrovanadium. The results allow it to be established that the thickness of the coatings grown on the D2 substrate is higher at all ferrovanadium concentrations, with the exception of 20%, than those grown on the H13 substrate.

XRD analysis, presented in a previous paper [16], revealed that the vanadium carbide formed is polycrystalline with a face-centered cubic (FCC) structure, of NaCl type, in which the vanadium atoms occupy the FCC phase lattice and the carbon atoms occupy the interstitial positions between the vanadium (PDF card 01-073-0476) on both substrates. Moreover, the relative intensities of the (200) and (111) planes are higher in the vanadium carbide coatings grown on H13 substrates than those grown on D2 substrates, and the relationship between these planes is approximately 0.8 in both cases. These results indicate that the vanadium carbide grew with a higher degree of crystallinity in the substrate with a lower concentration of carbon atoms. Fig. 1 shows the cross section of the VC coatings deposited on D2 and H13 steels; the coating grown on D2 steel is more compact.

3.2. Hardness

Fig. 2a-b shows the values of the hardness of the VC coatings that were deposited on AISI H13 and AISI D2 tool steels. In coatings deposited on AISI D2, higher hardness values are exhibited in the samples manufactured with 20% ferroalloy, with values close to 3000 HV. These hardness values were higher than those reported in the literature [4, 6-13, 16], in which hardness values of about 2372 HV and 2270,9 HV were reported.

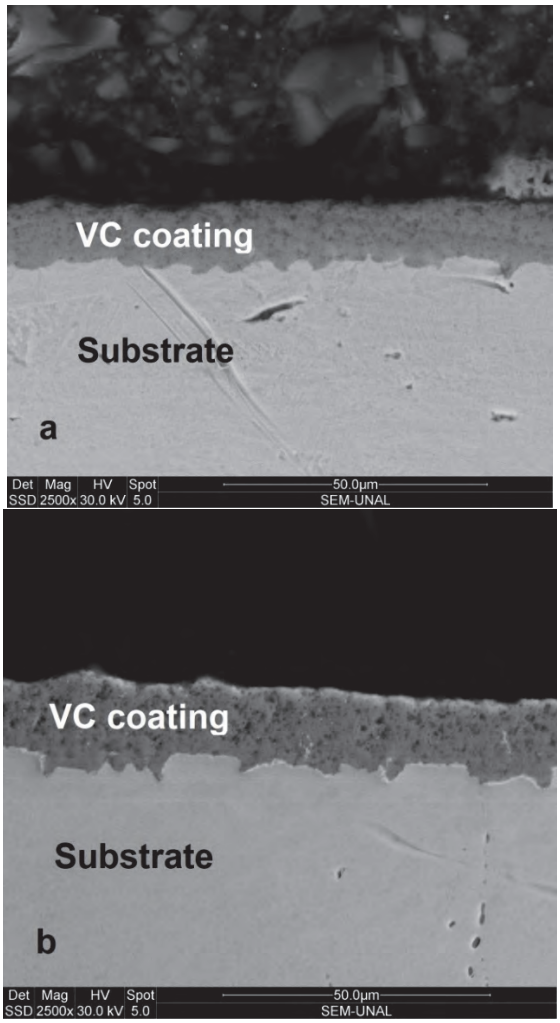


Figure 1. SEM images of the cross section of vanadium carbide coatings on a) AISI D2 steel and b) AISI H1, both obtained with 20% ferroalloy in the reactive mixture.
Source: The authors'.

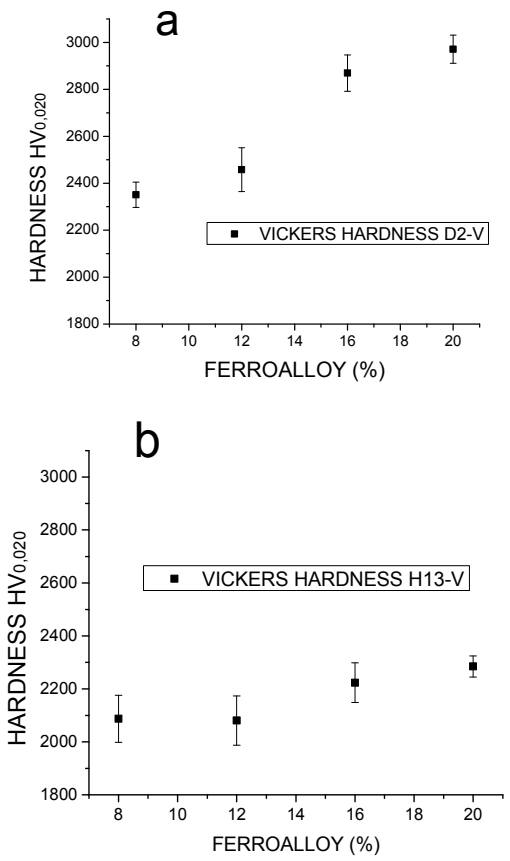


Figure 2. Hardness of VC coatings on steels a) AISI D2 and b) AISI H13 varying the ferrovanadium content.
Source: The authors'.

For vanadium carbide coatings deposited on AISI H13 steel, the highest hardness value was for the sample fabricated with 20% ferroalloy; however, this value is close to the average value of 2300 HV. Furthermore, one can observe that the type of steel significantly determines hardness results for these coatings. This can be explained by the amount of carbon necessary to form the carbide on each substrate, which sets the value of the carbon activity (Ac). This, in turn, significantly affects the solubility of carbon in the crystal structure of the carbide-forming element, and hence can influence the nucleation and growth of the vanadium carbide grains [7,14,17,18]. The AISI D2 steel can be characterized by a columnar microstructure of elongated grains. The high carbon content and its activity are capable of reducing the outward diffusion of carbon atoms on the growth surface. Under these manufacturing conditions, a low nucleation rate occurs, which hinders the continued growth of the coating. Furthermore, for AISI H13 steel it is possible to achieve an equiaxed grain microstructure, due to the decrease in the carbon content, which allows the value of the carbon activity to increase, favoring perpendicular growth so that it is approximately equal to the horizontal growth rate. Thus, an increase in the nucleation density reduces the grain size, and the formation of a compact microstructure is favored.

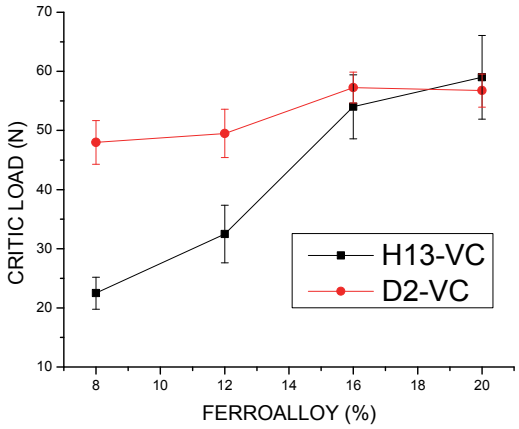


Figure 3. Critical load as a function of ferroalloy content two both steels.
Source: The authors'.

3.3. Adherence

Fig. 3 shows the adhesion results obtained for the coatings. It can be observed that critical loads are exhibited for the coatings produced with 20% ferroalloy, and lower critical loads were exhibited for vanadium carbide coatings on H13 steel produced with 8% ferroalloy. In general, all coatings exhibited a cohesive failure type characterized by ductile behavior in the scratch trace. Also, a small fracture area of the layer was observed, but not in the interphase substrate-coating, i.e. the phenomenon of widespread delamination in the coating was not present, allowing one to conclude that the coatings exhibit a high degree of adhesion and simultaneously good cohesion, since delamination failures or spallation were generally very mild and were present under relatively high critical loads.

Adhesion test results were characterized over a wide area by a buckling type deformation; see Fig. 4. This type of failure is related to the intrinsic fragility of the coating, and is observed in thick layers [18]. For all samples, the failure is buckling on the perpendicular scratching axis. This type of crack is characteristic of a solid Hertziana, where the fracture is fragile when a blunt indenter is used. It should also be noted that the coatings are produced by carbon diffusion from the substrate surface towards the coating, which may promote adhesion values of over 50 N, which are used for cutting tool applications [14,19-22].

3.4. Friction coefficient

Fig. 5, shows the SEM image taken with secondary electrons on the samples with 16 % ferroalloy. In the image it can be observed that there are cracks produced by a buckling of the tread surface, which is produced by application of a normal load on the sample. The results established that the wide track was possibly obtained by a plastic mechanism and oxidation with air.

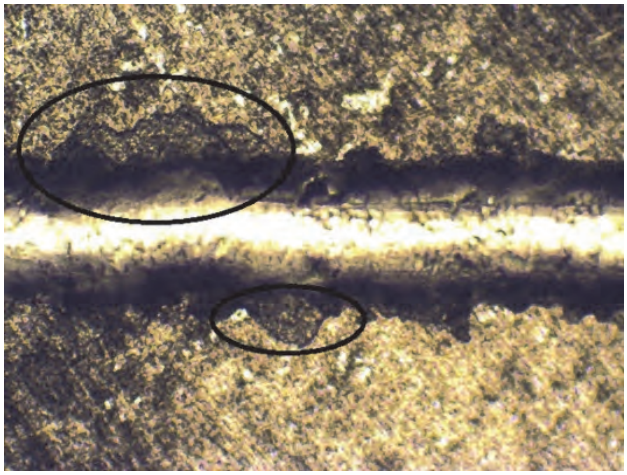


Figure 4. Footprint scratched upon layer of VC on D2 steel showing the type of fault.
Source: The authors'.

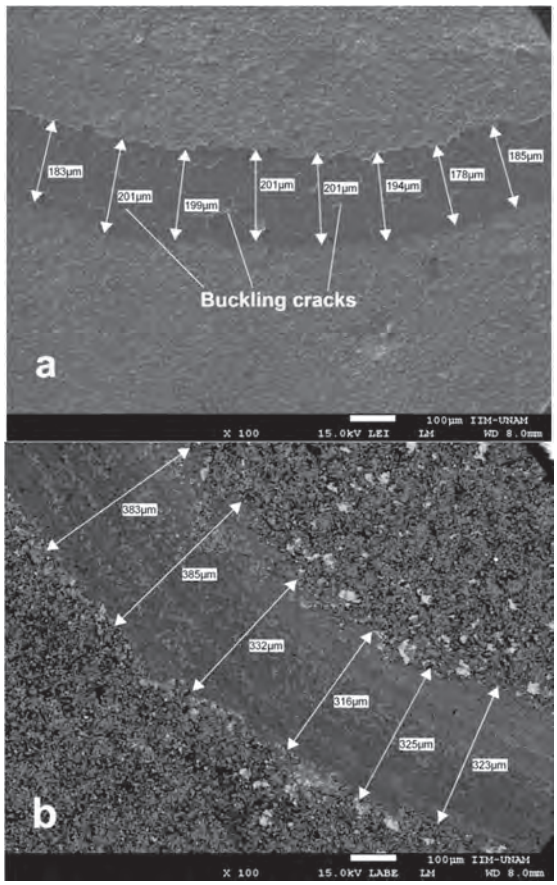


Figure 5. SEM micrograph of VC obtained on a) steel D2 b) steel H13
Source: The authors'.

The results for the friction coefficient (COF) for each of the layers studied are shown in Fig. 6. The results establish that for all coatings, the COF is improved relative to that of the substrate. In the coatings deposited on AISI D2 steel, the influence of the percentage of ferroalloy on the value of the COF is more evident, since it can be observed that increasing

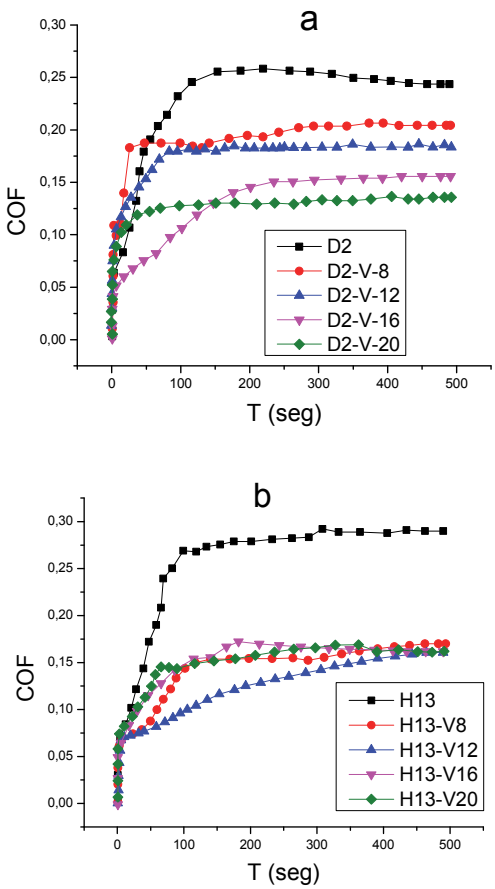


Figure 6. Coefficient of Friction of VC obtained on a) AISI D2 and b) AISI H13 steels.
Source: The authors'.

the ferroalloy content in the reactive mixture reduces the coefficient of friction to close to a value of 0.12. This behavior is possibly related to the formation of more compact and homogeneous layers. Additionally, samples deposited with 20% ferroalloy have the highest hardness and adhesion values.

The increased COF for the first 100 seconds of the test, observed in Fig. 6, can be explained by the plow mechanism, since when a load is applied to the system, the mechanical energy is dissipated by the deformation of the surfaces during sliding contact; if a hard roughness penetrates the softer surface, the plastic flow generated by the plow creates an increasing resistance to the movement and an increase in the friction coefficient [18,21]. The wear type that was exhibited by the carbide coatings was a combination of abrasive wear and adhesion wear. Adhesive wear is a form of deterioration that occurs between two surfaces in sliding contact, and it occurs when two surfaces are in contact, forming strong bonds between them. Due to the relative movement, bonds are either released and transferred between surfaces, or remain as free particles [18]. In Fig. 5, the optical micrographs of the typical signs of wear on these coatings can be observed. Also, the presence of alumina (Al2O3) particles that adhered to the surface thereof can be seen. For

all samples, adhesive and abrasive wear mechanisms due to debris or loose particles are present. [20,21]. The friction coefficient, adhesion, and hardness values obtained in the present research project are low and are comparable to hard coatings produced through techniques such as chemical vapor phase deposition. The coatings produced in the present research project lead to an excellent opportunity to produce coatings for cutting tools, improving their mechanical and tribological properties, enabling them to increase durability for fieldwork.

4. Conclusions

Vanadium carbide coatings were produced on AISI H13 and AISI D2 steel, varying the ferrovanadium content in the synthesis process. These coatings had a FCC cubic phase with orientation mainly in the planes (200) and (111). Upon increasing the vanadium content in the coating, the following was observed:

1. An increase in hardness, which reached values close to 3000 HV in the coatings deposited on AISI D2.
2. An increased coating adhesion, with the highest values of critical load higher than 50 N. This value can be explained by the process of diffusion of carbon on the coating surface and the chemical reaction with the vanadium.
3. The friction coefficient reached values close to 0.12, which can be explained by increased hardness and adhesion.

Acknowledgements

The authors gratefully acknowledge the financial support granted by the Departamento Administrativo de Ciencia, Tecnología e Innovación — COLCIENCIAS through project No. 338-2011. The authors acknowledge the support of the Universidad Nacional de Colombia (UNAL) and the Universidad “Los Libertadores”.

References

[1] Arai, T., Harper, S., Thermoreactive Deposition/Diffusion Process, ASM Handbook, 4, ASM International, Materials Park, OH, USA, p. 448, 1991.

[2] Liu, X., Wang. H., Li, D. and Wu, Y., Study on kinetics of carbide coating growth by thermal diffusion process, Surface & Coatings Technology 201, pp. 2414-2418, 2006. DOI: 10.1016/J.SURFCOAT.2006.04.028

[3] Arai, T., Fujita, H., Sugimoto, Y. and Ohta, Y., Diffusion carbide coatings formed in molten borax systems, J. Mater. Eng., 9(2), pp. 183-189, 1987.

[4] Aguzzoli, C., Figueroa, C.A., de Souza, F.S., Spinelli, A. and Baumvol, I.J.R., Corrosion and nanomechanical properties of vanadium carbide thin film coatings of tool steel. Surface & Coatings Technology. 206, 2725-2731, 2012. DOI: 10.1016/J.SURFCOAT.2011.11.042

[5] Fan, X.S., Yang, Z.G., Zhang, C. and Zhang, Y.D., Thermo-reactive deposition processed vanadium carbide coating: growth kinetics model and diffusion mechanism. Surface & Coatings Technology. 208, pp. 80-86, 2012. DOI: 10.1016/j.surfcoat.2012.08.010

[6] Fan, X.S., Yang, Z.G., Zhang, C., Zhang, Y.D. and Che, H.Q., Evaluation of vanadium carbide coatings on AISI H13 obtained by thermo-reactive deposition/diffusion technique. Surface & Coatings Technology. 205, pp. 641-646, 2010. DOI: 10.1016/j.surfcoat.2010.07.065

[7] Fan, X.S., Yang, Z.G., Xia, Z.X., Zhang, C. and Che, H.Q., The microstructure evolution of VC coatings on AISI H13 and 9Cr18 steel by thermo-reactive deposition process. Journal of Alloys and Compounds. 505, pp. L15-L18, 2010. DOI: 10.1016/j.jallcom.2010.06.064

[8] Castillejo, F.E. and Olaya J.J., Recubrimientos de VC y NbC producidos por DRT: Tecnología Económica, eficiente y ambientalmente limpia. Ciencia e Ingeniería Neogranadina. 22(1), pp. 95-105, 2012. ISSN 0124-8170

[9] Castillejo, F.E., Marulanda, D. and Olaya J.J., Estudio de recubrimientos de carburos ternarios de Niobio-Vanadio producidos sobre acero D2 usando la técnica de deposición por difusión termorreactiva. Revista Latinoamericana de Metalurgia y Meteriales. 34(2), pp. 230-239, 2014. ISSN: 0255-6952

[10] Sen, S. and Sen, U., Sliding wear behavior of niobium carbide coated AISI 1040 steel. Wear. 264, pp. 219-225, 2008. DOI: 10.1016/j.wear.2007.03.006

[11] Oliveira, C.K.N., Benassi, C.L. and Casteletti, L.C., Evaluation of hard coatings obtained on AISI D2 steel by thermo-reactive deposition treatment. Surface & Coatings Technology. 201, pp. 1880-1885, 2006. DOI: 10.1016/j.surfcoat.2006.03.036

[12] Gee, M.G., Gant, A., Hutchings, I., Bethke, R., Schiffman, K., Van Acker, K., Poulat, S., Gachon, Y. and von Stebut, J., Progress towards standardisation of ball cratering. Wear. 255, pp. 1-13, 2003. DOI: 10.1016/S0043-1648(03)00091-7

[13] Castillejo, F.E., Marulanda, D., Olaya J.J. and Alfonso, J.E., Wear and corrosion resistance of niobium–chromium carbide coatings on AISI D2 produced through TRD, Surface and Coatings Technology, 254(15), pp. 104-111, 2014. DOI: 10.1016/j.surfcoat.2014.05.069

[14] Orjuela A., Rincón, R. and Olaya, J.J., Corrosion resistance of niobium carbide coatings produced on AISI 1045 steel via thermo-reactive diffusion deposition, Surface and Coatings Technology, 259, pp. 667-675, 2014. DOI: 10.1016/j.surfcoat.2014.10.012

[15] DIN EN 1071–3, Methods of test for ceramic coatings, determination of adhesion and other mechanical failure modes by a scratch test. 2005.

[16] Castillejo, F., Marulanda, D., Rodriguez, O. and Olaya, J.J., Electrical furnace for producing carbide coatings using the thermoreactive deposition/diffusion technique. DYNA, 78(170), pp. 192-197. 2011, ISSN: 0012-7353

[17] Castillejo, F.E., Olaya, J.J. and Alfonso, E., Wear resistance of vanadium-niobium carbide layers grown via TRD. DYNA 81(184), pp. 1-2. 2014. DOI: 10.15446/dyna.v82n193.46657

[18] Orjuela, A., Resistencia a la corrosión en recubrimientos de carburo de vanadio y carburo de niobio depositados con la técnica TRD. Tesis de Maestría, Universidad Nacional de Colombia, Colombia, [En línea]. 2013. Disponible en: http://www.bdigital.unal.edu.co/10727/1/300281.

[19] Adachi, K.A. and Hutchings, I.M., Wear-mode mapping for the micro-scale abrasion test, Wear, 255, pp. 23-29, 2003. DOI: 10.1016/S0043-1648(03)00073-5

[20] Sen, U., Friction and wear properties of thermo-reactive diffusion coatings against titanium nitride coated steels Materials and Design 26, pp. 167-174, 2005. DOI: 10.1016/j.matdes.2004.05.010

[21] Devia, D., Mecanismos de desgaste en herramientas de conformado con recubrimientos de TiAlN por medio de sistemas PAPVD. Tesis de Doctorado. Universidad Nacional de Colombia, Facultad de Minas Medellín, Colombia, 2012.

[22] Taktak, S., Ulker, S. and Gunes, I., High temperature wear and friction properties of duplex surface treated bearing steels. Surface & Coatings Technology 202, pp. 3367-3377, 2008. DOI: 10.1016/j.surfcoat.2007.12.015

F.A. Orjuela-Guerrero received his BSc. Eng. in Mechanical Engineering in 2010, and his MSc. in Mechanical Engineering in 2013, both from the Universidad Nacional de Colombia, Bogotá, Colombia. He has worked in mechanical design programs and projects in the metal mechanic industry. In 2013 his is as he became a professor in the Engineering Department, at the Universidad Los Libertadores, Bogotá, Colombia, as well as a professor in

the Universidad Distrital Francisco José de Caldas, Bogota, Colombia. Since 2014, he has been a collaborator to a materials science and surfaces group that works with the publication of scientific papers.
ORCID: 0000-0003-4987-473X

J.E. Alfonso-Orjuela, completed his BSc. degree in Physics in 1987 and his MSc. degree in Science - Physics in 1991, both from the Universidad Nacional de Colombia, Colombia. In 1997 he completed his PhD in Science - Physics in the Universidad Autonoma de Madrid, Spain. He has taught at the Universidad Nacional de Colombia as a Professor since 2000, where his research has been focused on material science, particularly on thin film processing as well as performance characterization, and has studied thin film optical, electrical and mechanical properties.
ORCID: 0000-0003-4200-8329

J.J. Olaya-Flórez, is an associate professor at the Departamento de Ingeniería y Mecatrónica in the Universidad Nacional de Colombia, Bogotá, Colombia. He conducts research in the general area of development and applications of thin films deposited by plasma assisted techniques, corrosion, and wear. He received his PhD in 2005 from the Universidad Nacional Autonoma de México – UNAM, Mexico
ORCID: 0000-0002-4130-9675

UNIVERSIDAD NACIONAL DE COLOMBIA
SEDE MEDELLÍN
FACULTAD DE MINAS

Área Curricular de Ingeniería
Eléctrica e Ingeniería de Control

Oferta de Posgrados

Maestría en Ingeniería - Ingeniería Eléctrica

Mayor información:

E-mail: ingelcontro_med@unal.edu.co
Teléfono: (57-4) 425 52 64

UNIVERSIDAD NACIONAL DE COLOMBIA
SEDE MEDELLÍN
FACULTAD DE MINAS



DYNA
http://dyna.medellin.unal.edu.co/

Multi-level pedagogical model for the personalization of pedagogical strategies in intelligent tutoring systems

Manuel F. Caro [a], Darsana P. Josyula [b] & Jovani A. Jiménez [c]

[a] *Facultad de Educación y Ciencias Humana, Universidad de Córdoba, Montería, Colombia. mfcarop@unal.edu.co*
[b] *Department of Computer Science, Bowie State University, Bowie, USA. darsana@cs.umd.edu*
[c] *Facultad de Minas, Universidad Nacional de Colombia, Medellín, Colombia. jajimen1@unal.edu.co*

Received: February 20th, 2015. Received in revised form: May 8th, 2015. Accepted: October 21th, 2015.

Abstract
Pedagogic strategies are action plans designed to manage issues related to sequencing and content organization, specifying learning activities, and deciding how to deliver content and activities in teaching processes. In this paper, we present an approach to personalization of pedagogical strategies in Intelligent Tutoring Systems using pedagogical knowledge rules in a Web environment. The adaptation of pedagogical strategies is made based on a multilevel pedagogical model. An Intelligent Tutoring Systems called FUNPRO was developed to validate the multilevel pedagogical model. The results of empirical tests show that the multilevel pedagogical model enables FUNPRO to improve the process of personalization of pedagogical strategies, due to the reduction of inappropriate recommendations.

Keywords: Pedagogical strategy; Intelligent Tutoring System; multi-level pedagogical model; knowledge rules.

Modelo pedagógico multinivel para la personalización de estrategias pedagógicas en sistemas tutoriales inteligentes

Resumen
Las estrategias pedagógicas son los planes de acción encaminados a gestionar los aspectos relacionados con la secuenciación y organización de los contenidos, especificación de las actividades de aprendizaje, y decidir cómo entregar el contenido y las actividades en los procesos de enseñanza. En este artículo se presenta un enfoque para la personalización de las estrategias pedagógicas en Sistemas Tutoriales Inteligentes utilizando reglas de conocimientos pedagógicos en un entorno Web. La adaptación de las estrategias pedagógicas que se hace con base en un modelo pedagógico multinivel. Un Sistemas Tutorial Inteligente llamado FUNPRO fue desarrollado para la validación del modelo pedagógico multinivel. Los resultados de las pruebas empíricas muestran que el modelo pedagógico multinivel permite a FUNPRO mejorar el proceso de personalización de estrategias pedagógicas debido a la reducción de las recomendaciones inapropiadas..

Palabras clave: estrategia pedagógica; Sistema Tutor Inteligente; modelo pedagógico multinivel; reglas de conocimiento.

1. Introduction

An Intelligent Tutoring System (ITS) is an intelligent system that provides individualized instructions to students [1,2]. One of the main components in an ITS is the tutor module. The pedagogical model contained in the tutor module is responsible for determining the learning objectives and the selecting pedagogical strategies that are most appropriate to guide a particular student's learning process [3,4]. The pedagogical strategies are the set of actions performed to facilitate the instruction and learning of students.

Various approaches are discussed in the literature to develop individualized instructions in an ITS. The experts developed pedagogical strategies into static plans in the early versions of ITS [5]. The next step in the evolution of personalized instructions is the implementation of algorithms for the production of instructional plans [6-9]; however, these plans have been difficult to develop, maintain and modify.

Several approaches and proposals have been presented by various authors in order to improve the personalization of student instructions in ITS [10-12]. Karampiperis and Sampson [12] proposed an adaptive instructional plans

© The author; licensee Universidad Nacional de Colombia.

model, based on the use of ontologies. Although the instructional plan model can replan on its own when a student has trouble achieving his or her learning objectives, replanning takes place in terms of resources used and not in terms of pedagogical strategies.

Arias, Jiménez, and Ovalle proposed a model of instructional planning using Case-Based Reasoning (CBR) [13]. This model allows instructions to be adapted in order to meet the specific needs of each student. A major limitation of this model is that the activity plans that are generated can be incomplete if the case characteristics do not adequately cover the entire solution space.

More recently, personalization approaches have focused on the pedagogical model of the tutor module of the ITS. Barros [3] presented a pedagogical model designed using an ontology called pedagogical ontology. However, the model does not have mechanisms to auto adjust the strategies established by the ontology.

None of the studies reviewed to date has been designed with all three learning theories elements, teaching methods, and teaching tactics used in each stage of the lesson, within the same model.

The design of mechanisms for the formulation of pedagogical strategies in Intelligent Tutoring Systems is a complex task due to the number of variables involved. In particular, the selection of the methods or pedagogic tactics to be used for the development of a certain lesson requires the ITS to hold an extensive repertoire of pedagogical knowledge. In many cases, the ITS generates recommendations that are inappropriate for the student in terms of their profile or preferences. Inappropriate recommendations affect student performance in the lesson due to inconsistencies in the presentation of resources and an inadequate level of content or strategy to address the lesson.

In this context, the aim of this paper is to present a new approach to a pedagogical model for the personalization of pedagogical strategies in ITS. The proposed pedagogical model allows the ITS to personalize pedagogical strategies into five levels: learning resources, activity level, pedagogical tactics level, teaching methods, and educational theories level. Personalization can be based on student profile, dynamicity of student interaction, or be experience-based. The model allows the ITS a higher level of personalization of the pedagogical strategy in order to reduce the number of inappropriate recommendations for the student.

An ITS called FUNPRO was developed to validate the multilevel pedagogical model. The reasoning performed by the system is based on rules and pedagogical knowledge that is represented in the form of ontologies. The empirical tests results showed the high adaptive capacities that the multilayer model provides to FUNPRO.

The primary objective of the ITS is to provide personalized instruction [1,2]. Therefore, the main module of an ITS is the tutor module [14]. The tutor module is also known in the literature as the Instructional Planner [5,13,15].

The pedagogic model inside the tutor module has educational functions. It is responsible for guiding the teaching-learning process and deciding what pedagogical actions are undertaken, how, and when [1,13]. In ITS, the pedagogical model contained in the tutor module is responsible for determining the learning objectives and selecting pedagogical strategies that are most appropriate to guide the learning process of a particular student [3,4,16,17].

The instructional plan configures the pedagogic strategy used for each student. The purpose of the pedagogic strategies is to facilitate student instruction and learning [18]. Pedagogic strategies, in general, refer to abstract teaching methods [19]. Pedagogic strategies are oriented towards configuring activities and interfaces between the student and the imparting of learning process. In educational environments, the pedagogic strategies are action plans designed to manage issues related to sequencing and organizing instructional content [8], specifying learning activities, deciding how to deliver the content [19], and employing pedagogic tactics [4].

The main contribution of this work is the incorporation of levels of personalization in pedagogical strategies. Levels allow for a greater number of customization aspects in the pedagogical strategy. Each level of the model represents a component of the pedagogical strategy; at each level, the ITS collects data, undertakes reasoning and, if inappropriate, reconfigures recommendations that are generated.

This paper is organized as follows, Section 2 presents the architecture proposed for a pedagogic model in Intelligent Tutoring Systems, and the personalization rules implemented in this work are explained. Section 3 presents the methodology used to validate the pedagogical model. Section 4 presents an analysis of empirical data that was collected from the validation test. Finally, Section 5 discusses the main conclusions and future work

2. The multi-level pedagogical model

The pedagogical model is multilevel in order to enrich the possibilities for personalization of pedagogical strategies. The pedagogical strategy is personalized at each level according to each student's characteristics. The following five abstraction levels compose the proposed pedagogic model: Theory level, Method level, Tactic level, Activity level, and Resource level, see Fig. 1.

Each level of the pedagogical model is represented by ontologies. For the definition of educational domain terminology and for pre-selection of the teaching methods and pedagogical tactics, a literature review was carried out. Then, several meetings were held with a group of experts from the Department of Educational Psychology at the Universidad de Córdoba (COL). In these sessions, terminology was validated and the pedagogical tactics to be implemented were selected. In this way, elements of the pedagogical model's structure, described below, were defined.

2.1. Theory level

Learning theories are composed of a diverse set of theoretical frameworks, which try to explain how individuals access knowledge. Many features of pedagogical theories can be partially modeled by computer. In this paper, we have only included those characteristics that can be modeled computationally: the type

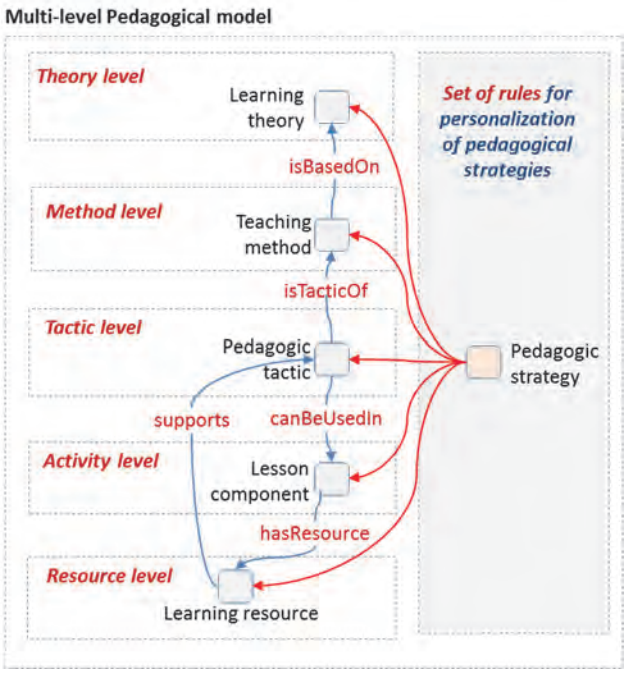


Figure 1. Multi-level pedagogical model
Source: The authors.

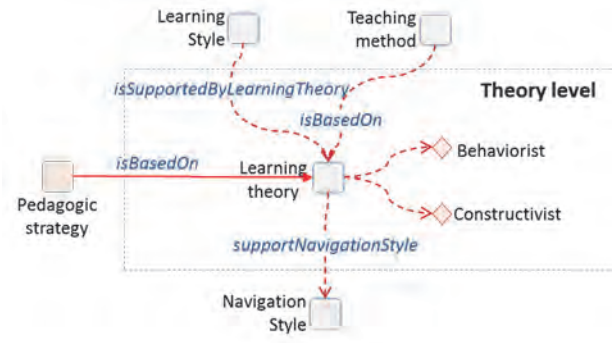


Figure 2. Ontology in Theory level
Source: The authors.

of content sequencing, the type of assistance provided to students, and the type of evaluation, see model in Fig. 2.

The proposed model supports two types of educational theories: behaviorism and constructivism. The characteristics of the behaviorism theory that are supported by the multilevel model are: linear navigation between contents, immediate reinforcement, and organization of content for levels with prerequisites.

Moreover, constructivist features supported by the multilevel model are: free navigation between content, content organization with minimal and necessary prerequisites, formative assessment, and activities for active student participation.

2.2. Method level

A teaching method is comprised by the principles that include an orderly logical arrangement of the tactics and

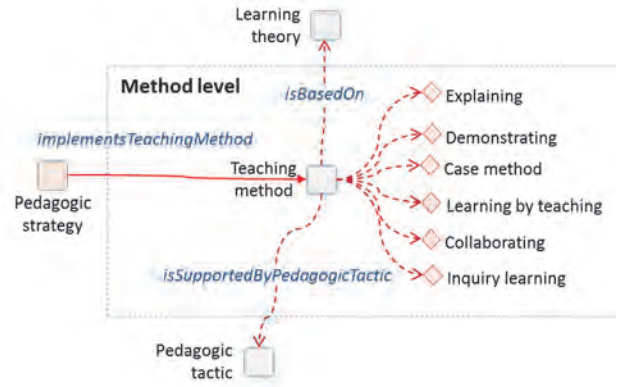


Figure 3. Ontology on a teaching method level
Source: The authors.

activities that are used in course lessons. The teaching methods are based on pedagogical theories; each method may contain all or part of the pedagogical principles in the theories, see Fig. 3.

The isBasedOn relationship determines the learning theory, which is based on a teaching method and establishes the content's organization. The is Supported By Pedagogical Tactic relationship, however, allows the association of the pedagogical tactics that will be used in the teaching method.

2.3. Tactic level

Tutor Module provides the learning objectives based on student characteristics. In addition, Tutor Module offers a range of pedagogic tactics for the student to achieve the learning objectives that have been established for him. Pedagogic Tactics are composed of actions and resources that are used in the interaction with the student [4] in order to provide a personalized teaching experience. The selection criteria used to include a pedagogic tactic in the Tutor Module was that such tactic can be modeled computationally [18,20]. In this work 19 pedagogic tactics were implemented (see Fig. 4).



Figure 4. Ontology on a pedagogical tactic level
Source: The authors.

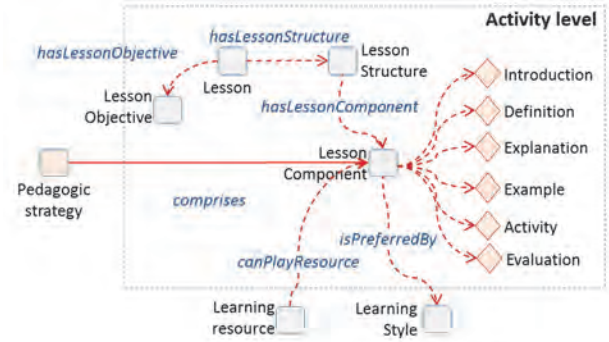


Figure 5. Ontology on an activity level
Source: The authors.

The canPlaysPedagogicalTactic relationship allows the pedagogical strategy to be associated with one or more lesson components. When a new learning resource is added, a new isResourceOfPedagogicalTactic relationship is created.

2.4. Activity level

The components of the lesson are the sections in which the lesson activities are organized. Fig. 5 shows the model of activity level.

The division of the lesson into sections has been widely used in the teaching practice [5,21,22]. Specifically, our proposal for lesson components is based on [22]; however, we make some modifications to adjust it to an education context in our university. Our proposed model suggests that there are six sections in the structure of a lesson: introduction, definition, explanation, example, activity, and evaluation.

In the Introduction section the objectives and information about the context of the lesson are presented. In the Description, the definitions and concepts related to the lesson are displayed. The Explanation section delves into concepts and issues relevant to the lesson. In the Example section, examples and demonstrations are provided that are related to the lesson's themes. In the Activity section, active pedagogical tactics, such as experiments, simulations, and exercises are employed. Finally, in the Evaluation section questionnaires and various types of tests to measure student achievement in the lessons are presented.

2.5. Resource level

Learning resources are digital objects such as images, animations, simulations, web pages, and more. Learning resources are the content carriers in the lesson and have different formats. Fig. 6 shows the relationship between the resource level and other of the model's components.

Students have the opportunity to assess the learning resources that the instructional planner recommends for each component of the lesson. The assessment is based on a scale of 1-5 as follows: (1) The resource was of no use in learning the lesson's subject, (2) the resource made little contribution to learning the lesson's topic, (3) the resource partially contributed in learning the lesson, (4) the resource was useful for the lesson, and (5) the resource was very useful for learning the lesson's topic.

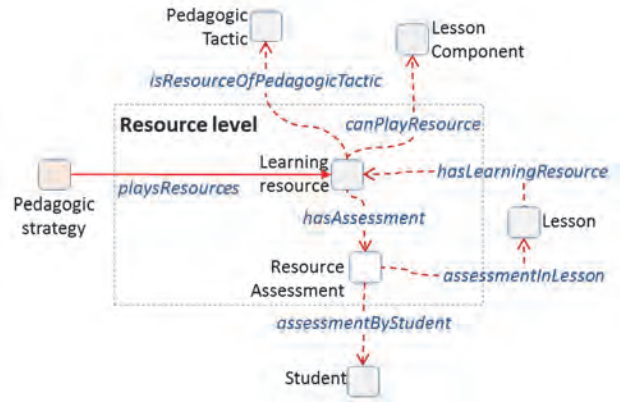


Figure 6. Ontology on a resource level
Source: The author'.

2.6. Personalization of pedagogical strategies

The pedagogical strategy has an internal representation consisting of three sections: context, recommendation, and performance, see Fig. 7.

The context section contains the input data used to configure the pedagogical strategy, which are: student information, course, and lesson. The recommendation section contains the settings for the pedagogical strategy, which are adapted to the student. This section consists of the navigation style, pedagogical theory, the teaching method, the components of the lesson that are enabled to students, and pedagogical tactics for each component. The performance section stores the result of the recommendation for a particular student's strategy. The performance of the strategy depends on the performance of the student in the lesson and has a scale of low, medium, and high.

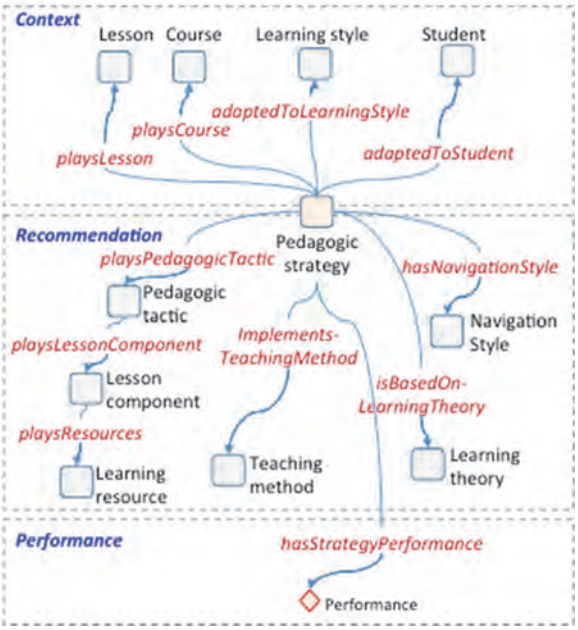


Figure 7. Ontological representation of a pedagogical strategy
Source: The authors.

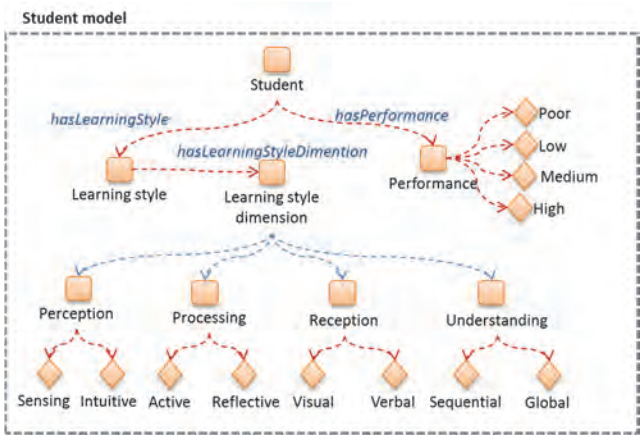


Figure 8. Ontology on a student model
Source: The authors.

Following the personalization process, the pedagogical strategy at each level of the model is described. Applying the rules of reasoning that comprise the pedagogical knowledge element of the model makes the personalization.

2.7. Personalization in learning theory's recommendations

The pedagogical strategies are implemented using learning theories criteria; otherwise, they would be limited to sequence of activities and tasks that do not have a clear educational purpose [23].

When a new student is registered, a profile is created immediately. The student fills out a form to generate his learning style profiles. When a registered student enters into the ITS, the pedagogical model activates the corresponding student model to adapt the teaching session. Preferences and indicators related to the student's level and learning style are obtained from the student model, see Fig. 8.

The approach used in this work to model the student learning style was based on the model developed by Felder [24]. Then, the following processes perform the personalization of pedagogical strategies on a learning theory level:

Profile-based adaptation: The adaptation takes the student's learning style into account as input parameters, including the dimension of understanding. For example, if the student has a predisposition that favors the sequential development of content, then the system will recommend a pedagogical strategy based on behaviorism. Otherwise, it will recommend a teaching strategy based on constructivism.

```
Rule 1:
Student (?s) ^ hasLearningStyle (?s,
sequential) ^
HaslearningStyleDimension (?ls,
understanding)
→ playsLearningTheory (?s, behaviorism)
(1)
```

Dynamic adaptation occurs when the recommended tactic for teaching a lesson is changed for a new one. If the new pedagogical tactic is based on a different pedagogical theory, the pedagogical strategy and student profile are updated.

```
Rule 2:
TeachingMethod (?tm) ^ TeachingMethod
(?new_tm) ^
isbasedOnLearningTheory (?tm , ?lt)  ^
isbasedOnLearningTheory (?new_tm, ?lt')
^
¬( LearningTheory (?lt) = LearningTheory
(?lt') )
→ playsLearningTheory (?s, ?lt')    (2)
```

2.8. Personalization in the teaching method recommendation

The adaptation at method level is performed in the following ways:

Adaptation is based on the theory of learning. Each teaching method is influenced by one or more learning theories. Thus, if it is recommended that the student use the constructivist theory of learning then this recommendation will be based on constructivist methods.

```
Rule 3:
Student (?s) ^ hasLearningStyle (?s,
?ls) ^ LearningStyle(?ls) ^
isSupportedByLearningTheory (?ls, ?lt) ^
LearningTheory (?lt) ^
isBasedOnLearningTheory(?ls, ?tm) ^
TeachingMethod (?tm)
→ implementsTeachingMethod (?s, ?tm) (3)
```

Dynamic adaptation occurs when the recommended tactic for teaching a lesson is changed for a new one. If the new pedagogical tactic is based on a different teaching method, the pedagogical strategy and student profile are updated.

```
Rule 4:
PedagogicTactic (?pt) ^
PedagogicTactic (?new_pt) ^
isSupportedByTeachingMethod (?pt , ?tm)
^
isSupportedByTeachingMethod (?new_pt,
?tm') ^
¬( TeachingMethod (?tm) = TeachingMethod
(?tm') )
→ implementsTeachingMethod (?s, ?tm')(4)
```

2.9. Personalization in the pedagogic tactic's recommendation

The personalization of pedagogical strategies on a pedagogical tactics level is performed in the following ways:

Profile-based adaptation: The pedagogical tactics recommendation of is carried out based on the student profile.

```
Rule 5:
Student (?s) ^ hasLearningStyle (?s,
?ls) ^ LearningStyle(?ls) ^
implementsTeachingMethod(?s, ?tm) ^
TeachingMethod(?tm) ^
givesSupportToPedagogicTactic(?tm, ?pt)
^
isSupportedByPedagogicTactic (?ls, ?pt)
^  PedagogicTactic (?pt) ^
canPlayInLessonComponent (?pt, ?lc)
→ playsPedagogicTactic (?lc, ?pt)   (5)
```

In this study, 19 pedagogic tactics were implemented, see Fig. 3. The selection of the pedagogical tactics was based on [4,18,20].

Dynamic Adaptation: This type of adaptation occurs when a student changes a recommended resource for a lesson with a new one. In this case, if the new resource supports a different kind of pedagogical tactic, the system reconfigures the recommendation preferences for the student and states that the tag recommendation is inappropriate.

```
Rule 6:
LearningResource (?current_lr) ^
LearningResource (?new_lr) ^
isResourceOfLessonComponent (?new_lr ,
?lc)  ^
isResourceOfPedagogicTactic (?new_lr,
?pt') ^
isResourceOfPedagogicTactic (?lr , ?pt)
^
¬( PedagogicTactic (?pt) =
PedagogicTactic (?pt') )
→ playsPedagogicTactic (?lc, ?pt')          (6)
```

2.10. Personalization in the learning resources recommendation

Adapting pedagogical strategies on a resource level occurs in the following cases:

Profile-based adaptation: Consists of the recommendation of resources according to the characteristics of the student profile.

```
Rule 7:
Student (?s) ^ hasLearningStyle (?s,
?ls) ^ LearningStyle(?ls) ^
canUseTeachingMethod(?s, ?tm) ^
TeachingMethod(?tm) ^
givesSupportToPedagogicTactic(?tm, ?pt)
^ PedagogicTactic (?pt) ^
isSupportedByPedagogicTactic (?ls, ?pt)
^  canPlayInLessonComponent (?pt, ?lc)
^ LearningResource (?lr) ^
isResourceOfLessonComponent (?lr , ?lc)
^
isResourceOfPedagogicTactic (?lr , ?pt)
→ playsLearningResource (?pt, ?lr)  (7)
```

Rule 7 is conditioned by the context of the pedagogical strategy and the result of the student evaluation for the learning resource after its use during the lesson. The resources are sorted from highest to lowest evaluation result. The model selects the resource with the highest performance.

Adaptation by preference: This type of recommendation occurs when a student changes the recommended learning resource to a different resource. In this case, the system updates the student's preferences according to the characteristics of the newly selected resource, and the new profile will be used to give new recommendations.

```
Rule 8:
LearningResource (?current_lr) ^
LearningResource (?new_lr) ^
isResourceOfLessonComponent (?new_lr ,
?lc)  ^
isResourceOfPedagogicTactic (?new_lr,
?pt) ^
isResourceOfPedagogicTactic (?lr , ?pt')
^
PedagogicTactic (?pt) = PedagogicTactic
(?pt')
→ playsLearningResource (?pt, ?new_lr)
(8)
```

3. Methodology

An ITS, to be used to learn Programming Fundamentals (FUNPRO) was developed using a MODESEC [25] methodology, and it is based on introspective learning [26]. FUNPRO was used to validate the multi-level pedagogic model and was developed entirely in SWI-Prolog. To edit the graphical interface, Notepad + + was used, see screenshot in Fig. 9.

3.1. Configuration of the experiment

A practical experiment was conducted in order to verify the personalization level of pedagogical strategies with respect to the preferences and profiles of students using FUNPRO. The experiment was conducted with 20 students undertaking an introductory course in programming. The course consisted of five lessons and had a basic level of complexity.

The performance metric used to measure the personalization level of pedagogical strategies was the average of changes made to the pedagogical strategies recommended at each model level. Changes in pedagogical strategies can be



Figure 9. FUNPRO screenshot
Source: The authors.

made directly by the student (e.g. when the student changes a learning resource) or dynamically (e.g., when the ITS detects a change in the student's learning preferences).

Changes made to the teaching strategy components, recommended for each student, will be interpreted as inappropriate recommendations. In this sense, if the amount of changes needed to adjust the pedagogical strategy according to the student's profile is high, and then the level of personalization of the teaching strategy will be low. Thus, the aims of the experiment were to see whether the multi-layer pedagogical model could increase the level of personalization of pedagogical strategies by reducing changes to the recommended strategy for each student in each lesson of the course, and also to observe if the reduction of inappropriate recommendations had a positive effect on student performance during the lesson.

4. Results

Data from the experiment will be described with respect to i) personalization of pedagogical strategies to the student profile at each level of the model and, ii) the relationship observed between the evaluation made by students in terms of learning resources and the changes made system to the pedagogical strategy.

i) Personalization of pedagogical strategies

In the data obtained from the experiment, with respect to the behavior of the adaptation of the pedagogical strategy to the student profile at each level of the model, the average number of adaptations per student observed at level of learning resources was 1.44. The average number of pedagogic tactic level adaptations was 0.82, the average number of adaptations at teaching method level was 0.35, and the average number of adaptations at learning theory level was 0.15.

Fig. 10 shows that the model level with the most number of adaptations was learning resource, and the level where there were fewer adjustments was learning theory.

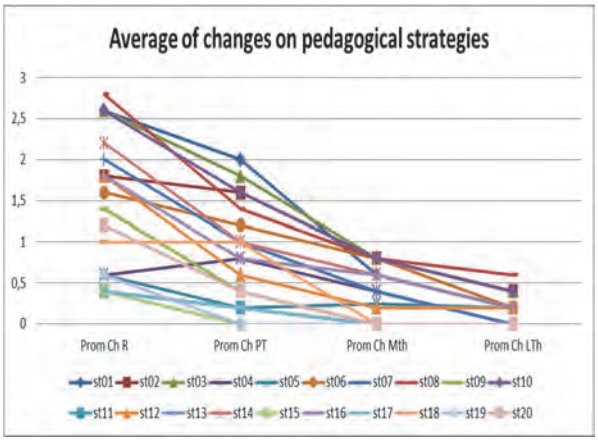
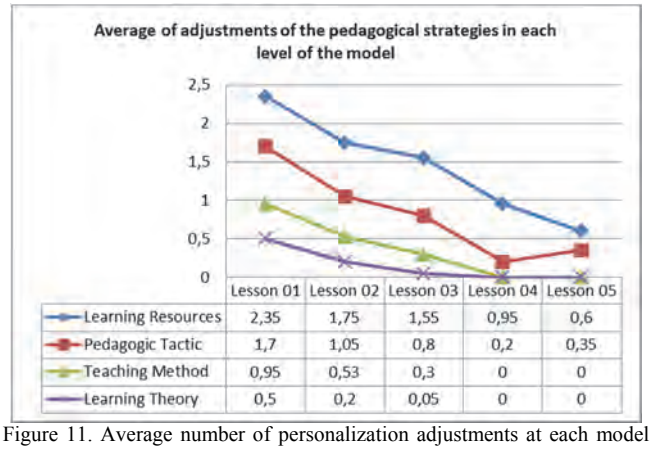


Figure 10. Average number of changes for pedagogical strategy
Source: The authors.



	Lesson 01	Lesson 02	Lesson 03	Lesson 04	Lesson 05
Learning Resources	2,35	1,75	1,55	0,95	0,6
Pedagogic Tactic	1,7	1,05	0,8	0,2	0,35
Teaching Method	0,95	0,53	0,3	0	0
Learning Theory	0,5	0,2	0,05	0	0

Figure 11. Average number of personalization adjustments at each model level
Source: The authors.

With respect to the occurrence of adaptation generated by the relationship between the levels, it can be said that 56.9% of resource changes made by the student generated changes in pedagogical tactics by applying rule (7). 42.7% of pedagogical tactic changes generated teaching method changes by applying rule (4), and 42.9% of teaching method changes generated Learning Theory changes for pedagogical strategy as a result of rule (2).

Fig. 11 shows the data on the average number of adaptations to the pedagogical strategy in each model level for each lesson in the course. With respect to the average of changes made to the pedagogical strategy recommended, a reduction of adaptations in each component of the strategy, while the student progresses in the course, is observed.

The results show that while the student's progress in the course, the system adapts its pedagogical strategy. Thus, for each new lesson the amount of required adjustments are minimal. Decreasing the number or adjustments indicates that as the student uses the system, the multilevel model improves recommendations for each component of the pedagogical strategy.

ii) Relationship between the resource evaluation and the changes made to the pedagogical strategy

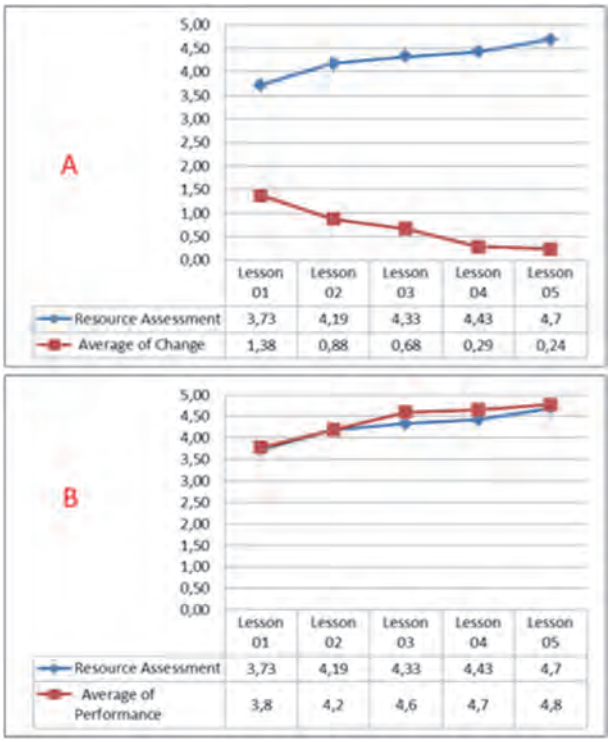


Figure 12. Relation between resource assessment and change average and performance average
Source: The authors.

Section (A) Fig. 12 shows the inverse relationship found between the average number of resources assessments made by student and the changes to the pedagogical strategy.

Students evaluate by giving the best score to which they prefer: the learning resources included in the teaching strategy in a new lesson or those learning resources that were recommended in a previous lesson. As the student evaluation of learning resources improves, there is a decrease in the percentage of adaptations required to personalize the pedagogical strategy. This is because the system learns with each adaptation to the pedagogical strategy, in turn producing better recommendations at each model level.

Section (B) of Fig. 12 shows the relationship between evaluations of learning resources and student performance in each lesson. When recommendations at each level of the pedagogical strategy are adapted to the profile of the student, an improvement in the student performance in the next lesson is observed.

5. Conclusions

In this paper, we have presented a multi-level pedagogical model-based on ontologies for the personalization of pedagogical strategies in ITS. Personalization of pedagogical strategies is made using rule-based reasoning. In this way, the structure of a pedagogical model for ITS, the main elements of which are the theories of learning, pedagogic strategies, and pedagogic tactics was defined.

The pedagogical tactics, teaching methods, and learning theories supported by the model, were determined by experts in Educational Psychology and supported by a literature review.

An ITS was used to learn about an introduction to programming (FUNPRO) by using MODESEC methodology. This was developed to validate the multi-level pedagogical model. Rules that create FUNPRO pedagogical knowledge were developed entirely in SWI-Prolog.

The results show that when the students' progress in the course the amount of required adjustments are minor. Decreasing the number of adjustments indicates that the multilevel model improves recommendations on each component of the pedagogical strategy as a result of rule (2, 4 and 7). The evidence found in the data produced in the experiment shows that the proposed multi-level model allows dynamic adaptation of the pedagogical strategy to each student's profile . Adaptations to each model level influence the improvement of student performance in the lessons that follow.

Acknowledgments

The authors thank the Department of Educational Psychology of the Universidad de Córdoba for the support and advice given throughout this work. The scholarship commission of doctoral studies from the University of Córdoba funded this research.

References

[1] Rongmei, Z. and Lingling, L., Research on internet intelligent tutoring system based on MAS and CBR, Conference: International Forum on Information Technology and Applications, IFITA 2009, Chengdu, China, pp. 15-17, May 2009. DOI: 10.1109/IFITA.2009.511, 2009. DOI: 10.1109/IFITA.2009.511

[2] Wang, Z., Design and implementation of an intelligent tutoring system for English instruction Xuejing Gu 1,2 Jie Hel Siyi Zhengl Wei Wangl 2., Intell. Comput. Intell. Syst. (ICIS), 2010 IEEE Int. Conf., (29-31) Oct, pp. 166-169, 2010.

[3] H. Barros, A. Silva, E. Costa, B. Ig, O. Holanda, and L. Sales, "Steps , techniques , and technologies for the development of intelligent applications based on Semantic Web Services : A case study in e-learning systems," Eng. Appl. Artif. Intell., vol. 24, no. 8, pp. 1355–1367, 2011. DOI: 10.1016/j.engappai.2011.05.007

[4] Bezerra-da Silva, C., Pedagogical model based on semantic web rule language, 12th Int. Conf. Comput. Sci. Its Appl., pp. 125-129, Jun. 2012.

[5] Viccari, R.M. and Jiménez, J.A., ALLEGRO : Teaching / Learning multi-agent environment using instructional planning and cases- based reasoning (CBR), CLEI Electron. Journal, 10(1), pp. 1-20, 2007.

[6] Jones, J.A. Intelligent tutoring systems: the first component of integrated information systems, Proceedings IEEE Int. Conf. Syst. Man, Cybern., pp. 531-536, 1992. DOI: 10.1109/icsmc.1992.271719

[7] Liu, J., The use of fuzzy reasoning in intelligent computer aided instructional systems, in Multiple-Valued Logic, 1988., Proceedings of the Eighteenth International Symposium on, 1988.

[8] Woo, C.W., Evens, M., Michael, J. and Rovick, A., Dynamic instructional planning for an intelligent physiology tutoring system, Comput. Med. Syst. - Proc. Fourth Annu. IEEE Symp., pp. 226-233, 1991.

[9] Specht, M. and Augustin, D.-S., ATS-adaptive teaching system a WWW-based ITS, Web-Based Knowl. Servers (Digest No. 1998/307), IEE Colloq., 1998.

[10] Espinosa, M.L., Sánchez, N.M., Valdivia, Z.G. and Pérez, R.B., Concept maps combined with case-based reasoning to elaborate intelligent teaching-learning systems, Computer (Long. Beach. Calif)., pp. 205-210, 2007. DOI: 10.1109/isda.2007.33

[11] Graham, C.R., Theoretical considerations for understanding technological pedagogical content knowledge (TPACK), Comput. Educ., 57(3), pp. 1953-1960, 2011. DOI: 10.1016/j.compedu.2011.04.010
[12] Karampiperis, P. and Sampson, D., Adaptive Instructional Planning using Ontologies, Proc. IEEE, 2004.
[13] Arias, F., Jiménez, J. and Ovalle, D., Arias, F., Jiménez, J. y Ovalle, D., Modelo de planificación instruccional en sistemas tutoriales inteligentes, Rev. Avances en Sistemas e Informática, 6(1), pp. 155-164, 2009.
[14] Soh, L. and Blank, T., Integrating case-based reasoning and meta-learning for a self-improving intelligent tutoring system, Int. J. Artif. Intell. Educ., 18(1), pp. 27-58, 2008.
[15] Aguilar, R., Muñoz, V., González, E.J., Noda, M., Bruno, A. and Moreno, L., Fuzzy and multiagent instructional planner for an intelligent tutorial system, Appl. Soft Comput., 11(2), pp. 2142-2150, 2011. DOI: 10.1016/j.asoc.2010.07.013
[16] Seridi, H., Sari, T., Khadir, T. and Sellami, M., Adaptive instructional planning in intelligent learning systems, Sixth IEEE Int. Conf. Adv. Learn. Technol., pp. 133-135, 2006.
[17] Cheung, K.S., Lam, J., Lau, N. and Shim, C., Instructional design practices for blended learning, Int. Conf. Comput. Intell. Softw. Eng., pp. 1-4, Dec. 2010. DOI: 10.1109/cise.2010.5676762
[18] Woo, C.W., Evens, M.W., Freedman, R., Glass, M., Shim, L.S., Zhang, Y., Zhou, Y. and Michael, J., An intelligent tutoring system that generates a natural language dialogue using dynamic multi-level planning., Artif. Intell. Med., 38(1), pp. 25-46, 2006. DOI: 10.1016/j.artmed.2005.10.004
[19] Mizoguchi, R., Hayashi, Y. and Bourdeau, J., Ontology-based formal modeling of the pedagogical world : Tutor modeling, Adv. Intell. Tutoring Syst. 308, pp. 229-247, 2010. DOI: 10.1007/978-3-642-14363-2_11
[20] Peña, C.I., Marzo, J., Lluís, J., Rosa, D. y Fabregat, R., Un sistema de tutoría inteligente adaptativo considerando estilos de aprendizaje, First Galecia Work., 2002.
[21] Amorim, R.R., Lama, M., Sánchez, E., Riera, A. and Vila, X.A., A learning design ontology based on the IMS specification the need for a learning design ontology. 9, pp. 38-57, 2006.
[22] Vesin, B., Ivanović, M., Klašnja-Milićević, A. and Budimac, Z., Protus 2.0: Ontology-based semantic recommendation in programming tutoring system, Expert Syst. Appl., 39(15), pp. 12229-12246, 2012. DOI: 10.1016/j.eswa.2012.04.052
[23] Ozdamli, F., Pedagogical framework of m-learning, Procedia - Soc. Behav. Sci., 31, pp. 927-931, 2012. 10.1016/j.sbspro.2011.12.171
[24] Felder, R.M. and Henriques, E.R., Learning and teaching styles in foreign and second language education, Foreign Lang. Ann., 28(1), pp. 21-31, 1995. 10.1111/j.1944-9720.1995.tb00767.x
[25] Caro, M.F., Toscano, R.E., Hermández, F. y David, M.E., Diseño de software educativo basado en competencias, Cienc. e Ing. Neogranadina, 19(1), pp. 71-98, 2009.
[26] Caro, M.F. and Jiménez, J.A., Analysis of models and metacognitive architectures in intelligent systems. DYNA, 80(180), pp. 50-59, 2013



M.F. Caro-Piñeres, is professor at the Department of Educational Informatics at the Universidad de Córdoba, Colombia. Coordinator of the Research Group on Cognitive Informatics and Cognitive Computing - Universidad de Córdoba – Colombia. His areas of interest: cognitive informatics, cognitive computing, metacognition in computation, design of educational software.
ORCID: 0000-0001-6594-2187



D.P. Josyula, is associate professor at the Department of Computer Science, in Bowie State University Bowie, USS. MSc. PhD. in Computer Science from the University of Maryland, College Park, USA. Her areas of interest: commonsense reasoning, philosophy of the mind, cognitive modeling, human-computer interaction, and dialog management.
ORCID: 0000-0001-7042-1028



J.A. Jiménez-Builes, he was born in Medellin and received his first BSc. degree in Computer Science and Informatics from the University of Medellin, Colombia. He then received his MSc. in Computer Science in 2001 and PhD. in Computer Science, in 2006, all of them from the Universidad Nacional de Colombia; Medellín, Colombia. He has been full time professor of the Faculty of Mines at the Universidad Nacional de Colombia, Medellín, Colombia, since 2005. Additionally, he is the director of the Artificial Intelligence for Education research group, based at the Universidad Nacional de Colombia.
ORCID: 0000-0001-7598-7696

UNIVERSIDAD NACIONAL DE COLOMBIA
SEDE MEDELLÍN
FACULTAD DE MINAS

Área Curricular de Ingeniería
de Sistemas e Informática

Oferta de Posgrados

Especialización en Sistemas
Especialización en Mercados de Energía
Maestría en Ingeniería - Ingeniería de Sistemas
Doctorado en Ingeniería- Sistema e Informática

Mayor información:

E-mail: acsei_med@unal.edu.co
Teléfono: (57-4) 425 5365

UNIVERSIDAD NACIONAL DE COLOMBIA
SEDE MEDELLÍN
FACULTAD DE MINAS



DYNA
http://dyna.medellin.unal.edu.co/

Impact of working conditions on the quality of working life: Case manufacturing sector colombian Caribbean Region

Laura Martínez-Buelvas [a], Oscar Oviedo-Trespalacios [a, b] & Carmenza Luna-Amaya [c]

[a] *Departamento de Ingeniería Industrial, Universidad del Norte, Barranquilla, Colombia. buelvasl@uninorte.edu.co*
[b] *Centre for Accident Research and Road Safety – Queensland (CARRS-Q), Institute of Health and Biomedical Innovation (IHBI), Queensland University of Technology (QUT), Brisbane, Australia oscar.oviedotrespalacios@qut.edu.au*
[c] *Departamento de Ingeniería Industrial, Universidad del Norte, Barranquilla, Colombia. cluna@uninorte.edu.co*

Received: February 22th, 2015. Received in revised form: June 1rd, 2015. Accepted: June 11th, 2015.

Abstract
This paper investigate the impact of Working Conditions on Quality of Working Life of human talent of manufacturing sector in the Colombian Caribbean region. To analyze this process interviewed 518 employees in the sector. The experimental design used was not descriptive cross type; each participant was applied an interview with the instrument of Working Conditions and Quality of Working Life Tool (Wage and Subjective Conditions). Data were analyzed using correlation analysis and logistic regression models. The results showed that the thermal environment and safety standard at work positively affects the Quality of Working Life. These results show that the relationship between working conditions and CVL is based on competition and far from linear or simple relationship relating to the consideration of the presence or absence of working conditions. This has implications when formulating policies, programs and interventions to prevent the negative effects of working conditions and enhance the industrial safety within industrial companies.

Keywords: Quality of Work Life, Working Conditions, Industrial Safety

Impacto de las condiciones de trabajo en calidad de vida laboral: Caso del sector manufacturero de la Región Caribe colombiana

Resumen
La presenta investigación centra su atención en evaluar el impacto de las Condiciones de Trabajo en la Calidad de Vida Laboral del talento humano de sector manufacturero de la región Caribe colombiana. Para analizar este proceso se entrevistaron a 518 empleados del sector. El diseño utilizado fue no experimental de tipo transversal descriptivo, puesto que a cada participante se le aplicó una entrevista con el instrumento de Condiciones de Trabajo y la Herramienta de Calidad de Vida Laboral (Condiciones Salariales y Subjetivas). Los datos fueron analizados mediante análisis de correlación y modelos de regresión logística. Los resultados mostraron que el ambiente térmico y las normas de seguridad en el trabajo afectan de forma positiva la Calidad de Vida Laboral de los empleados del sector. Estos resultados ponen de manifiesto que la relación entre las condiciones de trabajo y la CVL se basa en la competencia y distan de ser una relación lineal y simple relacionada con la consideración de la presencia o la ausencia de las condiciones de trabajo. Ello tiene implicaciones a la hora de formular políticas, programas e intervenciones para prevenir, erradicar y amortiguar los efectos negativos de las condiciones de trabajo y mejorar la seguridad industrial dentro de las empresas.

Palabras Claves: Calidad de Vida Laboral, Condiciones de Trabajo, Seguridad Industrial.

1. Introducción

La Gestión del Talento Humano y seguridad industrial han evolucionado de un enfoque taylorista (adaptar el hombre a la máquina) a modelos encaminados a satisfacer al capital humano (adaptar la máquina al hombre); soportados en herramientas que permitan desarrollar funciones gerenciales de alto desempeño donde las necesidades y expectativas de los empleados son el centro de la gestión [1-3]. No obstante y como consecuencia de las distintas problemáticas laborales observadas en diferentes momentos históricos, la perspectiva desde la que se evalúan los

© The author; licensee Universidad Nacional de Colombia.

resultados del ambiente de trabajo ha cambiado considerablemente [4, 5].

Durante los años sesenta, los estudios se centraron en conocer la intensidad y características de los procesos correspondientes a la generación de empleo y a la capacidad de ajuste a los diferentes ambientes de trabajo que permitieran conducir a un mejor rendimiento de los empleados [6-8]. Pero hoy día, existe un mayor protagonismo por una nueva perspectiva en la cual, la organización debe responder a las necesidades de los empleados mediante el desarrollo de mecanismos para la toma efectiva de decisiones con respecto a su vida en el trabajo [8].

La Calidad de Vida Laboral (CVL) en los últimos años se ha convertido en los países desarrollados en el elemento de referencia denominado "estado de bienestar", concepto afectado de manera compleja por múltiples factores, entre ellos, el estado psicológico, el nivel de dependencia, las relaciones sociales, las características del ambiente y la salud física [9]. Adicionalmente, se puede definir como la exigencia y el anhelo del empleado con lo que respecta a las condiciones de trabajo, la remuneración, las posibilidades de desarrollo profesional, el equilibrio entre el rol laboral y familiar, la seguridad y las interacciones sociales en el lugar de trabajo [10-12].

El término Calidad de Vida Laboral (CVL) abarca una variedad de programas, técnicas, teorías y estilos de gestión, a través de los cuales se diseñan las organizaciones y los puestos de trabajos, a fin de conceder a los trabajadores mayor autonomía, responsabilidad y autoridad [13]. Desde este punto de vista, la CVL es un concepto amplio y heterogéneo dado la riqueza y pluralidad de los diferentes temas estrechamente relacionados con el mundo laboral, como consecuencia de las diversas disciplinas, enfoques teóricos y áreas de estudio desde el cual se puede abordar [14,15].

En el actual escenario mundial de crisis económica, en donde las políticas gubernamentales se centralizan en lograr mayores tasas de empleo, como mecanismo para iniciar el crecimiento económico y garantizar el bienestar social, el estudio de las condiciones de trabajo y la CVL cobra un especial interés para los investigadores académicos, empresarios y en especial para el trabajador [16]. En Colombia, la persistencia de la tasa de desempleo superior al 8% desde 2013, la existencia del trabajo informal, la discriminación laboral, el incumplimiento de los estándares laborales establecidos por el Gobierno, entre otros factores, son muestra de la complejidad de los problemas asociados al mundo del trabajo y la insuficiencia de los esfuerzos implementados por el Estado para superarlos [17].

Hoy día las organizaciones en su afán de ser competitivas frente a un mercado que va cambiando aceleradamente, están obligadas a desarrollar estrategias de adaptación como opciones para garantizar su permanencia en el mercado [4,18]. En este sentido, para que la economía pueda crecer y lograr como resultado la posibilidad de generar trabajos decentes para cada persona económicamente activa se tendrá que mejorar la productividad [19]. Por tal motivo, aspectos tales como la satisfacción de los empleados, la tecnología, la eficacia, la eficiencia, el clima laboral, las condiciones de trabajo y los esquemas de gestión organizacional son eslabones de una misma cadena y por lo tanto determinantes dentro de una estrategia para elevar la productividad [4].

Ahora bien, las condiciones de trabajo son consideradas como un factor determinante en los procesos de salud-enfermedad a los cuales se exponen los trabajadores; en un sentido amplio, las condiciones de trabajo se definen como, cualquier aspecto circunstancial en el que se produce la actividad laboral, incluyendo tanto factores del entorno físico en el que se realiza como las circunstancias temporales en que se da [1,20,21]. Se hace hincapié en la necesidad de mejorar las condiciones de trabajo para disminuir los riesgos asociados a la actividad laboral, y con ello mejorar no solo la seguridad y salud de los trabajadores, sino también su calidad de vida. En este contexto, las condiciones de trabajo son concebidas como el conjunto de circunstancias y características materiales, ecológicas, económicas, políticas, organizacionales, entre otras, a través de las cuales se efectúan las relaciones laborales [16, 22].

No obstante, el mejorar las condiciones laborales de las personas ha venido disminuyendo los riesgos laborales dentro de las empresas, pero también el tener en cuenta el comportamiento humano promueve prácticas más seguras que impactan en la CVL [23,24]. Es claro que durante los últimos años los avances realizados en el campo de CVL han dado frutos y actualmente se están estimando nuevas metodologías y/o herramientas que permitan evaluar las condiciones a las cuales los trabajadores están expuestos y de esta manera involucrarlos a conseguir no sólo los objetivos financieros y de operaciones de la empresa sino también los beneficios en pro de su desarrollo personal y profesional.

La presente investigación pretende cuantificar y estudiar la forma en la cual las condiciones de trabajo y la CVL interactúan. Su contenido incluye aspectos de tales condiciones que, en función de su presencia e intensidad, pueden actuar como factores protectores y promotores de salud, bienestar y calidad de vida laboral o, por el contrario, como factores de riesgo psicosocial.

En la literatura, hay una necesidad general de desarrollar herramientas más sofisticadas y mediciones de auto-reporte sensibles de seguridad, ya que la prueba sobre el terreno podría arrojar resultados riesgosos o económicamente inviable [25]. Adicional, a la fecha en Colombia no se ha realizado estudios que evidencien el impacto de las condiciones de trabajo en la Calidad de Vida Laboral del talento humano del sector manufacturero, por lo que surge interés particular de realizar esta investigación, de tal manera, que los resultados se constituyan en un sustrato valioso para los empleadores para buscar estrategias que dignifiquen el trabajo en el sector, mejoren los modelos de gestión organizacional y asignen eficientemente los recursos.

2. Calidad de vida laboral

El estudio de la Calidad de Vida Laboral (CVL) es uno de los temas más investigado en los últimos años a nivel internacional, motivado porque la situación laboral en forma mundial pasa por un momento de crisis, donde se observa que el nivel precario aumenta y los logros laborales obtenidos en los dos últimos siglos ha disminuido, debido en gran parte al

capitalismo global [2,26,27]. En este sentido, este concepto representa una serie de problemas conceptuales, dado que se consideran factores objetivos derivados del entorno, la organización y la naturaleza de la tarea [28]. Sin embargo, a este concepto se le puede adicionar la perspectiva del trabajador, a quien parece importante considerar la valoración subjetiva a la hora de describir e indagar sobre los aspectos que influyen en su desarrollo laboral [26,29].

El término "Calidad de Vida Laboral" fue acuñado en 1970 por Louis Davis, quien describió la preocupación que debía suscitar en toda la organización el bienestar y la salud de todos sus empleados para que se desempeñaran exitosamente en sus tareas [30]. La revisión de la literatura muestra las definiciones más clásicas de la CVL desde una perspectiva amplia y genérica basada en la valoración del individuo con relación a su medio de trabajo, predominando factores como la satisfacción laboral, la experiencia en la organización, la motivación por el empleo, las necesidades personales, entre otras [14,31].

En este orden de ideas, Poza y Prior definen la Calidad de Vida Laboral, como la forma en que se produce la experiencia laboral en condiciones objetivas, incluyendo aspectos como la salud laboral o la seguridad, y en condiciones subjetivas del trabajador, en el sentido de cómo lo vive. Asimismo, Lau expone que la CVL es un conjunto de condiciones y ambientes de trabajo favorables que protegen y promueven la satisfacción de los empleados mediante recompensas, seguridad laboral y oportunidades de desarrollo personal. Por otra parte, Chiavenato expone que la CVL representa un concepto multidimensional con dos situaciones antagónicas: por una parte se hace referencia a reivindicar el bienestar y satisfacción del empleado, y por la otra, se evidencia el interés de la organización en términos del incremento de la productividad y calidad final de los productos/servicios que ofrece [32,33].

Las definiciones más recientes se caracterizan por la identificación de la CVL con la satisfacción que el trabajo le genera el empleado manteniéndose un enfoque centrado en el individuo; adicionalmente, éstas se ven influenciadas por las nuevas formas de gestionar el talento humano quienes representan un papel destacado en las organizaciones [30].

Actualmente, el estudio de la CVL se ha venido abordando desde dos perspectivas teóricas-metodológicas: la primera evalúa el entorno de trabajo y la segunda valora la perspectiva psicológica [14]. Estas difieren por los objetivos que persiguen en su propósito de mejorar la calidad de vida en el trabajo. La perspectiva encaminada a evaluar el entorno de trabajo tiene como meta mejorar la calidad de vida mediante el logro de los intereses organizacionales, mediante el análisis del la organización entendida como un sistema, llevando a cabo un nivel de análisis macro [14,31]. Por su parte, la perspectiva psicológica muestra mayor interés por el trabajador, desarrollando un análisis minucioso de aquellos elementos puntuales que conforman las diversas situaciones a las cuales se enfrenta el trabajador. En definitiva, mientras la última corriente teórica señala la importancia de los aspectos subjetivos de la vida laboral, la perspectiva del entorno laboral subordina tales aspectos a las condiciones de trabajo y a los elementos estructurales de la organización [14,31].

Las mediciones de CVL se pueden realizar mediante la utilización de métodos objetivos o subjetivos. En las aproximaciones objetivas se evalúan las condiciones físicas del entorno laboral a través de informaciones siempre cuantitativas, proporcionadas por los representantes y/o documentos procedentes de la organización. Entre los instrumentos más utilizados están listados, perfiles y *checklist* [31]. No obstante, la aproximación subjetiva posibilita la percepción, juicio y opinión que tienen los empleados con respecto a sus condiciones de trabajo y entorno laboral. Recoge información cualitativa o cuantitativa de variables individuales. Las técnicas más utilizadas son la observación, la entrevista y cuestionarios [14].

Ambas metodologías presentan limitaciones y por si solas son insuficientes para dar cuenta de un concepto multidimensional y complejo como el de la CVL. Por tal motivo, la presente investigación tiene como objetivo evaluar el impacto de las condiciones de trabajo en la satisfacción, la salud y el bienestar de los empleados, es decir, en la Calidad de Vida Laboral, anteponiendo los intereses individuales de la organización, esto con el fin de minimizar la fragmentación y el sesgo en las evaluaciones.

3. Metodología

Para la presente investigación se optó por un tipo de estudio instrumental, debido a que en este caso el diseño de los instrumentos fue resultado del ajuste y adaptación de la literatura revisada, así como también del análisis de las propiedades psicométricas de diferentes herramientas de evaluación previamente definidas. [34-37].

La segunda etapa de la investigación de acuerdo a los resultados obtenidos fue del tipo multivariado, correlacional, transversal y no experimental, dado que se evidenció una fiel representación del fenómeno de estudio, en un momento dado de tiempo y sin manipulación de las variables [36,37].

3.1. Procedimiento

Los datos obtenidos en el estudio forman parte de una investigación más amplia donde no sólo se analizaron dimensiones de carácter socio-demográfico sino también, se evaluaron variables asociadas a las condiciones de trabajo y a las condiciones salariales y subjetivas asociadas a la CVL. Las entrevistas se realizaron entre los meses de Abril y Junio de 2013. La información se obtuvo a través de una entrevista de aproximadamente 90 minutos de duración, la cual fue realizada por el equipo de trabajo de la investigación, conformado por un ingeniero industrial y el grupo de apoyo que fue previamente entrenado y capacitado para brindar orientación a los trabajadores que así lo solicitaran durante la sesión de evaluación. Los empleados firmaron el consentimiento en el que se les indicó de forma expresa que se haría uso agregado de los datos exclusivamente con fines de investigación, preservando el anonimato.

3.2. Participantes

Los participantes del estudio son trabajadores del sector manufacturero de la región Caribe colombiana. En total

fueron entrevistados 518 empleados de diferentes empresas del sector.

En cuanto a la distribución de los participantes en atención al sexo el 67,8% son hombres, mientras que el 32,2% son mujeres. Los encuestados tenían edades comprendidas entre 17 y 68 años (media = 37 y D.E. = 11,73) y llevaban trabajando en la organización una media de 1 a 3 años. Su selección se hizo de forma aleatoria en cada uno de los diversos subsectores y tamaños de empresas (grandes, medianas y pymes).

Con respecto al tamaño de las empresas tenemos que el 32% correspondía a Grandes Empresas, el 34% a Medianas y el porcentaje restante a Pymes. Adicional, el subsector con mayor participación fue el sector metalmecánico representado por un 45%, a este le seguían el subsector energético (14%), el de alimentos y bebidas (12%), el de la construcción (11%) y el textil (10%).

3.3. Instrumentos

Los instrumentos que se aplicaron fueron validados siguiendo las metodologías de [35,34].

Herramienta Condiciones de Trabajo: Los factores estudiados para medir el impacto de las condiciones de trabajo en el sector manufacturero en la región Caribe colombiana, fueron extraídos de una revisión documental y de herramientas previamente diseñadas a las cuales se les realizaron adaptaciones conforme a las necesidades de investigación [38]. Para el caso en el cual se evaluaban las condiciones de seguridad en el trabajo se adaptó el instrumento desarrollado por Hayes et al [39], a partir del cual se valoraban integralmente las dimensiones de la percepción de seguridad en el trabajo. No obstante, conforme a la clasificación emitida por Casas et al [40], se incluyeron las preguntas asociadas al ambiente físico al cual se encuentran expuestos los trabajadores, con el fin de determinar los potenciales riesgos presentes en su labor diaria. La escala constó de 44 ítems que los participantes debían responder en una escala tipo Likert de 1 a 10 en función de su grado de acuerdo con cada una de las afirmaciones que se le presentaban, siendo 1 Totalmente en Desacuerdo y 10 Totalmente de Acuerdo.

Finalmente, se comprobó la fiabilidad y validez del instrumento mediante análisis factorial exploratorio y análisis de componentes principales con rotación VARIMAX. El método de consistencia interna basado en el alfa de Cronbach permitió estimar la fiabilidad del instrumento de medida a través de un conjunto de ítems que se esperaba midieran el mismo constructo o dimensión teórica; cuanto más cerca se encontrara el valor del alfa a 1 mayor es la consistencia interna de los ítems analizados.

La investigación reportó que la escala de condiciones de trabajo presenta una media de 5,38 (D.E. = 3,22) y un alfa de Cronbach de 0.793 lo que indica que este instrumento tiene un alto grado de confiabilidad, validando su uso para la recolección de datos; la evaluación de homogeneidad fue elevada en todos los casos obteniéndose correlaciones de ítems total superiores a 0,60. Adicional, la adecuación de los datos a la matriz factorial fue satisfactoria, encontrándose un KMO = 0,785. Por otra parte, sólo fueron interpretables cinco factores, los cuales se explicaron en un 73,128% con respecto a la varianza total. La estructura factorial quedó representada por 17 ítems escalonados en cinco grupos, a saber: carga física, ambiente térmico, ruido, riesgos laborales y seguridad en el trabajo.

Herramienta de Calidad de Vida Laboral (Condiciones Salariales y Subjetivas): Esta herramienta fue diseñada y aplicada como un instrumento de evaluación de componentes psicológicos y psicosociales que impactan en la Calidad de Vida Laboral (CVL). La base conceptual para el diseño de esta herramienta provino de investigaciones anteriores como las de Casas et al [40], Segurado Torres & Agulló Tomás [14], Akranavičiūtė & Ruževičius [1] y Bagtasos [26], con el fin de conocer los factores de condiciones salariales y subjetivas que desde la perspectiva del empleado, afectan su CVL, y de esta manera analizar su impacto en el sector al cual se evaluó. La herramienta constó de 98 ítems que los participantes debían responder en una escala tipo Likert de 1 a 10, siendo 1 Totalmente en Desacuerdo y 10 Totalmente de Acuerdo.

La escala correspondiente a las condiciones salariales estuvo constituida por 34 ítems que evalúan la percepción de los empleados con respecto a su salario, a su estabilidad laboral; así como también, por aquellos factores propios de su desarrollo personal al interior de la organización, a saber, habilidad mental, promoción y formación. De igual forma, los ítems de la escala subjetiva miden la conexión del individuo con el mundo y la actividad laboral que se da a su alrededor, analizado las interacciones a nivel jerarquizo, organizacional y social. Para el caso de la variable satisfacción laboral se adaptó el instrumento de Spector [41].

Después del análisis factorial exploratorio y análisis de componentes principales con rotación VARIMAX, la investigación reportó que las escalas presentan una media de 7,99 (D.E. = 2,37) y un alfa de Cronbach de 0,898 lo que indica que este instrumento tiene un alto grado de confiabilidad, validando su uso para la recolección de datos.; la evaluación de homogeneidad fue elevada en todos los casos obteniéndose correlaciones de ítems total superiores a 0,60. La adecuación de los datos a la matriz factorial fue satisfactoria encontrándose un KMO de 0,888 y una varianza total de 71,298%. La estructura factorial quedó representada por 20 ítems de los 98 iniciales, escalonados en cinco grupos, representados en: salario, estabilidad laboral, plano individual, jerárquico y técnico.

3.4. Variables del Modelo

Los variables que servirán para evaluar el impacto de las condiciones de trabajo en la percepción de la CVL del talento humano del sector manufacturero en la región Caribe colombiana, fueron extraídos luego de la validación de los instrumentos aplicados por [42].

En general, el estudio de las condiciones de trabajo representa una característica prominente del entorno laboral en donde se involucran temas económicos, sociales, políticos, tecnológicos, ergonómicos, entre otros [22]. Adicional, las dimensiones por medio de las cuales se medirá el impacto de la CVL se agrupan en: condiciones salariales, desarrollo vocacional, condiciones subjetivas y satisfacción laboral, dado que éstas permiten una perspectiva general del ambiente físico y social al cual está expuesto el trabajador. A

continuación se explica la escogencia de estas dimensiones y en la Fig. 1 se representa gráficamente dicha clasificación:

- Carga Física: Para el caso de estudio, este factor se describe con un alfa de Cronbach de 0,820 y correlaciones estimadas en un 0,562; suponiendo un factor potencial que está formado por los diferentes requerimientos físicos a los que se ve sometido el trabajador a lo largo de la jornada de trabajo, cuando se ve obligado a ejercer un esfuerzo muscular dinámico o esfuerzo muscular estático excesivo.
- Ambiente Térmico: este es uno de los factores que hace efecto en el aumento o disminución en los índices de productividad, en la tasa de siniestros y especialmente en la eficiencia y eficacia en la actividad laboral de un trabajador. Luego de la validación el factor quedó representada por un alfa de Cronbach de 0,793 y correlaciones estimadas de 0,410.
- El ruido, no es más que un sonido que es molesto para el oído humano, por lo cual se pueden generar inconformidades en la realización de cualquier actividad o bien perjuicios en la salud. Para el caso de estudio, este factor se describe con un alfa de Cronbach de 0,805 y correlaciones estimadas en un 0,559.
- Riesgo Laboral: Para los empleados de este sector esta variable supone considerar los riesgos a los cuales ellos se encuentran expuestos desde la percepción de su trabajo a diario, los problemas de salud que se generan, hasta la frecuencia de accidentes de trabajo en las actividades encomendadas. Representado por un alfa de Cronbach de 0,884 y correlaciones estimadas en un 0,654.
- Seguridad en el Trabajo: este factor está formado por una serie de garantías individuales de carácter universal que tiene por ley cualquier trabajador. Para el caso de estudio, este factor se describe con un alfa de Cronbach de 0,876 y correlaciones estimadas en un 0,497; indicando que es un factor potencial para evaluar la seguridad, la salud y la calidad de vida en el empleo, las cuales le brindan al trabajador confianza para desempeñarse efectivamente dentro de la organización.
- Salario: en este se considera la percepción que tienen los empleados con respecto al salario recibido manifestándose como una motivación para su desempeño. Para el caso de estudio, este factor se describe con un alfa de Cronbach de 0,855 y correlaciones estimadas en un 0,452, lo cual indica que es un factor potencial para evaluar los incentivos dados por la organización a los empleados para satisfacer sus expectativas e impulsar a realizar mejor su trabajo.
- Estabilidad Laboral: Para los empleados del sector este factor supone una relación positiva con la satisfacción laboral y con el compromiso organizacional.
- Plano individual: Con un alfa de Cronbach de 0,828 y correlaciones estimadas en un 0,61, este factor explica que la autonomía y la participación activa en la toma de decisiones son factores que influyen positivamente en la percepción de la CVL del talento humano del sector de estudio.
- Plano Jerárquico y Técnico: La confianza, la comunicación y el apoyo mutuo se constituyen en determinantes para la percepción positiva de este factor en el talento humano del sector manufacturero de la región, el cual se justifica por un alfa de Cronbach de 0,902.

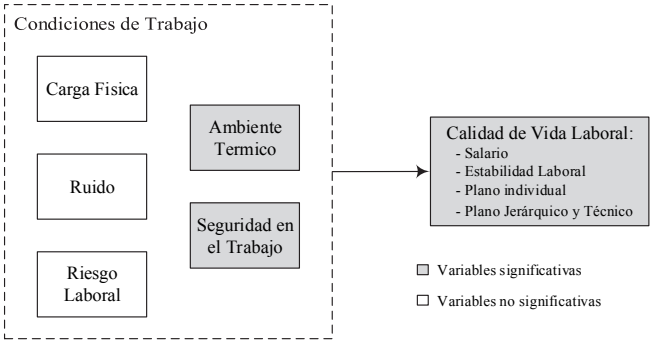


Figura 1. Clasificación de las variables de estudio
Fuente: Elaboración de los Autores

3.5. Análisis

La tabulación y depuración de los datos recopilados se hizo con el fin de verificar la utilidad de la data y posteriormente dar inicio al proceso de análisis estadístico. Inicialmente se realizó un análisis de correlación mediante el Estadígrafo de Correlación *r* de Pearson. Luego, se ajustaron una serie de modelos de regresión logística para la evaluación de la CVL. Estos modelos incluyeron una serie de variables relacionadas con la CVL, construidas a partir de la información obtenida con la aplicación de las herramientas previamente diseñadas. Los análisis se realizaron con el Paquete Estadístico para Ciencias Sociales (SPSS), versión 19.0 para Windows. Las variables incluidas inicialmente en el modelo por condiciones de trabajo fueron: (a) carga física, (b) ambiente térmico, (c) ruido, (d) riesgo laboral, (e) seguridad en el trabajo; y por condiciones salariales y subjetivas tenemos: (f) salario, (g) estabilidad laboral, (h) individuo, (i) plano jerárquico (j) plano técnico.

4. Resultados

4.1. Análisis de correlación

Para examinar la magnitud y la significación de las asociaciones entre las diferentes variables del estudio, se calcularon los coeficientes de correlación de Pearson [43], debido a que las variables de estudio seguían una distribución normal. Este análisis se realizó en tres grupos, en el primero se evaluará la relación entre las variables de condiciones de trabajo, en el segundo la relación entre las variables de CVL y en el tercero la relación entre las variables de Condiciones de Trabajo y las de CVL.

Correlación Variables Condiciones de Trabajo: En el análisis correlacional de las variables de condiciones de trabajo se encontró una relación positiva significativa con *p-value* menor a 0,01 entre: el riesgo laboral y la carga física (r = 0,262), seguridad en el trabajo y carga física (r = 0,292), riesgo laboral y ruido (r = 0,376), y por último, entre la seguridad en el trabajo y el ambiente térmico (r= 0,192).

Estas relaciones indican que cuando las estrategias de promoción y prevención son mayores la percepción positiva con respecto a los riesgos asociados a la carga física, el ruido y el ambiente térmico incrementan. Por otra parte, se encontró una relación negativa significativa con *p-value*

menor a 0,01 entre el riesgo laboral y el ambiente térmico (r = -0289). Esta relación negativa sugiere que a mejores condiciones térmicas se percibe buenas estrategias de prevención con relación a los riesgos laborales (ver Tabla 1).

Correlaciones Variables Calidad de Vida Laboral: En el análisis correlacional de las variables de Calidad de Vida Laboral se encontró una relación positiva significativa con *p-value* menor a 0,01 entre todas las variables, a saber: salario, estabilidad laboral, individuo, plano jerárquico y plano técnico (ver Tabla 2). Estas relaciones sugieren:

- A mayor estabilidad laboral la percepción de un buen salario recibido por la labor realizada incrementa (r = 0,414).
- La percepción del individuo conforme a su satisfacción laboral incrementa a medida que aumente su salario y estabilidad en la empresa (r = 0,172 y r = 0,385 respectivamente).
- Con respecto a las condiciones subjetivas representadas por el individuo y su relación con el plano jerárquico y técnico incrementa a medida que las condiciones básicas sean satisfechas por la organización, como es el salario y la estabilidad.

Correlaciones Variables Condiciones de Trabajo versus Calidad de Vida Laboral: En el análisis correlacional del cruce entre las variables de Condiciones de Trabajo y las variables de Calidad de Vida Laboral se encontró relaciones positivas significativas con p-value menor a 0,01 entre las siguientes variable indicando:

- Cuando las variables relacionadas al ambiente térmico son controladas la percepción con respecto al salario, la estabilidad laboral y las relaciones entre el individuo y la organización incrementan como se muestra en la Tabla 3.
- Adicional cuando los programas de promoción y prevención de seguridad en el trabajo al interior de la organización se encuentran debidamente documentados la percepción con respecto a las variables de Calidad de Vida es satisfactoria (ver Tabla 3).

Tabla 1.
Correlación de Pearson – Variables Condiciones de Trabajo

Variables	1	2	3	4	5
1. Carga Física	1				
2. Ambiente Térmico	-0,033	1			
3. Ruido	0,234**	-0,255**	1		
4. Riesgo Laboral	0,262**	-0,289**	0,376**	1	
5. Seguridad en el Trabajo	0,292**	0,192**	-0,002	0,032	1

** p < 0.01

Fuente: Elaboración de los Autores

Tabla 2.
Correlación de Pearson – Variables Calidad de Vida Laboral

Variables	6	7	8	9	10
6. Salario	1				
7. Estabilidad laboral	0,414**	1			
8. Individuo	0,172**	0,385**	1		
9. Plano Jerárquico	0,270**	0,401**	0,455**	1	
10. Plano Técnico	0,155**	0,338**	0,433**	0,477**	1

** p < 0.01

Fuente: Elaboración de los Autores

Tabla 3.
Correlación de Pearson – Variables Condiciones de Trabajo vs Calidad de Vida Laboral

Variables	1. Carga Física	2. Ambiente Térmico	3. Ruido	4. Riesgo Laboral	5. Seguridad en el Trabajo
6. Salario	0,028	0,196**	-0,178**	-0,141**	0,177**
7. Estabilidad laboral	0,148**	0,285**	-0,132**	-0,148**	0,359**
8. Individuo	0,010	0,151**	-0,076	-0,098*	0,215**
9. Plano Jerárquico	0,149**	0,224**	-0,100*	-0,118**	0,331**
10. Plano Técnico	0,128**	0,265**	-0,081	-0,010	0,211**

** p < 0.01
* p < 0.05

Fuente: Elaboración de los Autores

Por otra parte, se encontraron relaciones negativas significativas con *p-value* menores a 0,01 entre las siguientes variables sugiriendo:

- A medida que el ruido presente en las actividades que el personal realiza a diario incrementa, la percepción disminuye en cada una de las variables asociadas a las condiciones salariales y subjetivas como se muestra en la Tabla 3.
- Asimismo cuando el riesgo asociado a la actividad que se desempeña es alto la percepción de las condiciones salariales y subjetivas disminuye (ver Tabla 3).

4.2. Modelo del Impacto de las Condiciones de Trabajo en la CVL

El primer paso para la construcción del modelo fue probar diferentes modelos de regresión logística utilizando como variable dependiente la Calidad de Vida Laboral y como variables independientes las de Condiciones de Trabajo, a saber, carga física, ruido, ambiente térmico, riesgo laboral y seguridad en el trabajo. No obstante, antes de iniciar la modelación se debió hallar el punto de corte en el cual se seleccionan los mejores modelos independientemente del coste asociado a la distribución, esto mediante el análisis de la curva COR, es decir, por medio de la curva COR se establece el punto de corte para la dicotomización de la variable dependiente. [44].

La curva COR proporciona una representación global de la exactitud diagnóstica. Un gráfico de curva COR ilustra la sensibilidad y especificidad de cada uno de los posibles puntos de corte de un test diagnóstico cuya escala de medición es continua. La curva se construye en base a la unión de distintos puntos de corte, correspondiendo el eje Y a la sensibilidad y el eje X a (1-especificidad) de cada uno de ellos. Para el caso de estudio, el valor óptimo se encuentra en 0,85 aproximadamente tal como se muestra en la Fig. 2.

Del gráfico anterior se puede concluir que el área bajo la curva COR es el estadístico que proporciona una medida completa de la capacidad predictiva del instrumento. El valor que se obtiene tiene una interpretación directa, por ejemplo, en el caso de estudio un área de 0,85 significa que un individuo

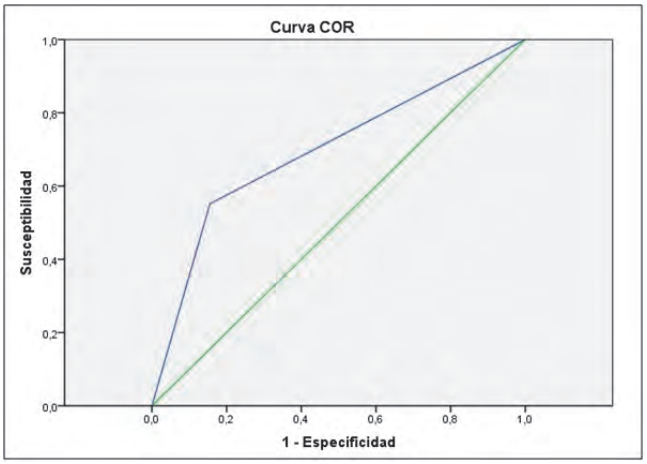


Figura 2. Curva COR para Modelado Condiciones de Trabajo en CVL
Fuente: Elaboración de los Autores

Tabla 4.
Modelo de Regresión para la Calidad de Vida Laboral

	Variables Incluidas	B	E.T.	gl	Sig.	Exp(B)
Paso 2	Ambiente Térmico	0,07	0,02	1	0,00	1,070
	Seguridad en el Trabajo	0,06	0,01	1	0,00	1,066
	Constante	-2,05	0,45	1	0,00	,129

Fuente: Elaboración de los Autores

seleccionado aleatoriamente del grupo positivo "tiene un valor en la prueba mayor que el de un individuo elegido aleatoriamente del grupo negativo un 85% de las veces".

El segundo paso fue categorizar la variable dependiente como una variable dicotómica con niveles bajo (0) y alto (1) para lograr un mejor ajuste a los modelos de regresión logística binaria. El número de casos finales incluidos en el análisis fue de 518 participantes que tenían mediciones completas en las variables de estudio. Para calcular el modelo de regresión logística, se utilizo el método de selección por pasos hacia delante de Wald que contrasta la entrada basándose en la significación del estadístico de puntuación y contrasta la eliminación basándose en la probabilidad del estadístico. En cada paso revalúa los coeficientes y su significación, pudiendo eliminar del modelo aquellos que no considera estadísticamente significativos. El último paso de estudio generó el modelo que se muestra en la Tabla 4.

A partir de este resultado el modelo queda representado como se muestra a continuación, este indica la percepción de la CVL de los empleados con respecto a las variables identificadas como significativas., para tal caso, cuando la probabilidad tienda a uno la percepción será positiva (1)

$$P_{(x)} = \frac{e^{-2.05+0,07X+0.06Y}}{1 + e^{-2.05+0,07X+0.06Y}} \qquad (1)$$

Para verificar el ajuste del modelo se analizó el estadístico de Wald, debido a que éste fue significativo (p-value <.0,5) el modelo presenta un buen ajuste. Por otro lado, se utilizó la prueba de Hosmer-Lemeshow con el fin de evaluar el ajuste global del modelo; en este caso, la ausencia de significación con un *p-value* igual a 0,058 indica igualmente un buen ajuste del modelo.

Los coeficientes de las variables de condiciones de trabajo y de la constante fueron evaluados por la prueba de Wald. Los valores de significancia se muestran en la Tabla 4. El porcentaje de casos clasificados por el modelo fue del 100%.

Aunque el R-cuadrado de Nagelkerke fue bajo (0,223) hay que tener en cuenta que otros estadísticos muestran la validez del modelo. En este sentido, la evidencia empírica sugiere que estos valores son intuitivos y suelen confundirse con los R-cuadrado de las regresiones ordinarias. En general esto indica que para tener mayor poder discriminativo sobre las condiciones de trabajo altas deberían entrar a evaluarse otras variables.

Los resultados muestran que el ambiente térmico y las normas de seguridad en el trabajo afectan de forma positiva la Calidad de Vida Laboral de los empleados del sector manufacturero de la región Caribe colombiana. Estos resultados ponen de manifiesto que la relación entre las condiciones de trabajo y la CVL se basa en la competencia y distan de ser una relación lineal y simple relacionada con la consideración de la presencia o la ausencia de las condiciones de trabajo. Ello tiene implicaciones a la hora de formular políticas, programas e intervenciones para prevenir, erradicar y amortiguar los efectos negativos de las condiciones de trabajo dentro de las empresas.

5. Discusión

La variable de Calidad de Vida (CVL) es una función de los esfuerzos que las empresas realizan para incrementar la productividad y mejorar el bienestar de los empleados y su entorno. En este sentido, hacer referencia al término "calidad" implica una connotación positiva o situación anhelada, resultado de una calificación en función de unos resultados y/o certezas [16]. Es decir, la CVL se ve afectada por la presencia de condiciones de trabajo más allá de su presencia o ausencia, que se relacionan con el conjunto de circunstancias y características materiales, ecológicas, económicas, políticas, organizacionales, entre otras, a través de las cuales se efectúan las relaciones laborales [22].

Trabajar en condiciones favorables relacionadas con el ambiente térmico conlleva a una mejora en la percepción de la CVL. En este sentido, cabe destacar la importancia del trabajo desarrollado en un ambiente agradable, dado que en el sector a temperaturas bajas se puede percibir disminución en la destreza manual, y a elevadas temperaturas se observa disminuciones en cuanto a la atención y estado de conciencia.

Por otro lado, las normas asociadas a la seguridad en el trabajo: está formada por una serie de garantías individuales de carácter universal que tiene por Ley cualquier trabajador; estas garantías incluyen la higiene y el control de riesgos en el trabajo, la atención médica, la asesoría legal, entre otros las cuales son fundamentales para los empleados del sector, quienes perciben que a medida que están condiciones son favorables así se verá afectada positivamente su CVL. Además, la mayoría de estudios sobre condiciones de trabajo

en Colombia se limitan a la caracterización de los factores de riesgo y posibles correlaciones de estos con la gestión organizacional a manera de diagnóstico, dejando de lado la proyección de los hallazgos identificados [17,45].

El propósito de esta investigación fue estudiar el impacto de las Condiciones de Trabajo en la CVL en el talento humano del sector manufacturero de la región Caribe colombiana, examinando la percepción de 518 empleados del sector. Los resultados se sitúan en la línea de estudios previos [38] en los cuales se señala que en los últimos años se han presentado avances con respecto al abordaje de esta temática, con miras no sólo a la observación de aquellos factores que se consideran afectan la CVL de los empleados, sino también a analizar desde diversas perspectivas las herramientas y/o metodologías que permitan mejorarla, y de esta manera cambiar la percepción que el trabajador tiene de la organización de un estado negativo a uno positivo.

Los resultados de correlación encontrados en esta investigación muestran que cuando las estrategias de promoción y prevención con respecto a la seguridad en el trabajo son mayores, la percepción positiva con respecto a los riesgos asociados a la carga física, el ruido y el ambiente térmico incrementan. Estas conclusiones se evidencian también en el estudio realizado por Hayes [39] en donde el autor mide la percepción de seguridad en el lugar de trabajo, estableciendo que existen correlaciones positivas significativas entre las condiciones de seguridad con los accidentes provocados por los diferentes riesgos a los cuales se puede enfrentar un empleado [39]. De igual manera, a mayor estabilidad laboral la percepción de un buen salario recibido por la labor realizada incrementa, estos resultados son congruentes y contrastan con los obtenidos por [10] quienes en su investigación exponen que existe una fuerte correlación entre variables como compensación y el trabajo realizado; indicando que la relación de estos factores es clave para el desempeño organizacional y el compromiso del trabajador hacia la tarea realizada, adicional una percepción positiva de la CVL facilita la gestión de la vida personal.

Con respecto al modelo, la construcción de una variable robusta de CVL que permitiera medir el impacto de las condiciones de trabajo llevó a establecer las dimensiones que afectan de modo positivo la CVL en los empleados del sector manufacturero de la región Caribe colombiana las cuales son el ambiente térmico y las normas de seguridad asociadas al trabajo que desempeñan. Estos resultados ponen en manifiesto que para los empleados es importante desarrollar sus actividades en un ambiente agradable, dado que en el sector a temperaturas bajas se puede percibir disminución en la destreza manual, y a elevadas temperaturas se observa disminuciones en cuanto a la atención y estado de conciencia. De igual forma, las normas asociadas a la seguridad en el trabajo son un complemento que hace que la percepción de la CVL sea positiva cuando las garantías dadas por Ley son cumplidas por las empresas. Adicional, los factores identificados por los empleados que a su saber afectan su calidad de vida tienen validez en el sector estudiado, dado que hay una escasa disponibilidad de estudios referentes a vigilancia o seguimiento de casos relacionados con enfermedades o lesiones derivadas de la actividad laboral [17], así como también, se evidencia la necesidad de implementar estrategias organizacionales que vayan más allá de lo contemplado en la literatura o la legislación disponible.

Finalmente, para mejorar la percepción de la calidad de vida en el trabajo se requieren cambios, los cuales no sólo debe propiciar el empresario sino también el Gobierno y el empleado. Estos cambios se pueden dar en la forma de ver y de hacer las cosas, en la manera de conducir la organización, en el contexto de responsabilidades, entre otros. Esto no significa que sea necesario cambiarlo todo, sino que el progreso en materia de calidad demanda adecuaciones en diferentes aspectos de la administración que constituyan un obstáculo para su logro. Del mismo modo, los directivos deben preocuparse de contar con las medidas solicitadas por los organismos gubernamentales y de seguridad, para que sus empleados puedan trabajar de manera adecuada, sin interferir en la productividad, como por ejemplo, diseñar estrategias que mitiguen la exposición del empleado a diferencias de temperatura o presión de vapor

Conforme a los resultados que se evidencian en el presente estudio, se recomienda concentrar los esfuerzos en la solución activa de los problemas cotidianos o en la toma de decisiones acerca del contenido del puesto desempeñado, confiriéndole al empleado la certidumbre de que sus opiniones cuentan y poseen valor. Entre las estrategias a desarrollar se proponen: incentivar espacios de reflexión sobre las tareas asignadas, movilizar recursos preexistentes, implementar cambios de naturaleza psicosocial en donde no sólo se vea afectada positivamente la organización sino todos los involucrados (internos y/o externos), y por último, ser integral en las actuaciones y decisiones que se efectúen a diario.

Adicional, cabe señalar que con este estudio es posible diseñar e implementar acciones orientadas a la mejora de la CVL del sector manufacturero de la región Caribe colombiana, con un impacto positivo en la productividad y reflexionar con respecto al sentido que se le quiere dar al trabajo. En materia de políticas en Salud Ocupacional, por ejemplo, se puede asegurar equidad en la salud (salud para todos), sumar vida a los años (mejorar la calidad de vida), sumar años a la vida (reducir la mortalidad) y sumar salud a la vida (reducir la morbilidad) [12,46]. Por tal motivo, es recomendable atender de manera especial al estilo de liderazgo, estableciendo una comunicación más fluida, fomentando la participación y la formación permanente de los empleados, estableciendo una visión compartida con relación al cambio y al desarrollo, estableciendo objetivos simples, pero desafiantes y alcanzables dentro de cada una de las empresas del sector [8].

5.1. Limitaciones y futuras investigaciones.

La singularidad del presente modelo en el país y sector, impide contrastar nuestros resultados con otros referentes. Este trabajo es un primer paso para continuar trabajando en herramientas y/o instrumentos robustos que permitan aplicar métodos analíticos más sofisticados para el análisis de la seguridad industrial y el bienestar de los trabajadores [42].

Referencias

[1] Akranavičiūtė, D. and Ruževičius, J., Quality of life and its components measurement, Engineering Economic, 2, pp. 43-48, 2007.

[2] Van der Berg, Y. and Martins, N., The relationship between organisational trust and quality of work life, South African Journal of Human Resource Management, 11(1), pp. 1-13, 2013. DOI: 10.4102/sajhrm.v11i1.392
[3] Darafsh, H., Relationship between learning organization and quality of work life: A comparative study of Iran and India, IUP Journal of Organizational Behavior, 11(4), pp. 21-27, 2012.
[4] Kleinhenz, J. and Smith, R., Regional competitiveness: Labor-management relations, workplace practices and workforce quality, Business Economics, 46, pp. 111-124, 2011. DOI: 10.1057/be.2011.6
[5] Zapata, A. y Sarache-Castro, W.A., Calidad y responsabilidad social empresarial: Un modelo de causalidad, DYNA [En línea], 80(177), pp. 31-39, 2013. Disponible en: http://www.revistas.unal.edu.co/index.php/dyna/article/view/27907
[6] Iglesias-Fernández, C., Llorente-Heras, R. y Dueñas-Fernández, D., Calidad del empleo y satisfacción laboral en las regiones españolas. Un estudio con especial referencia a la Comunidad de Madrid, Investigaciones Regionales, 19, pp. 25-49, 2011.
[7] Robone, S., Jones, A.M. and Rice, N., Contractual conditions, working conditions and their impact on health and well-being, The European Journal of Health Economics, 12(5), pp. 429-444, 2011. DOI: 10.1007/s10198-010-0256-0
[8] Sundaray, B.K., Sahoo, C.K. and Tripathy, S.K., Impact of Human resource interventions on quality of work life, International Employment Relations Review, 19(1), pp. 68-86, 2013.
[9] Márquez-Membrive, J., Granero-Molina, J., Solvas-Salmerón, M., Fernández-Sola, C., Rodríguez-López, C. and Parrón-Carreño, T., Quality of life in perimenopausal women working in the health and educational system, Rev. Latino-Am. Enfermagem, 19, pp. 1314-1321, 2011. DOI: 10.1590/S0104-11692011000600006
[10] Selahattin, K. and Sadullah, O., An empirical research on relationship quality of work life and work engagement, Procedia - Social and Behavioral Sciences, 62, pp. 360-366, 2012. DOI:10.1016/j.sbspro.2012.09.057
[11] Narehan, H., Hairunnisa, M., Norfadzillah R.A. and Freziamella, L., The effect of quality of work life (QWL) programs on quality of life (QOL) among employees at multinational companies in Malaysia, Procedia - Social and Behavioral Sciences, 112, pp. 24-34, 2014. DOI: 10.1016/j.sbspro.2014.01.1136
[12] Charu, M., Occupational stress and its impact on QWL with specific reference to hotel industry, Advances in Management, 5, pp. 50-54, 2012.
[13] Das, T.V. and Vijayalakshmi, Ch, Quality of work life: A strategy for good industrial relations, Advances in Management, 6, pp. 8-15, 2013.
[14] Segurado-Torres, A. y Agulló-Tomás, E., Calidad de vida laboral: Hacia un enfoque integrador desde la psicología social, Colegio Oficial de Psicólogos del Principado de Asturias, 14, pp. 828-836, 2002.
[15] Jagannathan, L. and Akhila P.R., Predictors of quality of work life of sales force in direct selling organizations, ICFAI Journal of Management Research, 8(6), pp. 51-59, 2009.
[16] Merino-Llorente, M.C., Somarriba-Arechavala, N. y Negro-Macho, A., Un análisis dinámico de la calidad del trabajo en España. Los efectos de la crisis económica, Estudios de Economía Aplicada, 30(1), pp. 261-282, 2012.
[17] Chaparro-Hernández, S.R. y Bernal-Uribe, C., Trabajo digno y decente en Colombia: Seguimiento y control preventivo a las políticas públicas, Procuraduría General de la Nación, 2007.
[18] Guthrie, J.P., Spell, C.S. and Ochoki-Nyamori R., Correlates y consequences of high involvement work practices: The role of competitive strategy, International Journal of Human Resource Management, 13, pp. 183-197, 2002. DOI: 10.1080/09585190110085071
[19] Ghiglione, C., El mejoramiento de la calidad de vida laboral como estrategia para vigorizar la capacidad de gestión municipal, Documentos y Aportes en Administración Pública y Gestión Estatal, 61, pp. 157-162, 2011. DOI: 10.14409/da.v1i16.1267
[20] Pailhé, A., Working conditions: How are older workers protected in France?, Population, 60, pp. 99-126, 2005. DOI: 10.3917/popu.501.0099
[21] Acevedo, G., Farias, A., Sánchez, J., Astegiano, C. y Fernández, A., Condiciones de trabajo del equipo de salud en centros de atención primaria desde la perspectiva del trabajo decente, Revista Argentina Salud Pública, 3(12), pp. 15-22, 2012.
[22] Blanch, J.M., Sahagún, M. y Cervantes, G., Estructura factorial del cuestionario de condiciones de trabajo, 26(3), pp. 175-189, 2010. DOI: 10.5093/tr2010v26n3a2
[23] Yeo, R.K. and Li, J., Working out the quality of work life: A career development perspective with insights for human resource management, Human Resource Management International Digest, 19, pp. 39, 2011. DOI: 10.1108/09670731111125952
[24] Stoetzer, U., Ahlberg, G., Bergman, P., Hallsten, L. and Lundberg I., Working conditions predicting interpersonal relationship problems at work, European Journal of Work & Organizational Psychology, 18, pp. 424-441, 2009. DOI: 10.1080/13594320802643616
[25] Anstery, K.J., Wood, J., Caldwell, H., Kerr, G., and Lord, S.R., Comparison of self-reported crashes, state crash records and an on-road driving assessment in a population-based sample of drivers aged 69-95 years, Traffic injury prevention, 10(1), pp. 84-90, 2009. DOI: 10.1080/15389580802486399
[26] Bagtasos, M.R., Quality of work life: A review of literature, DLSU Business & Economics Review, 20, pp. 1-8, 2011.
[27] Rathi, N., Relationship of quality of work life with employees' psychological well-being, International Journal of Business Insights & Transformation, 3, pp. 52-60, 2009.
[28] Quezada, F.Q., Castro A.S. y Cabezas, F.S., Diagnóstico de la calidad de vida laboral percibida por los trabajadores de cuatro servicios clínicos del complejo asistencial Dr. Víctor Ríos Ruiz, Horizontes Empresariales, 9, pp. 55-68, 2010.
[29] Celia, B.R. and Karthick, M., A study on quality of work life in the it sector, Asia Pacific Journal of Research in Business Management [Online]. 3(2), pp. 27-35, 2012. Disponible en: http://www.indianjournals.com/ijor.aspx?target=ijor:apjrbm&volume=3&issue=2&article=003
[30] Gomez Vélez, M.A., Calidad de vida laboral en empleados temporales del Valle de Aburrá - Colombia, Revista Ciencias Estratégicas [Online]. 18(24), pp. 225-236, 2010. Diponible en: https://revistas.upb.edu.co/index.php/cienciasestrategicas/article/view/708
[31] Silva, M.D., Nuevas perspectivas de la calidad de vida laboral y sus relaciones con la eficacia organizacional, PhD Tesis, Departamento de Psicología Social, Universitat de Barcelona, Barcelona, España, 2006.
[32] Argüelles-Ma, L.A., Quijano-Garcia, R.A., Fajardo, M.J., Magaña-Medina, D.E. y Sahui-Maldonado, J.A., Propuesta de modelo predictivo de la calidad de vida laboral en el sector turístico Campechano (México), Revista Internacional Administración & Finanzas, 7(5) pp. 61-76, 2014.
[33] Somarriba-Arechavala, N., Merino-Llorente, M.C., Ramos-Truchero, G. y Negro-Macho, A., La calidad del trabajo en la Unión Europea, Estudios de Economia Aplicada [Online], 28(3), pp. 1-22, 2010. Disponible en: http://www.redalyc.org/articulo.oa?id=30120334013
[34] Bello, A.M., Palacio, J., Vera-Villarroel, P., Oviedo-Trespalacios, O., Rodríguez, M. y Celis-Atenas, K., Presentación de una escala para evaluar actitudes y creencias sobre la sexualidad reproductiva en adolescentes varones de la región Caribe colombiana, Universitas Psychologica Panamerican Journal of Psychology, 13, 2014. DOI: 10.11144/Javeriana.UPSY13-1.peea
[35] Bello-Villanueva, A.M., Palacio, J., Rodríguez-Díaz, M. y Oviedo-Trespalacios, O., Medición de la intención en la actividad sexual en adolescentes: Una aproximación de acuerdo al género del Caribe colombiano, Terapia psicológica, 31, pp. 343-353, 2013. DOI: 10.4067/S0718-48082013000300009
[36] Hernandez-Sampieri, R., Fernández-Collado, C. y Baptista-Lucio, P., Metodología de la Investigación, McGraw Hill. México, 2006.
[37] Zorrilla, S., Torres, M., Cerro, A. y Bervian, P., Metodología de la Investigación.: McGraw Hill, México, 1997.
[38] Martinez-Buelvas, L., Oviedo-Trespalacios, O. y Luna-Amaya, C., Condiciones de trabajo que impactan en la calidad de vida laboral, Salud Uninorte [Online], 29, 2013. Disponible en: http://rcientificas.uninorte.edu.co/index.php/salud/article/viewArticle/5328

[39] Hayes, B.E., Peryer, J., Smecko, T. and Trask, J., Measuring perceptions of workplace safety: Development and validation of the work safety scale, Journal of Safety Research, 29, pp. 145-161, 1998. DOI: 10.1016/S0022-4375(98)00011-5
[40] Casas, J., Repullo, J.R., Lorenzo, S. y Cañas J.J., Dimensiones y medición de la calidad de vida laboral en profesionales sanitarios, Revista de Administración Sanitaria, 6, pp. 143-160, 2002.
[41] Spector, P.E., Job Satisfaction Survey, Thesis, Department of Psychology, University of South Florida, USA, 1994.
[42] Martínez, L., Evaluación del impacto de las condiciones de trabajo en la calidad de vida laboral en el sector manufacturero de la región Caribe colombiana**,** MSc. Thesis, Departamento de Ingeniería Industrial, Universidad del Norte, Barranquilla, Colombia, 2014.
[43] Castillo-Sierra, R., Oviedo-Trespalacios, O., Cyelo J. and Soto J., The influence of atmospheric conditions on the leakage current of ceramic insulators on the Colombian Caribbean coast, Environ Sci Pollut Res, 22, pp. 2526-2536, 2015. DOI: 10.1007/s11356-014-3729-3
[44] Holgado, D., Maya-Jariego, I., Ramos, I., Palacio, J., Oviedo-Trespalacios, Ó., Romero-Mendoza, V. and Amar, J. Impact of child labor on academic performance: Evidence from the program "Edúcame Primero Colombia", International Journal of Educational Development, 34, pp. 58-66, 2012. DOI: 10.1016/j.ijedudev.2012.08.004
[45] Tuesca-Molina, R., La Calidad de vida, su importancia y cómo medirla, Salud Uninorte [Online], 21, pp. 76-86, 2005. Disponible en: http://www.redalyc.org/articulo.oa?id=81702108
[46] Sarina-Muhamad, N. and Mohamad-Adli, A., Quality work life among factory workers in Malaysia, Procedia - Social and Behavioral Sciences, 35, pp. 739-745, 2012. DOI: 10.1016/j.sbspro.2012.02.144
[47] Costa, B.E. and Silva, N.L, Analysis of environmental factors affecting the quality of teacher's life of public schools from Umuarama, Work, 41, pp. 3693-3700, 2012. DOI: 10.3233/WOR-2012-0673-3693

L. Martínez-Buelvas, es Ing. industrial y MSc.en Ingeniería Industrial de la Universidad del Norte, Colombia. Catedrática e investigadora del Departamento de Ingeniería Industrial de la Universidad del Norte, Colombia y directora de proyectos de la empresa Medicina Alta Complejidad S.A., Colombia. Áreas de actuación en investigación, consultoría y docencia: planeación, programación y control de la producción, diseño de sistemas productivos, gestión de proyectos, y gestión del conocimiento. Pertenece al Grupo de Investigación Productividad y Competitividad de la Universidad del Norte, Colombia.
ORCID: 0000-0002-8349-1137

O. Oviedo-Trespalacios, es Ing. industrial y MSc. en Ingeniería Industrial de la Universidad del Norte, Colombia. Candidato a Dr. en Ingeniería de Factores Humanos de Queensland University of Technology, Australia. De 2012 a 2014, trabajó como profesor titular en el Departamento de Ingeniería Industrial de la División de Ingeniería de la Universidad del Norte, Colombia. Actualmente, es investigador en ingeniería de factores humanos aplicados a la seguridad en sistemas críticos del Centre for Accident Research and Road Safety – Queensland (CARRS-Q), Institute of Health and Biomedical Innovation (IHBI), Queensland University of Technology (QUT), Australia. Sus áreas de investigación incluyen: seguridad en transporte, métodos estadísticos aplicados a salud, Ingeniería de factores humanos, ingeniería cognitiva y seguridad industrial.
ORCID: 0000-0001-5916-3996

C. Luna- Amaya, es Ing. Industrial, de la Universidad Industrial de Santander, Colombia. Esp. en Gerencia de Empresas Comerciales, del ICESI, Colombia. Esp. en Gestión Industrial y Dra. en Ingeniería Industrial de la Universidad Politécnica de Valencia, UPV, España. Es profesora de tiempo completo, Universidad del Norte, Colombia. Áreas de actuación en investigación, consultoría y docencia: gestión del conocimiento, gestión por competencias, mejora y optimización de procesos, ingeniería concurrente, diseño modelos organizacionales. Pertenece al grupo de investigación Productividad y Competitividad de la Universidad del Norte, Colombia.
ORCID 0000-0002-3104-5151

UNIVERSIDAD NACIONAL DE COLOMBIA
SEDE MEDELLÍN
FACULTAD DE MINAS

Área Curricular de Ingeniería Administrativa e Ingeniería Industrial

Oferta de Posgrados

Especialización en Gestión Empresarial
Especialización en Ingeniería Financiera
Maestría en Ingeniería Administrativa
Maestría en Ingeniería Industrial
Doctorado en Ingeniería - Industria y Organizaciones

Mayor información:

E-mail: acia_med@unal.edu.co
Teléfono: (57-4) 425 52 02

UNIVERSIDAD NACIONAL DE COLOMBIA
SEDE MEDELLÍN
FACULTAD DE MINAS



DYNA
http://dyna.medellin.unal.edu.co/

Application of a prefeasibility study methodology in the selection of road infrastructure projects: The case of Manizales (Colombia)

Diego Alexander Escobar-García [a], Camilo Younes-Velosa [b] & Carlos Alberto Moncada-Aristizábal [c]

[a] *Facultad de Ingeniería y Arquitectura, Universidad Nacional de Colombia, Manizales, Colombia. daescobarga@unal.edu.co*
[b] *Facultad de Ingeniería y Arquitectura, Universidad Nacional de Colombia, Manizales, Colombia. cyounesv@unal.edu.co*
[c] *Facultad de Ingeniería, Universidad Nacional de Colombia, Bogotá, Colombia. camoncadaa@unal.edu.co*

Received: February 25th, 2015. Received in revised form: May 8th, 2015. Accepted: July 21th, 2015.

Abstract
Major cities in Colombia are currently generating urban transformation processes that involve the construction of major infrastructures, which mainly look to mitigate the adverse effects of ever-increasing road traffic. In addition, intermediate cities have made great efforts when it comes to urban planning and promote the application of prefeasibility study methodologies to make the appropriate decisions regarding the infrastructures to be built in specific places in the city. This paper discusses the results after applying a prioritization methodology as a comparative tool between two possible road infrastructures in the area of San Marcel in the city of Manizales, Colombia. The best proposal is selected based on the best coverage indicators and variables such as overall construction costs and life span: determined from information generated in traffic simulations.

Keywords: Accessibility, priorization analysis, coverage, geostatistics, urban planning.

Aplicación de una metodología a nivel de prefactibilidad para la selección de proyectos de infraestructura vial. El caso de Manizales (Colombia)

Resumen
Actualmente las grandes ciudades colombianas están generando procesos de transformación urbana que involucran la construcción de importantes infraestructuras, buscando en la mayoría de los casos, tratar de mitigar los efectos adversos del creciente tránsito automotor. Por su parte, las ciudades intermedias no ahorran esfuerzos en términos de planificación urbana, impulsando la aplicación de metodologías, que a nivel de prefactibilidad, permiten tomar decisiones respecto a las infraestructuras que se deben construir en determinados sitios de la ciudad. En este artículo se discuten los resultados de aplicar una metodología de priorización como instrumento comparativo entre dos posibles infraestructuras viales en el sector de San Marcel en la ciudad de Manizales, Colombia. Se determina cuál de las propuestas refiere mejores indicadores de cobertura, relacionando los mismos con variables como los costos globales de construcción y vida útil definida a partir de simulaciones de tránsito.

Palabras clave: Accesibilidad, análisis de priorización, cobertura, geoestadística, planeamiento urbano.

1. Introduction

Manizales is an intermediate city located in the west central region of Colombia on the central mountain chain at an altitude of 2,150 meters above sea level. It has a population of 361,422 inhabitants in an area close to 35 km^2.

Manizales is currently implementing a Mobility Plan (2010-2040) [1] and several infrastructure projects have been implemented during the last few years, which have changed the mobility characteristics in specific sectors of the city.

A Geographic Information System (GIS) was used in this research to collect current and future road network information based on each of the proposals.

The accessibility isochronous curves were calculated using the GIS geospatial visualization capabilities and geostatistical software. These curves were then used to calculate studies of geospatial coverage of the variables area, population and number of households.

© The author; licensee Universidad Nacional de Colombia.

Given its capacity to store information and to integrate the different models related to a specific territory [2] GIS facilitates understanding in greater detail of means of transport accessibility characteristics. The use of algorithms [3], such as the shortest path algorithm, provides researchers with the necessary tools to simulate the impact of insertion of a given infrastructure.

From the geographical point of view, accessibility is a measure of the ease of communication between a group of communities or activities, which is achieved by using different means of transport [4]. This concept has become very important in urban and regional planning, and has been applied in regional economic planning and in Location Theory since the second decade of the twentieth century. [5]. Accessibility has become a primary element of urban planning in the use of quantitave criteria to determine future land use in order to achieve greater social welfare through appropriate sector planning [6].

There are various definitions of the term, but the classic was provided by Hansen in the early second half of the last century ". "…the potential of Opportunities for interaction. "[7]. The models built on accessibility measures are commonly based on the distance and attraction between network nodes [8]. However, accessibility is nowadays more related to the distance of means of transport and the savings in connection time between different regions [9].

Factors such as location of the nodes, number of nodes, transportation network and population distribution affect accessibility [10]. However, the new mobility paradigm includes other factors such as the quality of means of transport, proximity to land use, and infrastructure characteristics such as cost, safety, comfort, and environment, among others [11].

Accessibility has been widely used in other fields of knowledge, such as analysis of service location [12-14], operation of means of transport [15,16], analysis of social cohesion [17,18], demographic analysis [19], economic development [20-22], sustainability [23,24], tourism [25], and social networks [26], among others.

Accessibility in Colombia has been a measure rarely used because the true potential of this type of analysis is not very well understood. However, there are some real examples of the application of these methodologies at both regional [27] and urban [28-30] levels.

Currently, accessibility analysis is becoming an important factor for plan evaluation and infrastructure projects [31], and in many cases the improvement of accessibility is one of the criteria used in evaluations [32]. Moreover, there are a variety of dynamic simulation models at urban levels [33-35] as well as accessibility models involving infrastructure insertion analysis [36,37] and its spatial-temporal impact on urban growth.

Therefore, accessibility must be recognized as a primary need [38] as it defines people's access to basic services such as health, education and employment as a priority. This shows how many countries can eliminate class differences by increasing access to basic services and satisfying basic needs as one of the objectives related to transportation [39].

This research includes an infrastructure prioritization methodology based on the following variables: accessibility, traffic microsimulation results and global and preliminary construction costs. The methodology, results and major conclusions are addressed in the following chapters.

2. Methodology

There are principally six phases in this methodology: In the first phase, the official network of the city of Manizales was obtained and the operating speed information was loaded in the database [1,29].

In the second phase the intervention alternatives in the road infrastructure were georeferenced.

In the third phase calculations were made of the Global Media Accessibility offered by the network of the existing transport infrastructure and the curves for each of the alternatives were evaluated.

In the fourth phase calculations were made on the impact on savings in Average Travel Time - ATT provided by each one of the alternatives.

In the fifth phase calculations were made of the percentages of area, population and number of households covered by ATT curves obtained from the analysis of global average accessibility in each one of the alternatives.

And in the sixth, a sensitivity analysis was undertaken according to the variability of the characteristics of life span, global construction costs and savings in ATT.

2.1. Secondary information

The infrastructure network for the Mobility Plan of Manizales, provided by the local administration, was instrumental in making the calculations for territorial accessibility. The network has loaded information relating to operating speeds, which was provided by GPS equipment installed in different types of vehicles.

2.2. Georeferencing of the alternatives

In this phase, the alternatives to infrastructure intervention were georeferenced using the road network as base information. Fig. 1 shows the sector under study and the arcs of the existing road network are highlighted.

New arcs, corresponding to each alternative, are incorporated taking into account the designs on phase II. The future operational features were defined in each alternative.

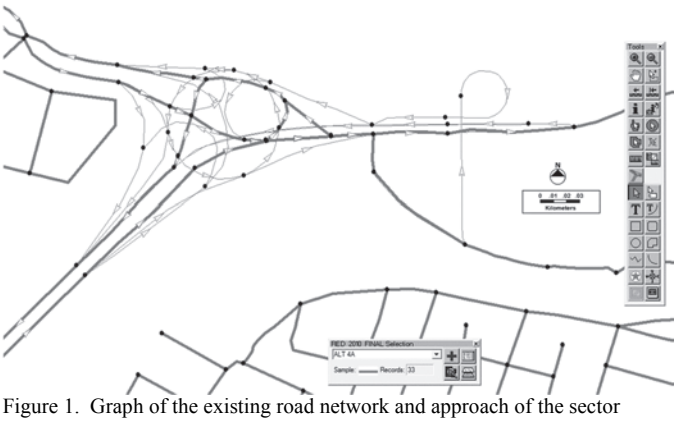


Figure 1. Graph of the existing road network and approach of the sector under study.
Source: Own source based on the graph provided by the Mobility Plan of Manizales [1].

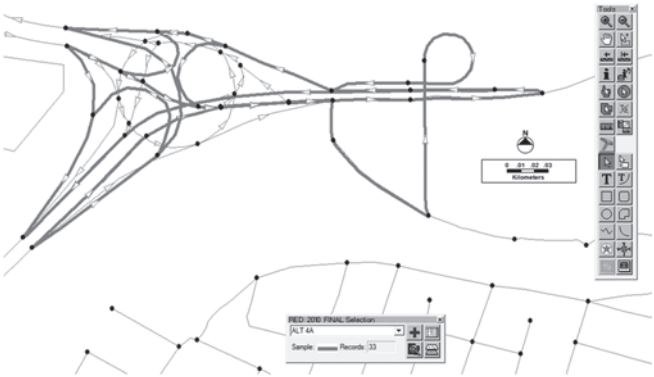


Figure 2. Graph of the road network including the insertion of alternative 4A. Source: Own source based on the graph provided by the Mobility Plan of Manizales [1].

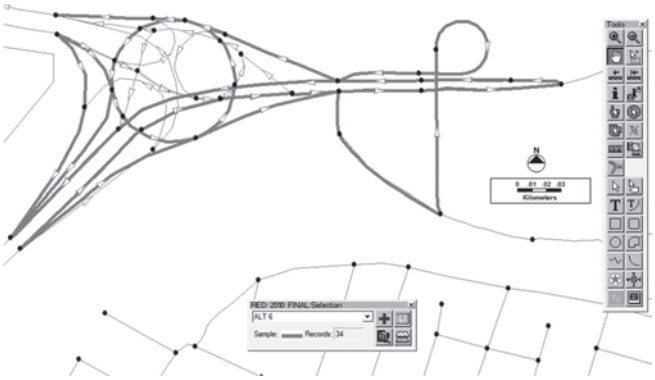


Figure 3. Graph of the road network including the insertion of alternative 6. Source: Own source based on the graphic provided by the Mobility Plan of Manizales [1].

Figs. 2 and 3 show an approach of each graph with the insertion of the alternatives to be evaluated: in this case alternative 4A and 6 respectively.

2.3. Calculation of urban territorial accessibility

The urban Territorial Accessibility was analyzed using the ATT vector (Tvi), which represents the average travel time from node i to the other network nodes. The GIS algorithm was used for this calculation to obtain the lower impedance (shortest path) between a specific node and the other nodes in the network, forming a unimodal matrix.

The matrix of minimum average travel time was designed using the unimodal matrix and also the information of average operating speed in each arc. The ATT is minimized between each and every node in the network. After that, the vector of average travel time (Tvi, eq.1) was obtained.

$$\overline{T_{vi}} = \frac{\sum_{j=1}^{m} t_{vi}}{(n-1)} i=1, 2, 3,..., n;\ j=1,2,3,..., m \qquad (1)$$

Where Tvi = minimum average travel time between node i and the other nodes in the network; i = number of network nodes. The ATT vector obtained (n x 1) is related to the geographical coordinates (longitude and latitude) of each of the nodes to generate a matrix of order (n x 3). Isochronous curves of average travel time were generated using this matrix to analyze urban Territorial Accessibility for both the current infrastructure and for each of the alternatives under consideration. The ordinary kriging method was used along with linear semivariogram as an average travel time prediction model.

2.4. Calculation of the impact on average travel time – ATT

Once the isochronous curves for the current infrastructure and for each of the other two alternatives of infrastructural intervention are calculated, the gradient on average travel times for each alternative was determined.

The gradient was calculated in terms of the percentage of ATT taking into account the hypothesis that there is an improvement in operating speeds of the vehicles in the new infrastructure. The ATT is reduced depending on the current average travel time.

2.5. Coverage analysis

The urban area of the city of Manizales is 35.1 Km2, has about 361,422 inhabitants, 83,868 households and approximately 115 neighborhoods.

The gradient curves of time savings in ATT in each of the alternatives under study were related using a GIS and taking into consideration the available demographic information. It was possible to estimate the percentage of population, area and number of households covered by a given gradient curve of time savings. Similar applications of coverage have been made in other contexts [40].

3. Results and discussion

3.1. Global Media Accessibility offered by the current network structure

The following will show excerpts from the analysis of global average accessibility for the city of Manizales. These results are the basis for the calculation of gradients in saving percentages in ATT. These excerpts have been documented in the Mobility Plan of the city of Manizales [1,28]. Fig. 4 shows the ATT isochronous curves in terms of Global Media Accessibility in Manizales. In general, the city is covered by isochronous curves of between 25 and 67.5 minutes.

The lowest isochronous curve is of 25 minutes covering a wide sector between Avenida Santander, Avenida Kevin Angel and the downtown area of Manizales. This area currently benefits from the best possible accessibility in the city. It is concluded that 50% of the population and 50% of the number of houses are covered by ATT of up to 29.5 minutes, while 50% of the urban area are covered by ATT of up to 32.5 minutes.

3.2. Gradient of global media accessibility. Alternative 4A

Once the Global Media Accessibility of Manizales is calculated, taking into account modifications to the graph corresponding to Alternative 4A, the vector of average travel time is compared in both the current infrastructure and in alternative 4A.



Figure 4. Global Media Accessibility curves in Manizales.
Source: Escobar and García (2012) [29].

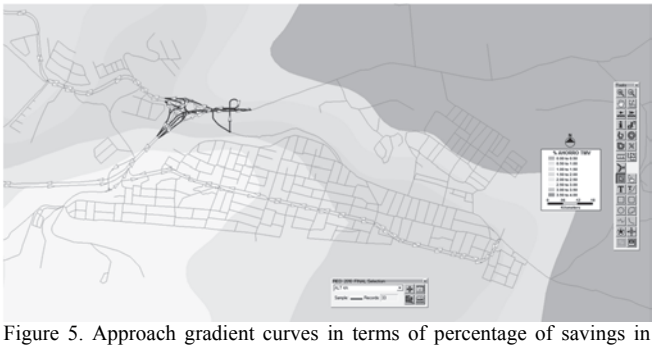


Figure 5. Approach gradient curves in terms of percentage of savings in ATT. Alternative 4A.
Source: Authors´own calculation.



Figure 6. Gradient curves in terms of percentage of savings in ATT. Alternative 4A.
Source: Authors´ own calculation.

A kriginig prediction model with linear semivariogram was applied in the geostatistical analysis. Fig. 5 shows an approach to the sector under study and the behavior of the curves is observed within the Enea neighborhood. Fig. 6 shows the configuration of these curves throughout the city of Manizales.

If chosen, Alternative 4A would provide a percentage of savings in ATT throughout the entire city and sectors located to the east (La Enea neighborhood) would have a percentage savings in ATT of maximum 3% of the current ATT. Table 1 shows the results of relating the gradient isochronous curves with the sociodemographic information of Manizales.

Fig. 7 was built using a more detailed analysis of the results. It shows the relationship between the percentage of coverage and the percentage of savings in ATT in each of the analyzed variables.

The percentage of area, population and number of households covered by each gradient isochronous curve was calculated. In the variable area, the gradient curve of 0.5% covers 70%. It is observed that 17% of the population might have an average saving of 1% in ATT regarding the initial ATT. Regarding the variable number of households, stratum 1, having the lower gradient curve, is the stratum reporting higher coverage percentages.

If chosen, Alternative 4A would have a final saving percentage of 0.8% in ATT in relation to the initial ATT for approximately 43% of coverage of the three variables.

3.3. Gradient of Global media accessibility. Alternative 6

Once the Global Media Accessibility is calculated taking into account the modifications done to the graph of Alternative 6, the same calculation of gradient is done in

Table 1.
Percentage of area, population and number of households covered by gradient curves in saving percentages of ATT in Alternative 4A.

Isochronous Curve % Savings	Area		Population		Households	
	Km^2	%	N° People	%	N° Houses	%
0,5	24,7	70%	283.510	78%	62.888	75%
1,0	8,3	24%	62.665	17%	17.215	21%
1,5	0,7	2%	1.623	0%	611	1%
2,0	0,5	2%	3.860	1%	984	1%
2,5	0,5	1%	4.520	1%	1.047	1%
3,0	0,4	1%	5.243	1%	1.128	1%
Total	35,1	100%	361.422	100%	83.873	100%

Source: Authors´own calculation.

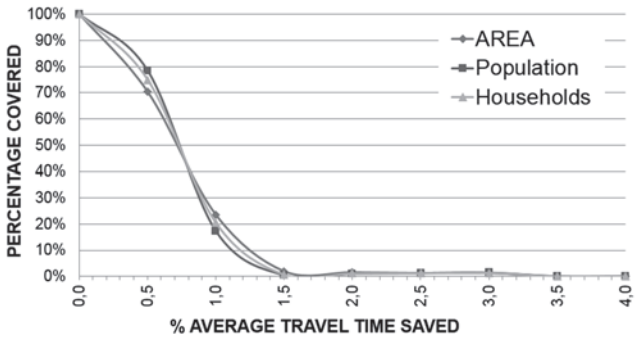


Figure 7. Relationship between the percentage of coverage and the percentage of savings in ATT. Alternative 4A.
Source: Authors´ own calculation.

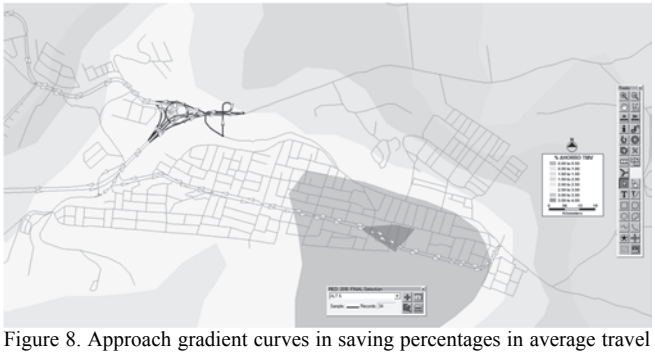


Figure 8. Approach gradient curves in saving percentages in average travel time. Alternative 6.
Source: Authors´ own calculation.



Figure 9. Gradient curves in saving percentages in average travel time. Alternative 6.
Source: Authors´ own calculation.

Alternative 4A. A kriginig prediction model with linear semivariogram is applied in the geostatistical analysis. Fig. 8 shows an approach to the sector under study and also the behavior of the curves in the Enea neighborhood.

A brief comparison of the curves obtained in Alternative 4A (see Fig. 5) shows that Alternative 6 would provide the Enea neighborhood with better service of transport given the fact that the gradient curves refer to a greater coverage in higher saving percentages of ATT. Fig. 9 shows the configuration of these curves throughout the city of Manizales.

If chosen, Alternative 6 would provide the entire city with saving percentages in ATT, and sectors located to the east (La Enea neighborhood) would benefit from savings percentages in ATT of maximum 4%; a value higher than the one obtained in Alternative 4A.

The percentage of area, population and number of households covered by each curve was calculated relating the gradient isochronous curves obtained from the sociodemographic data of Manizales. Table 2 shows the summary of the overlay data.

The gradient curve of 0.5% covers 54% in the variable area and 20% of the population could experience an average

Table 2.
Percentage of area, population and number of households covered by gradient curves in saving percentage of ATT in Alternative 6.

Isochronous curve % Savings	Area		Population		Households	
	Km^2	%	N° of people	%	N° Houses	%
0,5	18,8	54%	270.414	75%	59.921	71%
1,0	12,4	35%	72.307	20%	19.041	23%
1,5	1,6	4%	2.221	1%	862	1%
2,0	0,6	2%	1.511	0%	534	1%
2,5	0,6	2%	3.565	1%	931	1%
3,0	0,9	3%	8.414	2%	1.939	2%
3,5	0,2	1%	2.856	1%	616	1%
4,0	0,0	0%	136	0%	29	0%
Total	35,1	100%	361.422	100%	83.873	100%

Source: Authors´ own calculation.

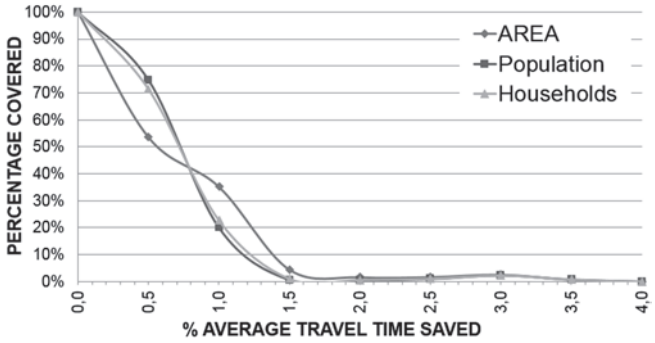


Figure 10. Relationship between the percentage of coverage and the percentage of savings in ATT. Alternative 6.
Source: Authors´ own calculation.

savings in ATT of 1% compared to the current infrastructure. The percentage distribution of coverage of number of households shows that stratum No. 1 manifests a higher percentage of number of households covered in the lower gradient curve; similar situation found in alternative 4A.

After making a more detailed analysis of the results, it was possible to find the relationship between the percentage of coverage and the percentage of savings in ATT for each of the variables. See Fig. 10.

Alternative 6, with approximately 41% coverage of the three variables, would provide a 0.8% of saving percentages in ATT compared to the initial ATT. It is to note that the percentage of coverage at the point where the area, population and number of households converge is slightly above 40% and very similar in both alternatives. However, the configuration of the curves is different.

3.4. Comparison of results for Global media accessibility and alternatives

An objective comparison is done regarding the percentages of coverage for each of the variables in each alternative. Fig. 11 separately and comparatively shows the results obtained while taking into account the variable area, population and number of households covered.

Regarding the variable area, there is a greater coverage in saving percentages, superior to 1%, in ATT. This is due to the characteristics of population density of the area covered

by such curves and to the differences in the configuration of the curves obtained in both intervention alternatives. The configuration of the curves is very similar in the variable urban population and number of households covered.

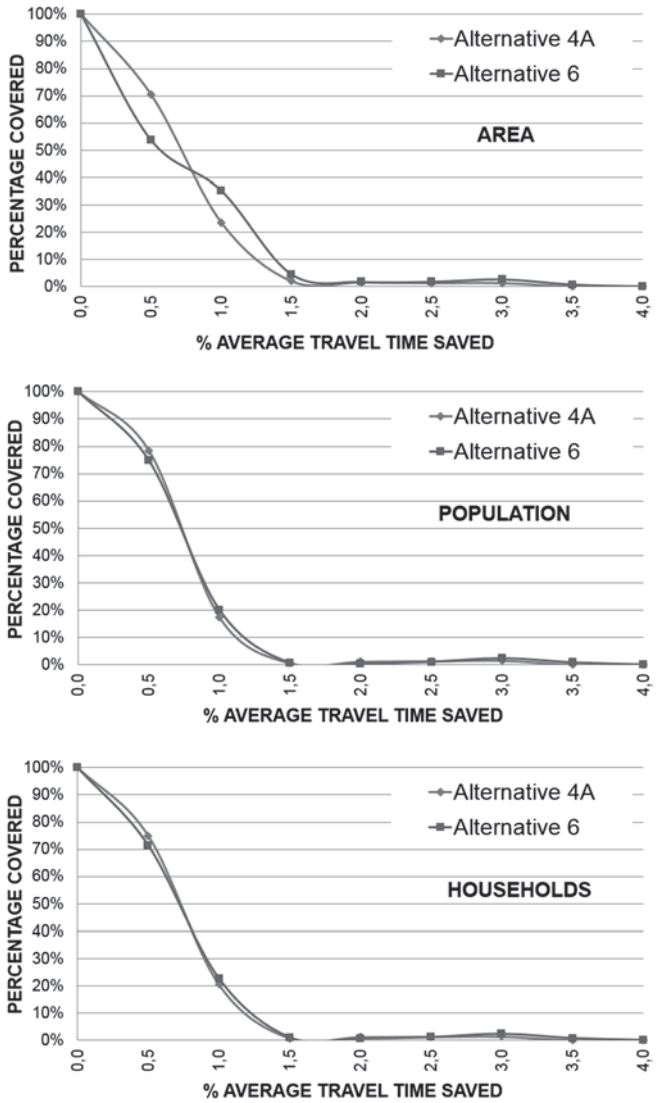


Figure 11. Comparison of results. Variables area, population and number of households.
Source: Authors´ own calculation.

Even though the percentage coverage of the variable population and number of households are similar due to their geospatial distribution, it is concluded that Alternative 6 demonstrates more favorable results than Alternative 4A in terms of a supply model of transport and saving percentages in ATT. These results are determined by the calculation of coverage percentages and cannot be verified simply by observing the graphs.

Calculating the number of households covered according to socioeconomic stratum manifests that the higher the stratum the higher the percentage of coverage of a gradient upper curve (see Fig. 12). For example, there is a high percentage of coverage (over 90%) for the gradient curve of 0.5%, in both alternatives for stratum 1. However, the percentage coverage decreases for stratum 6 (up to 60 %) but increases to almost 30% in the gradient curve of 1% in savings in ATT.

Coverage of households in stratum 3 was achieved with gradient curves exceeding 3% savings in average travel time. This result reflects residential activity in La Enea neighborhood. These results are higher in Alternative 6 than in Alternative 4A as this is the point in which the difference between the two alternatives is higher regarding supply models.

It is important to note the results obtained in stratum 5, where the gradient curve of 1% in ATT savings, presents greater coverage than the gradient curve of 0.5%. This is a very positive situation due to the fact that there is a strong possibility of further decreasing the average travel time in stratum 5, in which vehicle purchasing power is considered high. It was found that over 50% of households in Stratum 5 might reduce their average travel time by up to 1%.

Performing a weighted analysis of the saving percentage in ATT in each variable shows that Alternative 4A would provide a 0.66% saving in ATT regarding the variable population, while Alternative 6 would generate a 0.72% savings in ATT.

Performing the same analysis regarding the variable number of households gives that Alternative 4A reports a saving percentage of 0.69% while Alternative 6 reports a saving percentage of 0.74%.

Finally, performing the same analysis regarding the variable area demonstrates that Alternative 4A generates a percentage saving of 0.72% and Alternative 6 reaches 0.87%. Table 3 shows the results of weighing the saving percentage in ATT by socioeconomic strata and by Alternative regarding the variable number of households.

If chosen, Alternative 4A would provide stratum 3 with 0.82% and stratum 5 with 0.79% savings in ATT. However, if chosen, Alternative 6 would provide stratum 3 with 0.91% and stratum 5 with 0.81% savings in ATT. In general, Alternative 6 shows higher saving percentages in ATT than Alternative 4A.

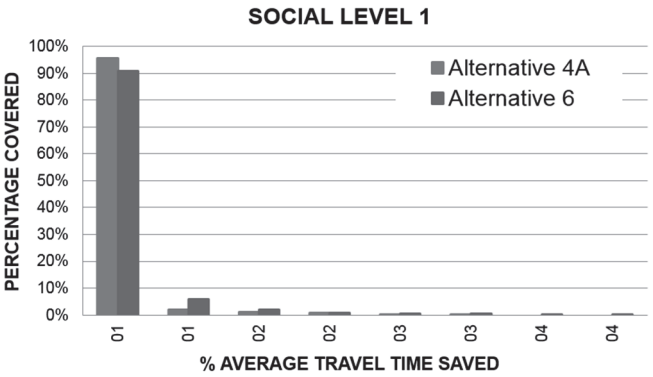
3.5. Prioritization analysis

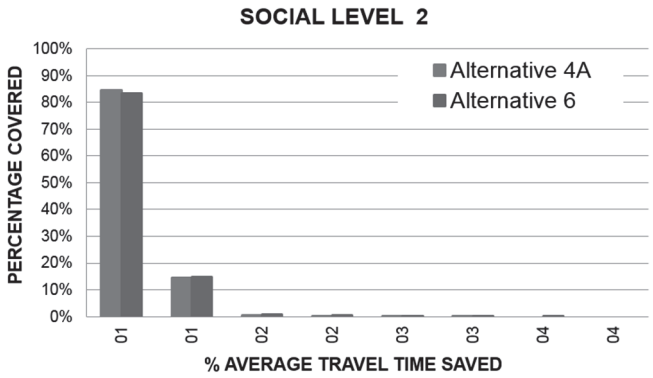
The prioritization analysis used in this research considers three variables that complement each other. The first deals with simulation results of traffic and demand, in other words, the life span calculated using traffic studies. The second deals with the analysis of urban territorial accessibility that defines the percentage saving in ATT obtained with the building of each alternative. The third deals with the preliminary construction cost of the alternatives. Alternative 4A yielded better results from the simulation and demand as it had a life span of twenty (20) years, while Alternative 6 had a life span of seven (7) years.

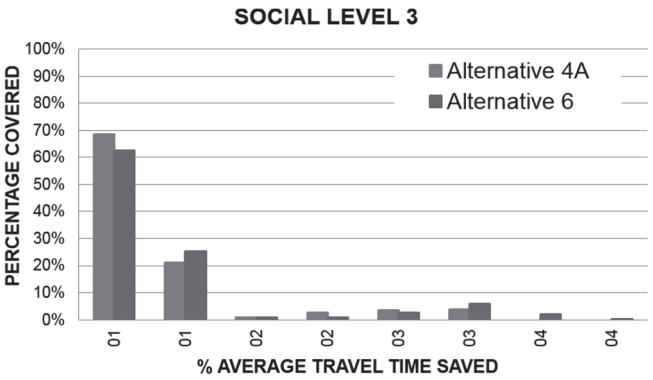
From the point of view of supply models, that is from the territorial accessibility analysis, and giving equal importance to the variables area, population and number of households, it was decided that Alternative 4A reported a weighted average saving percentage of 0.69% while Alternative 6 reported 0.78%.

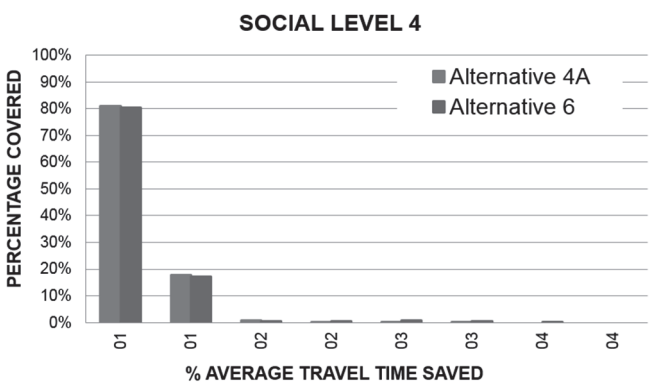
Alternative 4A reported preliminary costs of approximately $8 million U.S dollars while Alternative 6 reported preliminary costs of approximately $6.5 million U.S dollars (2014 prices).

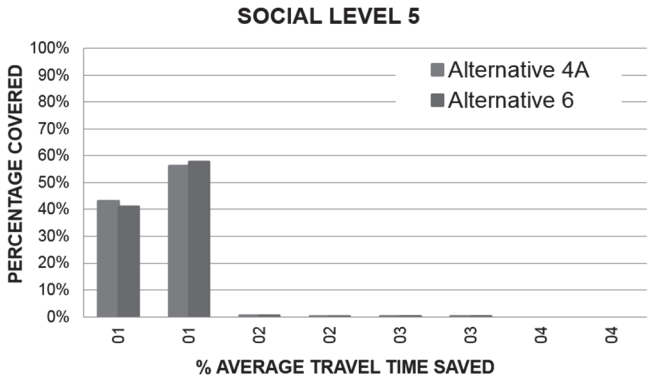
Table 4 shows the rating or scores in each alternative, assigning the best result a value of five points for each of the three variables that make up the prioritization study and provides a score directly proportional to the highest score in the second option.











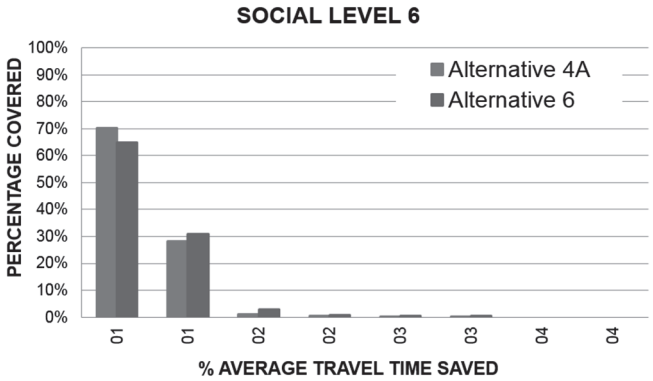


Figure 12. Comparison of results in terms of social levels. Variables area, population and households.
Source: Authors´ own calculation.

Table 3.
Saving Percentage in ATT weighted by the number of households in each socioeconomic stratum and each proposed alternative.

Social Level	Alternative 4A	Alternative 6
1	0,54	0,58
2	0,58	0,60
3	0,82	0,91
4	0,60	0,63
5	0,79	0,81
6	0,66	0,71
Total	0,69	0,74

Source: Authors´ own calculation.

Table 4.
Scores of the variables in the prioritization analysis in each alternative.

Alternative	Life span	% ATT savings	Preliminary costs
4A	5,0	4,4	4,1
6	1,8	5,0	5,0

Source: Authors´ own calculation.

Giving equal value to the life span, ATT savings and preliminary costs variables shows that Alternative 4A would have a final score of 4.5 (within a scale of 0 to 5, 5 being the highest and 0 the lowest) and Alternative 6 a score of 3.9. The recommendation is thus to build Alternative 4.

However, it would be possible to generate a sensitivity analysis by performing a gradual analysis of the weight of each of the variables to show the variation of the score assigned to each alternative depending on the weight defined

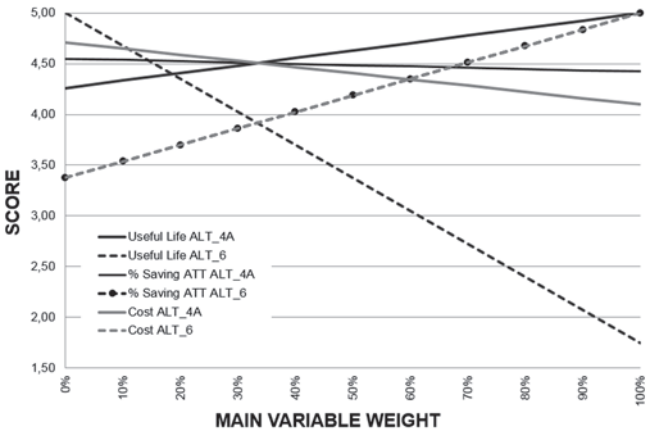


Figure 13. Sensitivity analysis according to gradual change of the main variable.
Source: Authors´ own calculation.

in each variable. Considering each of the variables to be the main variable of gradual change and equally distributing the weight of the remaining two variables, the values of the scores obtained are graphed.

Fig. 13 shows the sensitivity curves in each alternative according to the gradual change of the variable defined as the main one. For example, if life span is taken as the main variable it would refer to an important variation in the weight assigned to this variable according to the score, thus getting a greater score variation in Alternative 6.

4. Conclusions

It is concluded that the values of saving percentages in ATT seem low because they correspond to the comparative of a particular intervention point in the city regarding the current situation and not an intervention of an entire vehicular corridor as presented in the Mobility Plan. In other words, from the point of view of a transport model,, an insertion of an infrastructure that is configured as a mobility corridor, whether new or rehabilitated, is more visible than the insertion of an infrastructure on a specific site in the city.

However, it is considered that the results show global percentages of saving in ATT and these savings very well qualify the impact of each of the analyzed alternatives in the entire city of Manizales.

It is noted that depending on the weight given to the three variables analyzed, the result would be the recommendation to build either alternative. However, there are combinations of weights of the three variables that yield similar results in terms of the final score.

It was found that 4A is the best recommended Alternative to be built because even though this alternative offers lower saving percentages in ATT than Alternative 6, and preliminary construction costs higher than Alternative 6, its life span is much higher than the life span of Alternative 6. This was defined after microsimulation and demand analysis.

It is also concluded that the definition of the weight of the variables in the analysis of prioritization depends exclusively on the main purpose for the interventions or on the constraints identified in the global project.

After making the proper prioritization calculation of Alternatives 4A and 6 and after analyzing the results, it is considered that the construction of Alternative 4A is the most viable. It is necessary to clarify that this prioritization analysis did not include environmental issues that might impact the results one way or another.

References

[1] Alcaldía de Manizales, Secretaría de Tránsito y Transporte. Plan de Movilidad de la ciudad de Manizales 2010 – 2040. Universidad Nacional de Colombia – Sede Manizales. Manizales, Abril 2011.

[2] Gómez, M., y Barredor, J.I., Sistemas de información geográfica y evaluación multicriterio en la ordenación del territorio. Ra-Ma Editorial. 2da. Edición. Madrid, 2005.

[3] Zhang, H. and Gao, Z., Bilevel programming model and solution method for mixed transportation network design problem. Journal of Systems Science and Complexity, [Online]. 22 (3), pp. 446-459, 2009. [Date of reference July 24th of 2012]. Available at: http://www.sysmath.com/jweb_xtkxyfzx/EN/Y2009/V22/I3/446

[4] Morris, J., Dumble, P. and Wigan, M., Accessibility indicators in transport planning. Transportation Research, [Online]. A, 13, pp. 91-109, 1978. [Date of reference September 21th of 2012]. Available at: http://projectwaalbrug.pbworks.com/f/Transp+Accessib+-+Morris,+Dumble+and+Wigan+(1979).pdf

[5] Batty, M., Accessibility: In search of a unified theory. Environment and Planning B: Planning and Design, [Online]. 36, pp. 191-194, 2009. [Date of reference November 6th of 2012]. Available at: http://www.envplan.com/abstract.cgi?id=b3602ed

[6] Kibambe, J.P., Radoux, J. and Defourny, P., Multimodal accessibility modeling from coarse transportation networks in Africa. International Journal of Geographical Information Science, [Online]. 27 (5), pp. 1005-022, 2013. [Date of reference December 23th of 2012]. Available at: http://www.tandfonline.com/doi/abs/10.1080/13658816.2012.735673#.VHP5bPmG8uc

[7] Hansen, W., How accessibility shapes land use. Journal of the American Institute of Planners, [Online]. 25 (2), pp. 73-76, 1959. [Date of reference December 23th of 2012]. Available at: http://www.tandfonline.com/doi/abs/10.1080/01944365908978307#.VHPikfmG8uc

[8] Curl, A., Nelson, J. and Anable, J., Does Accessibility Planning address what matters?. Transportation Business & Management, [Online]. 2, pp. 3-11, 2011. [Date of reference September 22th of 2012]. Available at: http://www.sciencedirect.com/science/article/pii/S2210539512000041

[9] Gutiérrez, J., Redes, espacio y tiempo. Anales de geografía de la Universidad Complutense, [Online]. 18, pp. 65-86, 1998. [Date of reference May 9th of 2012]. Available at: http://revistas.ucm.es/index.php/AGUC/article/viewFile/AGUC9898110065A/31393

[10] Burkey, M., Decomposing geographic accessibility into component parts: methods and an application to hospitals. Annals of Regional science, [Online]. 48 (3), pp. 783-800, 2012. [Date of reference April 19th of 2012]. Available at: DOI: 10.1007/s00168-010-0415-3

[11] Litman, T., Beyond roadway level-of-service: Improving transport system impact evaluation. [Online]. Victoria Transport Policy Institute. February 2014. [Date of reference January 5th of 2015]. Available at: http://www.vtpi.org/CGOP_LOS.pdf

[12] Calcuttawala, Z., Landscapes of information and consumption: A Location analysis of public libraries in calcutta, in Edward D. Garten, Delmus E. Williams, James M. Nyce (eds.). Advances in Library Administration and Organization, [Online]. Vol. 24, Emerald Group Publishing Limited, pp.319-388, 2006. [Date of reference August 13th of 2012]. Available at: http://www.emeraldinsight.com/doi/pdfplus/10.1016/S0732-0671%2806%2924009-4. DOI: 10.1016/s0732-0671(06)24009-4

[13] Park, S., Measuring public library accessibility: A case study using GIS. Library & Information Science Research, [Online]. 34 (1), pp. 13-21, 2012. [Date of reference September 12th of 2012]. Available at: http://www.sciencedirect.com/science/article/pii/S0740818811000958

[14] Higgs, G., Langford, M. and Fry, R., Investigating variations in the provision of digital services in public libraries using network-based GIS models. Library & Information Science Research, [Online]. 35 (1), pp. 24-32, 2013. [Date of reference January 15th of 2013]. Available at: http://www.sciencedirect.com/science/article/pii/S0740818812000977

[15] Cao, X. and Li, L., Accessibility distribution impact of intercity rail transit development on Pearl River Delta Region in China. CICTP 2012: Multimodal Transportation Systems—Convenient, Safe, Cost-Effective, Efficient. Proceedings of the 12th International Conference of Transportation Professionals. Beijing, China, [Online]. pp. 1719-1730, 2012. [Date of reference August 12th of 2013]. Available at: http://ascelibrary.org/doi/abs/10.1061/9780784412442.175

[16] Botero, R., Murillo, J. and Jaramillo, C., Decision strategies for evaluating pedestrian accessibility. Revista DYNA, [Online]. 78 (168), pp. 28-35, 2011. [Date of reference September 14th of 2014]. Available at: http://dyna.unalmed.edu.co/en/ediciones/168/articulos/a03v78n168/a03v78n168.pdf

[17] Schürman, C., Spiekermann, K. and Wegener, M., Accessibility indicators. Berichte aus dem Institut für Raumplanung, [Online]. 39, IRPUD, Dortmund, 1997. [Date of reference November 23th of 2013]. Available at: http://spiekermann-wegener.de/pub/pdf/IRPUD_Ber39.pdf

[18] López, E., Gutierrez, J. and Gómez, G., Measuring regional cohesion effects of large-scale transport infrastructure investment: An accessibility approach, European Planning Studies, 16 (2), pp. 277-301, 2008. DOI: 10.1080/09654310701814629

[19] Kotavaara, O., Antikainen, H. and Rusanen, J., Population change and accessibility by road and rail networks: GIS and statistical approach to Finland 1970–2007. Journal of Transport Geography, [Online].19 (4), pp. 926-935, 2011. [Date of reference October 16 2012]. Available at: http://www.sciencedirect.com/science/article/pii/S0966692310001948

[20] Rietveld, P. and Nijkamp P., Transport and regional development. In: J. Polak and A. Heertje, Eds., European Transport Economics, European Conference of Ministers of Transport (ECMT), Blackwell Publishers, Oxford. 1993.

[21] Vickerman, R., Spiekermann, K. and Wegener, M., Accessibility and economic development in Europe. Regional Studies, 33 (1), pp. 1-15, 1999. DOI: 10.1080/00343409950118878

[22] Mackinnon, D., Pirie, G. and Gather, M., Transport and economic development. In: R. Knowles, J. Shaw, & I. Docherty, Eds., Transport Geographies: Mobilities, Flows and Spaces, Blackwell Publishers, Oxford, 2008, pp. 10-28.

[23] Cheng, J., Bertolini, L. and Clercq, F., Measuring sustainable accessibility. Transportation research board: Journal of the Transportation Research Board, 2017, pp. 16-25, 2007. DOI: 10.3141/2017-03

[24] Vega, A., A multi-modal approach to sustainable accessibility in Galway. Regional Insights, 2(2), pp. 15-17, 2011. DOI: 10.1080/20429843.2011.9727923

[25] Kastenholz, E., Eusébio, C., Figueiredo, E. and Lima, J., Accessibility as competitive advantage of a tourism destination: The case of Lousã, in Field guide to case study research in tourism, hospitality and leisure. In: K.F. Hyde, Ryan, C. and Woodside, A.G. (eds.). Advances in Culture, Tourism and Hospitality Research, 6, [Online]. Emerald Group Publishing Limited, pp. 369-385, 2012. [Date of reference April 15th of 2014]. Available at: http://www.emeraldinsight.com/doi/abs/10.1108/S1871-3173%282012%290000006023

[26] Sailer, K., Marmot A. and Penn, A., Spatial configuration, organisational change and academic networks. ASNA 2012 – Conference for 'Applied Social Network Analysis', Zürich, Switzerland, [Online]. 2012. [Date of reference December 18th of 2012]. Available at: http://discovery.ucl.ac.uk/1381761/

[27] Escobar, D., García, F. and Tolosa, R., Análisis de accesibilidad territorial a nivel regional. Tesis. Facultad de Ingeniería y Arquitectura. Universidad Nacional de Colombia. ISBN 9789587612776. Manizales, March 2013.

[28] Escobar, D. and García, F., Territorial accessibility analysis as a key variable for diagnosis of urban mobility: A case study Manizales (Colombia). Procedia - Social and Behavioral Sciences, [Online]. 48(0), pp. 1385-1394, 2012. [Date of reference April 10th of 2012]. Available at: http://www.sciencedirect.com/science/article/pii/S1877042812028509

[29] Escobar, D., García, F. y Tolosa, R., Diagnóstico de la Movilidad urbana de Manizales. Facultad de Ingeniería y Arquitectura. Universidad Nacional de Colombia. ISBN 9789587611281. Manizales, March 2012.

[30] Escobar, D. y Urazan, C., Accesibilidad territorial: Instrumento de planificación urbana y regional. Revista Tecnura, Edicion Especial, pp. 241-253, 2014.

[31] Gutiérrez, J., Condeco-Melhorado, A. and Martín, J., Using accessibility indicators and GIS to assess spatial spillovers of transport infraestructure investment. Journal of Transport Geography, 18, pp. 141-152, 2012. DOI: 10.1016/j.jtrangeo.2008.12.003

[32] Karou, S. and Hull, A., Accessibility modelling: predicting the impact of planned transport infrastructure on accessibility patterns in Edinburgh, UK. Journal of Transport Geography, [Online]. 35, pp. 1-11, 2014 [Date of reference July 5th of 2014]. Available at: DOI:10.1016/j.jtrangeo.2014.01.002

[33] Liévano, F. and Olaya, Y., Agent-based simulation approach to urban dynamics modeling. Revista DYNA, [Online]. 79(173), pp. 34-42, 2012. [Date of reference December 9th of 2014]. Available at: http://dyna.unalmed.edu.co/en/ediciones/173-II/articulos/a04v79n173-II/a04v79n173-II.pdf

[34] Li, Q., Zhang, T., Wang, H. and Zeng, Z., Dynamic accessibility mapping using floating car data: a network-constrained density estimation approach. Journal of Transport Geography, [Online]. 19, pp. 379-393, 2011. [Date of reference September 17th of 2014]. Available at: http://www.sciencedirect.com/science/article/pii/S0966692310001158

[35] Mesa, M., Valencia, J. y Olivar, G., Modelo para la dinámica de un vehículo a través de una secuencia de semáforos. Revista DYNA, [Online]. 81(184), pp. 138-145, 2014. [Date of reference October 17th of 2014]. Available at: http://dyna.unalmed.edu.co/en/ediciones/186/articulos/v81n186a19/v81n186a19.pdf

[36] Zhu, X. and Liu, S., Analysis of the impact of the MRT system on accesibility in Singapore using an integrated GIS tool. Journal of Transport Geography, 4(12), pp. 89-101, 2004. DOI: 10.1016/j.jtrangeo.2003.10.003

[37] Chen, S., Claramunt, C. and Ray, C., A spatio-temporal modelling approach for the study of the connectivity and accessibility of the Guangzhou metropolitan network. Journal of Transport Geography, [Online]. 36, pp. 12-23, 2014 [Date of reference August 15th of 2014]. Available at: DOI: 10.1016/j.jtrangeo.2014.02.006

[38] Halden, D., The use and abuse of accessibility measures in UK passenger transport planning. Transportation Business & Management, [Online]. 2, pp. 12-19, 2011. [Date of reference July 9th of 2013]. Available at: http://www.sciencedirect.com/science/article/pii/S2210539511000022

[39] Jones, P., Developing and applying interactive visual tools to enhance stakeholder engagement in accessibility planning for mobility disadvantaged groups. Transportation Business & Management, [Online]. 2, pp. 29-41, 2011. [Date of reference June 28th of 2013]. Available at: http://www.sciencedirect.com/science/article/pii/S2210539511000320

[40] Straatemeier, T., How to plan for regional accessibility?. Transport Policy, [Online].1, pp. 127-137, 2008. [Date of reference October of 2012]. Available at: http://projectwaalbrug.pbworks.com/f/Transp+Accessib+-+Straatemeier+(2007).pdf

D.A. Escobar-García, received his BSc. Eng in Civil Engineering in 1999 from the Universidad Nacional de Colombia, his MSc. degree in Civil

Engineering in 2001 from the Universidad de los Andes, Colombia, and his PhD in land management and transport infrastructure in 2008 from the Universidad Politécnica de Cataluña, España. From 1999 to 2001 he worked for road construction companies and since 2001 he has worked for the Universidad Nacional de Colombia. He is currently a professor in the Civil Engineering Department, of the Architecture and Engineering Faculty in the Universidad Nacional de Colombia, in Manizales, Colombia. His research interests include: accessibility, sustainable models transit and transport planning, simulation, modeling and forecasting in transport, and forecasting using geostatistical techniques.
ORCID: 0000-0001-9194-1831

C. Younes-Velosa, received his BSc. Eng in Electrical Engineering in 1999 from the Universidad Nacional de Colombia, his MSc. degree in High Voltage Engineering in 2002 from the Universidad Nacional de Colombia, PhD in Electrical Engineering from the Universidad Nacional de Colombia and received degree in Law from Universidad de Manizales in 2014. Since 2006 he has worked as a professor in the Electric, Electronic and Computing Engineering Department of the Architecture and Engineering Faculty in the Universidad Nacional de Colombia, in Manizales, Colombia. His research interests include: Energy Policy on lighting, Renewable Energy Sources and Transport Regulation, Electromagnetic Compatibility and Lightning Protection.
ORCID: 0000-0002-9685-8196

C. A. Moncada-Aristizábal, received his BSc. Eng in Civil Engineering in 2000 from the Universidad Nacional de Colombia, his MSc. degree in Transport Engineering in 2005 from the Universidad Nacional de Colombia and his MSc. degree in Infrastructure Planning in 2010 from the University of Stuttgart, Alemania. From 2013, he has been developing his PhD in transport at the Universidad de los Andes, Colombia. He worked as transport planner consultant for the Ministry of Transportation in medium and small sized cities. He is currently a Professor in the Civil and Agricultural Engineering Department -Faculty of Engineering- at the Universidad Nacional de Colombia, in Bogotá. His research interests include: transport demand models transit and transport planning, simulation, modeling and forecasting in transport.
ORCID: 0000-0003-3745-6880

UNIVERSIDAD NACIONAL DE COLOMBIA
SEDE MEDELLÍN
FACULTAD DE MINAS

Área Curricular de Ingeniería Civil

Oferta de Posgrados

Especialización en Vías y Transportes
Especialización en Estructuras
Maestría en Ingeniería - Infraestructura y Sistemas de Transporte
Maestría en Ingeniería – Geotecnia
Doctorado en Ingeniería - Ingeniería Civil

Mayor información:

E-mail: asisacic_med@unal.edu.co
Teléfono: (57-4) 425 5172

UNIVERSIDAD NACIONAL DE COLOMBIA
SEDE MEDELLÍN
FACULTAD DE MINAS



DYNA
http://dyna.medellin.unal.edu.co/

Simulation of a thermal environment in two buildings for the wet processing of coffee

Robinson Osorio-Hernandez [a], Lina Marcela Guerra-Garcia [b], Ilda de Fátima Ferreira-Tinôco [c], Jairo Alexander Osorio-Saraz [d] & Iván Darío Aristizábal-Torres [e]

[a] Departamento de Engenharia Agrícola, Universidade Federal de Viçosa, Viçosa, Brasil. robinson.hernandez@ufv.br
b Departamento de Engenharia Agrícola, Universidade Federal de Viçosa, Viçosa, Brasil. lina.garcia@ufv.br
c Departamento de Engenharia Agrícola, Universidade Federal de Viçosa, Viçosa, Brasil. iftinoco@ufv.br
d Departamento de Ingeniería Agrícola y Alimentos, Universidad Nacional de Colombia, Medellín, Colombia. aosorio@unal.edu.co
e Departamento de Ingeniería Agrícola y Alimentos, Universidad Nacional de Colombia, Medellín, Colombia. idaristi@unal.edu.co

Received: March 6th, 2015. Received in revised form: May 15th, 2015. Accepted: May 12th, 2015.

Abstract
This study aimed to compare the bioclimate and energy consumption of two coffee wet processing facilities in Colombia, with two typical types of Colombian coffee, using computer simulation. Specifically, we evaluated the effect of the heat generated by machines and the effect of the natural ventilation area on temperature and relative air humidity inside these buildings and their energy consumption. The postharvest plant with typology *b* gave the best results in terms of temperature and relative humidity suitable to preserve the quality of the coffee bean. Its approximate energy consumption was 30% of the total consumed by typology *a*.

Keywords: bioclimate, quality coffee, wet beneficio of coffee, coffee drying, energy consumption.

Simulación del ambiente térmico en dos edificaciones para beneficio húmedo de café

Resumen
Este estudio tuvo como objetivo hacer una comparación bioclimática y de consumo energético entre dos instalaciones de beneficio húmedo de café en Colombia, con dos tipologías típicas de la zona cafetera colombiana, por medio de simulación computacional, evaluando específicamente el efecto del calor generado por las máquinas y el efecto del área de ventilación natural sobre la temperatura y la humedad relativa del aire en el interior de éstas construcciones y su consumo energético. El beneficiadero de café de tipología *b* presentó los mejores resultados en términos de temperatura y humedad relativa para conservar la calidad del grano de café y su consumo energético aproximado fue 30% del total consumido por la tipología *a*.

Palabras clave: bioclima; calidad de café; beneficio húmedo de café; secado de café; consumo energético.

1. Introduction

Coffee has great economic and social importance [1,2]. It is the third most important food product in the world after wheat and sugar, and the coffee industry employs 125 million people worldwide [3]. Nearly 25 million households over 50 countries produce coffee in tropical and subtropical regions of Asia, Africa and Latin America. There are also coffee growing regions in the United States (Hawaii, Puerto Rico) and Australia [4].

Nowadays it is observed that the specialty coffee market (market value-added) is experiencing a continuous growth in demand, mainly because the world is increasingly enjoying good coffee and the highest quality beverages [5].

Various factors determine the formation of the flavors and aromas of the coffee beverage, the final appearance of the grain and thus the value of the final product. These factors include the genetic strain, variety, edaphological factors, the crop and climatic factors, but harvest and postharvest management are key issues [6].

The postharvest process is one of the primary points for the preservation of the qualitative characteristics of the coffee bean [7], as long as appropriate techniques that meet the

© The author; licensee Universidad Nacional de Colombia.

climatic conditions of the region and socioeconomics of the producer are used [6]. In Colombia the coffee is wet processed [8]. The wet processing of coffee includes depulping, fermentation, washing and drying the coffee bean.

The removal of the epicarp and mesocarp, depending on the environmental conditions in the drying coffee, can reduce the risk of unwanted fermentation [9]. Drying is considered a critical process step, which decreases the product moisture content from 55–60% wet basis (wb) to 10–12% wb (the grain moisture balance with the environment), the reduction being due to water activity and metabolic processes. The coffee is dried in the interest of maintaining its quality and storing it for extended periods of time [10,11].

The main problems in the cup (taste) arise from poor drying and storage. Some of these problems even present biological and chemical risks with the product and can lead to a product that is unfit for human consumption [12,13].

Although less than 10% of Colombian coffee growers use mechanical drying, they are responsible for approximately 70% of the volume of coffee that is produced in Colombia [14].

Furthermore, according to [15], solar drying is the most commonly used method for preserving agricultural products in most developing countries. Solar drying of coffee is used by 90% of Colombian coffee producers and uses a renewable energy source (the most abundant on the planet) it is also highly appreciated in the specialty coffee market. This is important to conserve the environment, but also because nowadays it is observed that the specialty coffee market is experiencing a continuous growth in demand [5].

Poor control and design of coffee postharvest plants (buildings for the wet processing of coffee) can compromise product quality due to inadequate bioclimatic environments. Humid environments and high temperatures during storage are risk conditions that can physically damage the grain, causing decomposition and deterioration in the quality of the product [13].

Temperatures higher than 50°C can kill the seed of coffee and begin the process of decomposition. According to [15], losses of fruits and vegetables during drying in developing countries are estimated at 30–40% of production, but they also report that postharvest losses can be reduced dramatically with optimal use (control) of well-designed solar drying systems.

In Arabica coffee storage, the discoloration defect has a rate that is directly related to the conditions of the storage environment; the higher the temperature and relative humidity, the faster the coffee bleaches. According to [16,17], a marked loss of color can be observed from the eighth day of storage conditions at temperatures above 20°C and with a relative humidity greater than 52%.

To analyze and suggest bioclimatic and air quality solutions within agro-industrial buildings, the application of mathematical and computational modeling is increasingly used and important [18]. Simulation is a very interesting tool in the design and evaluation of buildings, showing how those buildings involve very complex aspects such as energy flows, transient stochastic occupancy patterns, etc., that traditional design methods based on experience or experimentation cannot quantify satisfactorily [19].

Numerous analyses of the bioclimatic and air quality in rural buildings have been done with software based on CFD [18], but other software may also be used. One of the most popular computer programs for energy and bioclimatic simulation for buildings is EnergyPlus™ [20], which is a free open source software developed by the US Department of Energy (DoE).

Its main input variables are: 3D building design, construction materials, internal equipment, and climate variables of the site of the building. This program calculates the energy efficiency, bioclimatic variables and air quality within buildings, across balances of mass, energy and chemical composition.

This study aimed to make a simulation of the thermal environment in EnergyPlus™ software for two typical installations of the Colombian coffee postharvest, in order to compare and analyze the internal bioclimatic conditions for grain quality.

2. Material and methods

The two buildings are located in the municipality of Barbosa (Antioquia-Colombia) at coordinates 6°26'15"N, 75°19'50"W, at an altitude of 1700 m (the two buildings are neighboring properties). The two farms produce the same amount of coffee, with a coffee cherry production of about 125,000 kg/year^{-1} (yielding 25,000 kg/year^{-1} of parchment coffee). This study was conducted during the month of May 2014.

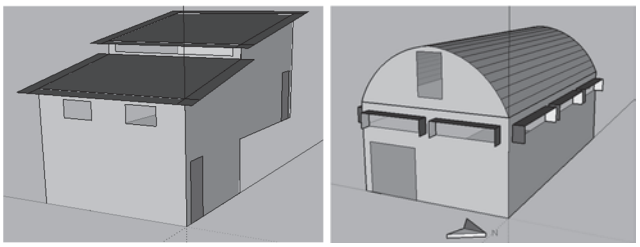
It was drawn in the 3D geometry SketchUp® program, for each of the two structures (Fig. 1). The first geometry, type *a*, has two floors (of equal size) in stepped form. On the first floor is the mechanical drying area, and the second floor is the area for pulped and fermented coffee; in this typology, all the coffee is mechanically dried. The dimensions of this building are: 5.50 m wide x 9.50 m long x 4 m high.

Type *b* has two separate floors: the first floor is the area for pulping, fermentation and mechanical drying of the coffee and has dimensions of 11 m long x 6 m wide x 3.5 m high. The second floor consists of a parabolic solar dryer with plastic covering, measuring 11m long x 6m wide x 2.30m high. Between the first and second floor, there is a lightweight concrete and brick slab.

Each floor of type *b* was analyzed as an independent thermal area, while type *a* was analyzed as a single thermal zone. The thermal zones were created using the plug-in Open Studio (EnergyPlus™), to generate an idf file for each type. In each thermal zone, the thermal characteristics of the materials and other details of each patterned surface are described [21].

Type *a* has 15 cm of unplastered brick cladding, with two windows on the western side of 1.15 m x 0.6 m, and a window in the roof discontinuity of 4.80 m x 0.30 m. These windows remain open all the time (unglazed). The roof is made of fiber cement tiles.

The first floor of type *b* has brick walls 0.15 m thick, without plaster, for the initial two meters. Between 2 m and 3.5 m height, the walls are of perforated brick, in the form of 10 windows. We calculated the air exchange area of the perforated brick windows and the interference with the passage of light.



a) b)

Figure 1. 3D geometries of two buildings for the wet processing of coffee - types a (a) and b (b).
Source: the authors.

To simplify the geometric model, 10 windows were made with the effective area of the perforated brick, and shading devices were inserted to simulate the interference with the light. The calculated area of the simplified windows was 1.92 m^2 for each window on the north and south walls, and 1.5 m^2 for each window on the east and west walls.

The first floor inside the building contains scales, fermentation tanks, and a coffee hydraulic classifier; these were added to the concrete at the bottom of the western wall, with a volume of 3.5 m^3 in order to account for the effect of thermal inertia of this mass. The same process was used for the type *a* building.

The second floor corresponds to the parabolic solar dryer of the coffee, which has a polyethylene plastic cover and a coffee layer with an average humidity of 33% wb and 0.03m thick on the slab. The solar dryer has two openings of 1.6 m^2 each for natural ventilation during the day. At night it is assumed that the solar dryer was closed.

In type *a* and on the first floor of type *b* there are lights, a humidity processing module to peel and sort coffee with a capacity of 2000 kg of coffee cherry per hour, and a mechanical drying machine with a capacity of 750 kg of parchment coffee per day for type *a*, and of 262.5 kg of parchment coffee per day for type *b*.

For the thermal properties of the stripped coffee we used equations 1 and 2 proposed by [22], for the specific heat (C_p, $J \cdot kg^{-1} \cdot °K^{-1}$) and density of the coffee (ρ_C, $kg.m^{-3}$) These properties are functions of the moisture content of the product on a dry basis (M_{db}, decimal dry basis).

$$C_p = 1.3556 + 5.7859 M_{db} \quad (1)$$

$$\rho_C = 365.884 + 2.7067 M_{db} \quad (2)$$

To calculate the thermal properties of composite materials and the thickness and equivalent thermal resistance of the various construction materials [23], we used the method of simplification layers of materials [24].

For calculation of the energy balance, it is necessary to calculate the heat generated within each building (heat generated by machines and human metabolism, the reaction energy generated in the fermentation process of coffee was not considered). Table 2 shows the heat values of the machines and lighting.

The heat exchanger drying machine "*a*" used coal (anthracite) as fuel, which, according to [25,26], has a consumption of 0.224 kg of coal per kg of dry parchment coffee, with a calorific value of 33440 kJ.kg-1. The heat exchanger drying machine "b" uses coffee husk as fuel which, according to [12] has a husk consumption of 0.352 kg per kg of dry parchment coffee with a calorific value of 17936 kJ.kg-1.

Table 1.
Thermal properties of materials.

Material	ρ($kg.m^3$)	K($W.m^{-1}.°K^{-1}$)	C_p($kJ.kg^{-1}.°K^{-1}$)
Mortar	2000	1.15	1.00
Concrete	2200	1.75	1.00
Brick	2200	0.95	0.84
Ceramics	1600	0.65	0.84
Polyethylene plastic	1600	0.90	0.92
Steel - Iron	920	0.04	1.59
Mortar	7800	55	0.46

Source: Adapted from NBR-15220 [25].

Table 2.
Power of coffee processing equipment.

Equipment	Power	Unit
Lighting	10	$W.m^{-2}$
Engine of processing module	1118	W
Engine of mechanical dryer *a*	1492	W
Engine of mechanical dryer *b*	746	W
Mechanical dryer heat exchanger *a*	104035	W
Mechanical dryer heat exchanger *b*	30690	W

Source: the authors.

The metabolic rate, i.e., the metabolic energy that the human body expends while performing physical activities, varies from person to person, according to the activity and working conditions performed. The value of 423 $W.person^{-1}$ was used in this study for the metabolic rate; according to [27], this value corresponds to heavy work activity and handling 50 kg sacks.

Table 3 shows the usage patterns of the coffee processing plant models "*a*" and "*b*". Mechanical drying and pulping require the same working hours for both typologies. The solar dryer (b-2f) is only opened during the day to encourage the mass exchange of water, and is closed at night to retain thermal energy, prevent condensation and prevent the ingress of moist air from outdoors.

The internal environment of the building was simulated for the month of May, which represents the first harvest of the year; the second harvest starts in October, coinciding with the bimodal behavior of rainfall in this part of Colombia [28].

A statistical analysis of variance ($p < 0.001$) and test media (Tukey, $p<0.050$) was made for the analysis of temperature and relative humidity (hourly), with four treatments: outdoor, type *a*, type *b-1f* (first floor), and type *b-2f* (second floor or solar dryer).

Finally, we made a graphical analysis of the behavior of temperature and relative humidity for the first experimental week and a comparative analysis of the energy consumption of the two coffee processing plants.

3. Results and discussion

Table 4 presents data on the volume of the buildings and their respective areas of natural ventilation. It is observed that the type *a* building has the smallest area of natural ventilation and a lower ratio of natural ventilation area to volume built.

Table 3.
Usage patterns.

Hours	Mechanical drying	Solar drying	Pulping coffee	Lighting	Occupants wet processing	Occupants solar dryer
00:00-06:00	off	off	off	off	0	0
06:00-07:00	on	off	off	on	2	0
07:00-07:30	on	on	off	off	0	1
07:30-09:00	on	on	off	off	0	0
09:00-10:00	on	on	off	off	1	0
10:00-10:30	on	on	off	off	0	1
10:30-12:00	on	on	off	off	0	0
12:00-13:00	on	on	on	off	2	0
13:00-13:30	on	on	off	off	0	1
13:30-14:00	on	on	off	off	0	0
14:00-15:00	on	on	off	off	0	0
15:00-15:30	on	on	off	off	1	1
15:30-16:00	on	on	off	off	1	0
16:00-17:30	on	on	off	off	0	0
17:30-18:00	on	on	on	on	0	0
18:00-19:00	on	off	on	on	1	1
19:00-20:00	on	off	off	on	2	0
20:00-21:00	on	off	off	on	2	0
21:00-24:00	off	off	off	off	0	0

Source: the authors.

Table 4.
Volume built and natural ventilation area.

Typology	Volume (m^3)	Vent area (m^2)	Area/volume (m^2m^{-3})
a	209	2.82	0.0135
b-1f	231	17.4	0.0753
b-2f	121	3.2	0.0264

Source: the authors.

To optimize the drying process, it not only requires energy transfer, but is important to provide optimum conditions for mass transfer, which in this context refers to having a sufficient area of natural ventilation to evacuate the vapor mass produced in the coffee drying process. According to [15] drying is defined as the process of moisture removal using simultaneous heat and mass transfer. In this context, the type *a* building has the worst conditions for mass exchange.

Table 5 shows the statistical analysis of the mean temperature, and it can be observed that warmer environments are present within type *a* and the solar dryer (type *b-2f*), between which there is no significant statistical difference. The type *a* building had higher temperature variance (indicative of scattering data), also presenting the highest maximum temperature and lowest minimum temperature of the four treatments.

Fig. 2 shows the thermal behavior during the first experimental week of building types *a* and *b*, and outdoors. It is observed that type *a* presents the warmest environment during the day and the coolest environment at night. This thermal behavior is because of the fiber cement roof, which has less thermal inertia than the concrete slab, and because this building has the smallest area of natural ventilation. Although the type *b-2f* has a plastic cover, it has the largest natural ventilation area during the day and at night is closed, retaining some heat, thus achieving higher thermal stability than type *a*.

The minimum peaks during the day are due to the door opening when employees come to work pulping or drying the coffee.

Table 5. Statistical data of mean temperature.

Group Name	N	Mean	Max	Min	Std Dev
Outdoor	744	23.08a	29.18	17.58	2.46
Type *a*	744	27.53b	41.11	18.02	6.39
Type *b - 1f*	744	24.36c	31.10	19.65	2.76
Type *b - 2f*	744	27.48db	33.13	22.79	2.16

Means followed by the same letters do not differ by the Tukey test at 0.05 probability.
Source: the authors.

Table 6.
Statistical data of mean relative humidity.

Group Name	N	Mean (%)	Max(%)	Min(%)	Std Dev
Outdoor	744	72.20 a	100.00	56.88	10.40
Type *a*	744	83.32 b	100.00	46.23	13.72
Type *b - 1f*	744	73.30 ca	98.76	56.87	8.91
Type *b - 2f*	744	75.22 d	99.68	51.82	10.25

Means followed by the same letters do not differ by the Tukey test at 0.05 probability.
Source: the authors.

Table 6 presents the statistical data of mean relative humidity content. As in the case of temperature, the type a building had the highest and most variable content of relative humidity, with a mean value of 83.32%, and a maximum value of 100%, i.e., condensation occurred within the construction. The type b showed similar behavior to the outdoors, but with less variance and without indoor saturation.

Fig. 3 shows the behavior of the relative humidity during the first experimental week, and it is observed that the internal environment of the type *a* building is saturated. The minimum peaks during the day are due to the door opening when employees come to work pulping or drying the coffee.

The saturation of the air makes the environment suffocating for the worker and thus uncomfortable to work in. This is also a dangerous environment for coffee quality, since it is conducive to the biological risk of the creation of fungi and bacteria (hot and humid environment), meaning that the grain may be re-moistened and damaged [13].

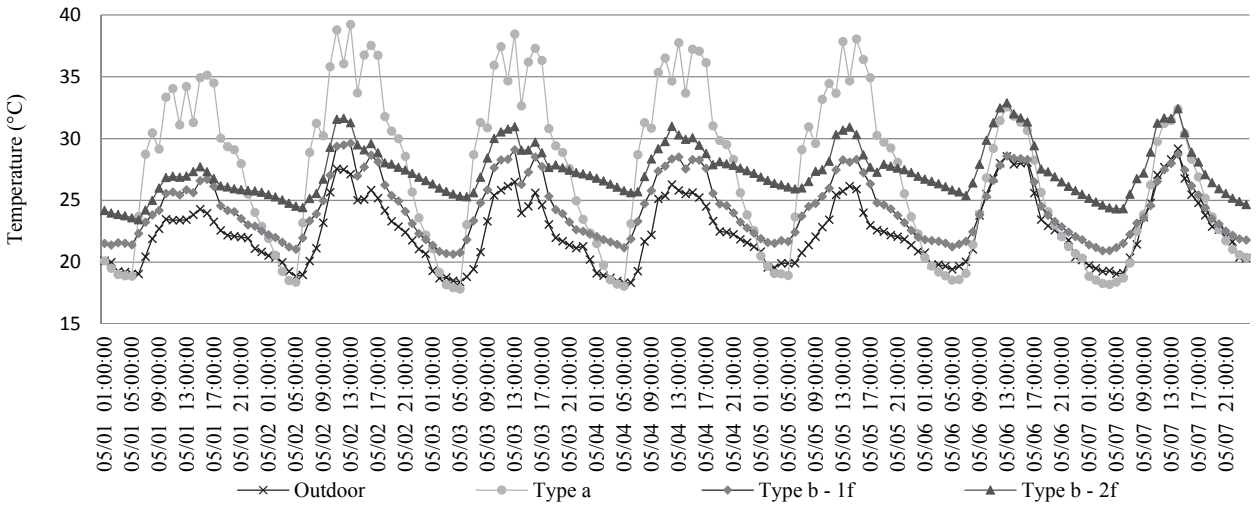


Figure 2. Thermal behavior - first week.
Source: the authors.

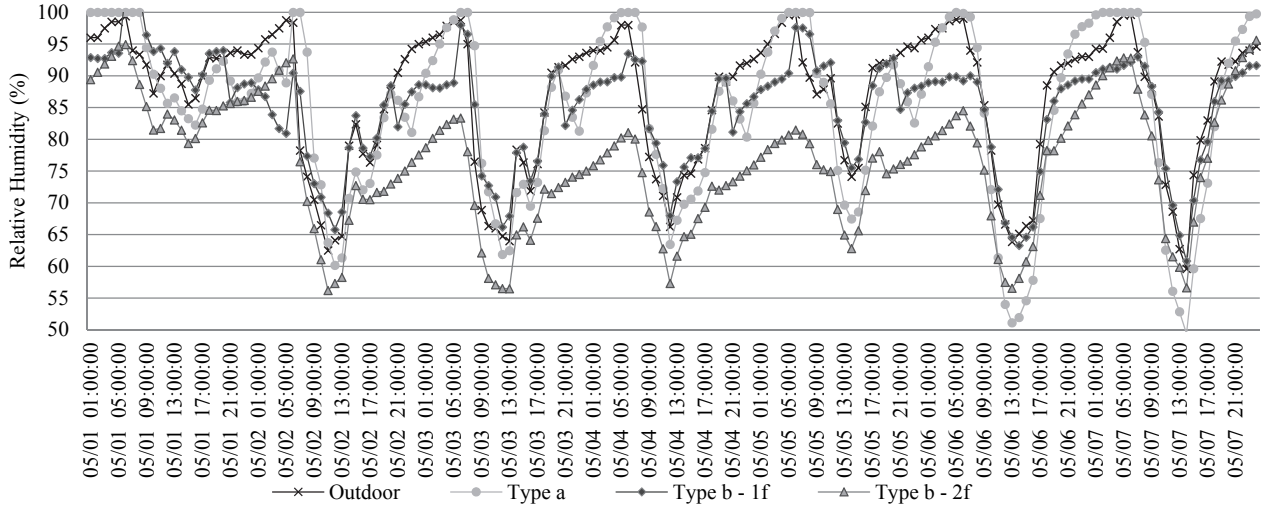


Figure 3. Relative humidity air - first week.
Source: The authors.

The type *b* building, on both the first and second floors, is at times close to saturation, but does not become fully saturated, and thus represents a more suitable environment for the quality of the coffee bean, especially in the solar dryer. But the wet and hot weather is a bioclimatic limitation for naturally ventilated facilities as in this case.

In Colombia, it is common to store dry parchment coffee during the harvest in wet processing coffee buildings for several weeks, in order to increase the volume of dry parchment coffee to transport and save money on freight costs.

According to [16] the coffee should not be stored for more than 8 days in an environment with a relative humidity above 52% and temperatures above 20°C. With this in mind, the two types of processing are not suitable for storing coffee for more than a week. The dried parchment coffee should be stored in suitable cellars.

Table 7 shows the energy consumption data of building types *a* and *b*, from which it can be observed that the highest power consumption was that of type *a*, with a value 3.3 times the consumption of type *b*.

Table 7.
Average power consumption.

Equipment	Consumption (kWh.day^{-1})	
	Type *a*	Type *b*
Lighting	2.3	3.0
Engine of processing module	3.4	3.4
Engine of mechanical dryer	22.4	11.2
Mechanical dryer heat exchanger	1560.5	460.4
Total energy consumption	1588.6	478.0

Source: the authors.

The biggest difference in power consumption is in the mechanical drying, since type *b* dries most of its coffee with the sun as the energy source. Although its mechanical dryer has 3 times less drying capacity (than type *a*), the heat exchanger uses coffee husk as an energy source, which according to [26] consumes only 84.3% of the energy consumed by the coal heat exchanger used in type *a*, making type *b* more energy-efficient in coffee processing and therefore more environmentally sustainable.

4. Conclusions

The type *a* building has the internal environment that offers the best compromise between the coffee bean quality and the highest temperatures and the highest relative indoor moisture content.

Type *b* is more energy-efficient than type *a*, as its power consumption is only 30% of the consumption of type *a*.

The weather conditions of the place where the two buildings are located (humid and hot) for both type *a* and type *b* are unsuitable for storing or keeping the coffee for periods longer than 8 days.

Acknowledgments

The authors thank the Departamento de Engenharia Agrícola - Universidade Federal de Viçosa, CAPES, FAPEMIG, CNPq, Departamento de Ingeniería Agrícola y Alimentos - Universidad Nacional de Colombia Sede Medellín, La Talega Coffee Company – Manuel Bolivar Coffee Farmer, and Federación Nacional de Cafeteros de Colombia for their valuable assistance in the development of this research.

References

[1] López, M.F., Sistemas de lógica difusa en el proceso de secado de café en lecho fluidizado, Revista Ingeniería e Investigación, 25(3), pp. 84-91, 2005.

[2] López, M.F., Secado de café en lecho fluidizado, Revista Ingeniería e Investigación, 26(1), pp. 25-29, 2006.

[3] Wintgens, J.N., Coffee: Growing, processing, sustainable production. A guidebook for growers, processors, traders and researchers., 2nd Ed. Wiley-Vch, 2009.

[4] Federación Nacional de Cafeteros de Colombia. About coffee. Much more than a drink social impact. [Online]. 2015. [date of reference February 17th of 2015]. Available at: http://www.cafedecolombia.com/particulares/en/sobre_el_cafe/mucho_mas_que_una_bebida/impacto_social/.

[5] Fonseca, J.J., Lacerda-Filho, A.F., Melo, E.C. and Teixeira, E.C., Secagem combinada de café cereja descascado, Rev. Eng. Na Agric. Viçosa, 17(3), pp. 244-258, 2009.

[6] Ribeiro, B.B., Mendonça, L.L., Dias, R.A.A., Assis, G.A. and Marques, A.C., Parâmetros qualitativos do café provenientes de diferentes processamentos na pós-colheita, Agrarian, 4(14), pp. 273-279, 2011.

[7] Carvajal, J.J. Aristizabal, I.D. y Oliveros, C.E., Evaluación de propiedades físicas y mecánicas del fruto de café (Coffea Arabica l. var. Colombia) durante su desarrollo y maduración, DYNA, 79(173), pp. 116-124, 2012.

[8] Buitrago, O.B. Ospina, M.E. y Álvarez, J.G., Implementación del secado mecánico de café en carros secadores, Revista Ingeniería e Investigación, 25, pp. 3-9, 1991.

[9] Borém, F.M., Ribeiro, D.M.A., Pereira, R.G.F., da Rosa, S.D.V.F. and de Morais, A.R., Qualidade do café submetido a diferentes temperaturas, fluxos de ar e períodos de pré-secagem, Ciênc. agrotec., Lavras., 32(5), pp.1609-1615, 2008.

[10] Ciro, H.J., Rodríguez, M.C. and Castaño, J.L.L., Secado de Café en Lecho Fijo con Intermitencia Térmica y Flujo de Aire Pulsado, Rev. Fac. Nac. Agron. Medellin, 64(2), pp. 6247-6255, 2011.

[11] Ciro, H.J., Abud, L.C. and Perez, L.R., Numerical simulation of thin layer coffee drying by control volumes, DYNA, 77(163), pp. 270-278, 2010.

[12] Oliveros, C.E. Peñuela, A. y Pabon, J., Gravimet SM: Tecnología para medir la humedad del café en el secado en silos, Cenicafé, 433, 1-8, 2013.

[13] Puerta, G.I., Riesgos para la calidad y la inocuidad del café en el secado, Cenicafé, 378, pp. 1-8, 2008.

[14] González, C., Sanz, J. y Oliveros, C.E. Control de caudal y temperatura de aire en el secado mecánico de café, Cenicafe, 61(4), pp. 281-296, 2010.

[15] El-Sebaii A.A. and Shalaby, S.M., Solar drying of agricultural products: A review, Renew. Sustain. Energy Rev., 16(1), pp. 37-43, 2012. DOI: 10.1016/j.rser.2011.07.134

[16] Vilela, E.R., Chandra, P.K. and de Oliveira, G., Efeito da temperatura e umidade relativa no branqueamento de grãos de café, Rev. Bras. Armazenamento, Especial-Café 1, pp. 31-37, 2000.

[17] Corrêa, P.C. Júnior, P. da Silva, F. and Ribeiro, D.M., Qualidade dos grãos de café (Coffea arabica L.) durante o armazenamento em condições diversas, Rev. Bras. Armazenamento Espec. Café Viçosa, 7(1), pp. 136-147, 2003.

[18] Norton, T., Grant, J., Fallon, R. and Sun, D.W., Assessing the ventilation effectiveness of naturally ventilated livestock buildings under wind dominated conditions using computational fluid dynamics, Biosyst. Eng., 103(1), pp. 78-99, 2009. DOI: 10.1016/j.biosystemseng.2009.02.007

[19] Bre, F. Fachinotti, V.D. y Bearzot, G., Simulación computacional para la mejora de la eficiencia energética en la climatización de viviendas, Mecánica Comput., 32(1), pp. 3107-3119, 2013.

[20] DoE, Energyplus engineering reference, Ref. EnergyPlus Calc., 2012.

[21] DoE, EnergyPlus, Input Output Reference: The Encyclopedic Reference to EnergyPlus Input and Output, USA Dep. Energy, 2014.

[22] Montoya, E.C., Oliveros, C.E. y Mejía, G., Optimización operacional del secador intermitente de flujos concurrentes para café pergamino. Cenicafé, 41(1), pp. 19-33, 1990.

[23] INMETRO, Qualidade e Tecnologia INMETRO, Anexo V - Portaria no. 50, de 01 de fevereiro de 2013. 2013.

[24] LabEEE., Laboratório de Eficiência Energética em Edificações, Florianópolis Universidade Fed. St. Catarina Sd Homepage Laboratório Pesqui. Disponível Em Httpwww Labeee Ufsc Br, 2015.

[25] ABNT, 15220-2. Desempenho Térmico de Edificações-Parte 2: Métodos de cálculo da transmitância térmica, da capacidade térmica, do atraso térmico e do fator de calor solar de elementos e componentes de edificações. Janeiro, 2003.

[26] Oliveros, C.E., Sanz, J.R., Ramirez, C.A. and Peñuela, A.E., Aprovechamiento eficiente de la energía en el secado mecánico del café, Cenicafé, 380, pp. 1-8, 2009.

[27] ASHRAE, Fundamentals, Am. Soc. Heat. Refrig. Air Cond. Eng. Atlanta, 111, 2001.

[28] Oviedo, N.E. y Torres, A., Atenuación hídrica y beneficios hidrológicos debido a la implementación de techos verdes ecoproductivos en zonas urbanas marginadas, Ing. Univ., 18(2), pp. 291-308, 2014. DOI: 10.11144/Javeriana.IYU18-2.hahb

R. Osorio-Hernandez, received the BSc. Eng in Agricultural Engineering in 2006 from the Universidad Nacional de Colombia - Medellin, Colombia, the MSc. degree in Agricultural Engineering in 2012 from the Universidade Federal de Viçosa, Brazil. Currently completing his doctoral studies in Agricultural Engineering at the Universidade Federal de Viçosa, Brazil. From 2006 to 2010, he worked for the National Federation Coffee Growers of Colombia, in Medellin, within the area of post-harvest and quality of coffee, at the same time, from 2007 to 2010, and 2012, he worked for the Universidad Nacional de Colombia, as ocasional professor of electrotechnics and rural constructions, and from 2012 to 2014, he worked for the National

Federation Coffee Growers of Colombia, in the area of quality assurance coffee, as an analyst in building design for coffee processing. His research areas include: bioclimatic simulation and energy of rural buildings, postharvest coffee, and energy in agriculture.
ORCID: 0000-0002-8698-7234

L.M. Guerra-Garcia, received the BSc. in Architecture in 2004 from the Universidad Nacional de Colombia - Medellin, Colombia, the MSc. degree in Agricultural Engineering in 2012 at the Universidade Federal de Viçosa, Brazil. Currently completing her doctoral studies in Agricultural Engineering, in rural constructions and ambience area, of the Universidade Federal de Viçosa, Brazil. From 2004 to 2009, she worked in different companies in design and / or construction of social housing, commercial buildings, religious and agricultural use. In 2014 she worked for the Universidad Nacional de Colombia - Medellin, as an occasional teacher in rural constructions. Her research interests include: bioclimatic simulation and energy of buildings, rural architecture and rural constructions and ambience.
ORCID: 0000-0001-9115-9057

I.F. Ferreira-Tinôco, has a BSc. in Agricultural Engineer in 1980, has a MSc degree in Agricultural Engineer in 1988, both achieved at the Federal University of Lavras, Brazil. Mrs. Tinôco has a DSc. degree in Animal Sciences in 1996, from the Federal University of Minas Gerais, Brazil. She is a full professor at the Department of Agricultural Engineering (DEA) of Federal University of Viçosa (UFV) and coordinates the UFV branch of the following scientific exchange programs: (1) CAPES/FIPSE Agreement involving the University of Illinois and University of Purdue, in the U.S.A.; (2) Umbrella Agreement amongst UFV and Iowa State University, University of Kentucky (both in the U.S.A.); (3) Scientific and Technical Agreement amongst UFV and University of Évora (Portugal), Universidad Nacional de Colombia (Colombia), Iowa State University, University of Kentucky (U.S.A.), and Erasmus agreement with the University of Florence (Italy). Professor Tinôco also coordinates the Center for Research in Animal Microenvironment and Agri-Industrial Systems Engineering (AMBIAGRO) and is the President of the DEA-UFV Internation Relations Committee. Her research areas are design of rural structures and evaporative cooling systems, thermal confort for animals, air quality and animal welfare.
ORCID: 0000-0002-4557-8071

J.A. Osorio Saraz, received the BSc. Eng in Agricultural Engineering in 1998 from the Universidad Nacional de Colombia – Medellin, Colombia, is Specialized in Environmental Legislation in 2001 from the Universidad de Medellin, Colombia, and has a MSc degree in Materials Engineering in 2006 from the Universidad Nacional de Colombia – Medellin, Colombia. In 2011 he achieved a Dr. degree in Agricultural Engineering from the Universidade Federal de Viçosa, Brazil. Since 2003 Dr. Osorio is professor at the Universidad Nacional de Colombia - Medellin, Colombia, teaching and rural constructions, bamboo constructions, computational modeling for livestock housing, air quality and animal welfare. Dr. Osorio is the Dean of the Faculty of Agricultural Sciences at Universidad Nacional de Colombia – Medellin, since 2012.
ORCID: orcid.org/0000-0002-4358-3600

I.D. Aristizábal-Torres, is BSc. Eng. in Agricultural Engineering in 1995 from Universidad Nacional de Colombia - Medellin, Colombia, Dr. in Agricultural Mechanization and Technology in 2006, of Universidad Politécnica de Valencia, Spain. Associate professor at the Universidad Nacional de Colombia – Medellin, since 2000- current, within Department of Agricultural and food engineering at the Faculty of Agricultural Sciences. Coordinator research group Agricultural Engineering (since 2012- current). Work areas; agricultural mechanization, agro-industrial processes and properties of agricultural products (fruits, grains).
ORCID: 0000-0003-1913-6832

UNIVERSIDAD NACIONAL DE COLOMBIA
SEDE MEDELLÍN
FACULTAD DE MINAS

Área Curricular de Medio Ambiente

Oferta de Posgrados

Especialización en Aprovechamiento de Recursos Hidráulicos
Especialización en Gestión Ambiental
Maestría en Ingeniería Recursos Hidráulicos
Maestría en Medio Ambiente y Desarrollo
Doctorado en Ingeniería - Recursos Hidráulicos
Doctorado Interinstitucional en Ciencias del Mar

Mayor información:

E-mail: acia_med@unal.edu.co
Teléfono: (57-4) 425 5105

UNIVERSIDAD NACIONAL DE COLOMBIA
SEDE MEDELLÍN
FACULTAD DE MINAS



DYNA
http://dyna.medellin.unal.edu.co/

A comparative study of multiobjective computational intelligence algorithms to find the solution to the RWA problem in WDM networks

Bryan Montes-Castañeda [a], Jorge Leonardo Patiño-Garzón [b] & Gustavo Adolfo Puerto-Leguizamón [c]

[a] *Facultad de Ingeniería, Universidad Distrital Francisco José de Caldas, Bogotá, Colombia, bmontesc@correo.udistrital.edu.co*
[b] *Facultad de Ingeniería, Universidad Distrital Francisco José de Caldas, Bogotá, Colombia, jlpatinog@correo.udistrital.edu.co*
[c] *Facultad de Ingeniería, Universidad Distrital Francisco José de Caldas, Bogotá, Colombia, gapuerto@udistrital.edu.co*

Received: March 16th, 2015. Received in revised form: May 27th, 2015. Accepted: June 11th, 2015.

Abstract
This paper presents a comparative study of multiobjective algorithms to solve the routing and wavelength assignment problem in optical networks. The study evaluates five computational intelligence algorithms, namely: the Firefly Algorithm, the Differential Evolutionary Algorithm, the Simulated Annealing Algorithm and two versions of the Particle Swarm Optimization algorithm. Each algorithm is assessed based on the performance provided by two different network topologies under different data traffic loads and with a different number of wavelengths available in the network. The impact of implementing wavelength conversion processes is also taken into account in this study. Simulated results show that, in general, the evaluated algorithms appropriately solve the problem in small-sized networks in which a similar performance was found. However, key differences were found when the size of the network is significant. This means that more suitable algorithms optimize the search space and the fall into local minimums is avoided.

Keywords: multiobjective algorithms; optical networks; heuristic algorithms; RWA problem.

Estudio comparativo de algoritmos de inteligencia computacional multiobjetivo para la solución del problema RWA en redes WDM

Resumen
Este artículo presenta un estudio comparativo de algoritmos multiobjetivo para la solución del problema de enrutamiento y asignación de longitudes de onda en redes ópticas. El estudio evalúa cinco algoritmos de inteligencia computacional, a saber: el algoritmo de luciérnaga, el algoritmo evolutivo diferencial, el algoritmo de enfriamiento simulado y dos versiones del algoritmo de optimización por enjambre de partículas. Cada algoritmo se evaluó teniendo en cuenta las prestaciones obtenidas sobre dos topologías de red con diferentes cargas de tráfico y diferente número de longitudes de onda disponibles. El impacto de incorporar procesos de conversión de longitud de onda también se tuvo en cuenta en este estudio. Los resultados de simulación muestran que los algoritmos estudiados resuelven apropiadamente el problema en redes con pocos nodos. Sin embargo, diferencias puntuales se encontraron en redes con un número significativo de nodos, lo cual hace más apropiados a los algoritmos que optimicen el espacio de búsqueda y eviten caer en mínimos locales.

Palabras clave: algoritmos multiobjetivo; algoritmos heurísticos; problema RWA; redes ópticas.

1. Introduction

Optical fiber has been consolidated as the preferred means of transmission in today's high-speed and long reach data networks. There have been several reasons for this situation, firstly, the increasing growth of data traffic consumption, which is expected to continue in the forthcoming years [1]. Secondly, the optical fiber systems have reached technological maturity and so they allow optical networks to be deployed, which are capable of managing huge amounts of bandwidth while providing more functions than just point-to-point transmission. These kinds of networks are known as wavelength-routing networks; their related advantages are based on some

© The author; licensee Universidad Nacional de Colombia.

switching and routing functions that are performed in the optical domain. These were previously performed in the network by electronics. A wavelength-routed network provides lightpaths to its clients i.e. optical connections carried end-to-end from a source node to a destination node using a wavelength on each intermediate link. Depending on the node capabilities, in some cases the lightpaths may be converted from one wavelength to another wavelength, allowing each optical channel to be spatially reused in different parts of the network. The key aspect of designing a wavelength-routing network is in the process that determines the wavelength or set of wavelengths that must be provided on each link that minimize the probability of network blocking from a given number of requests. This aspect is known as the wavelength-dimensioning problem or Routing and Wavelength Assignment (RWA) problem when the lightpath routing process is involved in the general solution of the problem.

In this context, two versions of the RWA problem can be considered. The first is called the *offline* RWA problem in which all the lightpaths are given at once. The solution to this form of the problem is mainly useful during network planning stages. However, when the network is operational the online RWA is a better answer, as the problem has to be solved for each lightpath at a time.

Solving this issue is not trivial. According to the computational complexity theory, the RWA problem is considered to be NP-complete; this means that it cannot be solved within a polynomial time (the required time to solve any problem by means of deterministic algorithms). For this reason, traditional methods using deterministic algorithms might not be good alternatives to solve the RWA problem. Some nondeterministic algorithms may offer acceptable results: heuristic algorithms represent an alternate solution despite their iterative behavior.

Different approaches from different perspectives have been proposed to solve the RWA problem. A first approach was based on Integer Linear Programming (ILP) in which the routing and wavelength assignment were treated separately. A description of the routing techniques using ILP is presented in [2,3] and the methods for routing and wavelength assignation are widely discussed in [4-10]. Nevertheless, for large networks with broad traffic to transport, the ILP solutions have shown some drawbacks, more precisely the potential assignation of a number of lightpaths to a given node higher than the number of wavelengths available in the network; something that brings about network blocking. Heuristic algorithms have shown to be more efficient in solving the RWA problem than the ILP approaches; in fact, one of the most used heuristics is the Tabu search [11]. Another heuristic method widely used is Genetic Algorithms (GA). Taking this into consideration, a comparative study between the GA and the Simulated Annealing (SA) concluded that GA produced better results. Different proposals have also been found in the literature to optimize the RWA problem. One of these is based on Ant Colony (ACO) algorithms, which have been used to solve both static RWA and dynamic RWA [12,13]. In this context, an ant-based agents approach that reduces the blocking probability to 0.33 and features a traffic load of 60 Erlangs and 8 wavelengths is presented in [14].

This paper focuses on evaluating the solution to the online RWA problem using multiobjective theory [15]. The reason for using such a paradigm is due to the necessity to solve more than one objective and it aims at finding routes that better adapt to the online requests and reduce the blocking probability when the network is operational. The targeted objectives defined in this work are summarized as follows:

- *Shortest number of hops*: This is the problem's main objective. The shorter the number of lightpaths the fewer the network resources used.
- *Low number of wavelength converters*: Reducing the number of wavelength converters results in both *cost-effective* networks while improving the Signal to Noise Ratio (SNR).
- *Average number of available wavelengths along the path*: This aims at assuring that the algorithm evenly uses all the nodes in the network, avoiding the overload of specific nodes.
- *Shortest physical path*: This aims at reducing the cumulative delays of the lightpath.

In order to assess the multiobjective optimization algorithms, an initial solution to the RWA problem that consists of 30 random paths, the objective of which is to produce a significant amount of potential solutions in order to generate the Pareto front, is carried out. The algorithm to set up the initial paths is based on the work described in [16], [17]. In this paper, the evaluation of five algorithms based on multiobjective computational intelligence used to solve the RWA problem is presented. The performance of the Firefly Algorithm (FA) [18], the Differential Evolutionary Algorithm (DEA) [19], the Simulated Annealing Algorithm (SAA) [20] and two modifications of the Particle Swarm Optimization (PSO) algorithm [21-24] will be evaluated by varying the number of available wavelengths in the network and the amount of nodes featuring wavelength conversion in two different network topologies.

2. Multiobjective optimization algorithms

This section presents the multiobjective computational intelligence algorithms that were considered in the comparative study, namely: FA, DEA, SAA and PSO.

2.1. Firefly Algorithm (FA)

The firefly algorithm is based on the behavior and characteristics of the fireflies. A firefly uses a luminescent flash pattern to attract other fireflies. The higher the luminescence the firefly exposes, the stronger the attraction. The algorithm modifies the initial worst solutions (the worst paths in our context) to bring them closer to the individuals that perform a better solution i.e. individuals belonging to the Pareto front. Table 1 shows the pseudocode used for modeling the FA approach.

Table 1.
Pseudocode for the Firelfly Algorithm.

```
//Generate initial population P = {X1, X2, …XN}
FOR  i = 1 to N
        Xi = Generate_Random_Route ()
End FOR
Define value for constants Alfa, Bo and Gamma
WHILE number_of_Iterations<N1 && timer<10ms
FOR i = 1 to N
        FOR j = 1 to N
                // if Xj dominates Xi move Xi to Xj
                IF Xj dominates Xi
                        rij = ||Xi − Xj|| =
√(∑_{k=1}^{d} (Xj^k − Xi^k)^2)
// Move Xi as long as such movement coincides with a valid route
WHILE   Xi^Const ~= Destination_Node
                        Xi^Const = Xi^Const +
Bo e^{−Gamma*rij^2} ( Xj^Const − Xi^Const) + alfa (rand[0,1] − 1/2

                                END WHILE
END IF
        END FOR
        END FOR
        // Update the Pareto vector and evaluates the routes that make
part of the Pareto Front
        PARETO(1 … N) = UpdatePareto()
//Evaluate which routes makes part of the Pareto front
FOR ii=1 to N
        IF PARETO = Make_part_of_the_ParetoFront
PARETOFRONTii=1
ELSE
                PARETOFrontii=0
        END IF
END FOR
END WHILE
// Selection among the routes that makes part of the Pareto front, giving
priority to the shortest route
Chosen_Route = Best_route_of_the_ParetoFront(PARETOFRONT)
//update network state matrix
State_of_the_network = update_state()
```

Source: The Authors

2.2. Differential Evolutionary Algorithm (DEA)

The genetic algorithms have been widely used to solve the RWA problem due to their relative ease in being implemented. In this work we propose a modification of the second-generation evolutionary algorithm called the Differential Evolutionary Algorithm [25]. The proposed adaptation aims at finding solutions following a multiobjective based operation in order to improve the performance of the solutions for the online version of the RWA problem. DEA is a modification of the traditional evolutionary algorithm that keeps a population of candidate solutions. Then, recombination and mutation procedures applied to these solutions produce new individuals to be chosen according to a performance function. In this work the initial population corresponds to the random lightpaths that generate the Pareto front, i.e. the performance function. The mutant population is generated by randomly taking groups of three individuals following the well-known Rand/1/bin variant [25,26]. From these recombined individuals, only those who represent valid lightpaths within the network are chosen. The generation of a new population is accomplished by comparing each recombined individual and the parent population; those individuals who dominate (parent or recombined individual) are chosen to be part of the Pareto front. This procedure guarantees that every new population generated is better than the previous one. The pseudocode defined for the DEA is shown in Table 2.

Table 2.
Pseudcode for the Differential Evolutionary Algorithm.

```
//Generate initial population P = {X1, X2, …XN}
FOR  i = 1 to N
        Xi = Generate_Random_Route()
End FOR
Define value for constants Mut, Crossing_Probability and Gamma
WHILE Number_of_Iterations<N1 && timer<10ms
        FOR i = 1 to N
// Three random routes are computed and recombination is accomplished
                X1 = choose_random_route()
X2 = choose_random_route()
X3 = choose_random_route()
Mutant=  X1 + Mut ( X2 – X3 )
// Recombination with Xi is done and it is evaluated if the route is valid
FOR J=1 to d
                IF Crossing_probability < rand(0,1)
                        Route_Productd = Xid
                ELSE
                         Ruta_Productd = Mutantd
                END IF
END FOR
// The best solutions for the next generations is chosen
                IF Xi dominates Route_Productd
                        Xi = Xi
                ELSE
                        Xi = Route_Product
                END IF
        END FOR
// Update the Pareto vector and evaluates the routes that make part of the
Pareto Front
        PARETO(1 … N) = UpdatePareto()
// Evaluate which routes makes part of the Pareto front
FOR ii=1 to N
        IF PARETO = Make_part_of_the_ParetoFront
PARETOFRONTii=1
ELSE
                PARETOFRONTii=0
        END IF
END FOR
END WHILE
// Selection among the routes that make part of the Pareto front, giving
priority to the shortest route
Chosen_Route = Best_route_of_the_ParetoFront(PARETOFRONT)
//update network state matrix
State_of_the_network = update_state()
```

Source: The Authors

2.3. Particle Swarm Optimization (PSO)

The PSO algorithm is based on the behavior of bees when they look for areas with a significant amount of pollen [21]. Each particle (bee) carries out a search and memorizes the best location they found, i.e. they remember the best solution they have discovered. In addition, each particle commits to memory the best solution provided by *k* amount of informers that they are connected to. The model is called *lbest* for low values of *k* and *gbest* for values of *k* as high as the swarm size. Both models were evaluated in this work, k=5 was used in the context of *lbest* (low number of particles with the basic amount of informers to carry out an efficient search), whereas k=30 was used to model *gbest* (each particle has as informers

Table 3.
Pseudocode for the Particle Swarm Optimization Algorithm.

```
//Generate initial population P = {X1, X2, …XN}
FOR  i = 1 to N
        Xi = Generate_Random_Route()
End FOR
Define value for constants w, c1 and c2
FOR  i = 1 to N
Vi = 0
Pi = Xi
// use method to find Gi in each neighboohood.
Gi = UpdateGi()
End FOR
WHILE Number_of_Iterations<N1 && timer<10ms
        FOR i = 1 to N
                // Move Xi and Vi
                Vi^{t+1} = wVi^t + c1 * Rand(0,1) * (Pi − Xi) +
c2 * Rand(0,1) * (Gi − Xi)
                Xi^{t+1} = Vi^{t+1} + Xi^t
                //Update Pi
IF  Xi^{t+1} dominates Pi
                        Pi = Xi^{t+1}
                END IF
        END FOR
        // method to update Gi in each neighborhood.
        Gi = UpdateGi()
END WHILE
// Selection among the routes that make part of the Pareto front and
belong to Gi, giving priority to the shortest route
Chosen_Route = Best_route (Gi)
// update network state matrix
State_of_the_network = update_state()
```

Source: The Authors

the remaining particles). Also, in the context of the proposed multiobjective algorithm, *Vi* is the velocity of the particle *Xi*, *Pi* is the best solution found by *Xi* and *Gi* is the best solution found by the swarm. The pseudocode to model the PSO algorithm is shown in Table 3.

2.1. Simulated Annealing Algorithm (SAA)

The simulated annealing algorithm is inspired by the annealing process of steel and ceramics in which the physical properties of the material is modified through heating (atoms increase its energy) and there is a subsequent controlled slow cooling processes (higher probabilities to re-crystallize in configurations featuring a lower energy than that featured at the beginning of the process). This procedure leads to a slow decrease in the probability of accepting worse solutions as it explores the solution space. For the sake of proposing an approach that follows multiobjective theory, random solutions are used instead of neighbor solutions. These solutions will be constantly compared with the initial results in order to expand the search space during the cooling process.

The SAA works on every one of the 30 initial lightpaths, i.e. each lightpath is compared with 30 different paths that are generated in the same way as the initial solution at every moment during the cooling process. If a solution generated in a given iteration is better than the initial, then the lightpath is updated, otherwise a probability is assigned for the particular lightpath to be chosen. The pseudocode for SAA is shown in Table 4.

Table 4.
Pseudocode for the Simulated Annealing Algorithm.

```
//Generate initial Population = {X1, X2, …XN}
FOR  i = 1 to N
        Xi = Generate_Random_Route()
End FOR
// Update the Pareto vector of the initial routes
PARETO(1 … N) = UpdatePareto()
Define value for constants Initial_temperature, Final_temperature, alfa y
N_iteraciones
Temp_actual= Initial_temperature
WHILE Temp_actual  > Final_Temperature && timer<10ms
        FOR i = 1 to N_iterations
//Generate random population P = {XX1, XX2, …XXN}
FOR  i = 1 to N
                XXi = Generate_Random_Route()
END FOR
// Update Pareto vector of routes XX
PARETOXX(1 … N) = UpdatePareto()
        delta = 0
         FOR  i = 1 to N
                //Evalaute which generated routes are better than
the former created
// and assings value to delta
IF Xi dominates XXi
                        delta = ||PARETO − PARETOXX||
                        delta =
sqrt(Σ_{k=1}^{d} (PARETOXXi^k − PARETOi^k)^2)
                ELSE
                        delta = −1
                END IF
                // with the value of delta a probability is assigned
to update new routes
                IF delta < 0
                        Xi = XXi
                ELSE
                        Probability = e^{−delta/Temp_actual}
                        IF  Probability > Rand(0,1)
                                Xi = XXi
END IF
                END IF
END FOR
//Update temperature
Temp_actual  =  Temp_actual * alfa
END WHILE
// Update Pareto vector and evaluates routes that make part of the Pareto front
PARETO(1 … N) = UpdatePareto()
//Evaluate which routes make part of the Pareto front
FOR ii=1 to N
        IF PARETO = Make_part_of_ParetoFront
PARETOFRONTii=1
ELSE
                PARETOFRONTii=0
        END IF
END FOR
// Selection among the routes that make part of the Pareto front, giving
priority to the shortest route
Chosen_Route = Best_route_of_the_ParetoFront(PARETOFRONT)
//update network state matrix
State_of_the_network = update_state()
```

Source: The Authors

3. Topology and traffic characteristics

In order to evaluate the proposed optimization algorithms, the conducted simulations were performed based on the topology characteristics of the National Science Foundation

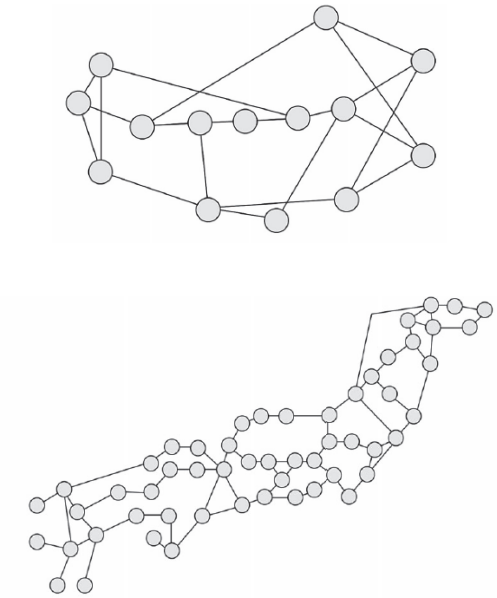


Figure 1. Network topologies used in the conducted simulations. (a) NSF Network. (b) NTT Network.
Source: The Authors

Network (NSFNet). This consists of 14 nodes and 42 optical links and the Nippon Telegraph and Telephone Network (NTT) that is comprised of 55 nodes and 144 links [27]. The significant differences in the number of nodes and links allow a more comprehensive understanding of the capabilities and performances of the evaluated algorithms. Fig. 1 shows the topology of the two networks considered in this work.

The evaluation of the algorithms is based on the normalized traffic load that is present in the networks. The normalized load in Erlangs is given by:

$$Load = \lambda_{total} T \tag{1}$$

Where T is the average time during which a given lightpath is active in the network, N is the initial number of nodes that generate traffic and λ_{total} is the average number of requests per unit of time that depends on the average number of requests from the initial node n (λ_n) as follows:

$$\lambda_{total} = \lambda_n N \tag{2}$$

In the context of this work, the online traffic is defined following a Poisson distribution such as that seen in [13,18,28,29]. Thus, the probability that k requests per unit time generated using λ_n is:

$$\mu(k, \lambda_n) = \frac{e^{\lambda_n} \lambda_n^{\ k}}{k!} \tag{3}$$

Once the number of requests per unit of time is chosen, the destination nodes are selected following a uniform distribution. Each request must state the amount of time for which it will be active. In this work an exponential distribution with a mean T of 50 seconds was used.

$$x = -\frac{1}{\lambda} \ln(1 - \mu) \tag{4}$$

Where T is defined by:

$$T = \frac{1}{\lambda} \tag{5}$$

4. Experimental results

Once the network topology and the data traffic are defined, the modeled algorithms are contrasted based on the capacity of the network to perform wavelength conversion. With this feature, a lightpath may be set up in such a way that several wavelengths are used along the path, which, in turn, provides flexibility to the network as the probability to set up such a lightpath is increased. The simulations conducted involved configurations in both network topologies featuring Full Wavelength Conversion (FWC), Limited Wavelength Conversion (LWC) and No Wavelength Conversion (NWC). FWC implies that all the nodes in the network have the capability to perform wavelength conversion while in LWC only some nodes have such capacity. NWC means that wavelength conversion processes are not performed in the network. The number of wavelengths available in the network was 8, 16 and 32 respectively, with traffic loads ranging from 0.28 to 0.83. The availability of optical channels is examined for the FWC, LWC and NWC configurations in the NSF Network. Performance results for the evaluated algorithms are shown in Fig. 2, 3, and 4 respectively. Fig. 2 shows the blocking probability as a function of the normalized load for the 8 wavelengths available on the network. Note that at high traffic loads, NWC leads to roughly 57% of blocking probability, whereas FWC derives approximately 42%. Overall, for 8 wavelength channels, the blocking probability is improved by 15% when the load is high (>0.8), 20% for medium traffic loads (0.5) and 13% for lost traffic loads (<0.3). As can be seen, the highest improvement is obtained in the medium zone, i.e. when the channel operates at half of its capacity. Low traffic loads lead to few inputs for the algorithms to find the best solution while the high traffic demand featured at high loads does not allow the algorithms to find an appropriate solution within the short time interval of each request. As far as the behavior of the evaluated algorithms is concerned, negligible differences between them were found in the FWC configuration. For NWC and LWC, the DEA and SAA respectively had a lower performance in comparison with the remaining algorithms.

When the networks incorporate 16 wavelengths, the blocking performance is improved, as can be seen in Fig. 3. Note that at high traffic load for NWC, the blocking probability is reduced to 28% (this is 29% less than the value obtained with 8 wavelengths).

It was also found that for medium to low traffic loads, the blocking probability is very low (less than 5%), while for medium to high loads the LWC and FWC configurations led to blocking probabilities that were lower than 12%. These had negligible differences between the evaluated algorithms in FWC. In this context, despite minimum differences in the obtained results, the algorithm that derived the lower performance was the SAA, while the best performance was

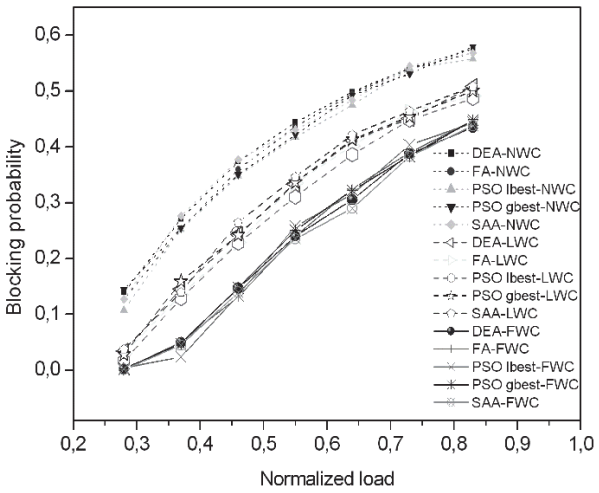


Figure 2. Blocking probability for the NSF network with 8 wavelength channels featuring NWC (dotted lines), LWC (dashed lines) and FWC (solid lines).
Source: The Authors

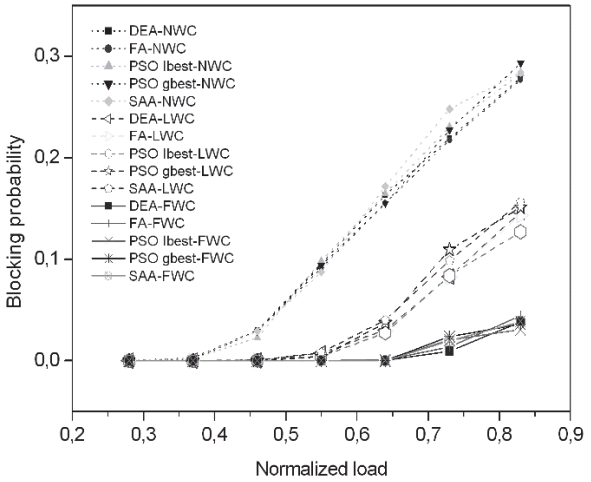


Figure 3. Blocking probability for the NSF network with 16 wavelength channels featuring NWC (dotted lines), LWC (dashed lines) and FWC (solid lines).
Source: The Authors

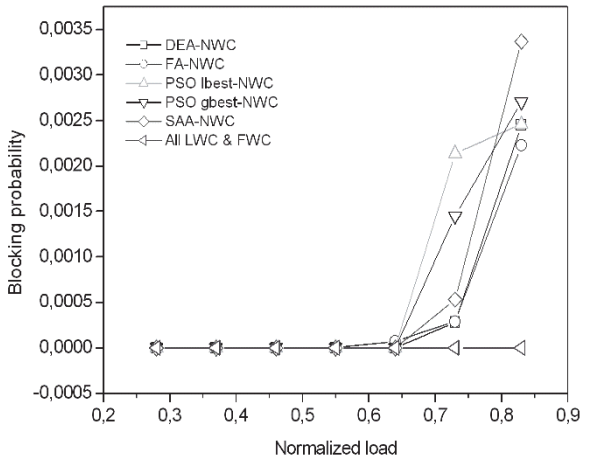


Figure 4. Blocking probability for the NSF network with 32 wavelength channels featuring NWC, LWC and FWC.
Source: The Authors

given by PSO *lbest*. Results obtained for the availability of 32 wavelengths in the network are shown in Fig. 4. While the LWC and FWC led to no blocking events, the NWC presented values as low as 0.35% at high traffic loads. Again, the SAA was the one with the lower performance.

Table 5 summarizes the blocking probability featured by the algorithms studied in low, medium and high traffic loads under NWC, LWC and FWC schemes with 8, 16 and 32 wavelengths.

As mentioned above, the algorithms were also evaluated in the topology characteristics of the NTT network. In order to give a comparative framework, the evaluation undertaken followed the same procedures and configuration that was accomplished in the NSF network. Fig. 5 shows the results for 8 wavelengths. Note that the fact of having more nodes and more links makes the NWC, LWC and FWC results more uniform, resulting in a rough average difference of 10% between the NWC and FWC configurations. Note that SAA presents a significantly different performance compared with the other algorithms, mainly for the NWC and LWC. It should be pointed out that for the LWC configuration, SAA has a similar performance to the FA in the NWC configuration. This fact demonstrates that SAA needs more network resources to offer functionalities similar to the remaining algorithms when the size of the network is significant. Also, note that blocking events appear for low traffic loads. This is caused by a low number of resources (wavelength channels) available in the moment of setting up the lightpaths. The blocking probability when the network uses 16 wavelengths is shown in Fig. 6. With this arrangement, the low performance of SAA in NWC, LWC and FWC configurations is more noticeable. Also, the blocking probability for a low traffic load falls to zero and the FWC leads to uniform behavior of the evaluated algorithms. A reduction of 17% for the blocking probability at high traffic loads (>0.8) in comparison to the NWC performance results was found.

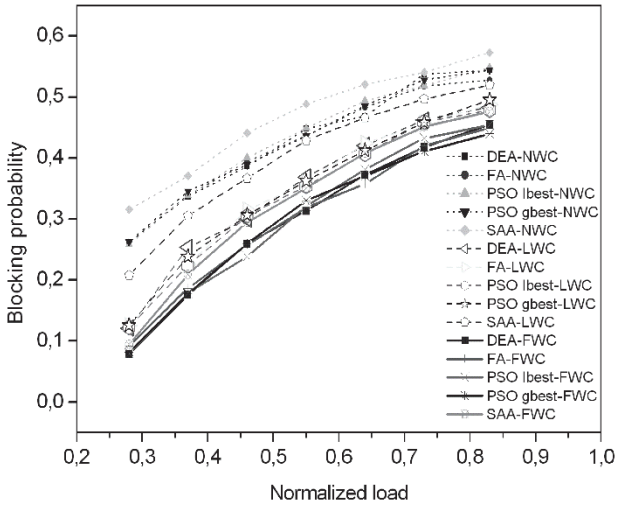


Figure 5. Blocking probability for the NTT network with 8 wavelength channels featuring NWC (dotted lines), LWC (dashed lines) and FWC (solid lines).
Source: The Authors

Table 5.
Blocking probability in the NSF network with 8, 16 and 32 wavelengths for low, medium and high traffic loads

No Wavelength Conversion															
			8 λ					16 λ					32 λ		
Load	DEA	FA	PSO lbest	PSO gbest	SAA	DEA	FA	PSO lbest	PSO gbest	SAA	DEA	FA	PSO lbest	PSO gbest	SAA
0.28	0.140	0.127	0.108	0.145	0.127	0.000	0.000	0.000	0.000	0.000	0.000	0.000	0.000	0.000	0.000
0.54	0.444	0.436	0.418	0.422	0.431	0.096	0.091	0.098	0.094	0.087	0.000	0.000	0.000	0.000	0.000
0.83	0.576	0.568	0.557	0.579	0.568	0.279	0.277	0.283	0.293	0.284	0.002	0.002	0.002	0.003	0.003

Limited Wavelength Conversion										
			8 λ					16 λ		
Load	DEA	FA	PSO lbest	PSO gbest	SAA	DEA	FA	PSO lbest	PSO gbest	SAA
0.28	0.034	0.029	0.017	0.028	0.038	0.000	0.000	0.000	0.000	0.000
0.54	0.333	0.335	0.311	0.336	0.346	0.007	0.004	0.004	0.004	0.008
0.83	0.508	0.491	0.487	0.501	0.509	0.147	0.143	0.127	0.151	0.157

Full Wavelength Conversion										
			8 λ					16 λ		
Load	DEA	FA	PSO lbest	PSO gbest	SAA	DEA	FA	PSO lbest	PSO gbest	SAA
0.28	0.002	0.001	0.004	0.002	0.002	0.192	0.000	0.000	0.000	0.000
0.54	0.240	0.240	0.252	0.250	0.235	0.384	0.000	0.000	0.000	0.000
0.83	0.435	0.447	0.444	0.448	0.438	0.577	0.038	0.034	0.031	0.036

Source: The Authors

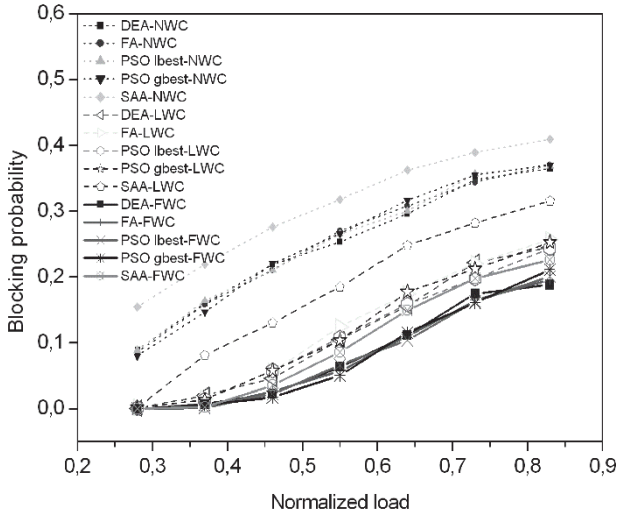


Figure 6. Blocking probability for the NTT network with 16 wavelength channels featuring NWC (dotted lines), LWC (dashed lines) and FWC (solid lines).
Source: The Authors

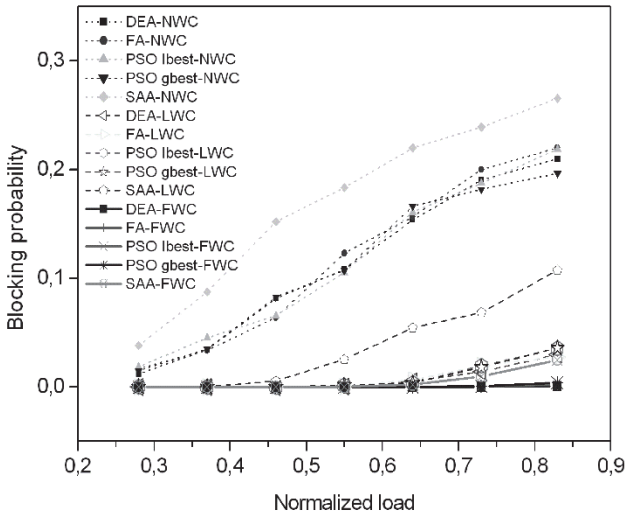


Figure 7. Blocking probability for the NTT network with 32 wavelength channels featuring NWC (dotted lines), LWC (dashed lines) and FWC (solid lines).
Source: The Authors

This comparative study, a significant number of wavelength resources in networks with a substantial number of nodes and links are shown in Fig. 7. Primarily, negligible differences were found in the LWC and FWC for all the evaluated algorithms except SAA. This showed the lowest performance, being up to an 8% less efficient for LWC configuration, PSO *lbest* is consistent and had a good performance. The blocking probability is, in general, reduced to values lower than 4% for LWC at high traffic load and nearly to zero for FWC configuration. Besides SAA, all the algorithms present no blocking from medium to low traffic loads in both LWC and FWC.

In order to make the outcomes clearer, Table 6 summarizes the blocking probability featured by the studied algorithms in low, medium and high traffic loads under NWC, LWC and FWC schemes with 8, 16 and 32 wavelengths.

5. Conclusions

Five heuristic algorithms based on multiobjective optimization were described and evaluated in this paper. The algorithms allow the problem of wavelength and routing assignment in optical networks to be solved from a dynamic behavior perspective. Each one of the evaluated algorithms offered positive results f to minimize, for example, the distance between nodes, number of hopes and availability of wavelength channels. These were taken into account simultaneously in order

Table 6.
Blocking probability in the NTT network with 8, 16 and 32 wavelengths for low, medium and high traffic loads

No Wavelength Conversion															
			8 λ					16 λ					32 λ		
Load	DEA	FA	PSO lbest	PSO gbest	SAA	DEA	FA	PSO lbest	PSO gbest	SAA	DEA	FA	PSO lbest	PSO gbest	SAA
0.28	0.262	0.262	0.258	0.263	0.316	0.090	0.086	0.087	0.080	0.155	0.012	0.017	0.018	0.015	0.038
0.54	0.448	0.437	0.446	0.436	0.488	0.254	0.270	0.265	0.266	0.318	0.108	0.123	0.105	0.107	0.183
0.83	0.544	0.527	0.530	0.544	0.573	0.365	0.370	0.369	0.371	0.409	0.210	0.220	0.219	0.197	0.266
Limited Wavelength Conversion															
			8 λ					16 λ					32 λ		
Load	DEA	FA	PSO lbest	PSO gbest	SAA	DEA	FA	PSO lbest	PSO gbest	SAA	DEA	FA	PSO lbest	PSO gbest	SAA
0.28	0.121	0.125	0.123	0.126	0.208	0.001	0.002	0.001	0.002	0.002	0.000	0.000	0.000	0.000	0.000
0.54	0.369	0.359	0.354	0.363	0.429	0.105	0.124	0.108	0.104	0.185	0.000	0.000	0.001	0.001	0.025
0.83	0.483	0.488	0.479	0.496	0.519	0.245	0.257	0.244	0.253	0.316	0.030	0.028	0.035	0.036	0.107
Full Wavelength Conversion															
			8 λ					16 λ					32 λ		
Load	DEA	FA	PSO lbest	PSO gbest	SAA	DEA	FA	PSO lbest	PSO gbest	SAA	DEA	FA	PSO lbest	PSO gbest	SAA
0.28	0.078	0.092	0.079	0.082	0.095	0.000	0.000	0.001	0.000	0.000	0.000	0.000	0.000	0.000	0.000
0.54	0.313	0.319	0.321	0.330	0.351	0.063	0.057	0.067	0.051	0.086	0.000	0.000	0.000	0.000	0.000
0.83	0.455	0.450	0.455	0.440	0.476	0.188	0.197	0.201	0.212	0.226	0.001	0.002	0.004	0.004	0.025

Source: The Authors

to provide a closer approximation to the operation of a real network. The algorithms were evaluated based on the traffic load presented in the network, thus, normalized loads from 0.28 to 0.83 were set up by changing the mean time duration of each lightpath. In general, the multiobjective nature of the evaluated algorithms appropriately solved the RWA problem, and similar results were found in all cases. However, the best results were given by the PSO lbest as each one of the six swarms used in the configuration carry out searches all over the optimization space. This fact avoided that the potential routes that could be chosen were not blocked or held back in a local minimum.

The available number of wavelengths, along with the capability of wavelength conversion, is an important feature to be implemented in optical networks. This feature allows the significant reduction of network blocking by reusing optical channels all along the end-to-end path. The wavelength conversion process allows the network control and management subsystem of the optical networks to be more adaptive to traffic changes while supporting better high data traffic loads.

Acknowledgement

The authors wish to acknowledge the Universidad Distrital Francisco José de Caldas for supporting the development of this paper.

References

[1] CISCO. Cisco Visual Networking Index: Global Mobile Data Traffic Forecast Update, 2013-2018, [Online]. White Paper, 2014, pp. 1-40. Available at: http://www.cisco.com/c/en/us/solutions/collateral/service-provider/visual-networking-index-vni/white_paper_c11-520862.pdf

[2] Guitart, F., Algoritmos de routing en redes totalmente opticas, [Online]. 2012. [Date of reference March 01th of 2015]. Available at: http://www.it.uc3m.es/muruenya/rba2/trabajos2009/Algoritmos_Routing_Redes_Totalmente_Opticas.pdf

[3] Vinolee, R. and Bhaskar, V., Performance analysis of mixed integer linear programming with wavelength division multiplexing, 2nd International Conference on Devices, Circuits and Systems (ICDCS), pp.1-6, 2014. DOI: 10.1109/ICDCSyst.2014.6926153.

[4] Le, D.D., Fen, Z. and Molnar, M., Minimizing blocking probability for the multicast routing and wavelength assignment problem in WDM networks: Exact solutions and heuristic algorithms, IEEE/OSA Journal of Optical Communications and Networking, 7(1), pp. 36-48, 2015. DOI: 10.1364/JOCN.7.000036

[5] Coiro, A., Listanti, M. and Matera, F., Energy-efficient routing and wavelength assignment in translucent optical networks, IEEE/OSA Journal of Optical Communications and Networking, 6(10), pp. 843-857, 2014. DOI: 10.1364/JOCN.6.000843

[6] Manousakis, K., Angeletou, A. and Varvarigos, E., Energy efficient RWA strategies for WDM optical networks, IEEE/OSA Journal of Optical Communications and Networking, 5(4), pp. 338-348, 2013. DOI: 10.1364/JOCN.5.000338

[7] Pavarangkoon, P. and Oki, E., A routing and wavelength assignment scheme supporting multiple light-source nodes in optical carrier-distributed networks, 4th IEEE International Conference on Network Infrastructure and Digital Content (IC-NIDC), pp. 168-173, 2014. DOI: 10.1109/ICNIDC.2014.7000287

[8] Balasis, F., Xin, W., Sugang, X. and Tanaka, Y., Dynamic physical impairment-aware routing and wavelength assignment in 10/40/100 Gbps mixed line rate optical networks, 16th International Conference on Advanced Communication Technology (ICACT), pp. 343-351, 2014. DOI: 10.1109/ICACT.2014.6779192

[9] Bandyopadhyay, A., Sarkar, A., Bhattacharya, U. and Chatterjee, M., Improved algorithms for dynamic routing and wavelength assignment in WDM all-optical mesh networks, Eleventh International Conference on Wireless and Optical Communications Networks (WOCN), pp. 1-5, 2014. DOI: 10.1109/WOCN.2014.6923050

[10] Sakthivel, P. and Sankar, P.K., Dynamic multi-path RWA algorithm for WDM based optical networks, International Conference on Electronics and Communication Systems (ICECS), pp. 1-5, 2014. DOI: 10.1109/ECS.2014.6892807

[11] Charbonneau, N. and Vokkarane, V.M., Tabu search meta-heuristic for static manycast routing and wavelength assignment over wavelength-routed optical WDM networks, IEEE International Conference on Communications (ICC), pp. 1-5, 2010. DOI: 10.1109/ICC.2010.5502241

[12] Al-Momin, M., Cosmas, J. and Amin, S., Enhanced ACO based RWA on WDM optical networks using requests accumulation and re-sorting method, Computer Science and Electronic Engineering Conference (CEEC), pp. 97-102, 2013. DOI: 10.1109/CEEC.2013.6659453

[13] Shen, J. and Cheng, X., An improved ant colony based algorithm for dynamic routing and wavelength assignment scheme in optical networks, The 2nd International Conference on Computer Application and System Modeling, [Online]. 2012. [Date of reference March 01th of 2015]. Available at: http://www.atlantis-press.com/php/download_paper.php?id=2481.

[14] Ngo, S., Jiang, X., Horiguchi, S. and Guo, M., Dynamic routing and wavelength assignment in WDM networks with ant-based agents, Springer Berlin Heidelberg, [Online]. 3207, pp 829-838, 2004. [Date of reference March 01rd of 2015]. Available at: http://link.springer.com/chapter/10.1007%2F978-3-540-30121-9_79#page-1

[15] Coello, C., Lamont, G. and Van, D., Evolutionary algorithms for solving multi-objective problems, [Online]. Springer Science+Business Media, LLC, 2007. [Date of reference March 01 rd of 2015]. Available at: http://www.inf.ufpr.br/aurora/disciplinas/topicosia2/livros/Evolutionary%20Algorithms%20For%20Solving%20Multi-Objective%20Problems%202Nd%20Edition.pdf

[16] Cui, Y., Xu, K., Wu, J. and Yu, Z., Multi-constrained routing based on simulated annealing, ICC '03, IEEE International Conference, 3, pp 1798-1722, 2003. DOI: 10.1109/ICC.2003.1203894

[17] Hai-Bo, M., Jian-Ning, Y. and Lin-Zhong, L., Shortest path algorithm for road network with traffic restriction, 2009 2nd International Conference, Power Electronics and Intelligent Transportation System (PEITS), 2, pp 381-384, 2009. DOI: 10.1109/PEITS.2009.5406759

[18] Rubio-Largo, A., Vega-Rodriguez, M.A., Gomez-Pulido, J.A. and Sanchez-Pérez, J.M., A Comparative study on multiobjective swarm intelligence for the routing and wavelength assignment problem, IEEE Transactions, Systems, Man, and Cybernetics, Part C: Applications and Reviews, 42(6), pp 1644-1655, 2012. DOI: 10.1109/TSMCC.2012.2212704

[19] Rubio-Largo, A., Vega-Rodríguez, M.A., Gómez-Pulido, J.A. and Sánchez-Pérez, J.M., A differential evolution with Pareto tournaments for solving the routing and wavelength assignment problem in WDM networks, IEEE Congress on Evolutionary Computation (CEC), pp. 1-8, 2010. DOI: 10.1109/CEC.2010.5586272

[20] Hernández, J., Hernández, S. y Flores, I., Algoritmo recocido simulado para el problema de la programación del tamaño del lote económico bajo el enfoque de ciclo básico, Revista chilena de ingeniería, [Online], 19(3), pp 473-485, 2011. [Date of reference March 01rd of 2015]. Available at: http://www.scielo.cl/pdf/ingeniare/v19n3/art15.pdf

[21] Bhushan, B. and Pillai, S., Particle swarm optimization and firefly algorithm: Performance analysis, 2013 IEEE 3rd International, Advance Computing Conference (IACC), pp 746-751, 2013. DOI: 10.1109/IAdCC.2013.6514320

[22] Amaya, I., Gómez, L. and Correa, R., Discrete particle swarm optimization in the numerical solution of a system of linear diophantine equations, DYNA, 81(185), pp. 139-144, 2014. DOI: 10.15446/dyna.v81n185.37244

[23] Bermeo, L.A., Caicedo, E., Clementi, L. andVega, J., Estimation of the particle size distribution of colloids from multiangle dynamic light scattering measurements with particle swarm optimization, Ingeniería e Investigación, 35(1), pp. 49-54. DOI: 10.15446/ing.investig.v35n1.45213

[24] Muñoz, M., López, J. y Caicedo, E., Inteligencia de enjambres: Sociedades para la solución de problemas (Una revisión), Ingeniería e Investigación, 28(2), pp. 119-130.

[25] Li, Y.-L., Zhan, Z.-H., Gong, Y.-J., Chen, W.-N., Zhang, J. and Li, Y., Differential evolution with an evolution path: A DEEP evolutionary algorithm, IEEE Transactions on Cybernetics, PP(99), pp. 1-13, 2014. DOI: 10.1109/TCYB.2014.2360752

[26] Villate, A., Rincon, D.E. y Melgarejo, M.A., Sintonización de sistemas difusos utilizando evolución diferencial. IEEE XVIII International Congress of Electronic and Systems Engineering. Lima: 2011, pp. 1-8.

[27] Rubio, A. and Vega, M., Optical network topologies and data sets for the RWA Problem, [Online]. [Date of reference March 01rd of 2015]. Available at: http://mstar.unex.es/mstar_documentos/RWA/RWA-Instances.html

[28] Bisbal, D., Dynamic routing and wavelength assignment in optical networks by means of genetic algorithms, Photonic Network Communications, [Online]. 7(1), pp.43-58, 2004. [Date of reference March 01rd of 2015]. Available at: http://link.springer.com/article/10.1023/A%3A1027401202391#page-1

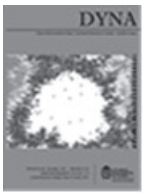
[29] Hassan, A., Phillips, C. and Zhiyuan L., Swarm intelligence based Dynamic Routing and Wavelength Assignment for wavelength constrained all-optical networks, ISCIT 2009, 9th International Symposium, pp 987-992, 2009. DOI: 10.1109/ISCIT.2009.5340993

B. Montes-Castañeda, received his BSc. in Electronic Engineering with an emphasis on Computational Intelligence, Telematics and Digital Signal Processing in 2015, from the Universidad Distrital Francisco José de Caldas, Colombia. In 2013 he joined the Microwave, Electromagnetism and Radiation Laboratory (LIMER) where he developed his undergraduate thesis. His research interests include telecommunications, optical networks and heuristic optimization.
ORCID: 0000-0003-4333-445X.

J.L. Patiño-Garzón, received his BSc. in Electronic Engineering with emphasis on Computational Intelligence, Telecommunications and Digital Signal Processing in 2015, from the Universidad Distrital Francisco José de Caldas, Colombia. In 2013 he joined the Microwave, Electromagnetism and Radiation Laboratory (LIMER) where he developed his undergraduate thesis. His research interests include heuristic algorithms, low and high level programming languages and optical networks.
ORCID: 0000-0002-8615-9447,

G.A. Puerto-Leguizamón, received his BSc. in Telecommunications Engineering in 2002. He joined the Institute of Telecommunications and Multimedia Applications at the Universitat Politècnica de València in Spain, where he completed his advanced research studies in 2005 and his PhD. in 2008. As a postdoctoral researcher he worked as co-leader of the task on the new generation of physical technologies for optical networks under the framework of the European funded project ALPHA (Architectures for Flexible Photonics Home and Access Networks). Since 2012 he has been an assistant professor at the Universidad Distrital Francisco José de Caldas in Bogotá, Colombia, where he works in the Microwave, Electromagnetism and Radiation Laboratory (LIMER). He has published more than 40 papers in journals and international conferences and he is a reviewer of the IEEE Journal on Lightwave Technologies and IEEE Photonic Technology Letters. His research interests include optical networking and radio over fiber systems.
ORCID: 0000-0002-6420-9693.

UNIVERSIDAD NACIONAL DE COLOMBIA
SEDE MEDELLÍN
FACULTAD DE MINAS



DYNA
http://dyna.medellin.unal.edu.co/

Determination of the Rayleigh damping coefficients of steel bristles and clusters of bristles of gutter brushes

Libardo V. Vanegas-Useche [a], Magd M. Abdel-Wahab [b] & Graham A. Parker [c]

[a] *Facultad de Ingeniería Mecánica, Universidad Tecnológica de Pereira, Pereira, Colombia. lvanegas@utp.edu.co*
[b] *Faculty of Engineering and Architecture, Ghent University, Gent, Belgium. magd.abdelwahab@ugent.be*
[c] *Faculty of Engineering and Physical Sciences, University of Surrey, Surrey, UK. G.parker@surrey.ac.uk*

Received: March 16th, 2015. Received in revised form: June 4th, 2015. Accepted: June 9th, 2015.

Abstract
Street sweeping is an important service that is usually performed by lorry-type vehicles that have a gutter brush, which is comprised of clusters of steel bristles that sweep the debris found in the road gutter. Effective operation of this brush is important, as most of the debris on roads is located in the gutter. In order to model a gutter brush by means of finite element dynamic analyses, it is necessary to determine appropriate values of the Rayleigh damping coefficients of both individual bristles and clusters of bristles. This paper presents the methodology and results of experimental tests that have been conducted to determine these coefficients. The results obtained are useful when studying the performance of conventional and oscillatory street sweeper gutter brushes by means of dynamic finite element modeling.

Keywords: Rayleigh damping coefficients; bristles of gutter brushes; street sweeping.

Determinación de los coeficientes de amortiguamiento de Rayleigh de cerdas y grupos de cerdas de acero de cepillos laterales

Resumen
El barrido de calles es un servicio importante que usualmente se realiza por medio de vehículos tipo camión que tienen un cepillo lateral conformado por grupos de cerdas de acero para barrer la basura que se encuentra en la cuneta de la carretera. Es importante que este cepillo funcione efectivamente, ya que la mayoría de la basura depositada en las carreteras se encuentra en la cuneta. Con el fin de modelar un cepillo lateral mediante análisis dinámico de elementos finitos, es necesario determinar valores apropiados de los coeficientes de amortiguación de Rayleigh tanto de cerdas individuales como de grupos de cerdas. En este trabajo se presenta la metodología y los resultados de pruebas experimentales que se han realizado para determinar estos coeficientes. Los resultados obtenidos son útiles para estudiar el desempeño de los cepillos laterales de las barredoras de calles mediante el modelado dinámico de elementos finitos.

Palabras clave: coeficientes de amortiguamiento de Rayleigh; cerdas de cepillos laterales; barrido de calles.

1. Introduction

Street sweeping is, in many cases, performed by lorry-type sweepers. There are different types of sweepers [1]; however, they usually comprise a suction unit, a wide broom, and a gutter brush (Fig. 1). There are two basic types of gutter brushes. These differ in the orientation of the bristle rectangular cross section; there are cutting brushes, whose bristles mainly deflect in a brush radial direction, and flicking brushes, whose bristles mainly deflect in a tangential direction. According to Peel *et al.* [2] and Michielen and Parker [3], around 80% of the debris found on roadways is in the gutter. Therefore, it is of interest to study the behavior and effectiveness of gutter brushes as they have to clear the large amount of debris that is located in the gutter and transfer it to the path of the suction unit or the wide broom.

Despite the relevance of studying gutter brush performance, there are a very limited amount of scientific papers written on the dynamics and performance of gutter brushes; in fact, it seems that research on this topic has only been performed by the Mechatronic Systems and Robotics Research Group at the University of Surrey [4-14]. This research has involved the development and

© The author; licensee Universidad Nacional de Colombia.



Figure 1. A street sweeper gutter brush.
Source: The authors'.

application of mathematical, numerical, and finite element models of gutter brushes, as well as experimental sweeping tests carried out in a gantry test rig. Reviews on this topic have been presented in previous works.

This work is concerned with the development of finite element models of conventional, as well as oscillatory gutter brushes [10]. In order to obtain useful results from the models, suitable values of several parameters have to be obtained, some of them experimentally. This article presents the procedure and results of a number of experimental tests that have been performed to obtain the Rayleigh damping coefficients of both a single bristle and of a cluster of bristles. These parameters, among others, are necessary for the dynamic Finite Element (FE) modeling of gutter brushes. Other parameters that have to be determined are the friction coefficient for bristle-bristle contact [9] and the normal contact stiffness for bristle-surface interaction.

The paper is organized as follows, some basic concepts of damping are introduced in Section 2. The procedure, results, and discussion of experiments for a single bristle are presented in Section 3. Then, the methodology, results, and discussion of experiments for a cluster of bristles are provided in Section 4. Finally, the conclusions are presented in Section 5.

2. Background on damping

Damping is the mechanism by which a system's kinetic energy is gradually converted into heat or sound [15]. Due to the reduction in energy, damping has the effect of gradually reducing the system's response, e.g., the displacement amplitude. Thus, in many cases, damping is a beneficial phenomenon without which the system may remain in a state of chaos [16]. There are different sources of damping, e.g., friction between two dry sliding surfaces, fluid resistance, and internal molecular friction. The internal molecular friction is the one that is of interest in this work. It is difficult to determine all the causes of damping in a practical system; therefore, damping is modeled in different ways: viscous damping, Coulomb or dry friction damping, and material or hysteretic damping.

The simplest form of damping is viscous damping, as it leads to linear equations of motion [15]. Because of this, many researchers use viscous damping (e.g., [17-24]). In this type of damping, the damping force is proportional to the velocity of the body. Rayleigh or proportional damping is a form of viscous damping that is proportional to a linear combination of the mass and stiffness dependent damping. Although the physical meaning of this type of damping is not clear, it is a very convenient way to represent damping in numerical models [25]. According to proportional damping:

$$\mathbf{C} = \alpha_D \mathbf{M} + \beta_D \mathbf{K} \tag{1}$$

where **C** is the damping matrix, **M** is the mass matrix, **K** is the stiffness matrix. α_D the mass proportional damping coefficient, and β_D the stiffness proportional damping coefficient are assumed to be constant.

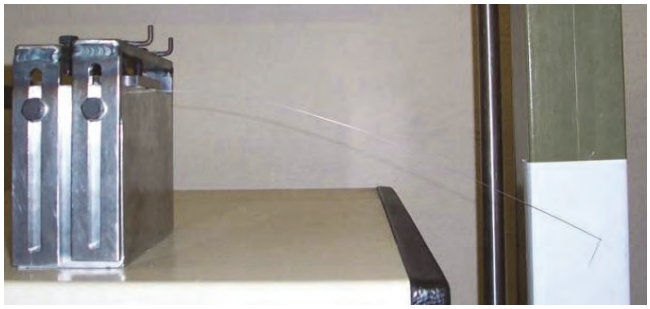
3. Rayleigh damping coefficients of a bristle

3.1. Overview

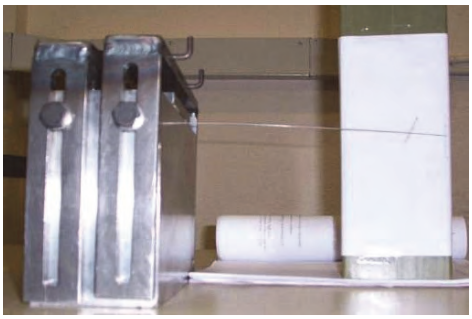
The bristles of a gutter brush, either conventional or oscillatory, deform and vibrate as they make contact, slide, and leave the road surface. During this process, the internal molecular friction in the bristles produces damping. This damping may be taken into account when modeling a gutter brush by means of FE analyses. In the ANSYS® software, this damping can be modeled as Rayleigh damping. In order to determine appropriate damping coefficients, the α_D and β_D of a bristle were subject to experimental tests. The procedure and results of these experiments are presented in Sections 3.2 and 3.3, respectively.

3.2. Methodology

The coefficients α_D and β_D are obtained experimentally, by analyzing the vibration amplitudes of steel bristles in cantilever's rate of decay. The experimental setup is shown in Fig. 2. The bristles were supported rigidly in a heavy clamping device, so that the damping associated with the clamping system is negligible. Free vibrations were produced by displacing the tip of the bristle downwards and then releasing it. It is assumed that the vibration of the bristle is dominated by the first mode. Therefore, the beam of infinite Degrees of Freedom (DOFs) is assumed to be equivalent to a single DOF system with viscous damping, and it is characterized by the motion of the free end. A measuring scale at the bristle tip enabled the decay of the vibration amplitudes to be tracked. The time Δt required for the deflection amplitude, y_{max}, to reduce from a certain value, y_i, to another value, y_f, (Fig. 3) was recorded three times, and the average was taken. This procedure was repeated for several pairs of values (y_i, y_f) and for three bristles (A, B, and C) of different lengths. The lengths and the first natural frequencies of the bristles are $l_{bA} = 481$ mm, $l_{bB} = 240$ mm, $l_{bC} = 95.8$ mm, $f_A = 1.89$ Hz, $f_B = 7.22$ Hz, and $f_C = 45.3$ Hz. The cross section of the bristles is 0.5×2 mm^2. The constants α_D and β_D are determined from a best fit of the experimental data. It should be noted that it was not possible to use signal analysis. This is because the wire that transmits the signal from the accelerometer generates a much higher level of damping than the bristles themselves.



(a) l_{bA} = 481 mm



(b) l_{bB} = 240 mm

Figure 2. Experimental setup for the determination of the damping coefficients of a bristle.
Source: The authors'.

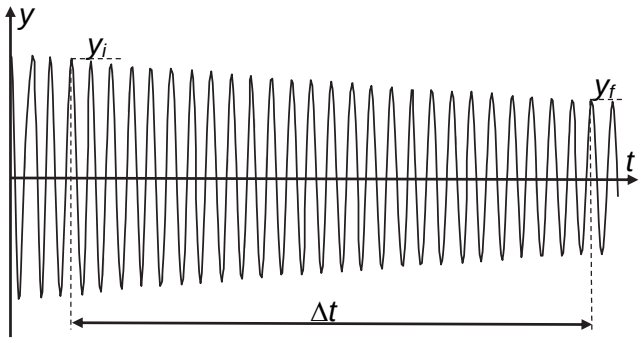


Figure 3. Bristle tip deflection against time. Variables measured in the experiments: y_i, y_f, and Δt.
Source: The authors'.

The number of cycles during the time Δt is estimated by:

$$N_c = f\ \Delta t \tag{2}$$

Where f is the frequency of bristle vibration. The frequency of bristle A was obtained experimentally, as it is small, and, therefore, corresponds to f_{Ad}, which is called the frequency of damped vibration. f_{Ad} = 1.891 Hz ± 0.009 Hz (standard error). The value of f_B and f_C given previously are the theoretical first natural frequencies. However, as [15]:

$$f_d = \sqrt{1-\zeta_D{}^2}\, f_i \tag{3}$$

and, it is anticipated that the damping ratio of the bristles, ζ_D, is small, and that the first natural frequency, f_i (i = 1), and the frequency of damped vibration, f_d, do not differ greatly. Hence, the natural frequencies may be used to estimate N_c (from eq. 2).

The logarithmic decrement, δ, which represents the rate at which the amplitude of free damped vibration decreases, may be expressed as [15]:

$$\delta = \frac{1}{N_c} \ln\left(\frac{y_i}{y_f}\right) \tag{4}$$

The damping ratio is defined as the ratio of the damping constant (or viscous damping coefficient), c, to the critical damping constant, c_c:

$$\zeta_D = \frac{c}{c_c} \tag{5}$$

and it is given by [15]:

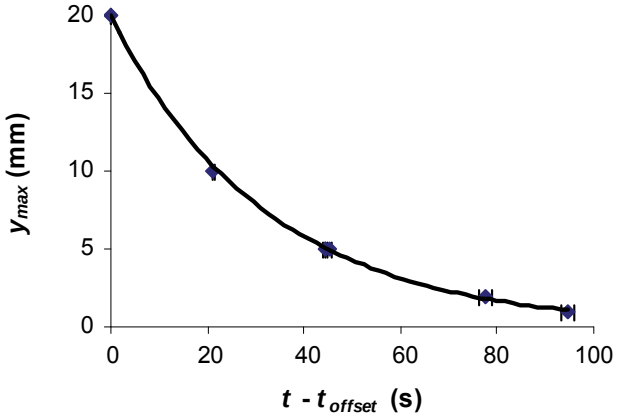
$$\zeta_D = \frac{\delta}{\sqrt{(2\pi)^2 + \delta^2}} \quad \text{or, when } \delta <\approx 1,\ \ \zeta_D \approx \frac{\delta}{2\pi} \tag{6}$$

Thus, from the measured values y_i, y_f, and Δt and the experimental or theoretical frequency, f, the damping ratio for each bristle can be calculated by using eq. (2), (4), (6).

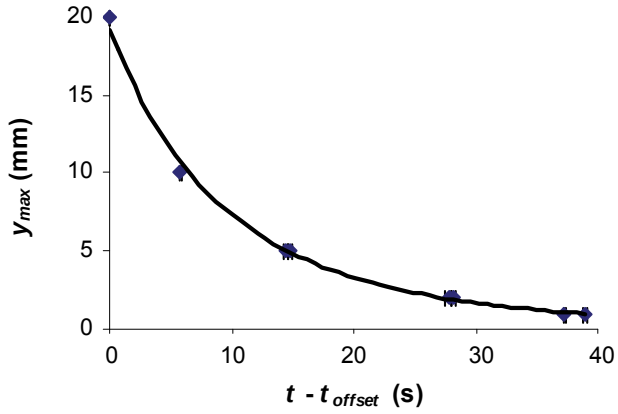
For each bristle, the experimental data were used to obtain a y_{max} - t curve. The experimental points (t, y_{max}) were fitted to a curve. Logarithmic, power, and exponential functions were considered. In general, the power equation provided the best fit, and it was selected, even though all the lines produced very similar results.

3.3. Results and discussion

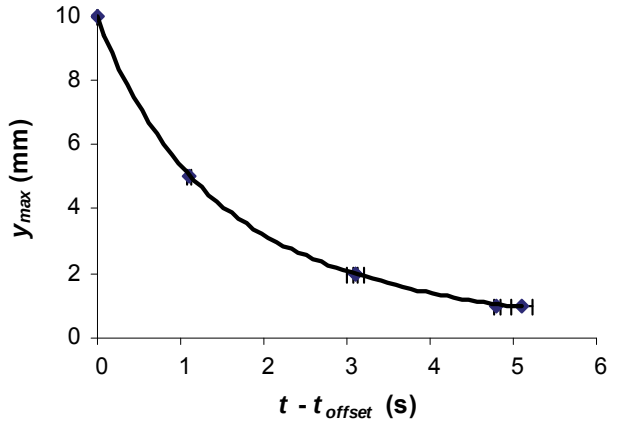
Fig. 4 presents the experimental data and the trend lines for the three bristles. The time t_{offset} is an offset obtained from the regression analyses. The logarithmic decrement, δ, and damping ratio, ζ_D, are, in theory, constant for a free viscously damped vibrating system. However, the experimental results suggest that they depend on the deflection amplitude, y_{max}. The trends in Fig. 4 indicate that δ and ζ_D are larger for higher values of y_{max}. However, for the longest bristle (l_{bA} = 481 mm, for which f_A = 1.89 Hz), δ and ζ_D are almost constant for the different amplitudes. The dependence of δ and ζ_D on the vibration amplitude may be partly due to the fact that the air resistance to which the bristles are subjected is proportional to the velocity raised to a power greater than 1. Higher deflections produce higher bristle speeds and, consequently, much higher aerodynamic forces. For each bristle, damping ratios for four values of y_{max} were calculated using the respective trend lines. These values are shown in the ζ_D - f curve in Fig. 5.



(a) l_{bA} = 481 mm



(b) l_{bB} = 240 mm



(c) l_{bC} = 95.8 mm

Figure 4. Decay of the deflection amplitude of a bristle. Error bars indicate standard errors.
Source: The authors'.

The damping ratio is related to the Rayleigh damping coefficients by [26]:

$$\zeta_{Di} = \frac{\alpha_{Di}}{2\omega_i} + \frac{\beta_{Di}\omega_i}{2} \tag{7}$$

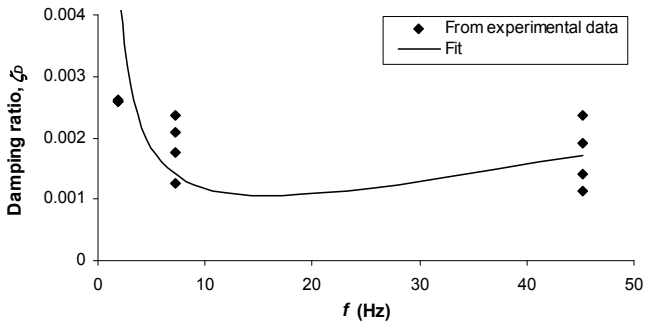


Figure 5. Damping ratio against frequency.
Source: The authors'.

where ω_i is a given angular frequency, and ζ_{Di}, α_{Di}, and β_{Di} are the values for that frequency.

In the ANSYS® software, only a value of each α_{Di} and β_{Di} can be input in a load step, regardless of the frequencies that are active in that load step. In this work, it is assumed that $\alpha_D = \alpha_{Di}$ and $\beta_D = \beta_{Di}$ are constant coefficients, i.e., they are independent of the frequency. This is not entirely satisfactory, but provided that the frequencies excited lie in a small range, acceptable results may be obtained.

Eq. (7) can be rearranged as follows:

$$2\omega_i \zeta_D = \alpha_D + \beta_D \omega_i^2 \tag{8}$$

$$e^{2\omega_i\zeta_D} = e^{\alpha_D + \beta_D\omega_i^2} \quad \text{or} \quad e^{2\omega_i\zeta_D} = e^{\alpha_D} e^{\beta_D\omega_i^2} \tag{9}$$

Eq. (9) is of the form:

$$y_D = A_1 e^{A_2 x_D}, \quad \text{where} \quad y_D = e^{2\omega_i\zeta_D}$$
$$A_1 = e^{\alpha_D},\ A_2 = \beta_D,\ \text{and}\ x_D = \omega_i^2 \tag{10}$$

Hence, the data points in Fig. 5 can be fitted to an exponential equation. The regression analysis yields the values $\alpha_D = 0.104\ s^{-1} \approx 0.1\ s^{-1}$ and $\beta_D = 1.07\times10^{-5}$ s ≈ 0.01 ms. The ζ_D - f curve that corresponds to these values is also shown in Fig. 5. Lastly, these values were used in a FE analysis for the free damped vibration of a cantilever beam as a means of verification. For l_b = 95.8 mm, y_i = 10 mm, and y_f = 5 mm, the damping ratios from eq. (7) and from the logarithmic decrement obtained from the FE results are 0.001599 and 0.001595, respectively (0.3% difference). This result seems satisfactory.

The mass component of Rayleigh damping ($\alpha_D\mathbf{M}$) damps rigid body motion [26], i.e., it is associated with the damping of inertial movements. Thus, it may be used when a structure is affected by fluid drag [27]. The bristles of a gutter brush, as well as those used in the experiments, are subjected to aerodynamic effects. Then, some mass proportional damping is expected. The bristles are also subjected to internal friction, which may be associated with stiffness proportional damping ($\beta_D\mathbf{K}$). The results of the experiments suggest that α_D and β_D can be assumed to be constant for a certain range of frequencies and equal to $\alpha_D \approx 0.1\ s^{-1}$ and $\beta_D \approx 0.01$ ms. Although this is a simplification,

hereinafter, the mass component of damping will be associated with aerodynamic effects and the stiffness component with internal friction (of a bristle or a cluster).

4. Rayleigh damping coefficients of a cluster

4.1. Overview

The modeling of an oscillatory gutter brush may be very complex. The bristles operate in non-steady state conditions, making contact with the surface, debris, neighboring bristles, and, possibly, bristles in other clusters. Thus, the bristles in a cluster should be modeled by several beams. However, the computational resources needed are huge. Consequently, it is of interest to model a cluster with a single beam. In order to do this, it is necessary to determine equivalent values of the damping coefficients of a cluster. These will take the internal friction into consideration in each bristle, as well as the energy dissipation caused by the interaction among bristles.

Experiments were carried out to estimate suitable values of α_D and β_D, to model a cluster of bristles as a single beam in a FE model. This was necessary because the computational resources needed to model the whole cluster, or even a small number of bristles per cluster, exceed the available resources by far. For example, a single 1 s simulation of a cluster of only five bristles may take about 20 days on an available PC.

4.2. Methodology

Several clusters of a number of brushes with steel bristles of different lengths were used. The cross section of the bristles is 0.5×2 mm^2. An initial deformation was applied to every cluster by deflecting the bristle tips an arbitrary amount. The cluster was then released so that the bristles withstood free damped vibrations. Due to the characteristics of the initial deformation and the interaction among bristles, the first mode is the dominant. Hence, the cluster is treated as a single DOF system characterized by the deflection of the tips. As the cluster oscillates, adjacent bristles slide on one another, generating friction forces, and they may also collide. Due to these interactions, the vibration amplitudes of a cluster's rate of decay tends to be much greater than its counterpart of a single bristle. However, a small fraction of the bristles are apart from other bristles, and the rate of decay of their vibrations is similar to that found in Section 3.

Due to the rapid decay, the procedure for a single bristle cannot be used reliably in this case. For this reason, a digital camera that captures 25 frames per second (fps) was used to capture the images of the vibrating cluster. In this way, the variation of the deflections with time could be obtained. As the bristles of a cluster are not tightly arranged but are dispersed at different angles, every bristle tip has its own decay of vibration amplitudes. A suitable bristle or part of the cluster was selected for each cluster to track its tip deflections. A measuring scale was used for this purpose. Also, a stopwatch was used to verify the number of fps recorded by the camera. Then, the recorded images were analyzed frame by frame, and approximate values of deflection were written down for a number of time points. Fig. 6 shows one of the setups that was prepared for one of the experiments.



(a) Equilibrium position



(b) Vibrating cluster

Figure 6. Experimental setup for the determination of α_D and β_D of a cluster. Source: The authors'.

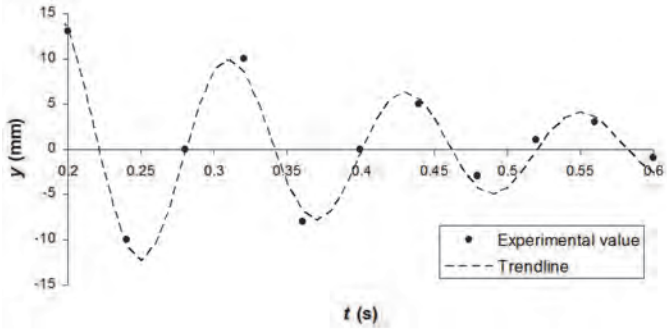


Figure 7. Deflection of a cluster ($l_b \approx 230$ mm) against time. Source: The authors'.

Fig. 7 shows, as an example, the experimental points obtained from the images of one of the experiments. The "best" fit of the experimental points, which is obtained as described in the following paragraphs, is also shown.

To obtain the logarithmic decrement, δ, the damping ratio, ζ_D, and the damping coefficients, α_D and β_D, it is necessary to fit the experimental points to a curve. The displacement of a single DOF underdamped system with viscous damper is given by [15]:

$$y(t) = \left\{ \begin{array}{l} y_0 \cos\left(2\pi\sqrt{1-\zeta_D{}^2}\, f_i t\right) + \\ \dfrac{\dot{y}_0 + \zeta_D 2\pi f_i y_0}{2\pi\sqrt{1-\zeta_D{}^2}\, f_i} \sin\left(2\pi\sqrt{1-\zeta_D{}^2}\, f_i t\right) \end{array} \right\} e^{-\zeta_D 2\pi f_i t} \quad (11)$$

where y_0 and $\dot{y}_0$ are the initial displacement and velocity ($t = 0$), respectively. It is anticipated that for all the results obtained ζ_D is very small ($\zeta_D < 0.09$). Taking this into account and by using the approximation in eq. (6), eq. (11) may be simplified:

$$y(t) = y_i \sin\left(2\pi\ f_i (t - t_i)\right) e^{-\delta\ f\ t} \quad (12)$$

where y_i and t_i are constant values that are obtained from the experimental data. This equation has four parameters: y_i, t_i, f_i, and δ. To obtain a suitable value of the logarithmic decrement, δ, it is necessary to test a large number of combinations of these four variables. After the required number of iterations, a value of δ is selected, and the damping ratio is calculated (eq. 6). The selected value of δ is the one that produces the minimum sum of the squared differences between the curve and the experimental points.

The procedure described in the preceding paragraph is suitable when the frequency is sufficiently small, e.g., when $l_b >\approx 220$ mm. This is because the camera is capable of recording enough frames to obtain a curve like the one shown in Fig. 7. For clusters of shorter bristles, the frequency of oscillation is higher, and the determination of the $y - t$ curve becomes more difficult, unless a camera with better control of the shutter speed and more fps were available. In view of this, for most of the brushes tested, a less accurate method of obtaining δ was used. The frames recorded were used to estimate the extreme positions of a certain part of the cluster. These deflection values were written down. As an example, Fig. 8 presents the experimental points for clusters of a cutting brush; the brush was tested three times. Eq. (13) was used to fit the experimental data by visual observation:

$$y_{max}(t) = y_i e^{-\delta\ f\ t} \quad (13)$$

The trend lines obtained with eq. (13) constitute upper bounds of the experimental points. Fig. 8 also shows the curves that seem to best fit the experimental data.

4.3. Results and discussion

For each of the five brushes tested, values of δ and ζ_D were obtained from at least three experiments. Table 1 presents the summary of the results. It should be noted that, to the authors' best knowledge, this is the first investigation into the damping of gutter brushes' steel bristles. It is of interest to note that the estimated frequencies of the brush in row 1 are higher than the theoretical natural frequency. This may be partly due to the propagation of impacts among bristles. They are initially dispersed, but the initial deformation forces the bristles to become close to each other. When the bristles are released, they tend to withstand vibrations with different amplitudes, generating wave propagations.

The points (f, ζ_D) are shown in Fig. 9. Similar to the case of the single-bristle experiments, it is assumed that the damping coefficients, α_D and β_D, are independent of the frequency. Hence, the data points are also fitted through an exponential equation (eq. 10). The regression analysis yields the values of the damping coefficients: $\alpha_D = 3.01\ s^{-1} \approx 3\ s^{-1}$ and $\beta_D = 0.396$ ms ≈ 0.4 ms. The ζ_D - f curve shown in Fig. 9 corresponds to these values. Taking into account the results and discussion in Section 3.3, for the case of single bristles, these results seem appropriate. These values are not accurate, as can be seen from the high dispersion of the experimental data. The dispersion is very high partly because, contrary to what has been assumed, the damping coefficients are not independent of the frequency. Damping coefficients also vary from one particular brush to another, from one particular cluster to another, and during brush life. Regarding the brush life, new brushes tend to have clusters with closely packed

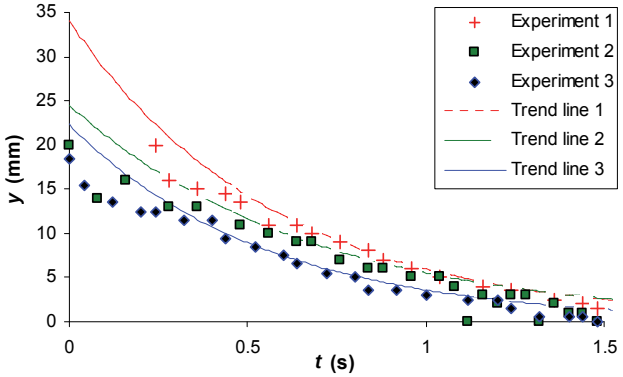


Figure 8. Experimental data and trend lines for the deflection of a cluster of a cutting brush ($l_b \approx 163$ mm).

Source: The authors'.

Table 1.
Results of the damping experiments with clusters of five brushes.

Brush type [a]	l_b (mm)	f_i [b] (Hz)	f (Hz) [c]			δ [d]			ζ_D [e] (eq. 6)
F128	230	7.9	8.3	8.2	8.4	0.45	0.44	0.53	0.075
F128	190	11.5	11.7	11.6	11.5	0.14	0.14	0.13	0.021
Cutting	165	15.3	15	15.5	15.6	0.12	0.10	0.12	0.018
F128	146	19.5	20.1	19.8	20.1	0.23	0.25	0.25	0.038
Cutting	133	23.5	23.5	23.5	23.5	0.23	0.26	0.30	0.042

[a] The brush named F128 has a flicking action
[b] Theoretical value of the first natural frequency of the bristles of the clusters
[c] Estimated from the "best" fit of the experimental data (brush in row 1) or assumed value based on f_i
[d] Estimated from the "best" fit of the experimental data
[e] Average of those calculated with the various logarithmic decrements
Source: The authors'.

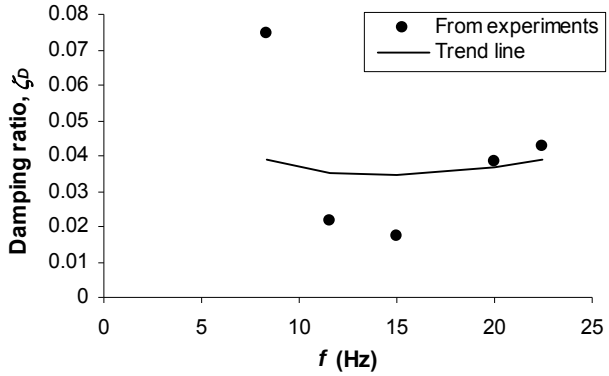


Figure 9. Damping ratio of a cluster of a gutter brush against frequency. Source: The authors'.

bristles, whereas used brushes tend to have clusters with bristles presenting high dispersion. All of this affects the way the vibrations are damped.

To conclude, due to its inherent complexities, damping is a physical phenomenon that has been dealt with by using equations that may not represent the reality. The determination of an accurate, unsophisticated model for the damping of the clusters of gutter brushes seems to be a very difficult task, if not impossible. Damping in a cluster is produced by aerodynamic forces, internal friction in the bristles, and the interaction among bristles. In addition, the characteristics of the clusters vary from one to another, e.g., each cluster may have a different number of bristles, and they are arranged in a different fashion, depending on the clamping conditions and the use to which they have been subjected. Due to the complexities involved in modeling damping, the damping coefficients determined from the experimental tests (both for clusters and for bristles) are rough estimates. However, the use of these values in FE analyses may provide a practical insight into the quantitative performance of oscillatory and non-oscillatory gutter brushes. Lastly, from an analysis of Newton's second law and eq. (1), it is concluded that the damping coefficients of a cluster can be used directly in a FE model of a gutter brush when the cluster is modeled with a single beam.

5. Conclusions

This article presented the methodology and results of experimental tests, as well as the accompanying FE analyses, to determine the Rayleigh damping coefficients of the bristles and clusters of gutter brushes used for road sweeping. In numerical analyses, damping is usually modeled as Rayleigh damping, in which the damping matrix is a linear combination of mass and stiffness dependent damping. The damping constants were obtained by subjecting bristles and clusters in cantilever to free damped vibrations. These were treated as single degree of freedom systems characterized by the motion of the tips. The results suggest that the damping coefficients of a bristle may be taken as $\alpha_D = 0.1$ s^{-1} and $\beta_D = 0.01$ ms, and those of a cluster as $\alpha_D = 3$ s^{-1} and $\beta_D = 0.4$ ms. Due to the complexities of the vibration of clusters of gutter brushes, the determined values of α_D and β_D are only estimates of the mean values; they may greatly vary depending on the arrangement of each particular cluster and the frequency of oscillation, among others aspects.

Acknowledgements

The authors acknowledge the support of the Universidad Tecnológica de Pereira (Colombia), the University of Surrey (UK), and the Programme Alβan, European Union Programme of High Level Scholarships for Latin America, identification number *(E03D04976CO)*.

References

[1] Vanegas-Useche, L.V. y Parker, G.A., Barrido de calles y vehículos barredores. Scientia et Technica, [Online] 26, pp. 85-90, 2004. Available at: http://www.redalyc. org/articulo.oa?id=84911640015

[2] Peel, G., Michielen, M. and Parker, G., Some aspects of road sweeping vehicle automation, Proc. 2001 IEEE/ASME Int. Conf. Adv. Intelligent Mechatronics, I-II, pp. 337-342, 2001. DOI: 10.1109/AIM. 2001.936477

[3] Michielen, M. and Parker, G.A., Detecting debris using forward looking sensors mounted on road sweeping vehicles, Proc. of Mechatronics 2000, paper number: M2000-094, 2000.

[4] Vanegas-Useche, L.V., Abdel-Wahab, M.M. and Parker, G.A., Effectiveness of gutter brushes in removing street sweeping waste. Waste Management, 30(2), pp. 174-184, 2010. DOI: 10.1016/j. wasman.2009.09.036

[5] Vanegas-Useche, L.V., Abdel-Wahab, M.M. and Parker, G.A., Modeling of an oscillatory freely-rotating cutting brush for street sweeping. DYNA, [Online] 78(170), pp. 204-213, 2011. Available at: http://www.revistas.unal.edu.co/index.php/dyna/article/view/29504/48793

[6] Vanegas-Useche, L.V., Abdel-Wahab, M.M. and Parker, G.A., Dynamics of a freely rotating cutting brush subjected to variable speed. International Journal of Mechanical Sciences, 50(4), pp. 804-816, 2008. DOI: 10.1016/j.ijmecsci.2007.11.004

[7] Vanegas-Useche, L.V., Abdel-Wahab, M.M. and Parker, G.A., Dynamics of an unconstrained oscillatory flicking brush for road sweeping. Journal of Sound and Vibration, 307(3-5), pp. 778-801, 2007. DOI: org/10.1016/j.jsv.2007.07.010

[8] Peel, G.A general theory for channel brush design for street sweeping, PhD. Thesis, University of Surrey, Guilford, UK, [Online]. 2002. Available at: http://epubs.surrey. ac.uk/792198/

[9] Vanegas-Useche, L.V., Abdel-Wahab, M.M. and Parker, G.A., Determination of friction coefficients, brush contact arcs, and brush penetrations for gutter brush-road interaction through FEM. Acta Mechanica, 221(1-2), pp. 119-132, 2011. DOI: 10.1007/s00707-011-0490-2

[10] Vanegas-Useche, L.V., Abdel-Wahab, M.M. and Parker, G.A., Dynamic finite element model of oscillatory brushes. Finite Elements in Analysis and Design, 47, pp. 771-783, 2011. DOI: org/10.1016/j. finel.2011.02.008

[11] Wang, C., Brush modelling and control techniques for automatic debris removal during road sweeping, PhD. Thesis, University of Surrey, Guilford, UK, [Online] 2005. Available at: http://ethos.bl.uk/OrderDetails.do?uin=uk.bl.ethos. 421309

[12] Abdel-Wahab, M., Parker, G. and Wang, C., Modelling rotary sweeping brushes and analyzing brush characteristic using finite element method. Finite Elements Ana. Des., 43(6-7), pp. 521-532, 2007. DOI: 10. 1016/j.finel.2006.12.003

[13] Abdel-Wahab, M.M., Wang, C., Vanegas-Useche, L.V. and Parker, G., Experimental determination of optimum gutter brush parameters and road sweeping criteria for different types of waste. Waste Management, 31, pp. 1109-1120, 2011. DOI: 10.1016/j.wasman.2010.12.014

[14] Vanegas-Useche, L.V., Abdel-Wahab, M.M. and Parker, G., Effectiveness of oscillatory gutter brushes in removing street

sweeping waste. Waste Management, In Press, Corrected Proof, 2015. DOI: 10.1016/j.wasman.2015.05.014

[15] Rao, S.S., Mechanical Vibrations, fourth edition. New Jersey: Pearson Education, Inc., 2004.

[16] Puthanpurayil, A.M., Dhakal, R.P. and Carr, A.J., Modelling of in-structure damping: a review of the state-of-the-art, Proc. Ninth Pacific Conf. Earthquake Engineering, [Online]. Paper Number 091, 2011. Available at: http://db.nzsee.org.nz/ 2011/091.pdf

[17] Ríos-Gutiérrez, M. and Silva-Navarro, G., Control activo de vibraciones en estructuras tipo edificio usando actuadores piezoeléctricos y retroalimentación positiva de la aceleración. DYNA, [Online]. 80(179), pp. 116-125, 2013. Available at: http://www.revistas.unal.edu.co/index.php/dyna/article/view/30733/html_33

[18] Carrillo, J., González, G. and Llano, L., Evaluation of mass-rig systems for shaking table experiments. DYNA, [Online]. 79(176), pp. 159-167, 2012. Available at: http://www.revistas.unal.edu.co/index.php/dyna/article/view/28509/43559

[19] Gómez-Pizano, D., Comparison of frequency response and neural network techniques for system identification of an actively controlled structure. DYNA, [Online]. 78 (170), pp. 79-89, 2011. Available at: http://www.revistas.unal.edu.co/index.php/dyna/article/view/29390/48778

[20] Valencia de Oro, A.L., Ramírez, J.M., Gómez, D. y Thomson, P., Aplicación interactiva para la educación en dinámica estructural. DYNA, [Online]. 78(165), pp. 72-83, 2011. Available at: http://www.revistas.unal.edu.co/index.php/dyna/article/view/25641/39139

[21] Hurtado-Cortés, L. y Villarreal-López, L., Control robusto de un sistema mecánico simple mediante una herramienta gráfica. DYNA, [Online]. 77(162), pp. 214-223, 2010. Available at: http://www.revistas.unal.edu.co/index.php/dyna/article/view/15852/36191

[22] Gómez, D., Marulanda, J. and Thomson, P., Sistemas de control para la protección de estructuras civiles sometidas a cargas dinámicas. DYNA, [Online]. 75 (155), pp. 77-89, 2008. Available at: http://www.redalyc.org/articulo.oa?id=49611953009

[23] Carrillo, J., Alcocer, S.M. and Gonzalez, G., Experimental assessment of damping factors in concrete housing walls. Ingeniería e Investigación, [Online]. 32(3), pp. 42-46, 2012. Available at: http://www.revistas.unal.edu.co/index.php/ingeinv/article/view/35939/37232

[24] Bedoya-Ruiz, D., Ortiz, G.A. and Álvarez, D.A., Behavior of precast ferrocement thin walls under cyclic loading: an experimental and analytical study. Ingeniería e Investigación, [Online]. 34(1), pp. 29-35, 2013. Available at: http://www.revistas.unal.edu.co/index.php/ingeinv/article/view/40420/44456

[25] Semblat, J.F., Rheological interpretation of Rayleigh damping. Journal of Sound and Vibration, [Online]. 206(5), pp. 741-744, 1997. Available at: http://arxiv.org/ftp/ arxiv/papers/0901/0901.3717.pdf

[26] SAS IP, Inc. Release 10.0 Documentation for ANSYS, 2005.

[27] NAFEMS, Earthquake rocking [Online]. 2004 [date of reference 2006]. Available at: http://www.nafems.org/publications/downloads/benchmark/october_2004/earthquake_rocking.pdf.

L.V. Vanegas-Useche, is a professor in the Mechanical Engineering Department at the Universidad Tecnológica de Pereira, Colombia. He received his BSc. in Mechanical Engineering in 1994, from the Universidad Tecnológica de Pereira, Pereira, Colombia, his MSc. in Advanced Manufacturing Technology and Systems Management in 1999, from the University of Manchester, Manchester, UK, and his PhD. in Mechanical Engineering in 2008, from the University of Surrey, Guildford, UK. He has published more than 50 scientific papers. His research interests include: Fracture Mechanics, Fatigue, Mechanical Design, and Finite Element Modeling of Machine Elements and Structures.
ORCID: 0000-0002-5891-8696

M.M. Abdel-Wahab, is a professor of applied mechanics at the Department of Mechanical Construction and Production at Ghent University, Belgium. He received his BSc. in1988, in Civil Engineering and his MSc. in1991, the Structural Mechanics, all of them from Cairo University. He completed his PhD. in Fracture Mechanics in 1995 at KU Leuven, Belgium. He was awarded his Dr. from the University of Surrey in 2008. He has published more than 200 scientific papers on Solid Mechanics and Dynamics of Structures. His research interests include Finite Element Analysis, Fracture Mechanics, Damage Mechanics, Fatigue of Materials, Durability, and Dynamics and Vibration.
ORCID: 0000-0002-3610-865X

G.A. Parker, is emeritus professor of Mechanical Engineering at the Department of Mechanical and Physical Sciences at the University of Surrey. He holds the following qualifications and titles: BSc., PhD., FIMechE, MEM.ASME, CEng, and Eur.Ing. He is also member of the EPSRC Mechanical Engineering College. His research interests include Virtual and Augmented Reality, Control and Systems Integration, Machine Vision, Brushing Technology, and Fluid Control Systems.
ORCID: 0000-0003-0677-6451

UNIVERSIDAD NACIONAL DE COLOMBIA
SEDE MEDELLÍN
FACULTAD DE MINAS

Área Curricular de Ingeniería Mecánica

Oferta de Posgrados

Maestría en Ingeniería - Ingeniería Mecánica

Mayor información:

E-mail: acmecanica_med@unal.edu.co
Teléfono: (57-4) 4259262

UNIVERSIDAD NACIONAL DE COLOMBIA
SEDE MEDELLÍN
FACULTAD DE MINAS



DYNA
http://dyna.medellin.unal.edu.co/

Estimate of induced stress during filling and discharge of metallic silos for cement storage

Wilmer Bayona-Carvajal [a] & Jairo Useche-Vivero [b]

[a] *Universidad Tecnológica de Bolívar, Cartagena, Colombia.*
[b] *Facultad de Ingeniería, Universidad Tecnológica de Bolívar, Cartagena, Colombia. usecheijk@yahoo.com*

Received: March 19th, 2015. Received in revised form: June 1rd, 2015. Accepted: June 16th, 2015.

Abstract
The present article show the structural analysis realized to metallic silo for storage cement through of the parametric model development in the finite element software ASNYS APDL, the fill and discharge pressures applied on the silo wall is determined with the Eurocode normative EN 1991-4.The model is development with type shell elements allowing that the structure silo fits to the cylindrical and conical geometric of the silo. It explains each of the phases having the development of the model and is made a detailed analysis of the results delivered by the software; different models are evaluated changing the sheet thickness for select the most appropriate. Also the results are analyzed when be changing the tilting the hopper and is reviewed the behavior of the silo when is analyzed with its structure.

Keywords: Cement silos, structural analysis, finite element, parametric model, Eurocode EN 1991-4, ANSYS APDL, type shell elements

Estimación de esfuerzos inducidos durante el llenado y vaciado de silos metálicos para almacenamiento de cemento

Resumen
El presente artículo describe el análisis estructural realizado a un silo metálico que almacena cemento por medio de un modelo paramétrico desarrollado en el software de elementos finitos ANSYS APDL, las presiones de llenado y vaciado que el material ejerce sobre las paredes del silo se determinan basados en la normativa del Eurocódigo EN 1991-4. El modelo se realiza con elementos tipos cáscara permitiendo que su estructura se ajuste que la geometría cilíndrica y cónica del silo. Se explica cada una de las fases involucradas en el desarrollo del modelo y se hace un análisis detallado de los resultados arrojados por el software, se evalúan diferentes modelos variando los espesores de lámina con el fin de seleccionar el más adecuado. También se analizan los resultados obtenidos cuando la tolva del silo cambia su ángulo de inclinación y se revisa el comportamiento que tiene el silo cuando es analizado en conjunto con su estructura soporte.

Palabras clave: Silo de cemento, análisis estructural, elementos finitos, modelo paramétrico, Eurocódigo EN 1991-4, ANSYS APDL, elementos tipo cáscara.

1. Introducción

El silo de cemento es el encargado de almacenar el material listo para empacar y para entregar al consumidor, también sirve de reserva para amortiguar los cambios de producción y paradas de mantenimiento, asegurando que todo el tiempo se puede entregar cemento al cliente.

Para realizar el diseño de un silo metálico de manera eficiente, se deben tener en cuenta diferentes variables que afectan el comportamiento del material dentro del esto es fundamental para determinar las cargas que determinaran el comportamiento estructural del silo. Inicialmente hay que tener claro que el material almacenado en el silo juega un papel crítico en el resultado del análisis estructural que se va a realizar, diferentes características físicas del material influyen sobre la resultante de las fuerzas que generan la presión sobre las caras del silo [5,6].

Actualmente existen diferentes normativas con las que se pueden determinar las presiones en las paredes de los silos, sin embargo el Eurocódigo EN 1991-4 ha ganado relevancia debido a su gran aplicación a nivel mundial y con resultados satisfactorios en los diseños realizados [1]. Con base en esta metodología se desarrolla una hoja de cálculo que involucra

© The author; licensee Universidad Nacional de Colombia.

cada una de las variables que están presentes en el cálculo de las presiones y desarrolladas con las normativas estándar estudiadas. Para determinar algunas variables del silo es necesario que se defina la geometría del mismo, por lo que la hoja de cálculo debe tener como entradas las dimensiones del silo además de las características del material a almacenar. Con estos valores y con la información contenida en ella, se obtienen como resultado del cálculo las presiones tanto de llenado como de vaciado en la parte cilíndrica y en la tolva del silo.

Con las presiones determinadas se puede realizar un análisis estructural con elementos finitos, no sin antes buscar el elemento más adecuado para representar la geometría metálica del silo. Los elementos tipos cáscara o más comúnmente conocidos como elementos tipo shell se describen en el desarrollo de este trabajo ya que son estos los elementos con los que se modela el silo [4,7].

El análisis estructural del silo se realiza por medio de un modelo computacional con elementos finitos para determinar el espesor de pared adecuado que debe tener el silo. Inicialmente se generan dos códigos con comandos de ANSYS-APDL en dos pestañas de la hoja de cálculo; uno para el modelo con presiones de llenado y el otro con presiones de vaciado. Cada código tiene como entrada todas las variables del silo que permiten parametrizar cualquier tipo de geometría que se desee. Adicionalmente en este archivo se pueden modificar las características de la malla al seleccionar el tipo, la cantidad y el tamaño de elementos que esta debe tener. El código esta enlazado con los resultados de las presiones de llenado y vaciado obtenidas con la misma hoja de cálculo. Mediante dos vínculos que tiene la hoja de cálculo se pueden generar los archivos de texto en formato txt, que contienen el código que se introduce en la línea de comandos de ANSYS-APDL, allí se corre el programa y son evaluados y analizados los resultados para obtener el diseño adecuado del silo [2,12].

También se analiza la variación de los esfuerzos que tiene el silo cuando cambia el ángulo de inclinación de la su tolva y finalmente se evalúa el comportamiento del silo cuando es analizado en conjunto con una estructura que lo soporte [13].

Con un modelo que pueda variar las propiedades del material almacenado y ajustar las características geométricas del silo, el diseñador estará en la capacidad de evaluar la mejor condición para determinado escenario, teniendo como resultado un diseño adecuado que se ajuste a las necesidades específicas de un caso.

2. Metodología

Para determinar los esfuerzos y deformaciones en el silo se trabaja una primera parte determinando las presiones de llenado y vaciado tanto en el cilindro como en la tolva y una segunda parte que es el modelo con elementos finitos de ANSYS-APDL.

2.1. Calculo de presiones con base en la normativa del Eurocodigo EN 1991-4

2.1.1. Especificaciones geométricas del silo

La Fig. 1 muestra la geometría del silo con las variables que afectan la curva de presiones y las cuales son entradas para el cálculo del silo [3,10].

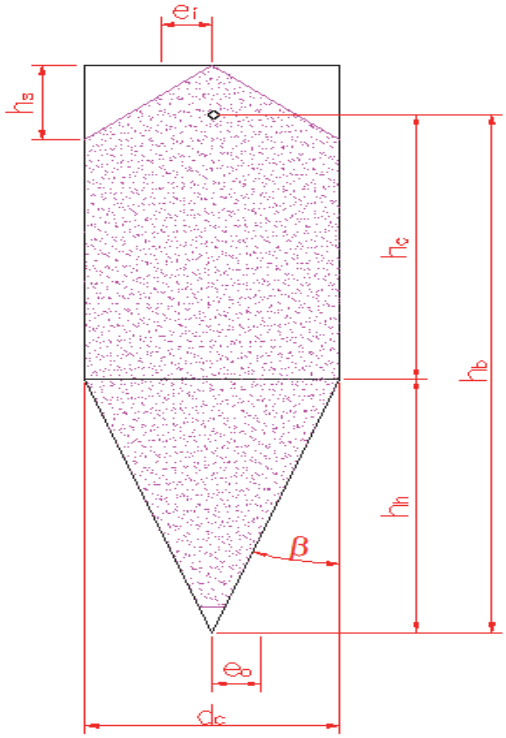


Figura 1. Geometría del silo a diseñar.
Fuente: Propia

Donde;
d_c = Diámetro del silo
h_b = Es la altura que tiene el material
h_c = Altura del material en la parte cilíndrica
h_h = Es la altura que tiene la tolva
h_s= Altura del cono superior que forma el material
β = Ángulo entre la pared de la tolva
e_i = Excentricidad del llenado
e_o = Excentricidad del vaciado

2.1.2. Propiedades de los materiales granulares en el cálculo del silo

Las propiedades del material que está contenido en el silo y que son necesarias para el calcular de las presiones sobre las paredes de este son:

→ Peso específico del material γ
→ Angulo de reposo con la horizontal ϕ_p
→ Angulo efectivo de fricción interno ϕ_t
→ Relación de presión lateral λ
→ Angulo de fricción con la pared ϕ_ω

Las propiedades para diferentes materiales granulares se pueden encontrar en el Eurocodigo EN 1991-4 en el anexo E [3,10].

2.1.3. Cálculo de presiones de llenado en el cilindro y tolva

En la Fig. 3 se aprecia la trayectoria z y las presiones que se ven involucradas en el llenado del silo en su parte cilíndrica [3,10].

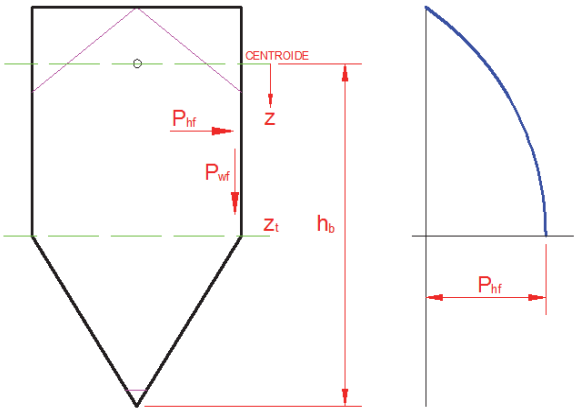


Figura 3. Presión de llenado sobre el cilindro
Fuente: Propia

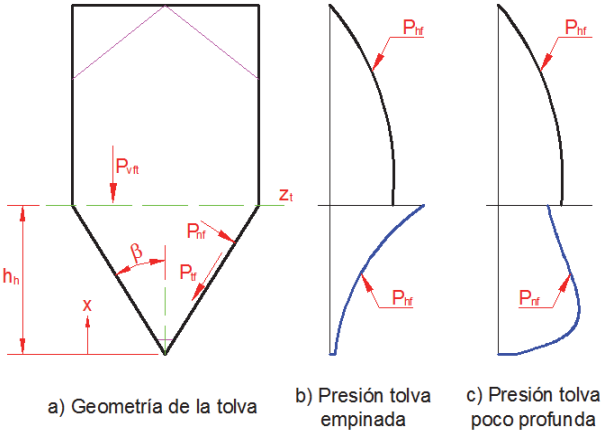


Figura 4. Presiones de llenado sobre la tolva
Fuente: Propia

Dónde:

$$P_{hf} = P_{ho}\,(1 - e^{-\frac{z}{z_o}})$$
$$P_{wf} = P_{vo}\,(1 - e^{-\frac{z}{z_o}})$$
$$P_{ho} = \frac{\gamma}{\mu}\frac{A}{U} = \frac{\gamma}{\mu}\frac{r}{2}$$
$$P_{vo} = \frac{\gamma}{\lambda\,\mu}\frac{A}{U} = \frac{\gamma}{\lambda\,\mu}\frac{r}{2}$$
$$z_o = \frac{1}{\lambda\,\mu}\frac{A}{U} = \frac{1}{\lambda\,\mu}\frac{r}{2}$$

Con:
A = Área de la sección transversal del silo.
U = Perímetro de las sección circular del silo.
r = Radio del silo.
z = Recorrido de la presión en el cilindro
γ = Peso específico del material.
λ = Relación de presión lateral.
μ = Coeficiente de fricción con la pared.

El cálculo de la presión libre se realiza mediante el aumento de la presión horizontal mediante la siguiente relación:

$$P_{pf} = 0.2\,\beta\,P_{hf}$$
$$\beta = 1 + \frac{e_i}{2r}$$

Dónde:
e_i = excentricidad del llenado.
La presión total horizontal es la suma de las dos presiones horizontales determinadas anteriormente, la presión fija y la presión libre.

$$P'_{hf} = P_{hf} + P_{pf}$$

La presión horizontal de llenado viene dada por:

$$P_{hf,s} = P'_{hf}\,(1 + 0.1\,\beta)$$

Y la presión horizontal por:

$$P_{wf,s} = P_{wf}\,(1 + 0.2\,\beta)$$

La Fig. 4 describe la trayectoria x y las presiones que se ven involucradas en el llenado del silo en su parte cónica [3,10].

Dónde:

$$P_{vft} = P_{vo}\,(1 - e^{-\frac{z_t}{z_o}})$$
$$P_{hf} = F_f\,P_{vf} \quad y \quad P_{tf} = \mu_h\,P_{hf}$$

$$P_{vf} = \frac{\gamma\,h_h}{n-1}\left\{\left(\frac{x}{h_h}\right) - \left(\frac{x}{h_h}\right)^n\right\} + P_{vft}\left(\frac{x}{h_h}\right)^n$$

Con:

$$n = 2(F_f\,\mu_h\,\cot\beta + F_f - 1)$$

Dónde:
γ = Peso específico del material.
h_h = Altura de la tolva, desde la punta del cono hasta la unión con el cilindro.
x = Recorrido de la presión en la tolva.
μ_h = Coeficiente de fricción con la pared de la tolva.
β = Ángulo de la tolva.
P_{vft} = presión vertical de la sección cilíndrica.

$$F_f = \frac{1 + a\,\mu\,\cot\beta}{1 + \mu\,\cot\beta}$$

a = 0.8 para presiones de llenado.

2.1.4. Cálculo de presiones de vaciado en el cilindro y tolva

La Fig. 5 muestra las presiones involucradas en el vaciado del silo en su parte cilíndrica. A continuación sus ecuaciones [3,10].

$$P_{he} = C_h\,P_{hf} \quad y \quad P_{we} = C_w\,P_{wf}$$

$$C_h = C_o \quad y \quad C_w = 1.1$$
$$P_{ne} = F_e\, P_{ve} \quad y \quad P_{te} = \mu_h\, P_{ne}$$
$$C_o = 1.35 + 0.02\,(\varphi_i - 30°)$$

$$P_{pe} = 0.2\,\beta\,P_{he} \qquad P'_{he} = P_{he} + P_{pe}$$

La Fig. 6 muestra las presiones involucradas en el vaciado del silo en su parte cónica. A continuación sus ecuaciones.

$$P_{ve} = \frac{\gamma\, h_h}{n-1}\left\{\left(\frac{x}{h_h}\right) - \left(\frac{x}{h_h}\right)^n\right\} + P_{vft}\left(\frac{x}{h_h}\right)^n$$

$$n = 2(F_f\,\mu_h\cot\beta + F_e - 1)$$

$$F_e = \frac{1 + \sin\varphi_i + \cos\varepsilon}{1 + \sin\varphi_i\,\cos(2\beta + \varepsilon)}$$
$$\varepsilon = \varphi_{wh} + \sin^{-1}\left\{\frac{\sin\varphi_{wh}}{\sin\varphi_i}\right\}$$

Donde;
μ_s = coeficiente de fricción de pared de la tolva
ϕ_{wh} = ángulo de fricción de la pared de la tolva
ϕ_i = Ángulo efectivo de fricción interna del material solido

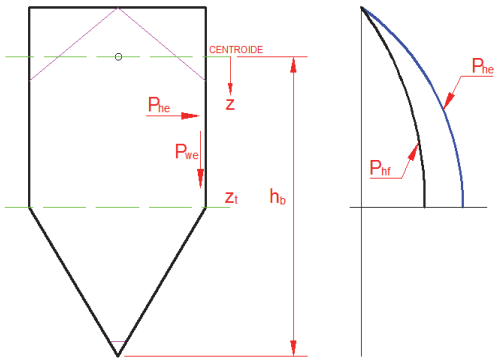


Figura 5. Presiones de vaciado en el cilindro
Fuente: Propia

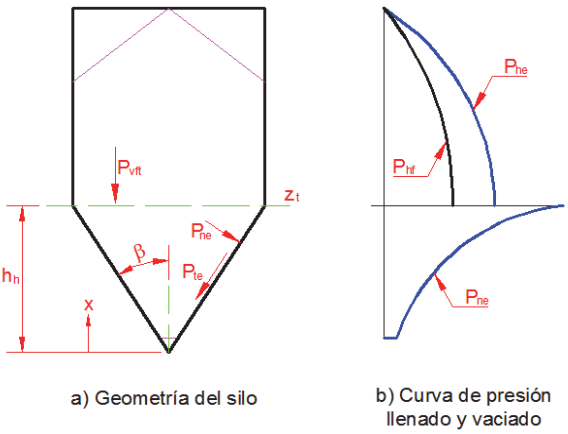


Figura 6. Presiones de vaciado en la tolva
Fuente: Propia

2.2. *Modelo con elementos finitos en ANSYS-APDL*

Para este proyecto se eligió la plataforma de Mechanical APDL (lenguaje de diseño paramétrico) porque permite desarrollar un código de comandos donde se estructuran cada una de las fases del análisis estructural y donde se puede parametrizar las entradas geométricas, características de material, tipo y tamaño del elemento a utilizar, detallado del mallado y características de las cargas sobre el modelo, además permite proporcionar al modelo una curva de presiones, caso que no es posible en Worckbench ya que este permite únicamente presiones hidrostáticas[2,12].

2.2.1. Procedimiento para generar el mallado del silo

Antes de realizar el mallado se nombran las variables que geométricas del silo para que el modelo quede paramétrico, en esta parte también se nombra el tipo de elemento a usar (shell 281, para que se ajuste mejor a las curvaturas del silo), tamaño del elemento y las propiedades del material del silo. La Fig. 7 muestra estas variables.

Una vez definidas las variables de la geometría del silo se procede a ubicar puntos estratégicos en el espacio (keypont) con el fin de dibujar la geometría del silo, con los keypont se generan líneas y cuando se hacen rotar en el eje del silo estas líneas se obtienen las superficies del silo, la Fig. 8 muestra este resultado.

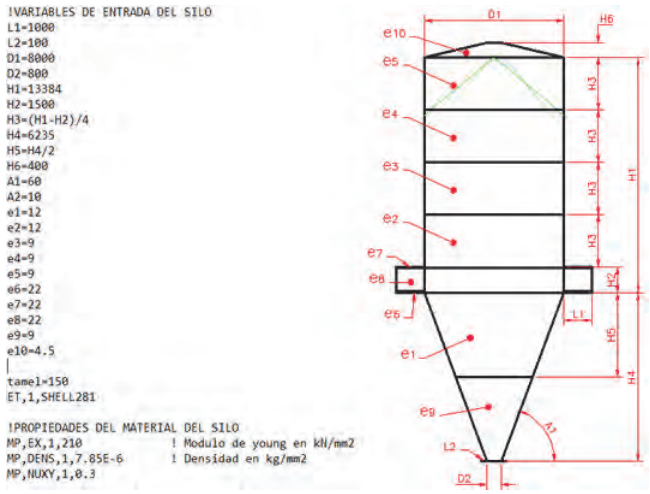


Figura 7. Variables de entrada del silo.
Fuente: Propia

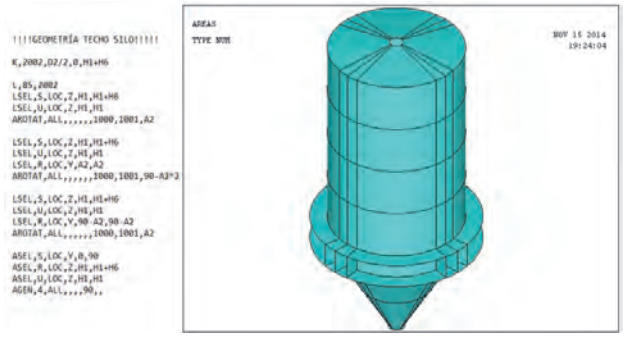


Figura 8. Geometría del silo en superficies
Fuente: Propia

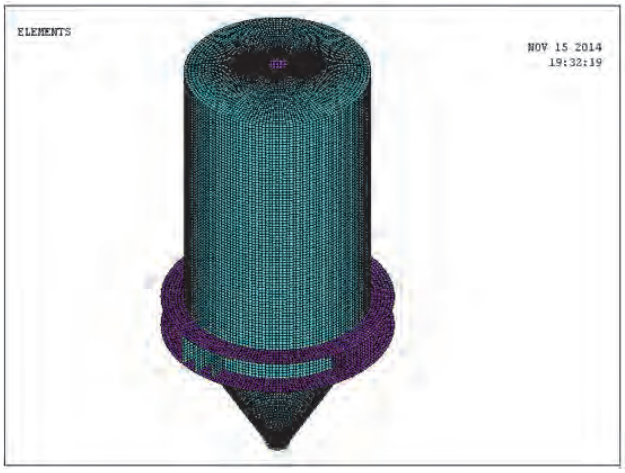


Figura 9. Visualización de la mala del silo
Fuente: Propia

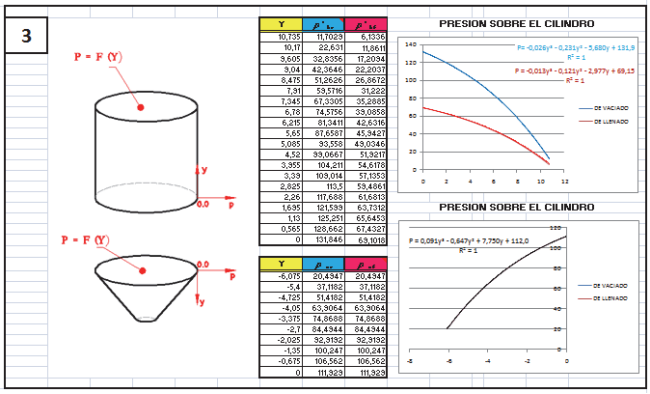


Figura 10. Curvas de presiones sobre el silo.
Fuente: Propia

Para realizar el mallado se selecciona las diferentes superficies del silo y se les asigna las propiedades físicas del material, el espesor y el tamaño del elemento, en la Fig. 9 se puede apreciar el mallado.

2.2.2. Asignación de cargas al modelo

Las ecuaciones usadas en el numeral 2.1.3 y 2.1.4 son ingresadas a una hoja de cálculo donde se determinan las presiones de llenado y vaciado del cilindro y de la tolva del silo, de allí se determinan las constante de una curva de tercer orden para graficar las curvas de presión y se pueden apreciar en la Fig. 10. Con estas constantes y relacionando el área donde es aplicada la presión, se asignan cargas a los nodos del modelo mediante dos ecuaciones que varían con la altura; una para la parte cilíndrica y otra para la parte cónica. La Fig. 11 representa la asignación de cargas en el cilindro.

Finalmente se le asignan las condiciones de frontera a los nodos que representan la base soporte del silo impidiendo su movimiento en cualquier sentido. Una vez terminado este código se copia en la línea de comandos de ANSYS y se digita SOLVE, de esta manera el programa calcula los esfuerzos y deformaciones del silo.

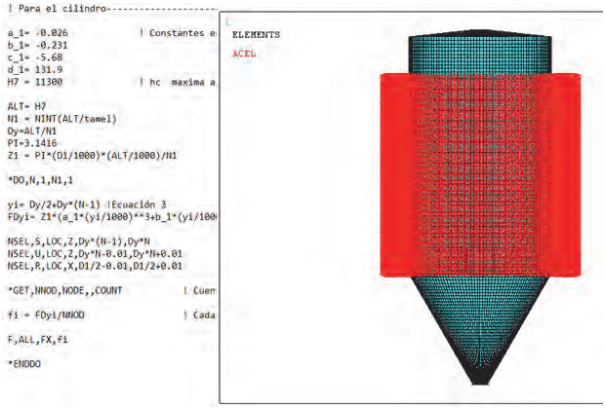


Figura 11. Asignación de cargas en el cilindro.
Fuente: Propia

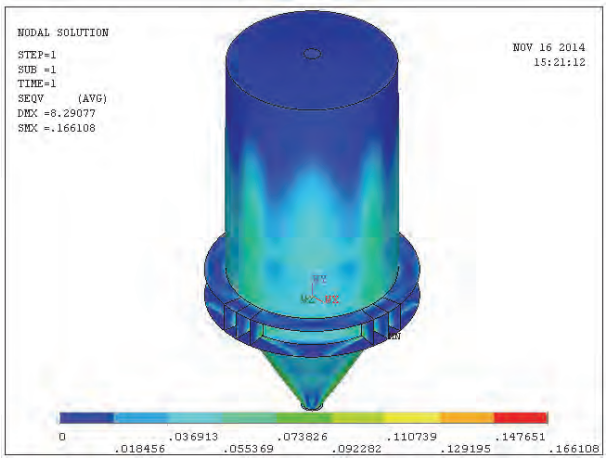


Figura 12. Esfuerzo Von Mises - General
Fuente: Propia

3. Resultados

3.1. *Esfuerzo.s y deformaciones del silo estudiado*

Las Figs. 12 y 13 muestran el esfuerzo de Von Mises producido por la presión de vaciado, se evidencia que su máximo valor de 0.166Mpa está ubicado en los refuerzos del

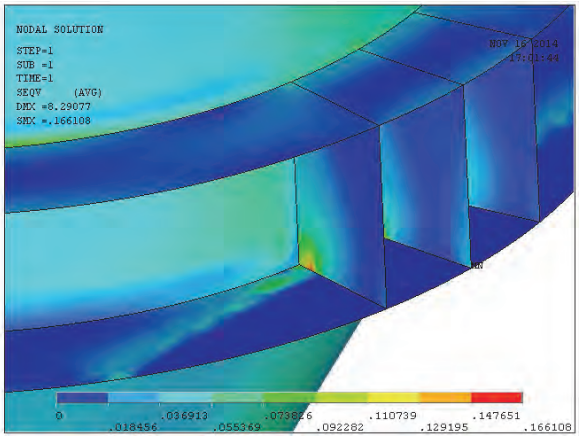


Figura 13. Esfuerzo Von Mises – Detalle
Fuente: Propia

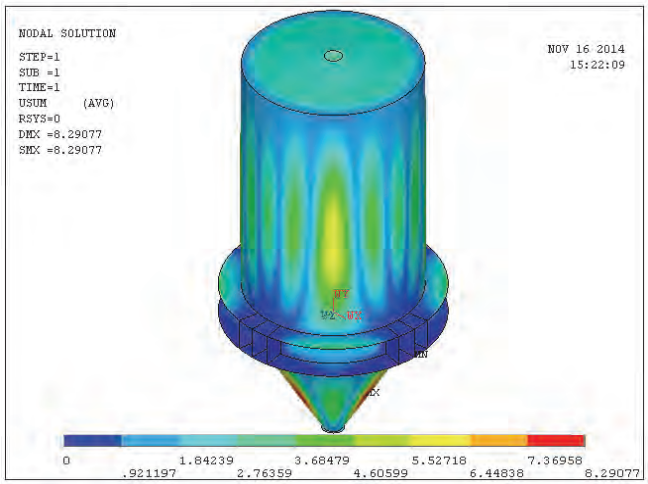


Figura 14. Suma de desplazamientos - General
Fuente: Propia

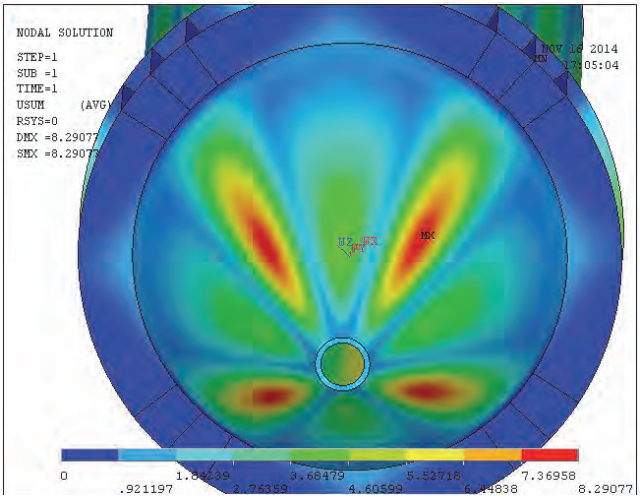


Figura 15. Suma de desplazamientos - Detalle
Fuente: Propia

cinturón, esto es lógico si se tiene en cuenta que el apoyo del silo está ubicado en esta parte y que allí soporta toda la carga

En cuanto a las deformaciones las Figs. 14 y 15 muestran que el valor máximo de 8.29mm está presente en la tolva y justamente bajo los refuerzos del cinturón, fenómeno que ocurre por la restricción de movimiento que tiene el soporte.

3.2. Selección del modelo más conveniente

Se realizaron análisis a 6 modelos de silos de igual geometría pero con diferentes espesores, para poder evaluar cual ofrece un mejor factor de seguridad y es menos pesado, esto con el fin de reducir sus costos de fabricación y montaje. Se encuentra que el modelo 5 es el adecuado debido a que arroja factores de seguridad de 1.51 para llenado y 1.37 para vaciado y su peso es de 40256kg. La Tabla 1 muestra estos resultados.

Tabla 1.
Resultados de varios modelos de un silo

ANALISIS SILO DE 1020 Ton						
VARIABLE	MODELO 1	MODELO 2	MODELO 3	MODELO 4	MODELO 5	MODELO 6
L1(mm)	1000	1000	1000	1000	1000	1000
L2 (mm)	100	100	100	100	100	100
D1(mm)	8000	8000	8000	8000	8000	8000
D2 (mm)	800	800	800	800	800	800
H1(mm)	13384	13384	13384	13384	13384	13384
H2 (mm)	1500	1200	1200	1200	1200	1000
H3 (mm)	2971	3046	3046	3046	3046	3096
H4 (mm)	6235	6235	6235	6235	6235	6235
H5 (mm)	3117,5	3117,5	3117,5	3117,5	3117,5	3117,5
H6 (mm)	400	400	400	400	400	400
A1(grados)	60	60	60	60	60	60
e1(mm)	12	12	11	12	12	14
e2 (mm)	12	12	11	11	12	14
e3 (mm)	9	9	11	11	9	9
e4 (mm)	9	9	9	9	9	9
e5 (mm)	9	9	9	9	9	9
e6 (mm)	22	19	19	19	19	19
e7 (mm)	22	19	19	19	19	19
e8 (mm)	22	19	25	25	25	25
e9 (mm)	12	12	11	12	12	12
e10 (mm)	4,5	4,5	4,5	4,5	4,5	4,5
Peso (kg)	40673	39578	39839	40620	40256	42875
DMXe (MPa)	167	202	170	171	166	164
DMXe (mm)	6,44	6,86	7,59	6,87	6,74	6,69
F.S.vaciado	*1,50*	*1,24*	*1,47*	*1,46*	*1,51*	*1,52*
DMXf (MPa)	184	217	186	187	182	178
DMXf (mm)	6,7	7,18	7,92	7,18	7,06	6,71
F.S llenado	*1,36*	*1,15*	*1,34*	*1,34*	*1,37*	*1,40*

Fuente: Propia

3.3. Análisis de un esfuerzo en un silo con tolvas de diferente inclinación

Tomando como referencia el silo del modelo 5 se realizan dos análisis modificando el ángulo de inclinación de la tolva (valor A1 de la Tabla 1 = 60 grados), caso 1 para tolva con 70 grados y caso 2 con 50 grados.

Las Figs. 16 y 17 muestran el esfuerzo de Von Mises generado por la presión de llenado para el caso 1 y 2 respectivamente y en las Figs. 18 y 19 para las cargas de vaciado.

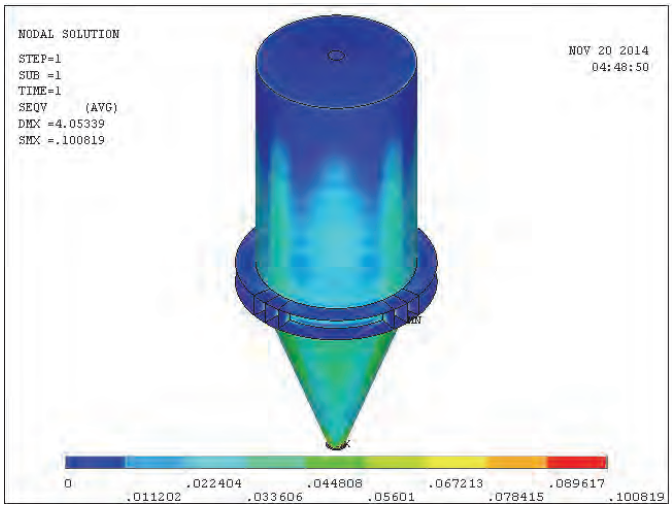


Figura 16. Silo con tolva 70 grados – Presión llenado
Fuente: Propia

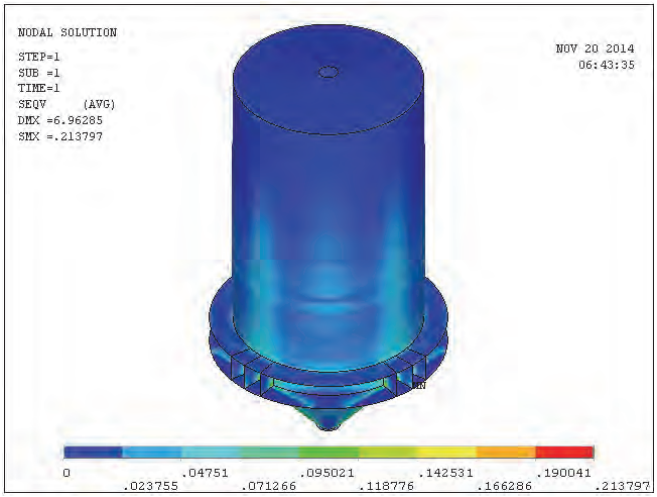


Figura 17. Silo con tolva 50 grados – Presión llenado
Fuente: Propia

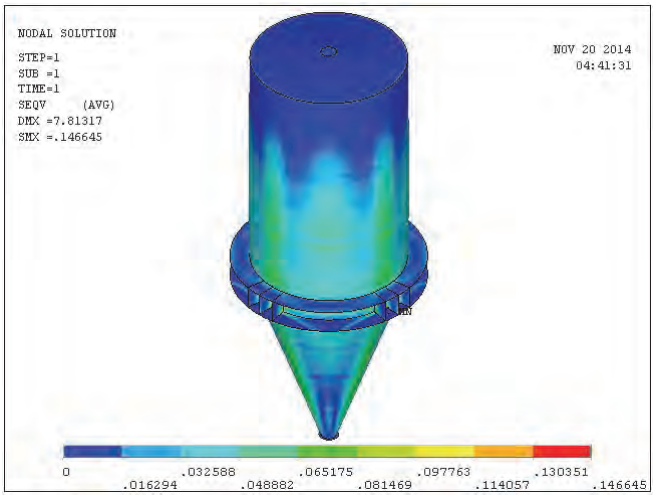


Figura 18. Silo con tolva 70 grados – Presión vaciado
Fuente: Propia

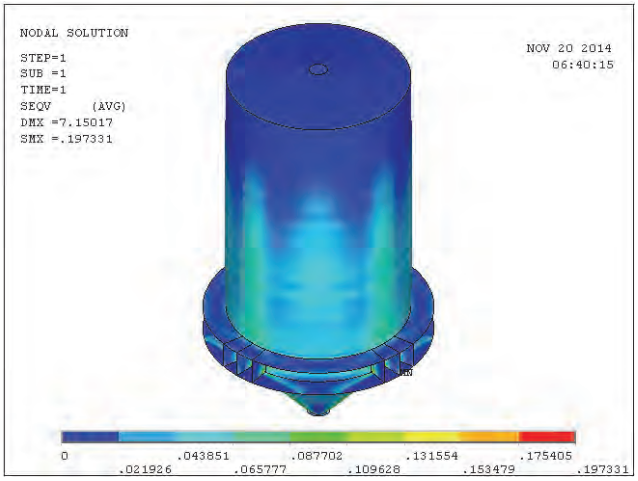


Figura 19. Silo con tolva 50 grados – Presión vaciado
Fuente: Propia

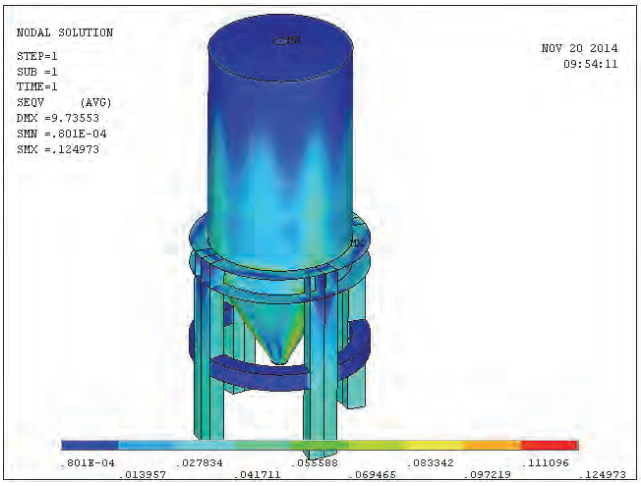


Figura 20. Esfuerzo Von mises con presión llenado
Fuente: Propia

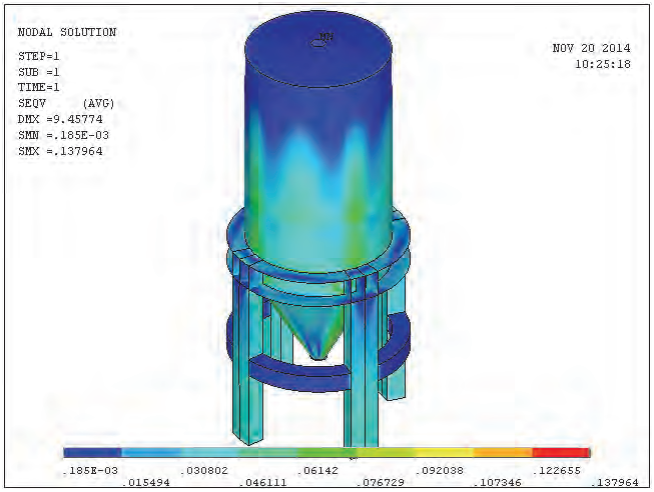


Figura 21. Esfuerzo Von mises con presión vaciado
Fuente: Propia

Nótese que para el caso 1 el esfuerzo de Von Mises es mayor para el vaciado (0.146GPa vs 0.100GPa), esto ocurre porque la tolva tiene mayor inclinación y las fuerzas verticales son menores, caso opuesto ocurre en el caso 2 donde el esfuerzo de Von Mises es de 0.197GPa para el vaciado 0.213GPa para el llenado.

3.4. Análisis de un silo con estructura

Como se pudo apreciar en los análisis anteriores el silo mostró sus esfuerzos máximos en cinturón y las deformaciones máximas en la tolva, por este motivo se realiza un análisis del silo contemplando una estructura de soporte de 10 metros de altura, dimensión comúnmente usada para este tipo de silos en el proceso de empaque del cemento. Se usa como base el código de ANSYS del modelo 5 adicionándole la geometría de las columnas y vigas de la estructura.

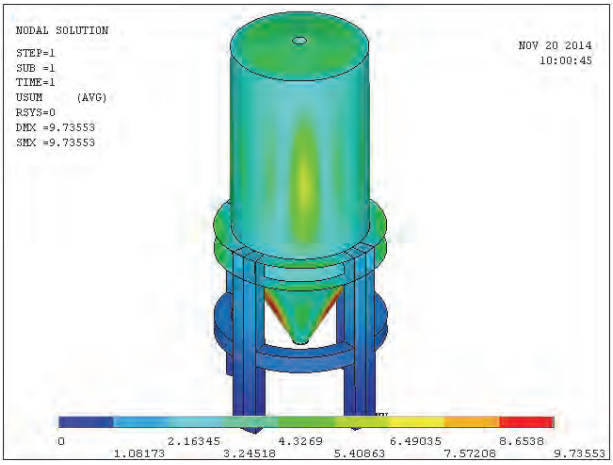


Figura 22. Suma de deformaciones con presión llenado
Fuente: Propia

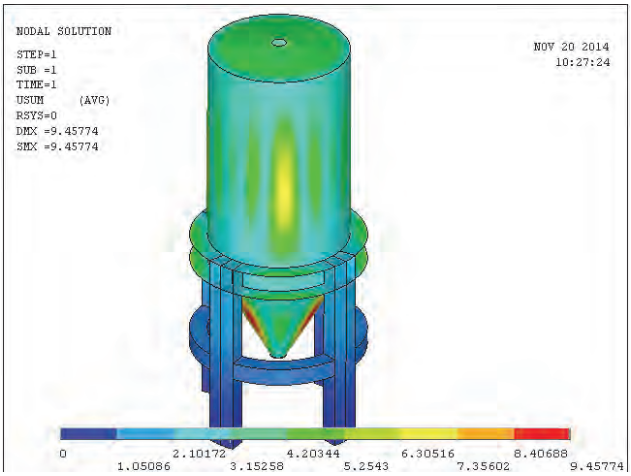


Figura 23. Suma de deformaciones con presión vaciado
Fuente: Propia

Las Figs. 20 y 21 representan el esfuerzo de Von Mises para presiones de llenado y vaciado respectivamente y las figuras 22 y 23 las deformaciones en los mismos casos.

De los resultados obtenidos se puede deducir que los esfuerzos en el silo son menores cuando se analiza en conjunto con su estructura, lo anterior se debe al efecto que se induce las dos diferentes condiciones de contorno de cada modelo.

Cuando se analiza únicamente el silo sus puntos de apoyo no tienen ningún grado de libertad, mientras que en el caso silo-estructura estos mismo puntos tienen grados de libertad y su desplazamiento depende de la rigidez de la estructura.

4. Conclusiones

El modelo paramétrico desarrollado con un código y en el software de elementos finitos ASNYS APDL permite realizar el cálculo de un silo con cualquier geometría, tamaño, espesores de lámina y tipo de material, tamaño y tipo de elemento finito a usar. En este modelo se pueden manipular los espesores de diferentes secciones del silo para realizar un análisis comparativo y evaluar la conveniencia de uno u otro diseño, permitiendo al calculista desarrollar un modelo adecuado y que se ajuste a las condiciones de fabricación y montaje del silo.

Al determinar las presiones ejercidas por el material y que están aplicadas en las paredes del silo, tanto en su parte cilíndrica como en su parte cónica, se encuentra que hay dos tipos de comportamiento en lo referente a las presiones en la parte cónica, encontrando que para tolvas con inclinaciones altas las presiones de vaciado son notoriamente mayores que las de llenado, caso contrario ocurre en las tolvas con una inclinación pequeña donde las presiones de llenado y vaciado son similares.

Los entornos gráficos, que son bastante amigables pero poco manipulables, de los principales software de elementos finitos no tienen la opción de ingresar al modelo presiones con variación respecto a una altura, lo más cercano que ofrecen es aplicación de presión hidrostática la cual es lineal. Como las curvas de presión determinadas son de orden tres, se hace necesario realizar un código que remplace la presión por una rutina de aplicación de fuerzas equivalentes sobre los nodos de cada área, parte cilíndrica y parte cónica. Lo anterior es otra razón por la cual se escogió ANSYS APDL como software para realizar el análisis por elementos finitos, su plataforma permite cualquier tipo de aplicación de carga.

Realizado el análisis estructural se encontró que no necesariamente las presiones de vaciado pueden ocasionar fallas en un silo, es fácil sesgar esta información ya que las presiones de vaciado siempre son mayores en el silo, pueda que en la tolva se dé la salvedad anteriormente descrita, pero en el total del silo siempre es mayor. El caso específico ocurre en una de las partes importantes del silo y que muchas veces se relega; es el cinturón que se encarga de unir el silo a una estructura. Se encontró que los valores los esfuerzos eran mayores cuando se aplicaba la carga de llenado, esto ocurre porque justo en ese punto hay un equilibrio entre las cargas de la tolva y del cilindro, si se disminuyen las del cilindro las de la tolva empiezas a pandear mas esta área, haciendo que se incrementen los esfuerzos en este punto. Es importante aclarar que los esfuerzos en el cuerpo del silo si son mayores en el vaciado que en el llenado.

Para describir el comportamiento de superficies curvadas del silo el modelo se desarrolla con elementos tipo cáscara más conocidos como "shell" ya que estos simultáneamente muestra esfuerzos de flexión y tensiones de membrana, los primeros corresponden a los esfuerzos de flexión de una placa produciendo momentos de flexión y momentos de torsión y los segundos corresponden a los esfuerzos en un problema de tensión plana, los cuales actúan tangentemente a la superficie media y producen fuerzas tangentes en la membrana.

Referencias

[1] Aguado, P., Métodos avanzados de cálculo de presiones en silos agrícolas mediante la técnica de los elementos finitos. El vaciado de silos y las paredes de chapa ondulada. PhD Thesis, Escuela Técnica Superior de Ingenieros Agrónomos UPM, España. 1997.

[2] Ansys,Inc., Ansys Mechanical APDL Introductory Tutorials. Canonsburg, USA, 2013.

[3] CEN (European Committee For Standardization). Eurocode EN 1991-4. Bruselas, Bélgica. Actions on structures - Part 4: Silos and tanks, 2005.
[4] Cook, R., Malkus, D., Plesla, M. and Witt, R., Concepts and applications of finite element analysis, University of Wisconsin, Madison, 2001.
[5] Ding, S., Rotter, M., Ooi J. and Enstad, G., Development of normal pressure and frictional traction along the walls of a steep conical hopper during filling: Thin-Walled Structures 49, pp. 1246-1250, 2011. DOI: 10.1016/j.tws.2011.05.010
[6] Ercoli, N, Ciancio, P. y Massey, L., Evaluación de la interacción grano-pared en el comportamiento estructural de silos. Mecánica Computacional XXVII, pp.161-180, 2007.
[7] Ercoli, N., Ciancio, N. y Berardo, C., Análisis para el diseño de un silo de clinker y su implementación computacional, en: Buscaglia, G., Dari, E. and Zamonsky, O., (Eds.), Mecánica Computacional. XXIII, pp. 619-638, 2004.
[8] Jürgen, T., Assessment of mechanical properties of cohesive particulate solids – Part 2. Particulate science and technology, 19, pp. 111-129, 2001. DOI: 10.1080/02726350152772065
[9] Rodriguez, W. y Pallares, R., Modelado tridimensional de un pavimento bajo carga dual con elementos finitos. Revista DYNA, 82(189), pp. 30-38, 2015. DOI: 10.15446/dyna.v82n189.41872
[10] Rotter, J., Guide for the economic design of circular metal silos. CRC Press. London and New York, 2001.
[11] Ulrich, H. and Josef, E., Numerical investigations on discharging silos. Journal Of Engineering Mechanics, 110, pp. 957-971, 1984. DOI: 10.1061/(ASCE)0733-9399(1984)110:6(957)
[12] University of Alberta – ANSYS tutorials. Canada. [Online]- Available at: http://www.mece.ualberta.ca/tutorials/ansys/
[13] Yanes, Á., Fernández, M. y López, P., Análisis de la distribución de presiones estáticas en silos cilíndricos con tolva excéntrica mediante el M.E.F. influencia de la excentricidad y comparación con el eurocódigo 1. Informes de la Construcción, 52, 2001, 472 P.

Bayona, W., Recibió su BSc. en Ingeniería Electromecánica en 2004 en la Universidad Pedagógica y Tecnológica de Colombia, por más de 10 años se ha desempeñado en el área del diseño mecánico desarrollando ingenierías conceptuales, básicas y de detalle de diferentes plantas del sector energético, metalmecánico, siderúrgico, cementero y del petróleo. Áreas de investigación de interés: análisis de esfuerzos y deformaciones por el método de elementos finitos, estudio del comportamiento de los fluidos y materiales pulverizados por medio de fluodinámica computacional, diseño de silos, tanques y recipientes a presión.
ORCID: 0000-0001-5799-5246

Useche, J., es profesor de ingeniería mecánica de la Universidad Tecnológica de Bolívar (UTB), Colombia, es coordinador del Grupo de Investigación de Materiales y Estructuras Continuas de la UTB. Es PhD en Ingeniería Mecánica de la Universidad Estatal de Campinas, Brasil. Recibió su BSc en Ingeniería Mecánica en la Universidad Tecnológica de Bolívar, Colombia y es MSc. en Ingeniería Mecánica de la Universidad de los Andes, Colombia. Áreas de investigación de interés: método de elementos finitos, método de elementos de frontera y métodos libres de malla para análisis de esfuerzos y deformaciones, mecánica del daño y evaluación de la vida residual.
ORCID: 0000-0002-9761-2067



UNIVERSIDAD NACIONAL DE COLOMBIA
SEDE MEDELLÍN
FACULTAD DE MINAS

Área Curricular de Ingeniería Mecánica

Oferta de Posgrados

Maestría en Ingeniería - Ingeniería Mecánica

Mayor información:

E-mail: acmecanica_med@unal.edu.co
Teléfono: (57-4) 4259262

UNIVERSIDAD NACIONAL DE COLOMBIA
SEDE MEDELLÍN
FACULTAD DE MINAS



DYNA
http://dyna.medellin.unal.edu.co/

An early view of the barriers to entry and career development in Building Engineering

Margarita Infante-Perea [a], Marisa Román-Onsalo [b] & Elena Navarro-Astor [c]

[a] *Escuela Técnica Superior de Ingeniería de Edificación, Universidad de Sevilla, Sevilla, España. minfante1@us.es*
[b] *Facultad de Ciencias del Trabajo, Universidad de Sevilla, Sevilla, España. onsalo@us.es*
[c] *Escuela Técnica Superior de Ingeniería de Edificación, Universitat Politècnica de València, Valencia, España. enavarro@omp.upv.es*

Received: April 5th, 2015. Received in revised form: August 11th, 2015. Accepted: September 04th, 2015

Abstract
The construction sector plays an important role in the global economy since it generates approximately 10% of the world GDP and employs around 7% of the workforce. Professional profiles for building engineers and barriers they may encounter when accessing the labor market as well as in their career development in the sector are researched. Having identified some variables as relevant barriers, this empirical research is exploratory in nature and adopts a descriptive and inferential approach, in order to analyze the influence of gender in the perception of barriers in two Spanish universities. Results show more difficult working circumstances for women, which allows us to reflect on the consequences of these early perceptions on the career development of the next generation of both male and female building engineers.

Keywords: career barriers; construction; professional development; gender; building engineering; women.

Una visión temprana de los obstáculos de acceso y desarrollo profesional en Ingeniería de edificación

Resumen
El sector de la construcción desempeña un importante rol en la economía mundial, ya que genera alrededor del 10% del PIB y da trabajo en torno al 7% de las personas empleadas. Se investigan las salidas profesionales de los ingenieros(as) de edificación y las barreras de carrera que pueden encontrar en su acceso al mercado de trabajo y en su desarrollo profesional en el sector. A partir de la identificación de variables como barreras relevantes, se adopta un enfoque descriptivo e inferencial de carácter exploratorio para analizar la influencia del género en la percepción de dichas barreras en dos universidades españolas. Los resultados muestran un escenario laboral más difícil para ellas y nos permiten reflexionar sobre las repercusiones que estas percepciones tempranas pueden tener en el desarrollo profesional de la próxima generación de ingenieros(as) de la edificación.

Palabras clave: barreras de carrera; construcción; desarrollo profesional; género; ingeniería de edificación; mujeres.

1. Introducción

El sector de la construcción juega un importante papel en la economía ya que genera alrededor del 10% del PIB mundial y da trabajo en torno al 7% de las personas empleadas en el mundo [1]. Este sector fue uno de los más dinámicos de la economía española entre 2000 y 2007, representando en 2004 casi una cuarta parte de todos los puestos de trabajo creados en España [2], siendo actualmente uno de los sectores más afectados por la crisis económica que atraviesa el país. Dentro del mismo, la edificación ha sido caracterizada por ser tradicionalmente masculina y por su imagen general de ser dura, pesada, sucia y orientada a la maquinaria [3]. Bajo la perspectiva de género, son numerosas las investigaciones que ponen de manifiesto la existencia de obstáculos de carrera en este sector en numerosos países [4]. Entre éstos encontramos las condiciones de trabajo propias de esta industria, que responden a un "modelo masculino": muchas horas de trabajo, trabajo inflexible (no es común el trabajo a tiempo parcial ni el trabajo compartido, exigiéndose una dedicación al 100%), cultura de presencia en el puesto, naturaleza nómada del trabajo en obra, entre otras. A estas condiciones se suma el paternalismo que hace que las mujeres sean asignadas a unos puestos (diseño, servicios de

© The author; licensee Universidad Nacional de Colombia.

apoyo, interiorismo y arquitectura doméstica) y los hombres a otros (control de las obras, relaciones con los clientes, diseño de exteriores y forma de los edificios), provocando una segregación ocupacional dentro de la industria [5].

Por otro lado, y principalmente en la obra, las mujeres soportan conductas inaceptables como el acoso verbal (comentarios obscenos, silbidos, palabrotas, lenguaje ofensivo, chistes), peticiones de intimidad sexual e incluso acoso sexual (tocamientos) [6-9]. Este ambiente ha sido descrito como una cultura de vestuario ("locker room"), una cultura excluyente en la que se hacen referencias sexuales explícitas para confirmar la heterosexualidad masculina dominante [9].

Las responsabilidades familiares obligan a las mujeres de esta industria a tener pausas en su carrera profesional. Para ellas sigue existiendo la necesidad de elegir entre familia o carrera [5,10-11], tienen miedo a perder el trabajo o a ser degradadas por tener hijas/os, o se quedan atrás en el desarrollo profesional cuando se reincorporan al trabajo [12]. Así, la dificultad de equilibrar vida profesional y familiar es identificada como otra barrera.

La falta de profesionalidad en la gestión de los recursos humanos implica la existencia de frenos en el reclutamiento y la selección. La invisibilidad de las mujeres y la falta de modelos femeninos, hacen que propietarios y empleadores duden a la hora de contratarlas [13]. Además, las redes de contactos juegan un importante papel y las mujeres suelen estar fuera [11,14]. Algunas investigaciones subrayan que se prefiere expresamente a hombres y se rechaza a las mujeres [15-16].

La prevalencia de redes informales frente al mérito [17-18], siendo frecuente acceder a un trabajo a través de recomendaciones de amigos o familiares, en ocasiones no siendo imprescindible presentar el título profesional [19], la preferencia hacia empleados varones [20], la intolerancia de la industria a pausas en la carrera [13], la falta de reconocimiento, e incluso la apropiación de las contribuciones de las mujeres [12], son ejemplos de la discriminación y de los frenos en la promoción que sufren las mujeres. Dificultades que finalmente constituyen un techo de cristal. Como señalan Dainty et al. [11], las mujeres tienden a progresar en su carrera un paso por detrás de sus compañeros varones.

Otra barrera es una retribución inferior por un trabajo equivalente [14], y ser considerada baja o injusta, carente de transparencia en la estructura salarial, y donde las habilidades y experiencia de las mujeres son ignoradas y menospreciadas [12].

En relación al desempeño, la dificultad para que se reconozca la labor profesional de las mujeres y el tener que realizar mayor nivel de esfuerzo y de trabajo que sus colegas varones [21-23] es una práctica que dificulta el desarrollo, empequeñece a las mujeres y demuestra un sistema injusto.

A esto hay que añadir los estereotipos de género que aún perduran en la industria, siendo dos los más citados [4]: la mujer no tiene las cualidades físicas para desenvolverse adecuadamente en obra porque carece de fuerza física y/o porque no se atreve a subir a las alturas, y la obra no es un trabajo para la mujer porque las condiciones y el ambiente son hostiles para ella.

Pese a estos obstáculos, cada vez son más las mujeres que estudian carreras universitarias y oficios especializados que cualifican para trabajar en la edificación. Por ejemplo en Colombia, en 1966, las mujeres representaban solo el 3,8% del alumnado inscrito en Ingeniería [24]; en el período 1984-89, en el área de Ingeniería, Arquitectura, Urbanismo y afines, la presencia de la mujer era del 10,55%, con un incremento paulatino hasta alcanzar el 16,12% en 2000-2004 [25]. En España, en el curso 2012-2013 la proporción de mujeres matriculadas en Grado en la rama de Ingeniería y Arquitectura es del 26.1%, y en Máster del 30.6% [26].

Sin embargo, el número de mujeres que trabajan en la industria es pequeño. En Malasia, por ejemplo, el porcentaje de mujeres que estudian grados de ingeniería y construcción en 2010 fue del 45%, mientras que sólo un 5,4% de los trabajadores de la construcción eran mujeres (incluyendo a profesionales y gestores) [27]. En Bangladesh y Tailandia tampoco hay una relación lineal entre la proporción de mujeres que estudian ingenierías y su empleabilidad [28]. En España, en el año 2009, el sector de la construcción solo representa el 1,76% de las mujeres ocupadas a nivel nacional [29].

Este contraste nos hace cuestionarnos qué ocurre con las mujeres que se han cualificado para desempeñar una ocupación en la industria, ¿la abandonan o ni siquiera han llegado a acceder? Nuestro objetivo es explorar si los futuros (as) ingenieros (as) de edificación perciben que a lo largo de su carrera encontrarán los obstáculos descritos, y los supuestos de partida que influirán en el empeño con que buscarán empleo e intentarán promocionarse en las distintas ocupaciones.

Dado que estas barreras pueden condicionar la elección de determinadas ocupaciones y el rechazo de otras [30], el análisis se llevará a cabo en función de la variable sexo, para saber si las barreras percibidas por las mujeres son diferentes a las que perciben los hombres. Si así fuera, se estaría contribuyendo a perpetuar la segregación ocupacional dentro de la propia industria. De este modo pretendemos responder a las siguientes preguntas: ¿la variable sexo se revela como determinante en las percepciones de las barreras de carrera? De ser así, ¿cuáles son las barreras percibidas como más importantes?

De las diferentes ocupaciones nos centramos en aquellas más directamente relacionadas con trabajos en obra dada su relevancia e incidencia [31].

2. Metodología

La investigación realizada adopta un enfoque descriptivo e inferencial de carácter exploratorio, a partir del estudio de variables identificadas como barreras relevantes en el desarrollo profesional de los/las estudiantes.

La población objeto de estudio la constituyen las alumnas y alumnos de 4º curso de las Escuelas Técnicas Superiores de Ingeniería de Edificación de las universidades españolas de Sevilla y Valencia. Entendemos que dicho alumnado ha casi completado su formación, están próximos a su incorporación al mercado de trabajo y, en consecuencia, tienen más claras las diferentes ocupaciones a las que pueden optar y una imagen más formada de lo que puede acontecer en ellas.

Teniendo en cuenta que se trata de un estudio piloto cuyo objetivo es realizar un acercamiento inicial a la realidad, no se ha buscado la representatividad en la muestra. El alumnado seleccionado corresponde al matriculado en dos grupos (uno de cada universidad) de una de las asignaturas obligatorias de último curso. Para evitar sesgos en los resultados, derivados de las circunstancias particulares de cada Escuela, se ha optado por igualar en número los/las estudiantes integrantes de Sevilla y Valencia.

Finalmente, la muestra ha quedado conformada por 58 estudiantes, 29 de cada provincia, siendo un 44,83% mujeres y el restante 55,17% hombres. Este desequilibrio entre sexos es lógico en una carrera universitaria tradicionalmente masculinizada, donde a pesar de que la brecha se ha ido reduciendo en la última década, sigue habiendo un mayor número de hombres que eligen estos estudios [32].

La técnica utilizada para la recogida de información es la encuesta. El cuestionario empleado ha sido diseñado para la toma de datos de una investigación más amplia, sometido a una validación interjueces y a varias pruebas experimentales previas con diversos grupos reducidos de participantes. Para su elaboración se han tenido en consideración las sugerencias de cinco expertas/os de tres áreas de conocimiento diferentes: igualdad y género, la profesión objeto de estudio y sector construcción, y estadística y manejo de la herramienta SPSS.

El cuestionario está estructurado en dos partes. En la primera se solicitan datos socio-demográficos de interés a través de preguntas abiertas y cerradas, de respuestas dicotómicas. Para este estudio sólo vamos a considerar la variable sexo.

En la segunda se incluye una única pregunta que tiene como objetivo recoger las percepciones sobre los obstáculos que pueden encontrar en su desarrollo profesional futuro. Dicha pregunta se estructura en seis secciones y quince ítems que se repiten en cada sección. Cada sección corresponde a una de las seis salidas profesionales recogidas en el Libro Blanco de la Edificación [33] (ver Tabla 1) y los 15 ítems se corresponden al inventario de barreras de carrera diseñado por Swanson et al. [34] (ver Tabla 2). Las/os participantes valoran mediante escala Likert de razón 1 a 4, donde 1 es nada y 4 mucho, el alcance potencial que tiene cada barrera para cada salida laboral. En otras palabras, el alumno/a valorará el grado en el que cada barrera indicada puede limitar su desarrollo profesional en cada una de las seis salidas laborales existentes para la Ingeniería de Edificación.

Hay que subrayar que de las 13 barreras originales de Swanson et al. [34] se eliminaron dos, relacionadas con discriminaciones por razón de raza y minusvalía. El motivo principal fue la homogeneidad de la muestra en relación a estos aspectos, siendo la presencia de alumnado de diferentes razas y con minusvalías anecdótica.

Con el objetivo de obtener mayor riqueza de información, la primera barrera de Swanson "discriminación sexual" se desglosó en cinco sub-barreras: el acoso sexual, la discriminación salarial y los retrasos en la promoción con respecto a personas del sexo opuesto, el tener un jefe/a sesgado en contra de las personas de tu mismo sexo y la discriminación sexual en la contratación, todas ellas extraídas de un inventario de barreras más amplio diseñado por el mismo autor y recogido en [35].

Tabla 1.
Salidas profesionales del Grado en Ingeniería de Edificación.

Perfiles profesionales	Ocupaciones del perfil
1. Dirección técnica de la obra	- Director de la ejecución de la obra - Director de obra - Técnico de planificación y organización de la obra - Técnico de control y gestión de la calidad - Técnico de control y gestión económicos
2. Gestión de la producción de la obra	- Jefe de obra - Jefe de producción - Técnico responsable de estudios - Técnico responsable de gestión de compras y recursos - Técnico de calidad y medio ambiente
3. Prevención y Seguridad y Salud	- Coordinador de seguridad y salud en fases de proyecto y de ejecución - Técnico en redacción de estudios y planes de seguridad - Técnico de prevención de riesgos laborales - Auditor de planes de prevención de riesgos laborales y su gestión
4. Explotación del edificio	- Director de explotación de edificios - Responsable de la conservación y mantenimiento - Técnico redactor de documentos sobre la gestión del uso, conservación y mantenimiento, así como planes de emergencia y evacuación del edificio - Técnico en estudios de ciclo de vida útil, evaluación energética y sostenibilidad de los edificios
5. Consultoría, Asesoramiento y Auditorias técnicas	- Auditor técnico de proyectos y de ejecución de obra - Auditor de sistemas de gestión de calidad y medio ambiente - Experto o consultor técnico en informes, peritaciones, dictámenes, tasaciones, valoraciones y estudios de viabilidad económica - Asesor urbanístico.
6. Redacción y desarrollo de proyectos técnicos	- Técnico en proyectos de demolición - Técnico de proyectos de reforma, interiorismo, rehabilitación. - Técnico de proyectos de obra nueva

Fuente: Libro Blanco del Título de Grado en Ingeniería de Edificación [33]

Para el análisis de percepciones del conjunto de estudiantes se ha realizado un estudio descriptivo básico según distribuciones de frecuencia. La valoración de la significatividad de posibles diferencias de percepción de barreras por sexo, se ha llevado a cabo mediante la prueba no paramétrica de contraste para dos muestras independientes de Mann-Whitney.

Con la finalidad de estudiar los perfiles profesionales más relacionados con la obra, se han seleccionado los tres primeros de la Tabla 1. Dirección técnica de la obra, Gestión de la producción de la obra, Prevención y Seguridad y Salud. La dimensión de las diferencias encontradas entre sexos (tamaño del efecto) se ha calculado mediante la "d" de Cohen. Finalmente, el análisis de la distribución de frecuencias por sexos permite conocer las barreras en las que la mayoría de mujeres y/o hombres asignan puntuaciones de

Tabla 2.
Inventario de Barreras de Carrera.

1. Discriminación sexual en la contratación
2. Acoso sexual
3. Retrasos en la promoción con respecto a personas del sexo opuesto
4. Tener un jefe/a sesgado en contra de las personas de tu mismo sexo
5. Percepción de salarios inferiores a los de compañeros/as del sexo opuesto
6. Falta de confianza (falta de autoestima, no sentirte capacitado para realizar tu trabajo)
7. Conflictos de múltiples tareas (equilibrando las responsabilidades laborales y no laborales; estrés en un rol afectando al rendimiento en otro)
8. Conflicto entre los hijos y las exigencias profesionales (recursos inadecuados para cuidar hijos, horarios inflexibles para formación, programación de reuniones antes y después del horario regular de trabajo…)
9. Preparación inadecuada (sensación de una preparación inadecuada para todos los aspectos de un trabajo)
10. Desaprobación por parte de una persona significativa (opiniones negativas de personas significativas en tu vida y familia)
11. Dificultades para tomar decisiones
12. Insatisfacción con la carrera profesional (decepción con el progreso personal y oportunidades disponibles, aburrimiento con la carrera profesional)
13. Falta de apoyo a la hora de elegir una carrera profesional no tradicional
14. Restricciones en el mercado laboral (economía restrictiva con pocas oportunidades; opciones limitadas dentro de un campo específico)
15. Dificultades de comunicación o socialización (No hay modelos de conducta o mentores disponibles, no hay acceso directo a las personas adecuadas o no puedes acceder a las personas que te pueden ayudar)

Fuente: Adaptado de Swanson et al. [34]

percepción positiva (valores 3 y 4) o negativas (1 y 2), afirmando o no la percepción de la existencia de cada barrera.

El estudio estadístico descrito se ha realizado mediante el paquete informático SPSS Statistics v. 20.

3. Resultados

Teniendo en cuenta la totalidad de la muestra, sin diferenciar por sexo, los resultados globales para las seis salidas profesionales muestran dos barreras principales: "Preparación inadecuada" y "Restricciones en el mercado laboral" u opciones limitadas que ofrece el sector, con una media del 58,92%, y 76,4% del alumnado asignando a estos items valores 3 y 4 de la escala Likert. Ambas barreras son percibidas por los(as) futuros(as) ingenieros de edificación como obstáculos determinantes para el desarrollo de su futura carrera profesional. Las restricciones económicas alcanzan su máxima valoración en la salida 2 de la Tabla 1, Gestión de la producción de la obra, con un 81,03% de los alumnos/as que así lo reconocen.

Para los perfiles profesionales más estrechamente relacionados con trabajos en obra, la prueba de Mann-Whitney muestra que la variable sexo determina la percepción que el alumnado tiene de algunas barreras. Como muestra las Tablas 3 y 4, para Gestión de la producción de la obra y Prevención y Seguridad y Salud existen diferencias significativas en las respuestas de mujeres y hombres para las siguientes cinco barreras, con un 99% de confianza: "Tener un jefe/a o supervisor/a sesgado", "Falta de confianza", "Experimentar acoso sexual", "Percepción de salarios inferiores" y "Discriminación sexual en la contratación". Para la barrera "Retrasos en la promoción" las diferencias también son significativas con un 95% de confianza ($0,01<p<0,05$). El cálculo de la "d" de Cohen confirma que las diferencias entre las percepciones de barreras de mujeres y hombres son grandes en todos los casos donde $d>0,8$. La excepción la encontramos en la barrera "Retrasos en la promoción" para la que las diferencias entre sexos se pueden considerar moderadas, $0,5< d<0,8$ (Tablas 3 y 4).

Para el perfil Dirección Técnica de la obra existen diferencias significativas entre las respuestas de mujeres y hombres en siete de las quince barreras de carrera analizadas. Para las barreras "Tener un jefe sesgado", "Acoso sexual", "Salarios inferiores" y "Discriminación sexual en la contratación", el análisis de los datos arroja unos valores de p=0,002, p=0,000, p=0,001, p=0,000 respectivamente, pudiendo afirmar con un nivel de confianza del 99% que la variable sexo es determinante en la percepción de los alumnos y alumnas. En el caso de "Inadecuada preparación", "Falta de confianza" y "Retrasos en la promoción", los valores son p=0,032, p=0,048, p=0,021, por lo que, con un nivel de confianza del 95%, afirmamos que las percepciones también difieren. El cálculo del tamaño del efecto refleja que las diferencias producidas entre hombres y mujeres son grandes en las cuatro primeras barreras y moderadas en las tres últimas (ver Tabla 5).

Tabla 3.
Prueba de contraste Mann-Withney y tamaño del efecto. Resultados para la salida Gestión de la Producción de Obra

	Gestión de la Producción de Obra		
Barreras de carrera	Mann-Whitney U	p	d
Inadecuada preparación	314,000	,089	
Restricciones en el mercado laboral	306,500	,057	
Jefe sesgado	169,500	,000**	1,20
Falta de confianza	232,500	,003**	0,81
Desaprobación persona significativa	314,500	,118	
Acoso sexual	213,000	,001**	0,91
Dificultades de socialización	345,000	,240	
Conflictos múltiples tareas	406,500	,872	
Dificultades para tomar decisiones	330,000	,155	
Conflicto entre hijos-trabajo	363,000	,377	
Retrasos en la promoción con respecto a personas del sexo opuesto	268,500	,012*	0,71
Insatisfacción con la carrera profesional	382,500	,585	
Percepción de salarios inferiores a los del sexo opuesto	210,500	,001**	0,92
Falta de apoyo	369,500	,419	
Discriminación sexual en la contratación	226,500	,002**	0,91

Fuente: Elaboración propia
Nota: Para el cálculo de la "d" de Cohen se han calculado desviaciones típicas combinadas. (Cohen 1988).
*p<0,05 **p<0,01

Tabla 4.
Prueba de contraste Mann-Withney y tamaño del efecto. Resultados para la salida de Prevención y Seguridad y salud

	Prevención y Seguridad y Salud		
Barreras de carrera	Mann-Whitney U	p	d
Inadecuada preparación	312,500	,093	
Restricciones en el mercado laboral	349,000	,267	
Jefe sesgado	161,500	,000**	1,42
Falta de confianza	235,500	,004**	1,17
Desaprobación persona significativa	386,000	,605	
Acoso sexual	168,000	,000**	1,30
Dificultades de socialización	339,000	,202	
Conflictos múltiples tareas	335,500	,277	
Dificultades para tomar decisiones	301,500	,063	
Conflicto entre hijos-trabajo	383,500	,591	
Retrasos en la promoción con respecto a personas del sexo opuesto	275,000	,018*	0,50
Insatisfacción con la carrera profesional	389,000	,661	
Percepción de salarios inferiores a los del sexo opuesto	213,500	,001**	1,11
Falta de apoyo	394,500	,714	
Discriminación sexual en la contratación	183,500	,000**	1,33

Fuente: Elaboración propia
Nota: Para el cálculo de la "d" de Cohen se han calculado desviaciones típicas combinadas. (Cohen 1988).
*p<0,05 **p<0,01

Tabla 5.
Prueba de contraste Mann-Withney y tamaño del efecto. Resultados para la salida Dirección técnica de la obra

	Dirección Técnica de la Obra		
Barreras de carrera	Mann-Whitney U	p	d
Inadecuada preparación	284,000	,032*	0,59
Restricciones en el mercado laboral	337,500	,183	
Jefe sesgado	228,500	,002**	0,80
Falta de confianza	296,000	,048*	0,51
Desaprobación persona significativa	389,500	,622	
Acoso sexual	166,000	,000**	1,11
Dificultades de socialización	289,000	,054	
Conflictos múltiples tareas	399,000	,781	
Dificultades para tomar decisiones	359,500	,359	
Conflicto entre hijos-trabajo	356,500	,454	
Retrasos en la promoción con respecto a personas del sexo opuesto	280,000	,021*	0,53
Insatisfacción con la carrera profesional	413,500	,967	
Percepción de salarios inferiores a los del sexo opuesto	205,500	,001**	0,94
Falta de apoyo	382,000	,885	
Discriminación sexual en la contratación	152,500	,000**	1,38

Fuente: Elaboración propia
Nota: Para el cálculo de la "d" de Cohen se han calculado desviaciones típicas combinadas. (Cohen 1988).
*p<0,05 **p<0,01

A continuación, en la Tabla 6, se muestran las barreras que son percibidas como más importantes para cada sexo, excluyendo, por no encontrarse determinante, aquellas en las que los porcentajes de estudiantes que confirman dicha percepción están muy próximos al 50%. Los hombres, para las tres salidas profesionales bajo estudio, perciben una única barrera como importante, las "Restricciones en el mercado laboral". De hecho, un aproximado 83% de estudiantes así lo reconoce. Es importante destacar que ellos no perciben ninguna barrera que haga alusión expresa al sexo, entendiendo que su condición de hombre no supondrá un obstáculo en su carrera profesional.

Tabla 6.
Barreras percibidas en salidas estrechamente relacionadas con trabajos en obra

Sexo	Gestión de la producción de la obra	Prevención y Seguridad y salud	Dirección técnica de la obra
Mujer	· Restricciones en el mercado laboral · Inadecuada preparación · Falta de confianza · Jefe sesgado contra las personas de mi sexo · Discriminación sexual en la contratación	· Falta de confianza · Restricciones en el mercado laboral · Inadecuada preparación · Jefe sesgado contra las personas de mi sexo · Dificultades para tomar decisiones · Discriminación sexual en la contratación	· Restricciones en el mercado laboral · Inadecuada preparación · Falta de confianza · Dificultades para tomar decisiones
Hombre	· Restricciones en el mercado laboral	· Restricciones en el mercado laboral	· Restricciones en el mercado laboral

Fuente: Elaboración propia

Las mujeres perciben tres barreras comunes a las salidas de obra, que a su vez son las que cobran mayor importancia en cada una: "Restricciones en el mercado laboral" (alrededor del 70-72%), "Inadecuada preparación" (64%) y "Falta de confianza" (percibida de forma más irregular, siendo la barrera más valorada en el perfil de Prevención y seguridad y salud). Esto nos indica que en esta salida laboral, a pesar de la crisis económica que afecta tan de lleno a la industria de la construcción, para las mujeres encuestadas la sensación de no sentirse capacitadas para realizar este trabajo es el principal obstáculo en su futuro laboral.

La siguiente barrera de carrera percibida por las mujeres es "Tener un jefe sesgado", que se pone de manifiesto para Gestión de la producción de obra (con un 57,7%) y para Prevención y seguridad y salud (65,4%). Ambas salidas comparten también la barrera "Discriminación sexual en la contratación" con alrededor del 60% de mujeres anticipándola. De igual modo, en torno al 60% de mujeres perciben "Dificultades para tomar decisiones" en las salidas Prevención y Seguridad y salud y Dirección técnica de la obra.

Esta barrera puede estar relacionada con la "Falta de confianza" o su baja autoestima, y la sensación de poseer una "Preparación inadecuada" para desarrollar un trabajo, desencadenando una suma de obstáculos que se retroalimentan y que no benefician su desarrollo profesional.

4. Conclusiones y reflexiones

El estudio realizado pone de manifiesto que tanto las mujeres como los hombres perciben que los principales obstáculos que van a dificultar el desarrollo de su vida laboral

futura en las seis salidas profesionales de la edificación, son una economía restrictiva con pocas oportunidades y opciones limitadas, así como la sensación de una preparación inadecuada.

En España desde mediados de 2007, se vive una profunda crisis económica que ha afectado duramente al sector de la edificación. Como es lógico, el alumnado conoce la situación y percibe que las restricciones económicas es la barrera más incidente en el sector, alcanzando su máxima valoración en la salida Gestión de la producción de la obra.

La próxima generación de ingenieros de la edificación también siente no estar suficientemente preparada y cualificada para ejercer la profesión. Esto es consistente con otras investigaciones que ponen de manifiesto que los egresados de estudios similares sienten que carecen de conocimientos prácticos aplicables a la ingeniería cuando acceden a su primer trabajo en el sector [36]. También confirma los resultados de trabajos previos que muestran la existencia de importantes desajustes educativos entre la formación universitaria y el desempeño profesional para el caso del jefe (a) de obra [37].

En las tres salidas profesionales de obra, el escenario laboral futuro es vislumbrado como más difícil para las futuras ingenieras de edificación. Mientras que ellos perciben que encontrarán un único obstáculo importante: las "Restricciones en el mercado laboral", ellas perciben tres: "Restricciones en el mercado laboral", "Inadecuada preparación" y "Falta de confianza".

La variable sexo determina la percepción que el alumnado tiene de numerosas barreras relacionadas, principalmente, con las discriminaciones por el hecho de ser mujer. Así, las alumnas anticipan que van a encontrar jefes sesgados a favor de los hombres y que serán discriminadas en la contratación en las salidas profesionales Gestión de la producción y Seguridad y salud. Sin embargo, no identifican ninguna en la Dirección técnica de la obra.

El resto de barreras que la literatura pone de manifiesto que encuentran las mujeres en el ejercicio de la profesión en edificación [4-5,10-11], no son previstas por estas alumnas, quizá por el desconocimiento de una realidad que está aún por venir.

Los resultados obtenidos nos permiten reflexionar sobre las repercusiones que estas percepciones tempranas pueden tener en el desarrollo profesional de esta próxima generación de ingenieros(as) de la edificación. De acuerdo con Gottfredson [30], posiblemente las mujeres excluirán de su abanico de ocupaciones aquéllas en las que perciban más obstáculos, pudiendo descartar la Gestión de la producción de la obra y Seguridad y Salud; o bien, afrontarán un escenario a priori percibido como más hostil en el que tendrán que desarrollar estrategias para no ser discriminadas en los procesos de selección y en su posterior desarrollo profesional. Ante este escenario, es posible que dirijan sus esfuerzos a buscar empleo en ocupaciones de la edificación ajenas a la obra, provocando a su vez, segregación ocupacional dentro de la edificación. No obstante, las conclusiones expuestas se basan en resultados de un estudio temprano, por lo que los resultados alcanzados no son generalizables a toda la población y serán confirmados o no con la totalidad de la muestra.

Bajo la perspectiva de género, la importancia de hacer visibles estas barreras en el sector radica en su condición fundamental para la búsqueda de soluciones que contribuyan al ejercicio de una profesión más equitativa e igualitaria, donde no tenga cabida la discriminación por razón de sexo, etnia, religión, discapacidad, orientación sexual, u otras; y donde la igualdad de oportunidades sea un hecho real.

Referencias

[1] Rivas, H., Análisis del sector de la construcción a escala internacional. Caso de Estados Unidos. Tesis, Facultad de Dirección y Administración de Empresas, Departamento de Organización de Empresas, Universidad Politécnica de Valencia. 2014.

[2] De Felipe-Blanch, J.J., Freijo-Álvarez, M., Alfonso, P., Sanmiquel-Pera, Ll. and Vintró-Sánchez, C., Occupational injuries in the mining sector (2000-2010). Comparison with the construction sector. DYNA, 81(186), pp. 153-158, 2014. DOI: 10.15446/DYNA.V81N186.39771

[3] Enshassi, A., Ihsen, S. and Al Hallaq, K., The perception of women engineers in the construction industry in Palestine. European Journal of Engineering Education, 33(1), pp. 13-20, 2008. DOI: 10.1080/03043790701745944

[4] Román-Onsalo, M., Navarro-Astor, E. and Infante-Perea, M., Barreras de carrera en la industria de la construcción. V Congreso universitario internacional "Investigación y género", Sevilla, 3-4 Julio 2014.

[5] Caven, V. and Navarro-Astor, E. The potential for gender equality in architecture: An Anglo-Spanish comparison, Construction Management and Economics, 31(8), pp. 874-882, 2013. DOI: 10.1080/01446193.2013.766358

[6] Choudhury, T., Experiences of women as workers: A study of construction workers in Bangladesh. Construction Management and Economics, 31(8), pp. 883-898, 2013. DOI.: 10.1080/01446193.2012.756143

[7] Wright, T., Uncovering sexuality and gender: an intersectional examination of women's experience in UK construction. Construction Management and Economics, 31(8), pp. 832-844, 2013. DOI: 10.1080/01446193.2013.794297

[8] Denissen, A.M., Crossing the line: how women in the building trades interpret and respond to sexual conduct at work. Journal of Contemporary Ethnography, 39(3), pp. 297-327, 2010. DOI: 10.1177/0891241609341827

[9] Bagilhole, B., Dainty, A. and Neale, R., A woman engineer's experiences of working on British Construction Sites. International Journal of Engineering Education, [Online]. 18(4), pp. 422-429, 2002. Available at: http://www.ijee.ie/articles/Vol18-4/IJEE1292.pdf

[10] Navarro-Astor, E., Work-family balance issues among construction professionals in Spain. Proceedings of 27th Annual ARCOM Conference, 5-7 September. Leeds, UK, Association of Researchers in Construction Management, [Online]. pp. 177-186, 2011. Available at: http://www.arcom.ac.uk/-docs/proceedings/ar2011-0177-0186_Navarro-Astor.pdf

[11] Dainty, A.R.J., Bagihole, B.M. and Neale, R.H., A grounded theory of women's career under-achievement in large UK construction companies. Construction Management and Economics, 18(2), pp. 239-250, 2000. DOI: 10.1080/014461900370861

[12] De Graft-Johnson, A., Manley, S. and Greed, C., Diversity or the lack of it in the architectural profession. Construction Management and Economics, [Online]. 23(10), pp. 1035-1043, 2005. Available at: http://www.tandfonline.com/doi/abs/10.1080/01446190500394233

[13] English, J. and Le Jeune, K., Do professional women and tradeswomen in the South African construction industry share common employment barriers despite progressive government legislation?. Journal of Professional Issues in Engineering Education and Practice, 138(2), pp. 145-152, 2012. DOI: 10.1061/(ASCE)EI.1943-5541.0000095

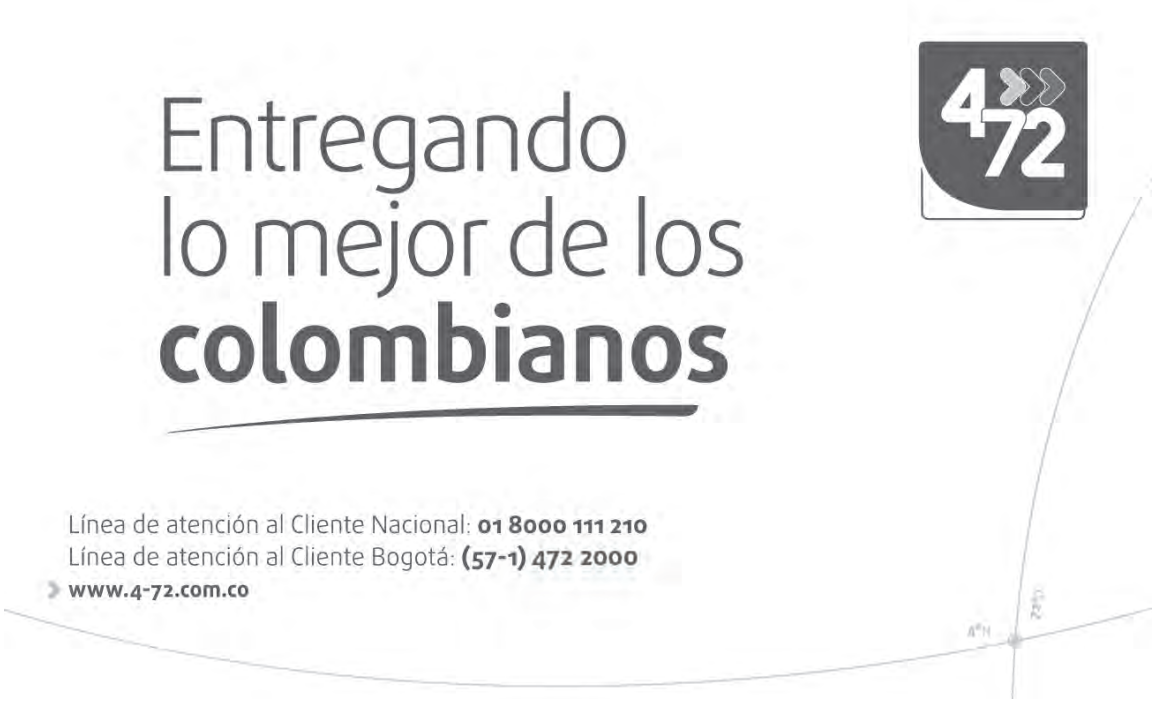
[14] Greed. C., Women in the construction professions: achieving critical mass. Gender, Work and Organization, 7(3), pp. 181-196, 2000. DOI: 10.1111/1468-0432.00106

[15] Arslan, G. and Kivrak, S., The lower employment of women in Turkish construction sector. Building and Environment, [Online]. 39(11), pp. 379-387, 2004. Available at: http://www.sciencedirect.com/science/article/pii/S0360132304001106
[16] Whittock, M., Women's experiences of non-traditional employment: Is gender equality in this area possible?. Construction Management and Economics, 20(5), pp. 449-456, 2002. DOI: 10.1080/01446190210140197
[17] Dainty, A. and Lingard, H., Indirect discrimination in construction organisations and the impact on women's careers. Journal of Management in Engineering, 22(3), pp. 108-118, 2006. DOI: 10.1061/(ASCE)0742-597X(2006)22:3(108)
[18] Watts, J., Leaders of men: Women "managing" in construction. Work, Employment and Society, 23(3), pp. 512-530, 2009. DOI: 10.1177/0950017009337074
[19] Solís, R., González, J.A. y Pacheco, J., Estudio de egresados de Ingeniería Civil en una Universidad de México. Revista Ingeniería e Investigación, 26(3), pp. 129-134, 2006.
[20] Kehinde, J.O. and Okoli, O.G., Professional women and career impediments in the construction industry in Nigeria. Journal of Professional Issues in Engineering Education and Practice, 130(2), pp. 115-119, 2004. DOI: 10.1061/(ASCE)1052-3928(2004)130:2(115)
[21] Borrás, G. y Bucci, I., La inserción laboral de las profesionales ingenieras en el ámbito público, privado y académico. VI Congreso Nacional de Estudios del Trabajo, [Online]. Asociación Nacional de Especialistas en Estudios del Trabajo. Buenos Aires, Argentina, 2003. Disponible en: http://www.aset.org.ar/congresos/6/archivosPDF/grupoTematico05/024.pdf
[22] Construction Sector Council. The state of women in construction in Canada. Ottawa: CSC. [Online]. 2010. Available at: http://www.cawic.ca/Resources/Documents/Recruitment_Women_English_State_of_Women_in_Construction_in_Canada%5B1%5D.pdf
[23] Ayre, M., Mills, J. and Gill, J., Yes, I do belong: The women who stay in engineering. Engineering Studies, [Online]. 5(3), pp. 216-232, 2013. Available at: http://www.tandfonline.com/doi/abs/10.1080/19378629.2013.855781
[24] Arango, L.G., Género e Ingeniería: La identidad profesional en discusión. Reflexiones a partir del caso de la Ingeniería de Sistemas en la Universidad Nacional de Colombia. Revista Latinoamericana de Estudios del Trabajo, [Online]. 18, pp. 199-223, 2006. Disponible en: http://relet.iesp.uerj.br/Relet_18/art9.pdf
[25] Olarte, MEC. La feminización de la educación superior y las implicaciones en el mercado laboral y los centros de decisión política. UNESCO, IESALC. 2005.
[26] Ministerio de Educación, Cultura y Deporte. Datos y cifras del sistema universitario Español. Curso 2013-2014. Gobierno de España. [Online]. 2015, 148 p. Disponible en: http://www.mecd.gob.es/dms/mecd/educacion-mecd/areas-educacion/universidades/estadisticas-informes/datos-cifras/DATOS_CIFRAS_13_14.pdf
[27] Abdullah, N.Z., Arshad, R.A. and Ariffin M.H., Technical female graduates in the Malaysan construction industry: Attrition Issues. International Surveying Research Journal, 3(1), pp. 33-43, 2013.
[28] Hossain, J. and Kusakabe, K., Sex segregation in construction organizations in Bangladesh and Thailand. Construction Management and Economics, [Online]. 23(6), pp. 609-619, 2005. Available at: http://www.tandfonline.com/doi/abs/10.1080/01446190500127062
[29] Infante-Perea, M., Román-Onsalo, M., Traverso-Cortés, J., La educación universitaria: Un factor de empleabilidad y estabilidad laboral de la mujer en el sector de la construcción. Revista Iberoamericana de Educación, RIE [En línea]. 56 (4), pp. 2-11, 2011. Disponible en: http://www.rieoei.org/deloslectores/4202Perea.pdf
[30] Gottfredson, L., Circumscription and compromise: A developmental theory of occupational aspirations. Journal of counselling psychology, 28(6), pp. 545- 579, 1981.
[31] Worrall, L., Organizational cultures: Obstacles to women in the UK construction industry, Journal of Psychological Issues in Organizational Culture, 2(4), pp. 6-21, 2012. DOI: 10.1002/jpoc.20088
[32] Román, M., Infante, M., Traverso, J. y Gil, M.R., Segregación ocupacional y empleabilidad femenina en el sector andaluz de la construcción. Libro de actas 1er. Congreso Universitario de Investigación y Género. Universidad de Sevilla. pp. 1191-1210. 2009.
[33] ANECA, Libro Blanco. Título de Grado en Ingeniería de Edificación. Agencia Nacional de Evaluación de la Calidad y Acreditación, 2004.
[34] Swanson, J.L., Daniels, K.K. and Tokar, D.M., Assessing perceptions of career related barriers: The Career Barriers Inventory. Journal of Career Assessment, 4(2), pp. 219-244, 1996.
[35] Bester, J., The perception of career barriers among South African university students. Thesis MSc of Arts (Psychology) in the Faculty of Arts and Social. Sciences at Stellenbosch University, Stellenbosch, Sudáfrica, [Online]. 2011. Available at: http://scholar.sun.ac.za/handle/10019.1/6719
[36] Solís, R. y Arcudia, C., Estudio de caso en México: Los alumnos de ingeniería civil opinan sobre las debilidades de egreso. Revista Ingeniería e Investigación, 24(2), pp. 27-34, 2004.
[37] Fuentes-del-Burgo, J. and Navarro-Astor, Do educational mismatches influence job satisfaction? The case of spanish building engineering graduates working as site managers. Proceedings of 29th Annual ARCOM Conference, Reading, UK, Association of Researchers in Construction Management, [Online]. pp. 237-247, 2013. Available at: http://www.arcom.ac.uk/-docs/proceedings/ar2013-0237-0247_Fuentes-del-Burgo_Navarro-Astor.pdf

M. Infante-Perea, obtuvo el título de Arquitecta Técnica en 2006 y el de Graduada en Ingeniería de Edificación en 2010, ambos por la Universidad de Sevilla. Así mismo en 2010 obtuvo también el título de MSc. en Seguridad Integral en la Edificación por la misma Universidad. Actualmente se encuentra realizando la Tesis Doctoral. En el campo profesional trabajó como arquitecta técnica para la Diputación de Huelva (Andalucía, España), realizó diversos trabajos en estudio de arquitectura y se dedicó durante unos años a las tasaciones y valoraciones inmobiliarias. En la actualidad es miembro del Departamento de Ingeniería Gráfica de la Universidad de Sevilla, España, e imparte clases en la Escuela Técnica Superior de Ingeniería de Edificación de la misma Universidad. Su principal línea de investigación es el sector de la construcción bajo la perspectiva de género.
ORCID: 0000-0002-1880-3069

M. Román-Onsalo, recibió su título de Dra. en Dirección y Administración de Empresas en 1997 y desde el año 1989 es profesora de la Universidad de Sevilla, España. Sus últimas publicaciones en revistas científicas se centran en el estudio del mercado laboral en el sector de la construcción. Incorporar la perspectiva de género a estas investigaciones es su principal foco de interés en la actualidad. Desde 2009 es coordinadora del Máster Agente de Igualdad para la intervención social con enfoque de género, Título Propio de la Universidad de Sevilla, España.

E. Navarro-Astor, es profesora titular de Escuela Universitaria de la Universitat Politècnica de València (UPV) desde 2002, adscrita a la Escuela Técnica Superior de Ingeniería de Edificación, y pertenece al Departamento de Organización de Empresas. Licenciada en Ciencias Económicas y Empresariales por la Universidad de Valencia, España, es doctora en Gestión de Empresas por la UPV desde 2008. Toda su trayectoria académica e investigadora se caracteriza por el intento de aportar al área de la Ingeniería y la Arquitectura aspectos relacionados con la gestión de personas que quizás, hasta la fecha, han sido poco tratados y considerados menos relevantes, como por ejemplo la motivación y la satisfacción laboral. Asimismo, en los últimos años, ha incorporado la perspectiva de género a muchas de sus investigaciones que se han centrado en el sector de la construcción, un sector tradicionalmente muy masculinizado en el que la mujer ha sido históricamente invisible.
ORCID: 0000-0002-1588-9186



DYNA
82 (194), December, 2015
is an edition consisting of 250 printed issues
which was finished printing in the month of October of 2015
in Todograficas Ltda. Medellín - Colombia

The cover was printed on Propalcote C1S 250 g,
the interior pages on Hanno Mate 90 g.
The fonts used are Times New Roman, Imprint MT Shadow

- Simulation of a hydrogen hybrid battery-fuel cell vehicle
- Using waste energy from the Organic Rankine Cycle cogeneration in the Portland cement industry
- The production, molecular weight and viscosifying power of alginate produced by Azotobacter vinelandii is affected by the carbon source in submerged cultures
- Supply chain knowledge management: A linked data-based approach using SKOS
- The green supplier selection as a key element in a supply chain: A review of cases studies
- The effect of crosswinds on ride comfort in high speed trains running on curves
- Valorization of vinasse as binder modifier in asphalt mixtures
- Comparison of consistency assessment models for isolated horizontal curves in two-lane rural highways
- Competition between anisotropy and dipolar interaction in multicore nanoparticles: Monte Carlo simulation
- Broad-Range tunable optical wavelength converter for next generation optical superchannels
- Numerical analysis of the influence of sample stiffness and plate shape in the Brazilian test
- Validating the University of Delaware's precipitation and temperature database for northern South America
- Experimental behavior of a masonry wall supported on a RC two-way slab
- Synthesis of ternary geopolymers based on metakaolin, boiler slag and rice husk ash
- New tuning rules for PID controllers based on IMC with minimum IAE for inverse response processes
- Low-cost platform for the evaluation of single phase electromagnetic phenomena of power quality according to the IEEE 1159 standard
- Self-assessment: A critical competence for Industrial Engineering
- Maintenance management program through the implementation of predictive tools and TPM as a contribution to improving energy efficiency in power plants
- Numerical modelling of Alto Verde landslide using the material point method
- The energy trilemma in the policy design of the electricity market
- Influence of seawater immersion in low energy impact behavior of a novel colombian fique fiber reinforced bio-resin laminate
- Effect of V addition on the hardness, adherence and friction coefficient of VC coatings produced by thermo-reactive diffusion deposition
- Multi-level pedagogical model for the personalization of pedagogical strategies in intelligent tutoring systems
- Impact of working conditions on the quality of working life: Case manufacturing sector colombian Caribbean Region
- Application of a prefeasibility study methodology in the selection of road infrastructure projects: The case of Manizales (Colombia)
- Simulation of a thermal environment in two buildings for the wet processing of coffee
- A comparative study of multiobjective computational intelligence algorithms to find the solution to the RWA problem in WDM networks
- Determination of the Rayleigh damping coefficients of steel bristles and clusters of bristles of gutter brushes
- Estimate of induced stress during filling and discharge of metallic silos for cement storage
- An early view of the barriers to entry and career development in Building Engineering

- Simulación de un vehículo híbrido de hidrógeno con batería y pila de combustible
- Aprovechamiento del calor residual por cogeneración con Ciclo Rankine Orgánico en la industria del cemento Portland
- La producción, el peso molecular y el poder viscosificante del alginato producido por Azotobacter vinelandii es afectado por la fuente de carbono en cultivos sumergidos
- Administración del conocimiento en cadenas de suministro: Un enfoque basado en Linked Data usando SKOS
- Selección de proveedores verde como un elemento clave en la cadena de suministro: Una revisión de casos de estudio
- Influencia del viento lateral en el confort de vehículos ferroviarios de alta velocidad circulando en curvas
- Revalorización de la vinaza como modificador de betún para mezclas bituminosas
- Comparación de modelos de análisis de consistencia para curvas horizontales aisladas en carreteras de dos carriles
- Competición entre la anisotropía y la interacción dipolar en nanopartículas multi-núcleo: simulación Monte Carlo
- Conversor de longitud de onda óptico sintonizable de banda ancha para la siguiente generación de supercanales ópticos
- Análisis numérico de la influencia de la dureza de la muestra y la forma de placa en el ensayo Brasileño
- Validación de la precipitación y temperatura de la base de datos de la Universidad de Delaware en el norte de Suramérica
- Comportamiento experimental de un muro de mampostería apoyado sobre una losa de concreto reforzado
- Síntesis de geopolímeros ternarios basados en metakaolin, escoria de parrilla y ceniza de cascarilla de arroz
- Nuevas reglas de sintonía basadas en IMC para un controlador PID con IAE mínimo en procesos con respuesta inversa
- Plataforma de bajo costo para la evaluación de fenómenos electromagnéticos monofásicos de calidad de la energía según el estándar IEEE 1159
- Autoevaluación: Una competencia crítica para la Ingeniería Industrial
- Programa de gestión de mantenimiento a través de la implementación de herramientas predictivas y de TPM como contribución a la mejora de la eficiencia energética en plantas termoeléctricas
- Modelamiento numérico del deslizamiento Alto Verde usando el método del punto material
- El trilema energético en el diseño de políticas del mercado eléctrico
- Influencia del agua de mar en el comportamiento frente a impacto de baja energía de un nuevo laminado de resina natural reforzada con fibra de fique colombiano
- Efecto de la adición de V en la dureza, adherencia y el coeficiente de fricción de recubrimientos de VC producidos mediante deposito termo-reactiva/difusión
- Modelo pedagógico multinivel para la personalización de estrategias pedagógicas en sistemas tutoriales inteligentes
- Impacto de las condiciones de trabajo en calidad de vida laboral: Caso del sector manufacturero de la Región Caribe colombiana
- Aplicación de una metodología a nivel de prefactibilidad para la selección de proyectos de infraestructura vial. El caso de Manizales (Colombia)
- Simulación del ambiente térmico en dos edificaciones para beneficio húmedo de café
- Estudio comparativo de algoritmos de inteligencia computacional multiobjetivo para la solución del problema RWA en redes WDM
- Determinación de los coeficientes de amortiguamiento de Rayleigh de cerdas y grupos de cerdas de acero de cepillos laterales
- Estimación de esfuerzos inducidos durante el llenado y vaciado de silos metálicos para almacenamiento de cemento
- Una visión temprana de los obstáculos de acceso y deqsarrollo profesional en Ingeniería de edificación

DYNA
Publication admitted to the
Sistema Nacional de Indexación y Homologación de
Revistas Especializadas CT+I - PUBLINDEX, Category A1

Red Colombiana de Revistas de Ingeniería

UNIVERSIDAD NACIONAL DE COLOMBIA
SEDE MEDELLÍN
FACULTAD DE MINAS